

The action of flecainide on the wild-type cardiac ryanodine receptor

Emma Jane Steer, BSc

Submitted in accordance with the requirements for the degree of
Doctor of Philosophy

University of Leeds
Faculty of Biological Sciences
School of Biomedical Sciences

May 2017

The candidate confirms that the work submitted is his/her own and that appropriate credit has been given where reference has been made to the work of others.

This copy had been supplied on the understanding that it is copyright material and that no quotation from the thesis may be published without proper acknowledgement.

Acknowledgments

Foremost, I would like to thank my supervisor, Prof Derek Steele, for the opportunity to undertake this project and the time that you have given to support me through it. Thank you for always having an open door to discuss the latest developments; your guidance has been invaluable.

To my co-supervisor and mentor, Prof Ed White, thank you for your time in supporting me during both my Undergraduate degree and throughout this project. I would not be here without your help and advice.

My thanks also go to all the members of the Cellular Cardiology research group and others with whom I have had the pleasure of working with. In particular I would like to thank Dr Al Benson, for writing the analysis code and your timely help during the last lap of this project. Thank you to Dr Sebastien Sikora for writing the other half of the analysis code and your thoughts throughout this project. Thank you to Dr Sarah Calaghan, for your generosity and encouragement in forming scientific collaborations and sharing your baking delights. Thank you to Dr Moza Al Owais for the electrophysiological measurements and your excellent gardening tips. Thank you to Dr Hannah Kirton for the Western blots, all the beautiful cells you've given me and the interesting chats we've had throughout these last few years. Thank you to Dr Zhaokang Yang for all of your help in the lab, being so open to answering even the silliest of questions and all of our engaging discussions. Thank you to Dr Isuru Jayasinghe, for giving your time to read over my thesis, introducing me to the Airyscan microscope and the advice that you have given me. Thank you to Prof Arun Holden for your support and advice both during and after my Undergraduate projects with you. Thank you to Dr John Colyer, for your genuine interest in the work and help in understanding the molecular side of things. Thanks to Dr Kathleen Wright for involving me in your excellent outreach projects. Thanks to Dr Matt Hardy for your curious anecdotes and positive outlook, which have always kept me smiling. Thanks to everyone in Hull for the encouragement during the last steps. An important thank you also goes to Prof John Lydon, for the incredibly inspiring chats, city tours and Christmas parties, I have learnt so much.

I have also had the privilege of working alongside my friends Ewan, Ruth and Sabine, whose weekly debriefs over a (half) pint have kept me going when I needed it most. Thanks to Ewan, for your discerning scientific observations, for introducing me to some excellent ceilidhs and impressive ability to conjure up excellent cardiac-related jokes. What DID happen to the cardiomyocyte that drank too much coffee? Thank you to Sabine, for your unrelenting patience with all my silly questions, continuous smiley demeanour and love of good cheese which should always be commended. We'll try to smuggle you some unpasteurised goodness somehow! To Ruth, thanks for being there 'til the end! For motivating me to exercise once in a blue moon, providing continual bear-attack-training and for letting me in on the keyboard short cut secrets. We did it!

A special thank you to all my girls, spread near and far. For all your support when I was there and understanding when I was not. Tea, soon?

Of course, I would like to thank my family: To Jan and Gary for your open ears and green space when the city became too grey. To Rob, Sarah, Owen, Lucy and Pippa for reminding me that there is a life away from flecainide, and it's wonderful. To Nan and Grampy, scientific thinkers through and through; thank you for your pride in all of us, with everything that we do. Danke zu meine liebe Oma, lieber Opa und alle die ich lieb habe in Deutschland. Ich freue mich Euch wiederzusehen!

Thank you to Seb, for your endless patience, love, practical advice and hot meals. You are my rock.

Thanks also to James for sending me silly cat videos and making me laugh when I most needed it - I'll return the favour in a year or so! Most importantly, thank you to my Mum and Dad, Esther and Alan, for your unwavering love and support throughout my life. Thank you for encouraging me to continue with science and with what I love. I am truly thankful that these are one and the same. I wouldn't be here without you.

Published abstracts

Steer E, Yang Z, White E, Steele DS (2016) Flecainide accumulates within intact ventricular cardiomyocytes and its intracellular effect on RyR2 is potentiated by SR counter-current block. Proceeding Abstracts of the Physiological Society **37**, PCB053.

Lotteau S, Yang Z, Venturi E, **Steer E**, Witschas K, Sitsapesan R, Steele D, Calaghan S (2016) Differential effects of statins on Ca²⁺ sparks in permeabilised rat skeletal and cardiac muscle: A mechanism for statin-induced myopathy. Proceeding Abstracts of the Physiological Society **37**, PCB021.

Venturi E, Witschas K, Lotteau S, **Steer E**, Steele D, Calaghan S, Sitsapesan R (2016) Simvastatin differentially modulates single cardiac and skeletal ryanodine receptor channels Proceeding Abstracts of the Physiological Society **37**, PCA052.

Lotteau S, Yang Z, Venturi E, **Steer E**, Witschas K, Sitsapesan R, Steele D, Calaghan S (2016) Simvastatin has profound effects on sarcoplasmic reticulum Ca²⁺ leak in skeletal but not cardiac muscle: A mechanism for myopathy. 2016 Biophysical Society Meeting Abstracts. Biophysical Journal, **110**, 1319-Pos.

Venturi E, Witschas K, Lotteau S, **Steer E**, Steele D, Calaghan S, Sitsapesan R (2016) Simvastatin activates single skeletal RyR1 channels but exerts more complex regulation of the cardiac isoform, RyR2. 2016 Biophysical Society Meeting Abstracts. Biophysical Journal, **110**, 1318-Pos.

Steer E, Yang Z, Steele DS (2015) Effects of flecainide on Ca²⁺ sparks and waves in saponin permeabilised rat ventricular myocytes. Proceeding Abstracts of the Physiological Society **34**, PC031.

Fowler E, Norman R, **Steer E**, Pervolaraki E, Stones R, Drinkhill M, Calaghan S, Steele D, White E (2015) The β 1 adrenergic receptor blocker metoprolol improves survival and partially restores Ca²⁺ handling abnormalities in rat pulmonary artery hypertension Proceeding Abstracts of the Physiological Society **34**, C03.

Communications

Oral

Flecainide is protective against spontaneous Ca^{2+} wave development yet does not alter Ca^{2+} spark properties in intact rat ventricular myocytes. September 2014. Early Career Research Conference in Cardiovascular and Diabetes Research. Leeds, UK. **Oral Communication Prize**

Posters

Flecainide accumulates within intact ventricular cardiomyocytes and its intracellular effect on RyR2 is potentiated by SR counter-current block. June 2016. *The Physiological Society Annual Meeting 2016*. Dublin, Ireland.

Flecainide acts on RyR2 to reduce spontaneous Ca^{2+} wave frequency and this is potentiated by SR K^+ counter-current block. April 2016. *Northern Cardiovascular Research Group*. Leeds, UK.

Effects of flecainide on Ca^{2+} sparks and waves in saponin permeabilised rat ventricular myocytes. July 2015. *The Physiological Society Annual Meeting 2015*. Cardiff, UK.

Effects of flecainide in permeabilised rat ventricular myocyte depend on the severity of Ca^{2+} overload. April 2015. *Northern Cardiovascular Research Group*. Newcastle, UK.

The effect of flecainide on spontaneous Ca^{2+} waves and sparks in wild-type rat ventricular cells. November 2014. *German Centre for Cardiovascular Research Symposium*. Berlin, Germany.

Abstract

The genetic disorder catecholaminergic polymorphic ventricular tachycardia (CPVT) causes the function of the sarcoplasmic reticulum (SR) Ca^{2+} release channel (RyR2) to be altered and induces fatal arrhythmias during stress or exercise. Flecainide, a class 1C sodium channel ($\text{Na}_v1.5$) inhibitor and anti-arrhythmic agent, was recently observed to be effective against CPVT arrhythmias. Controversially, it was suggested that flecainide acted directly on RyR2, alongside its action on $\text{Na}_v1.5$. The present study sought to establish whether flecainide affected RyR2 activity to prevent pro-arrhythmic Ca^{2+} waves in wild type (WT) cardiomyocytes and if so, to elucidate the mechanisms responsible.

Flecainide or flecainide-FITC was applied to intact or saponin permeabilised cardiomyocytes isolated from WT rat ventricle. Confocal microscopy was used to image SR Ca^{2+} release after application of flecainide or trans-sarcolemmal movement of fluorescent flecainide-FITC.

In intact myocytes, flecainide decreased pro-arrhythmic Ca^{2+} wave frequency although Ca^{2+} spark properties were unchanged, indicating no effect on RyR2 despite prolonged flecainide exposure (45 min). Flecainide-FITC traversed the sarcolemma over a period of hours and primarily accumulated in the mitochondria. In permeabilised myocytes, where flecainide had immediate access to RyR2 and $\text{Na}_v1.5$ was non-functional, a 10-20% decrease in wave frequency was apparent, accompanied by sustained changes in Ca^{2+} spark properties. The effect on waves was potentiated when the SR counter-current was inhibited by substitution of K^+ with Cs^+ .

These results suggest that flecainide has an anti-arrhythmic effect on RyR2 in permeabilised WT cardiomyocytes. However, slow cytosolic accumulation and the requirement for an increased drug concentration may explain the absence of an effect on RyR2 in intact cells. Nevertheless, these findings support the concept that RyR2 channel activity can be pharmacologically manipulated and that RyR2 represents a potential pharmacological target in patients with arrhythmia.

Contents

Acknowledgments.....	iii
Published abstracts	v
Communications	vi
Abstract	vii
Contents	viii
Figures	xiv
Tables	xviii
Main abbreviations and agents	xix
Chapter 1: General introduction	1
1.1 General introduction.....	1
1.2 The structure and function of the heart	2
1.3 The cardiomyocyte	4
1.3.1 The sarcolemma and transverse-tubules.....	6
1.3.2 The sarcoplasmic reticulum.....	7
1.3.3 The mitochondria.....	8
1.3.4 The sarcomere	10
1.3.5 The nucleus.....	12
1.4 Electrical excitation of the heart	13
1.4.1 Excitation contraction coupling and the action potential.....	13
1.4.2 The electrical conduction system.....	18
1.4.3 Autonomic modulation of heart rate	19
1.4.4 Sympathetic system	19
1.4.5 Parasympathetic system	20
1.5 Ca ²⁺ release from the sarcoplasmic reticulum	21
1.5.1 Ca ²⁺ induced Ca ²⁺ release	21
1.5.2 Ca ²⁺ waves	23
1.5.3 Ca ²⁺ sparks	24
1.5.4 Non-spark Ca ²⁺ release	26
1.5.5 Modulation of ryanodine receptor function	26
1.5.6 SR Autoregulation	29

1.6 Cardiac arrhythmias.....	31
1.6.1 Arrhythmic mechanisms at the single cell level	32
1.6.2 Arrhythmias at the tissue level	33
1.7 Catecholaminergic polymorphic ventricular tachycardia (CPVT).....	34
1.7.1 CPVT phenotype and characterisation	34
1.7.2 CPVT genotype.....	36
1.7.3 CPVT therapy	39
1.8 Flecainide.....	41
1.8.1 Flecainide induced inhibition of the cardiac Na ⁺ current	41
1.8.2 Flecainide inhibition of cardiac K ⁺ currents.....	45
1.8.3 Effects of flecainide on RyR2.....	45
1.9 Study aims	47

Chapter 2: General Methods 48

2.1 Solutions.....	48
2.2 Myocyte Isolation.....	48
2.3 Confocal microscopy imaging of live myocytes	56
2.4 Confocal microscopy Ca ²⁺ imaging of intact myocytes.....	58
2.4.1 Fluo-4-acetoxymethyl ester loading.....	58
2.4.2 Intact myocyte selection.....	58
2.4.3 XY imaging of intact myocytes.....	59
2.4.4 Line scan imaging of intact myocytes.....	59
2.5 Confocal microscopy of permeabilised myocytes.....	60
2.5.1 Saponin permeabilisation	60
2.5.2 Triton X-100 permeabilisation.....	61
2.5.3 Intracellular perfusion and Ca ²⁺ imaging in saponin permeabilised cells.....	61
2.5.4 Saponin permeabilised myocyte selection and confocal imaging	62
2.6 Confocal microscopy analysis	63
2.6.1 Analysis of intracellular Ca ²⁺ wave frequency in intact and saponin permeabilised myocytes	63
2.6.2 Semi-automated Ca ²⁺ wave dimension analysis in saponin permeabilised myocytes	63
2.6.3 Semi-automated Ca ²⁺ wave propagation velocity analysis in saponin permeabilised myocytes	65
2.6.4 Ca ²⁺ spark analysis.....	68
2.6.5 Analysis of flecainide-FITC in intact and permeabilised cells.....	70

2.7 Western blotting	71
2.7.1 Sample preparation.....	71
2.7.2 Bicinchoninic acid assay.....	71
2.7.3 Gel electrophoresis	72
2.7.4 Protein transfer.....	74
2.7.5 Membrane blocking and protein probing.....	75
2.7.6 Western blot analysis	75
2.8 Voltage clamp of cardiomyocytes	76
2.9 Monocrotaline model of right sided heart failure	77
2.10 Statistical analysis.....	77

Chapter 3: The effect of flecainide on Ca²⁺ handling in intact ventricular myocytes from wild type rat..... 78

3.1 Introduction	78
3.2 Methods	80
3.2.1 Myocyte imaging protocol	80
3.2.2 Voltage clamp of cardiomyocytes.....	81
3.2.3 Line scan analysis	81
3.2.4 Statistics	82
3.3 Results.....	83
3.3.1 The effect of 100 nM isoprenaline on Ca ²⁺ wave frequency and spark properties ...	83
3.3.2 The effect of field stimulation frequency on Ca ²⁺ wave frequency and spark properties in the presence of isoprenaline	84
3.3.3 The effect of flecainide on triggered Ca ²⁺ transients	91
3.3.4 The effect of flecainide on Ca ²⁺ waves during and after electrical pacing.....	91
3.3.5 The effect of flecainide on Ca ²⁺ sparks.....	93
3.3.6 The effect of flecainide after a 2 hour incubation period, including 35 min at 37°C	101
3.3.7 The effect of flecainide in a monocrotaline model of heart failure	101
3.3.8 The effect of flecainide on the cardiac peak Na ⁺ current.....	103
3.4 Discussion.....	114
3.4.1 The effects of isoprenaline on Ca ²⁺ wave and spark release.....	114
3.4.2 The effects of pacing frequency on Ca ²⁺ waves and sparks	116
3.4.3 The effects of flecainide on SR Ca ²⁺ release	116
3.4.4 Conclusions and summary	119

Chapter 4: Flecainide-FITC accumulation within intact and permeabilised ventricular myocytes..... 120

4.1 Introduction	120
4.2 Methods	122
4.2.1 Intact myocyte imaging protocol	122
4.2.2 Saponin and Triton X-100 permeabilised myocyte imaging protocol.....	122
4.2.3 Flecainide-FITC effects on $\text{Na}_v1.5$	123
4.2.4 Analysis and statistics	123
4.3 Results.....	125
4.3.1 Flecainide-FITC accumulation within intact myocytes	125
4.3.2 -FITC entry into intact cardiomyocytes.....	126
4.3.3 Flecainide-FITC accumulation within saponin permeabilised myocytes.....	132
4.3.4 Flecainide-FITC in Triton X-100 permeabilised myocytes.....	138
4.3.5 Effect of flecainide-FITC on cardiac Na^+ current.....	139
4.4 Discussion	145
4.4.1 Flecainide-FITC entry into intact cardiomyocytes.....	145
4.4.2 Flecainide-FITC within permeabilised cardiomyocytes	147
4.4.3 Flecainide-FITC properties.....	149
4.4.4 Conclusions and summary	151

Chapter 5: The effect of flecainide on Ca^{2+} handling in permeabilised ventricular myocytes..... 153

5.1 Introduction	153
5.2 Methods	155
5.2.1 Permeabilised myocyte imaging protocol.....	155
5.2.2 Application of exogenous CaM.....	156
5.2.3 Semi-quantification of CaM in intact and permeabilised ventricular myocytes	156
5.2.4 Analysis	157
5.2.5 Statistics	158
5.3 Results.....	159
5.3.1 The effect of $[\text{Ca}^{2+}]$ on permeabilised myocyte Ca^{2+} release	159
5.3.2 The effect of flecainide on Ca^{2+} waves	164
5.3.3 The effect of flecainide on Ca^{2+} sparks.....	176
5.3.4 The effect of flecainide on Ca^{2+} SR content.....	176

5.3.5 The effect of calmodulin on permeabilised myocyte Ca^{2+} release with and without flecainide	177
5.4 Discussion	190
5.4.1 The effect of intracellular $[\text{Ca}^{2+}]$ on Ca^{2+} waves and sparks	190
5.4.2 The effect of flecainide on Ca^{2+} waves, sparks and transients	191
5.4.3 The effect of flecainide on Ca^{2+} waves in the presence of calmodulin	193
5.4.4 Conclusions and Summary	195

Chapter 6: The effect of flecainide on RyR2 after inhibition of the SR counter-current in permeabilised myocytes 197

6.1 Introduction	197
6.2 Methods	199
6.2.1 SR K^+ counter-current block protocol	199
6.2.2 Valinomycin protocol	200
6.2.3 Analysis and statistics	200
6.3 Results	202
6.3.1 Cs^+ ion exchange decreased wave frequency and prolonged wave duration	202
6.3.2 Flecainide decreased wave frequency after counter-current inhibition	202
6.3.3 Flecainide countered the decrease in wave frequency caused by valinomycin	203
6.4 Discussion	215
6.4.1 Channels which mediate the K^+ SR counter-current	215
6.4.2 Block of SR counter-current with Cs^+ and effect on Ca^{2+} release	217
6.4.3 The effect of flecainide on wave frequency was exacerbated when SR counter-current was slowed with Cs^+	218
6.4.4 The effect of flecainide on wave frequency when SR counter-current was increased with valinomycin	220
6.4.5 The effect on wave frequency in the presence of valinomycin and flecainide	221
6.4.6 Limitations	222
6.4.7 Conclusions and Summary	224

Chapter 7: General Discussion 225

7.1 Introduction	225
7.2 The diffusion of flecainide across the sarcolemma and its effects in intact and permeabilised myocytes	225
7.3 Proposed mechanism of action of flecainide on RyR2	227
7.4 The effect of flecainide on other intracellular membrane bound proteins	228

7.5 Differences in effect seen with flecainide in WT and CPVT animal models.....	232
7.6 Future perspectives.....	233
7.7 Clinical implications.....	234
Appendix.....	236
References.....	237

Figures

Chapter 1

Figure 1.1 Ultra-structure of the heart and ventricular tissue.....	3
Figure 1.2: Schematic arrangement of the proteins involved in the mitochondrial electron transfer chain and ATP production.....	9
Figure 1.3: Sarcomere ultrastructure and cross-bridge cycling.....	11
Figure 1.4: Action potentials and corresponding current fluxes.....	14
Figure 1.5: The peak and late Na^+ current.....	15
Figure 1.6: Markov model of $\text{Na}_v1.5$ gating kinetics.....	16
Figure 1.7: The cardiac conduction system and action potential morphologies at each tissue type.....	17
Figure 1.8: Schematic of the channel proteins and ion movements associated with EC coupling and CICR.....	22
Figure 1.9: Experimental evidence documenting SR Ca^{2+} autoregulation.....	31
Figure 1.10: ECG readings from human participants with or without CPVT before, during and after exercise.....	35
Figure 1.11: Overview of the RyR2 structure and schematic of a RyR2 intra-protein interaction.....	38
Figure 1.12: Skeletal schematic of the molecular structure of flecainide.....	42
Figure 1.13: Changes in action potential morphology upon application of flecainide in the sub-epicardium and sub-endocardium.....	43

Chapter 2

Figure 2.1: Schematic of a Langendorff Perfusion System.....	49
Figure 2.2: Imaging and perfusion of live cardiomyocytes.....	57
Figure 2.3: A pictorial representation of the semi-automated Ca^{2+} wave analysis.....	64
Figure 2.4: Detection of a wave front at different wave fluorescent amplitudes using the semi-automated Ca^{2+} wave analysis.....	66
Figure 2.5: Detection of the wave front at five threshold parameters using the semi-automated Ca^{2+} wave analysis.....	67
Figure 2.6: Example of a Ca^{2+} spark and relevant dimensions analysed by Sparkmaster.....	69
Figure 2.7: Examples of sparks identified by Sparkmaster including erroneously identified sparks.....	69
Figure 2.8: XY scans of a flecainide-FITC loaded cell and analysed areas.....	70
Figure 2.9: Schematic of the transfer stack in which protein was transferred from the gel onto the PVDF membrane.....	74
Figure 2.10: Schematic of the square wave pulse used in patch clamp experiments.....	76

Chapter 3

Figure 3.1: Effect of 100 nM isoprenaline on Ca ²⁺ wave frequency during field stimulation at 0.5 and 1.5 Hz	85
Figure 3.2: Effect of 100 nM isoprenaline on Ca ²⁺ wave frequency after field stimulation at 0.5 and 1.5 Hz	86
Figure 3.3: Effects of 100 nM isoprenaline on spark size and frequency after field stimulation at 0.5 and 1.5 Hz	87
Figure 3.4: Effect of field stimulation frequency on Ca ²⁺ wave frequency during pacing in cardiomyocytes superfused with 100 nM isoprenaline	88
Figure 3.5: Effect of field stimulation frequency on Ca ²⁺ wave frequency post-pacing in cardiomyocytes superfused with 100 nM isoprenaline	89
Figure 3.6: Effects of field stimulation frequency on spark properties in the presence of 100 nM isoprenaline superfusion	90
Figure 3.7: The effect of flecainide on cell response to field stimulation in cardiomyocytes superfused with 100 nM isoprenaline	94
Figure 3.8: The effect of flecainide on Ca ²⁺ transient disruption during pacing in cardiomyocytes superfused with 100 nM isoprenaline	95
Figure 3.9: The effect of flecainide on Ca ²⁺ wave frequency during field stimulation in cardiomyocytes superfused with 100 nM isoprenaline	96
Figure 3.10: The effect of flecainide on Ca ²⁺ wave frequency post-pacing in cardiomyocytes superfused with 100 nM isoprenaline	97
Figure 3.11: The effect of flecainide on the time between the last triggered field stimulation and the first Ca ²⁺ wave in cardiomyocytes superfused with 100 nM isoprenaline	98
Figure 3.12: The effect of flecainide on the occurrence spontaneous Ca ²⁺ transients in cardiomyocytes superfused with 100 nM isoprenaline	99
Figure 3.13: The effect of flecainide on spark properties in cardiomyocytes superfused with 100 nM isoprenaline	100
Figure 3.14: The effect of flecainide on Ca ²⁺ waves during 1.5 Hz field stimulation after 2 hours of incubation, including 25 min at 37 °C in cardiomyocytes superfused with 100 nM isoprenaline.....	104
Figure 3.15: The effect of flecainide on Ca ²⁺ waves after 1.5 Hz field stimulation stopped and after 2 hours of incubation, including 25 min at 37 °C in cardiomyocytes superfused with 100 nM isoprenaline.....	105
Figure 3.16: The effect of flecainide on spark properties after 2 hours of incubation, including 25 min at 37 °C in cardiomyocytes superfused with 100 nM isoprenaline	106
Figure 3.17: The effect of MCT induction of HF in Ca ²⁺ waves and Ca ²⁺ transients during 1.5 Hz field stimulation, superfused with 100 nM isoprenaline	107
Figure 3.18: The effect of MCT induction of HF on Ca ²⁺ waves and Ca ²⁺ transients after 1.5 Hz field stimulation, superfused with 100 nM isoprenaline	108
Figure 3.19: The effect of MCT induction of HF on spark size and frequency after 1.5 Hz field stimulation and superfused with 100 nM isoprenaline	109
Figure 3.20: The effect of flecainide on Ca ²⁺ waves and Ca ²⁺ transients during 1.5 Hz field stimulation in cells from a MCT model of HF and superfused with 100 nM isoprenaline	110
Figure 3.21: The effect of flecainide on Ca ²⁺ waves and Ca ²⁺ transients after 1.5 Hz field stimulation in cells from a MCT model of HF and superfused with 100 nM isoprenaline	111

Figure 3.22: The effect of flecainide on spark size and frequency after 1.5 Hz field stimulation in cells from a MCT model of HF and superfused with 100 nM isoprenaline	112
Figure 3.23: The effect of flecainide on the peak cardiac Na ⁺ current using patch clamp recording.....	113

Chapter 4

Figure 4.1: Slow accumulation of 6 μM flecainide-FITC within intact cardiomyocytes.....	127
Figure 4.2: Slow accumulation of 25 μM flecainide-FITC within intact cardiomyocytes	128
Figure 4.3: Accumulation of 6 μM flecainide-FITC within intact cardiomyocytes with or without the OCTN1 blocker cimetidine	129
Figure 4.4: Accumulation of 25 μM flecainide-FITC within intact cardiomyocytes with or without the OCTN1 blocker cimetidine.....	130
Figure 4.5: 6 and 25 μM -FITC entry into cardiomyocytes	131
Figure 4.6: Accumulation of 6 μM flecainide-FITC (F-F) within intracellular organelles of saponin permeabilised cardiomyocytes	134
Figure 4.7: Accumulation of 25 μM flecainide-FITC (F-F) within intracellular organelles of saponin permeabilised cardiomyocytes.....	135
Figure 4.8: Accumulation of 6 μM flecainide-FITC (F-F) within intracellular organelles of saponin permeabilised cardiomyocytes was disrupted by FCCP.....	136
Figure 4.9: Accumulation of 25 μM flecainide-FITC (F-F) within intracellular organelles of saponin permeabilised cardiomyocytes was disrupted by FCCP	137
Figure 4.10: Fluorescence pattern of 6 μM flecainide-FITC within Triton-X100 permeabilised cardiomyocytes	140
Figure 4.11: Fluorescence pattern of 25 μM flecainide-FITC within Triton-X 100 permeabilised cardiomyocytes	141
Figure 4.12: Transverse striations visible after 6 μM FITC-flecainide washout with or without 100 μM non-fluorescent flecainide in Triton-X 100 permeabilised cardiomyocytes	142
Figure 4.13: Transverse striations visible in Triton-X100 permeabilised cardiomyocytes after 25 μM flecainide-FITC washout with or without 100 μM non-fluorescent flecainide.....	143
Figure 4.14: Flecainide-FITC block of the cardiac Na ⁺ current using patch clamp recording	144
Figure 4.15: Molecular drug structures.....	150

Chapter 5

Figure 5.1: The effect of free [Ca ²⁺] on wave frequency and propagation velocity	160
Figure 5.2: The effect of free [Ca ²⁺] on wave properties.....	161
Figure 5.3: The effect of intracellular [Ca ²⁺] and Ca ²⁺ buffering on spark properties.....	162
Figure 5.4: The effect of intracellular [Ca ²⁺] and Ca ²⁺ buffering on spark properties.....	163
Figure 5.5: The effect of flecainide on wave frequency and propagation velocity over 3 min at LOW free [Ca ²⁺].....	167
Figure 5.6: The effect of flecainide on wave amplitude and upstroke rate at LOW free [Ca ²⁺]	168
Figure 5.7: The effect of flecainide on wave duration and relaxation time constant at LOW free [Ca ²⁺].....	169
Figure 5.8: The effect of flecainide on wave frequency over 3 min at HIGH free [Ca ²⁺].....	170

Figure 5.9: The effect of flecainide on wave amplitude and upstroke rate at HIGH free $[Ca^{2+}]$	171
Figure 5.10: Effect of flecainide on wave duration and relaxation time constant at HIGH free $[Ca^{2+}]$	172
Figure 5.11: The effect of flecainide on wave frequency and propagation velocity over 5 min at HIGH free $[Ca^{2+}]$	173
Figure 5.12: The effect of flecainide on wave peak amplitude and upstroke rate over 5 min at HIGH free $[Ca^{2+}]$	174
Figure 5.13: The effect of flecainide on wave duration and relaxation constant over 5 min at HIGH free $[Ca^{2+}]$	175
Figure 5.14: The effect of flecainide on spark frequency over 3 min.....	179
Figure 5.15: The effect of flecainide on spark amplitude over 3 min.....	180
Figure 5.16: The effect of flecainide on spark FWHM over 3 min.....	181
Figure 5.17: Effect of flecainide on spark FDHM over 3 min.....	182
Figure 5.18: The effect of flecainide on SR Ca^{2+} content over 5 min.....	183
Figure 5.19: The effect of saponin permeabilisation on relative quantity of endogenous intracellular CaM.....	184
Figure 5.20: The effect of exogenous CaM on wave frequency and propagation velocity.....	185
Figure 5.21: The effect of exogenous CaM on wave dimensions.....	186
Figure 5.22: The effect of flecainide on wave frequency and propagation velocity in the presence of exogenous CaM.....	187
Figure 5.23: The effect of flecainide on wave amplitude and upstroke rate in the presence of exogenous CaM.....	188
Figure 5.24: The effect of flecainide on wave duration and relaxation time constant in the presence of exogenous CaM.....	189

Chapter 6

Figure 6.1: Effect of Cs^+ on wave frequency and wave propagation.....	204
Figure 6.2: Effect of Cs^+ on wave properties.....	205
Figure 6.3: Effect of flecainide on wave frequency in the presence of Cs^+	206
Figure 6.4: Effect of flecainide on wave propagation in the presence of Cs^+	207
Figure 6.5: Effect of flecainide on wave properties in the presence of Cs^+	208
Figure 6.6: Effect of flecainide on wave properties in the presence of Cs^+	209
Figure 6.7: Effect of valinomycin or valinomycin + flecainide on wave frequency.....	211
Figure 6.8: Effect of valinomycin or valinomycin + flecainide on wave propagation.....	212
Figure 6.9: Effect of valinomycin or valinomycin + flecainide on wave properties.....	213
Figure 6.10: Effect of valinomycin or valinomycin + flecainide on wave properties.....	214

Chapter 7

Figure 7.1: Hypothesised transient changes in SR membrane potential during a Ca^{2+} wave....	229
Figure 7.2: Hypothesised block of RyR2 by flecainide during SR Ca^{2+} release.....	230

Tables

Chapter 2

Table 2.1: Composition of solutions used for myocyte isolation.	50
Table 2.2: Composition of solutions used for intact cell Ca ²⁺ imaging.....	51
Table 2.3: Composition of solutions used for permeabilised cell Ca ²⁺ imaging.....	52
Table 2.4: Total and free concentrations of ions and ligands in intracellular solutions which give rise to different Ca ²⁺ release characteristics.....	53
Table 2.5: Chemical concentrations required for Western blot experiments.	54
Table 2.6: Composition of solutions used for intact cell patch clamp.....	55

Appendix

Table 8.1: Chemical names and sources	236
---	-----

Main abbreviations and agents

ADP	Adenosine diphosphate
ANOVA	Analysis of variance
APD	Action potential duration
ATP	Adenosine triphosphate
BSA	Bovine serum albumin
Ca ²⁺	Calcium
CaCl ₂	Calcium chloride
Caffeine	Caffeine
CaM	Calmodulin
CAMKII	Ca ²⁺ /calmodulin-dependent protein kinase II
cAMP	Cyclic adenosine monophosphate
Casq	Calsequestrin
Casq2 ^{-/-}	Calsequestrin knockout mutant mouse model
CAST	Cardiac Arrhythmia Suppression Trial
CICR	Calcium-induced calcium release
CIM	Cimetidine
Cl ⁻	Chloride
Collagenase	Collagenase type 2
CON	Control
CPVT	Catecholaminergic polymorphic ventricular tachycardia
Creatine	Creatine
CRU	Calcium release unit
Cs hydroxide hydrate	Caesium hydroxide hydrate (4 M)
Cs methanesulfonate	Caesium methanesulfonate
Cs ⁺	Caesium
DAD	Delayed after depolarisation
Di-8-ANEPP	Di-8-aminonaphthylethylenylpyridinium
EAD	Early after depolarisation
ECC	Excitation contraction coupling
EGTA	Ethylene glycol tetraacetic acid
E _m	Equilibrium potential
Ethanol	Ethanol
Exogenous CaM	Exogenous CaM isolated from bovine brain
FADH ₂	Flavin adenine dinucleotide
FCCP	Carbonyl cyanide-4-(trifluoromethoxy)phenylhydrazone
FITC	Fluorescein isothiocyanate
FKBP12.6	Peptidyl-prolyl cis-trans isomerase
FLEC	Flecainide acetate
Fluo-3PentaK ⁺	Fluo3 pentapotassium salt
Fluo-4AM	Fluo-4 acetoxymethyl ester
Glucose	Glucose

GPCR	G-protein coupled receptor
HEPES	4-(2-Hydroxyethyl)-1-piperazineethanesulfonic acid
HF	Heart failure
hERG	Human Ether-à-go-go
Isoprenaline	Isoprenaline (Isoproterenol USA)
K ⁺	Potassium
K _{ATP}	Potassium adenosine triphosphate channel
KCl	Potassium chloride
KOH	Potassium hydroxide (4M)
K _v 11.1	Voltage-gated potassium channel
K _v 2.1	Voltage-gated potassium channel
LQT	Long Q-T
LTCC	L-type calcium channel
MCF	Mitochondrial carrier family
MCT	Monocrotaline
MCU	Mitochondrial calcium uniporter
Mg sulphate	Magnesium sulphate
Mg ²⁺	Magnesium
MgCl ₂	Magnesium chloride
mitcoBK _{Ca}	Mitochondrial calcium activated potassium channel
mitoK _{ATP}	Mitochondrial adenosine triphosphate dependent potassium channel
mitoK _v 1.3	Mitochondrial voltage-gated potassium channel
mitoTASK	Mitochondrial two pore domain potassium channel
Na ⁺	Sodium
Na ₂ ATP	ATP disodium salt hydrate
Na ₂ CrP	Creatine phosphate disodium salt tetrahydrate
NaCl	Sodium chloride
NAD ⁺	Oxidized nicotinamide adenine dinucleotide
NADH	Reduced nicotinamide adenine dinucleotide
NaH ₂ PO ₄	Sodium dihydrogen orthophosphate
NaOH	Sodium hydroxide
Na _v 1.5	Voltage-gated sodium channel
NCX	Sodium-calcium exchanger
NUC	Nucleus
NU-FL	Neutral derivative of flecainide
OCTN1	Organic cation transporter 1
PBS	Phosphate buffered solution
PHOS	Phosphorylated
P _i	Inorganic phosphate
PKA	Protein kinase A
pK _a	Acid dissociation constant
PLB	Phospholamban
P _o	Open probability
Protease	Protease from <i>Streptomyces griseus</i>

QH ₂	Quinol
QX-FL	Fully-charged derivative of flecainide
R4496C ^{+/-}	RyR2 mutant mouse model
ROS	Reactive oxygen species
RyR1	Skeletal muscle ryanodine receptor
RyR2	Cardiac ryanodine receptor
SAN	Sino atrial node
Saponin	Saponin from quillaja bark
SCD	Sudden cardiac death
SDS	Sodium dodecyl sulphate
SERCA/SERCA2a	Cardiac SR calcium ATP-ase
SR	Sarcoplasmic reticulum
T X-100	Triton X-100
Tank buffer	TRIS/Glycine/SDS commercial mix
Taurine	Taurine
TEMED	Tetramethylethylenediamine
TMRM	Tetramethylrhodamine methyl ester
TNF- α	Tumour necrosis factor alpha
TRIC	Trimeric intracellular cation-specific channels
T-tubule	Transverse tubule
VAL	Valinomycin
VDAC	Voltage dependent anion channel
VEH	Vehicle
WT	Wild type

Chapter 1: General introduction

1.1 General introduction

Flecainide is a clinically prescribed, anti-arrhythmic drug with a controversial history. Pro-arrhythmic effects and increased mortality in patients with structural heart disease were first identified in the 1989 Cardiac Arrhythmia Suppression Trial (CAST) (CAST, 1989). These negative findings underlie the highly conservative approach towards the clinical use of flecainide (Hayward et al., 2016). However, in patients with little or no structural heart disease, flecainide is a safe and potent anti-arrhythmic agent (Lafuente-Lafuente et al., 2015, Vigneswaran et al., 2014, van der Werf et al., 2011a).

In recent years, flecainide has shown itself to be highly effective in the treatment of catecholaminergic polymorphic ventricular tachycardia (CPVT), a genetic disorder that causes potentially fatal ventricular arrhythmias in response to normal adrenergic drive (van der Werf et al., 2011a). However, flecainide's mechanism of action in CPVT is controversial; in addition to its well-characterised role as a class 1C sodium channel inhibitor, flecainide has been reported to act directly on the sarcoplasmic reticulum (SR) Ca^{2+} release channel or ryanodine receptor (RyR2) (Hwang et al., 2011a, Savio-Galimberti and Knollmann, 2015, Hilliard et al., 2010).

If flecainide's primary antiarrhythmic mechanism does involve a direct action on RyR2, it would represent a new therapeutic approach to the treatment of arrhythmias. However, subsequent studies have fuelled disagreement between research groups regarding flecainide's site of action (Sikkel et al., 2013, Bannister et al., 2015, Bannister et al., 2016). Resolution of this issue is important because confirmation of an action on RyR2 would likely stimulate the development of novel and more effective drugs to target pro-arrhythmic SR Ca^{2+} release both in CPVT and other pathological conditions.

In this chapter, the structural and functional properties of the heart and individual cardiomyocytes will be summarised. Following this, important cellular mechanisms such as the cardiac electrophysiology and the control of intracellular Ca^{2+} will be discussed. The role of these mechanisms in pathological conditions will be presented with a particular focus on CPVT. Finally, the inhibitory effects of flecainide on the cardiac Na^+ channel ($\text{Na}_v1.5$) will be reviewed alongside the controversy surrounding the effect of flecainide on RyR2.

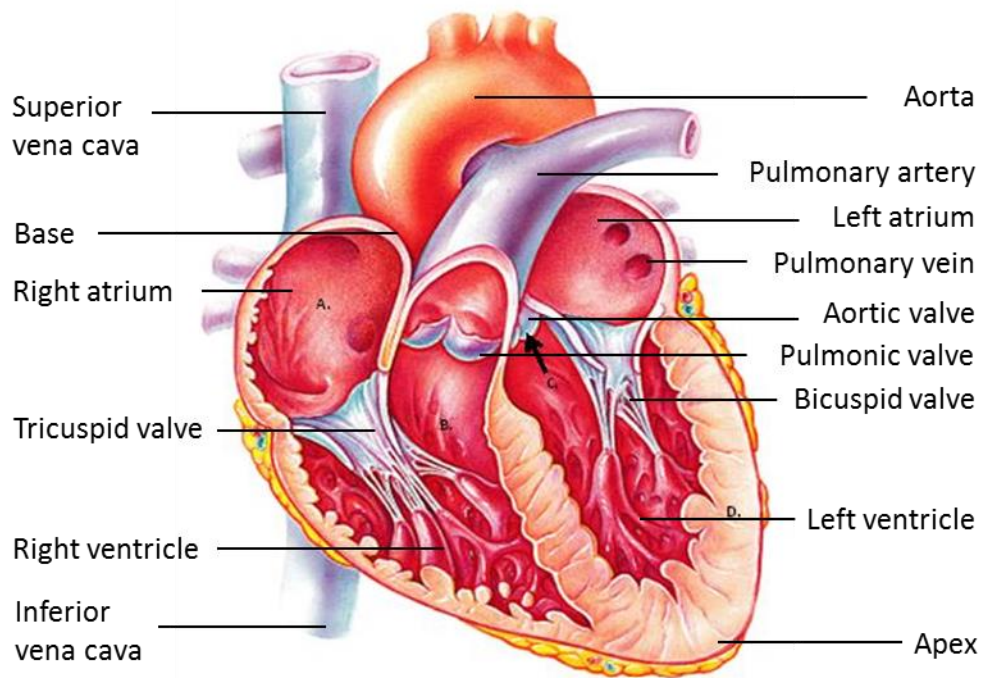
1.2 The structure and function of the heart

The heart is a muscular pump, located posterior to the sternum, within the thorax. The base of the heart lies at the second intercostal space and the cardiac apex is situated at the fifth intercostal space (Iaizzo, 2015). The heart pumps blood through the circulatory system to provide the body with oxygen and nutrients. Metabolic waste such as CO₂ is also removed from these tissues. Other circulating factors such as endogenous hormones and cells of the immune system are transported through the body by the pumping action of the heart. In addition, the cardiovascular system is crucial for thermal control, helping to maintain the tissues at 37 °C (Opie, 2004).

The mammalian heart consists of four chambers, with inlets into each of the atria and an outlet from each ventricle (Figure 1.1 A). Deoxygenated blood, returning from the body enters the right atrium via the superior and inferior vena cava. Large volumes of blood are able to flow directly into the right ventricle through the tricuspid valve; however atrial contraction ensures maximal entry of blood into the ventricles. Co-ordinated ventricular contraction from the apex of the heart pumps de-oxygenated blood through the semilunar valve and into the pulmonary artery, where blood is transported to the lungs (Opie, 2004). Within the pulmonary capillary system, oxygen binds to haemoglobin in red blood cells and newly oxygenated blood is transported into the left atrium via the pulmonary veins. Blood moves through the bicuspid valve into the left ventricle. The left ventricle is the largest and most muscular chamber, responsible for pumping large volumes of blood into the systemic circulation through the aortic valve and aorta (Redington et al., 1988). A proportion (4-5%) of the cardiac output is pumped into the coronary circulation, oxygenating the cardiac muscle itself (Schampaert et al., 2013, Hall and Guyton, 2016).

The right and left ventricles are separated via the ventricular septum (Arnould-Taylor, 1998). The walls of both ventricular chambers consist of tissue layers referred to as the sub-epicardium, mid-myocardium and sub-endocardium (Figure 1.1 B). The sub-epicardium is the external most layer of cardiac muscle, proximate to the pericardium or heart sac and is comprised primarily of connective tissue (Ovalle and Nahirney, 2013). The mid-myocardium is the thick layer of myocardial muscle, situated between the sub-epicardium and sub-endocardium. The sub-endocardium is located closest to the chambers of the ventricles and is comprised primarily of endothelial smooth muscle (Ovalle and Nahirney, 2013).

A



B

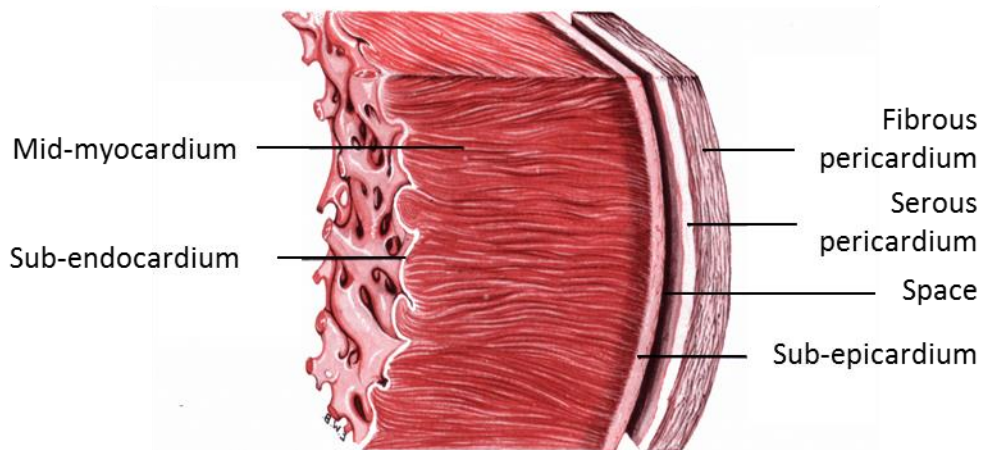


Figure 1.1 Ultra-structure of the heart and ventricular tissue

A) Schematic of the cardiac chambers, valves and major vessels. Note the thick left ventricle wall and ventricular septum. **B)** The layers of ventricular tissue and pericardial sac as in the ventricular wall. Images adapted from www.newhealthadvisor.com and www.proprofs.com.

1.3 The cardiomyocyte

The heart is comprised of cardiomyocytes, fibroblasts and a small proportion of other cell types including cardiac stem cells, vascular smooth muscle cells and endothelial cells (Banerjee et al., 2007, Nag, 1980, Smith et al., 2014). In rat hearts, 30% of cells are cardiomyocytes whereas 64% are fibroblasts. In human hearts, this proportion shifts such that 27% of cells are cardiomyocytes and 72% are fibroblasts (Banerjee et al., 2007, Nag, 1980). Cardiomyocytes alone facilitate cardiac contraction, yet fibroblast activation and proliferation following myocardial ischaemia aids in cardiac wound healing and improves post-ischaemic cardiac performance (Duan et al., 2012, Cartledge et al., 2015). Recent evidence suggests that fibroblasts also have the capacity to increase or decrease Ca^{2+} transient amplitude in cardiomyocytes, via soluble mediators (Cartledge et al., 2015). However, the role of fibroblasts within the myocardium will not be considered further in this study.

Mammalian ventricular myocytes have a rod-shaped appearance (Bensley et al., 2016). When isolated from wild-type (WT) rat, their dimensions range between 80 – 128 μm in length and 16 – 25 μm in width; and myocyte size is positively correlated with the age and size of the animal (Korecky and Rakusan, 1978). One distinctive characteristic of ventricular cardiomyocytes is their myofibrillar structure, which can be visualised under a light microscope as striations running parallel along the cell axis (Frisk et al., 2014, Peeters et al., 1995). Sarcolemmal invaginations known as transverse tubules (t-tubules) radiate into the centre of the cytosol. T-tubules can be viewed as regularly spaced transverse striations, after application of the membrane potential dye DI-8-ANEPPS. Isolated atrial myocytes share the rod-shaped appearance of ventricular cardiomyocytes but are longer and thinner (Dibb et al., 2013). Discrepancies exist in the literature as to whether t-tubules exist within atrial cardiomyocytes (Kirk et al., 2003, Dibb et al., 2009). Species differences may explain these inconsistencies as atrial t-tubules are more prevalent in large animal models such as sheep and horse (Dibb et al., 2013). Additionally, anatomical variances may play a role; atrial cardiomyocytes isolated from the rat sub-epicardium of the right atria display a more organised t-tubule system than the rest of the atria (Frisk et al., 2014).

Cardiomyocytes are electrically excitable cells and ionic concentrations differ greatly across the myocyte sarcolemma. The two main ionic species are potassium (K^+) and sodium (Na^+). The cytosol contains ~ 140 mM K^+ and ~ 20 mM Na^+ , whereas the extracellular environment has ~ 5 mM K^+ and ~ 140 mM Na^+ (Opie, 2004). Under diastolic conditions, the sarcolemma is primarily permeable to K^+ therefore the resting membrane potential is largely controlled by the K^+ equilibrium potential. This can be calculated using the Nernst equation:

$$E_m = \frac{RT}{zF} \ln \left(\frac{[X]_o}{[X]_i} \right)$$

whereby E_m is the equilibrium potential; R is the universal gas constant ($8.314 \text{ J.K}^{-1}.\text{mol}^{-1}$); T is the temperature in Kelvin (K); z is the valency of the ion; F is Faraday's constant (96485 C.mol^{-1}); and X is the concentration of the relevant ion inside (i) and outside (o) the cell. In ventricular cardiomyocytes, the K^+ equilibrium potential is -80 mV at 37°C (310 K).

The membrane potential can be calculated using an extension of the Nernst equation, the Goldman-Hodgkin-Katz equation. This equation considers all ionic concentration differences across the membrane potential and relative ionic permeability:

$$E_{rev} = \frac{RT}{zF} \ln \left(\frac{PX_1[X_1]_o + PX_2[X_2]_o + PX_3[X_3]_o}{PX_1[X_1]_i + PX_2[X_2]_i + PX_3[X_3]_i} \right)$$

whereby P is the relative permeability of the relevant ion. As Na^+ , Ca^{2+} and chloride (Cl^-) are relatively impermeable to the cardiomyocyte sarcolemma during diastole, the membrane potential (~ -85 mV), reflects the K^+ equilibrium potential (Fozzard and Sheu, 1982).

Changes in membrane depolarisation are coupled between cardiomyocytes via gap junctions at the intercalated discs to form an electrical and functional syncytium (Mayama et al., 2007). Gap junctions consist of 6 connexins arranged in a hemichannel, which allow the passage of ions and small cytoplasmic solutes (< 900 Da) (Beyer et al., 1987, Gros and Jongsma, 1996). Connexin isoforms Cx40, Cx43 and Cx45 are present within the myocardium and Cx43 is the most prevalent in the ventricle (Beyer et al., 1989, Gourdie et al., 1993, Bao et al., 2011). Ventricular myocytes are arranged in sheets, which rotate in orientation through the depth of the myocardial wall (Helm et al., 2005, Gilbert et al., 2007).

1.3.1 The sarcolemma and transverse-tubules

The cardiomyocyte membrane, or sarcolemma, comprises of an external sarcolemma and continuous membrane invaginations called t-tubules. The sarcolemma acts to separate the cytosol from the extracellular medium, as well as to integrate membrane proteins into its lipid bilayer sheet. β -adrenergic signalling proteins, such as adenylyl cyclase and the β_2 -adrenoceptor, are compartmentalised by caveolae; cholesterol-rich lipid rafts that form small membrane invaginations (Head et al., 2005, Calaghan and White, 2006). Ion channels, antiporters and pumps are also located throughout the sarcolemma, although their relative fractions may differ between the external and t-tubular portions. For example, the Ca^{2+} ATPase and the Na^+ - Ca^{2+} exchanger (NCX), Ca^{2+} removal transporters and antiporters respectively, are preferentially located in the t-tubules (Chase and Orchard, 2011, Yang et al., 2002). Alongside this, voltage gated L-type Ca^{2+} channels (LTCC) are also concentrated within the t-tubules (Kawai et al., 1999).

The t-tubular network is a highly complex membrane structure which consists primarily of radial invaginations into the centre of the cytosol, although a smaller proportion of longitudinal tubules are apparent (Soeller and Cannell, 1999). T-tubules are ~ 450 nm in diameter (Savio-Galimberti et al., 2008). The structure and location of t-tubules are of great importance with regard to their function. The extended t-tubule invaginations are proximal to the SR, the internal Ca^{2+} storage organelle (Section 1.3.2) and facilitate the penetration of action potentials into the centre of the cell (Section 1.4.1). The cytosolic space between the t-tubule and the SR membrane, known as the dyadic cleft, measures ~ 12 nm (Radermacher et al., 1994). This short distance facilitates fast signalling between proteins located at these membranes. For example, the diffusion of Ca^{2+} from the sarcolemmal LTCC pore opening to opposing RyR2 channels in the SR. The resulting cardiomyocyte twitch is therefore synchronous (Section 1.5.1).

Interestingly, in heart failure or after myocardial infarction, when cardiac contractility is reported to decline, the ratio of transverse to longitudinal tubules decreases and the t-tubules become more disorganised (Louch et al., 2006, Crossman et al., 2015). In these cases, coupling of LTCC to RyR2 is decreased, which impairs excitation contraction coupling (EC coupling) and Ca^{2+} induced Ca^{2+} release (CICR) efficacy and function (Sections 1.4.1 and 1.5.1) (Louch et al., 2006, Crossman et al., 2015).

1.3.2 The sarcoplasmic reticulum

The SR is a lattice-like internal membrane compartment comprising 3.5% of the cell volume (Page et al., 1971), which accumulates and releases Ca^{2+} into the cytosol. The SR can be categorised as either longitudinal or junctional. The junctional SR lies proximal to the t-tubule membrane and facilitates the functional coupling between RyR2 and the LTCC channels, with a ratio of 1:7.3 respectively (Bers and Stiffel, 1993). Longitudinal SR is distant from the t-tubule and is devoid of RyR2, but contains the cardiac SR Ca^{2+} -ATPase (SERCA) (Inui et al., 1988).

The primary Ca^{2+} release channel associated with the cardiac SR membrane is RyR2 (Section 1.5). RyR2 is a large channel protein (~2.2 mDa) comprised of 4 homomeric subunits (565 kDa each), arranged to form a single pore (Radermacher et al., 1994, Liu et al., 2002, Tunwell et al., 1996). RyR2 opens in response to Ca^{2+} entering the cytosol via LTCC during the processes of EC coupling and CICR Sections (1.4.1 and 1.5.1) (Altamirano and Bers, 2007). Transport of two Ca^{2+} ions from the cytosol into the SR via SERCA requires the binding and hydrolysis of one ATP molecule. Considering the vast number of SERCA proteins within the SR membrane (up to 100 $\mu\text{mol/L}$ cytosol in rat) it has been suggested that SERCA need only cycle once to take up cytosolic Ca^{2+} (Bers, 2001). However, the rate of SERCA cycling is inhibited by another SR membrane protein, phospholamban (PLB). PLB can be phosphorylated via protein kinase A (PKA) or CaMKII. PKA mediated phosphorylation of PLB in response to increased sympathetic drive to the heart decreases inhibition of SERCA, leading to stronger and more forceful ventricular contractions (Li et al., 2000, Hagemann et al., 2000). Once within the SR, Ca^{2+} is strongly buffered by Casq, a SR luminal protein which polymerises upon increased luminal Ca^{2+} concentration ($[\text{Ca}^{2+}]$) (Park et al., 2003). In addition to its buffering role, Casq and the closely associated proteins triadin and junctin can directly modulate RyR2 mediated Ca^{2+} release (Jones et al., 1995, Kobayashi et al., 2000, Terentyev et al., 2007).

During Ca^{2+} uptake or release by the SR, a K^+ flux occurs in the opposite direction to the movement of Ca^{2+} . This counter-current is hypothesised to be facilitated by both RyR2 and SR K^+ (TRIC) channels and serves to reduce the build-up of charge across the SR membrane, which would otherwise limit SR Ca^{2+} release (Yazawa et al., 2007, Guo et al., 2013). The SR counter-current will be discussed in more detail in Chapter 6. Other SR channels are reported to exist in cardiomyocytes, and may modulate EC coupling to some extent. For example, the Ca^{2+} release channel IP_3 is expressed in atrial and ventricular cardiomyocytes and a modulatory role in atrial EC coupling has been described (Zima and Blatter, 2004). However, expression of IP_3 receptors in the outer nuclear envelope, proximal to the SR complicates this interpretation and it may be

that the primary role of IP₃ in cardiomyocytes is to facilitate long term nuclear Ca²⁺ signalling (Zima et al., 2007, Ljubojevic and Bers, 2015).

1.3.3 The mitochondria

The mitochondria constitute ~30% of the cell volume (Page et al., 1971). In mammalian cardiomyocytes, the majority of the mitochondria are densely packed and highly ordered in parallel rows between the sarcomeres (Birkedal et al., 2006). A second population of sub-sarcolemmal mitochondria also exist in the cytosolic space, immediately opposing the sarcolemma and caveolae structures (Fridolfsson et al., 2014). Each mitochondrion comprises of an inner and an outer membrane, and their inner matrix is highly negatively charged (Perry et al., 2011). Their major role within the cardiomyocyte is to produce ATP, the most dominant chemical energy store, via the electron transfer chain, which is summarised in Figure 1.2. The electron transfer chain is a set of simultaneous reduction and oxidation reactions, which give rise to a high proton gradient between the mitochondrial matrix and inter-membrane space. Controlled proton influx drives the synthesis of ATP via ADP.

Nicotinamide adenine dinucleotide (NADH) is reduced by Complex I, an enzyme located on the inner mitochondrial membrane, to produce quinol (QH₂) and two electrons. These electrons are transferred by Complex I to coenzyme Q, a lipid soluble electron carrier within the inner mitochondrial membrane. Additionally, four protons are translocated across the inner mitochondrial membrane to the inter-membrane space, contributing to the proton gradient. Alongside this mechanism, Complex II reduces flavin adenine dinucleotide (FADH₂) and the two electrons produced are transferred to coenzyme Q. Less energy is contributed to the overall reaction as protons are not translocated. Coenzyme Q transfers electrons to Complex III.

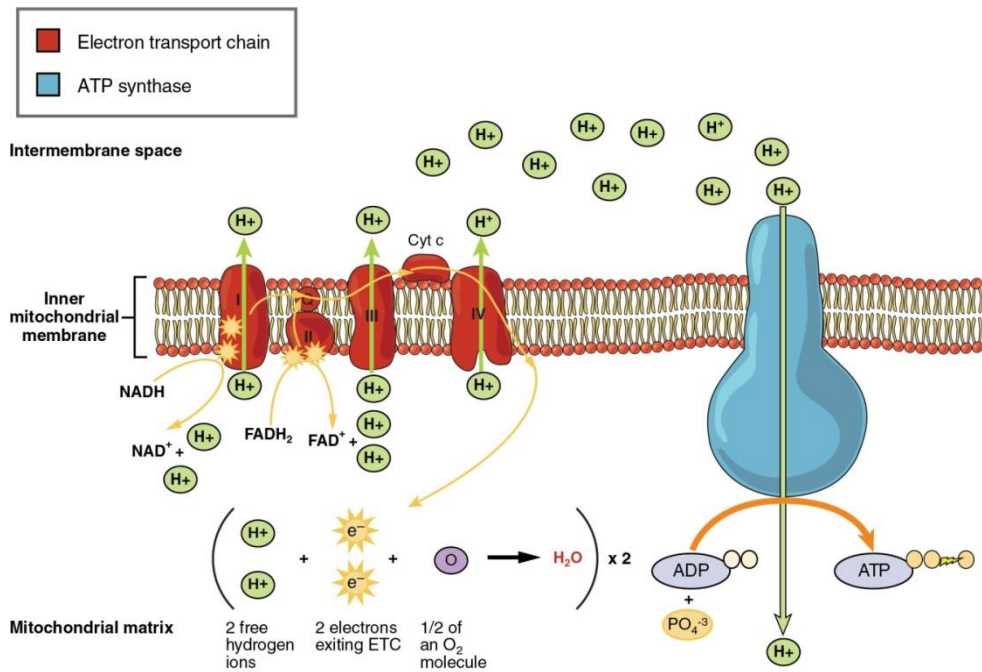


Figure 1.2: Schematic arrangement of the proteins involved in the mitochondrial electron transfer chain and ATP production

A) Electrons are removed from NADH and FADH₂ and transferred from Complex I or II to Coenzyme Q. Electrons are further transferred to Complex III and Complex IV via cytochrome C. Electron transfer drives proton translocation from the mitochondrial matrix to the inter-membrane space creating a proton gradient. ATP production is controlled by proton movement through ATP synthase down its concentration gradient. Image taken from www.archive.cnx.org.

These electrons are further transported to Complex IV via cytochrome C. At both Complex III and IV, protons are translocated to the inter-membrane space. The final transfer of electrons occurs at Complex IV when electrons are transferred to molecular oxygen (O_2) and two molecules of water are produced. The influx of protons from the inter-membrane space to the mitochondrial matrix drives the production of adenosine triphosphate (ATP) from adenosine diphosphate (ADP) and inorganic phosphate (P_i) via ATP synthase. Production of reactive oxygen species (ROS), such as superoxide ($O_2^{\bullet-}$) and subsequently hydrogen peroxide (H_2O_2), can occur during electron transfer, primarily at Complex I and partially at Complex III (Murphy, 2009).

In addition to the SR, Ca^{2+} can also be accumulated into the mitochondria via the mitochondrial Ca^{2+} uniporter (MCU) (Kirichok et al., 2004). Mitochondrial Ca^{2+} uptake is limited on the timescale of cardiac excitation and contraction (Boyman et al., 2014b). Instead, at high heart rates when a sustained increase in cytosolic $[Ca^{2+}]$ occurs, mitochondrial Ca^{2+} also increases, leading to the increased production of ATP (Unitt et al., 1989). This indicates that mitochondrial Ca^{2+} may act as a regulator of oxidative phosphorylation. Many other channels, antiporters and transporters exist in the mitochondrial membrane. Ca^{2+} is extruded from the mitochondria via the Na^+/Ca^{2+} antiporter (Jung et al., 1995). The voltage dependent anion channel (VDAC), situated at the outer mitochondrial membrane allows the passage of molecules <5000 Da into the inter-membrane space (Colombini, 1979). Additionally, a large variety of K^+ channels also exist within the inner mitochondrial membrane (Laskowski et al., 2016), despite low K^+ permeability (Bednarczyk et al., 2008) and their function is not fully understood.

1.3.4 The sarcomere

Sarcomeres are contractile units organised throughout the cardiomyocyte in parallel rows alongside the mitochondria (Kanzaki et al., 2010, Birkedal et al., 2006). Sarcomeres include several myofilament proteins (Figure 1.3 A). The thin filament proteins comprise actin, tropomyosin and the troponin C, T and I complex. Myosin makes up the thick filament. The thin filaments are attached at the Z lines and are interdigitated with the thick filaments. During SR Ca^{2+} release, the thin and thick filaments interact in an ATP dependent manner. This is referred to as the sliding myofilament theory or cross-bridge cycling and causes contraction along the length of the cell (Figure 1.3 B) (Huxley, 1967).

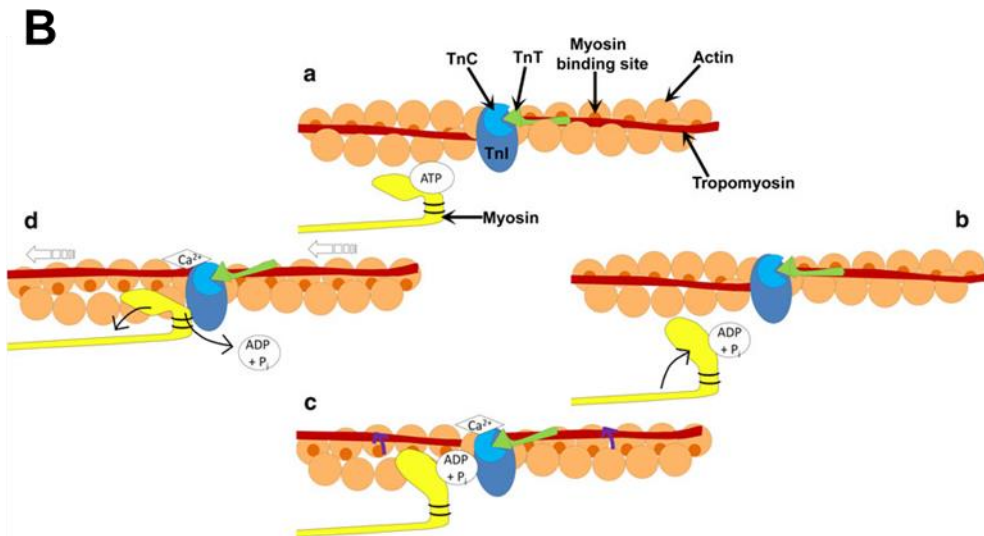
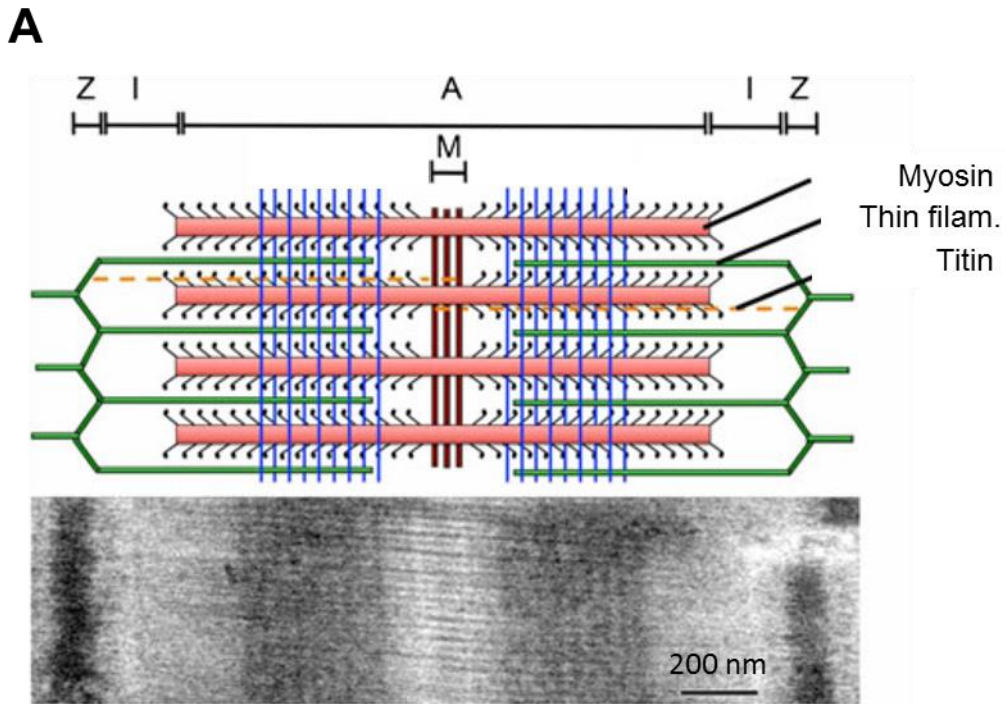


Figure 1.3: Sarcomere ultrastructure and cross-bridge cycling

A) Schematic of a cardiac sarcomere coupled with an electron micrograph of a cardiac sarcomere. Sarcomeres are 1.7 – 1.8 μm in length (Jayasinghe et al., 2009, Bub et al., 2010). Thin filaments include actin, tropomyosin and the troponin C, T and I complex. Thin filaments are joined at the z discs. Myosin thick filaments interdigitate with the thin filaments. Passive elasticity of the cell is regulated by titin. **B)** A schematic of the cross-bridge cycle. At a) ATP is bound to the myosin head, which is then detached from the actin binding site.; b) ATP is hydrolysed into ADP and P_i , and the myosin head becomes cocked; c) the myosin head binds to the binding site on actin d) P_i is released from the myosin head, strengthening the bond with actin. ADP is released, sliding the actin filament towards the sarcomere centre. ATP must bind to the myosin head to detach it from actin. Images taken and adapted from (Sadayappan and de Tombe, 2012) and (England and Loughna, 2013).

Ca^{2+} released from the SR binds to troponin C. This induces a conformational change in the troponin complex which causes tropomyosin to move away from the myosin binding sites located on the actin filament (Miki et al., 2012). Myosin heads which protrude from the myosin rod, bind ATP. ATP is hydrolysed to form ADP and P_i and the energy released causes the myosin head to cock and bind to the actin filament, forming a cross-bridge. Release of P_i from myosin strengthens the actin-myosin bond. Further release of ADP induces the myosin head to pivot and slide the actin filament to the centre of the sarcomere. In the absence of ADP and P_i , ATP can bind to the myosin head, weakening and releasing the cross-bridge. Individual myosin heads can move the filament 0.25–0.5% of the sarcomere length (5-10 nm) with each stroke (Tyska et al., 1999). When combined, isolated cells are shortened by ~9% of their diastolic length when stimulated at 1 Hz (Mukherjee et al., 1993).

1.3.5 The nucleus

Consistent with the majority of mammalian cells, the nucleus contains DNA required for the expression of relevant proteins. Within the nucleus, DNA is transcribed to mRNA which in turn is translated into amino acid chains and proteins, outside of the nucleus. In human cardiomyocytes, mono-, bi-, tri-, and tetra-nucleated ventricular cardiomyocytes are present at a ratio of 74 : 25.5 : 0.4 : 0.1 (Olivetti et al., 1996). Interestingly, mono-nucleated cells isolated from the left atria display larger Ca^{2+} transients compared with bi-nucleated cells from the same region. This may be due to differences in protein expression caused by nuclear differences (Huang et al., 2012).

1.4 Electrical excitation of the heart

1.4.1 Excitation contraction coupling and the action potential

EC coupling is the mechanism by which the cardiomyocyte contracts in response to electrical stimulation. EC coupling is reliant upon action potentials; electrical depolarisations of the cardiomyocyte, which are functionally coupled to the process of CICR. An action potential is a wave of sarcolemmal depolarisation, followed by sarcolemmal repolarisation which initiates synchronous myocyte contraction. Cells of the cardiac conduction system, atria, ventricles, SAN and AV node all exhibit action potentials, although their morphologies are varied. The characteristic ventricular and atrial action potentials are summarised in Figure 1.4 A and B. The ventricular action potential will be described in 5 phases (Nerbonne and Kass, 2005). Deviations from the ventricular action potential morphology will also be briefly introduced.

Depolarisation of the membrane to a level more positive than the action potential threshold (~ -55 mV), initiates voltage-gated $\text{Na}_v1.5$ to open, allowing a rapid influx of Na^+ (Phase 0). This is referred to as the fast Na^+ current (Figure 1.5 A). Within 1 ms of opening, 99% of $\text{Na}_v1.5$ are inactivated, thereby contributing to the initial repolarisation of the cell (Phase 1) (O'Leary et al., 1995). Immediately after the initiation of an action potential, the cardiomyocyte enters a refractory period, during which time another action potential cannot be initiated. This is in part due to $\text{Na}_v1.5$ inactivation, which prevents further depolarisation of the cardiomyocyte. $\text{Na}_v1.5$ gating kinetics are summarised by Markov probability models in Figure 1.6 (Patlak, 1991, Zhang et al., 2013). These models illustrate the probability of $\text{Na}_v1.5$ occupying an open, closed or inactivated state, which in turn determines Na^+ permeability. Additionally, voltage gated K^+ channels open, which facilitate the transient outward current (I_{to}), further repolarising the cell. During Phase 2, the action potential plateaus due to Ca^{2+} influx via voltage-gated LTCC. At this time, 1% of $\text{Na}_v1.5$ channels are still open, allowing the late Na^+ current entry into the cytosol (Figure 1.5 A). The development of heart failure or the existence of congenital mutations can increase the late Na^+ current and pre-dispose to arrhythmias (Hu et al., 2013, Toischer et al., 2013). During the plateau phase, voltage-gated repolarising K^+ channels which facilitate the delayed rectifier K^+ currents, open (Phase 3). These K^+ currents are classified as rapidly activating (I_{kr}) and slowly activating (I_{ks}). This causes complete repolarisation as LTCCs close. The cell membrane is then maintained at its stable resting membrane potential (~ -85 mV) by inwardly rectifying K^+ currents (I_{k1}) (Phase 4).

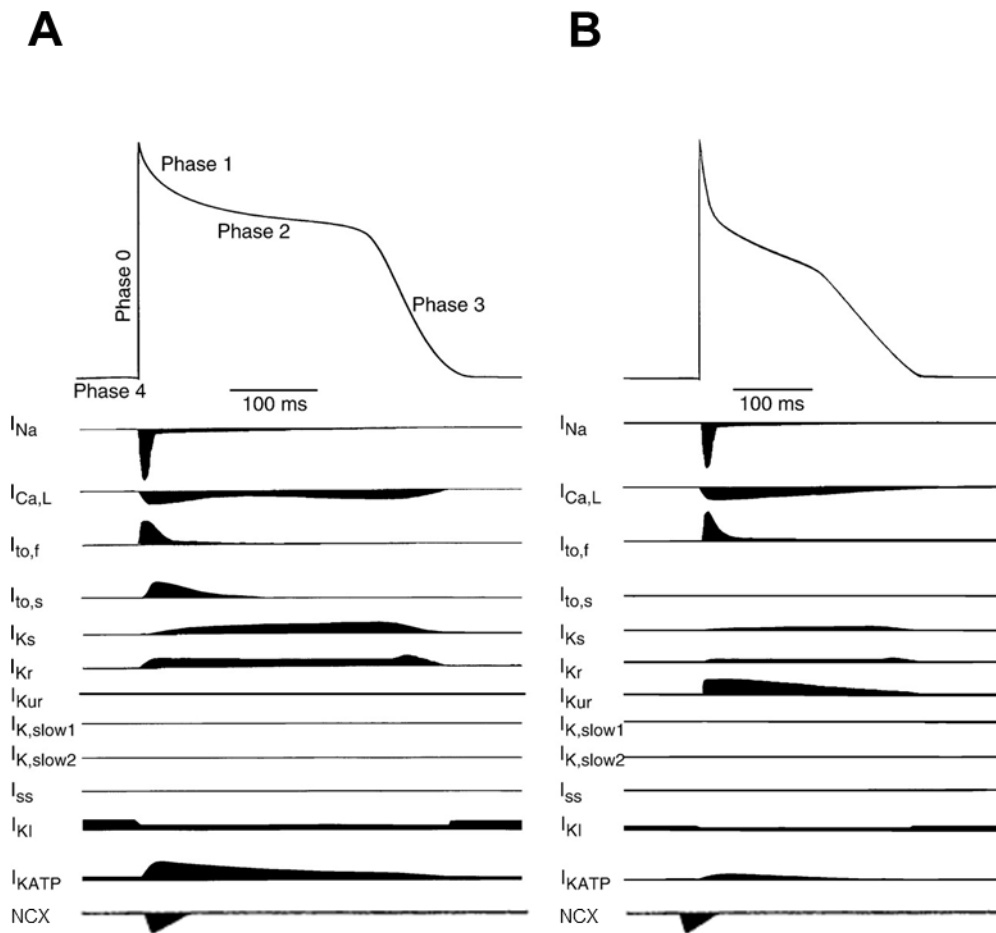


Figure 1.4: Action potentials and corresponding current fluxes.

A) Ventricular action potential and current fluxes which occur during the upstroke (Phase 0); initial repolarisation (Phase 1); plateau (Phase 2); repolarisation (Phase 3); and resting membrane potential (Phase 4). **B)** Atrial action potential and current fluxes which occur during each phase. Atrial phases are the same as those labelled on the ventricular action potential. Schematic taken from (Nerbonne and Kass, 2005).

A

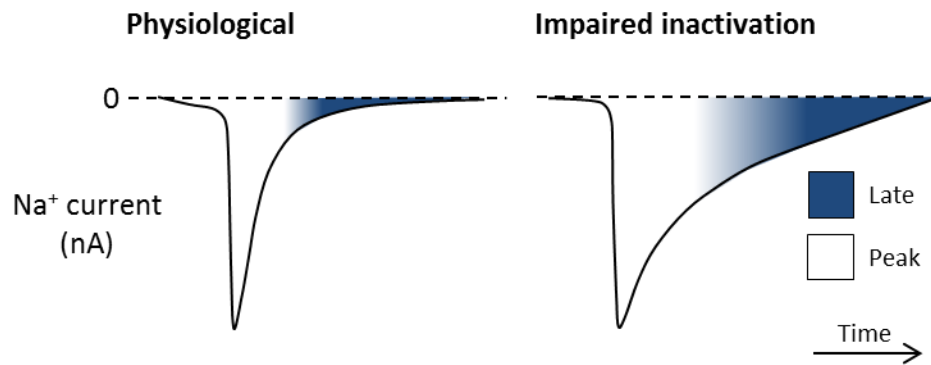
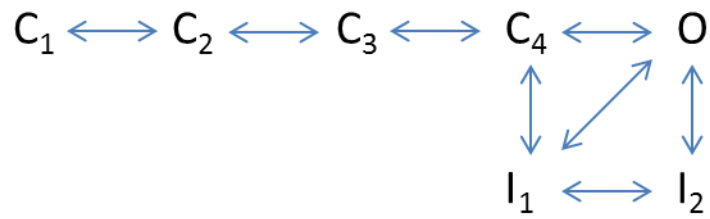


Figure 1.5: The peak and late Na⁺ current.

A) Schematic traces of physiological Na_v1.5 mediated I_{Na} and pathological Na_v1.5 mediated I_{Na} whereby the inactivation states of Na_v1.5 are impaired. Peak current shown in white and the late current in blue. Adapted from Vadnais and Wenger 2010 and are not real recordings (Vadnais and Wenger, 2010).

A



B

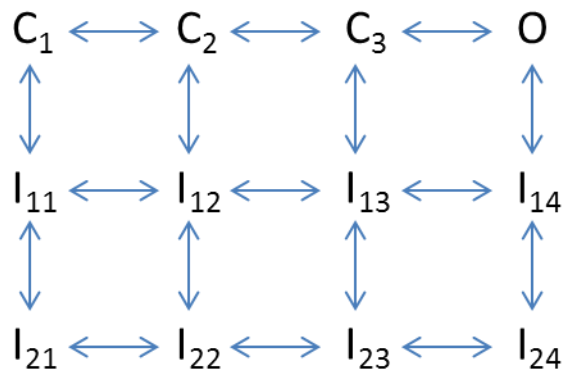


Figure 1.6: Markov model of $Na_v1.5$ gating kinetics.

A) Markov model hypothesised by Patlak showing 4 closed states (C); 1 open state (O); and 2 inactivated states (I). **B)** The revised model by Zhang et al. which includes 3 closed states; 1 open state; and 8 inactivated states, thereby better modelling the slow inactivation state of $Na_v1.5$. Schematics adapted from Patlak, 1991 and Zhang et al., 2013.

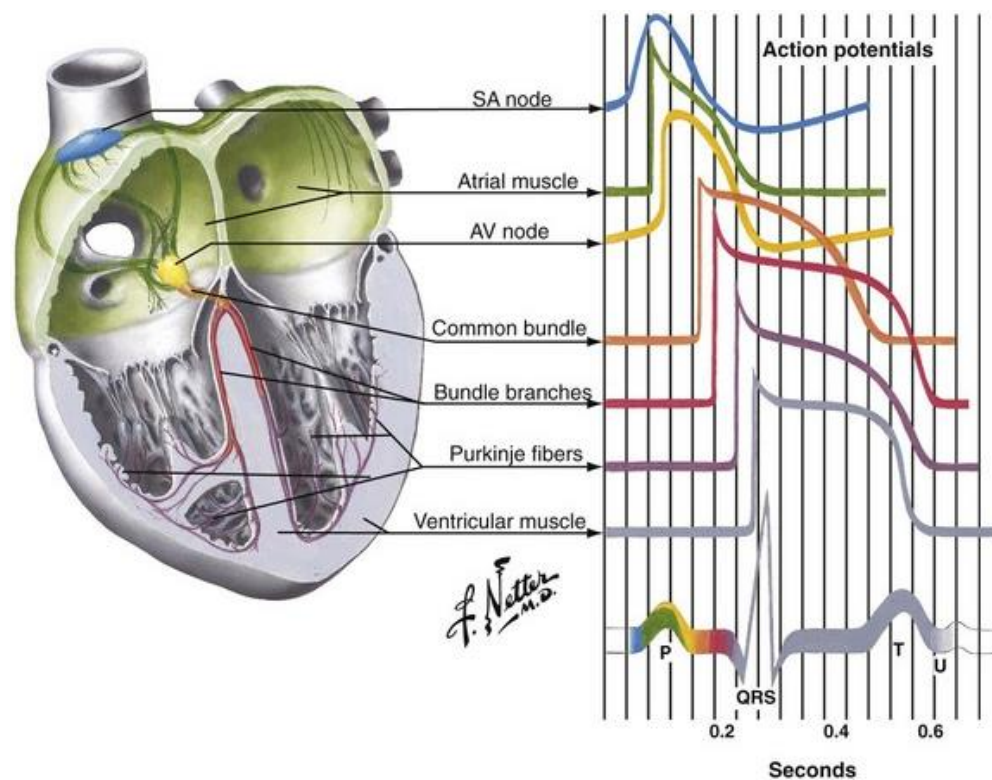


Figure 1.7: The cardiac conduction system and action potential morphologies at each tissue type. Action potentials initiate from SAN cells and propagate across the atria to the AV node. Conduction continues along the Bundle of His within the ventricular septum before branching into the Purkinje fibres and conducting through the ventricular muscle. Action potential morphologies change throughout different tissues due to changes in ion channel expression and ionic currents. Image from (Netter, 2014) (F. N. Netter 2014).

As is apparent in the summary schematic (Figure 1.7), action potential morphology within the cardiac tissue is heterogeneous. The atrial action potential is generally similar in morphology to the ventricular action potential. All 5 phases are apparent, however the plateau phase and overall action potential duration (APD) is shorter (Nerbonne and Kass, 2005). This is due to differing combinations and proportions of K^+ currents. For example in some species, including rat and human, the presence of a third delayed rectifier K^+ current with an “ultra-rapid” activation (I_{Kur}) is present in the atria only (Wang et al., 1993a, Boyle and Nerbonne, 1991). Additionally, action potentials within the atria increase in duration as the wave front travels from the SAN to the AVN (Spach et al., 1989). It has been hypothesised that this is a cardioprotective mechanism, which protects the atria from spontaneous, pathological depolarisations which may occur within close proximity of the SAN (Spach et al., 1989). Additionally, the presence of a “notch” or “spike and dome” morphology observed uniquely in ventricular sub-epicardial layers (Figure 1.12 A; solid), occurs primarily because of the presence of I_{to} (Wang et al., 1993b). Action potentials recorded from the SAN and AV node pacemaker cells do not exhibit a stable resting membrane potential. Instead, Phase 4 continuously depolarises until the threshold for action potential activation is reached. This is due to the presence of the funny current (I_f); a mixed Na^+ and K^+ current that causes SAN and AV node cell automaticity and regulates heart rate through the rate of Phase 4 depolarisation (Brown et al., 1976, Bucchi et al., 2007).

The action potential duration measured in rat ventricular myocytes is shorter than that observed in other mammals (Bassani et al., 2004). This is due to a species dependent increase in sarcolemmal ion channels that contribute towards the transient outward current (I_{to}). In rat ventricular cardiomyocytes, these channels include the voltage-gated K^+ channels $K_v4.2$ and $K_v1.4$ (Yeola and Snyders, 1997). Increased I_{to} quickly repolarises the membrane and limits the plateau phase (phase 2) thereby shortening the action potential (Bers, 2001) (Josephson et al., 1984b, Josephson et al., 1984a, Shattock and Bers, 1989).

1.4.2 The electrical conduction system

Regular contraction of the heart is under autonomic control. Myocytes of the SAN, located within the right atrial wall (Dobrzynski et al., 2005) regularly and spontaneously fire action potentials, which travel along the cardiac conduction system and through the myocardium (Figure 1.7). Action potential conduction pathways ensure contraction of the cardiac muscle at

the appropriate time in the cardiac cycle. Loss of regular conduction and contraction causes arrhythmias and inefficient cardiac pumping inducing a reduced cardiac output.

SAN cells exhibit an intrinsic spontaneous action potential firing rate. The action potential front is conducted through the atrial tissue, primarily along the Bachmann bundle pathway that runs through the inner wall of the left atrium. This electrical conduction causes the atria to contract, forcing blood into the ventricles. Next, the action potential passes into the AV node, located at the interatrial septum, close to the coronary sinus (Matsuyama et al., 2012). The AVN acts similarly to the SAN, in that it is auto-rhythmic and can initiate action potentials, albeit at a slower rate than SAN. Electrical conduction of the action potential is delayed at the AVN to allow the ventricles to fill. Thereafter, the action potential conducts through the left and right Bundles of His, located within the ventricular septum. Once reaching the apex of the heart, action potentials travel through Purkinje fibres and into the left and right ventricular muscle.

1.4.3 Autonomic modulation of heart rate

Whilst SAN cells display an intrinsic firing rate, this is regulated by the autonomic nervous system. Activation of the cardiac parasympathetic nervous system initiates a bradycardic response, for example during digestion. Conversely, activation of the sympathetic nervous system initiates a tachycardic response, during exercise or emotional stress.

1.4.4 Sympathetic system

Adrenergic stimulation of the heart occurs via the sympathetic nervous system and circulating catecholamines. Post-ganglionic, spinal sympathetic afferent nerves run along the sub-epicardial coronary system and penetrate the myocardium to reach the sub-endocardium. Sympathetic innervation is apparent throughout the atria and ventricles, yet is most dense in the atria (Vaseghi and Shivkumar, 2008).

Noradrenaline released into the neuromuscular junctions and circulating adrenaline, released by the adrenal glands superior to the kidneys, increase heart rate. Both signalling molecules activate β_1 , and to a lesser extent β_2 , adrenoceptors. These adrenoceptors are located at the sarcolemma, primarily within caveolae (Calaghan and White, 2006). They are coupled to the activation of $G_s\alpha$ subunit and the corresponding stimulatory signalling pathway. $G_s\alpha$

translocates within the sarcolemma to activate adenylyl cyclase to convert ATP into cyclic adenosine monophosphate (cAMP) (Yu and Rasenick, 2002). Four cAMP molecules are required to remove the regulatory subunits attached to PKA and allow PKA to phosphorylate a wide range of proteins. Phosphorylation of PLB, decreases its inhibition of SERCA, inducing faster uptake of Ca^{2+} into the SR (Negash et al., 2000, Calaghan et al., 1998); cross-bridge cycling kinetics can be increased via phosphorylation of troponin I (Kentish et al., 2001); and RyR2 phosphorylation is increased, although the subsequent effects on RyR2 function and Ca^{2+} release are still controversial (Ullrich et al., 2012, Houser, 2014).

1.4.5 Parasympathetic system

The divisions of the post-ganglionic vagus nerve innervate the heart via the cardiac plexus. Acetylcholine is released into neuromuscular junctions located primarily in the SAN and AV node. Some atrial and ventricular innervation is apparent, although parasympathetic control of the ventricle is less compared with the atria and is subject to desensitisation (McMorn et al., 1993, Vaseghi and Shivkumar, 2008).

Acetylcholine binds to muscarinic acetylcholine M2 receptors at the sarcolemma (Nenasheva et al., 2013). This initiates G_i protein coupled subunits to dissociate. The $G_{i\alpha}$ subunit inhibits adenylyl cyclase and therefore the production of cAMP; in this case, PKA-mediated phosphorylation of PLB, troponin I and RyR2 is prevented. Additionally, $G_{\beta\gamma}$ subunits bind to acetylcholine-dependent K^+ channels at the sarcolemma (Logothetis et al., 1987). This increases $I_{\text{K,Ach}}$, shortening action potential duration (APD) and hyperpolarising the membrane in atrial cells, without a significant effect on ventricular cells (Calloe et al., 2013). As well as directly affecting cardiomyocytes, acetylcholine can initiate parasympathetic effects by inhibiting the sympathetic nerve (Vanhoutte and Levy, 1980).

1.5 Ca²⁺ release from the sarcoplasmic reticulum

1.5.1 Ca²⁺ induced Ca²⁺ release

The primary SR Ca²⁺ release channel in cardiomyocytes is RyR2; a large channel protein (~2.2 mDa) comprised of 4 homomeric subunits (565 kDa each), arranged to form a single pore (Radermacher et al., 1994, Liu et al., 2002, Tunwell et al., 1996). RyR2 homomers are primarily located at the junctional SR membrane in close proximity to LTCC on the sarcolemma (Scriven et al., 2010). The primary physiological function of RyR2 is during the processes of EC coupling and CICR. During cell diastole, RyR2 clusters can spontaneously open to release relatively small, localised amounts of Ca²⁺, termed Ca²⁺ sparks (Section 1.5.3). Propagation of sparks across the length of the cell can cause pro-arrhythmic, spontaneous Ca²⁺ waves to occur (Section 1.5.2).

Atrial and ventricular cardiomyocyte contraction is Ca²⁺ dependent upon CICR (Figure 1.8). In response to Na_v1.5 opening and myocyte depolarisation as part of the cardiac action potential, Ca²⁺ influxes via LTCC (Egom et al., 2016). Importantly, LTCCs are positioned at the t-tubule, directly adjacent to clusters of cardiac RyR2 at the SR membrane to form couplons (Bers and Stiffel, 1993, Hayashi et al., 2009). This close proximity allows for the rapid diffusion of Ca²⁺ from the LTCC pore to activate RyR2 and release Ca²⁺ (Näbauer et al., 1989, Winslow et al., 2006). It is important to note that RyR2 opens in response to Ca²⁺ influx and not membrane depolarisation (Näbauer et al., 1989). RyR2 opening and release of Ca²⁺ from the SR is rapid and amplifies the cytosolic [Ca²⁺] from ~100 nM to 1 μM within tens of milliseconds (Dzbek and Korzeniewski, 2007). Importantly, CICR induces a synchronous release of Ca²⁺ throughout the myocyte, to ensure uniform contraction and this is known as a Ca²⁺ transient. Upon release from the SR, cytosolic Ca²⁺ binds to troponin C on the thin filament to facilitate ATP-dependent actin-myosin cross-bridge cycling (Figure 1.3B).

To ensure a return to the diastolic state and to allow ventricular filling, Ca²⁺ is extruded from the cytosol via ATP dependent SERCA located at the SR membrane; NCX at the sarcolemma; and to a much lesser extent MCU transporters on the inner mitochondrial membrane and Ca²⁺-ATPase at the sarcolemma (Bers, 2001, Kirichok et al., 2004, Bers et al., 2006b). SERCA is the predominant extrusion pathway, contributing ~60% in humans and >85% in rat (Pieske et al., 1999, Choi and Eisner, 1999). ~1% of Ca²⁺ is taken up by the mitochondria and then only at the mitochondrial ends adjacent to RyR2 clusters, or during high cytosolic [Ca²⁺] (>2 μM) whereby mitochondrial Ca²⁺ uptake may serve to blunt Ca²⁺ wave amplitude (Andrienko et al., 2009, Williams et al., 2013, Boyman et al., 2014b, Loughrey et al., 2002). Ca²⁺ (~1%) is also extruded

by sarcolemmal Ca^{2+} -ATPase (Bers, 2001). The remaining Ca^{2+} is removed via the electrogenic NCX antiporter which transports 1 Ca^{2+} out of the cell in exchange for 3 Na^+ ions into the cell.

The amount of Ca^{2+} released with each Ca^{2+} transient is dependent upon the sensitivity of RyR2 to Ca^{2+} . Alteration of this, for example by pharmacological modulation by caffeine or tetracaine can transiently affect Ca^{2+} transient amplitude (Eisner et al. 1999). This effect is transient due to the negative feedback mechanism, termed autoregulation, which is further discussed in Section 1.5.6.

A

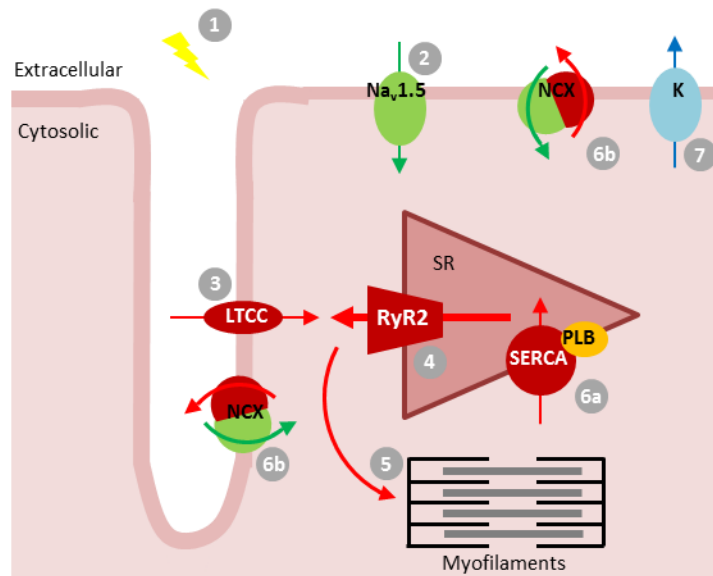


Figure 1.8: Schematic of the channel proteins and ion movements associated with EC coupling and CICR

A) Schematic of a cardiomyocyte t-tubule, sarcoplasmic reticulum (SR) and myofilaments with associated channel proteins and ion movements. 1. Depolarisation of the cell from a neighbouring cell initiates 2. $\text{Na}_v1.5$ to open and Na^+ influxes. 3. LTCC opens and Ca^{2+} influxes, 4. initiating the opening of RyR2. Ca^{2+} is released into the cytosol and 5. binds to troponin C at the sarcomeres, causing contraction of the myocyte. 6) Ca^{2+} is primarily extruded from the cytosol via a) SERCA and b) NCX. 7) The cell repolarises due to K^+ efflux via K^+ channels. Channels and ion movements are labelled red = Ca^{2+} ; green = Na^+ ; blue = K^+ . Schematic adapted from (Bers, 2001).

1.5.2 Ca²⁺ waves

In addition to physiological action potential evoked Ca²⁺ transients, spontaneous Ca²⁺ waves can occur which result in asynchronous and pathological contractions. Ca²⁺ waves occur at a threshold SR luminal [Ca²⁺] at which Ca²⁺ spark release is initiated and the propagation of a Ca²⁺ wave is facilitated by an increased cytosolic [Ca²⁺] (Lukyanenko et al., 1996). This threshold for Ca²⁺ wave release can be pharmacologically altered by increasing or decreasing the sensitivity of RyR2 to Ca²⁺. For example, decreasing the sensitivity of RyR2 to Ca²⁺ with application of tetracaine requires there to be a higher SR Ca²⁺ content for spontaneous waves to be initiated (Eisner et al., 2013). Wave frequency is initially decreased, however, upon continued SR loading by SERCA, the new threshold for wave release is reached wave frequency returns to control levels. This negative feedback mechanism is discussed in more detail in Section 1.5.6.

Spontaneous waves may arise for at least three possible reasons 1) increased cytosolic [Ca²⁺], 2) SR Ca²⁺ overload or 3) RyR2 or Casq mutations, such as those seen in CPVT patients which increase RyR2 sensitivity to SR Ca²⁺ (Savio-Galimberti and Knollmann, 2015, Kort et al., 1985, Bers et al., 2006a). Increased resting cytosolic [Ca²⁺] can activate RyR2 to open and can be caused by a decreased extrusion of Ca²⁺ from the cytosol via the two main extrusion mechanisms; SERCA and NCX. This could occur due to inhibition of SERCA or NCX activity, as seen in models of heart failure (Bers et al., 2006a). Conversely, SR Ca²⁺ overload can occur due to an increased reuptake of Ca²⁺ into the SR via SERCA, for example, when SERCA is stimulated during sympathetic stimulation. Catecholamine bound β_1 adrenoceptors initiate the stimulatory G-protein coupled receptor mechanism, which results in the phosphorylation of the SERCA inhibitor protein, PLB. Thereby, the inhibitory protein is itself inhibited, increasing Ca²⁺ re-uptake into the SR (Negash et al., 2000). CPVT mutations affect RyR2 function via a mutation of the RyR2 protein or the associated luminal protein Casq. The resultant increase in sensitivity of RyR2 to Ca²⁺ increases spark frequency and the probability of spontaneous, propagating Ca²⁺ waves (Liu et al., 2013a). In failing hearts, hyper-phosphorylation by PKA or CAMKII can also lead to a sustained increase in the RyR2 mediated Ca²⁺ leak giving rise to an increased incidence of arrhythmia (Walweel et al., 2017). Ca²⁺ waves can affect contraction in numerous ways. In the isolated cardiomyocyte, a spontaneous wave causes asynchronous contraction, which is much slower than the synchronous response to an action potential. A spontaneous Ca²⁺ wave arising immediately prior to physiological CICR can decrease the strength of a subsequent contraction because the SR Ca²⁺ available for release is decreased (Capogrossi et al., 1986). Additionally, Ca²⁺ waves can invoke tissue wide arrhythmias via the initiation of a delayed after depolarisation (DAD; Section 1.6) (Fujiwara et al., 2008).

1.5.3 Ca²⁺ sparks

During cell diastole, distinct, solitary Ca²⁺ sparks can be visualised at 40x magnification in the presence of a Ca²⁺ dependent fluorophore (e.g. fluo-4) using line scan confocal microscopy imaging. These sparks contribute to diastolic SR Ca²⁺ leak, which balances SR Ca²⁺ uptake via SERCA (Westcott et al., 2016). Spark initiation is thought to occur via the random opening of a single RyR2 channel and subsequent activation of neighbouring RyR2 by the initially released Ca²⁺ (Bovo et al. 2015). Under physiological conditions, this very localised CICR does not usually continue to propagate along the length of the cell (Cheng et al., 1996). However pathological conditions such as increased intracellular [Ca²⁺] or increased RyR2 sensitivity to Ca²⁺ can cause sparks to propagate further to form waves or aborted wavelets (Cheng et al., 1996, Savio-Galimberti and Knollmann, 2015, Kort et al., 1985, Bers et al., 2006a). The principle of the spatio-temporal summation of sparks can also be applied to Ca²⁺ transients (Cheng et al., 1996, Shkryl and Blatter, 2013). During EC coupling, the influx of Ca²⁺ via LTCC initiates the release of many sparks from RyR2 clusters to form a Ca²⁺ transient (Cannell and Soeller, 1998).

The mechanisms underlying spark termination have been computationally modelled and several theories have been reviewed. These include emptying of SR Ca²⁺; inactivation of RyR2 channels; 'stochastic attrition', the spontaneous dosing of RyR2 clusters; and 'cooperativity', whereby the random closing of one RyR2 channel increases the probability that more channels will close (Jafri, 2012, Stern and Cheng, 2004, Westcott et al., 2016). Experimentally it has been reported that local decreases to ~60% of the initial SR [Ca²⁺] contribute to spark termination in permeabilised rabbit ventricular cardiomyocytes (Bovo et al., 2015) (al. 2015). Alongside this decrease in local SR load, the spatio-temporal spread of released Ca²⁺ depletes and thereby limits inter-duster CICR (Gillespie and Fill, 2013). In summary, spark termination is multifactorial and, at least, dependent upon both cytosolic and luminal [Ca²⁺]. These termination mechanisms prevent positive feedback during EC coupling and the propagation of spontaneous waves.

High frequency Ca²⁺ sparking sites exist within the cardiomyocyte, however during diastolic conditions sparks are generated at a low frequency (Santiago et al., 2010, Zima et al., 2010). Spark width is typically ~2 μm and peak fluorescence is ~1.85 ΔF/F₀, (Cheng et al., 1996, Cheng and Lederer, 2008). The peak fluorescence amplitude units, ΔF/F₀, represents the difference between the spark amplitude (F) and the diastolic cell background fluorescence (F₀), divided by F₀, thereby normalising for differences in cell background fluorescence. However spark parameters are likely to be dependent upon RyR2 cluster size and density (Soeller and Cannell, 2002). Super resolution confocal microscopy has shown cluster size to be highly variable

(Baddeley et al. 2009, Hou et al. 2015). The majority of clusters within cardiomyocytes are relatively small and are made up of ~14 RyR2s (Baddeley et al., 2009). Yet the existence of larger clusters (>100 RyR2s) and superclusters (~1500 RyR2s) dominate transverse sectioned images and it is estimated that >90% of RyR2s contribute to these clusters (Hou et al., 2015). Computational models investigating spark parameters and RyR2 cluster size indicate that this relationship is complex due to subtle changes in $[Ca^{2+}]$ within the RyR2 sub-space and variations in RyR2 cluster size and density (Walker et al., 2014, Stern et al., 2013). Further to this, 'rogue' RyR2s or single RyR2s located away from clusters, have also been reported. Ca^{2+} release from these channels is hypothesised to be uncoupled from larger RyR2 clusters and computer simulations indicate that spontaneous non-spark Ca^{2+} releases from rogue RyR2s may preclude pro-arrhythmic cell behaviour (Section 1.5.5) (Sobie et al., 2006, Lu et al., 2012). Additionally t-tubule remodelling, reported to occur during heart failure, can cause 'orphaned RyR2'. Orphaned RyR2 clusters are left without a dyadic cleft which functionally links them to sarcolemmal LTCC. This causes dyssynchronous Ca^{2+} sparks and increases the risk of arrhythmia (Song et al., 2006).

Spark dimensions and frequency are also dependent upon many modulators that affect RyR2 function (Section 1.5.5). The measurement of Ca^{2+} spark parameters allows the effects of chemical modulators or induced pathology on RyR2 function to be studied whilst the channel is *in situ*. For example, an increased SR Ca^{2+} content or cytosolic $[Ca^{2+}]$, induces an increase in spontaneous Ca^{2+} spark amplitude, width and frequency (Cheng et al., 1996). Spark frequency can also be modulated pharmacologically by caffeine or tetracaine. However due to SR autoregulation, these changes are transient (Section 1.5.6) (Gyorke et al., 1997, Overend et al., 1997). Pathological changes to RyR2 function, such as that seen in CPVT (Section 1.7) also alter spark parameters. Cardiomyocytes isolated from mouse models of CPVT show an increase in spark frequency and duration when compared with WT cells (Savio-Galimberti and Knollmann, 2015, Westcott et al., 2016, Fernandez-Velasco et al., 2009b). In this diseased state, there is an increased probability that sparks can initiate further release of sparks from adjacent RyR2 leading to the formation of macro-sparks, aborted wavelets, or spontaneous waves, which may then propagate the length of the myocyte (Petrovic et al., 2015).

1.5.4 Non-spark Ca²⁺ release

Another form of RyR2 mediated SR Ca²⁺ leak has been identified, which may account for approximately half of the diastolic SR Ca²⁺ leak (Santiago et al., 2010, Lipp and Bootman, 1997). Ca²⁺ quarks or blinks are extremely small releases of SR Ca²⁺, almost unidentifiable against diastolic background noise. Dual Ca²⁺ imaging, which measures changes in intra SR Ca²⁺ in parallel with cytosolic Ca²⁺ has indicated that Ca²⁺ quarks are distinct Ca²⁺ release events, much smaller and more frequent than diastolic spontaneous spark release (Brochet et al., 2011). It is currently hypothesised that quarks originate from rogue RyR2 channels, located at the junctional SR but further away from larger clusters of RyR2 (Brochet et al., 2011, Williams et al., 2011). The pathological implication of Ca²⁺ quarks and their potential to be pharmacologically manipulated is currently unclear. Technical advancements in super-resolution microscopy may begin to clarify this (Xu et al., 2016).

1.5.5 Modulation of ryanodine receptor function

RyR2 activity can be modulated by different proteins and ions, located at both the cytosolic and luminal faces of RyR2. Within the SR lumen are three proteins, calsequestrin (Casq), triadin and junctin that modulate RyR2 activity (Dries et al., 2013, Terentyev et al., 2007, Wehrens et al., 2003). Casq can modulate RyR2 open probability both directly and indirectly. Casq sequesters Ca²⁺ and in doing so may act as a Ca²⁺ buffer, attenuating the [Ca²⁺] in the microdomain surrounding the luminal face of RyR2 (Kalyanasundaram et al., 2010). However, Casq can also directly bind to the luminal face of RyR2 (Handhke et al., 2016). Decreasing Casq to 75% of normally expressed levels, and thereby decreasing RyR2-Casq binding, increases the amount of spontaneous Ca²⁺ waves in single ventricular cardiomyocytes and increases the number of pro-arrhythmogenic spontaneous ventricular beats (Chopra et al., 2007). In complete Casq knockout mouse models, CPVT like arrhythmias are also exhibited upon initiation of exercise or adrenaline injection (Song et al., 2007, Chen et al., 2013, Alcalai et al., 2011). Triadin binds directly to Casq (Kobayashi et al., 2000) and this interaction closes the RyR2 pore (Terentyev et al. 2007). This inhibition of RyR2 by triadin is likely to be a necessary for the appropriate control of SR Ca²⁺ release, as individuals with triadin mutations show arrhythmogenic CPVT activity, indicative of unregulated SR Ca²⁺ release (Section 1.7.1) (Roux-Buisson et al., 2012, Walsh et al., 2016). Unlike Casq and triadin, junctin directly interacts with RyR2 at its cytosolic and luminal domains (Li et al., 2015, Altschafli et al., 2011). The role of

junction on RyR2 modulation is complex and dependent upon $[Ca^{2+}]$; increasing RyR2 activity at low luminal $[Ca^{2+}]$ and inhibiting RyR2 activity at high luminal $[Ca^{2+}]$ (>1 mM) (Altschafli et al., 2011). Despite this complexity, complete loss of junction in knock out mouse models exhibit CPVT-like behaviour (Altschafli et al., 2011).

Cytosolic proteins can also modulate RyR2 activity. For example, FKBP12.6, a 12.6 kDa cytosolic protein, regulates RyR2 function via a protein-protein interaction (Oda et al., 2013a, Wehrens et al., 2003). It is reported that FKBP12.6-RyR2 binding inhibits RyR2 opening. Dissociation of FKBP12.6 from RyR2, which is reported to occur within heart failure models, causes an increase in RyR2 open probability (Marx et al., 2000). Alongside this, an FKBP12.6^{-/-} knockout mutant mouse model causes significantly increased RyR2 open probability and an increased incidence of DADs (Wehrens et al., 2003).

Another cytosolic modulator of RyR2 is CaM, a Ca^{2+} binding protein that also directly binds to and regulates RyR2 (Yang et al., 2014, Xu et al., 2010). Within the structure of CaM, there are two Ca^{2+} binding sites at each of the two helix-loop-helix domains (EF hands) located within the C and N terminal lobes respectively (Chattopadhyaya et al., 1992). In its Ca^{2+} bound state, the inter-protein interaction between CaM and RyR2 stabilises RyR2 activity by promoting interactions between the central and N-terminal domains to preferentially close the channel (Figure 1.11) (Oda et al., 2013b). CaM bound to RyR2 causes RyR2 opening times to decrease by ~20% (Smith et al., 1989, Oda et al., 2013b, Huang et al., 2012). Additionally, the threshold for wave termination was increased with CaM (Tian et al., 2013). Mutations in CaM specific genes such as CALM 1-3 have been reported to cause arrhythmogenic disorders with CPVT phenotypes (Nyegaard et al., 2012). These CaM mutations disrupt the direct binding of CaM to the RyR2-CaM binding domain and thereby disrupt appropriate CaM modulation of SR Ca^{2+} release (Rebeck et al., 2016, Sondergaard et al., 2015). In its Ca^{2+} unbound form (apoCaM), RyR2 inhibition is diminished (Fruen et al., 2003).

RyR2 phosphorylation can modulate RyR2 activity. However, the function of RyR2 in response to different phosphorylation states is highly contentious within the literature and there are several phosphorylation and dephosphorylation mediators which may also complicate this issue (Wehrens et al., 2004, Terentyev et al., 2003b, Terentyev et al., 2007, Marx et al., 2000, Dobrev and Wehrens, 2014). There are three identified RyR2 phosphorylation sites located at serines 2030, 2808 and 2814 (Huke and Bers, 2008). Serines 2808 and 2814 are phosphorylated by CAMKII. CAMKII phosphorylation causes an increase in RyR2 open probability and sensitivity to Ca^{2+} (Wehrens et al., 2004). Serines 2808 and 2030 are phosphorylated by PKA (Huke and Bers, 2008). In single channel lipid bilayer models, PKA

phosphorylation of RyR2 has been reported to increase RyR2 channel activity due to consequential FKBP12.6 dissociation from RyR2 (Marx et al., 2000). However, in permeabilised myocytes, RyR2 channel activity is increased at both maximal and minimal levels of PKA phosphorylation (Bovo et al., 2017).

Availability of protein phosphatases PP1 and PP2, proteins that remove phosphate groups from RyR2, can also alter RyR2 phosphorylation state. For example, experimental application of PP1 or PP2 in permeabilised cardiomyocytes initially increased Ca^{2+} spark frequency (duBell et al., 2002, Terentyev et al., 2003b). The availability of other cytosolic proteins such as phosphodiesterase IV (PDE4) can also indirectly affect the phosphorylation status of RyR2, as inhibition of PDE4 slows cAMP degradation, thereby increasing PKA levels (Li et al., 2006, Ullrich et al., 2012). Additionally, both PKA and CAMKII can affect the function of other SR membrane bound proteins such as SERCA and PLB, which may in turn indirectly affect RyR2 function.

Perhaps the most important modulator of RyR2 activity is Ca^{2+} . Both luminal and cytosolic Ca^{2+} can act on RyR2 to open or close the channel pore. At its cytosolic side, RyR2 has an activating site and an inactivating site that Ca^{2+} can bind to, to respectively activate or inactivate the channel (Laver et al., 1997). Relatively low concentrations of Ca^{2+} ($\sim 1 \mu\text{M}$) are required to activate RyR2, whereas high concentrations (1 mM) cause RyR2 inactivation (Gusev and Niggli, 2008). Bilayer experiments have also revealed Ca^{2+} activating and inactivating sites at the luminal face of RyR2 (Ching et al., 2000) with a specific luminal Ca^{2+} activation site identified at the helix bundle channel gate (Jiang et al., 2007, Chen et al., 2014). The open probability of RyR2 increases with increasing luminal $[\text{Ca}^{2+}]$ (Gyorke and Gyorke, 1998, Tencerova et al., 2012, Sitsapesan and Williams, 1994b) which in cardiomyocytes causes an increase in the frequency of Ca^{2+} sparks (Section 1.5.3) and, during SR Ca^{2+} overload, can initiate spontaneous Ca^{2+} waves (Section 1.5.2) (Venetucci et al., 2008).

Another ion that modulates RyR2 activity is Mg^{2+} . Mg^{2+} competes with Ca^{2+} for access to the RyR2 channel pore and in doing so decreases the amount of Ca^{2+} that is released from the SR (Gillespie et al., 2012). Mg^{2+} also competes with Ca^{2+} for access to the activating and inactivating sites on the cytosolic side of RyR2. Displacement of Ca^{2+} for Mg^{2+} at either site results in a decrease in channel opening (Gusev and Niggli, 2008, Laver and Honen, 2008).

Whilst RyR2 conducts divalent cations, predominantly Ca^{2+} , monovalent cations such as K^+ can also be conducted through the same pore. This has been shown using single channel lipid bilayer experiments, in which native or recombinant RyR2 proteins were embedded into a

bilayer membrane and single channel current measurements were taken using patch clamp electrophysiology (Sitsapesan and Williams, 1994a). K^+ can be used as a charge-carrying ion in place of Ca^{2+} to increase the signal to noise ratio (Bannister et al. 2015)(Sitsapesan and Williams, 1994a). However, K^+ conductance via RyR2 can also occur under physiological conditions, during and immediately after Ca^{2+} release, as part of the SR counter-current (Gillespie and Fill, 2008, Guo et al., 2013). This counter-current opposes the large movement of charge carried by Ca^{2+} ions, with each Ca^{2+} transient or wave (Coronado et al., 1980). Without it, the SR membrane would rapidly polarise towards the Ca^{2+} equilibrium potential resulting in cessation of Ca^{2+} release within <1 ms (Gillespie and Fill, 2008).

1.5.6 SR Autoregulation

Ca^{2+} sparks, waves and transients are all subject to the negative feedback mechanism termed auto-regulation. Autoregulation ensures that SR Ca^{2+} release remains consistent from beat to beat and prevents long-term changes in SR Ca^{2+} release from occurring, for example due to pharmacological RyR2 modulation (Eisner et al., 1998, Dibb et al., 2007).

In the intact cardiomyocyte, cytosolic $[Ca^{2+}]$ is controlled by SR and sarcolemmal channels, transporters and antiporters. At the SR membrane, intracellular $[Ca^{2+}]$ is controlled by RyR2 and SERCA; Ca^{2+} is released from the SR via RyR2, and transported back by SERCA. At the sarcolemma, Ca^{2+} influx is controlled by LTCC whereas Ca^{2+} efflux is primarily controlled by NCX. Together, the function of these proteins maintains the net balance of Ca^{2+} within both the cytosol and SR lumen during steady state pacing. Disruption of this system, for example by pharmacological manipulation of RyR2, demonstrates how autoregulation of SR Ca^{2+} can occur. Application of caffeine (0.5 – 1.0 mM) to electrically paced, isolated cardiomyocytes sensitises RyR2 to Ca^{2+} and thereby initially increases the amount of Ca^{2+} released from the SR with each Ca^{2+} transient (Eisner et al., 1998). In single cell experiments measuring cell shortening, this is observed as a near immediate increase in cell shortening (Figure 1.9A). However, within one minute, cell shortening has returned to baseline levels, despite the continued presence of caffeine (Figure 1.9A). This is due to a net decrease in $[Ca^{2+}]$ that occurs after each release of SR Ca^{2+} . Released Ca^{2+} is extruded from the cytosol via the normal mechanisms; in rat cardiomyocytes, this equates to ~85% taken into the SR via SERCA and ~15% extruded from the cell via NCX (Choi and Eisner 1999). The proportional amount of Ca^{2+} extruded from the cell remains unchanged in the presence of caffeine; however, the total amount of Ca^{2+} extruded is increased, as more Ca^{2+} is being released by the SR. This results in a net decrease in cytosolic

[Ca²⁺] as Ca²⁺ influx via LTCC remains unaffected by caffeine application (Eisner et al. 1998). The opposite is true of tetracaine (Figure 1.9B). Tetracaine partially inhibits RyR2 and in doing so initially decreases the amount of Ca²⁺ released from the SR (Laver and van Helden, 2011). This causes a net gain in cellular [Ca²⁺] as Ca²⁺ influx via LTCC during the subsequent paced stimulations is relatively greater than that being extruded by NCX (Figure 1.9B). Ca²⁺ released by the SR is then increased to control levels (Eisner et al., 1998).

In the case of permeabilised cells, sarcolemmal proteins are functionless and cytosolic [Ca²⁺] can be experimentally controlled and maintained at a constant level. Within this reduced cell model, the effects of Ca²⁺ autoregulation can also be demonstrated (Gyorke et al., 1997, Overend et al., 1997). Application of caffeine to permeabilised cells increases the sensitivity of RyR2 to Ca²⁺, transiently increasing Ca²⁺ spark frequency (Figure 1.9C). This increase in spark frequency depletes SR Ca²⁺ content below the RyR2 activation threshold and spark release ceases. However, as SERCA function remains unaffected by caffeine application, and the [Ca²⁺] outside of the SR is maintained by the experimental solution, so SR loading continues until the new RyR2 threshold for Ca²⁺ release is reached and sparks are released at a rate comparable to control (Lukyanenko et al., 2001, Porta et al., 2011) (Gyorke et al., 1997, Overend et al., 1997). Again, the opposite is true of tetracaine. Partial inhibition of RyR2 initially decreases spark frequency but the continued uptake of Ca²⁺ by SERCA causes a rise in SR Ca²⁺ content, which overrides the inhibition by tetracaine (Figure 1.9D). Spark frequency is ultimately restored to the control level (Gyorke et al., 1997, Overend et al., 1997).

Under physiological conditions such as the increased sympathetic drive to the heart, any effects on RyR2 are combined with increased SR Ca²⁺ uptake via SERCA, allowing sustained effects on Ca²⁺ release (Lukyanenko et al., 2001). Overall, these findings appeared to suggest that drugs or interventions that result in moderate changes in RyR2 gating, without concomitant changes in SERCA function, do not have sustained effects on SR Ca²⁺ release.

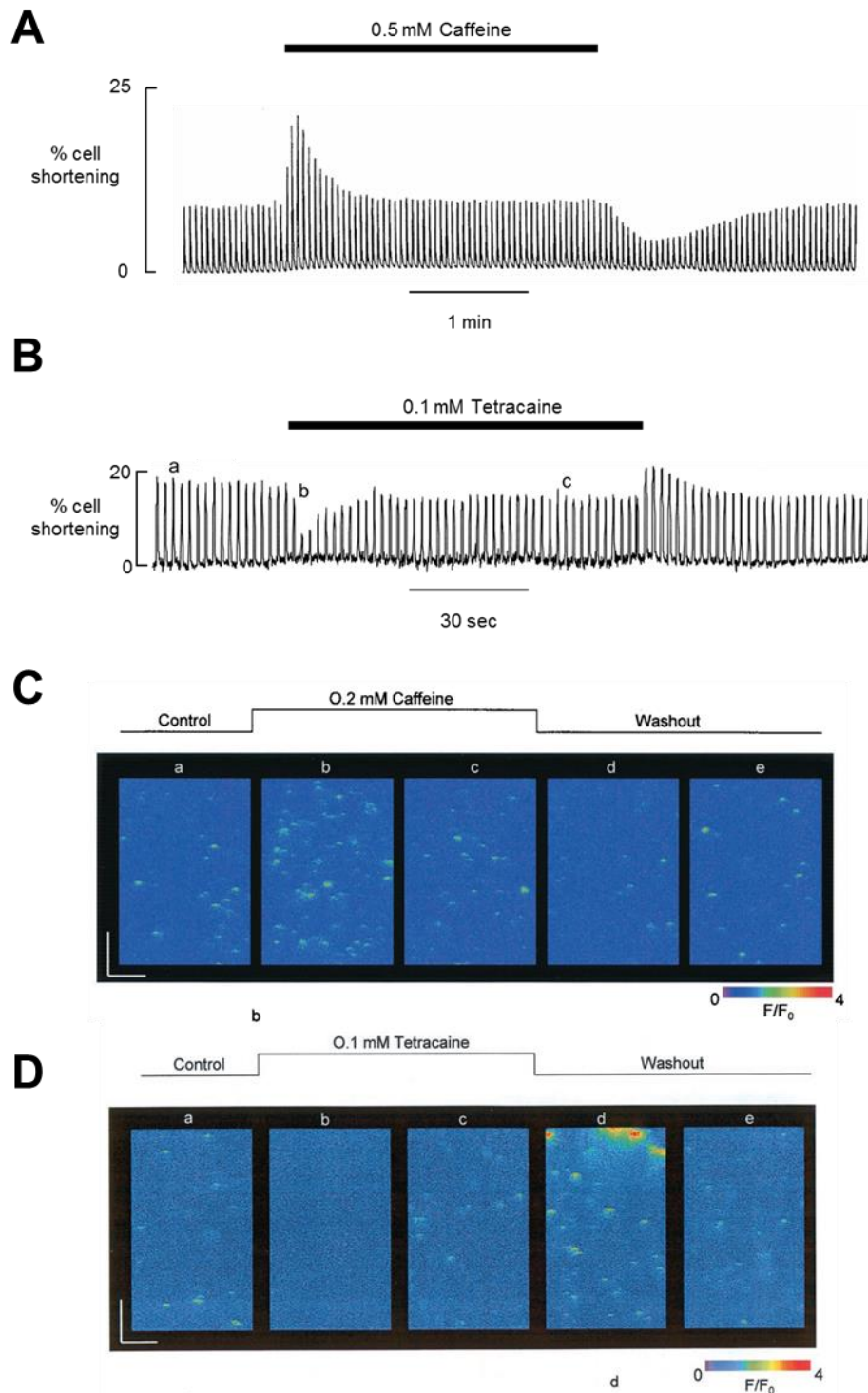


Figure 1.9: Experimental evidence documenting SR Ca^{2+} autoregulation
 A) Percentage of cell shortening recorded in intact, paced cardiomyocytes during application of 0.5 mM caffeine or **B)** 0,1 mM tetracaine. **C)** Spark frequency imaged in permeabilised cardiomyocytes during application of 0.2 mM caffeine or **D)** 0.1 mM tetracaine. Figures adapted from Eisner et al. 1998 and Lukyanenko et al. 2001.

1.6 Cardiac arrhythmias

Cardiac arrhythmias are a pathological change in heart rate or the development of irregular cardiac rhythms. Arrhythmias in either the atria or ventricles are caused by a range of underlying problems. Healthy ageing can slow conduction of the action potential wave front due to decreased Cx43 gap junction proteins (Jones and Lancaster, 2015). Heart failure or a previous myocardial infarction may alter the structure of the cardiac tissue giving rise to heterogeneous electrical activity (Yao et al., 1999). In certain individuals, some prescribed drugs may be pro-arrhythmic. Counter-intuitively this can include anti-arrhythmic drugs such as flecainide (Section 1.8) (Krishnan and Antzelevitch, 1993). Additionally, genetic disorders, which alter the function of proteins integral to the action potential or Ca^{2+} release, can cause arrhythmias. For example, CPVT causes arrhythmias in response to physiological adrenergic drive due to functional alterations of RyR2, caused by mutations in RyR2 or its regulatory protein Casq (Section 1.7.2) (Liu et al., 2013a, Gray et al., 2016).

1.6.1 Arrhythmic mechanisms at the single cell level

At the single cell level, cytosolic and SR Ca^{2+} overload can induce Ca^{2+} waves and in turn cause spontaneous depolarisations and inappropriate firing of an action potential (Fujiwara et al., 2008, Capogrossi et al., 1986). Pathological depolarisations, which occur after cell repolarisation, are DADs and are primarily dependent upon the electrogenic antiporter, NCX (Nagy et al., 2004). Aside from reversing briefly during the initial depolarisation phase of an action potential, NCX moves Ca^{2+} out of the cytosol in exchange for Na^+ at a ratio of 1:3 (Bridge et al., 1990). Given the valency of each ion, this results in a net inward movement of current; the transient inward current (I_{ti}) (Schlotthauer and Bers, 2000). If cytosolic Ca^{2+} increases during the diastolic period due to spontaneous SR Ca^{2+} release, the resulting efflux of Ca^{2+} via NCX results in depolarisation of the sarcolemma. If the threshold for an action potential is reached, an action potential is initiated and an arrhythmic contraction of the myocyte occurs (Fujiwara et al., 2008).

Early after depolarisations (EADs) are inappropriate, sometimes oscillatory depolarisations, which occur during the plateau phase of an action potential. EADs primarily occur due to the reactivation of I_{Ca} at membrane potentials more positive than -40 mV when APD is prolonged (January and Riddle, 1989). This may be due to decreased repolarisation of the cell due to pathological alterations in I_{K} such as in the genetic disorders LQT1 and LQT2 (Long QT Syndrome 1 and 2) (Viitasalo et al., 2006).

1.6.2 Arrhythmias at the tissue level

Both DADs and EADS originating from a neighbouring cluster of spontaneous cardiomyocytes can give rise to ectopic beats, which under certain conditions induce tissue wide arrhythmias (Fujiwara et al., 2008, Chang et al., 2013, Myles et al., 2012). In CPVT, ectopic beats tend only to arise from action potentials triggered by DADs during catecholamine treatment and tachycardia (Liu et al., 2006, Nam et al., 2005). Triggered ectopic activity can propagate through ventricular tissue that is no longer refractory and need not follow the physiological conduction pathway. This can give rise to re-entrant arrhythmias and ventricular fibrillation (Roses-Noguer et al., 2014, Nam et al., 2005). In the case of structural heart disease, the risk of re-entrant arrhythmias is increased when coupled with a large dispersion of refractory periods and an increase in APD (Krishnan and Antzelevitch, 1993).

Self-sustaining re-entrant arrhythmias or fibrillation can also be induced by atrial or ventricular tachycardia, such as in CPVT (Nair et al., 2011, Matsuyama et al., 2013, Clayton and Holden, 2002, Napolitano et al., 1993, Nam et al., 2005). While atrial fibrillation can result in relatively mild symptoms, the risk of developing a stroke is increased (Wolf et al., 1991). In contrast, ventricular fibrillation is rapidly fatal as the heart ceases to operate effectively as a pump and sudden cardiac death (SCD) is common in undiagnosed CPVT individuals (Napolitano et al., 1993).

1.7 Catecholaminergic polymorphic ventricular tachycardia (CPVT)

1.7.1 CPVT phenotype and characterisation

CPVT is a rare and often fatal genetic disorder. It affects 1 in 10,000 individuals, 75% of which present with clinical symptoms by 20 years of age (Pflaumer and Davis, 2012). Individuals have a normal heart rhythm at rest, yet suffer from inappropriate cardiac responses to adrenergic drive and circulating catecholamines, induced by either exercise or emotion. Sufferers may present with mild symptoms such as dizziness, palpitations, or exercise and emotion induced syncope. Unfortunately, however, sudden cardiac death may be the first clinical symptom in severe cases (Pflaumer and Davis, 2012, Napolitano et al., 1993).

Individuals with CPVT do not present with structural cardiac abnormalities. Therefore diagnosis is achieved through provocative stress testing whereby heart rate and rhythm is monitored during controlled exercise or adrenaline infusion (Krahn et al., 2005). Isolated premature ventricular beats are apparent at heart rates between 100–130 bpm. Other cardiac anomalies such as non-sustained ventricular tachycardia, bi-directional ventricular tachycardia and supraventricular arrhythmias such as atrial fibrillation may also be present at exercise induced high heart rates and can be visualised with ECG monitoring (Figure 1.10). Within an ECG, the P wave represents atrial depolarisation; the QRS complex represents ventricular depolarisation; and the T wave represents ventricular repolarisation (Figure 1.10 A). Bi-directional tachycardias are a classic symptom of CPVT whereby the QRS complex of each alternate beat shifts 180° (Figure 1.10 C) (Baheer et al., 2011). In cases where exercise testing is not possible or is inconclusive, continuous cardiac recording for a period of up to two weeks may be undertaken, using a Holter monitor (Napolitano et al., 1993).

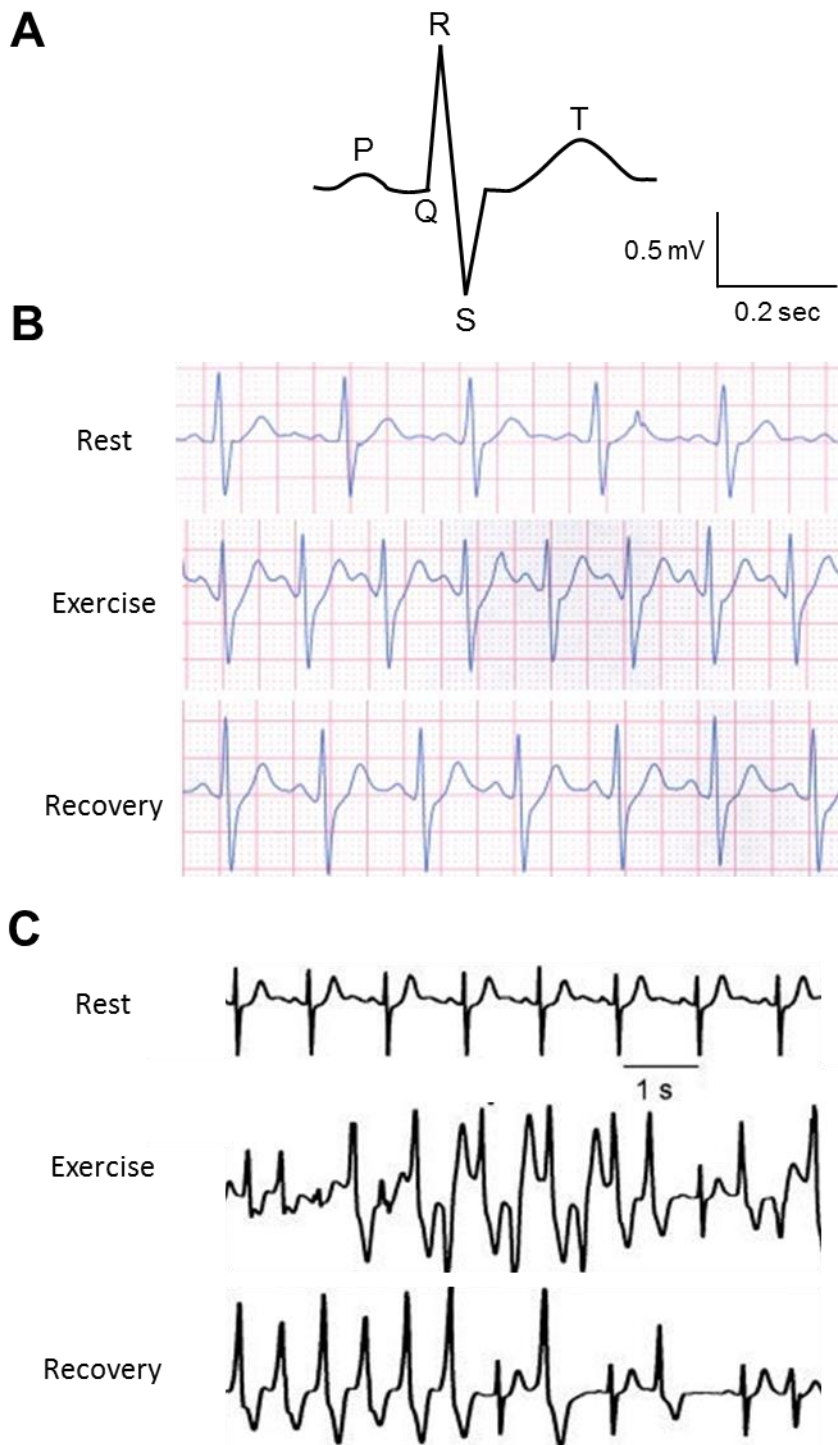


Figure 1.10: ECG readings from human participants with or without CPVT before, during and after exercise.

A) ECG schematic illustrating the P wave, QRS complex and T wave. **B)** ECG reading from a healthy individual. An increase in heart rate is apparent in response to exercise and heart rate slows after exercise is stopped. Normal P wave, QRS complex and T wave are apparent throughout ECG monitoring. **C)** In the CPVT patient, ECG is normal at rest with defined P wave, QRS complex and T wave. During exercise, polymorphic tachycardias, including bidirectional tachycardia is apparent. During bidirectional tachycardia, the QRS complex shifts 180° at every alternate heartbeat. Polymorphic tachycardias begin to subside during exercise recovery. ECGs adapted from Grier, 2008 and Burns, 2017.

1.7.2 CPVT genotype

As CPVT is predominantly an inherited disorder, genetic testing is available for suspected patients and their immediate family members. This can confirm suspected diagnoses and preempt potential cardiac incidences in siblings who may also carry the defective gene. Additionally, it may be discovered that asymptomatic family members also carry the defective gene (Beery et al., 2009). However, despite this strong familial link, 20% of reported CPVT mutations are *de novo* (van der Werf and Wilde, 2013). It is estimated that the prevalence of CPVT is 1 in 10,000, however the true prevalence is unknown (Napolitano et al., 2016).

The most common CPVT mutations are mutations of the RYR2 gene, located on chromosome 1 q42.1-43 (OMIM# 604772). RYR2 gene encodes the RyR2 protein (Marks et al., 2002, Allouis et al., 2005, Postma et al., 2005, Marjamaa et al., 2011). Inheritance of these mutations is autosomal dominant and the majority of mutations lead to a gain in function of RyR2. There are currently over 150 known RYR2 mutations, the majority of which are located at “hot-spots” on the RyR2 protein (Medeiros-Domingo et al., 2009, Priori and Chen, 2011). A number of RyR2 mutations have been investigated in experimental cell models including the missense mutations R4496C and G230C. Both mutations were associated with increases in Ca²⁺ spark and wave frequency in isolated cardiomyocytes (Fernandez-Velasco et al., 2009b, Savio-Galimberti and Knollmann, 2015, Liu et al., 2013b).

Much rarer CPVT mutations affect the CASQ2 gene, located on chromosome 1 p11-13.3 (OMIM# 61193). CASQ2 gene encodes the protein, Casq (Otsu et al., 1993). Inheritance of these mutations is autosomal recessive and most commonly seen in consanguineous families (Al-Hassnan et al., 2013). It has been hypothesised that changes in inter-protein binding between Casq, junctin and triadin account for the dissociation of Casq from RyR2, leading to increased RyR2 Ca²⁺ sensitivity and increased SR Ca²⁺ release (Chen et al., 2013). In Casq knockout or mutant mouse models, CPVT like arrhythmias are exhibited upon initiation of exercise or adrenaline injection (Song et al., 2007, Chen et al., 2013, Alcalai et al., 2011).

Rarer still are genetic mutations affecting the expression of triadin protein on chromosome 6 q22.31 (OMIM# 603283). To date, triadin mutations have been identified and reported in four CPVT individuals with severe ventricular fibrillation (Roux-Buisson et al., 2012, Walsh et al., 2016). One of the triadin mutations induced a premature stop codon leading to protein instability and subsequent protein degradation (Roux-Buisson et al., 2012). It is unknown exactly what effect triadin degradation has on Ca²⁺ handling within the single cell. However,

considering the clinical signs and association with CPVT it may be presumed that release of Ca^{2+} from the cardiomyocyte is increased within this mutation.

A common factor with all CPVT mutations is their ability to increase the Ca^{2+} sensitivity of RyR2. In essence, CPVT mutations decrease the threshold for spontaneous and potentially arrhythmogenic Ca^{2+} release (Priori and Chen, 2011). There are currently two theories which may explain the pathological changes in RyR2 sensitivity; dissociation of FKBP12.6 from RyR2 or changes in intra-protein interactions within the RyR2 structure.

FKBP12.6 is a 12.6 kDa protein which regulates RyR2 function via a protein-protein interaction (Oda et al., 2013a, Wehrens et al., 2003). Dissociation of FKBP12.6 from RyR2 is implicated as a consequence of long-term PKA-mediated RyR2 phosphorylation during heart failure and increases RyR2 open probability (Marx et al., 2000). Indeed, in an FKBP12.6^{-/-} mutant mouse model, DADs and RyR2 open probability was significantly increased and at least three RYR2 mutants decreased FKBP12.6 binding to RyR2 causing a CPVT phenotype (Wehrens et al., 2003). However, disruption in FKBP12.6-RyR2 binding may only account for some of the pathological increases in Ca^{2+} sensitivity; in other CPVT RyR2 mutations, the RyR2-FKBP12.6 interactions remained stable, despite increased Ca^{2+} sensitivity (George et al., 2003).

Another explanation for increased RyR2 Ca^{2+} sensitivity could be the reduced interaction between RyR2 domains. Interaction between the N-terminus and central domain is important in controlling the open and closed probability of the channel forming C-terminal (Figure 1.11) (Yamamoto and Ikemoto, 2002). Interestingly, RyR2 mutation hotspots correspond with the N-terminal and central domains (Figure 1.11). When this intra-protein interaction is compromised, as is the case in RyR2 mutations affecting these domains, channel opening is facilitated allowing Ca^{2+} to leak from the SR into the cytosol (Liu et al., 2010). Indeed, disruption of the N-terminal and central domain using the synthetic peptide DPc10 caused an increase in Ca^{2+} sensitivity and spontaneous Ca^{2+} release in WT ventricular cardiomyocytes (Yang et al., 2006).

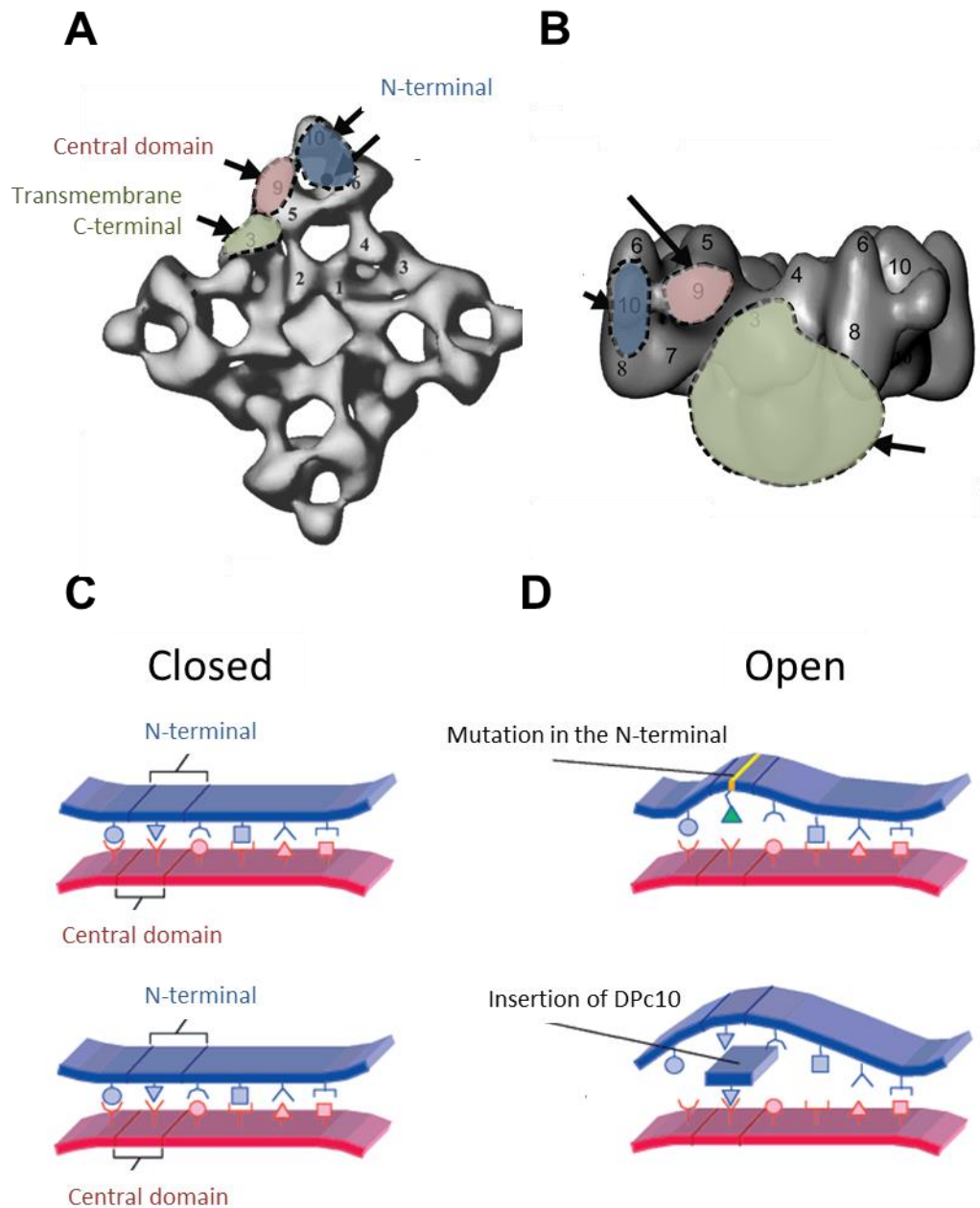


Figure 1.11: Overview of the RyR2 structure and schematic of a RyR2 intra-protein interaction
A) Cytoplasmic view of a 3D surface representation of a RyR2 tetramer. Mutation hot spots and the corresponding protein domains are highlighted. The N-terminal is shown in blue, the central domain in pink and the transmembrane C-terminal is shown in green. **B)** Side view of a 3D surface representation of a RyR2 tetramer with RyR2 domains indicated as before. Images adapted from (Bagattin et al., 2004) and (Stokes and Wagenknecht, 2000). **C)** Schematic of the N-terminal and central domain interaction under physiological conditions, whereby these domains are “zipped” and RyR2 is predominantly in its closed state. **D)** Schematic of the N-terminal and central domain interaction under pathological conditions whereby an increase in Ca^{2+} sensitivity and RyR2 open probability occurs. Top panel shows a structural mutation and the lower panel shows the insertion of the synthetic peptide DPc10. Images adapted from (Yamamoto and Ikemoto, 2002).

1.7.3 CPVT therapy

To reduce the incidence of cardiac arrhythmias, CPVT patients are told to avoid exercise and highly emotional or stressful situations but other prophylactic treatment is necessary. Invasive therapies, such as denervation of the left sympathetic cervical nerve or implantation of a cardioverter defibrillator (ICD) are considered (Roses-Noguer et al., 2014). However, denervation is irreversible and ICD shocks (appropriate or inappropriate) are stressful for the patient and can induce further catecholamine induced arrhythmias. Therefore pharmacological intervention is the first choice of treatment (Pflaumer and Davis, 2012).

High doses of non-selective β -blockers, such as propranolol or nadolol, are the conventional first line therapy for all CPVT sufferers. Missed doses can prove lethal, yet when administered correctly, β -blockers are effective at controlling catecholamine induced cardiac arrhythmias in the majority of CPVT patients. Non-selective β -blockers inhibit the β_1 and β_2 adrenoceptors located at the myocyte membrane and the downstream adrenergic effects which induce CPVT arrhythmias (Leren et al., 2016). For example, β -blockers inhibit an increase in SR Ca^{2+} uptake via SERCA by preventing PKA-mediated PLB phosphorylation (Negash et al., 2000). β -blockers also inhibit further RyR2 phosphorylation, which may prevent excess Ca^{2+} release via RyR2 (Marx et al., 2000). Additionally, β -blockers also blunt the increased Ca^{2+} influx via the LTCC Ca^{2+} current, thereby limiting the potential for Ca^{2+} overload (Farkas et al., 2012).

Interestingly, two other β -blockers, carvedilol and nebivolol, may have an additional mechanism of action not observed in other β -blockers. It has been suggested that carvedilol may act directly on the RyR2 to decrease pro-arrhythmic Ca^{2+} release (Zhou et al., 2011, Zhang et al., 2015). In single-channel lipid bilayer experiments, RyR2 open duration times were decreased and whole hearts perfused with R-carvedilol showed suppression of ventricular tachycardia and Ca^{2+} waves in epicardial cardiomyocytes (Zhang et al., 2015). This effect was enantiomer-dependent and R-carvedilol alone suppresses Ca^{2+} waves and ventricular arrhythmias without changing heart rate or blood pressure as would be expected of a standard β -blocker (Zhang et al., 2015, Stoschitzky et al., 2001). In similar single-channel lipid bilayer experiments, complemented by whole heart drug perfusions, nebivolol showed similar enantiomer-dependent block of RyR2; suppression of Ca^{2+} waves and ventricular arrhythmias occurs without an effect on heart rate and blood pressure (Tan et al., 2016). Importantly, these anti-arrhythmic effects of carvedilol and nebivolol are not observed in at least 12 other β -blockers (Tan et al., 2016).

Another pharmacological therapy used in combination with β -blockers is the LTCC channel blocker, verapamil. Verapamil has been reported to prevent ventricular arrhythmias in CPVT patients in small clinical studies (Rosso et al., 2007, Alcalai et al., 2011, Fagundes et al., 2010). The anti-arrhythmic action of verapamil may be caused by dual inhibition of LTCC within the SA and AV nodes and an inhibition of LTCC in ventricular myocytes. Verapamil slows SAN pacing and electrical conduction through the AVN, thereby limiting the conduction of atrial arrhythmias into the ventricles (Ning and Wit, 1983). Additionally, isolated ventricular myocytes from the *Casq2*^{-/-} mutant mouse model treated with verapamil showed suppression of Ca^{2+} oscillations (Alcalai et al. 2011).

Finally, there is clinical evidence to suggest that flecainide is effective and safe in the treatment of CPVT. One pilot study reported complete or partial suppression of exercise induced ventricular arrhythmias by flecainide in 76% of CPVT patients (van der Werf et al., 2011b). Similar results are apparent in other small trials and case reports (Khoury et al., 2013, Mantziari et al., 2013, Lieve et al., 2016) although the results of the largest clinical trial are still awaited (Kannankeril, 2010). However, the mechanism of action by which flecainide inhibits CPVT induced ventricular arrhythmias is controversial in the current literature.

1.8 Flecainide

Flecainide is a class 1c antiarrhythmic drug. Its chemical structure (N-(2-piperidylmethyl)-2,5-bis(2,2,2-trifluoroethoxy) benzamide acetate) consists of two amide groups, connected to either the piperidine or benzamide rings (Figure 1.12) (Banitt et al., 1977). The primary antiarrhythmic effect of flecainide is its use-dependent block of cardiac $\text{Na}_v1.5$. The active binding site of flecainide to $\text{Na}_v1.5$ is still unknown, although both the piperidine and benzamide rings have been implicated in binding to K^+ channels (Madeja et al., 2010, Melgari et al., 2015b). Alongside its potent anti-arrhythmic properties (Anderson et al., 1981), flecainide has proven itself to be fatally pro-arrhythmic in patients with structural ventricular abnormalities (CAST, 1989). Controversy surrounding the action of flecainide is resurfacing as additional mechanisms of action are investigated (Hilliard et al., 2010).

1.8.1 Flecainide induced inhibition of the cardiac Na^+ current

Flecainide blocks $\text{Na}_v1.5$ in its open state by entering the pore region via the extracellular side of the sarcolemma (Ramos and O'Leary, 2004, Nitta et al., 1992). During inactivated and closed states, flecainide becomes trapped within the pore region, and drug dissociation from the channel is slow (Ramos and O'Leary, 2004). High frequency stimulation encourages further high affinity binding of flecainide to $\text{Na}_v1.5$, and this underlies flecainide's use-dependent properties. In this way, flecainide inhibits both the peak and late I_{Na} (Nagatomo et al., 2000).

Flecainide block of I_{Na} is beneficial in the treatment of atrial fibrillation, LQT syndrome and Wolff-Parkinson White Syndrome (Aliot et al., 2011, Benito et al., 2008, Moss et al., 2005, BNF, 2015). In the case of LQT3, flecainide is particularly effective at inhibiting the late I_{Na} of the mutated $\text{Na}_v1.5$ channel, ΔKPQ (Nagatomo et al., 2000). Clinically this exhibits as a shortening of the pathologically prolonged QT segment of the ECG (Moss et al., 2005, Antzelevitch et al., 2014). However the safety of flecainide within these patients has been questioned due to the occurrence of Brugada-like ECG traces, in which the ST interval is elevated (Moss et al., 2005).

Flecainide is contraindicated in patients with structural cardiac abnormalities, for example those with a history of myocardial infarction or heart failure (CAST, 1989, Anderson et al., 1994). This is due to the pro-arrhythmic and sometimes fatal effects of flecainide (CAST, 1989). In the ventricular tissue, flecainide causes heterogeneous and opposing effects on action

A

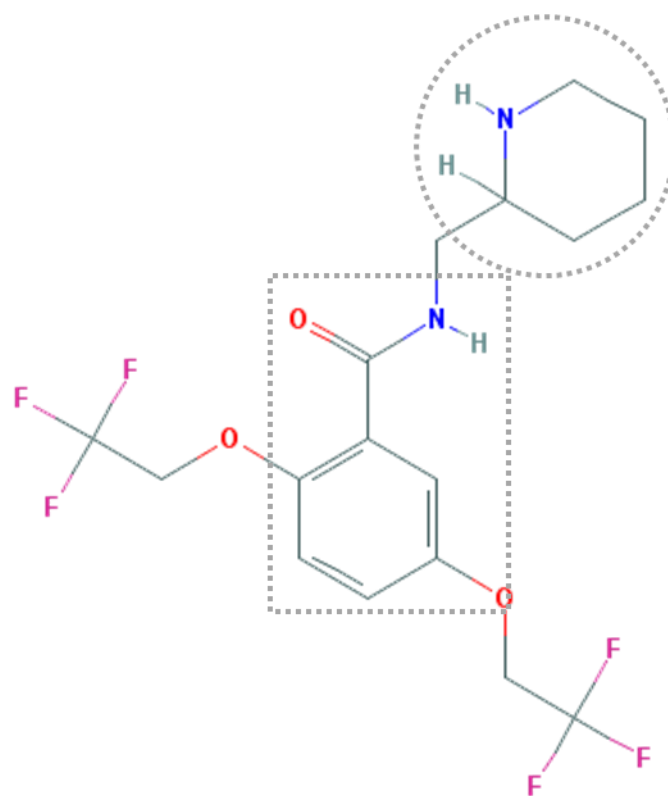


Figure 1.12: Skeletal schematic of the molecular structure of flecainide

A) Molecular structure of flecainide, with piperidine ring (circle) and bezamide ring (rectangle) emphasised. Structure images taken from <http://pubchem.ncbi.nlm.nih.gov>.

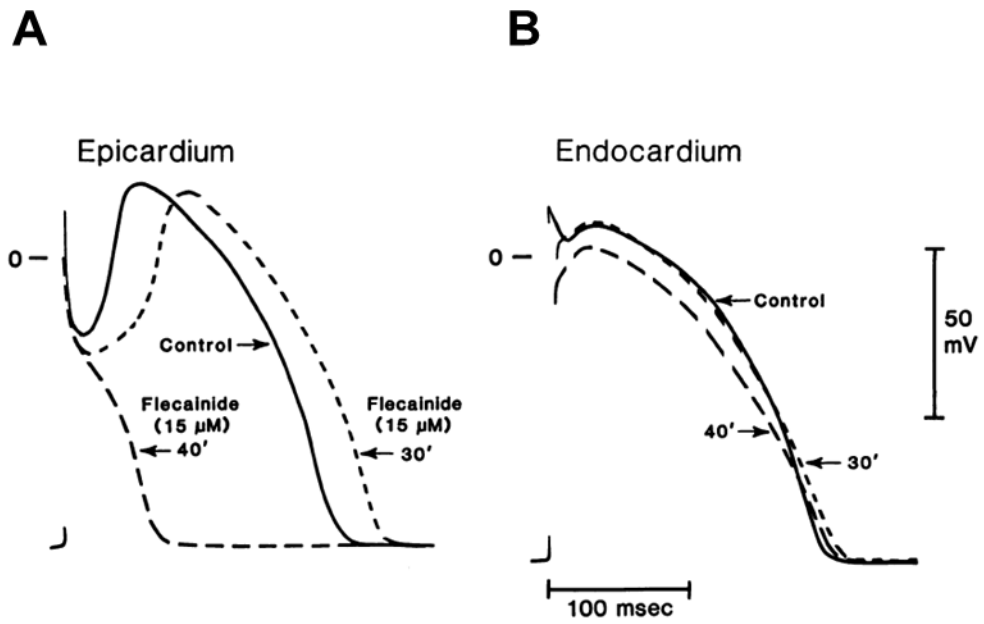


Figure 1.13: Changes in action potential morphology upon application of flecainide in the sub-epicardium and sub-endocardium

A) Action potential of the sub-epicardium (solid) with flecainide-dependent changes in action potential morphology and prolongation or curtailment of APD (dashed). **B)** Action potential of the sub-endocardium (solid) with smaller flecainide-dependent changes in action potential morphology and duration (dashed). Images taken from Krishnan and Antzelevitch, 1993.

potential duration (APD) in the sub-epicardium and sub-endocardium (Stokoe et al., 2007, Krishnan and Antzelevitch, 1991, Krishnan and Antzelevitch, 1993). In the presence of flecainide, block of peak I_{Na} and premature termination of Phase 0 at more negative potentials may delay the activation of I_{Ca} , thereby increasing APD. Conversely, early termination of the action potential upstroke by flecainide may minimise I_{Ca} resulting in the marked shortening of the APD (Figure 1.13) (Krishnan and Antzelevitch, 1993). Prolongation of the APD is coupled with an increase in the post-repolarisation refractory period (PRR), which helps to prevent the initiation of pro-arrhythmic depolarisations (Krishnan and Antzelevitch, 1991). However, when coupled with a wide dispersion of refractory periods, due to APD shortening and a relatively shorter PRR in the sub-endocardium and sections of the sub-epicardium, re-entrant arrhythmias in ventricular tissue are encouraged (Krishnan and Antzelevitch, 1993). In post-ischaemic or infarcted hearts where action potential heterogeneity is inherently increased (Antzelevitch et al., 1991), further variability of action potential morphology by flecainide increases the risk of phase 2 re-entrant arrhythmias (Krishnan and Antzelevitch, 1993, Coromilas et al., 1995).

Some variability in APD is also apparent within the atria (Spach et al., 1989). However, arrhythmogenic initiation points are apparent only at specific anatomical sites where the APD heterogeneity is steep, such as at the pulmonary vein-left atrial junction (Spach et al., 1989, Varela et al., 2016). Flecainide inhibition of I_{Na} in atrial tissue increases APD at all stimulation rates with further APD prolongation at fast stimulation rates (Wang et al., 1993b, Kirchhof et al., 2005). In this way, flecainide reverses the pathological shortening of the APD caused by ionic remodelling during atrial fibrillation (Kirchhof et al., 2005). Unlike that reported in the ventricle, dispersion of RPP is not increased enough to become pro-arrhythmogenic.

Although flecainide blocks both the peak and late I_{Na} , it is the peak I_{Na} block which elicits flecainide's pro-arrhythmic effects. Relatively specific inhibitors of the ventricular late I_{Na} , such as ranolazine (Antzelevitch et al., 2004) and the novel pharmaceutical GS-6615 (Rajamani et al., 2016), do not display the same pro-arrhythmic characteristics of flecainide (Rajamani et al., 2016, Song et al., 2004, Mason and Sossalla, 2016, Antzelevitch et al., 2004).

1.8.2 Flecainide inhibition of cardiac K⁺ currents

Alongside its prominent I_{Na} block, flecainide also inhibits the repolarising delayed rectifier K⁺ current, I_K/I_{HERG} (Melgari et al., 2015b, Follmer et al., 1992) which acts to repolarise the membrane potential during phase 3 of the action potential. The transient outward K⁺ current (I_{to}), which contributes to the “spike and dome” morphology of the sub-epicardial action potential is also blocked by flecainide (Wang et al., 1993b). I_K/I_{HERG} and I_{to} block by flecainide may partially contribute to the increased APD observed within a proportion of ventricular myocytes by prolonging the time for membrane repolarisation (Wang et al., 1993b, Paul et al., 2002).

1.8.3 Effects of flecainide on RyR2

An effect of flecainide on RyR2 was first postulated by Watanabe et al. (Watanabe et al., 2009). In these experiments, flecainide decreased spontaneous Ca²⁺ waves by ~39% and decreased DADs by ~69% in cardiomyocytes isolated from the Casq2^{-/-} CPVT mouse model. The decrease in Ca²⁺ wave frequency remained significant even after NCX block, indicating that flecainide inhibition of Na_v1.5 did not fully account for flecainide’s anti-arrhythmic mechanism (Sikkel et al., 2013, Watanabe et al., 2009). Additionally, application of flecainide to single channel RyR2 embedded within a lipid bilayer decreased channel opening times, suggesting that RyR2 may be a target of flecainide’s action (Watanabe et al., 2009).

The effects of flecainide on spontaneous waves and single channel current flow were also studied by Hilliard et al. (Hilliard et al., 2010). An additional effect of flecainide on Ca²⁺ sparks was apparent in Casq2^{-/-} myocytes, whereby spark frequency was increased in combination with a decrease in amplitude and width, thus, further supporting the hypothesis that flecainide acted on RyR2 to block Ca²⁺ waves (Hilliard et al., 2010). A similar effect of flecainide on wave frequency and spark properties was also reported recently in a second CPVT mutant mouse model affecting RyR2 (R4496C^{+/-}) (Savio-Galimberti and Knollmann, 2015). Interestingly, flecainide, and to a lesser extent, the R-propafenone enantiomer, were the only Na_v1.5 inhibitors that decreased the frequency of spontaneous Ca²⁺ waves in Casq2^{-/-} cardiomyocytes. No effect on waves was seen upon application of other Na_v1.5 inhibitors procainamide, quinidine, lidocaine, tetrodotoxin or ranolazine (Hwang et al., 2011a).

However, other groups have been unable to replicate effects consistent with an action of flecainide on RyR2 in either WT cardiomyocytes or cells from CPVT mutant R4496C^{+/-} mice (Liu et al., 2011, Sikkell et al., 2013, Bannister et al., 2015). There are several reasons why this may be the case including differences in experimental protocol, which may not be relevant to clinical administration of flecainide. For example, the time taken for flecainide to cross the sarcolemma is relatively high because it is mostly charged at physiological pH (Liu et al., 2003). Some studies applied flecainide too briefly to cardiac myocytes to allow an intracellular action (discussed further in Chapters 3 and 4). Additionally, flecainide can accumulate within tissue over time (Latini et al., 1987), meaning that effects seen experimentally in permeabilised cells at levels above the normal plasma concentration may have clinical relevance where regular dosing is routine (discussed further in Chapter 4). Another factor is that flecainide may affect mutant and WT RyR2 differently, such that any anti-arrhythmic effect of flecainide may be more difficult to identify in WT cells (discussed further in Chapter 7) (Savio-Galimberti and Knollmann, 2015).

These discrepancies suggest a need for further investigation into the mechanism of action for flecainide. Since the 'golden age' of pharmaceutical development in the 1970s, new pharmacological targets have lacking (Walker, 2006). The possibility of a novel and potentially highly beneficial anti-arrhythmic mechanism of action on RyR2 merits further investigation.

1.9 Study aims

The overarching aim of this thesis is to investigate the hypothesis that flecainide modulates RyR2 channel activity to prevent pro-arrhythmic SR Ca^{2+} release in isolated WT rat ventricular cardiomyocytes. The current clinical evidence suggests that flecainide can enable CPVT individuals to live longer by suppressing arrhythmias. However, age is a primary risk factor for myocardial infarction and structural heart failure (Jousilahti et al., 1999). Under these circumstances, flecainide is contraindicated because of the high risk of fatal arrhythmias linked to the action of the drug on $\text{Na}_v1.5$. If flecainide's antiarrhythmic action does involve a direct action on RyR2, it may be possible to develop new drugs which selectively target RyR2, thereby providing an effective antiarrhythmic treatment for patients with structural heart disease. However, the current uncertainty regarding flecainide's effect on RyR2 is an obstacle to development of novel RyR2 modulators. Therefore, this study will investigate:

- I. The effect of flecainide on isoprenaline-induced spontaneous Ca^{2+} waves and sparks in intact WT cardiomyocytes.
- II. The time taken for flecainide to enter the intact cardiomyocyte, the method of cell entry and localisation of flecainide within the myocyte.
- III. The effect of flecainide on spontaneous Ca^{2+} waves and sparks in permeabilised WT myocytes cardiomyocytes.
- IV. Whether flecainide's effect on Ca^{2+} waves is dependent upon the modulatory protein CaM.
- V. The effect of flecainide on spontaneous Ca^{2+} waves when the SR membrane potential is pharmacologically altered.

There is continued controversy as to the effects of flecainide on RyR2 and the subsequent effects on pro-arrhythmic Ca^{2+} release from the SR. This study aims to clarify some of the discrepancies present within the literature, whilst furthering the current understanding of flecainide on RyR2.

Chapter 2: General Methods

2.1 Solutions

The compositions of all solutions are given in Tables 2.1-2.6. A list of full chemical names and sources are given in Table 8.1, Appendix A.

2.2 Myocyte Isolation

Ventricular cardiomyocytes were isolated from male Wistar rats (160 ± 20 g) using a Langendorff perfusion system (Figure 2.1). Rats were sacrificed by concussion followed by cervical dislocation according to Schedule 1 of the UK Animals (Scientific Procedures) Act, 1986. The rib cage was opened and the heart excised, ensuring that the remaining aorta was sufficient to allow cannulation. The open end of the aorta was attached to the Langendorff perfusion rig thereby allowing retrograde perfusion at 37°C . Isolation solution I (Table 2.1) was initially perfused through the coronary system at a flow rate of 10.9 ml/min until the effluent ran clear, indicating removal of blood from the coronary system. At this point, a strong, regular beat dictated by the SAN discharge rate was observed. Subsequent perfusion with zero Ca^{2+} isolation solution II (Table 2.1) for 2 min at 5.7 ml/min caused a progressive decrease in cardiac contraction. Enzymatic digestion of the interstitial cardiac tissue was then initiated by perfusion with protease and collagenase enzyme isolation solution III (Table 2.1) for 10 min at 5.7 ml/min. The atria were then discarded and the remaining right and left ventricles were cut open and shaken (450 osc/min, 5 min) in 5 ml of isolation solution IV (Table 2.1), which contained both enzymes and bovine serum albumin (BSA). The temperature was maintained at 37°C throughout. Thereafter, any undigested ventricular tissue was removed by passing the solution through a 200 μm nylon mesh leaving a suspension of mostly rod shaped myocytes.

Isolated myocytes in solution IV (Table 2.1) were incrementally re-introduced to extracellular calcium. Initially, the $[\text{Ca}^{2+}]$ was increased from zero to 0.56 mM. Myocytes were then centrifuged at 53 G for 40 sec to form a pellet. The supernatant was removed and the pellet re-suspended in 5 ml of filtered isolation solution I (Table 2.1), with a $[\text{Ca}^{2+}]$ of 0.75 mM. To ensure complete removal of the enzyme solution, centrifugation and re-suspension of the myocytes in Isolation Solution I was repeated. The process of shaking the tissue was repeated until the interstitial tissue was fully digested resulting in a yield of 60-90 % rod shaped ventricular cardiomyocytes.

A

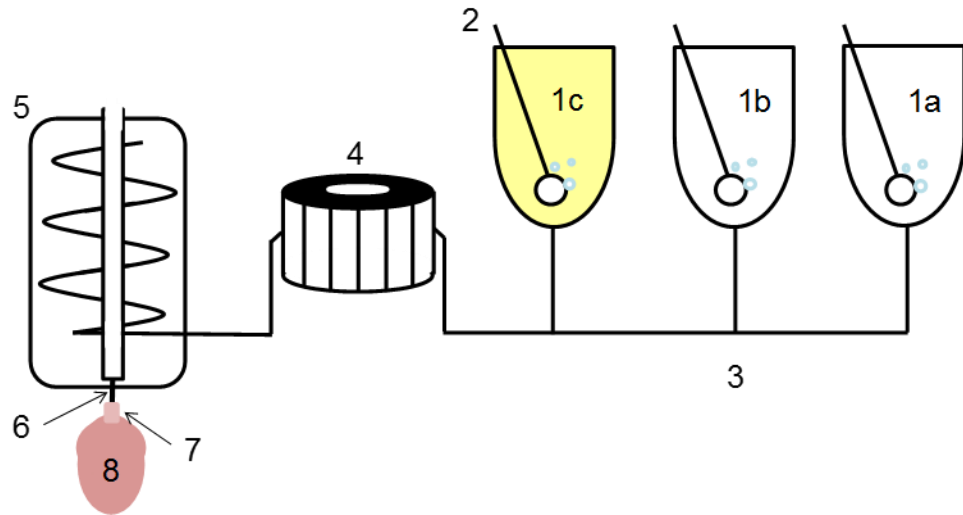


Figure 2.1: Schematic of a Langendorff Perfusion System

A) *1a)* Vessel containing Isolation Solution; *1b)* Vessel containing Zero Ca^{2+} Isolation Solution; *1c)* Vessel containing Enzyme Solution; *2)* oxygenation system; *3)* silicon tubing; *4)* peristaltic pump and; *5)* bubble trap; *6)* aortic cannula; *7)* aorta; *8)* isolated rat heart. All solutions were warmed to 37°C throughout the system with warmed water jackets surrounding the vessels and bubble trap.

Chemical	Isolation Solution I	Zero Ca ²⁺ Isolation Solution II	Enzyme Solution III	Enzyme Solution + BSA IV
NaCl	130	130	130	130
KCl	5.4	5.4	5.4	5.4
MgCl ₂	1.4	1.4	1.4	1.4
NaH ₂ PO ₄	0.4	0.4	0.4	0.4
HEPES	10	10	10	10
Glucose	10	10	10	10
Taurine	20	20	20	20
Creatine	10	10	10	10
EGTA	-	0.1	-	-
CaCl ₂	0.75	-	-	-
Collagenase	-	-	1.0 mg/ml	1.0 mg/ml
Protease	-	-	0.1 mg/ml	0.1 mg/ml
BSA	-	-	-	1.43 mg/ml
pH to 7.1 (37 °C)	NaOH	NaOH	NaOH	NaOH

Table 2.1: Composition of solutions used for myocyte isolation. All values displayed as mM except where specified. A list of full chemical names and sources can be found in Table 8.1

Chemical	Tyrode's Solution	Control Solution	Flecainide Solution
NaCl	136.9	136.9	136.9
KCl	5.4	5.4	5.4
MgCl ₂	0.5	0.5	0.5
NaH ₂ PO ₄	0.5	0.5	0.5
HEPES	1.0	1.0	1.0
Glucose	11.1	11.1	11.1
CaCl ₂	1.0	1.8	1.8
Ethanol	-	0.001%	-
Isoprenaline	-	1x10 ⁻⁴	1x10 ⁻⁴
Flecainide	-	-	0.015
pH to 7.1 (22 °C)	NaOH	NaOH	NaOH

Table 2.2: Composition of solutions used for intact cell Ca²⁺ imaging. All values displayed as mM except where specified. A list of full chemical names and sources can be found in Table 8.1.

Chemical	Permeabilisation Solution	Intracellular solution (zero waves)	Intracellular solution (low frequency waves)	Intracellular solution (high frequency waves)	Cs ⁺ replacement Solution
KCl	100	100	100	100	-
MgCl ₂	5.72	5.72	5.72	5.72	-
HEPES	25	25	25	25	25
Na ₂ ATP	5	5	5	5	5
Na ₂ CrP	10	10	10	10	10
CaCl ₂	-	0.05	0.008	0.02	0.008
EGTA	0.1	0.35	0.1	0.1	0.1
Fluo-3 free acid	-	0.015	0.010	0.010	0.010
Cs ⁺ methanesulfonate	-	-	-	-	100
Mg ²⁺ sulphate	-	-	-	-	5.72
pH to 7.0 (22 °C)	KOH	KOH	KOH	KOH	Cs ⁺ hydroxide hydrate

Table 2.3: Composition of solutions used for permeabilised cell Ca²⁺ imaging. All values displayed as mM except where specified. A list of full chemical names and sources can be found in Table 8.1

Chemical	Intracellular solution (zero waves)		Intracellular solution (low frequency waves)		Intracellular solution (high frequency waves)	
	[Total]	[Free]	[Total]	[Free]	[Total]	[Free]
Ca ²⁺	0.060	1.39 × 10 ⁻⁴	0.018	1.46 × 10 ⁻⁴	0.030	2.86 × 10 ⁻⁴
Mg ²⁺	5.72	1.00	5.72	1.00	5.72	1.00
K ⁺	100	99.9	100	99.9	100	99.9
Na ⁺	15	15	15	15	15	15
EGTA	0.340	11.2 × 10 ⁻⁶	0.098	3.18 × 10 ⁻⁶	0.098	2.71 × 10 ⁻⁶
ATP	5	0.151	5	0.150	5	0.150
CrP	10	9.82	10	9.81	10	9.81

Table 2.4: Total and free concentrations of ions and ligands in intracellular solutions which give rise to different Ca²⁺ release characteristics. All values displayed as mM except where specified. Free concentrations of ions and ligands were calculated using the REACT software assuming at 22 °C and pH 7.0 (Duncan et al., 1999). The calculation assumes a contamination level of Ca²⁺ of 10 μM (Orchard et al., 1998) and EGTA at 97% purity.

Chemical	Homogenisation buffer	Sample buffer	Tank buffer	Transfer buffer	Blocking buffer	Washing buffer	Resolving gel	Stacking gel
TRIS/HCl	62.5 mM	62.5 mM	-	-	50 mM	-	-	-
Glycerol	10% v/v	10% v/v	-	-	-	-	-	-
SDS	2% v/v	2% v/v	-	0.0375% v/v	-	-	-	-
Protease inhibitor mix	1 tablet/10 ml	1 tablet/10 ml	-	-	-	-	-	-
β-mercaptoethanol	-	5% v/v	-	-	-	-	-	-
Bromophenol blue	-	0.01% v/v	-	-	-	-	-	-
Commercial tank buffer	-	-	10% v/v	-	-	-	-	-
Glycine	-	-	-	39 mM	-	-	-	-
TRIS	-	-	-	48 mM	-	-	-	-
Methanol	-	-	-	20% v/v	-	-	-	-
NaCl	-	-	-	-	150 mM	-	-	-
TWEEN-20	-	-	-	-	0.1% v/v	0.1% v/v	-	-
Dried milk	-	-	-	-	5% w/v	-	-	-
30% acrylamide	-	-	-	-	-	-	40% v/v	13% v/v
PBS	-	-	-	-	-	1% v/v	-	-
Protogel Resolving buffer	-	-	-	-	-	-	25% v/v	-
Protogel Stacking buffer	-	-	-	-	-	-	-	25% v/v
Ammonium persulphate	-	-	-	-	-	-	2.3% v/v	5% v/v
TEMED	-	-	-	-	-	-	0.09% v/v	0.13% v/v
pH to 7.4 (22 °C)	-	-	-	-	HCl	HCl	-	-

Table 2.5: Chemical concentrations required for Western blot experiments. Quantities displayed as a concentration (mM) or a percentage (%) of the final volume (volume/volume, v/v; or weight/volume, w/v). A list of full chemical names and sources can be found in Table 8.1.

Chemical	Extracellular solution	Intracellular Solution
NaCl	140	-
CsCl	5.4	115
HEPES	5.5	10
CaCl ₂	2.5	1
MgCl ₂	0.5	-
Glucose	11	-
EGTA	-	10
Tetraethylammonium chloride	-	20
MgATP	-	5
TRIS-GTP	-	0.1
pH (22 °C)	7.4	7.05

Table 2.6: Composition of solutions used for intact cell patch clamp. All values displayed as mM except where specified. A list of full chemical names and sources can be found in Table 8.1.

2.3 Confocal microscopy imaging of live myocytes

Confocal microscopy allows the collection of high resolution, high magnification images of both live and fixed cells, stained or probed with various fluorescent dyes or antibodies (Figure 2.2 A). Confocal microscopy is dependent upon a primary beam splitter (also known as a dichroic mirror) which is capable of reflecting excitatory light and passing light emitted by the fluorescent dyes staining the cells (Callamaras and Parker, 1999). The light emitted from the focal plane of the cell passes through a pinhole and light emitted from outside the focal plane is blocked. Individual photons are detected in a vacuum by a photomultiplier tube (PMT) and are digitally converted to appear on the computer screen (Hamamatsu-Photonics, 2007). The laser light source scans the specimen in parallel lines, also known as a raster pattern. The specimen is scanned along its horizontal (X) axis as a fast line scan. A slower frame scan offsets each line scan from the top to the bottom of the specimen, forming the vertical (Y) axis. The Z axis is defined as the focal plane of the specimen (Digman et al., 2013). In this way, XY scanning forms an image with size as both dimensions. During line scanning, the Y scan axis remains unchanged, thereby creating an image whereby the X axis is size and the Y axis is time. This increases the temporal resolution and allows the visualisation of small and fast changes in intracellular Ca^{2+} , such as Ca^{2+} sparks (Cheng et al., 1996). Line scans depicting waves are rotated 90° left throughout this thesis.

The Nikon Eclipse TE2000-U confocal microscope was equipped with a 40x magnification oil immersion lens. The dye was excited with a 20 mW 488 nm diode laser, which was typically attenuated to 7%. Fluorescence was measured at 520–540 nm and was detected using a photomultiplier tube. All images were visualised using LaserSharp 2000 or ImageJ software. Confocal imaging of live cells was used to measure fast changes in intracellular Ca^{2+} in intact and permeabilised cardiomyocytes over time in line scan mode. XY mode was used to image intracellular accumulation of fluorescently labelled flecainide (flecainide-FITC).

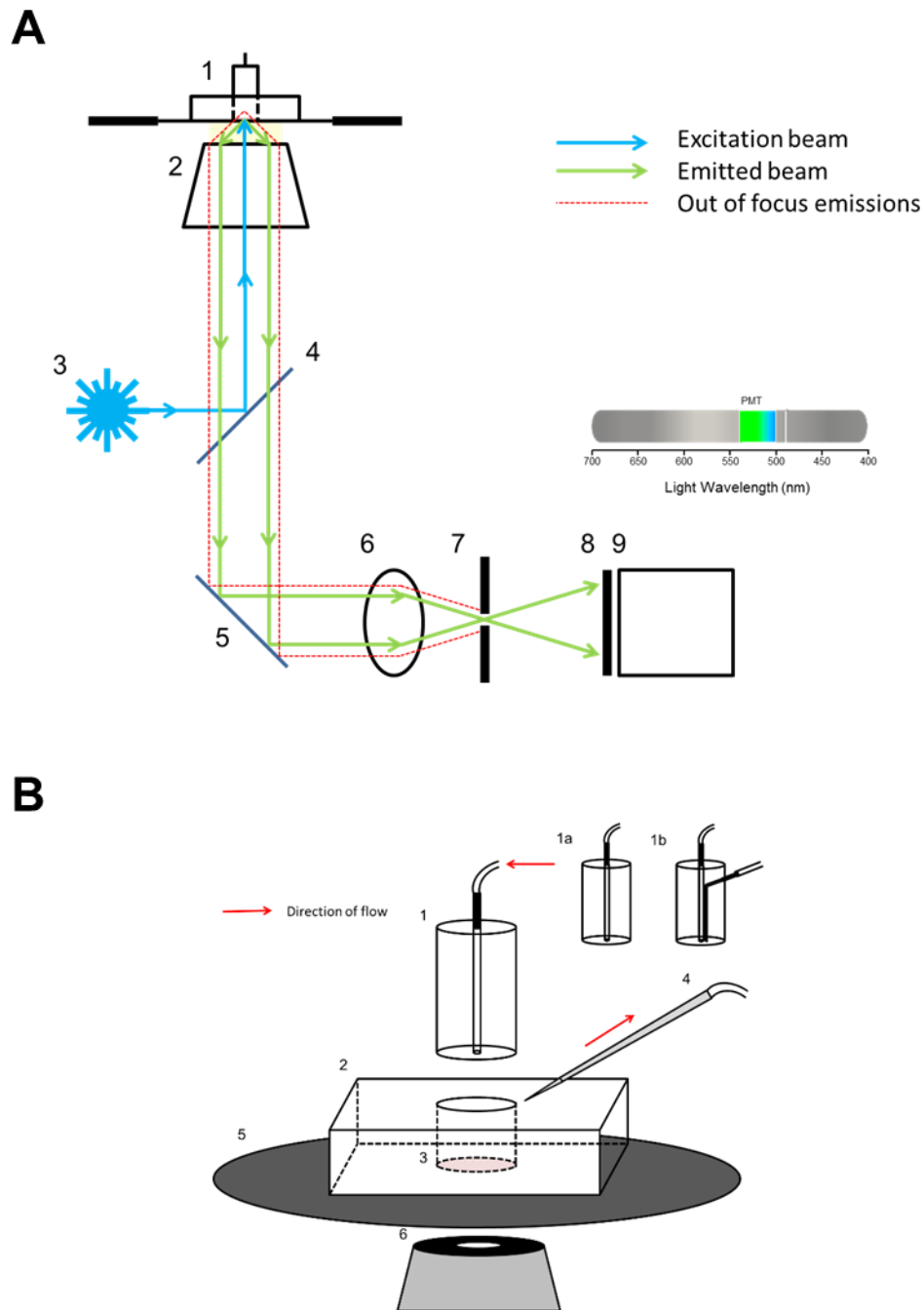


Figure 2.2: Imaging and perfusion of live cardiomyocytes

A) A schematic of the laser light pathways within a confocal microscope 1) Perfusion column and cell bath on microscope stage, connected to peristaltic pump; 2) 40x objective under oil; 3) laser light source; 4) primary dichroic mirror; 5) mirror; 6) lens; 7) pinhole; 8) emission filter 520/40 9) photomultiplier tube. Adapted from the LaserScan 2000 Software schematic. **B)** A schematic of the live cell imaging and perfusion bath set up 1) Entry of perfusion solution through the Perspex column via a peristaltic pump; 1a) standard perfusion column; 1b) column for use in caffeine puff experiments to allow dual application of solutions; 2) Perspex cell bath; 3) cells on coverslip of cell bath; 4) perfusion suction system attached to peristaltic pump; 5) microscope stage; 6) objective lens of microscope.

2.4 Confocal microscopy Ca²⁺ imaging of intact myocytes

2.4.1 Fluo-4-acetoxy methyl ester loading

In preparation for confocal microscopy Ca²⁺ imaging, intact myocytes were loaded with fluo-4-acetoxy methyl ester (fluo-4-AM). The attached AM moiety enables fluo-4 to enter the cytosolic space through the sarcolemma. Once within the cytosol, the AM moiety is cleaved by endogenous esterases in the process of de-esterification, leaving the membrane impermeant form of the dye trapped within the cell (Blatter and Wier, 1990). Fluo-4 was excited at 488 nm and when bound to cytosolic Ca²⁺, emitted fluorescence which was collected at 520 - 540 nm (Gee et al., 2000).

During the loading procedure, myocytes suspended in isolation solution 1 (Table 2.1) were centrifuged at 53 G for 40 sec and the supernatant removed. Myocytes were re-suspended in 2 ml of 1 mM Ca²⁺ Tyrode's solution (Table 2.2). Fluo-4-AM solubilised in DMSO was added to the myocyte suspension to give a final concentration of 6 µM. Myocytes were rocked for 20 min at 10 rpm to allow fluo-4-AM to pass through the myocyte membrane. Thereafter, myocytes were centrifuged at 53 G for 40 sec and supernatant removed. Myocytes were re-suspended in 2 ml of 1 mM Ca²⁺ Tyrode's solution (Table 2.2). Washing of the myocytes was repeated. Myocytes were left at 4 °C for a minimum of 45 min to allow de-esterification of intracellular fluo-4-AM into fluo-4 by endogenous esterases. All experiments using fluo-4 loaded myocytes were undertaken within 3 hours of dye loading.

2.4.2 Intact myocyte selection

Myocytes were placed in the cell bath on the microscope stage (Figure 2.2 B) and allowed to settle onto the cover slip for 2 min. The Perspex column (7 mm diameter) was lowered close to the surface of the cells and perfusion with control solution (Table 2.2) initiated. During this time, intact myocytes were selected if quiescent; displayed clear striations; and elicited a strong contractile response to electrical field-stimulation. Myocytes with obvious cytoplasmic vesicles, rounded edges or major structural defects, including disrupted extracellular membranes were excluded. Platinum electrodes embedded between the cover slip bottom and Perspex wall of the cell bath were used to field-stimulate the cells. A 10 ms square wave pulse at 30 V (~20 % above average threshold for response) was emitted to test field-stimulation response.

2.4.3 XY imaging of intact myocytes

In preparation for line scan imaging, selected myocytes were initially scanned in XY mode at 750 lines/second (lps). Laser intensity was kept between 0.5-2% of the total intensity and laser exposure time was limited to <10 sec. Within this time, the image of the myocyte was rotated using the scan-rotate feature within the LaserScan 2000 software and the scan line was positioned longitudinally across the cell. The position of the scan line was adjusted to avoid the nuclei and outer edges of the myocyte. XY images were collected at 512 X 512 pixels. All experiments were carried out at 22 ± 2 °C. Experiments performed at 37 °C may more appropriately model physiological WT cell function as protein and channel activity can be temperature dependent. In the rat cardiomyocyte, SERCA activity in isolated SR vesicles was slowed by ~50% when temperature was decreased from 37 °C to 25 °C (Liu et al. 1997). However, the proportion of SERCA activity contributing to Ca^{2+} extrusion from the cytosol remained unchanged at 24 °C compared with 37 °C (Mackiewicz and Lewartowski, 2006). In single channel lipid bilayer studies, RyR2 conductance was decreased alongside an increase in channel P_o at cooler temperatures, giving rise to a net increase in current flow (Sitsapesan et al., 1991). This was supported by experiments performed in isolated cardiomyocytes, when RyR2 is *in situ*, in which rapid cooling of the cells induced opening of RyR2 (McCall et al., 1996).

2.4.4 Line scan imaging of intact myocytes

After XY scanning, line scan images were obtained at 188 lps with a time interval of 5.3 ms. Laser intensity was 7% of the total laser intensity. Scanning protocols, including line scan duration are documented in detail within each relevant results chapter. Between experiments, the tubing and cell bath were washed with 30 ml ultra-pure water to prevent contamination. Experiments which used carbonyl cyanide-4-(trifluoromethoxy) phenylhydrazone (FCCP) or valinomycin, were additionally washed out with 30 ml 100 % ethanol and 30 ml 70 % ethanol. All experiments were carried out at 22 ± 2 °C.

2.5 Confocal microscopy of permeabilised myocytes

2.5.1 Saponin permeabilisation

Treatment of cardiomyocytes with saponin causes the perforation of cholesterol-rich regions of cellular membranes (Shany et al., 1974, Goldenthal et al., 1985, Saka et al., 2014). Mitochondrial and SR membranes contain less cholesterol than in the sarcolemma, therefore saponin relatively selectively permeabilised the sarcolemma (Severs, 1982). The free movement of large cytosolic proteins (800 kDa) through the permeabilised sarcolemma has been reported (Hudder et al., 2003). An equilibrium is formed between the cytosol and the surrounding solution; therefore, experimental solutions were designed to mimic the ionic composition of the ventricular myocyte cytosol. Solutions contained a high concentration of K^+ (100 mM) and a relatively low concentration of Na^+ (15 mM) (Table 2.3) (Opie, 2004). The free concentration of Mg^{2+} was maintained at 1 mM. This was important in the current study as Mg^{2+} influences RyR2 gating (Gusev and Niggli, 2008). Adenosine triphosphate (ATP) and creatine phosphate (CrP) were present to support the metabolic requirements of the cell (Yang and Steele, 2002). pH was set at physiological pH 7.0 by addition of KOH and was strongly buffered by HEPES. The physiological concentration of free Ca^{2+} during cell diastole has been measured to be ~ 100 nM with high Ca^{2+} buffering by proteins such as troponin C and calmodulin (Bers, 2000). Whilst troponin C is present in permeabilised myocytes, free cytosolic proteins such as calmodulin were likely lost during the permeabilisation process. Within the intracellular solution, Ca^{2+} buffering was provided by ethylene glycol-bis (β -aminoethyl ether-N,N,N',N'-tetraacetic acid (EGTA) and to a lesser extent ATP and CrP (Bers, 2000). ATP also strongly buffers Mg^{2+} (Fabiato and Fabiato, 1975). Given the complexity of the solutions, the binding of Ca^{2+} , Mg^{2+} , K^+ and Na^+ ions with EGTA, ATP and CrP was calculated using REACT software (Duncan et al., 1999). The output provided the free and complexed concentrations of all ions and ligands (Table 2.4).

For permeabilisation, myocytes suspended in isolation solution I (Table 2.1) were centrifuged at 53 G for 40 sec and the supernatant was removed. Myocytes were then re-suspended in 1 ml of permeabilisation solution (Table 2.3) and the cell wash was repeated. Saponin (0.01%) was added to the cell suspension and this was rocked at 10 rpm for 15 min. Myocytes were pelleted down in the centrifuge at 53 G for 40 sec and re-suspended in permeabilisation solution. The cell wash was repeated. All experiments using saponin permeabilised myocytes were undertaken within one hour of permeabilisation.

2.5.2 Triton X-100 permeabilisation

Myocytes were treated with the non-ionic detergent Triton X-100 to permeabilise the sarcolemmal, mitochondrial and SR membranes of cardiomyocytes (Solaro et al., 1971). An equilibrium is formed between the intracellular space and the surrounding solution; therefore, permeabilisation and intracellular solutions were utilised to mimic the ionic composition of the ventricular myocyte cytosol (Table 2.3). Myocytes suspended in isolation solution were centrifuged at 53 G for 40 sec and the supernatant removed. Myocytes were re-suspended in 1 ml of permeabilisation solution (Table 2.3). Centrifugation and re-suspension was repeated. Triton X-100 was added to the cell suspension to ensure a working solution of 1% and cells were rocked at 10 rpm for 30 min. The cells were pelleted down in the centrifuge at 53 G for 40 sec and re-suspended in intracellular solution. The cell wash was repeated to remove all Triton X-100. All experiments using Triton X-100 permeabilised myocytes were undertaken within 30 min of permeabilisation.

2.5.3 Intracellular perfusion and Ca²⁺ imaging in saponin permeabilised cells

Saponin permeabilised myocytes were placed in the cell bath on the microscope stage and allowed to settle onto the cover slip for 2 min. The Perspex column was lowered and the cells perfused with intracellular solution (Table 2.3). When visualising spontaneous Ca²⁺ waves, the solution contained 10 µM fluo-3 in its free acid form. This was increased to 15 µM in experiments visualising only sparks. Fluo-3 was excited at 488 nm and emitted fluorescence was collected at 520-540 nm when bound to cytosolic Ca²⁺ (Gee et al., 2000)

Free Ca²⁺ concentration was maintained at 146 nM to induce low frequency Ca²⁺ waves, or 286 nM to induce high frequency Ca²⁺ waves to investigate if the effect of flecainide was dependent upon these Ca²⁺ concentrations. (Table 2.4). In experiments investigating only Ca²⁺ sparks, the concentration of the Ca²⁺ buffer EGTA was increased from 0.1 to 0.35 mM to prevent the spatiotemporal summation of sparks into waves. Free Ca²⁺ concentration was maintained at 139 nM (Table 2.4). It must be noted that all documented free Ca²⁺ concentrations included unavoidable Ca²⁺ contamination which was previously estimated at 20 µM (Orchard et al., 1998). In the current experiments, disposable plastic equipment was used instead of glassware, thereby minimising this problem and limiting inconsistencies between experiments. Thus, Ca²⁺ contamination was assumed at 10 µM in all intracellular solutions (Table 2.4).

2.5.4 Saponin permeabilised myocyte selection and confocal imaging

Using the microscope's bright-field mode, saponin permeabilised myocytes were selected if their rod-like shape was maintained and blebbing at the cell membrane was apparent, indicating permeabilisation. Myocytes were confirmed to be permeabilised if there was no response to electrical field stimulation (10 ms square wave pulse, 30 V), due to the abolition of a membrane potential difference across the plasma membrane. Additionally, appropriately permeabilised cells exhibited a background fluorescence that was greater than the bath fluorescence in the presence of fluo-3 free acid. Permeabilised myocytes were XY and line scan imaged as described for intact myocytes (Section 2.4.3 and 2.4.4). All experiments were carried out at 22 ± 2 °C. Similarly to intact cells, experiments performed at 37 °C may more appropriately model physiological WT cell function and performing these experiments at a lower temperature may increase RyR2 P_o (Sitsapesan et al., 1991, McCall et al., 1996). Specific scanning protocols are documented in detail within each relevant chapter.

2.6 Confocal microscopy analysis

2.6.1 Analysis of intracellular Ca²⁺ wave frequency in intact and saponin permeabilised myocytes

Analysis of wave frequency was measured using the open source software ImageJ (Schneider et al., 2012) and the frequency was calculated as waves/min. In saponin permeabilised cells, line scans were viewed in ImageJ and the time between each wave was measured using the Line Tool. The number of waves were then presented as a frequency (waves/min).

2.6.2 Semi-automated Ca²⁺ wave dimension analysis in saponin permeabilised myocytes

Analysis of wave peak amplitude, mean upstroke rate, total duration from the wave peak to 90% of the Ca²⁺ decline and Ca²⁺ decline time constant was semi-automated using ImageJ and a C script written by Dr A Benson (Benson, 2016). Waves were cropped from the original line scan, ensuring a minimum 1 sec of quiescent cell background either side of the wave and the removal of non-cell background. Cropped waves were saved as both .tif and .txt files, and the .txt file was used as the input for the C script. For each pixel in the line scan, the fluorescence value (F) was described in the .txt file and then calculated as a $\Delta F/F_0$ value. F_0 was determined to be the mean fluorescence of the initial 100 ms of the scan, which corresponded to the cell background fluorescence during cell quiescence. Wave characteristics were calculated for each spatial location in the line scan as follows: a five-point moving average filter was first applied to the $\Delta F/F_0$ data. Mean and standard deviation $\Delta F/F_0$ values were then calculated for the first and last 100 ms of the cropped image; these corresponded to the resting values prior to and after a wave respectively. T_2 was the time at which the peak amplitude $\Delta F/F_0$ occurred. Working backwards from T_2 , the start time of the wave (T_1) was taken as the point when $\Delta F/F_0$ crossed below the mean + 2SD pre-wave resting value. To determine wave end time (T_3), all data from T_2 onwards were fit with an exponential equation of the form

$$y = y_0 - \Delta y(1.0 - e^{-x/\tau})$$

whereby y_0 is the starting value of the exponential, Δy is the difference between the starting value and the exponential asymptote, and τ is a time constant. The wave duration from the wave peak to 63% (relaxation time constant) and 90% of the exponential curve was recorded (Figure 2.3).

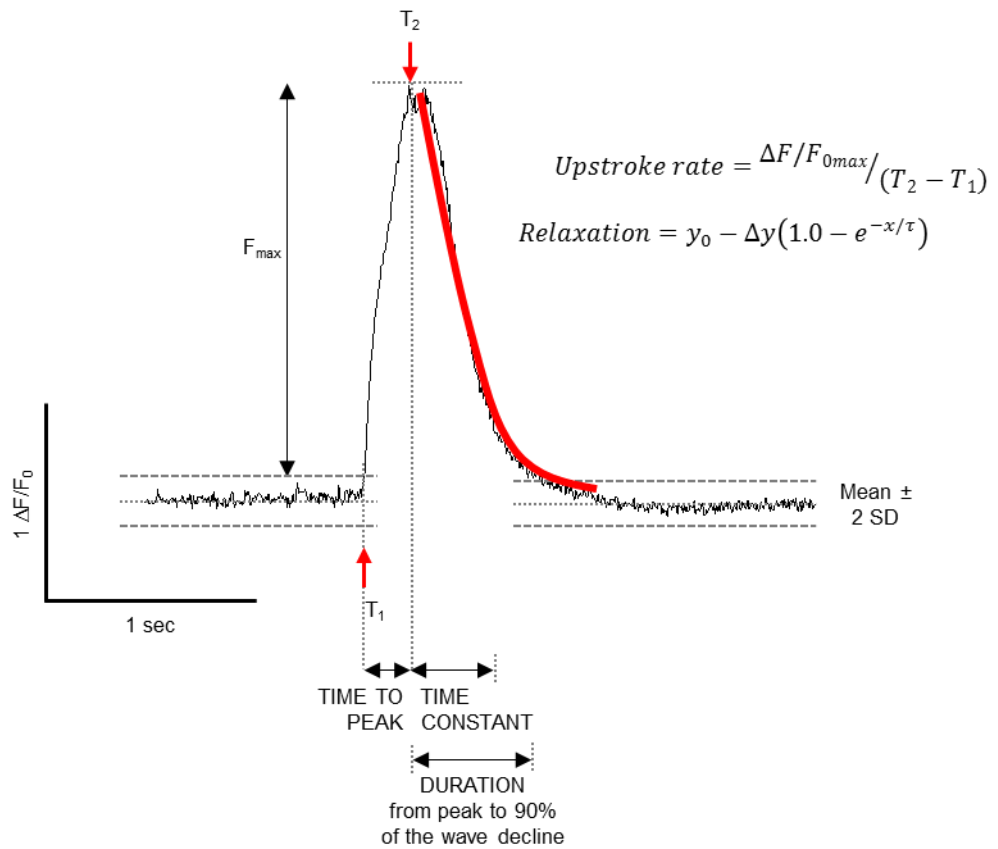
A

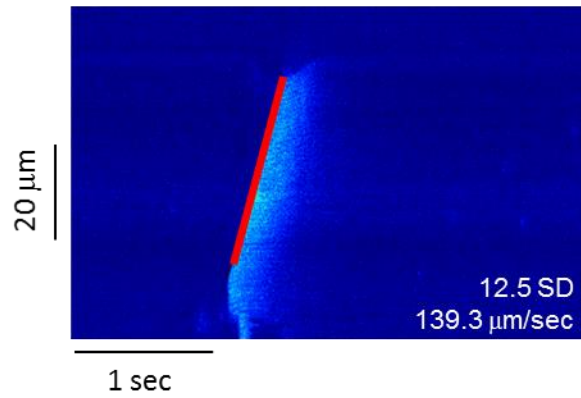
Figure 2.3: A pictorial representation of the semi-automated Ca^{2+} wave analysis

A) T_1 = time at wave start; T_2 = time at wave peak amplitude. Red curve indicates exponential fit of Ca^{2+} wave decline. The semi-automated analysis was performed at each row of pixels along the line scan and averaged. Analysis script written by Dr A Benson (Benson, 2016).

2.6.3 Semi-automated Ca²⁺ wave propagation velocity analysis in saponin permeabilised myocytes

The velocity of the wave front was analysed using a semi-automated, Python encoded image analysis tool written by Dr S Sikora (Sikora, 2016). Individual waves were manually cropped from the original line scan using ImageJ. It was ensured that a minimum of 1 sec of cell 'diastole' was included immediately before and after a wave. All waves were saved as .tif files and input into the analysis tool. A Gaussian smoothing filter was applied to each image to minimise noise and avoid the erroneous identification of sparks preceding a wave front. The mean fluorescence of the first 100 ms was averaged over all rows and columns to give the mean fluorescence of the quiescent cell background. The wave front within each row of pixels was identified as the first pixel with a fluorescence value greater than 10, 12.5, 15, 17.5 or 20 SD above the quiescent background mean. These threshold parameters were included to ensure that the sensitivity of the tool to detect a wave front was appropriate across a range of wave amplitudes (Figure 2.4). Next, a linear function was fitted to the pixels identified as the wave front in the upper and lower halves of the image and the gradient for each was measured. Each gradient was calculated as a velocity by multiplying by 37.6 which corresponded to the scaled pixel dimensions. Each wave was output as five images, each relating to the five different threshold parameters. Within each image, the identified wave front, linear fit, gradient value, calculated velocity and r^2 values were hard coded into the image. Additionally, an Excel spreadsheet was produced, which contained the wave front gradient, calculated velocity and r^2 value at each threshold parameter. All output images with an r^2 value of less than 0.9 or a propagation velocity of less than 90 $\mu\text{m}/\text{sec}$ were highlighted as potentially problematic but were not omitted from the dataset until they had been manually viewed. Unsuccessful analyses were omitted from the dataset if large sparks were inappropriately detected as the wave front at low threshold parameters (Figure 2.5). 2.1% of waves were unsuccessfully analysed at all threshold parameters.

A



B

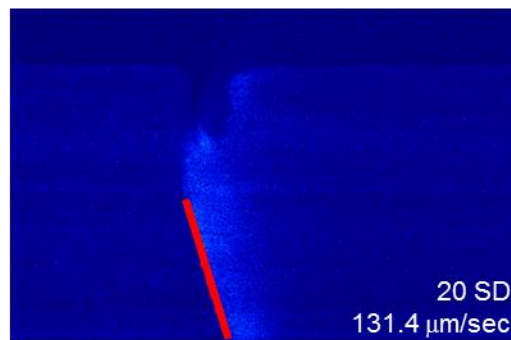


Figure 2.4: Detection of a wave front at different wave fluorescent amplitudes using the semi-automated Ca^{2+} wave analysis

A) Representative output images showing a wave with an amplitude of $2.7 \Delta F/F_0$ detected at 12.5 SD above the diastolic fluorescent mean and **B)** a wave with an amplitude of $1.7 \Delta F/F_0$ detected at 20 SD above the diastolic fluorescent mean. The detected wave front was shown in red. Analysis script written by Dr S Sikora (Sikora, 2016).

A

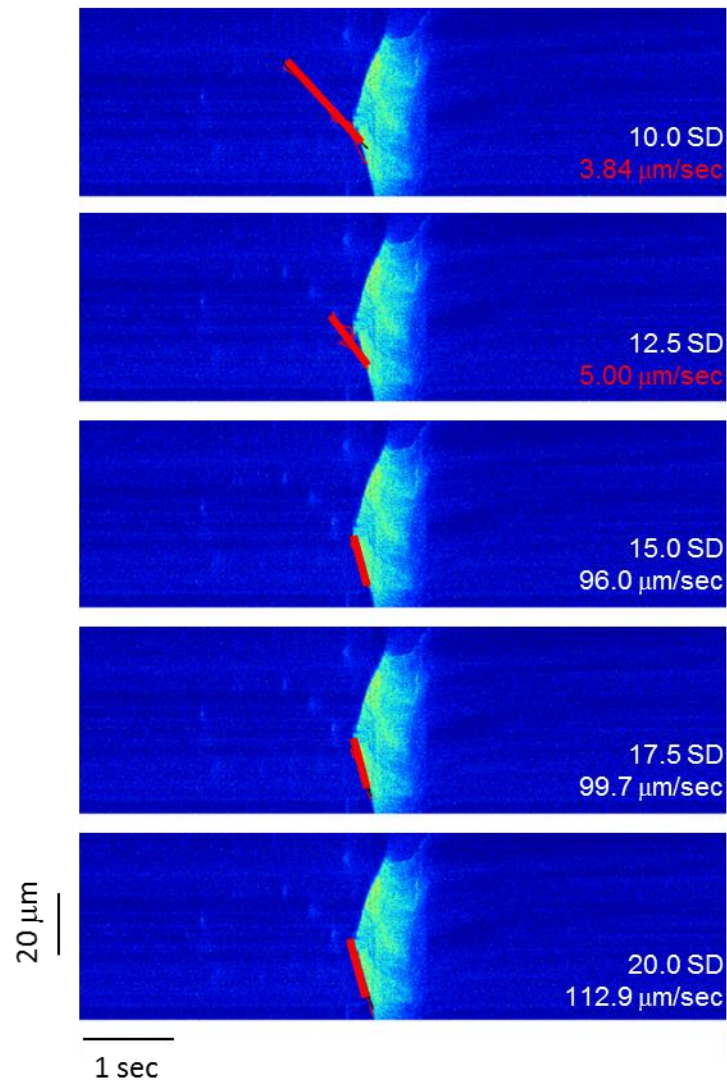


Figure 2.5: Detection of the wave front at five threshold parameters using the semi-automated Ca^{2+} wave analysis

A) Output images of a wave front detected at 10, 12.5, 15, 17.5 and 20 SD above the calculated background value during cell diastole (diastolic mean). The detected wave front was shown in red. At the two lowest threshold parameters (10 and 12.5 SD + diastolic mean) sparks were erroneously detected as the wave front and wave velocity was skewed. An average velocity of the three subsequent threshold parameters was included within the dataset. Analysis script written by Dr S Sikora (Sikora, 2016).

2.6.4 Ca²⁺ spark analysis

Ca²⁺ sparks were analysed using the open source software ImageJ and the plugin Sparkmaster (Picht et al., 2007). Line scans were cropped according to individual protocols, detailed within each relevant chapter. All cropped scans excluded spontaneous waves and Ca²⁺ transients.

The scanning speed (188 lps) and pixel size (0.2 μm) were constant throughout. The criteria value (3.8) and number of intervals (5) also remained constant at the recommended values (Picht et al., 2007). The criteria value (3.8) determined the fluorescence value above which a pixel was considered part of a spark. The standard deviation of the background noise was multiplied by this value and divided by the mean value of the background. In experiments by Picht et al. (2007) which aimed to validate SparkMaster, the criteria value of 3.8 was shown to minimise the occurrence of false positives whilst still allowing sensitivity in detecting small or low amplitude sparks (Picht et al. 2007). To remove the non-cell background from the image analysis, a threshold fluorescence value was set between the lowest fluorescence value of the cell and the highest fluorescence value of the non-cell background. A smoothing filter was applied to the remaining image to remove excess background noise. Image regions where the fluorescence values exceeded the mean + 2 SD were identified as potential sparks and initially removed from the analysis. A second mean and SD were calculated on the remaining pixels as this calculation more appropriately represented the diastolic cell background fluorescence. Sparks were then confirmed if regions of potential sparks had a fluorescence greater than the second calculated SD, multiplied by the threshold criteria (3.8) plus the cell background mean (Picht et al., 2007).

Spark amplitude ($\Delta F/F_0$), full width at half maximal amplitude (FWHM; μm) and full duration at half maximal amplitude (FDHM; ms) were calculated for each spark and averaged for each cell (Figure 2.6). Spark frequency is provided as the number of sparks that occurred per 100 μm per second. Each Sparkmaster output was manually checked to identify obvious errors. Sparks were removed from the analysis output if Sparkmaster detected one spark as two or more sparks (Figure 2.7 A); two sparks were detected as one spark (Figure 2.7 B); or sparks were immediately adjacent to the cell border (Figure 2.7 C). An example of correctly identified sparks is shown in Figure 2.7 D.

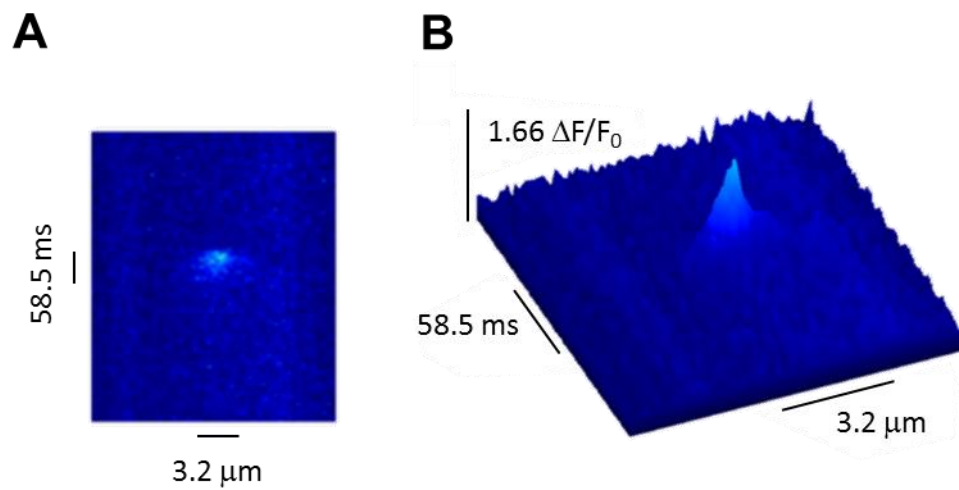


Figure 2.6: Example of a Ca^{2+} spark and relevant dimensions analysed by Sparkmaster
A) Line scan image crop of a Ca^{2+} spark with distance on the X axis and time on the Y axis. **B)** Surface profile plot of the same spark including amplitude on the Z axis.

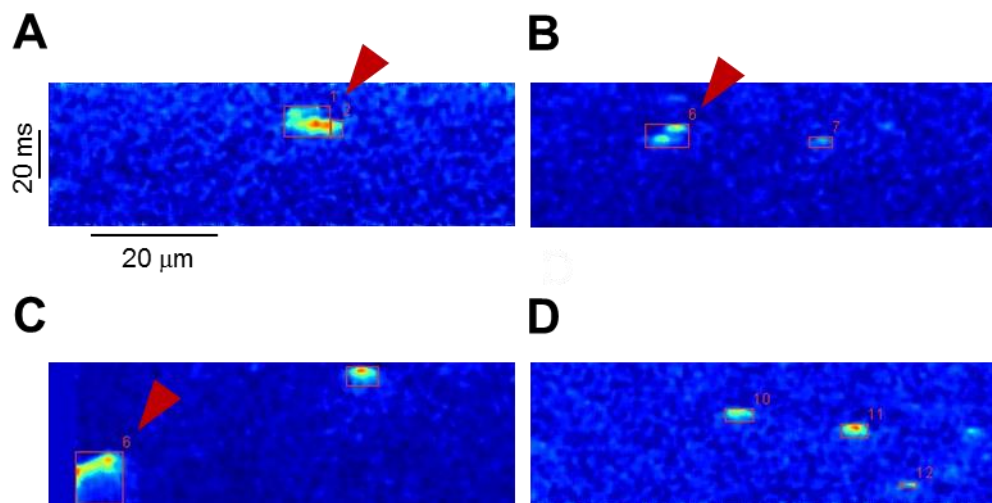


Figure 2.7: Examples of sparks identified by Sparkmaster including erroneously identified sparks
A) One spark was detected as two sparks; **B)** Two sparks were identified as one spark; **C)** spark directly adjacent to the cell border; **D)** well identified sparks (Picht et al., 2007).

2.6.5 Analysis of flecainide-FITC in intact and permeabilised cells

Flecainide-FITC fluorescence was analysed using the open source software ImageJ. The edge of the cell was identified and manually marked using the Polygon Sections tool and the mean cell fluorescence recorded ($F_{(c)}$; Figure 2.8). The selected area was inverted to give the non-cell background fluorescence (F_0) (Figure 2.8 B). If artefacts were present in the XY scan then the polygon tool was used to draw around the clear background area. Nuclei edges were identified and manually marked. The mean fluorescence was recorded if bright, block-like staining was not apparent within this region ($F_{(nuc)}$; Figure 2.8 C). This methodology was used for both intact and permeabilised myocytes.

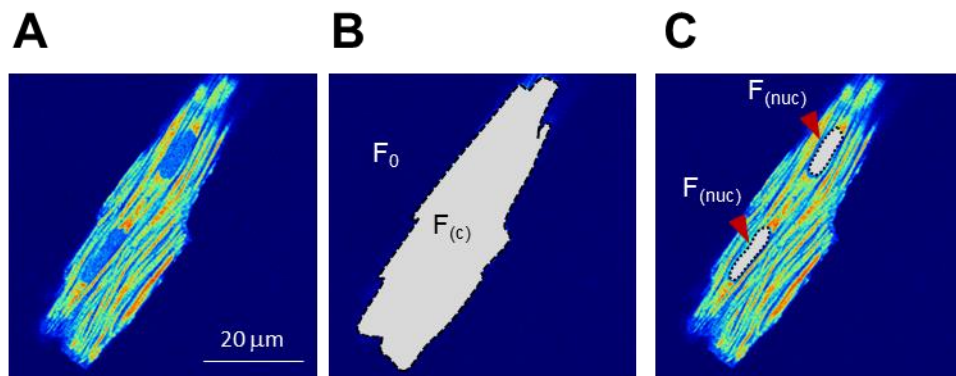


Figure 2.8: XY scans of a flecainide-FITC loaded cell and analysed areas

A) Unanalysed flecainide-FITC loaded cell. **B)** Whole cell identified and fluorescence determined ($F_{(c)}$) by subtracting non-cell background fluorescence (F_0). **C)** Nuclei identified and fluorescence determined ($F_{(nuc)}$). F_0 remained the same.

2.7 Western blotting

2.7.1 Sample preparation

All Western blotting was performed by Hannah M. Kirton. Rat ventricular myocytes were isolated as described in Section 2.2. The myocyte yields were combined and then washed and re-suspended in isolation solution (Table 2.1). Prior to homogenisation, the myocytes were divided into three experimental groups. Group 1 were kept at 4 °C and remained intact; Group 2 were permeabilised in 0.01% saponin for 15 min at room temperature with gentle rotation; and Group 3 were permeabilised in 0.01% saponin for 15 min at room temperature and were retained in intracellular solution for a further 15 min thereafter. After treatment, cells were centrifuged (53 G for 40 sec) with intracellular solution and the supernatant was discarded. This wash was repeated. Homogenisation buffer (2 ml) (Table 2.5) was applied to each sample and the cells were re-suspended and gently triturated. Cells remained on ice (4 °C) for 30 min. The lysed cells were then centrifuged at 10 °C for 15 min at 16,000 G. The supernatant was collected and the pellet was discarded.

Homogenisation buffer containing tris(hydroxymethyl)aminomethane-hydrochloric acid (TRIS-HCl) (Table 2.5) facilitated the extraction of cytosolic and membrane proteins and allowed their semi-quantification during Western blot. Sodium dodecyl sulphate (SDS) was present as an anionic detergent that coats proteins with a negative charge that is proportional to their length. Glycerol acted to increase the density of the protein solution to facilitate gel well loading. Protease and phosphatase inhibitors (G Bioscience) were included to prevent endogenous proteases and phosphatases from degrading proteins during the cell lysis process. Lysates were then assessed for their protein concentration via bicinchoninic acid assay technique.

2.7.2 Bicinchoninic acid assay

The bicinchoninic acid (BCA) assay relies on two chemical reactions that enable the protein concentration of each sample to be determined. Peptide bonds within the protein sample reduce copper (II) sulphate to Cu^+ which then reacts with two molecules of bicinchoninic acid to form $\text{BCA-Cu}^{1+}\text{-BCA}$, a chromogenic purple complex (Huang et al., 2010). This complex absorbs light at a wavelength of 562 nm. The colour intensity of the reaction product is correlated with protein quantity (Olson and Markwell, 2007). Therefore, the amount of protein

in each sample could be spectrophotometrically quantified and compared relative to the standard calibration curve.

In a 96 well plate, the calibration standards contained known concentrations of bovine serum albumin (BSA) at 0, 200, 400, 600, 800 and 1000 µg/ml. Protein samples were loaded onto the plate at their original concentrations and at a 50% dilution with water. Standards were loaded in duplicate while the protein samples were loaded in triplicate. Copper (II) sulphate and bicinchoninic acid were mixed at a ratio of 1:50 as a working reagent (Micro BCA Protein Assay Kit, Thermo Scientific, UK). The plate was incubated at 37 °C for 30 min. Each well was read using a 570 nm wavelength emitted light (Varioskan, SkanIT, Thermo Fisher, UK). The light absorbed by each sample was quantified using the Beer-Lambert law:

$$A = \epsilon bC$$

where A is the absorbance of the emitted light, ϵ is the molar absorptivity of the dye (L/mol cm), b is the distance of the light path (cm) and C is the concentration of the dye in solution (M). All absorbance readings were compared against the calibration standard. All calibration standards produced a linear best fit with an r^2 value >0.95.

2.7.3 Gel electrophoresis

During gel electrophoresis, negatively charged proteins are pulled towards the positive cathode within the polymerised acrylamide gel mesh. Larger proteins move through the gel slower than smaller proteins. In this way, proteins are separated according to their size and the relative amount of protein can be quantified. The density of the resolving gel was prepared according to the molecular weight of the protein of interest. A 12% resolving gel was made to separate proteins with a low molecular weight (e.g. CaM; 16.7 kDa) (Mini-PROTEAN gel cast, Bio-Rad, UK) (Table 2.5). The stacking gel (Table 2.5) was prepared and the 12 well comb was placed into the top of the gel. Protein samples (25 µg) were mixed with sample buffer containing β-mercaptoethanol and bromophenol blue. β-mercaptoethanol is a reducing agent that cleaves disulphide bonds, disrupting the quaternary and tertiary protein structure. Bromophenol blue allows the samples to be visualised as they migrate through the gel. Samples were boiled at 95 °C for 5 min, vortexed and allowed to cool on ice. Thereafter, samples were stored at -20 °C or mixed and pipetted into the gel wells (25 µg protein per well). A protein ladder of known molecular weight (Precision Plus Protein, Bio-Rad, UK) was present in all gels. The proteins were run on the gel at a constant voltage of 50 V for ~30 min. This

encouraged the proteins to migrate through the stacking gel at an even rate. Once the protein samples had reached the resolving gel, a constant voltage of 120 V was applied. The electrophoresis was terminated after the 10 kDa MW ladder marker had run off the gel to establish sufficient resolution of the protein bands.

2.7.4 Protein transfer

The resolved protein gel was transferred to a polyvinylidene difluoride (PVDF) membrane (FluoroTrans, PALL, UK; 0.2 μm pore size) using the semi-dry blotting method (BioRad). The resolving gel was removed from the gel cast and the stacking gel discarded. A transfer stack was created between the positive anode and negative cathode plates of the semi-dry transfer machine (Figure 2.9). All layers within the transfer stack were pre-soaked in transfer buffer (Table 2.5) and the PVDF membrane was activated with methanol. Proteins were transferred onto the PVDF membrane at a constant 60 mA (60mA per 6 x 5 cm PVDF membrane) for 90 min in a semi-dry transfer machine (Trans-blot SD, Bio-Rad, UK).

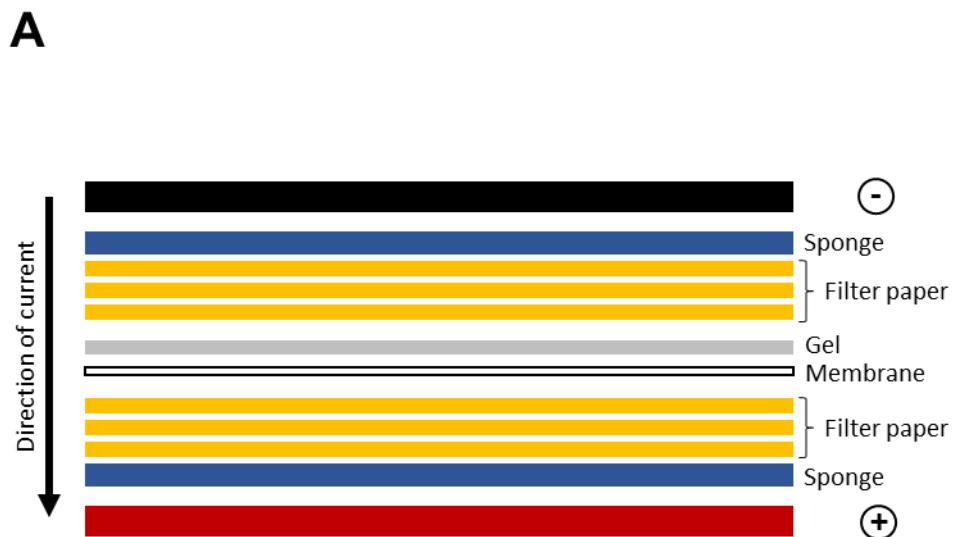


Figure 2.9: Schematic of the transfer stack in which protein was transferred from the gel onto the PVDF membrane

A) The transfer stack was layered onto an anode (+) plate and comprised of (from bottom to top) a layer of sponge, three sheets of filter paper, an activated PVDF membrane, the gel, three sheets of filter paper and a layer of sponge. The cathode (-) plate was placed over the sandwich and current (60 mA per 6 x 5 cm PVDF membrane) moved from the cathode through the stack to the anode, thereby facilitating protein transfer from the gel to the membrane.

2.7.5 Membrane blocking and protein probing

Once the proteins were transferred to the membrane, the membrane was blocked in blocking buffer (Table 2.5) for 90 min at room temperature. This blocking procedure prevents non-specific antibody binding. After blocking, the membrane was cut in two to detect for the presence and relative quantities of the protein of interest (CaM) and the house keeping protein (β -actin). Rabbit monodonal anti-CaM primary antibody (AbCaM [EP799Y], ab45689) was used to probe for CaM (16.7 kDa), or mouse monoclonal anti- β -actin primary antibody (Sigma, A5441) was used to probe for β -actin (42 kDa). Each primary antibody was diluted to 1:1000 in blocking buffer and membranes were incubated in their respective primary antibodies overnight at 4 °C. Thereafter, the membranes were washed in washing buffer (Table 2.5) for 2 x 15 min and 4 x 5 min at room temperature to remove excess primary antibody. Membranes were then incubated for 90 min at room temperature in secondary antibody conjugated to horseradish peroxidase (HRP). Anti-rabbit HRP (Jackson Lab, UK) or anti-mouse HRP (Jackson Lab, UK) secondary antibodies were used to amplify the signal of the primary antibodies probing for CaM or β -actin respectively. Secondary antibodies were diluted to 1:2500 in blocking buffer. Thereafter, the membranes were washed in washing buffer (Table 2.5) for 2 x 15 min and 4 x 5 min at room temperature to remove excess secondary antibody.

Protein bands were detected via an enhanced chemiluminescence (ECL) commercial kit (GE Healthcare Life Sciences, Amersham, UK) using reagents A and B at a ratio of 1:1. The ECL reagent mix was pipetted onto the membrane and left for ~5 min. The membrane was imaged using the G:BOX Genesys, Syngene, UK. Membranes were exposed for 5–60 sec. The image immediately prior to saturation of the digital signal was used for analysis.

2.7.6 Western blot analysis

Imaged membranes were opened in ImageJ. Bands representing the protein of interest were identified by comparing the location of the bands with the protein ladder marker. Images were converted to 8-bit grayscale. Using the Line Profile tool in ImageJ, a line profile was positioned across each band and the mean grey value described the relative protein content. The line profile was then positioned away from the bands and the mean grey value described the background intensity. The background intensity was subsequently subtracted from the protein band intensity. This method for analysing protein bands was repeated for β -actin, and all corresponding protein samples were normalised to β -actin.

2.8 Voltage clamp of cardiomyocytes

All electrophysiological experiments were performed by Moza Al-Owais. Myocytes were patch clamped using whole cell configuration of the patch-clamp technique in the voltage-clamp mode. Isolated, intact ventricular rat myocytes were transferred to the bath recording chamber mounted on the stage of an Olympus CK40 inverted microscope and allowed to settle for 10min. Following that, cells were continually perfused (3-5 ml/min) with extracellular electrophysiological solution (Table 2.6). Patch pipettes had resistances of 3-6 M Ω and filled with intracellular electrophysiological solution (Table 2.6). Na⁺ currents were evoked by a 200 ms step from -80 mV to -30 mV every 10 sec (Figure 2.10), and measured for their peak amplitude under control conditions and then in the presence of 10, 30 and 100 μ M flecainide or flecainide-FITC. All experiments were carried out at 22 ± 1 °C. Series resistance was compensated by 60-70% and monitored after breaking into the whole cell configuration throughout the duration of experiments. If a significant increase in series resistance occurred (> 20%), the experiment was terminated. Electrical signals were measured with an axopatch 200 patch-clamp amplifier, controlled by a personal computer using a Digidata 1322A interface and driven by pCLAMP 10 software (Molecular Devices, Foster City, CA). Voltage clamp signals were sampled at 50 kHz and low pass filtered at 20 kHz.



Figure 2.10: Schematic of the square wave pulse used in patch clamp experiments

A) Na⁺ currents were evoked during a 200 ms pulse from -80 mV to -30 mV which was triggered every 10sec.

2.9 Monocrotaline model of right sided heart failure

Monocrotaline (MCT) rats were induced and maintained by Ewan Fowler and Ruth Norman. MCT right ventricular myocytes were isolated by Ewan Fowler. Right sided heart failure developed 3-4 weeks after intraperitoneal injection of monocrotaline (MCT). MCT is oxidised by the liver to produce the reactive MCT pyrrole compound. During the first pass of active MCT pyrrole through the pulmonary vascular bed, apoptosis of pulmonary arteriole endothelial cells occurs. This induces lung fibrosis, which ultimately causes development of pulmonary hypertension and right sided heart failure (Sahara et al., 2007, Benoist et al., 2012). MCT rats were culled and cardiomyocytes isolated upon the development of heart failure symptoms, which included rapid weight loss, lethargy, dyspnoea, cold extremities or piloerection. For an extensive report on the characterisation of MCT model, please see Fowler 2015 and Benoist 2012.

2.10 Statistical analysis

Microsoft Excel (Microsoft Excel, Redmond, WA, USA) was used to tabulate numerical outputs from all software analysis tools. SPSS (SPSS, Inc., Chicago, IL, USA) was used to test for normality using the Shapiro-Wilk test. Non-normal data were Log transformed and normality was re-tested. Parametric and non-parametric analyses were applied where appropriate. GraphPad (La Jolla, CA, USA) was used to plot histograms and curve fit the data. Sigma Stat 3.5 (Systat software, San Jose, CA, USA) was used to perform all other statistical analyses and Origin (OriginLab, Northampton, MA, USA) was used to graph all other data.

Two independent groups were compared using an unpaired Student's t-test. Two dependent groups were compared using a paired Student's t-test. More than two independent groups were compared using a one way analysis of variance (ANOVA) and Holm-Sidak *post hoc* test. When two groups, each with repeated measurements from the same cell were compared, a two way repeated measures ANOVA was used and a Holm-Sidak *post hoc* test applied. Groups with a binary outcome were compared using an N-1 chi-squared test. An extra sum of squares F test was applied to test the difference between histogram distributions. Each relevant statistical test was documented in the relevant figure legend.

All data were presented as mean \pm SEM and significance was considered when $p < 0.05$. The following conventions illustrated significant differences between groups: * = $p < 0.05$; ** = $p < 0.01$; *** = $p < 0.001$. Sample sizes were calculated *a priori* from preliminary data or previously published results from within the Steele group. The number of cells and hearts used in each experiment were documented in the corresponding figure legend and text as 'cells, (hearts)'

Chapter 3: The effect of flecainide on Ca²⁺ handling in intact ventricular myocytes from wild type rat

3.1 Introduction

The class 1C antiarrhythmic agent flecainide is a well characterised inhibitor of the sarcolemmal cardiac Na⁺ channel, Na_v1.5 (Nitta et al., 1992, Ramos and O'Leary, 2004). However, a series of recent studies provided evidence that flecainide also modulates SR Ca²⁺ release via a direct action on RyR2 (Watanabe et al., 2009, Hwang et al., 2011a, Hilliard et al., 2010). The initial evidence for an effect on RyR2 was based in part, on Ca²⁺ spark measurements in intact and permeabilised cardiomyocytes isolated from a calsequestrin knockout (Casq2^{-/-}) mouse model of CPVT (Hilliard et al., 2010). Flecainide decreased Ca²⁺ spark width and amplitude thereby suppressing the formation of pro-arrhythmic Ca²⁺ waves (Hilliard et al., 2010). These authors suggested that RyR2 modulation was the primary antiarrhythmic mechanism of the drug in CPVT because flecainide prevented the Ca²⁺ waves that initiate DADs. The inhibitory effect on Na_v1.5 would provide only secondary protection should occasional DADs still occur.

A sustained anti-arrhythmic effect of flecainide involving an action on RyR2 is a novel concept. Not least because most drugs shown to experimentally modulate RyR2 have only transient effects on Ca²⁺ release at sub-millimolar concentrations (Lukyanenko et al., 2001, Diaz et al., 1997). For example, partial inhibition of RyR2 with tetracaine initially decreases triggered SR Ca²⁺ release and resting Ca²⁺ spark frequency. However, the decrease in Ca²⁺ efflux leads to an increase in SR Ca²⁺ content, which ultimately restores SR Ca²⁺ release to the control level (Lukyanenko et al., 2001, Overend et al., 1997). The sustained effect of flecainide on RyR2 may indicate that it affects SR Ca²⁺ release more subtly. Specifically, the decrease in Ca²⁺ spark mass in the presence of the drug was accompanied by an increase spark frequency, such that there was no overall effect on the SR Ca²⁺ content (Hilliard et al., 2010). Without a change in SR Ca²⁺ content, autoregulation should not be influenced thus allowing a sustained effect of flecainide on SR Ca²⁺ sparks and hence waves.

In contrast to these findings, a recent study on cardiomyocytes isolated from WT rat hearts challenged the suggestion that flecainide modifies RyR2 function (Sikkel et al., 2013). While flecainide was reported to decrease Ca²⁺ wave frequency, the characteristic changes in Ca²⁺ spark properties (Hilliard et al., 2010) were not apparent. This led the authors to conclude that the antiarrhythmic effect of flecainide on Ca²⁺ waves must involve its established action on

Na_v1.5 alone (Sikkel et al., 2013). One possible explanation for this is that flecainide might have a much more potent effect on abnormal RyR2 channels present in CPVT. However, a limitation of these experiments was that myocytes were incubated with the drug for only 5 minutes, whereas the effect of flecainide on RyR2 has been reported to take 20-30 minutes to become apparent in intact cells (Hwang et al., 2011b). This delay likely reflects the slow diffusion of flecainide through the cell membrane (Liu et al., 2003). Flecainide is 99% protonated at physiological pH and only the neutral fraction can enter the cytosol freely (Liu et al., 2003). Therefore, an effect on RyR2 might not be expected after such a short incubation period. Whilst Sikkel et al. (2013) also provided data showing a decrease in Ca²⁺ wave frequency after 30 min incubation with flecainide, Ca²⁺ spark properties were not studied after this longer period of drug incubation.

The aim of this chapter was to investigate the effect of flecainide on spontaneous Ca²⁺ release and RyR2 function in WT rat cardiomyocytes during prolonged (>45 min) drug incubation. Myocytes from WT rat ventricle were electrically paced and perfused with isoprenaline to mimic β-adrenergic drive and induce pro-arrhythmic Ca²⁺ waves. Thus, the pathological state described within CPVT individuals was partially simulated. Confocal line scan imaging was used to visualise SR Ca²⁺ release in the form of field stimulated Ca²⁺ transients, spontaneous Ca²⁺ waves and spontaneous Ca²⁺ sparks.

3.2 Methods

3.2.1 Myocyte imaging protocol

Rat ventricular cardiomyocytes were isolated via retrograde perfusion and enzymatic digestion on a Langendorff perfusion system (Chapter 2.2). CON cardiomyocytes were isolated from the right and left ventricles whereas MCT cardiomyocytes were isolated from the right ventricle only (Section 2.9). Isolated cells were loaded with fluo-4 AM for 15 min in 1 mM Ca²⁺ Tyrode's solution. Excess fluo-4 AM was removed and intracellular fluo-4 AM was left to de-esterify for a minimum of 45 min at 4 °C. Fluo-4 loaded cells were incubated with 15 µM flecainide or vehicle for 35 min at room temperature in 1.8 mM Ca²⁺ Tyrode's solution. Cells were then placed in the experimental chamber on the stage of a Nikon Diaphot inverted microscope and myocytes were viewed with a ×40 oil immersion lens (Nikon Plan Fluor DLL, numerical aperture 1.3). A confocal laser-scanning unit (Bio-Rad, Cellmap) was attached to the side port of the microscope.

Cells were left for 2 min to settle onto the glass cover slip of the experimental chamber. 4 – 6 cells of regular size and shape were identified in the plane of view and their response to field stimulus was tested (10 ms square wave pulse; 30 mV). 10 min of electrical pacing at 0.5, 1.5 or 2.5 Hz began with perfusion of 1.8 mM Ca²⁺ Tyrode's solution containing 15 µM flecainide or vehicle; and 100 nM isoprenaline or vehicle. The concentration of flecainide used exceeded physiological plasma concentrations (0.2 – 5 µM). However, it was considered that a supraphysiological concentration might decrease the time taken for flecainide to cross the sarcolemma bilayer and access RyR2 (discussed further in Chapter 4). Flecainide was solubilised in ethanol (0.01%) and isoprenaline was solubilised in ultra-purified water. All experiments were performed at 22 ± 2 °C unless stated otherwise.

After 10 min of pacing, fluo-4 was excited with the 488 nm line of a diode laser and fluorescence was measured at >520 – 540 nm. Images were acquired in line-scan mode at 188 lines/sec with an interval time of 5.3 ms between lines along the longitudinal axis of the cell for 90 sec. The first 10 sec of each line scan included cell responses to electrical field stimulation. For the remaining 80 sec, electrical pacing was stopped and information on spontaneous waves and sparks was collected. The above protocol was altered to increase flecainide translocation across the sarcolemma. The cell incubation period was increased to 2 hours, including 35 min at 37 °C. The initial protocol was also repeated in cells isolated from a monocrotaline treated rat model of right sided heart failure (MCT). Comprehensive characterisations of this model are documented (Fowler, 2015, Benoist, 2012) For the

purposes of this study it is important to note that MCT Ca^{2+} wave and spark frequencies were significantly increased when compared with myocytes isolated from saline control animals, indicating an increased RyR2P_o (Fowler, 2015).

3.2.2 Voltage clamp of cardiomyocytes

Myocytes were patch clamped using whole cell configuration of the patch-clamp technique in the voltage-clamp mode. An Olympus CK40 inverted microscope was used to visualise the myocytes. Cells were continually perfused (3-5 ml/min) with extracellular electrophysiological solution. Patch pipettes had resistances of 3-6 M Ω and filled with intracellular electrophysiological solution. Na^+ currents were evoked by a 200 ms step from -80 mV to -30 mV every 10 secs, and measured for their peak amplitude under control conditions and then in the presence of 20 μM flecainide. All experiments were carried out at 22 ± 1 °C.

3.2.3 Line scan analysis

Incubation with the Ca^{2+} sensitive dye fluo-4 AM and confocal microscopy line scanning allowed the visualisation of SR Ca^{2+} release in the form of transients, waves and sparks. All images were analysed using ImageJ software. Electrically paced transients were counted and the proportion of missing or disrupted transients was recorded. Ca^{2+} wave frequency was analysed during and post-pacing. All waves were counted and wave frequency calculated as waves/min. Waves which began immediately prior to a paced Ca^{2+} transient, but which were interrupted by the paced transient were included in this total. Post-pacing, Ca^{2+} waves were counted and the frequency calculated within the first 30 sec, the second 30 sec and the final 20 sec. Post-pacing wave frequency was displayed as a combined and separate value.

Sparks occurred spontaneously throughout each trace however their presence was predominantly apparent immediately prior to Ca^{2+} wave formation. Spark analysis was therefore limited to 5 sec prior to the each Ca^{2+} wave. If the time between Ca^{2+} waves was less than 5 sec, sparks were analysed down to 1 sec prior to Ca^{2+} wave formation. It was not possible to analyse sparks <1 sec from the start of a wave due to the presence of artefacts caused by the increased background amplitude from the previous Ca^{2+} wave. Sparks were then analysed using the ImageJ plugin Sparkmaster (Picht et al., 2007).

3.2.4 Statistics

Data distribution was tested using the Shapiro-Wilk test of normality. Data with a Shapiro-Wilk p value < 0.05 were Log transformed and the normality of the data was re-tested. Independent data were analysed using unpaired Student's t-tests or one way ANOVA with a Holm Sidak multiple comparison *post hoc* test. Proportions were compared using N-1 Chi-squared test with Bonferroni correction if comparing more than 3 groups. Statistical analyses were documented in each figure legend. Significance was considered when $p < 0.05$. All data were displayed as mean \pm SEM.

3.3 Results

3.3.1 The effect of 100 nM isoprenaline on Ca²⁺ wave frequency and spark properties

Figure 3.1 A shows representative line scan images and associated line profiles of myocytes which were field stimulated at 1.5 Hz, in the presence or absence of isoprenaline. Each stimulus was associated with a rapid, uniform increase in Ca²⁺ concentration. In the presence of isoprenaline, spontaneous Ca²⁺ waves (red triangles) were present in between field stimulations and sometimes disrupted the triggered Ca²⁺ transient. Spontaneous Ca²⁺ waves did not occur at any field stimulation frequency in the absence of isoprenaline, however differences between 0 ISO and 100 ISO were only significant at 1.5 Hz field stimulation. ($p < 0.05$; Figure 3.1 B). Within these cells, Ca²⁺ wave frequency was 14.0 ± 5.29 waves/min (0.5 Hz) and 52.5 ± 14.4 waves/min (1.5 Hz; Figure 3.1 C; $n = 5$ cells (0 ISO, 0.5 Hz); 9 cells (100 nM ISO, 0.5 Hz); 9 cells (0 ISO, 1.5 Hz); 9 cells (100 nM ISO, 1.5 Hz)).

Spontaneous Ca²⁺ waves also occurred following cessation of pacing at 1.5 Hz, both in control cells and in cells incubated with isoprenaline (Figure 3.2 A). The time between the final triggered Ca²⁺ transient and the first spontaneous Ca²⁺ wave was significantly decreased in the presence of isoprenaline after stimulation at both 0.5 Hz ($p < 0.01$) and 1.5 Hz ($p < 0.001$; Figure 3.2 B). In the absence of isoprenaline, 80% of cells paced at 0.5 Hz subsequently exhibited Ca²⁺ waves. In contrast, all cells displayed Ca²⁺ waves when superfused with isoprenaline or when paced at 1.5 Hz (Figure 3.2 C). At 0.5 Hz field stimulation, the presence of isoprenaline did not significantly change Ca²⁺ wave frequency ($p > 0.05$; Figure 3.2 D). However, at 1.5 Hz wave frequency was significantly increased >3 fold in the presence of isoprenaline ($p < 0.001$; Figure 3.2 D). Each line scan was split into three groups; 0-30 sec; 30-60 sec; and 60-80 sec post-pacing and the wave frequency was analysed (Figure 3.2 E). After pacing at 0.5 Hz and 1.5 Hz, Ca²⁺ wave frequency was increased by isoprenaline in the first 30 sec post-pacing ($p = 0.06$ and $p < 0.001$ respectively). However, there was no change in wave frequency with isoprenaline >30 sec after pacing was stopped (Figure 3.2 E; $p > 0.05$; $n = 5$ cells, (1) heart (0 ISO, 0.5 Hz); 9, (2) (100 nM ISO, 0.5 Hz); 9, (2) (0 ISO, 1.5 Hz); 9, (2) (100 nM ISO, 1.5 Hz)).

Ca²⁺ sparks (red triangles) were analysed 5 sec prior to the release of a Ca²⁺ wave in the presence or absence of isoprenaline (Figure 3.3 A). In the presence of isoprenaline, spark amplitude was significantly increased by 30.9% after pacing at 0.5 Hz ($p < 0.05$); or by 34.0% after pacing at 1.5 Hz ($p < 0.01$; Figure 3.3 B). Isoprenaline did not change spark FWHM at either 0.5 Hz or 1.5 Hz (Figure 3.3 C). Spark FDHM was significantly decreased in the presence of isoprenaline by 21.5% after pacing at 0.5 Hz ($p < 0.001$) and decreased by 21.4% after pacing

at 1.5 Hz ($p < 0.001$; Figure 3.3 D). Spark frequency did not significantly change in the presence of isoprenaline after pacing at 0.5 Hz or 1.5 Hz ($p > 0.05$; Figure 3.3 E; $n = 5$ cells, (1) heart (0 ISO, 0.5 Hz); 9, (2)(100 nM ISO, 0.5 Hz); 9, (2) (0 ISO, 1.5 Hz); 9, (2) (100 nM ISO, 1.5 Hz)).

3.3.2 The effect of field stimulation frequency on Ca^{2+} wave frequency and spark properties in the presence of isoprenaline

Figure 3.4 A shows representative line scans and fluorescence profiles of cells field stimulated at 0.5, 1.5 or 2.5 Hz in the presence of isoprenaline. Triggered Ca^{2+} transients (grey triangles) and spontaneous Ca^{2+} waves (red triangles) were apparent at all field stimulation frequencies. During electrical pacing, 53.5%, 50.7% and 24.2% of cells exhibited spontaneous Ca^{2+} waves at 0.5, 1.5 and 2.5 Hz respectively (Figure 3.4 B). Significantly fewer cells exhibited Ca^{2+} waves when paced at 2.5 Hz, when compared with cells paced at 0.5 Hz or 1.5 Hz ($p < 0.01$; Figure 3.4 B). Wave frequency was significantly greater when cells were paced at 1.5 Hz compared with cells paced at 0.5 Hz (67.6 ± 7.09 waves/min vs 26.1 ± 2.95 waves/min respectively; Figure 3.4 C; $p < 0.001$). This trend was apparent between cells paced at 2.5 Hz and 0.5 Hz (67.9 ± 19.3 waves/min vs 26.1 ± 2.95 waves/min) yet did not reach significance ($p = 0.08$; Figure 3.4 C). There was no significant difference in wave frequency between cells stimulated at 1.5 Hz and 2.5 Hz ($p > 0.05$; Figure 3.4 C; $n = 71$ cells (0.5 Hz); 67 cells (1.5 Hz); 66 cells (2.5 Hz)).

After field stimulation was stopped, spontaneous Ca^{2+} waves were apparent at all pacing frequencies (Figure 3.5 A). Ca^{2+} waves occurred in 94.2%, 100% and 98.5 % of cells at 0.5, 1.5 and 2.5 Hz respectively (Figure 3.5 B). Wave frequency was significantly greater when cells were paced at 1.5 Hz compared with cells paced at 0.5 Hz (6.57 ± 1.87 waves/min vs 3.54 ± 0.32 waves/min respectively; Figure 3.5 C; $p < 0.05$). Cells paced at 2.5 Hz more than doubled Ca^{2+} wave frequency when compared with cells paced at 0.5 Hz (7.59 ± 1.40 waves/min vs 3.54 ± 0.32 waves/min respectively; Figure 3.5 C; $p < 0.05$). However, there was no significant difference in Ca^{2+} wave frequency between cells paced at 1.5 Hz or 2.5 Hz (Figure 3.5 C; $p > 0.05$; $n = 71$ cells, (6) hearts (0.5 Hz); 67, (10) (1.5 Hz); 66, (9) (2.5 Hz)).

Ca^{2+} sparks (red triangles) were analysed 5 sec prior to the release of a Ca^{2+} wave after pacing at 0.5, 1.5 or 2.5 Hz (Figure 3.6 A). Sparks showed no significant differences in amplitude (Figure 3.6 B), FWHM (Figure 3.6 C), FDHM (Figure 3.6 D) or frequency (Figure 3.6 E) as a function of field stimulation frequency ($p > 0.05$; $n = 71$ cells, (6) hearts (0.5 Hz); 67, (10) (1.5 Hz); 66, (9) (2.5 Hz)).

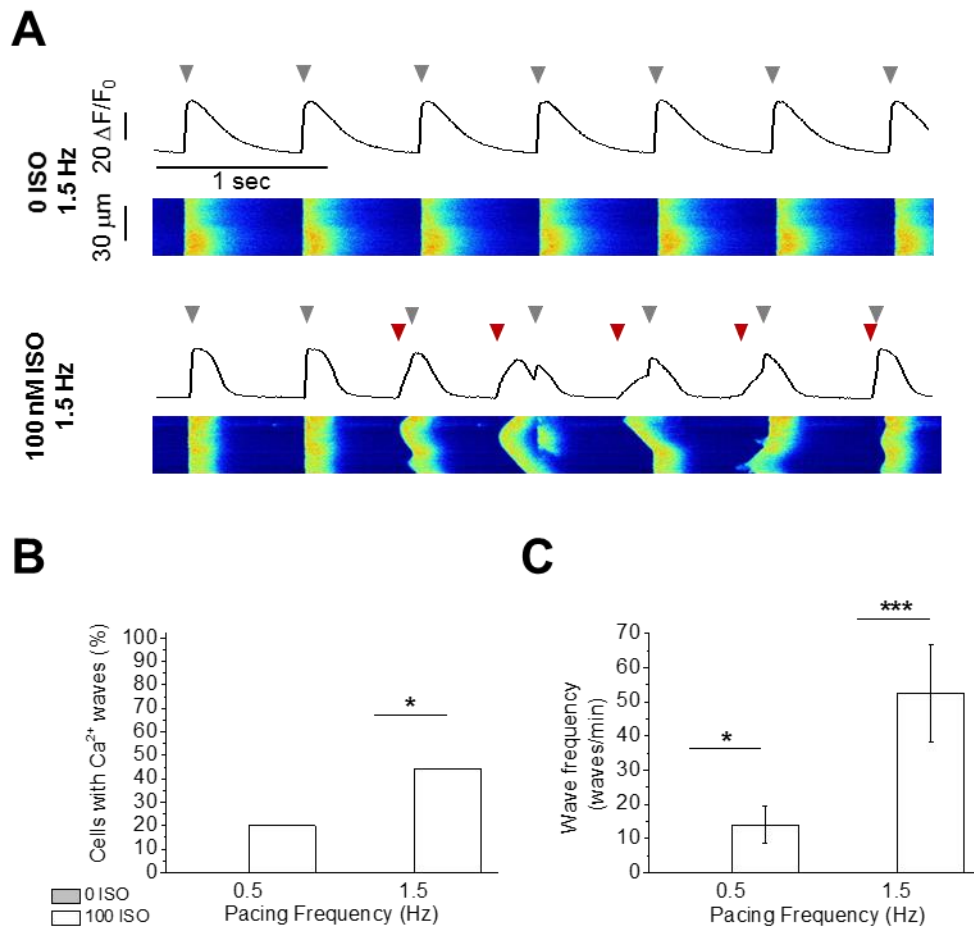


Figure 3.1: Effect of 100 nM isoprenaline on Ca^{2+} wave frequency during field stimulation at 0.5 and 1.5 Hz

A) Representative line scans and fluorescence profiles of cells field stimulated at 1.5 Hz with or without 100 nM isoprenaline (ISO). Grey triangles indicate field stimulation pulse and red triangles represent the start of a Ca^{2+} wave. **B)** Percentage of cells exhibiting Ca^{2+} waves during 0.5 or 1.5 Hz field-stimulation, with or without 100 nM isoprenaline. **C)** Ca^{2+} wave frequency at 0.5 or 1.5 Hz field stimulation frequency with or without 100 nM isoprenaline. N-1 chi-squared test or two tailed unpaired Student's t-test. * = $p < 0.05$; *** $p < 0.001$. 0 ISO, 0.5 Hz n = 5 (1); 0 ISO, 1.5 Hz n = 9 (2); 100 ISO, 0.5 Hz n = 9 (2); 100 ISO, 1.5 Hz n = 9 (2).

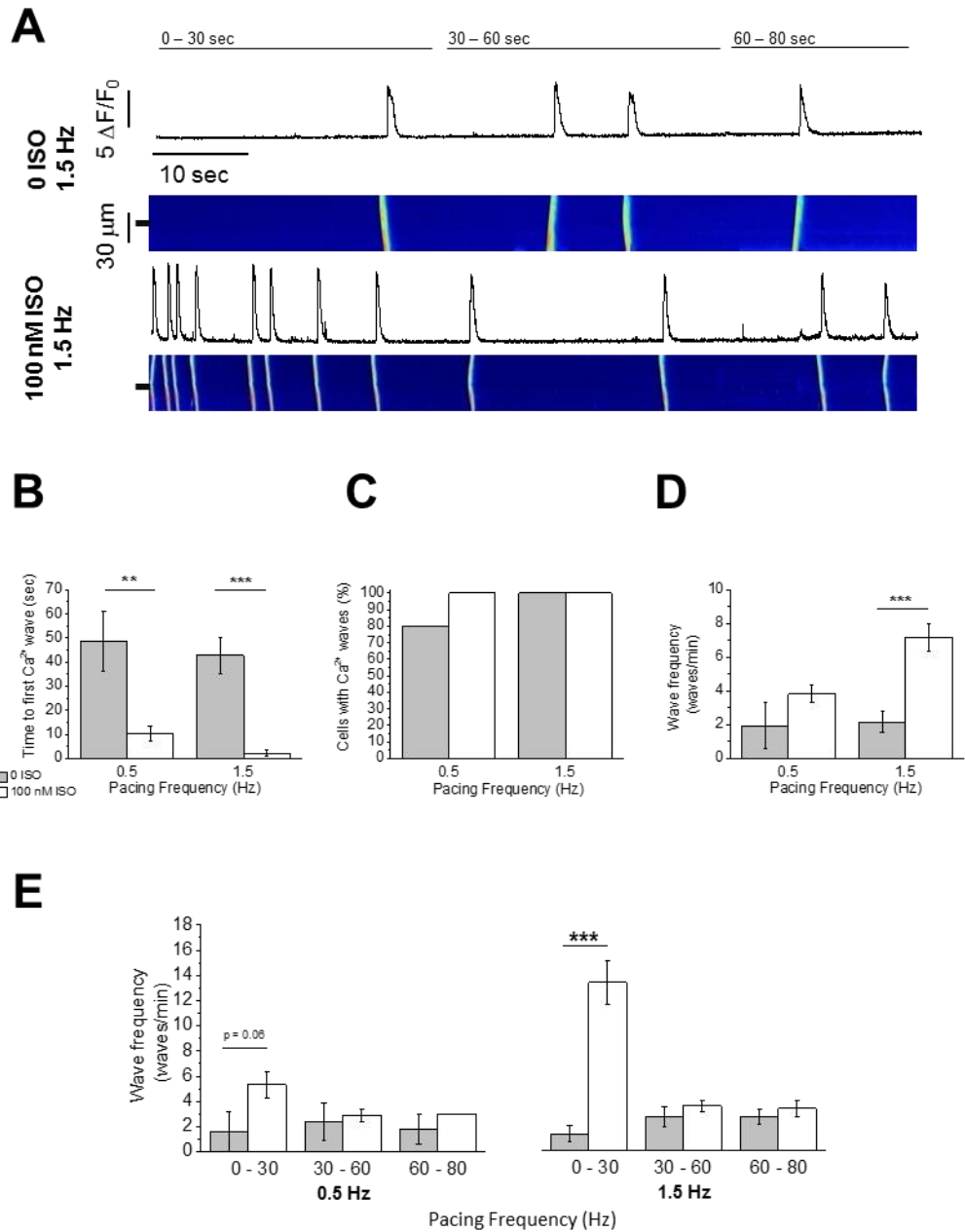


Figure 3.2: Effect of 100 nM isoprenaline on Ca^{2+} wave frequency after field stimulation at 0.5 and 1.5 Hz

A) Representative line scans and fluorescence profiles of cells immediately after field stimulation at 1.5 Hz with or without 100 nM isoprenaline (ISO). **B)** Time between the final field-stimulated Ca^{2+} transient and the first Ca^{2+} wave **C)** Percentage of cells exhibiting Ca^{2+} waves **D)** Ca^{2+} wave frequency **E)** Ca^{2+} wave frequency 0-30 sec 30-60 sec or 60-80 sec after field stimulation was stopped. N-1 chi-squared test or two tailed unpaired Student's t-test. *** $p < 0.001$. 0 ISO, 0.5 Hz $n = 5$ (1); 0 ISO, 1.5 Hz $n = 9$ (2); 100 ISO, 0.5 Hz $n = 9$ (2); 100 ISO, 1.5 Hz $n = 9$ (2).

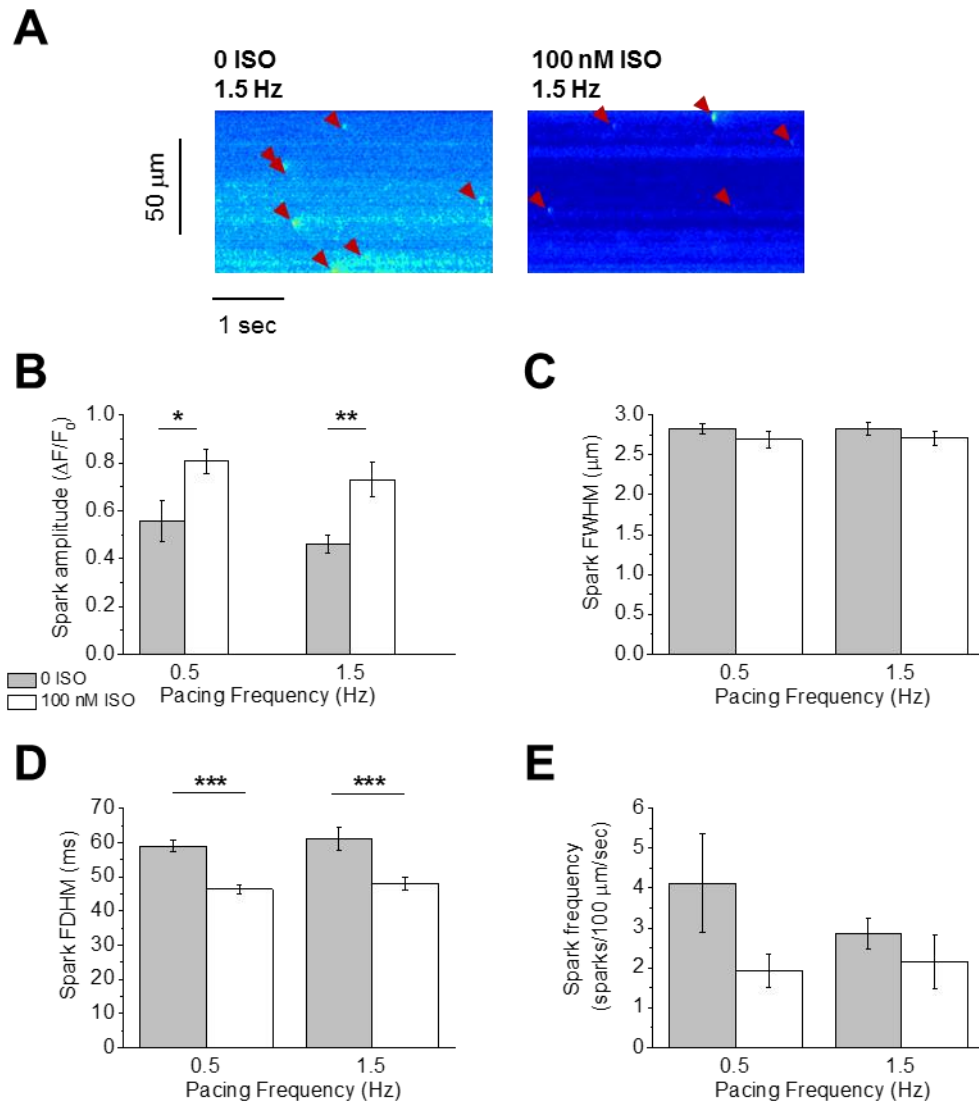


Figure 3.3: Effects of 100 nM isoprenaline on spark size and frequency after field stimulation at 0.5 and 1.5 Hz

A) Representative line scans of sparks after field stimulation at 1.5 Hz, with or without 100 nM isoprenaline (ISO). Red triangles indicate sparks identified by Sparkmaster **B)** Mean data for spark amplitude, **C)** spark FWHM **D)** spark FDHM and **E)** spark frequency. Two tailed unpaired Student's t-test. * = $p < 0.05$; ** = $p < 0.01$; *** $p < 0.001$. 0 ISO, 0.5 Hz $n = 5$ (1); 0 ISO, 1.5 Hz $n = 9$ (2); 100 ISO, 0.5 Hz $n = 9$ (2); 100 ISO, 1.5 Hz $n = 9$ (2).

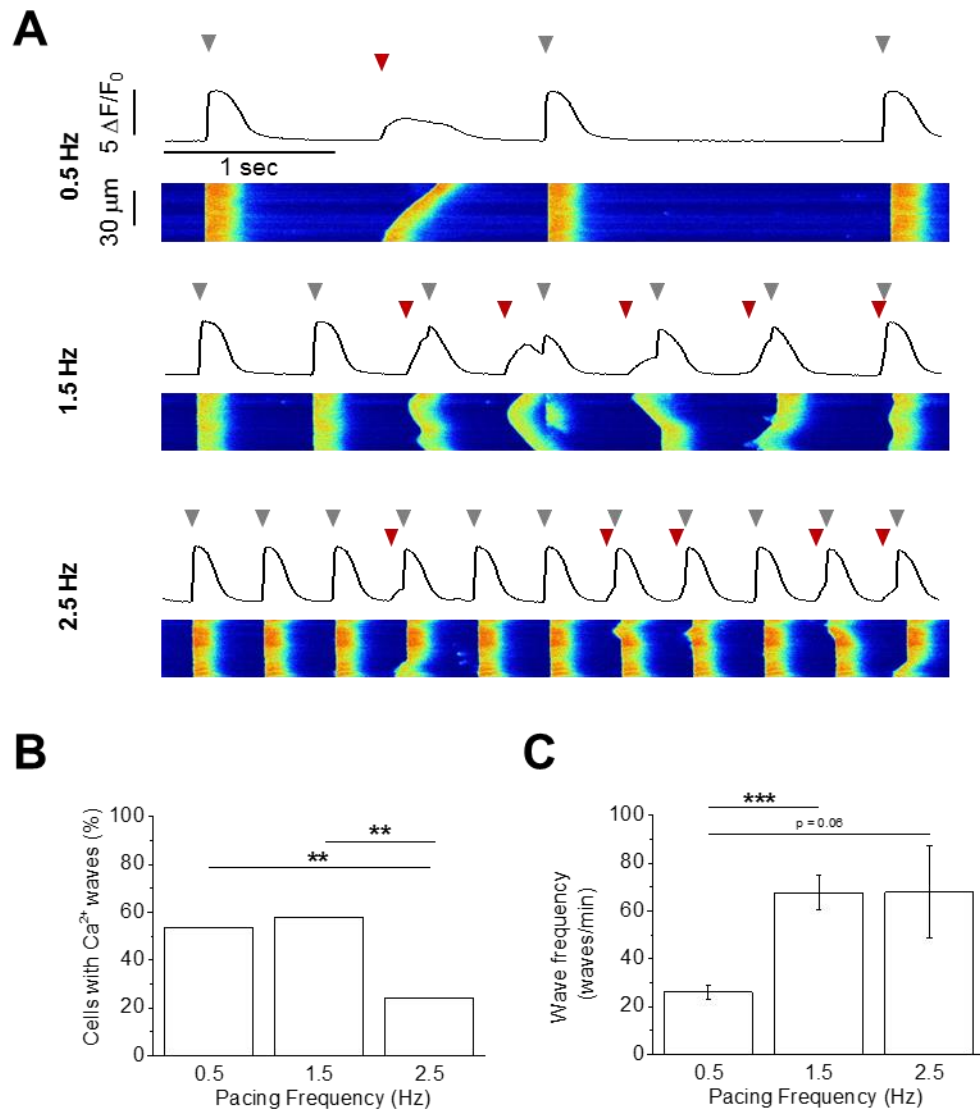


Figure 3.4: Effect of field stimulation frequency on Ca^{2+} wave frequency during pacing in cardiomyocytes superfused with 100 nM isoprenaline

A) Representative line scans and fluorescence profiles of Ca^{2+} waves during 0.5, 1.5 or 2.5 Hz field-stimulation. Grey triangles indicate field stimulation pulses and red triangles indicate the start of a Ca^{2+} wave. **B)** Percentage of cells exhibiting Ca^{2+} waves during field stimulation **C)** Ca^{2+} wave frequency at each field stimulation frequency. N-1 chi-squared test with Bonferroni correction or one way ANOVA + Holm Sidak multiple comparisons *post hoc* test performed on Log transformed data. * = $p < 0.05$. 0.5 Hz n = 71 (6); 1.5 Hz n = 67 (10); 2.5 Hz n = 66 (9).

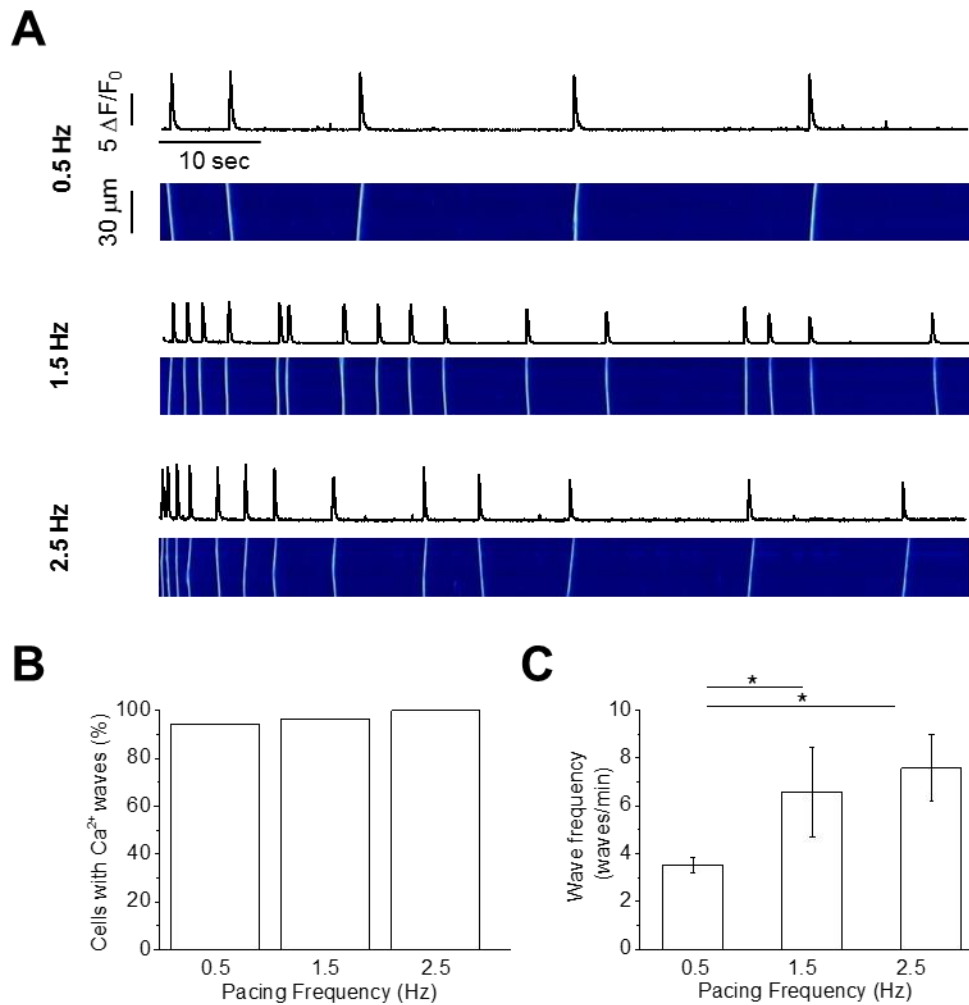


Figure 3.5: Effect of field stimulation frequency on Ca^{2+} wave frequency post-pacing in cardiomyocytes superfused with 100 nM isoprenaline

A) Representative line scans and fluorescence profiles of Ca^{2+} waves after 0.5, 1.5 or 2.5 Hz field-stimulation. **B)** Percentage of cells exhibiting Ca^{2+} waves **C)** Ca^{2+} wave frequency at each field stimulation frequency. N-1 chi-squared test with Bonferroni correction or one way ANOVA + Holm Sidak multiple comparisons *post hoc* test performed on Log transformed data. * = $p < 0.05$. 0.5 Hz n = 71 (6); 1.5 Hz n = 67 (10); 2.5 Hz n = 66 (9).

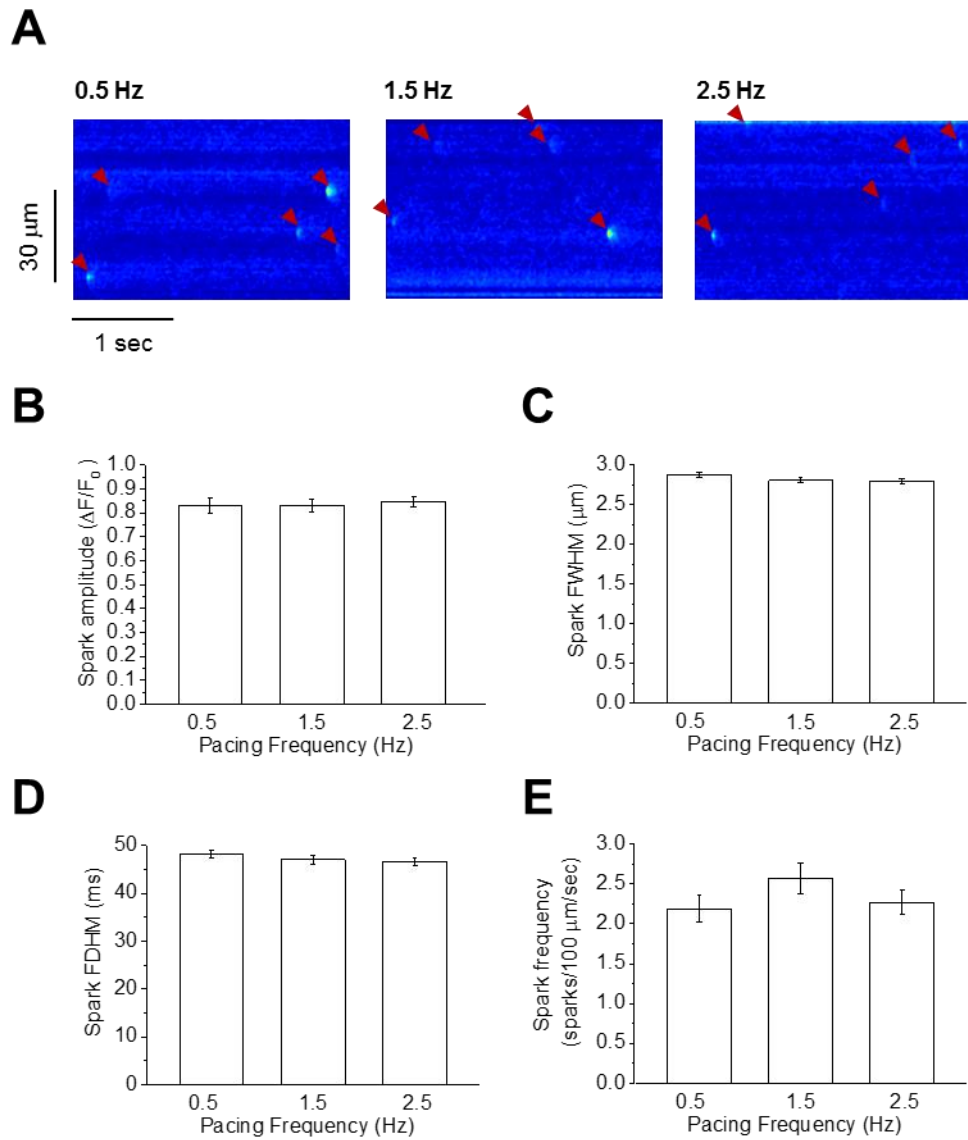


Figure 3.6: Effects of field stimulation frequency on spark properties in the presence of 100 nM isoprenaline superfusion

A) Representative line scans of cells at 0.5, 1.5 and 2.5 Hz. Red triangles indicate sparks identified by Sparkmaster. **B)** Mean data for spark amplitude, **C)** spark FWHM, **D)** spark FDHM and **E)** spark frequency for sparks occurring after field-stimulation at either 0.5, 1.5 or 2.5 Hz. One-way ANOVA performed. 0.5 Hz n = 61 (6); 1.5 Hz n = 60 (10); 2.5 Hz n = 62 (8).

3.3.3 The effect of flecainide on triggered Ca²⁺ transients

Cardiomyocytes were incubated with 15 μ M flecainide or vehicle control for 35 min at room temperature. Cells were then paced at 0.5, 1.5 or 2.5 Hz for 10 min in the presence of 100 nM isoprenaline and 15 μ M flecainide or vehicle. Within this period, some cells became unresponsive to electrical pacing and failed to trigger a Ca²⁺ transient. Less than 5% of control cells were unresponsive to field stimulation, across all pacing frequencies. In contrast, 6.36%, 13.9% and 51.6% of flecainide treated cells became unresponsive to field stimulation at 0.5, 1.5 and 2.5 Hz respectively (Figure 3.7 A). Flecainide significantly increased the proportion of unresponsive cells, in cells paced at 1.5 Hz ($p < 0.05$) or 2.5 Hz ($p < 0.001$; $n = 67$ cells, (6) hearts (VEH, 0.5 Hz); 36, (4)(VEH, 1.5 Hz); 29, (4) (VEH, 2.5 Hz); 77, (6) (FLEC, 0.5 Hz); 36, (4) (FLEC, 1.5 Hz); 31, (4)(FLEC; 2.5 Hz)). Unresponsive cells were not included in the following dataset.

A small proportion of cells were identified as responsive to pacing; however missing or disrupted Ca²⁺ transients were apparent in the line scans (red triangles; Figure 3.8 A). At 0.5 Hz pacing frequency, only one vehicle and zero flecainide treated cells did not respond to all stimulation pulses. At 1.5 Hz and 2.5 Hz, 24.3% and 17.7% of flecainide treated cells respectively displayed missing or disrupted Ca²⁺ transients compared with <10% of all vehicle treated cells (Figure 3.8 B). The differences between vehicle and flecainide treated cells were significant at 0.5 Hz ($p < 0.01$) and 1.5 Hz ($p < 0.001$; Figure 3.8 C; $n = 71$ cells, (6) hearts (VEH, 0.5 Hz); 67, (10) (VEH, 1.5 Hz); 66, (9) (VEH, 2.5 Hz); 72, (6) (FLEC, 0.5 Hz); 68, (10) (FLEC, 1.5 Hz); 62, (9) (FLEC; 2.5 Hz)).

3.3.4 The effect of flecainide on Ca²⁺ waves during and after electrical pacing

Ca²⁺ waves were line scanned during the final 10 sec of pacing at 1.5 Hz in the presence or absence of flecainide (Figure 3.9 A). During 0.5 Hz and 1.5 Hz field stimulation ~50% of cells exhibited Ca²⁺ waves and there was no difference between vehicle and flecainide treated cells (Figure 3.9 B). At 2.5 Hz only 21.5% of vehicle treated cells and 33.9% of flecainide treated cells exhibited Ca²⁺ waves, again with no significant difference between vehicle and flecainide treated groups (Figure 3.9 B). Cells exhibiting one or more Ca²⁺ waves were included in the data presented in Figure 3.9 C to prevent skewing of the data towards zero. At 1.5 Hz, there was a trend for Ca²⁺ wave frequency to decrease with flecainide during field stimulation ($p = 0.06$). However this trend was not apparent at 0.5 or 2.5 Hz ($p > 0.05$; Figure 3.9 C; $n = 71$ cells,

(6) hearts (VEH, 0.5 Hz); 67, (10) (VEH, 1.5 Hz); 66, (9) (VEH, 2.5 Hz); 72, (6)(FLEC, 0.5 Hz); 68, (10) (FLEC, 1.5 Hz); 62, (9) (FLEC; 2.5 Hz)).

Ca²⁺ waves were line scanned for 80 sec immediately after electrical pacing at 1.5 Hz in the presence or absence of flecainide. Post-pacing scan time was divided into three groups; 0-30 sec, 30-60 sec and 60-80 sec after pacing was stopped (Figure 3.10 A). Within all experimental groups, >90% of cells displayed Ca²⁺ waves within 80 sec of pacing being stopped (Figure 3.10 B). Flecainide decreased Ca²⁺ wave frequency by 18.9% after pacing at 0.5 Hz (p = 0.07) and significantly decreased wave frequency by 51.4% (p < 0.001) and 26.0 % (p < 0.05) at 1.5 and 2.5 Hz respectively (Figure 3.10 C). Interestingly, after pacing at 1.5 or 2.5 Hz, flecainide significantly (or near significantly) decreased Ca²⁺ wave frequency at each post-pacing time point (Figure 3.10 D; n = 71 cells, (6) hearts (VEH, 0.5 Hz); 67, (10) (VEH, 1.5 Hz); 66, (9) (VEH, 2.5 Hz); 72, (6)(FLEC, 0.5 Hz); 68, (10)(FLEC, 1.5 Hz); 62, (9)(FLEC; 2.5 Hz)).

The time from the last triggered Ca²⁺ transient to the start of the first Ca²⁺ wave was calculated in the presence or absence of flecainide (Figure 3.11 A). There were no significant differences between control and flecainide treated cells (p > 0.05; Figure 3.11 B). Figure 3.12 A shows a close up line scan fluorescence profile of (i) a spontaneous Ca²⁺ wave and (ii) a spontaneous Ca²⁺ wave initiating a rapid uniform Ca²⁺ transient. This phenomenon was more prevalent within vehicle treated cells than flecainide treated cells, although this trend reached significance only after pacing at 1.5 Hz (p < 0.01; Figure 3.12 B). Of these cells, the percentage of waves which triggered Ca²⁺ transients showed no clear differences between vehicle and flecainide treated cells (p > 0.05; Figure 3.12 C; n = 71 cells, (6) hearts (VEH, 0.5 Hz); 67, (10) (VEH, 1.5 Hz); 66, (9) (VEH, 2.5 Hz); 72, (6) (FLEC, 0.5 Hz); 68, (10) (FLEC, 1.5 Hz); 62, (9) (FLEC; 2.5 Hz)).

3.3.5 The effect of flecainide on Ca²⁺ sparks

Ca²⁺ sparks (red triangles) were analysed 5 sec prior to the release of a Ca²⁺ wave in the presence or absence of flecainide (Figure 3.13 A). In cells electrically paced at 2.5 Hz, flecainide significantly decreased spark amplitude from $0.85 \pm 0.02 \Delta F/F_0$ to $0.78 \pm 0.03 \Delta F/F_0$ ($p < 0.05$). However, there was no change in spark amplitude in cells paced at 0.5 Hz or 1.5 Hz (Figure 3.13 B). Spark FWHM (Figure 3.13 B), FDHM (Figure 3.13 C) or frequency (Figure 3.13 D) was not significantly affected by flecainide at any field stimulation frequency ($p > 0.05$; $n = 61$ cells, (6) hearts (VEH, 0.5 Hz); 60, (10) (VEH, 1.5 Hz); 62, (8) (VEH, 2.5 Hz); 64, (6) (FLEC, 0.5 Hz); 65, (10) (FLEC, 1.5 Hz); 54, (8) (FLEC; 2.5 Hz)).

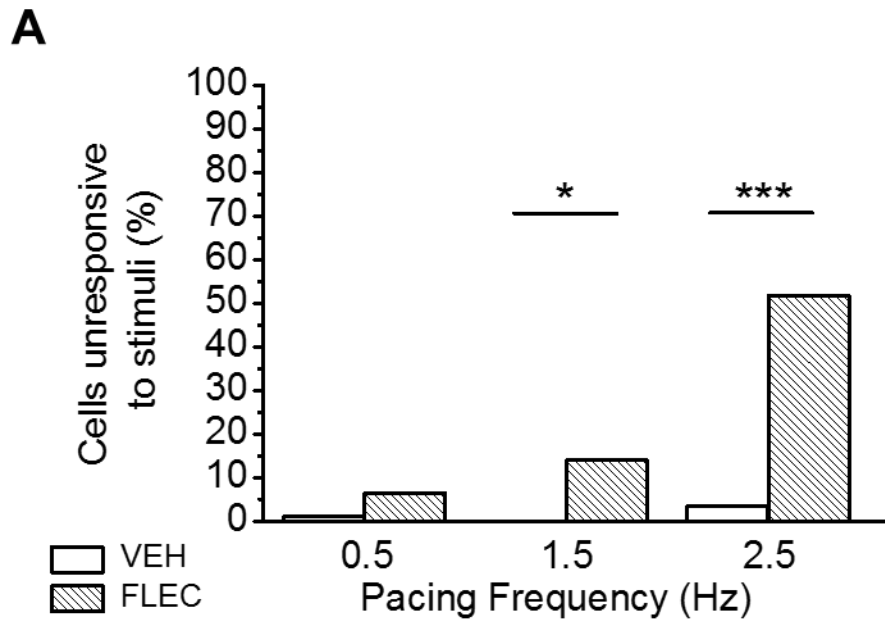


Figure 3.7: The effect of flecainide on cell response to field stimulation in cardiomyocytes superfused with 100 nM isoprenaline

A) Percentage of cells responsive to field-stimulation at 0.5, 1.5 or 2.5 Hz with (FLEC) or without (VEH) 15 μ M flecainide. All experiments were in the presence of 100 nM isoprenaline. N-1 chi-squared test. * = $p < 0.05$; *** = $p < 0.01$. VEH, 0.5 Hz $n = 67$ (6); VEH, 1.5 Hz $n = 36$ (4); VEH, 2.5 Hz $n = 29$ (4). FLEC, 0.5 Hz $n = 77$ (6); FLEC, 1.5 Hz = 36 (4); FLEC, 2.5 Hz = 31 (4).

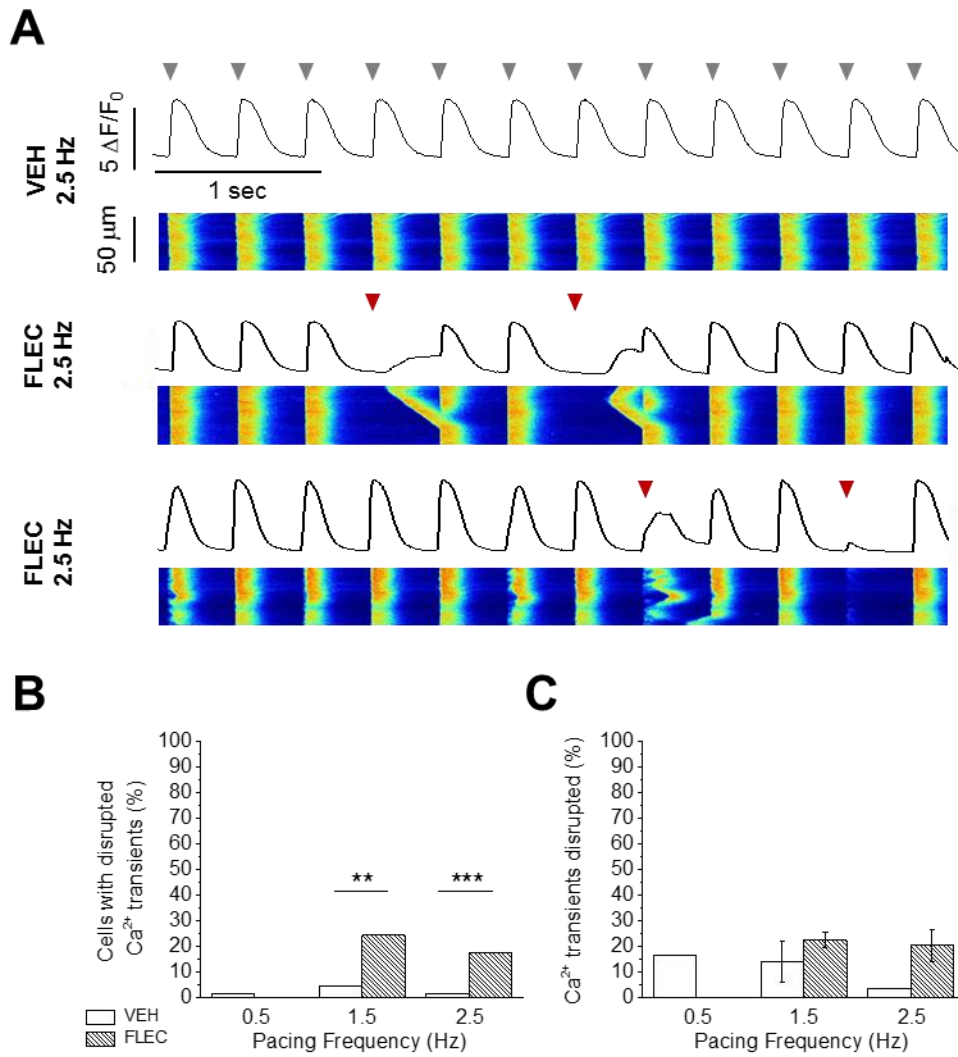


Figure 3.8: The effect of flecainide on Ca^{2+} transient disruption during pacing in cardiomyocytes superfused with 100 nM isoprenaline

A) Example line scans and fluorescence profiles of vehicle (VEH) and flecainide (FLEC) treated cells with and without disrupted Ca^{2+} transients during 2.5 Hz field stimulation. Grey triangles indicated field stimulation pulses and red triangles indicated missing or disrupted Ca^{2+} transients. **B)** Percentage of cells with disrupted Ca^{2+} transients **C)** Percentage of Ca^{2+} transients disrupted within a cell. Only cells exhibiting this phenomena were included. N-1 chi-squared test or two tailed unpaired Student's t-test applied. ** = $p < 0.01$; *** = $p < 0.001$. VEH, 0.5 Hz $n = 71$ (6); VEH, 1.5 Hz $n = 67$ (10); VEH, 2.5 Hz $n = 66$ (9). FLEC, $n = 72$ (6); FLEC, 1.5 Hz $n = 68$ (10); 2.5 Hz = 62 (9).

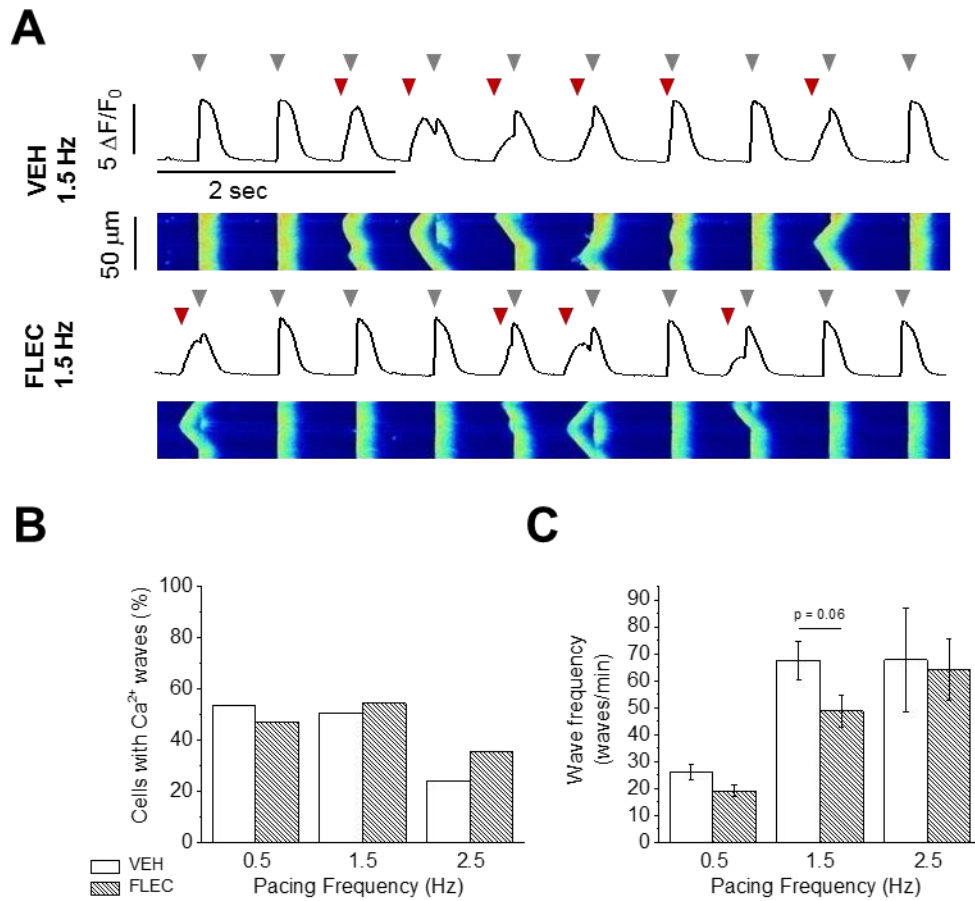


Figure 3.9: The effect of flecainide on Ca^{2+} wave frequency during field stimulation in cardiomyocytes superfused with 100 nM isoprenaline

A) Representative line scans and fluorescence profiles of vehicle (VEH) and flecainide (FLEC) treated cells during 1.5 Hz field stimulation. Grey triangles indicated field stimulation pulses and red triangles indicated the start of a Ca^{2+} wave. **B)** Percentage of cells exhibiting Ca^{2+} waves during field stimulation. **C)** Frequency of Ca^{2+} waves during field stimulation. Only cells exhibiting Ca^{2+} waves during field stimulation were included. N-1 chi-squared test or two tailed unpaired Student's t-tests. VEH, 0.5 Hz n = 71 (6); VEH, 1.5 Hz n = 67 (10); VEH, 2.5 Hz n = 66 (9). FLEC, 0.5 Hz n = 72 (6); FLEC, 1.5 Hz n = 68 (10); FLEC, 2.5 Hz n = 62 (9).

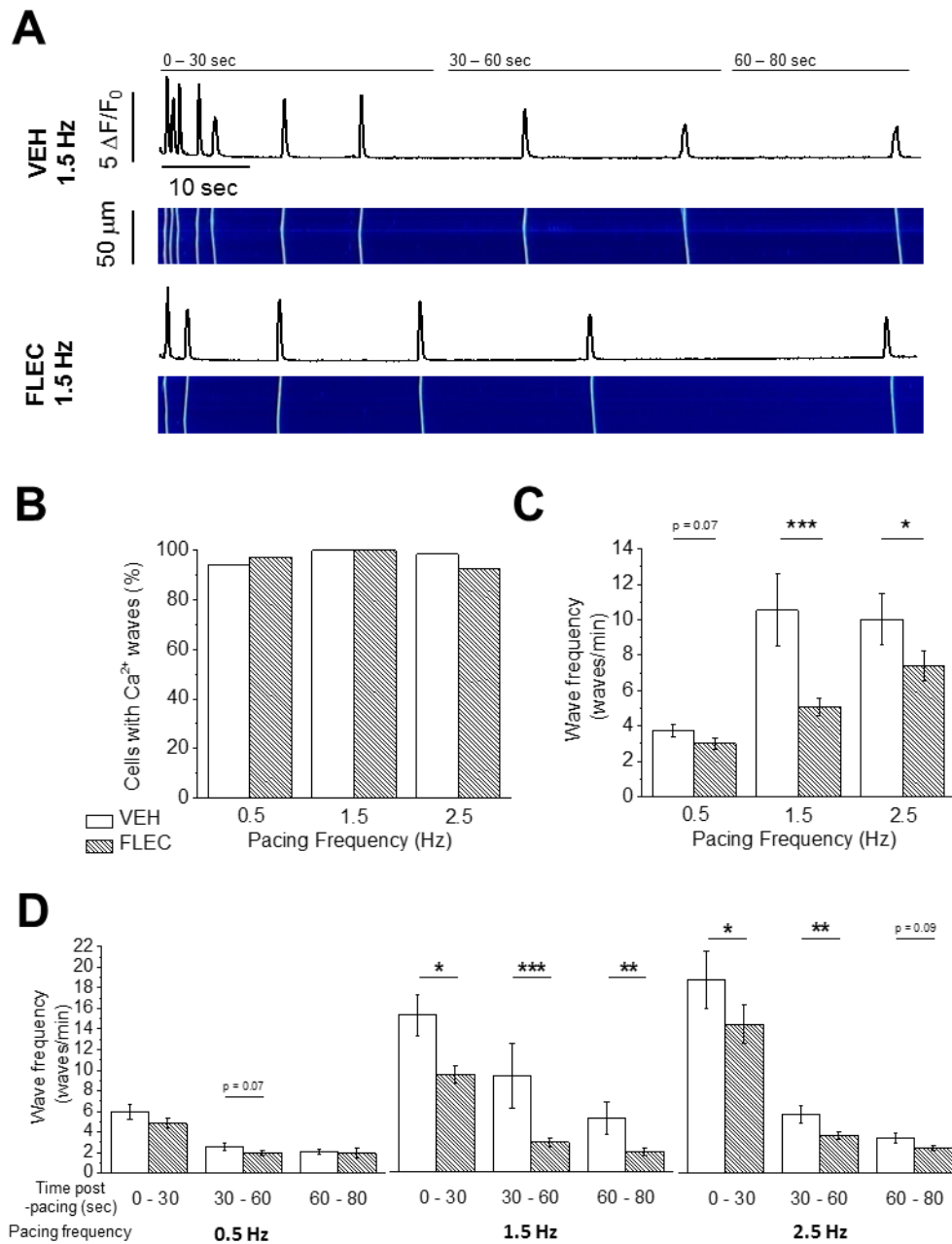


Figure 3.10: The effect of flecainide on Ca^{2+} wave frequency post-pacing in cardiomyocytes superfused with 100 nM isoprenaline

A) Representative line scans and fluorescence profiles of vehicle (VEH) and flecainide (FLEC) treated cells after 1.5 Hz stimulation **B)** Percentage of cells exhibiting Ca^{2+} waves after 0.5, 1.5 or 2.5 Hz field stimulation **C)** Frequency of Ca^{2+} waves **D)** Frequency of Ca^{2+} waves at 0-30 sec, 30-60 sec and 60-80 sec post-pacing. N-1 chi-squared test or two tailed unpaired Student's t-tests. * = $p < 0.05$; ** = $p < 0.01$; *** = $p < 0.001$. VEH, 0.5 Hz $n = 71$ (6); VEH, 1.5 Hz = 67 (10); VEH, 2.5 Hz = 66 (9). FLEC, 0.5 Hz $n = 72$ (6); FLEC, 1.5 Hz = 68 (10); FLEC, 2.5 Hz = 62 (9).

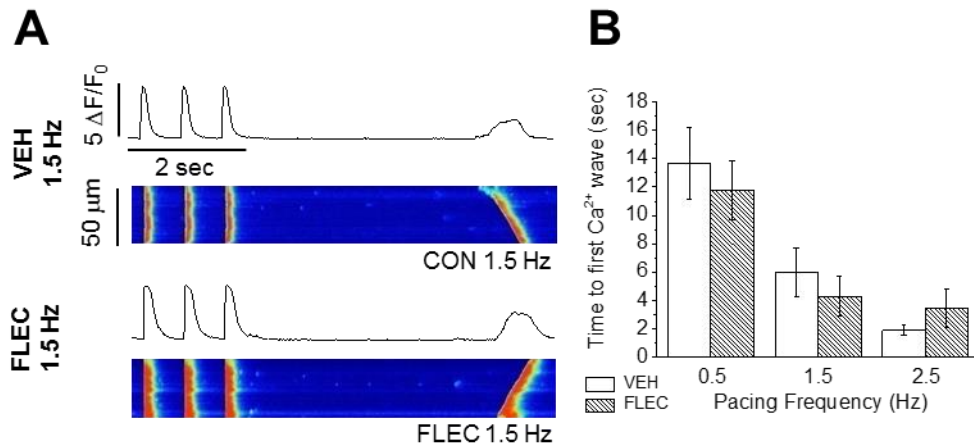


Figure 3.11: The effect of flecainide on the time between the last triggered field stimulation and the first Ca^{2+} wave in cardiomyocytes superfused with 100 nM isoprenaline

A) Representative line scans and fluorescence profiles of vehicle (VEH) and flecainide (FLEC) treated cells immediately after 1.5 Hz stimulation. **B)** The time between the last triggered field-stimulation and first Ca^{2+} wave in cells field stimulated at 0.5, 1.5 and 2.5 Hz, with or without 15 μM flecainide. Two tailed unpaired Student's t-tests. VEH, 0.5 Hz n = 71 (6); VEH, 1.5 Hz = 67 (10); VEH, 2.5 Hz = 66 (9). FLEC, 0.5 Hz n = 72 (6); FLEC, 1.5 Hz n = 68 (10); FLEC, 2.5 Hz n = 62 (9).

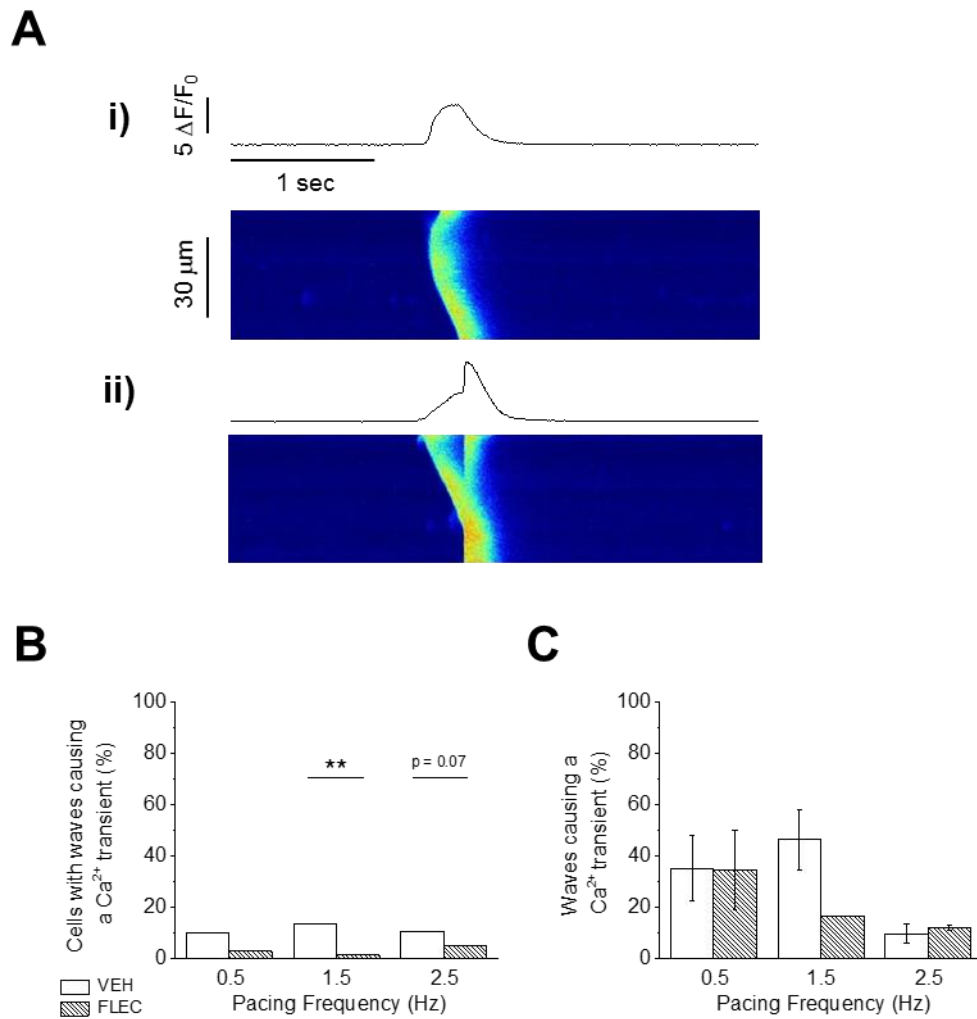


Figure 3.12: The effect of flecainide on the occurrence spontaneous Ca^{2+} transients in cardiomyocytes superfused with 100 nM isoprenaline

A) Representative line scans and fluorescence profiles illustrating the differences between **i)** a Ca^{2+} wave and **ii)** a Ca^{2+} wave which triggers a synchronous Ca^{2+} transient **B)** Percentage of vehicle (VEH) or flecainide (FLEC) treated cells exhibiting spontaneous Ca^{2+} transients **C)** Percentage of Ca^{2+} waves which caused a spontaneous Ca^{2+} transient. Only cells exhibiting this phenomenon were included. N-1 chi-squared test or two tailed unpaired Student's t-test. ** = $p < 0.01$. VEH, 0.5 Hz $n = 71$ (6); VEH, 1.5 Hz $n = 67$ (10); VEH, 2.5 Hz $n = 66$ (9). FLEC, 0.5 Hz $n = 72$ (6); FLEC, 1.5 Hz $n = 68$ (10); FLEC, 2.5 Hz $n = 62$ (9).

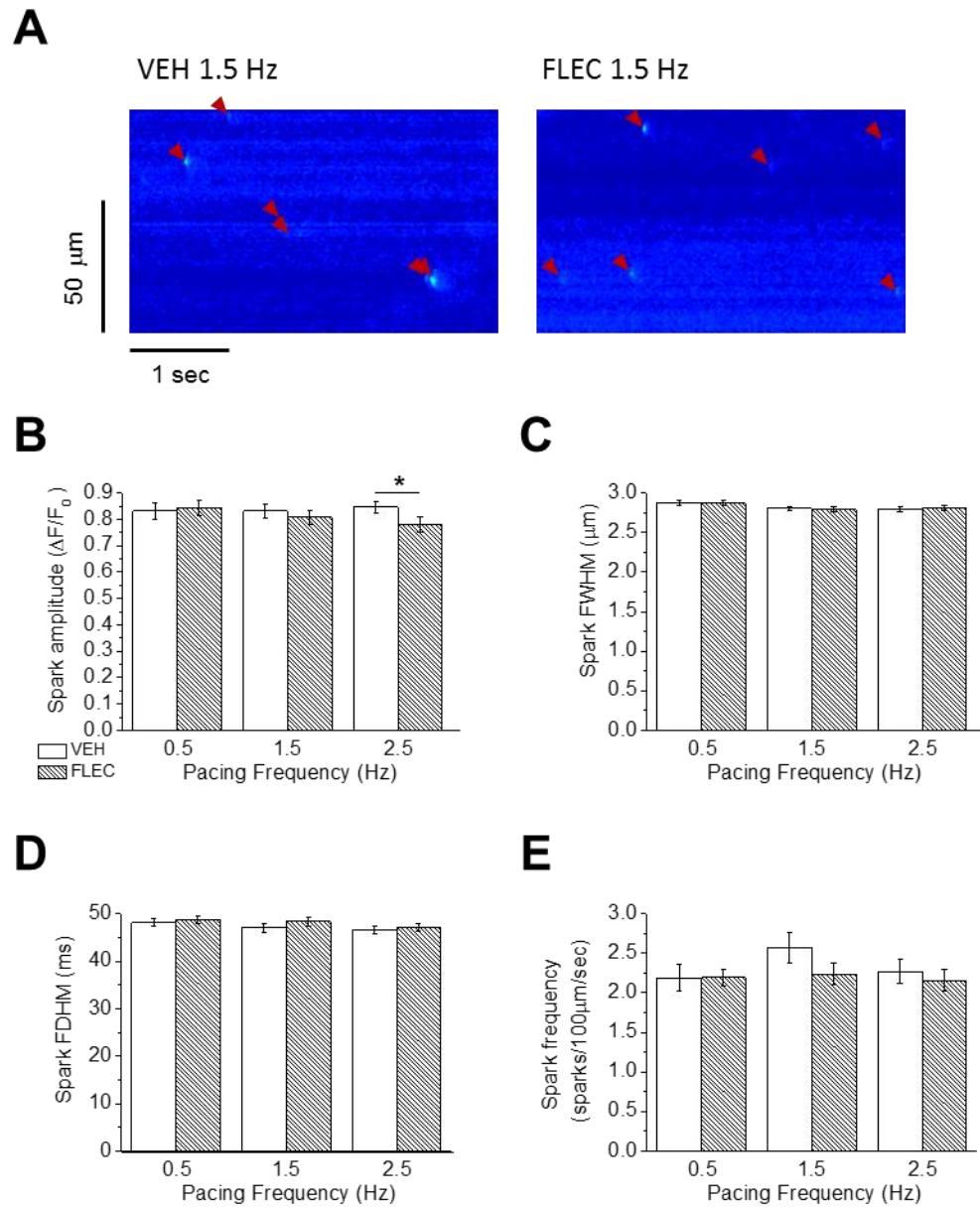


Figure 3.13: The effect of flecainide on spark properties in cardiomyocytes superfused with 100 nM isoprenaline

A) Representative line scans of sparks from vehicle (VEH) and flecainide (FLEC) treated cells after field stimulation at 1.5 Hz. Red triangles indicate sparks identified by Sparkmaster. **B)** Mean data for spark amplitude, **C)** spark FWHM, **D)** spark FDHM and **E)** spark frequency. Two tailed unpaired Student's t-test. VEH, 0.5 Hz n = 61 (6); VEH, 1.5 Hz n = 60 (10); VEH, 2.5 Hz n = 62 (8). FLEC, 0.5 Hz n = 64 (6); FLEC, 1.5 Hz n = 65 (10); FLEC, 2.5 Hz n = 54 (8).

3.3.6 The effect of flecainide after a 2 hour incubation period, including 35 min at 37°C

Flecainide significantly decreased post-pacing Ca^{2+} wave frequency; however, a significant effect of flecainide on sparks was not apparent. As will be elaborated upon in the Discussion, these results are indicative of flecainide inhibition of sarcolemmal $\text{Na}_v1.5$, rather than an effect on RyR2, located at the SR membrane. To facilitate flecainide entry into the cell, the previous experiments were repeated with an increased incubation period of 2 hours, including 35 min at 37 °C. In the following experiments, cells were paced at 1.5 Hz only.

During field stimulation at 1.5 Hz, ~30% of vehicle or flecainide treated cells exhibited spontaneous Ca^{2+} waves ($p > 0.05$; Figure 3.14 A). Of these cells, Ca^{2+} wave frequency was ~65 waves/min within each experimental group ($p > 0.05$; Figure 3.14 B). Interestingly, <10% of cells displayed missing or disrupted Ca^{2+} transients during pacing within each experimental group ($p > 0.05$; Figure 3.14 C) and of these cells, 20-30% of Ca^{2+} transients were missing or disrupted in each experimental group ($p > 0.05$; Figure 3.14 D). Post-pacing, Ca^{2+} waves were apparent in 100% and 92.3% of vehicle and flecainide treated cells respectively (Figure 3.15 A). Flecainide significantly decreased post pacing wave frequency by 36.8% ($p < 0.01$; Figure 3.15 B). This significant decrease in Ca^{2+} wave frequency was apparent at each time point after pacing was stopped (Figure 3.15 C). There was a trend to indicate that flecainide increased the time between the final Ca^{2+} transient and first Ca^{2+} wave ($p = 0.08$; Figure 3.15 D). Only one vehicle treated cell and zero flecainide treated cells exhibited Ca^{2+} waves which initiated a Ca^{2+} transient (Figure 3.15 E and F). Similar to the previous experiments, flecainide did not significantly alter spark amplitude ($p > 0.05$; Figure 3.16 A), FWHM ($p > 0.05$; Figure 3.16 B), FDHM ($p > 0.05$; Figure 3.16 C) or spark frequency ($p > 0.05$; Figure 3.16 D; $n = 25$ cells (VEH, 1.5 Hz); 26 cells (FLEC, 1.5 Hz)).

3.3.7 The effect of flecainide in a monocrotaline model of heart failure

The spontaneous releases of Ca^{2+} waves and sparks were compared between cardiomyocytes isolated from the MCT model of right-sided heart failure and cardiomyocytes isolated from CON rat. In cells from the MCT model, 67% of cells displayed Ca^{2+} waves during field stimulation, compared with 50% of CON cells (Figure 3.17 A). Of the cells that exhibited wave behaviour during field stimulation, there was no significant difference in wave frequency between these groups ($p > 0.05$; Figure 3.17 B). Ca^{2+} transients, caused by field stimulation

pulses were disrupted in ~4% of WT cells and zero MCT cells (Figure 3.17 C and D). In both groups, all cells exhibited Ca^{2+} waves post-pacing (Figure 3.18 A). However wave frequency was significantly increased in the MCT model, compared with CON cells (~136% increase, $p < 0.05$, Figure 3.18 B). This difference was apparent at all time points post-pacing ($p < 0.05$, Figure 3.18 C). There was a trend for the time between the final field stimulation Ca^{2+} transient and first spontaneous Ca^{2+} wave to decrease in the MCT model, however this was not significant ($p > 0.05$; Figure 3.18 D). MCT cells displayed spontaneous Ca^{2+} transients arising from a Ca^{2+} wave in 77.8% of cells, an almost 6 fold significant increase when compared with CON vehicle treated cells ($p < 0.05$, Figure 3.18 E). Despite this, when only affected cells were measured, the frequency of waves which became Ca^{2+} transients was comparable between MCT and CON cells ($p > 0.05$, Figure 3.18 F). Spark parameters in MCT and CON cells were compared (Figure 3.19). No significant differences in spark amplitude or FWHM were apparent between MCT and CON cells ($p > 0.05$, Figure 3.19 A and B). There was a trend for spark duration to increase in MCT cells ($p < 0.1$, Figure 3.19 C) however there was no significant difference in spark frequency between MCT and CON groups ($p > 0.05$, Figure 3.19 D).

The effect of flecainide on Ca^{2+} waves and sparks was investigated in MCT cells through repetition of experiments documented in Section 3.3.3 – 3.3.5. During field stimulation at 1.5 Hz, ~66% of vehicle or flecainide treated cells exhibited spontaneous Ca^{2+} waves (Figure 3.20 A). Of these cells, Ca^{2+} wave frequency was ~55 waves/min within each experimental group ($p > 0.05$; Figure 3.20 B). Response to electrical stimulation was disrupted in zero vehicle treated cells and two flecainide treated cells (Figure 3.20 C and D). All cells displayed Ca^{2+} waves after pacing was stopped (Figure 3.21 A). Flecainide significantly decreased Ca^{2+} wave frequency by 65.3% ($p < 0.05$; Figure 3.21 B). This decrease in wave frequency was significant at each post-pacing time point ($p < 0.05$; Figure 3.21 C). There was no significant difference between vehicle and flecainide treated cells in the time between the final triggered Ca^{2+} transient and the first Ca^{2+} wave ($p > 0.05$; Figure 3.21 D). Vehicle treated MCT cells displayed spontaneous Ca^{2+} transients arising from a Ca^{2+} wave in 77.8% of cells (Figure 3.21 E). This was an almost 6 fold increase when compared with WT vehicle treated cells (Figure 3.12 B). Only 43.8 % of MCT flecainide treated cells displayed this phenomenon ($p < 0.05$; Figure 3.21 E). Of these cells, flecainide did not alter the total amount of Ca^{2+} waves affected ($p > 0.05$; Figure 3.21 F). Flecainide did not change spark amplitude ($p > 0.05$; Figure 3.22 A), FWHM ($p > 0.05$; Figure 3.22 B), FDHM ($p > 0.05$; Figure 3.22 C) or spark frequency ($p > 0.05$; Figure 3.22 D; $n = 18$ cells (VEH, 1.5 Hz); 16 cells (FLEC, 1.5 Hz)).

3.3.8 The effect of flecainide on the cardiac peak Na⁺ current

Peak I_{Na} was recorded in ventricular cardiomyocytes in the presence and absence of 20 μ M flecainide by Dr M Al Owais (Figure 3.23). After 8 min, flecainide decreased peak I_{Na} by $73.0 \pm 2.36\%$ (Figure 3.23 B and C). Partial recovery of the peak I_{Na} to $55.6 \pm 8.15\%$ of the control current was apparent after 8 min of flecainide wash out (Figure 3.23 B and C; n = 4 cells).

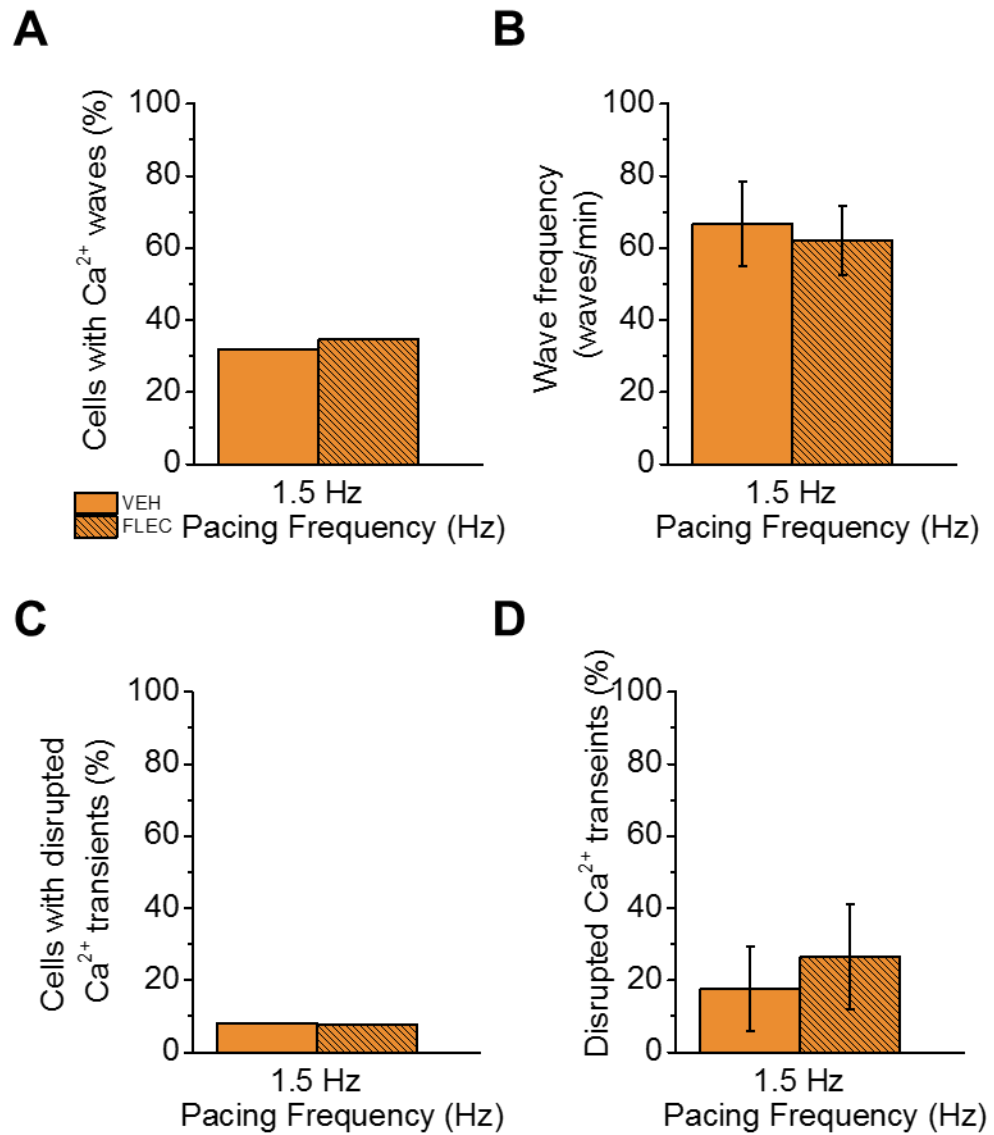


Figure 3.14: The effect of flecainide on Ca²⁺ waves during 1.5 Hz field stimulation after 2 hours of incubation, including 25 min at 37 °C in cardiomyocytes superfused with 100 nM isoprenaline **A)** Percentage of vehicle (VEH) and flecainide (FLEC) treated cells exhibiting Ca²⁺ waves during field stimulation. **B)** Frequency of Ca²⁺ waves during field stimulation **C)** Percentage of cells with disrupted Ca²⁺ transients **D)** Percentage of disrupted Ca²⁺ transients. Only cells exhibiting this phenomenon were included. N-1 chi-squared test or two tailed unpaired Student's t-test. VEH n = 25 (4); FLEC n = 26 (4).

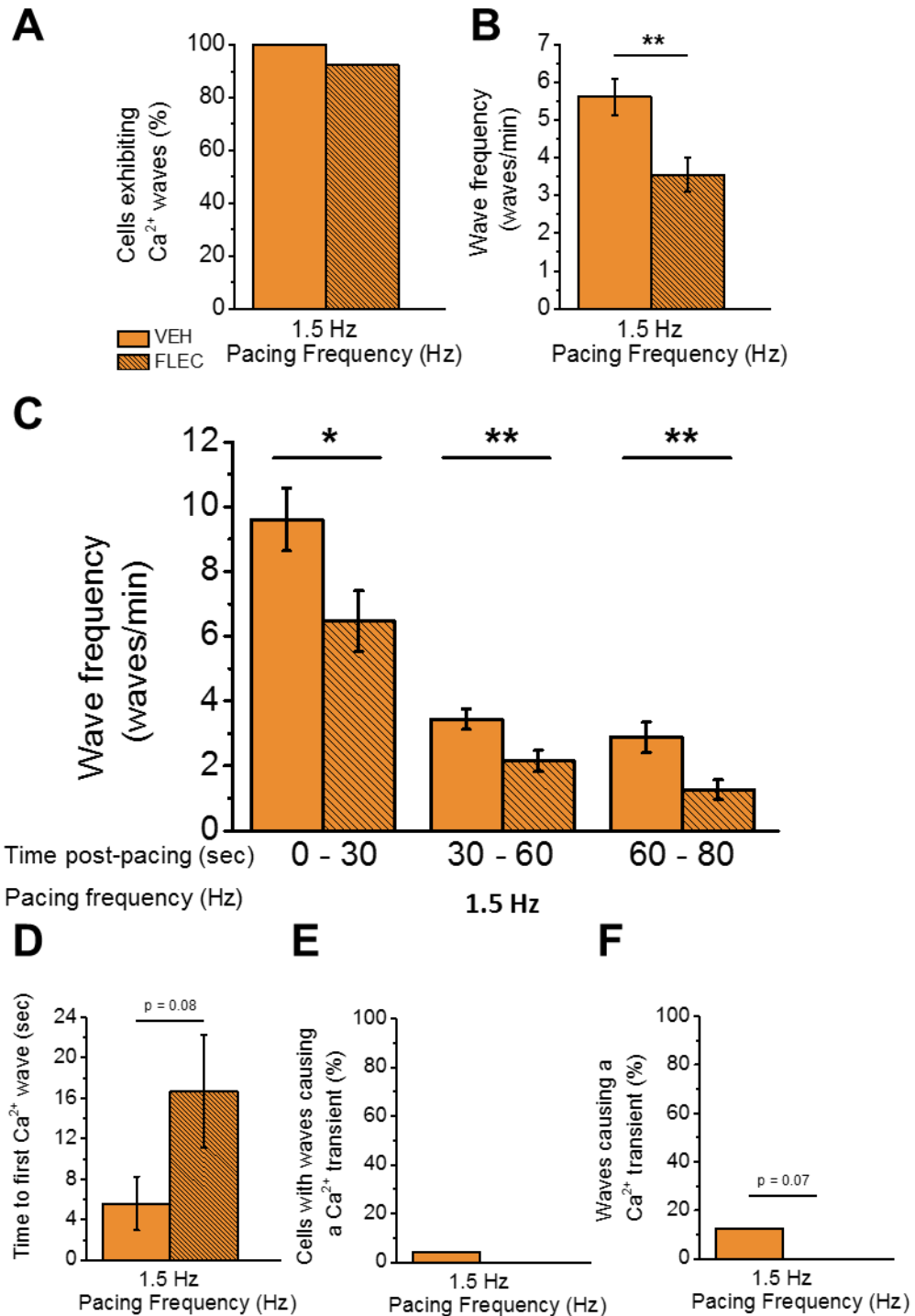


Figure 3.15: The effect of flecainide on Ca^{2+} waves after 1.5 Hz field stimulation stopped and after 2 hours of incubation, including 25 min at 37 °C in cardiomyocytes superfused with 100 nM isoprenaline

A) Percentage of vehicle (VEH) and flecainide (FLEC) treated cells exhibiting Ca^{2+} waves **B)** Frequency of Ca^{2+} waves after 1.5 Hz field stimulation stopped. **C)** Frequency of Ca^{2+} waves at 0-30 sec, 30-60 sec and 60-90 sec after field stimulation stopped **D)** Time between the last triggered field-stimulation and first Ca^{2+} wave **E)** Percentage of cells triggering spontaneous Ca^{2+} transients **F)** Percentage of Ca^{2+} waves that triggered spontaneous Ca^{2+} transients. N-1 chi-squared test or two tailed unpaired Student's t-test. * = $p < 0.05$; ** = $p < 0.01$. VEH n = 25 (4); FLEC n = 26 (4).

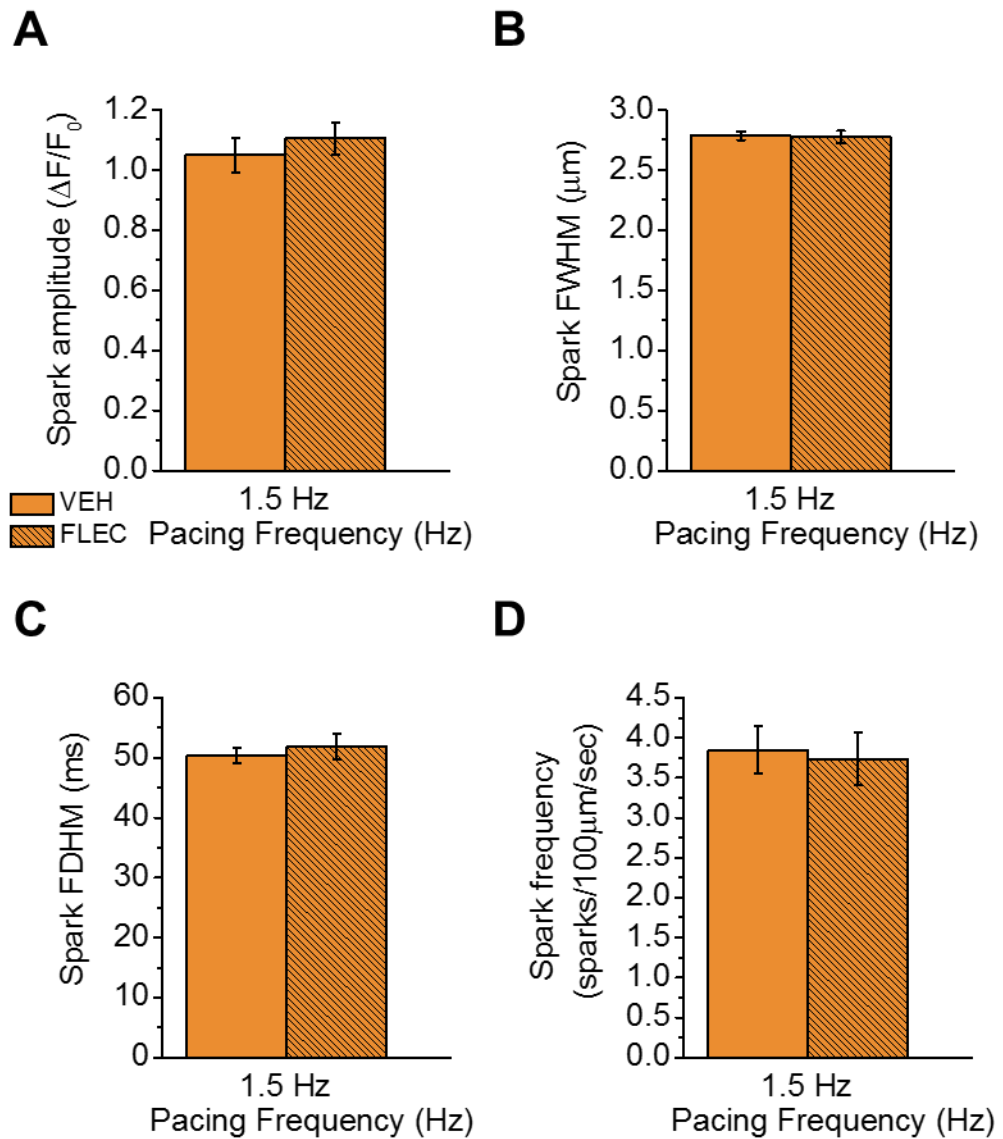


Figure 3.16: The effect of flecainide on spark properties after 2 hours of incubation, including 25 min at 37 °C in cardiomyocytes superfused with 100 nM isoprenaline
A) Mean data for spark amplitude, **B)** spark FWHM, **C)** spark FDHM, **D)** or spark frequency in vehicle (VEH) and flecainide (FLEC) treated cells. Two-tailed unpaired Student's t-test. CON n = 25 (4); FLEC n = 26 (4).

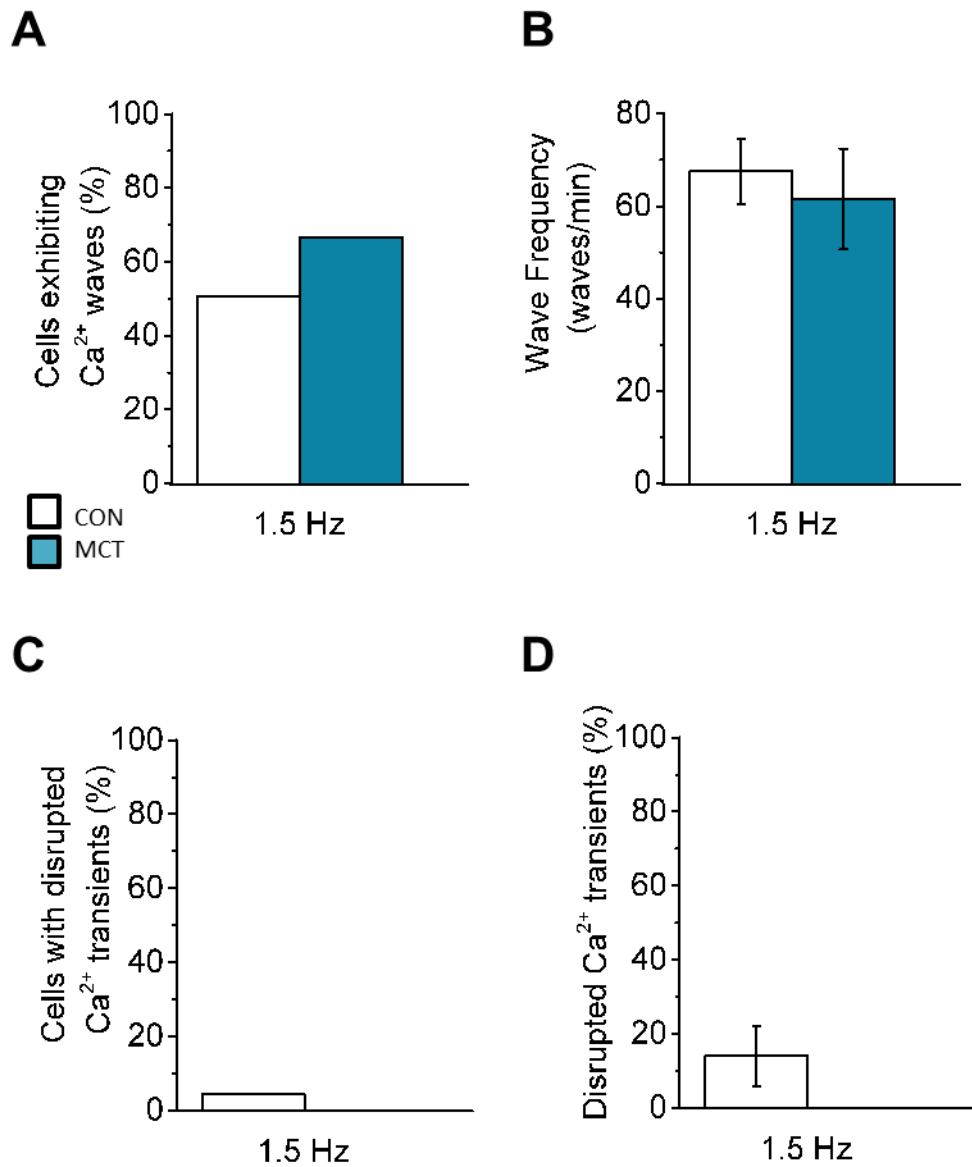


Figure 3.17: The effect of MCT induction of HF in Ca²⁺ waves and Ca²⁺ transients during 1.5 Hz field stimulation, superfused with 100 nM isoprenaline

A) Percentage of CON (white) and MCT (blue) cells exhibiting Ca²⁺ waves during 1.5 Hz field stimulation. **B)** Frequency of Ca²⁺ waves during 1.5 Hz field stimulation. **C)** Percentage of cells with disrupted Ca²⁺ transients **D)** Percentage of disrupted Ca²⁺ transients. Only cells displaying this phenomena were included. N-1 chi-squared test or two tailed unpaired Student's t-test. CON n = 67 (10); MCT n = 18 (3).

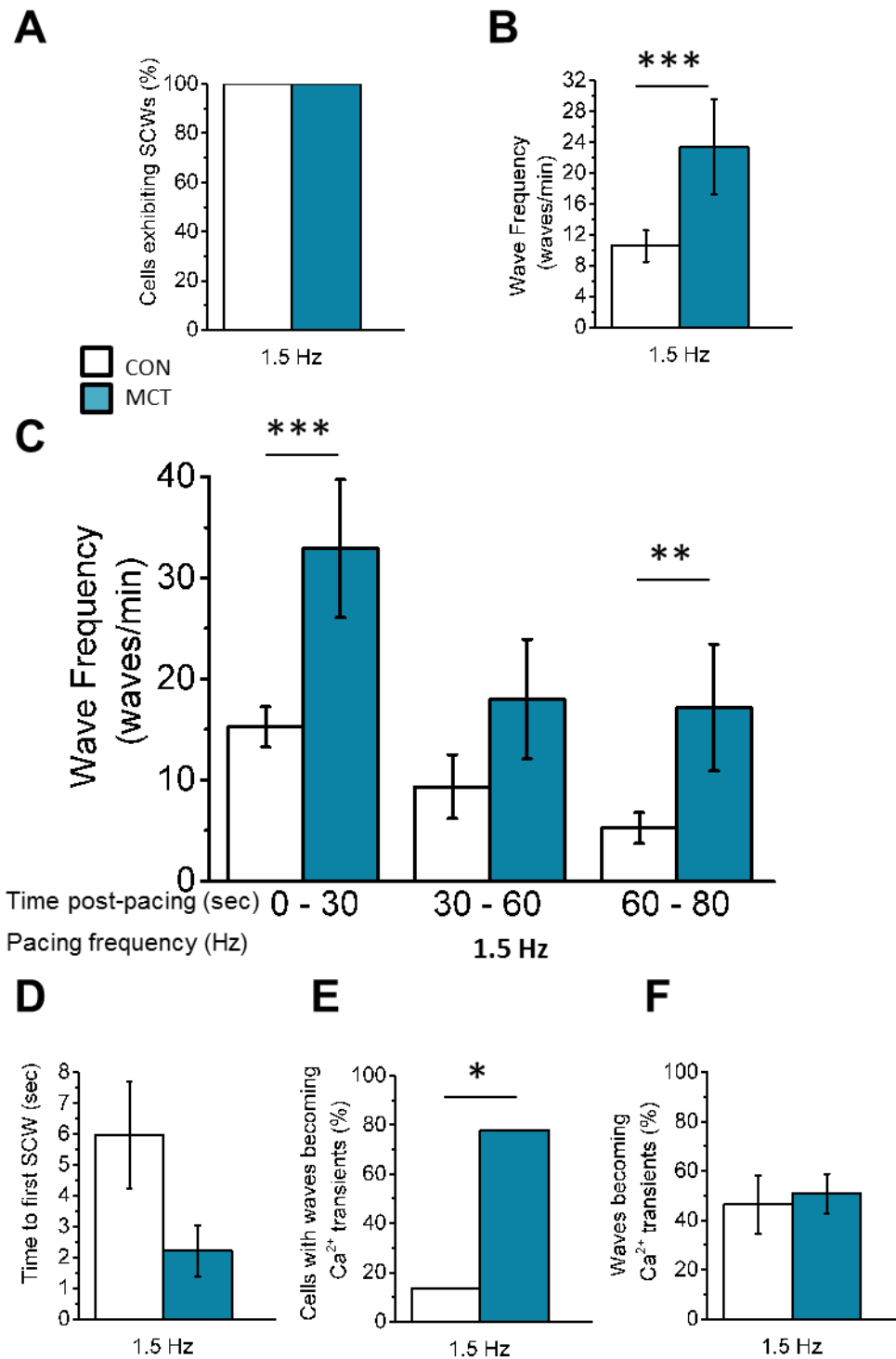


Figure 3.18: The effect of MCT induction of HF on Ca²⁺ waves and Ca²⁺ transients after 1.5 Hz field stimulation, superfused with 100 nM isoprenaline

A) Percentage of CON (white) and MCT (blue) cells exhibiting Ca²⁺ waves **B)** Frequency of Ca²⁺ waves after 1.5 Hz field stimulation was stopped. **C)** Frequency of Ca²⁺ waves at 0-30 sec, 30-60 sec and 60-90 sec post pacing **D)** Time between the last triggered field-stimulation and first Ca²⁺ wave **E)** Percentage of cells triggering spontaneous Ca²⁺ transients **F)** Percentage of Ca²⁺ waves that triggered spontaneous Ca²⁺ transients. N-1 chi-squared test or two tailed unpaired Student's t-test. * = p < 0.05. CON n = 67 (10); MCT n = 18 (3).

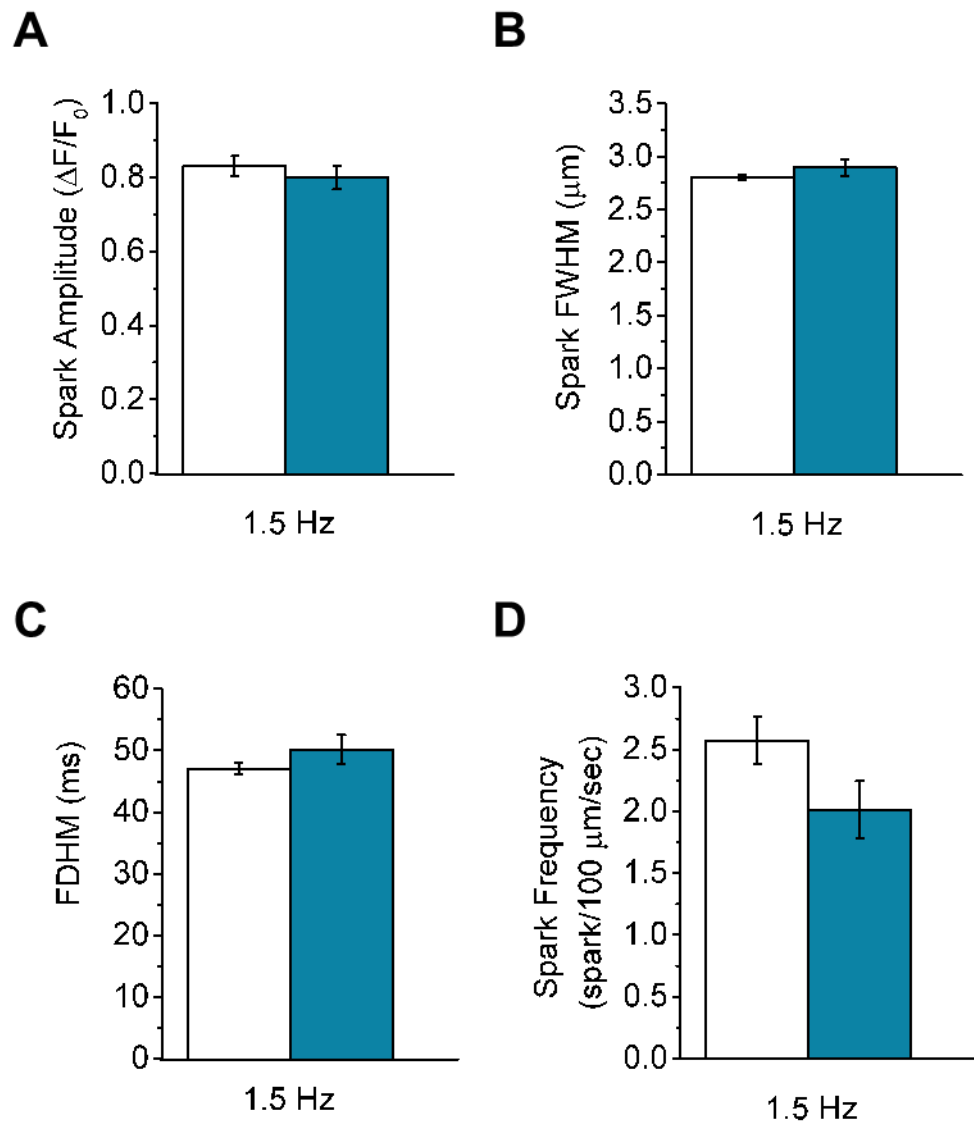


Figure 3.19: The effect of MCT induction of HF on spark size and frequency after 1.5 Hz field stimulation and superfused with 100 nM isoprenaline

A) Comparing CON (white) and MCT (blue) mean data for spark amplitude, **B)** spark FWHM, **C)** spark FDHM, **D)** or spark frequency. Two-tailed unpaired Student's t-test. CON n = 67 (10); MCT n = 18 (3).

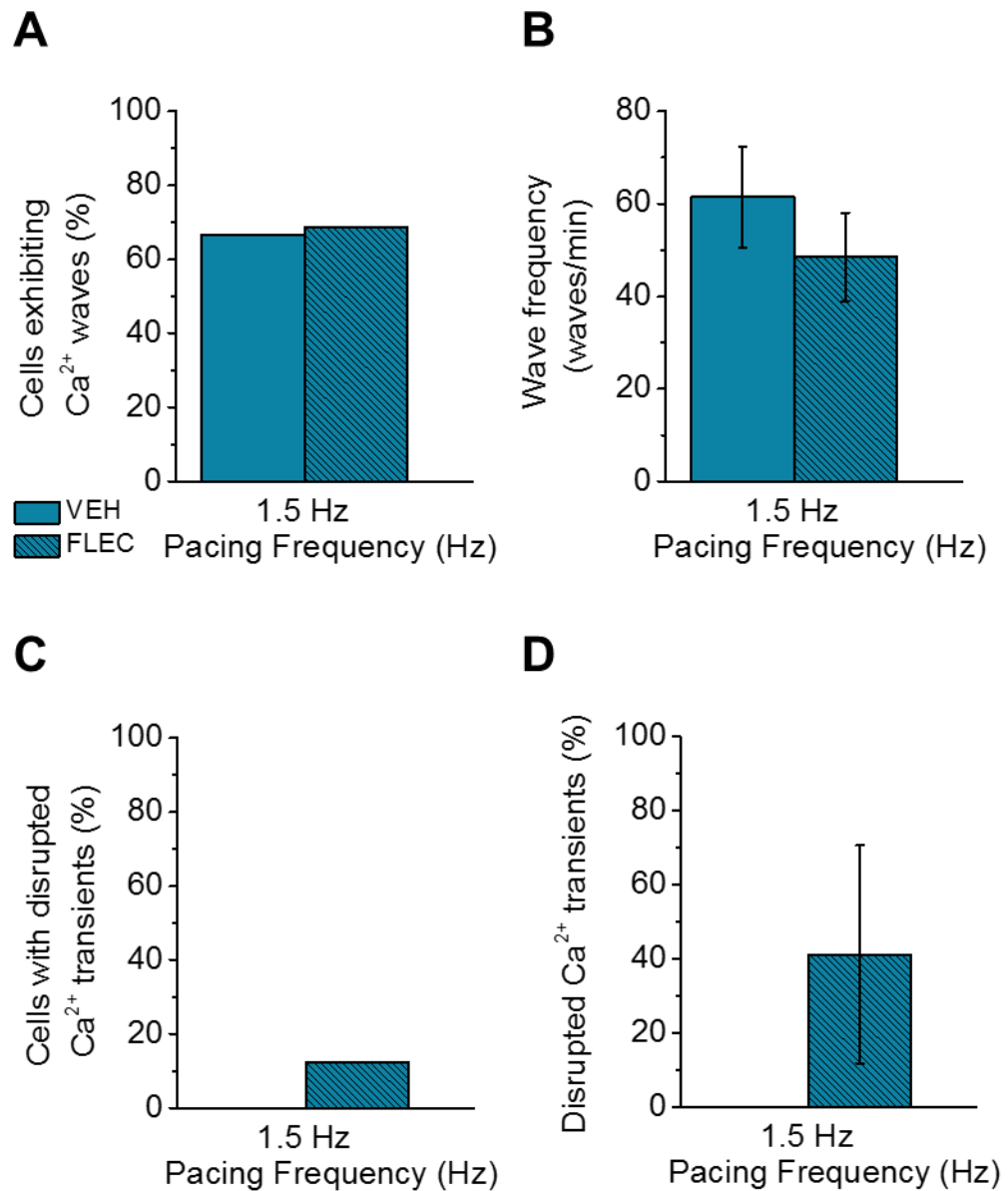


Figure 3.20: The effect of flecainide on Ca^{2+} waves and Ca^{2+} transients during 1.5 Hz field stimulation in cells from a MCT model of HF and superfused with 100 nM isoprenaline
A) Percentage of vehicle (VEH) and flecainide (FLEC) treated MCT cells exhibiting Ca^{2+} waves during 1.5 Hz field stimulation. **B)** Frequency of Ca^{2+} waves during 1.5 Hz field stimulation. **C)** Percentage of cells with disrupted Ca^{2+} transients **D)** Percentage of disrupted Ca^{2+} transients. Only cells displaying this phenomena were included. N-1 chi-squared test or two tailed unpaired Student's t-test. VEH n = 18 (3); FLEC n = 16 (3).

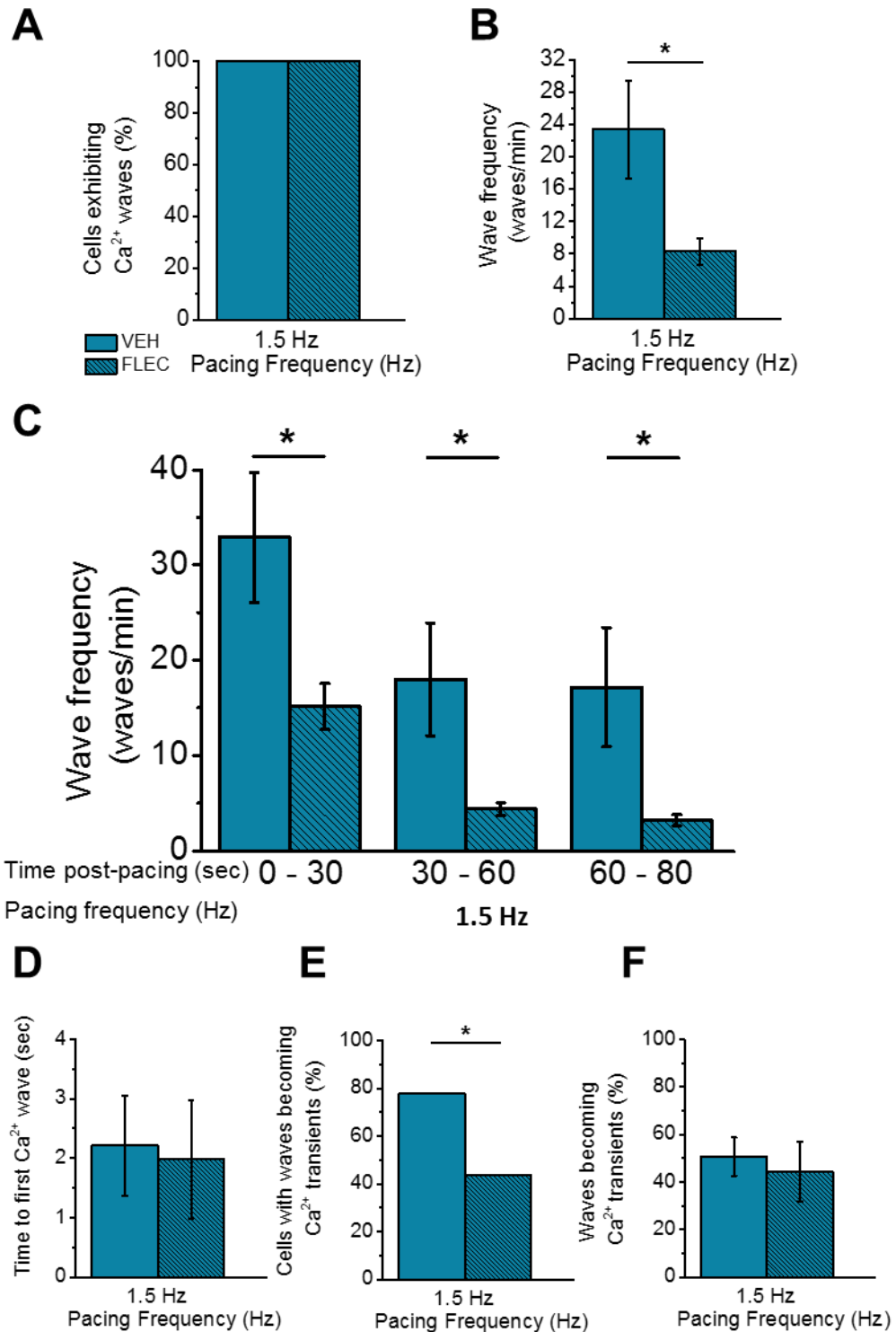


Figure 3.21: The effect of flecainide on Ca²⁺ waves and Ca²⁺ transients after 1.5 Hz field stimulation in cells from a MCT model of HF and superfused with 100 nM isoprenaline

A) Percentage of vehicle (VEH) and flecainide (FLEC) treated cells exhibiting Ca²⁺ waves **B)** Frequency of Ca²⁺ waves after 1.5 Hz field stimulation was stopped. **C)** Frequency of Ca²⁺ waves at 0-30 sec, 30-60 sec and 60-90 sec post pacing **D)** Time between the last triggered field-stimulation and first Ca²⁺ wave **E)** Percentage of cells triggering spontaneous Ca²⁺ transients **F)** Percentage of Ca²⁺ waves that triggered spontaneous Ca²⁺ transients. N-1 chi-squared test or two tailed unpaired Student's t-test. * = p < 0.05. VEH n = 18 (3); FLEC n = 16 (3).

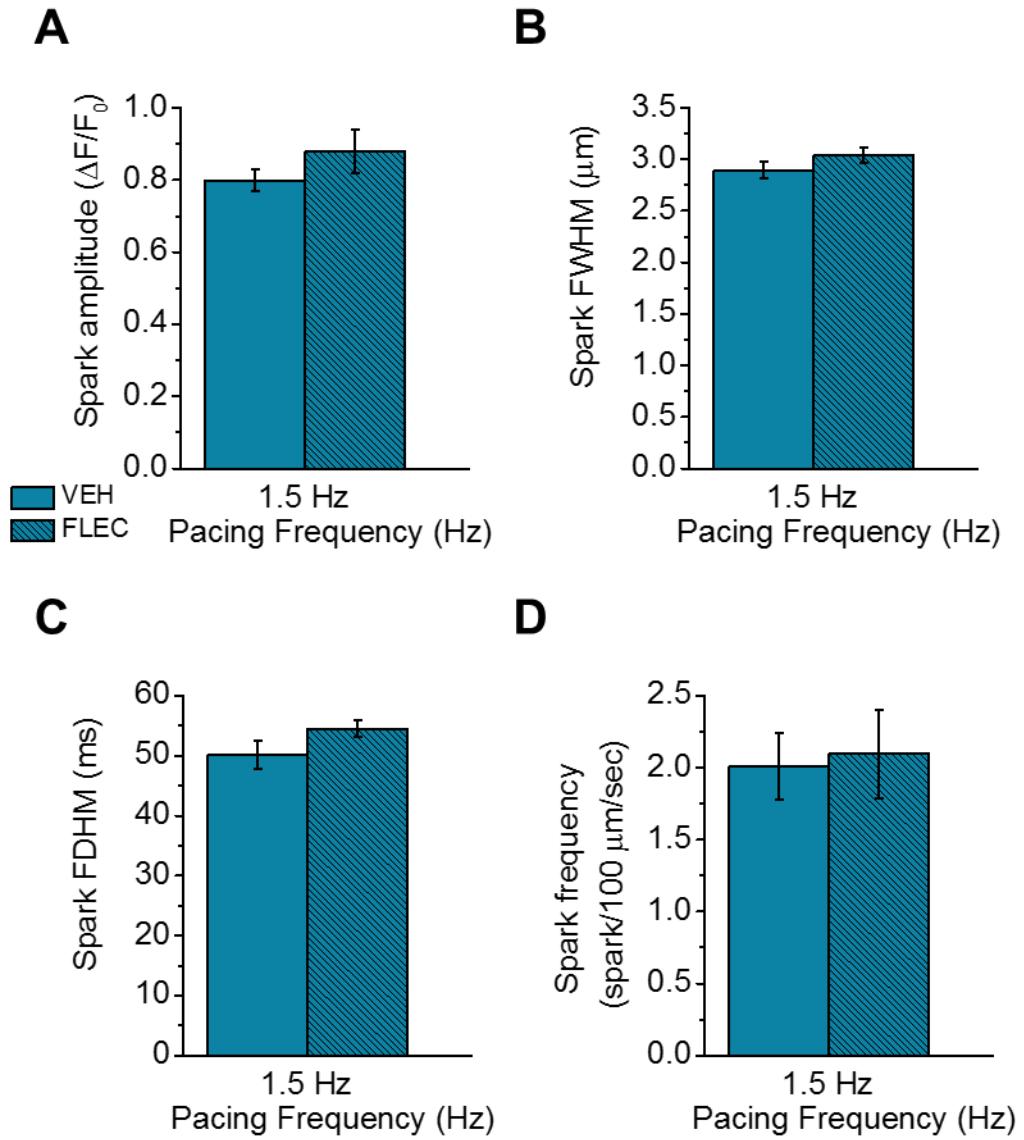


Figure 3.22: The effect of flecainide on spark size and frequency after 1.5 Hz field stimulation in cells from a MCT model of HF and superfused with 100 nM isoprenaline
A) Mean data for spark amplitude, **B)** spark FWHM, **C)** spark FDHM, **D)** or spark frequency in vehicle (VEH) and flecainide (FLEC) treated cells. Two-tailed unpaired Student's t-test. VEH n = 18 (3); FLEC n = 16 (3).

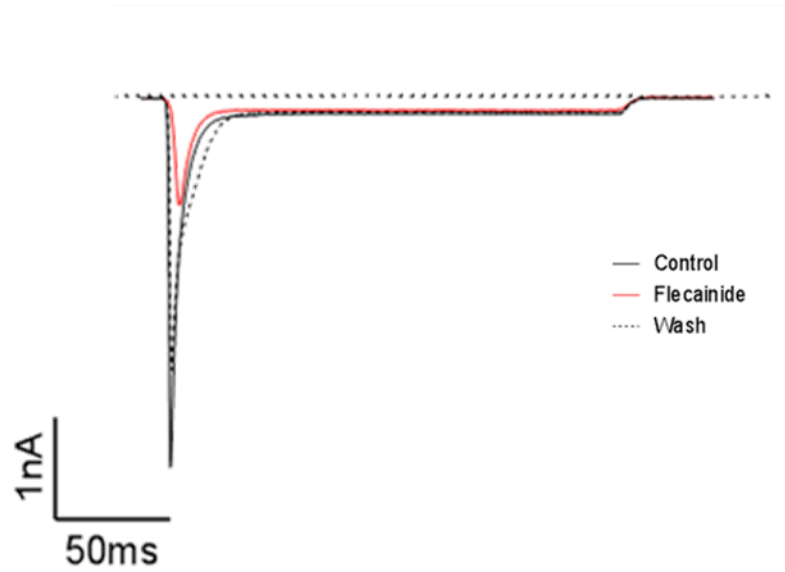
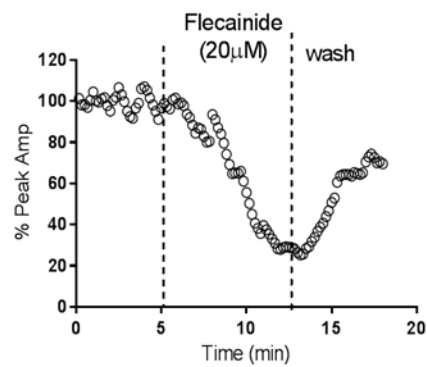
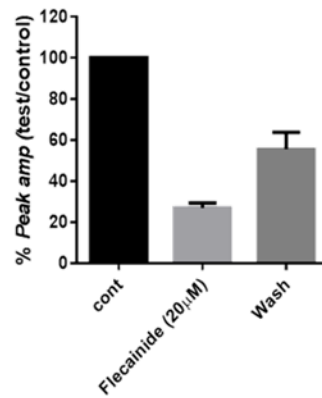
A**B****C**

Figure 3.23: The effect of flecainide on the peak cardiac Na⁺ current using patch clamp recording
A) Representative recordings of the peak Na⁺ current under control (CON, black) and flecainide treated (FLEC, red) conditions. **B)** Changes in Na⁺ peak amplitude over time in one cell. **C)** Mean data showing peak amplitude upon flecainide application and wash out. n = 4 (1). Patch clamp recordings by Dr M Al Owais.

3.4 Discussion

3.4.1 The effects of isoprenaline on Ca^{2+} wave and spark release

Isolated rat ventricular myocytes were electrically paced and perfused with isoprenaline to induce Ca^{2+} waves and mimic the conditions that precipitate arrhythmias in CPVT patients. Isoprenaline mimics the actions and effects of the endogenous sympathetic neurotransmitter noradrenaline and the circulating catecholamine, adrenaline (Weitl and Seifert, 2008). Isoprenaline binds to β_1 and, to a lesser extent, β_2 adrenoceptors at the sarcolemma to initiate the $\text{G}\alpha_s$ stimulatory G-protein coupled receptor signalling pathway (Ponick et al., 2003). The $\text{G}\alpha$ subunit coupled to the adrenoceptor translocates to sarcolemmal bound adenylyl cyclase to catalyse the production of cAMP from ATP (Calaghan et al., 1998). In turn, cAMP removes the PKA regulatory subunits, activating PKA and resulting in numerous downstream cellular effects (Negash et al., 2000, Kentish et al., 2001, Ullrich et al., 2012, Houser, 2014, Calaghan et al., 1998).

PKA mediated phosphorylation increases LTCC mediated I_{Ca} to increase cytosolic $[\text{Ca}^{2+}]$, which in turn increases Ca^{2+} activation of the RyR2 at its cytosolic face. SR Ca^{2+} release is increased in the form of sparks and waves (Farkas et al., 2012, Viatchenko-Kapinski and Gyorke, 2001, Bovo et al., 2011). Notably, PKA phosphorylates PLB, (Frank et al., 2000, Li et al., 2002), inducing SR Ca^{2+} overload, such that the SR Ca^{2+} content exceeds the threshold for Ca^{2+} wave formation (Domeier et al., 2012, Kashimura et al., 2010). Additionally, PKA can directly phosphorylate RyR2 at serine (2808). This has been reported to alter SR luminal Ca^{2+} sensing via dissociation of the RyR2 modulatory protein FKBP12.6 (Marx et al., 2000, Ullrich et al., 2012). However, other groups have reported that β -adrenergic mediated RyR2 phosphorylation remains independent of PKA and is instead facilitated by CAMKII (Li et al., 2002, Curran et al., 2007, Ogrodnik and Niggli, 2010) or isoprenaline may also activate CAMKII via PKA (for review see (Grimm and Brown, 2010)). It is a combination of these simultaneous cellular effects of isoprenaline that give rise to the increased incidence of pro-arrhythmic Ca^{2+} waves both during and immediately after electrical pacing. In the present study, isoprenaline increased post-pacing wave frequency in the first 30 sec post-pacing only; thereafter, no difference in spontaneous wave frequency was apparent. In this quiescent period (>30 sec post-pacing) it may be that SR Ca^{2+} overload was reduced due to decreased CAMKII phosphorylation of PLB (Bassani et al., 1995b, Hagemann et al., 2000) and a slow loss of SR Ca^{2+} (Bassani et al., 1995a).

Published results on Ca^{2+} sparks in the presence of β -adrenergic stimulation are contradictory. In one report, isoprenaline did not affect spark amplitude (Santiago et al., 2013). Yet similarly

to the current results, spark amplitude was also found to be increased with isoprenaline (Gomez et al., 1996, Li et al., 2002), potentially due to an increased SR Ca^{2+} load (Zima et al., 2010, Li et al., 2002). It was anticipated that isoprenaline would induce an increase in the frequency of Ca^{2+} sparks due to the SR Ca^{2+} content induced by pacing and β -adrenergic stimulation (Ogrodnik and Niggli, 2010, Santiago et al., 2013, Li et al., 2002). However, in the current experiments, spark frequency did not change significantly in the presence of isoprenaline. An increase in spark width and duration has been reported (Santiago et al., 2013) due to an increased RyR2 sensitivity to Ca^{2+} (Santiago et al., 2013) or increased SR content (Zima et al., 2010). Contradictory to this, isoprenaline was also reported to decrease spark width and duration due to the increased SERCA uptake of Ca^{2+} limiting Ca^{2+} propagation (Gomez et al., 1996). Under the conditions of the present study, isoprenaline did not significantly change spark width and significantly decreased duration.

One possible explanation for these results may be that increased SERCA uptake decreases spark duration but in doing so increases SR Ca^{2+} content and spark amplitude (Gomez et al., 1996). Selectively analysing sparks immediately prior to a wave might have ensured that spark width was maximal and that any wider spark would tend to initiate a wave in both control and isoprenaline treated cells. Indeed, spark FWHM reported in this study was $\sim 2.8 \mu\text{m}$ in both control and isoprenaline groups. This was greater than the spark widths reported by Santiago et al. ($\sim 2.5 \mu\text{m}$ in the presence of isoprenaline). Additionally, in the presence of isoprenaline, wave frequency was extremely high and two thirds of cells initiated a Ca^{2+} wave within 1 sec post-pacing. Therefore appropriate analysis of sparks by Sparkmaster was compromised due to the presence of waves and an unstable cell background fluorescence (Picht et al., 2007). It is hypothesised that under these conditions, SR Ca^{2+} release may be so great as to immediately cause the release of Ca^{2+} waves due to the fast spatio-temporal summation of Ca^{2+} sparks (Cheng et al., 1996). This would indicate that Ca^{2+} waves rather than sparks were the predominant form of spontaneous Ca^{2+} release under the current conditions and spark frequency would be difficult to interpret.

This discussion has focussed predominantly upon the effect of isoprenaline when cells were paced at 1.5 Hz. Similar, yet less pronounced effects of isoprenaline on spontaneous Ca^{2+} waves were apparent at 0.5 Hz indicating that the effect of isoprenaline on Ca^{2+} wave frequency is dependent upon pacing frequency. Interestingly however, the increase in spark amplitude and decrease in spark duration was of a similar magnitude between pacing frequencies.

3.4.2 The effects of pacing frequency on Ca²⁺ waves and sparks

An increase in stimulation frequency from 0.5 Hz to 1.5 Hz significantly increased Ca²⁺ wave frequency during and immediately after electrical pacing. This increase in Ca²⁺ wave frequency might reflect an increased diastolic [Ca²⁺] within the cytosol and SR at higher pacing frequencies. Indeed, a positive relationship between cellular Ca²⁺ content and pacing frequency has been reported in rat cardiomyocytes (Layland and Kentish, 1999, Frampton et al., 1991, Baartscheer et al., 2003, Fowler, 2015). This is achieved on a cellular level by increased SR Ca²⁺ load via increased SERCA uptake (Frampton et al., 1991) facilitated by CAMKII phosphorylation of PLB at the threonine (17) site (Hagemann et al., 2000, Gattoni et al., 2016). However, a further increase in pacing frequency to 2.5 Hz did not further increase Ca²⁺ wave frequency. It may be that at 2.5 Hz field stimulation and in the presence of 100 nM isoprenaline, SR Ca²⁺ overload was so great that cells went into hypercontracture. However, physiological heart rates within rat are 5.5-8 Hz indicating instead that in the current cardiomyocytes, the Ca²⁺ frequency relationship may plateau between 1.5 and 2.5 Hz (Szigligeti et al., 1996).

As Ca²⁺ wave frequency increased with increased pacing frequency (0.5 to 1.5 Hz), it was expected that the likely increase in SR Ca²⁺ load would also increase Ca²⁺ spark size or frequency. However, all spark parameters were unchanged with an increase in pacing frequency. As previously discussed (Section 3.4.1), it may be that analysing sparks 1-5 sec prior to the release of a Ca²⁺ wave in the presence of isoprenaline maximised spark size and frequency.

3.4.3 The effects of flecainide on SR Ca²⁺ release

Flecainide increased the proportion of cells that failed to respond to electrical stimulation, at all pacing frequencies. This was particularly apparent at 2.5 Hz whereby 51.6 % of cells were unresponsive to pacing. Additionally, the proportion of cells with missing or disrupted triggered Ca²⁺ transients was greater at 1.5 and 2.5 Hz, than at 0.5 Hz, all in the presence of flecainide. These frequency dependent effects are indicative of flecainide's use dependent block of Na_v1.5 (Wang et al., 2003, Anno and Hondeghem, 1989). An increase in pacing frequency from 0.02 Hz to 10 Hz, increased flecainide inhibition of peak I_{Na} by ~70% (Ramos and O'Leary, 2004). Flecainide also progressively increased I_{Na} inhibition as a function of pacing duration, until a steady state inhibition was reached (Ramos and O'Leary, 2004). This

progressive inhibition was also apparent in electrophysiological experiments. Flecainide blocked peak I_{Na} amplitude by ~20% after 3 min of pacing at 0.1 Hz. However, by 5 min of pacing at 0.1 Hz, I_{Na} was inhibited by ~70%. The use-dependence of flecainide's action reflects a high binding affinity of flecainide to $Na_v1.5$ in its open state. Flecainide competes with Na^+ for access to its binding site within the channel pore and remains bound even after $Na_v1.5$ has closed. During fast pacing, dissociation from $Na_v1.5$ is slow (Ramos and O'Leary, 2004, Anno and Hondeghem, 1989), thereby trapping flecainide within the channel and inhibiting peak I_{Na} (Ramos and O'Leary, 2004, Nitta et al., 1992, Belardinelli et al., 2013, Nagatomo et al., 2000).

During line scan imaging it is possible to identify when a DAD triggers an action potential because a slowly propagating Ca^{2+} wave suddenly changes into a rapid and uniform Ca^{2+} transient (Figure 3.12 Aii) (Schlotthauer and Bers, 2000). DADs occur because NCX removes Ca^{2+} from the cytosol in exchange for Na^+ at a ratio of 1:3. During a wave, Ca^{2+} efflux via NCX induces a net inward movement of positive ions which depolarizes the cell and causes a 'triggered' action potential if the action potential threshold is exceeded (Schlotthauer and Bers, 2000). Despite the high spontaneous wave frequency seen in vehicle treated cells, the proportion of cells displaying this triggered activity was low (~10%). Even so, flecainide decreased the proportion of cells that exhibited rapid uniform Ca^{2+} transients triggered by a preceding wave. This is indicative of anti-arrhythmic behavior in the whole heart as triggered ectopic beats and can induce severe arrhythmias including VF in CPVT patients (Nam et al., 2005).

Flecainide did not decrease the probability of a wave occurring between field stimulated Ca^{2+} transients. However, flecainide was highly effective at suppressing spontaneous Ca^{2+} waves that occurred after field stimulation at 1.5 or 2.5 Hz, at each subsequent time point. It may be that this discrepancy in the effect of flecainide on wave frequency was due to differences in SR Ca^{2+} content. During pacing and in the presence of isoprenaline, SR Ca^{2+} content has previously been reported to be maximal (Dibb et al., 2007). This high SR Ca^{2+} content is likely to be similar in the current experiments due to the high wave frequency apparent between, and immediately prior to, paced Ca^{2+} transients. However, Ca^{2+} content was not directly measured using caffeine puffs. Upon cessation of stimulation, wave frequency decreased in both control and flecainide groups indicating a decrease in the average SR Ca^{2+} content. Only under these conditions did flecainide significantly decrease Ca^{2+} wave frequency indicating a potential dependency upon $[Ca^{2+}]$. Suppression of Ca^{2+} waves by flecainide has previously been documented in CPVT mouse myocytes and in rat WT cells (Hwang et al., 2011a, Sikkel et al., 2013), although the mechanism underlying this result is controversial. Sikkel et al. (2013)

suggested that following brief (5 min) exposure to flecainide, inhibition of I_{Na} lowers cellular $[Na^+]$ which in turn facilitates Na^+ influx and Ca^{2+} efflux via NCX. The resultant decrease in cytosolic $[Ca^{2+}]$ may then reduce the probability of sparks forming waves (Sikkel et al., 2013). This conclusion is at variance with a number of papers suggesting that flecainide can act directly on RyR2 to disrupt Ca^{2+} waves by reducing spark mass in $Casq2^{-/-}$ myocytes and reducing the probability of saltatory propagation of Ca^{2+} sparks across RyR2 clusters (Watanabe and Knollmann, 2011, Hwang et al., 2011a, Watanabe et al., 2009, Hilliard et al., 2010, Savio-Galimberti and Knollmann, 2015). In permeabilised cells where an effect on $Na_v1.5$ is entirely absent, flecainide modified Ca^{2+} sparks and waves (Savio-Galimberti and Knollmann, 2015). In addition, flecainide also inhibited isolated RyR2 channels incorporated into lipid bilayers (Hwang et al., 2011a, Watanabe et al., 2009, Hilliard et al., 2010). In contrast, experiments by Liu et al (2011) reported no change in Ca^{2+} spark, wave or DAD frequency upon treatment with flecainide in permeabilised or intact $R4496C^{+/+}$ myocytes. However, flecainide did significantly decrease the occurrence of pathologically triggered action potentials (Liu et al., 2011). This was reported to be due to flecainide's use-dependent inhibition of $Na_v1.5$ causing an increased threshold for triggered activity (Liu et al., 2011).

As recently discussed (Steele et al., 2013), it is possible that all effects of flecainide on I_{Na} and RyR2 could occur under the appropriate conditions. It is certainly the case that $Na_v1.5$ inhibition occurs and that this could lower intracellular $[Na^+]$ to decrease intracellular $[Ca^{2+}]$ or alter the action potential threshold (Sikkel et al., 2013, Liu et al., 2011, Belardinelli et al., 2013, Nitta et al., 1992). Yet when directly compared against other clinical $Na_v1.5$ inhibitors, only flecainide (and to a lesser extent R-propafenone) was capable of inhibiting Ca^{2+} waves in $Casq2^{-/-}$ myocytes, indicating an additional or alternative mechanism of action (Hwang et al., 2011a). Given also that Sikkel et al. (2013) only exposed cells to flecainide for 5 minutes, an RyR2 mediated effect would not be expected to occur as a necessary incubation period of 20-30 min has been reported (Hwang et al., 2011b).

In the experiments presented in this chapter, WT rat myocytes were exposed to flecainide for a prolonged period (>45 min). However, although there was a clear inhibitory effect on the frequency of Ca^{2+} waves post-pacing, there were no consistent, significant effects on Ca^{2+} spark properties. These data suggest that under these conditions in WT rat myocytes, there is no effect on RyR2 and that the primary anti-arrhythmic action is most likely mediated via inhibition of $Na_v1.5$. However, depending on flecainide's rate of entry, an incubation period for 45 min at room temperature may not allow sufficient access of flecainide to RyR2, located at the SR membrane. To investigate this further, the protocol was modified and flecainide was

incubated within cells for 2 hours, including 30 min at 37 °C to increase drug uptake into the cells (Sugano et al., 2010). The overall effect of flecainide on wave frequency was very similar between the two incubation protocols; flecainide significantly decreased wave frequency post-pacing at each time point and there was no change in spark characteristics.

It is possible that the effect of flecainide on RyR2 and Ca²⁺ sparks would be apparent when an abnormal RyR2 Ca²⁺ leak is present, as occurs in CPVT (Savio-Galimberti and Knollmann, 2015). Therefore, the effects of flecainide were investigated in the MCT rat model of right-sided heart failure, which is known to display increased Ca²⁺ leak (Fowler, 2015). When comparing MCT and CON cells, Ca²⁺ wave frequency post-pacing and the proportion of cells displaying wave triggered Ca²⁺ transients was greater in MCT cells, potentially due to the increased I_{Na} reported in MCT cardiomyocytes (Rocchetti et al., 2014). In the current experiments, spark characteristics were unchanged between MCT and CON cells. However, when spark parameters were directly investigated comparing sham and MCT animals in the absence of isoprenaline, there was an ~85% increase in spark frequency in MCT cells (Fowler et al., In preparation). Despite this, flecainide did not significantly affect spark characteristics in MCT cells, indicating a negligible effect of flecainide on RyR2 under these conditions.

3.4.4 Conclusions and summary

The current data, reported in intact, WT cardiomyocytes, indicated that whilst flecainide had a pronounced anti-arrhythmic effect on Ca²⁺ wave suppression, there was no clear evidence of an effect on RyR2. Flecainide elicited no effect on Ca²⁺ sparks indicating that an effect on RyR2 was too small to detect under these conditions or absent completely in WT rat myocytes. It is possible that species differences could account for the difference in effect of flecainide seen in mouse or rat. Additionally, a marked effect of flecainide on RyR2 might require the presence of a CPVT mutation. Another possibility is that flecainide was unable to accumulate to a high enough concentration within the cytosol to affect WT RyR2 with the experimental period. To investigate these possibilities further, subsequent chapters will characterise the accumulation and localization of cellular flecainide using a fluorescently tagged version of the drug (Chapter 4) and investigate the effects of flecainide on RyR2 in permeabilised rat myocytes (Chapters 5 and 6).

Chapter 4: Flecainide-FITC accumulation within intact and permeabilised ventricular myocytes

4.1 Introduction

Inhibition of $\text{Na}_v1.5$ by flecainide has been widely characterised in cardiomyocytes and cultured cell lines (Ikeda et al., 1985, Belardinelli et al., 2013, Wang et al., 2003, Ramos and O'Leary, 2004). $\text{Na}_v1.5$ is incorporated into the sarcolemma and spans the depth of the cell lipid bilayer to form an internal aqueous channel pore (Rook et al., 2012). Whilst inhibition of $\text{Na}_v1.5$ by flecainide has been reported to occur via external cell application only (Nitta et al., 1992), flecainide's actual binding site is believed to be situated at the cytoplasmic side of the $\text{Na}_v1.5$ channel pore (Ramos and O'Leary, 2004). Access to the binding site may be facilitated by channel opening, which allows the entry and movement of flecainide along the aqueous pathway (Ramos and O'Leary, 2004). While it is currently unknown whether flecainide can enter the cytosol via this pathway, approximately 1% of flecainide is in its neutral form at physiological pH and will slowly permeate the cell membrane (Liu et al., 2003). Studies addressing the effects of flecainide on the K^+ human Ether-à-go-go (hERG) current, have also suggested that the OCTN1 transporter may contribute to flecainide uptake (McBride et al., 2009).

An interaction of flecainide with RyR2 has recently been described (Hilliard et al., 2010, Watanabe et al., 2009, Hwang et al., 2011a). As RyR2 is located at the dyadic junction on the SR membrane (Jayasinghe et al., 2009) substantial cytosolic accumulation of the drug must precede any observed effect. Consistent with this, an initial study addressing the effects of flecainide on RyR2 in myocytes from CPVT mice concluded that at least 15-30 min pre-incubation with flecainide was required for effects on RyR2 to be observed (Hwang et al., 2011b).

The requirement for cellular accumulation might explain the reported absence of RyR2 mediated effects in WT cardiomyocytes exposed to flecainide for only 5 min (Sikkel et al., 2013). However in the present study on WT rat myocytes, RyR2 mediated effects were not apparent despite exposure to relatively high levels of the drug (15 μM) for a minimum of 45 min (Chapter 3). A possible explanation for this is that despite the prolonged incubation period, flecainide might not have permeated the sarcolemma and accumulated sufficiently to modulate the WT RyR2. While previous studies have provided evidence of marked flecainide concentration in the heart (Latini et al., 1987, Mishima et al., 1999), the magnitude of this effect and the subcellular localisation of the drug remain uncertain.

In this chapter, the time scale, mechanism and extent of flecainide accumulation within intact WT cardiomyocytes was investigated using a fluorescent bioconjugate of flecainide and fluorescein isothiocyanate (flecainide-FITC). Additionally, the subcellular localisation of flecainide was studied by exposing permeabilised myocytes to flecainide-FITC.

4.2 Methods

4.2.1 Intact myocyte imaging protocol

Rat ventricular cardiomyocytes were isolated via retrograde perfusion and enzymatic digestion on a Langendorff apparatus (Chapter 2.2). The isolation solution, in which isolated cells were stored, was then switched to Tyrode's solution (1.8 mM Ca^{2+}) containing 6 or 25 μM flecainide-FITC. Cells were placed immediately in the experimental chamber on the microscope stage and left for 1 min to settle onto the glass cover slip. 4-6 cells were imaged in XY scanning mode at a scanning speed of 188 lps and a final resolution of 1280 pixels x 1024 lines (103 x 82 μm). Cardiomyocytes were incubated with either 6 or 25 μM flecainide-FITC. Flecainide-FITC was applied to cells at a concentration of 6 μM to ensure consistency with initial studies investigating the effect of flecainide on RyR2 (Sikkel et al. 2013, Hilliard et al. 2011). This concentration of flecainide has been detected at peak plasma levels (Mano et al., 2015, 3M, 2016). Increasing the concentration of flecainide-FITC to 25 μM was done to investigate if the rate of flecainide-FITC uptake into the cell and sub-cellular compartments was concentration dependent. Cells incubated in 6 μM flecainide-FITC were scanned at 0.2% of the maximum laser power (20 mW). Cells which were incubated at 25 μM flecainide-FITC were scanned at 0.1% maximum laser scanning power to avoid signal saturation. Laser power was minimised and each cell was scanned once to avoid bleaching of the FITC signal. Flecainide-FITC was excited with the 488 nm line of a diode laser and fluorescence was measured at 520-540 nm. Cells were XY scanned every 20 min for a total of 180 min. These experiments were repeated with 6 or 25 μM FITC. Cimetidine (100 μM) or its vehicle (DMSO; 0.001%) was added to the solutions to investigate the possible role of the OCTN1 transporter on flecainide-FITC uptake (McBride et al., 2009). Cimetidine was solubilised on the day of the experiment.

4.2.2 Saponin and Triton X-100 permeabilised myocyte imaging protocol

Isolated myocytes were permeabilised using saponin or Triton X-100 as detailed in Chapters 2.5.1 and 2.5.2 and were left to settle on the coverslip base of the experimental chamber. XY scans of cells under control conditions were obtained during perfusion with an intracellular solution (146 nM free Ca^{2+} ; Table 2.3 and 2.4). Repeat XY scans of cells were recorded at 5, 20, 40, 60 and 120 sec after perfusion with intracellular solution containing 6 or 25 μM flecainide-FITC. In washout experiments, saponin permeabilised cells were loaded with 6 or 25 μM flecainide-FITC for 2 min within the experimental chamber. Perfusion solution was switched

back to the control solution for 2 min to remove extracellular drug from within the cytosol. The solution was switched again to intracellular solution containing the mitochondrial uncoupler, carbonyl cyanide-4-(trifluoromethoxy)phenylhydrazone (FCCP; 30 μ M) or vehicle for 10 min. XY scans were recorded 5 and 30 sec after the second solution change and then every minute thereafter. Cardiomyocytes were repeatedly scanned during this protocol, however laser intensity was maintained at <0.2% of the maximum laser power (20 mW) to minimise signal bleaching.

In washout experiments involving brief treatment with Triton X-100, permeabilised cells were exposed to 6 or 25 μ M flecainide-FITC for 2 min within the experimental chamber. The perfusion solution was then switched to either the control intracellular solution or an intracellular solution containing 100 μ M flecainide for 7 min. Thereafter, different cells were XY scanned for a further 5 min. Perfusion was maintained at 0.7 ml/min and all experiments were done at 22 ± 2 °C.

4.2.3 Flecainide-FITC effects on $\text{Na}_v1.5$

Isolated, intact myocytes were patch clamped using whole cell configuration of the patch-clamp technique in voltage-clamp mode. Cells were continually perfused (3-5 ml/min) with extracellular electrophysiological solution (Chapter 2, Table 4). Patch pipettes had resistances of 3-6 M Ω and were filled with intracellular electrophysiological solution (Chapter 2, Table 2.6). I_{Na} was evoked by a 200 ms step from -80mV to -30 mV every 10 sec, peak amplitude was measured under control conditions and then in the presence of 10, 30 and 100 μ M flecainide-FITC at 22 ± 1 °C.

4.2.4 Analysis and statistics

XY scans were viewed and analysed using ImageJ software. Cells were outlined using the Polygon Tool and the mean cell fluorescence (F) measured. A representative region of extracellular fluorescence (F_e) was also selected and measured, ensuring other cells or debris were not included within the visual field. The final cell fluorescence was calculated as F/F_e , i.e. the intracellular fluorescence relative to the extracellular fluorescence. In all recorded groups, differences in uptake rate during the incubation and scan time were apparent. For this reason a Boltzmann Curve rather than a linear fit was applied to the data points.

Two tailed unpaired and paired Student's t-tests were used where appropriate to test for differences in intact cell fluorescence or nuclei cell fluorescence at two time points. A two way ANOVA was used to test for differences between control and cimetidine groups at different time points. Two way repeated measures ANOVA was used to test for differences between FCCP washout and the vehicle time control at different time points. Two tailed unpaired Student's t-test was used to test for differences between control and flecainide washout groups in experiments in which cells were permeabilised with Triton X-100. Tests which analysed more than two groups used a Holm-Sidak multiple comparisons procedure to isolate significantly different time points. Significance was considered when $p < 0.05$.

4.3 Results

4.3.1 Flecainide-FITC accumulation within intact myocytes

Experiments to investigate the rate of flecainide-FITC entry into intact WT rat ventricular myocytes were performed. Figure 4.1 A shows cardiomyocytes at control (CON) and after, 60, 120 and 180 min incubation with 6 μ M flecainide-FITC. On average, 6 μ M flecainide-FITC accumulated within intact cardiomyocytes at a rate of 1.65 F/F_e/hour within the first hour (Figure 4.1 B, solid). This accumulation rate slowed to 0.73 F/F_e/hour in the third hour and there was a 4.3 fold increase in cell fluorescence over 180 min (0.81 \pm 0.04 F/F_e to 3.48 \pm 0.42 F/F_e; $p < 0.001$; Figure 4.1 C; $n = 7-12$ cells at each time point). Compared with whole cell fluorescence, flecainide-FITC increased in the nucleoplasm at a slower rate; 0.70 F/F_e/hour in the first hour and 0.38 F/F_e/hour in the third hour (Figure 4.1 B, dashed). There was a 2.76 fold increase in nuclear fluorescence over 180 min (0.71 \pm 0.03 to 1.96 \pm 0.28 F/F_e; $p < 0.001$; Figure 4.1 C). At 0 and 180 min, whole cell fluorescence was significantly greater than nuclei fluorescence ($p < 0.001$; Figure 4.1 C; $n = 7-12$ cells at each time point).

Qualitatively similar results were obtained in cells incubated with 25 μ M flecainide-FITC (Figure 4.2 A). Flecainide-FITC accumulated in cells at a rate of 3.59 F/F_e/hour and 1.02 F/F_e/hour in the first and third hour respectively (Figure 4.2 B, solid; $n = 9-15$ cells). These rates of accumulation were 2.18 and 1.40 fold greater than the accumulation rate at 6 μ M flecainide-FITC respectively. Accumulation of 25 μ M flecainide-FITC into the nucleoplasm was 1.87 F/F_e/hour and 0.51 F/F_e/hour in the first and third hour respectively (Figure 4.2 B, dashed; $n = 9-11$ cells at each time point). The rate of nuclear accumulation was 2.67 and 1.34 fold greater at 25 μ M than 6 μ M flecainide-FITC. At 180 min, there was a 9.83 fold increase in whole cell fluorescence (0.71 \pm 0.05 F/F_e to 6.98 \pm 0.55 F/F_e; $p < 0.001$; Figure 4.2 C) and a 6.84 fold increase in nuclear fluorescence (0.57 \pm 0.03 F/F_e to 3.97 \pm 0.58 F/F_e; $p < 0.001$; Figure 4.2 C) relative to control values at 0 min. At 0 and 180 min, whole cell fluorescence was significantly greater than the nuclear fluorescence ($p < 0.001$; Figure 4.2 C; $n = 9-11$ cells at each time point).

It has been suggested that the uptake of flecainide may be facilitated by the OCTN1 transporter (McBride et al., 2009). Flecainide-FITC uptake rate was therefore measured in the presence of flecainide-FITC (F-F) or with the added presence of the OCTN1 inhibitor, cimetidine (F-F+CIM) over 3 hours (Figure 4.3 A) (Yang et al., 2010). Following the introduction of 6 μ M flecainide-FITC, cimetidine had no effect on cell or nuclear fluorescence at any time point ($p > 0.05$; Figure 4.3 B; $n = 8-15$ cells at each time point). At 25 μ M flecainide-FITC (Figure 4.4 A)

there was a significant difference between cimetidine and control groups for whole cell ($p < 0.01$) and nuclei fluorescence ($p < 0.05$; Figure 4.4 B; $n = 7-15$ cells at each time point). However, a significant decrease in fluorescence with cimetidine was only apparent at 80 min (whole cell and nuclei) and 160 min (whole cell only) when the Holm-Sidak *post hoc* test was applied.

4.3.2 FITC entry into intact cardiomyocytes

Entry of FITC into the intact cell was also investigated to consider the cell permeability properties of FITC, in the absence of bioconjugation with flecainide. In these experiments, FITC entry into intact cells was investigated using 6 and 25 μM FITC. Cell fluorescence increased during 180 min incubation of FITC with intact cardiomyocytes (Figure 4.5 A). However, FITC fluorescence was significantly lower at each time point between 60 and 180 min compared with flecainide-FITC fluorescence at both 6 and 25 μM ($p < 0.001$; Figure 4.5 B and C; $n = 7-12$ cells at each time point). This difference continued as a strong trend at time points prior to 60 min ($p > 0.05$). These results were mirrored in the uptake rate of 6 μM FITC. In the first and third hours of 6 μM FITC uptake, the rates were 1.06 $F/F_0/\text{hour}$ and 0.47 $F/F_0/\text{hour}$ respectively, which were considerably slower than those previously quoted for flecainide-FITC (Figure 4.5 B). The same is true for 25 μM FITC whereby the uptake rate was 2.67 $F/F_0/\text{hour}$ in the first hour and 1.02 $F/F_0/\text{hour}$ in the third hour (Figure 4.5 C). Although the pattern produced by unconjugated FITC was qualitatively similar to that produced by flecainide-FITC, it should be noted that the level of contaminating free FITC present in the flecainide-FITC drug sample was essentially undetectable in the analysis provided by the company (Severn-Biotech, 2016).

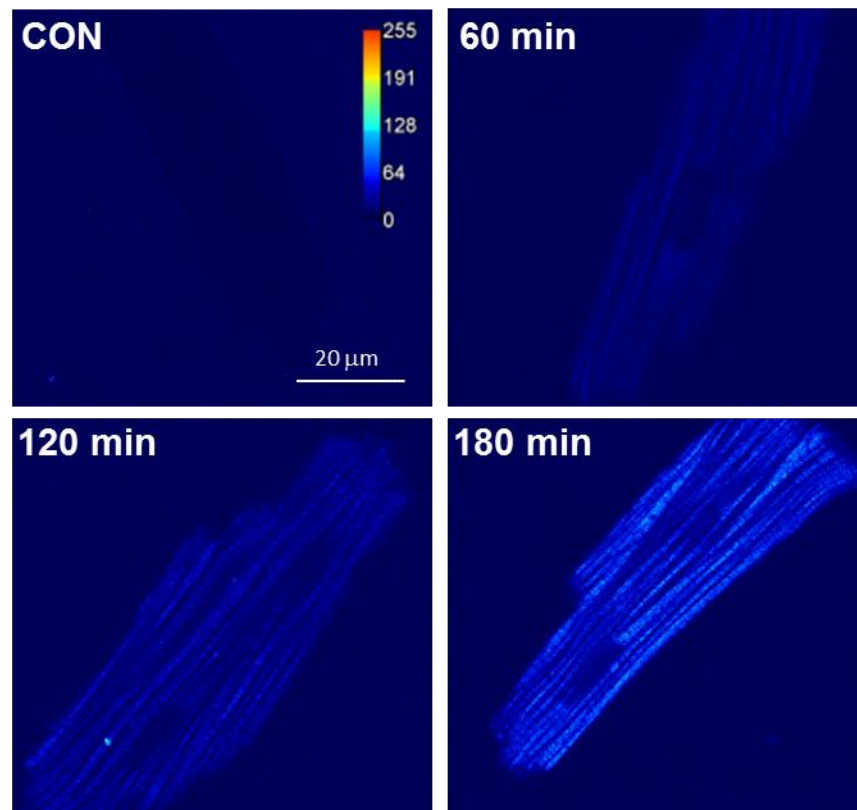
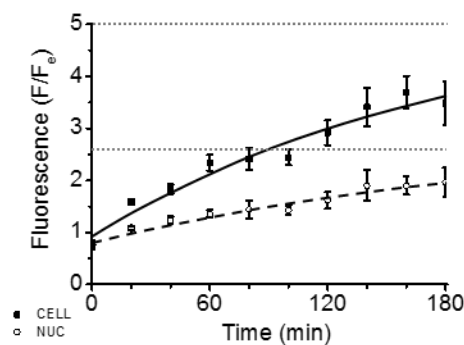
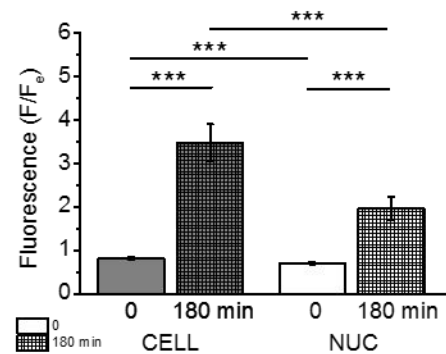
A**B****C**

Figure 4.1: Slow accumulation of 6 μ M flecainide-FITC within intact cardiomyocytes

A) Representative XY scans of cells at control and after, 60, 120 and 180 min incubation with 6 μ M flecainide-FITC. **B)** Change in whole cell fluorescence (CELL) and nucleoplasmic fluorescence (NUC) over 180 min. Grey dotted lines represent 90% of the upper asymptote of the Boltzmann fitted curve. **C)** Differences in CELL and NUC fluorescence within control groups and after 180 min incubation with flecainide-FITC. Two-tailed paired or unpaired Student's t-test where appropriate. *** = $p < 0.001$. $n = 7-12$ (3) at each time point. $n = \text{CELL } 0 = 7$ (3); $\text{CELL } 180 = 15$ (3); $\text{NUC } 0 = 7$ (2); $\text{NUC } 180 = 11$ (3).

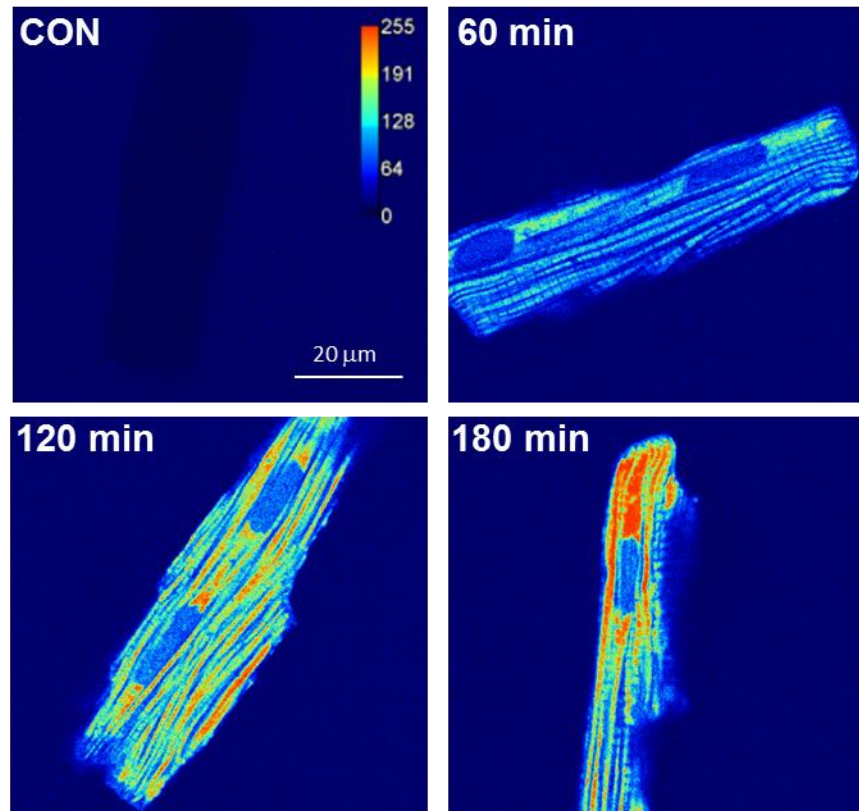
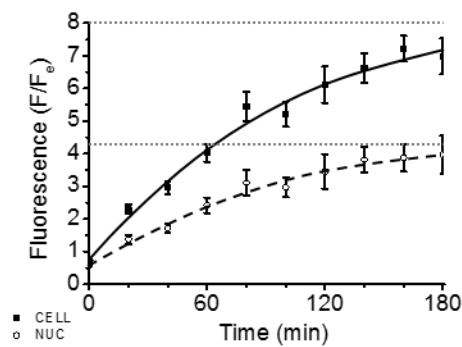
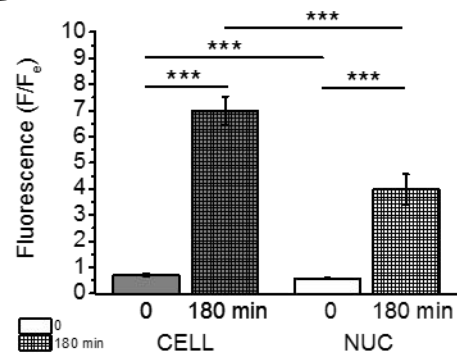
A**B****C**

Figure 4.2: Slow accumulation of 25 μ M flecainide-FITC within intact cardiomyocytes

A) Representative XY scans of cells at control and after, 60, 120 and 180 min incubation with 25 μ M flecainide-FITC. **B** Change in whole cell fluorescence (CELL) and nucleoplasmic fluorescence (NUC) over 180 min. Grey dotted lines represent 90% of the upper asymptote of the Boltzmann fitted curve. **C** Differences in CELL and NUC fluorescence within control groups and after 180 min incubation with flecainide-FITC. Two-tailed paired or unpaired Student's t-test where appropriate. *** < 0.001. n = 7-12 (3) at each time point. n = CELL 0 = 9 (3); CELL 180 = 15 (3); NUC 0 = 9 (3); NUC 180 = 11 (3).

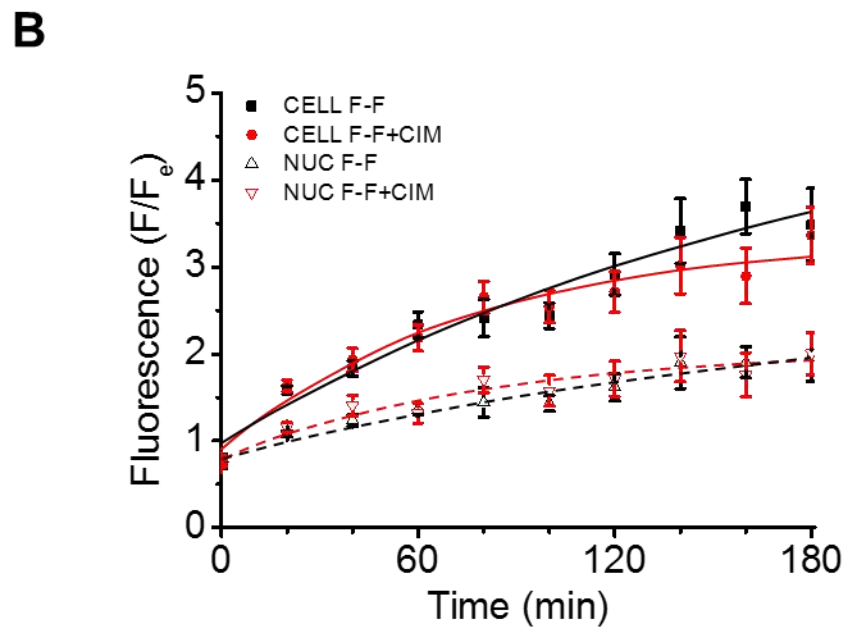
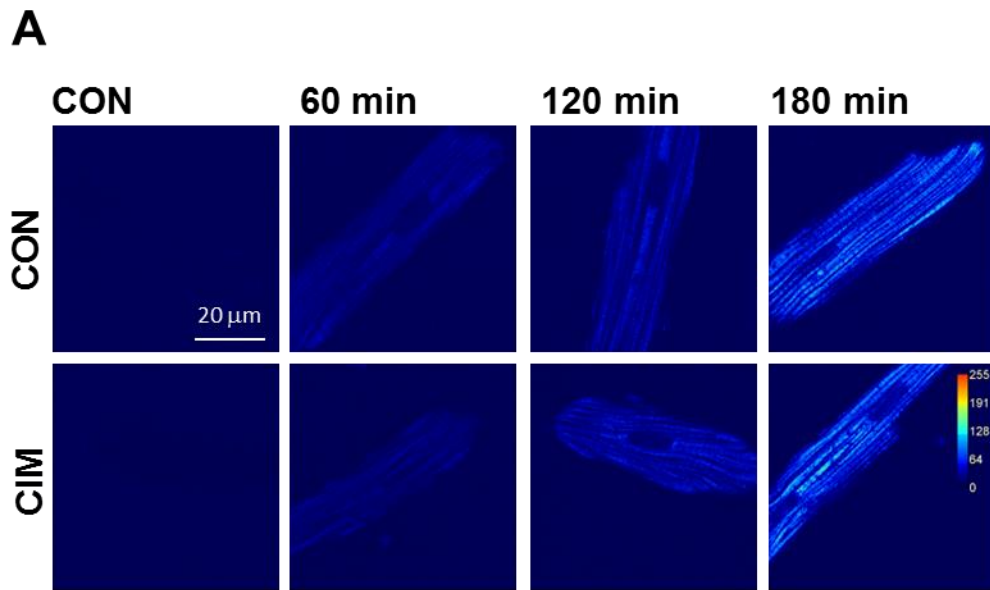


Figure 4.3: Accumulation of 6 μ M flecainide-FITC within intact cardiomyocytes with or without the OCTN1 blocker cimetidine

A) Representative XY scans of cells at control and after 60, 120 and 180 min incubation with 6 μ M flecainide-FITC with 100 μ M cimetidine (F-F+CIM) or without (F-F). **B)** Change in whole cell fluorescence (CELL; closed) and nucleoplasmic fluorescence (NUC; open, dashed) over time in F-F (black) and F-F+CIM (red) groups. Two way ANOVA. n = CELL F-F = 8 – 15 (3); CELL F-F +CIM = 10 – 15 (3); NUC F-F = 7 – 15 (3); NUC F-F+CIM = 9 – 15 (3).

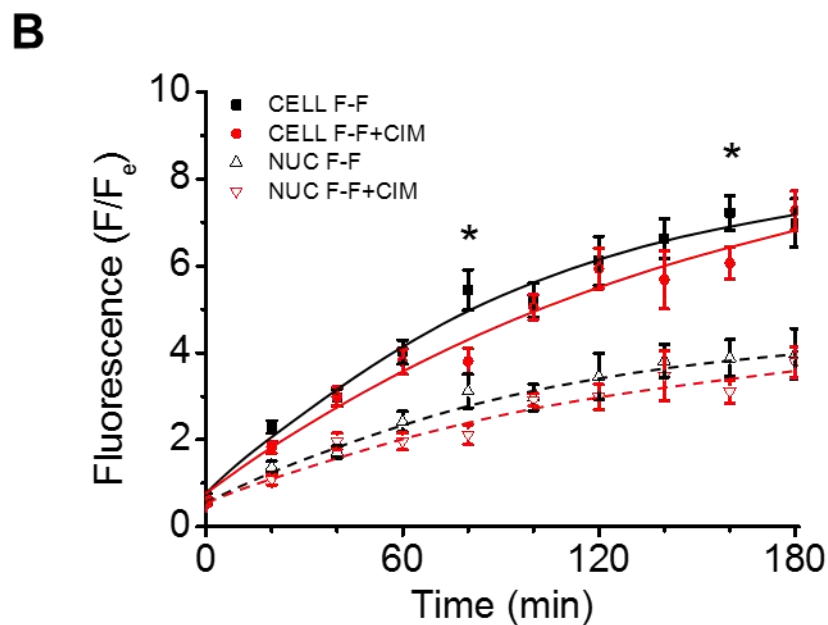
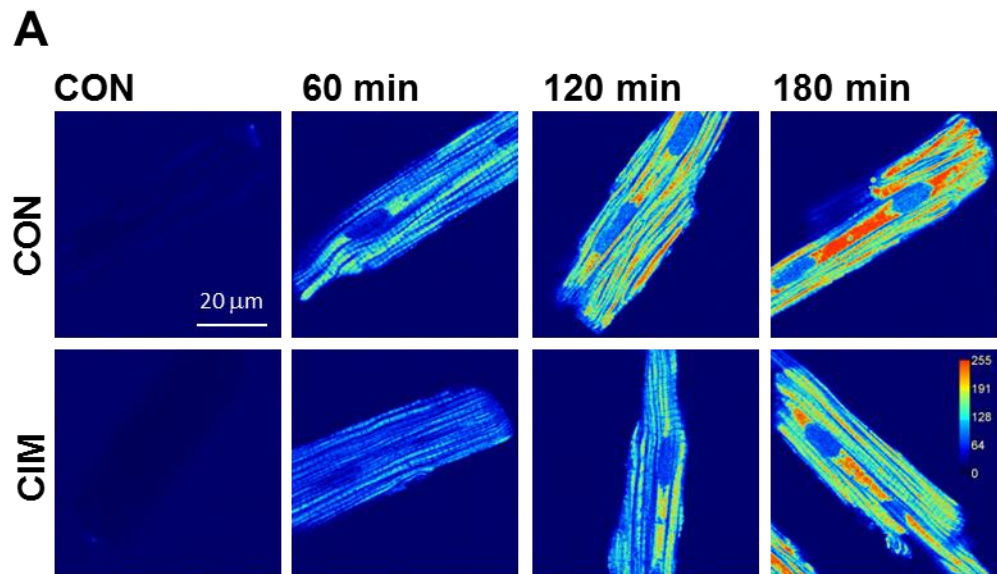


Figure 4.4: Accumulation of 25 μ M flecainide-FITC within intact cardiomyocytes with or without the OCTN1 blocker cimetidine

A) Representative XY scans of cells at control and after 60, 120 and 180 min incubation with 25 μ M flecainide-FITC with 100 μ M cimetidine (F-F+CIM) or without (F-F). **B)** Change in whole cell fluorescence (CELL; closed) and nucleoplasmic fluorescence (NUC; open, dashed) over time in F-F (black) and F-F+CIM (red) groups. Two way ANOVA + Holm-Sidak *post hoc* test. * = $p < 0.05$. $n =$ CELL F-F = 9 – 16 (3); CELL F-F+CIM = 11 – 15 (3); NUC F-F = 9 – 14 (3); NUC F-F+CIM = 7 – 14 (3).

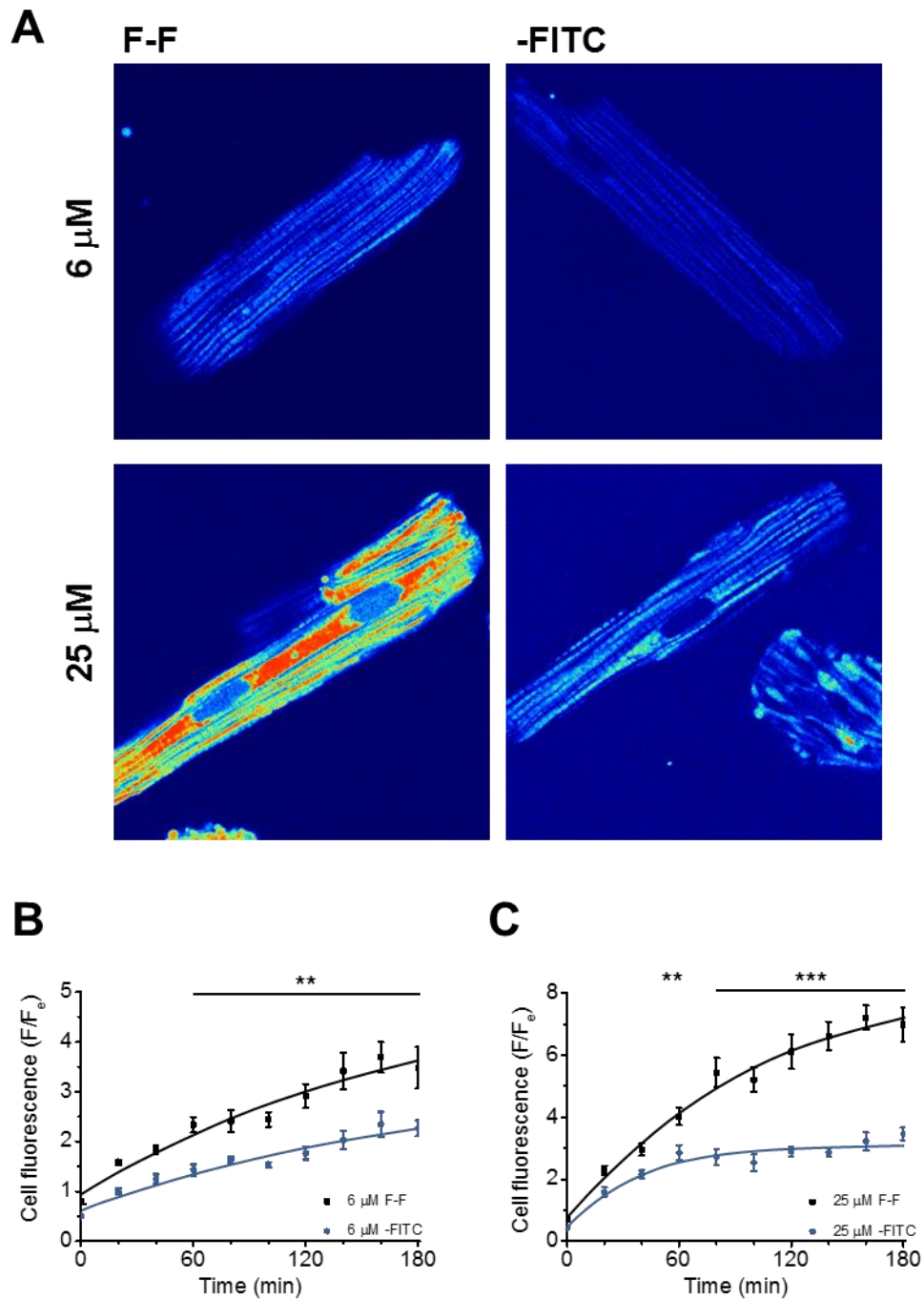


Figure 4.5: 6 and 25 μ M -FITC entry into cardiomyocytes

A) Representative XY scans of cells after 180 min incubation with either (top) 6 μ M flecainide-FITC (F-F) or -FITC; or (bottom) 25 μ M F-F or -FITC. **B)** Changes in cell fluorescence over 180 min with 6 μ M F-F (black) or -FITC (blue). **C)** Changes in cell fluorescence over 180 min with 25 μ M F-F (black) or -FITC (blue). Two way ANOVA + Holm-Sidak *post hoc* test. ** = $p < 0.01$; *** = $p < 0.001$. $n = 6 \mu$ M F-F = 7-12 (3); 6 μ M FITC = 8-10 (2); 25 μ M F-F = 7-12 (3); 25 μ M FITC = 8-10 (2) at each time point.

4.3.3 Flecainide-FITC accumulation within saponin permeabilised myocytes

In the experiments shown in Figures 4.1 - 4.4, the drug fluorescence exhibited a pattern consistent with mitochondrial accumulation (Boyman et al., 2014a, Swift and Sarvazyan, 2000). Therefore, this was studied in more detail using cells permeabilised with saponin, where flecainide should have unrestricted access to the cytosol and organelles.

Following saponin treatment, flecainide-FITC (6 μ M) rapidly concentrated into an intracellular compartment. As in intact cells, the pattern was consistent with mitochondrial localisation (Figure 4.6 A). Whole cell fluorescence approached 90% of the upper asymptote of the fitted Boltzmann curve at 60.9 sec and the time to half maximal fluorescence was 18.7 sec (Figure 4.6 B, solid; n = 12 cells (CELL)). Flecainide-FITC accumulated more slowly in the nucleoplasm than the whole cell and the time to half maximal fluorescence was at 45.5 sec (Figure 4.6 B, dashed; n = 8 cells (NUC)). Flecainide-FITC fluorescence accumulated into the intracellular compartment faster at 25 μ M than at 6 μ M (Figure 4.7 A). Whole cell fluorescence approached 90% of the upper asymptote of the Boltzmann curve at 6.5 sec and the time to half maximal fluorescence was 4.5 sec (Figure 4.7 B, solid; n = 15 cells (CELL)). Again, nuclear fluorescence increased more slowly than whole cell fluorescence, reaching 90% of the upper asymptote at 42.7 sec and the time to half maximal fluorescence was 12.7 sec (Figure 4.7 B, dashed; n = 11 cells (NUC)).

To confirm mitochondrial localization, saponin permeabilised cells were exposed to flecainide-FITC for 2 min until the block-like fluorescence was apparent. The solution was then replaced with cytosolic solution which lacked flecainide-FITC (CON) in either the presence or absence of the mitochondrial uncoupler FCCP (30 μ M) (Figure 4.8 A). CON washout decreased the whole cell fluorescence to 74.5% of the initial fluorescence value over 10 min, however cell fluorescence decreased much more rapidly in the presence of FCCP (Figure 4.8 B; n = 5 cells (FCCP)): 10 min of FCCP washout rapidly decreased whole cell fluorescence to 17.0% of the initial fluorescence value. The time to half maximum fluorescence was 25.2 sec (Figure 4.8 B, blue; n = 4 cells (CON)). All fluorescent values between the FCCP and control groups were significantly different except at 0 ($p < 0.001$; Figure 4.8 B). Figure 4.9 A shows saponin permeabilised cells loaded with 25 μ M flecainide-FITC before and during washout with CON or FCCP. After loading with 25 μ M flecainide-FITC, washout under CON conditions decreased the whole cell fluorescence to 53.4% of the initial fluorescence value and the time to half minimal fluorescence was 3.3 sec (Figure 4.9 B, black; n = 5 cells (CON)). FCCP washout rapidly decreased whole cell fluorescence after cell loading at 25 μ M. Whole cell fluorescence was

decreased to 25.1% of the initial fluorescence value after 10 min and the time to half minimal fluorescence was 21.0 sec (Figure 4.9 B, blue; n = 5 cells (FCCP)). All fluorescence values between the FCCP and CON groups were significantly different except at 0 ($p < 0.01$; Figure 4.9 B).

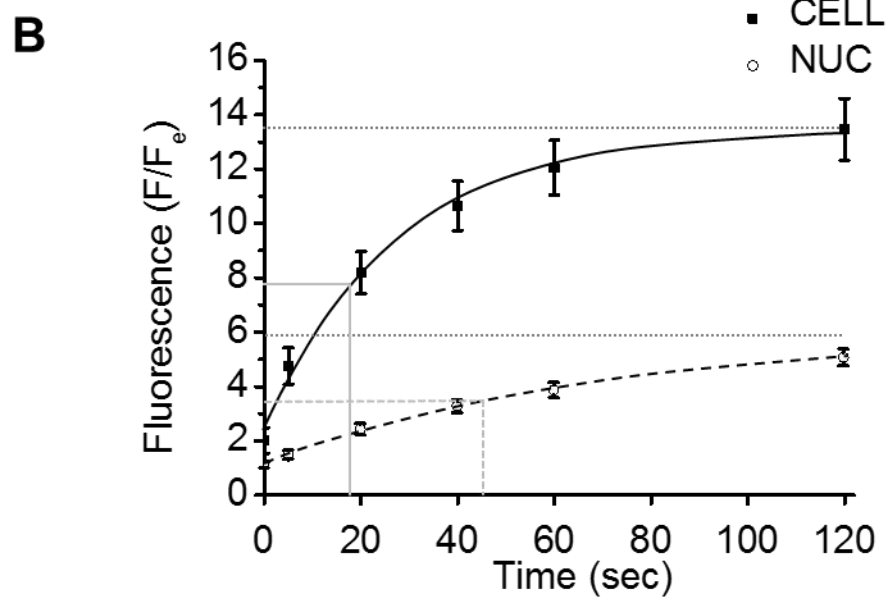
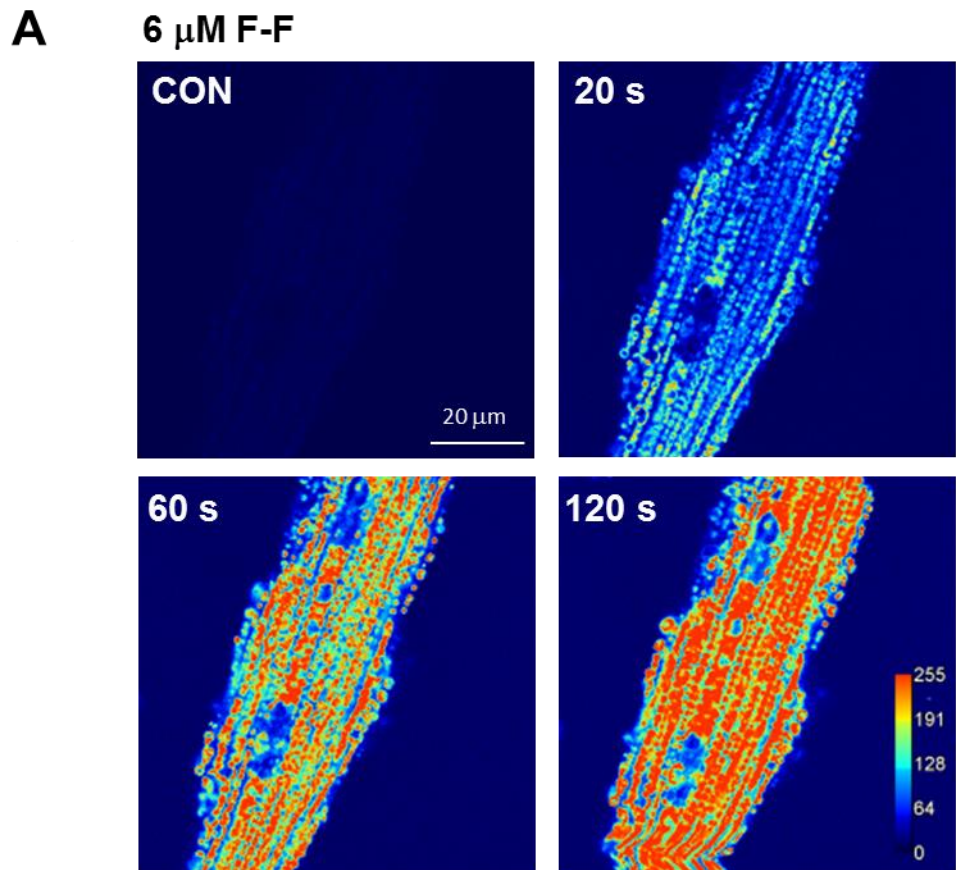


Figure 4.6: Accumulation of 6 μM flecainide-FITC (F-F) within intracellular organelles of saponin permeabilised cardiomyocytes

A) Representative XY scans of cells at control and after 20, 60 and 120 sec of perfusion with 6 μM flecainide-FITC. **B)** Mean increase in total cell fluorescence (CELL; closed) and nucleoplasmic fluorescence (NUC; open, dashed) in the presence of 6 μM flecainide-FITC over 120 sec. Grey dotted lines represent 90% of the upper asymptote of the Boltzmann fitted curve. Grey filled lines represent 50% of the upper asymptote. $n = \text{CELL} = 12$ (5); $\text{NUC} = 8$ (4).

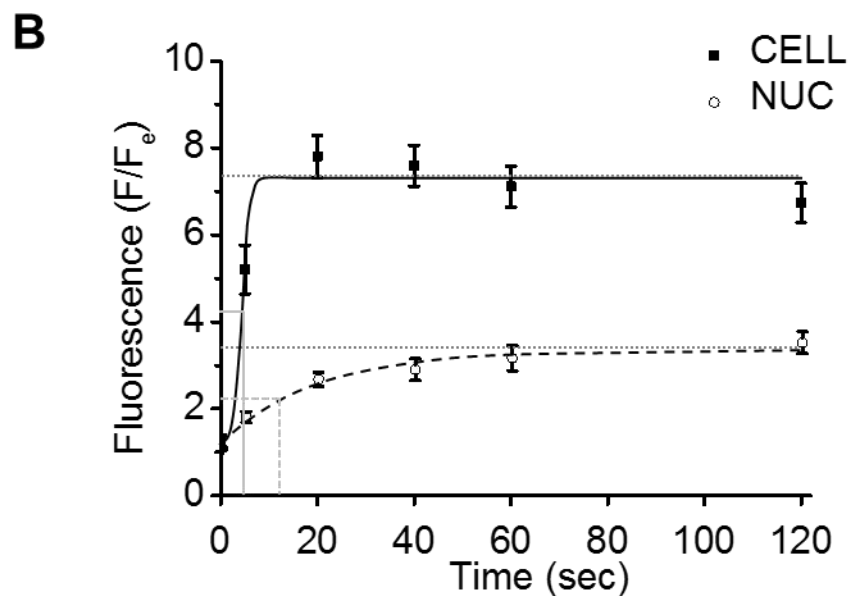
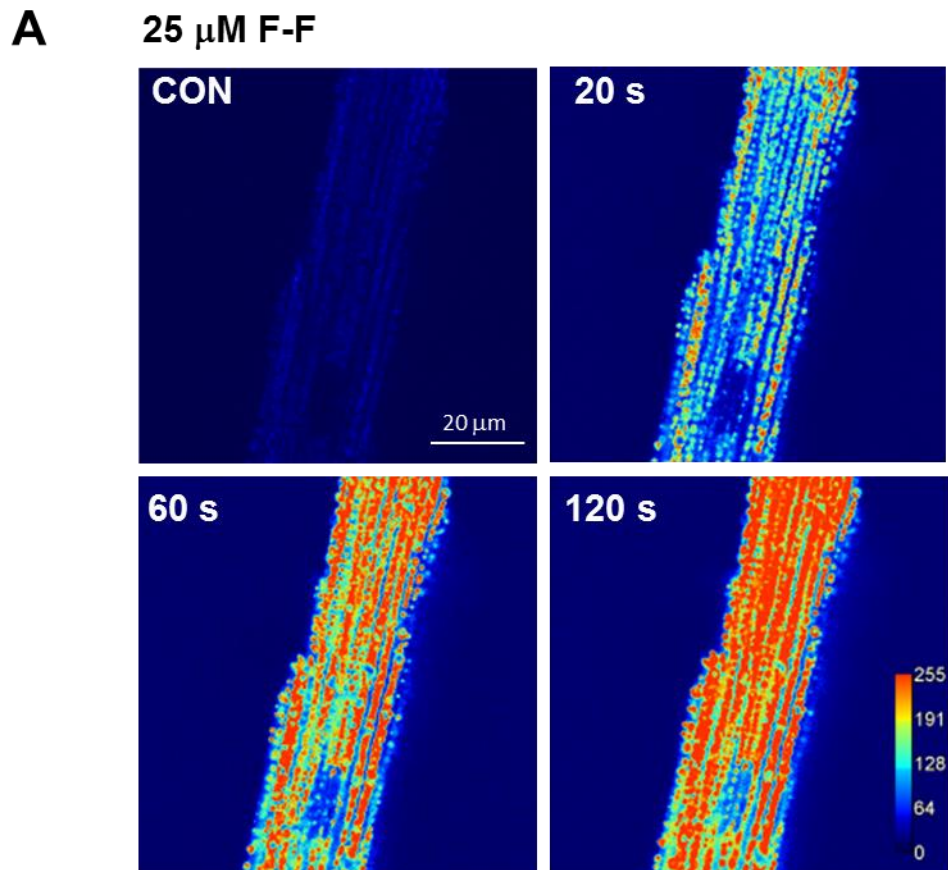


Figure 4.7: Accumulation of 25 μ M flecainide-FITC (F-F) within intracellular organelles of saponin permeabilised cardiomyocytes

A) Representative XY scans of cells at control and after 20, 60 and 120 sec of perfusion with 25 μ M flecainide-FITC. **B)** Mean increase in total cell fluorescence (CELL; closed) and nucleoplasmic fluorescence (NUC; open, dashed) in the presence of 25 μ M F-F over 120 sec. Grey dotted lines represent 90% of the upper asymptote of the Boltzman fitted curve. Grey filled lines represent 50% of the upper asymptote. $n = \text{CELL} = 15$ (4); $\text{NUC} = 11$ (4).

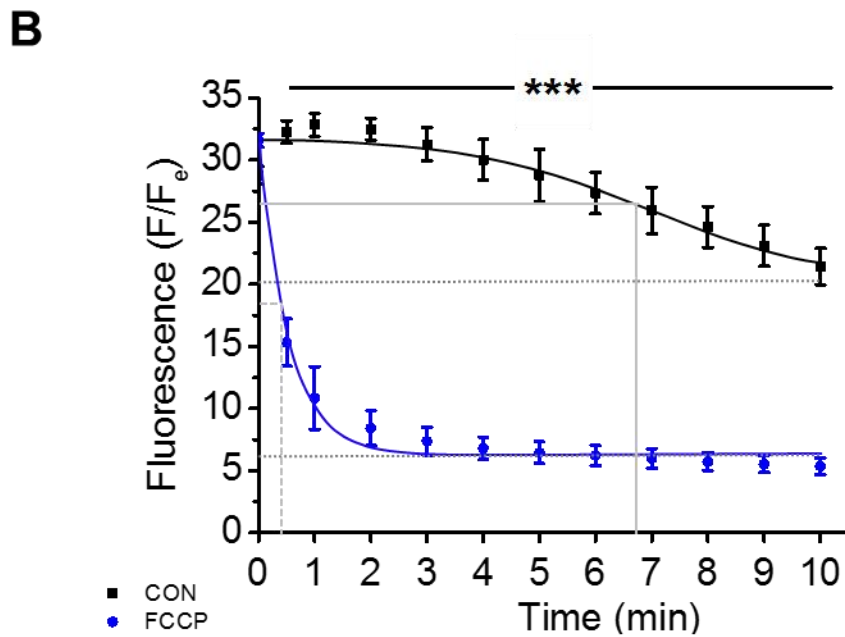
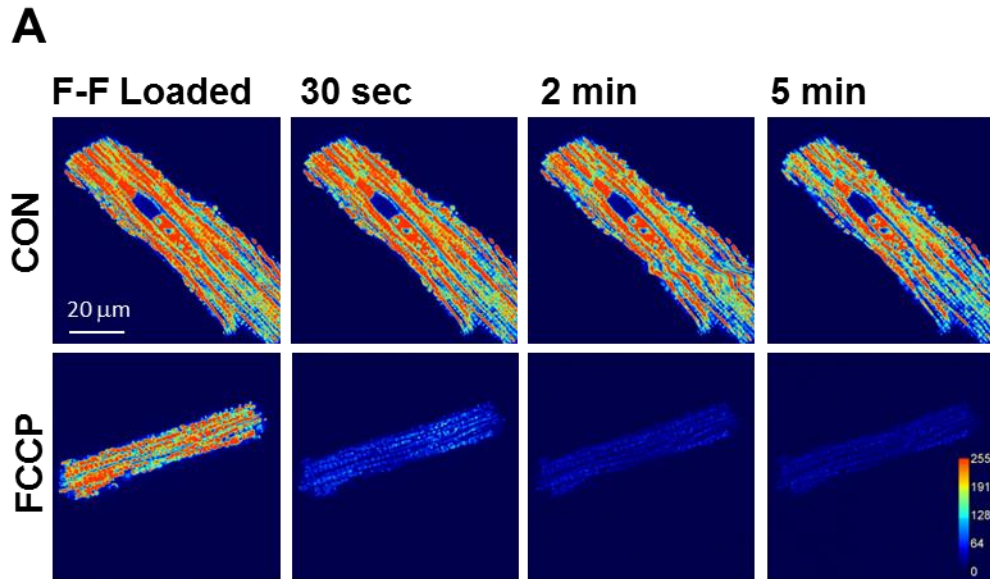


Figure 4.8: Accumulation of 6 μM flecainide-FITC (F-F) within intracellular organelles of saponin permeabilised cardiomyocytes was disrupted by FCCP

A) Representative XY scans of cells after 2 min of loading with flecainide-FITC, then 30 sec, 2 min and 5 min after perfusion with 30 μM FCCP (FCCP) or without (CON). **B)** Mean change in flecainide-FITC loaded whole cell fluorescence in FCCP (blue) and CON (black) groups. Grey dotted lines represent 90% of the lower asymptote of the Boltzman fitted curve. Grey filled lines represent 50% of the lower asymptote. Two way repeated measures ANOVA + Holm-Sidak *post hoc* test. *** = $p < 0.001$. $n = \text{CON} = 5$ (3), FCCP = 4 (3).

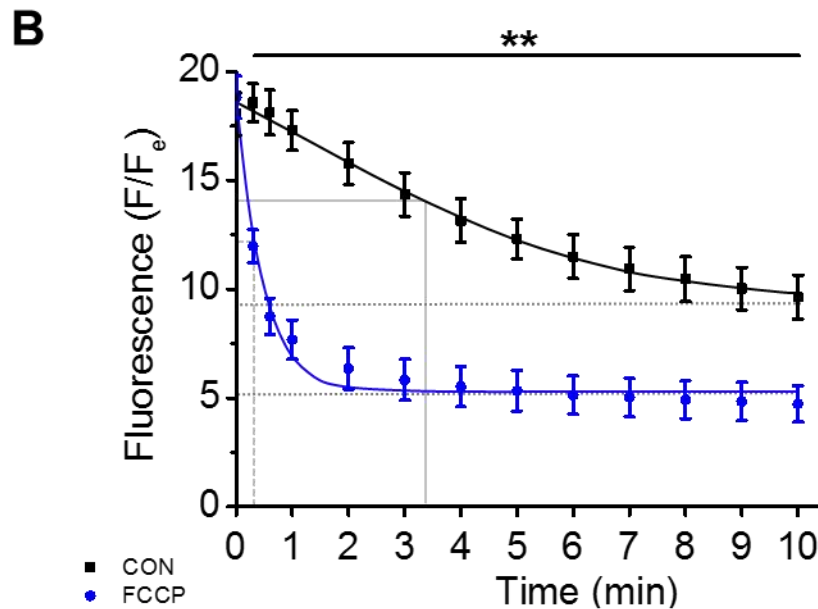
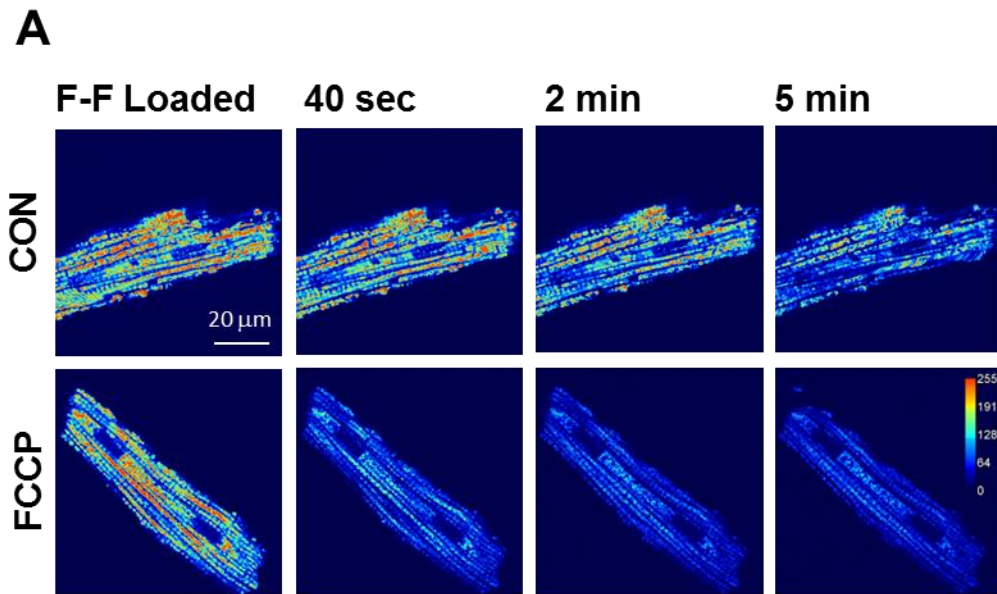


Figure 4.9: Accumulation of 25 μM flecainide-FITC (F-F) within intracellular organelles of saponin permeabilised cardiomyocytes was disrupted by FCCP

A) Representative XY scans of cells after 2 min of loading with flecainide-FITC, then 40 sec, 2 min and 5 min after washout with 30 μM FCCP (FCCP) or without (CON). **B)** Mean change in flecainide-FITC loaded whole cell fluorescence in FCCP (blue) and CON (black) groups. Grey dotted lines represent 90% of the lower asymptote of the Boltzman fitted curve. Grey filled lines represent 50% of the lower asymptote. Two way repeated measures ANOVA + Holm-Sidak *post hoc* test. ** = $p < 0.01$. $n = \text{CON} = 5$ (3), $\text{FCCP} = 5$ (3).

4.3.4 Flecainide-FITC in Triton X-100 permeabilised myocytes

The experiments with FCCP strongly suggest that flecainide-FITC accumulates within the mitochondria. However, a faint mitochondrial pattern was still typically present after FCCP treatment, suggesting that some flecainide-FITC remained within the mitochondria. This residual mitochondrial signal might obscure flecainide binding to other cellular structures. Therefore, cells were exposed to Triton X-100, a non-ionic detergent, which non-selectively disrupts all cellular membranes (Solaro et al., 1971).

Exposure of Triton X-100 treated myocytes to 6 μ M flecainide-FITC resulted in rapid diffuse staining coupled with faint transverse striations (Figure 4.10 A and B). In myocytes loaded with 6 μ M flecainide-FITC, whole cell fluorescence neared 90% of the upper asymptote of the fitted Boltzmann curve at 13.5 sec and the time to half maximal fluorescence was 4.2 sec (Figure 4.10 C; n = 7 cells). Similarly at 25 μ M flecainide-FITC, diffuse staining coupled with faint transverse striations was apparent (Figure 4.11 A and B). Whole cell fluorescence reached 90% of the upper asymptote of the fitted Boltzmann curve at 9.8 sec and the time to half maximum fluorescence was 3.0 sec (Figure 4.11 C; n = 10 cells). Upon cytosolic washout of 6 μ M flecainide-FITC, transverse striations of alternating high and low fluorescent peaks were apparent (Figure 4.12 A). Under these conditions, transverse striations in cells initially loaded with 6 μ M flecainide-FITC were distanced $1.91 \pm 0.02 \mu\text{m}$ and $1.92 \pm 0.02 \mu\text{m}$ apart in high and low fluorescent peaks respectively.

Intracellular solution containing a high concentration of non-fluorescent flecainide was applied to Triton X-100 permeabilised cells as a washout solution to investigate if flecainide-FITC could be competitively displaced. In these experiments, the distances between transverse striations was similar (high, $1.93 \pm 0.02 \mu\text{m}$ and low, $1.94 \pm 0.01 \mu\text{m}$; $p > 0.05$; Figure 4.11 B). The peak to trough ratio of the high fluorescent peaks in control washout cells was 1.88 ± 0.04 (Figure 4.12 C; n = 21 cells (CON)). This was significantly decreased to 1.75 ± 0.05 in cells washed out in the presence of 100 μ M flecainide ($p < 0.05$; Figure 4.12 C, red; n = 26 cells (FLEC)). A similar trend was seen in the peak to trough ratio of the low fluorescent peaks (CON, 1.36 ± 0.02 vs FLEC, 1.31 ± 0.02) although this did not reach statistical significance ($p = 0.07$; Figure 4.12 C, grey).

Upon cytosolic washout of 25 μ M flecainide-FITC, transverse striations of alternating high and low fluorescent peaks were apparent (Figure 4.13 A). All transverse striations were distanced $\sim 1.91 \mu\text{m}$ apart (Figure 4.13 B, from left to right; $1.89 \pm 0.02 \mu\text{m}$; $1.91 \pm 0.03 \mu\text{m}$; $1.91 \pm 0.02 \mu\text{m}$; $1.92 \pm 0.02 \mu\text{m}$). There was no change between CON and FLEC wash out groups when comparing the peak to trough ratios ($1.80 \pm 0.05 \mu\text{m}$ and $1.77 \pm 0.07 \mu\text{m}$ respectively; $p > 0.05$;

Figure 4.13 C, red). There was also no significant change in low fluorescent peak to trough ratio between control and flecainide groups (1.37 ± 0.04 and 1.34 ± 0.05 respectively; $p > 0.05$; Figure 4.13 C, grey; $n = 12$ cells for both groups).

4.3.5 Effect of flecainide-FITC on cardiac Na^+ current

In intact cells, 20 μM flecainide blocked the peak Na^+ current by 71.7% after 12 min incubation at 22.0 ± 2 °C (Figure 3.23). However, flecainide-FITC showed little block of the peak Na^+ current at 10 or 30 μM (Figure 4.14 A-C; $n = 2$ cells). After 5 min incubation with 100 μM flecainide-FITC there was a ~18% decrease in the percent of the peak amplitude.

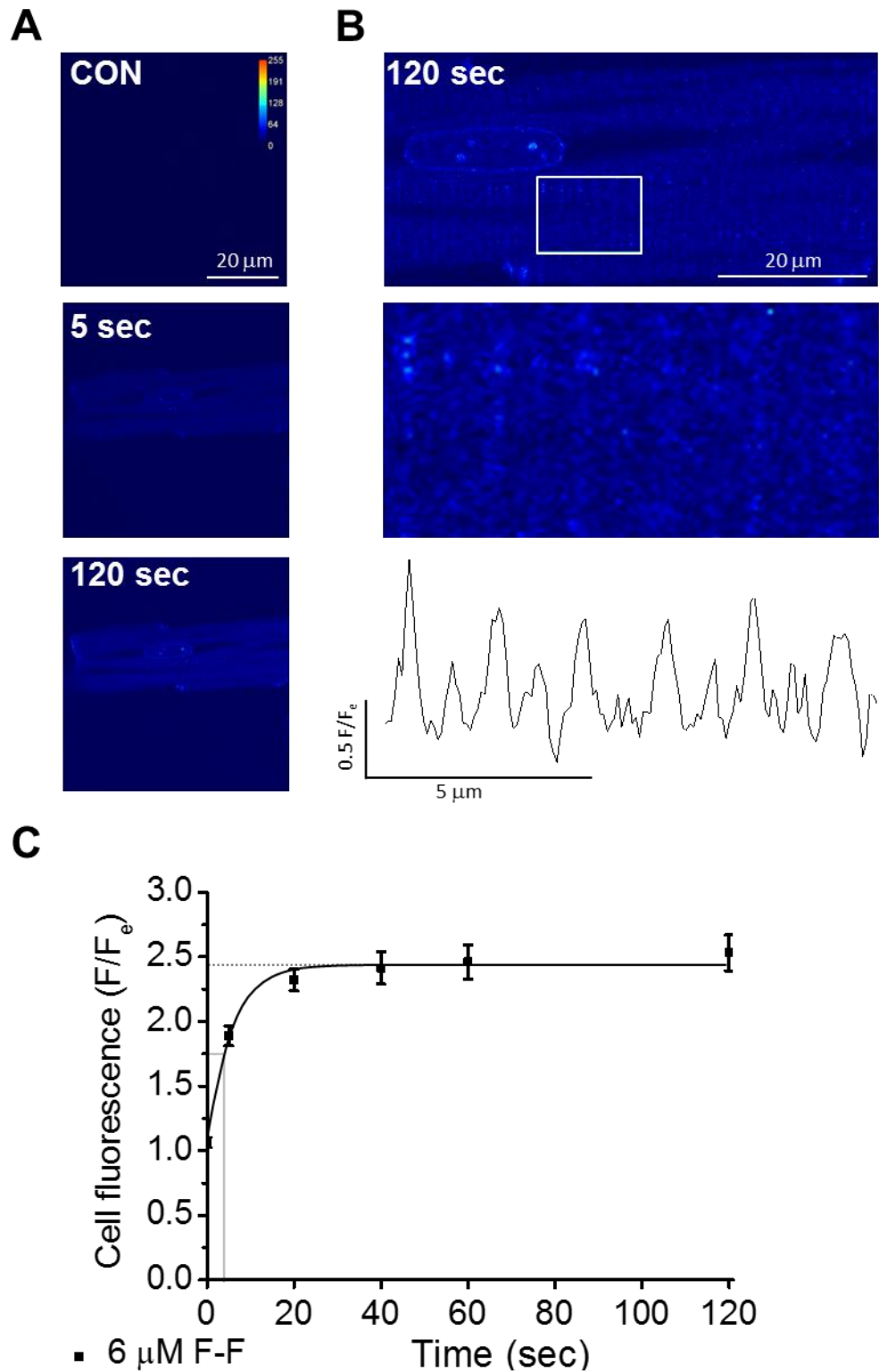


Figure 4.10: Fluorescence pattern of 6 μM flecainide-FITC within Triton-X 100 permeabilised cardiomyocytes

A) Representative XY scans of cells at control and after 5 and 120 sec perfusion with 6 μM flecainide-FITC. **B)** Close up cell section after 120 sec perfusion with flecainide-FITC and fluorescence trace showing transverse striations. **C)** Mean change in whole cell fluorescence in the presence of F-F over 120 sec. $n = 7$ (3).

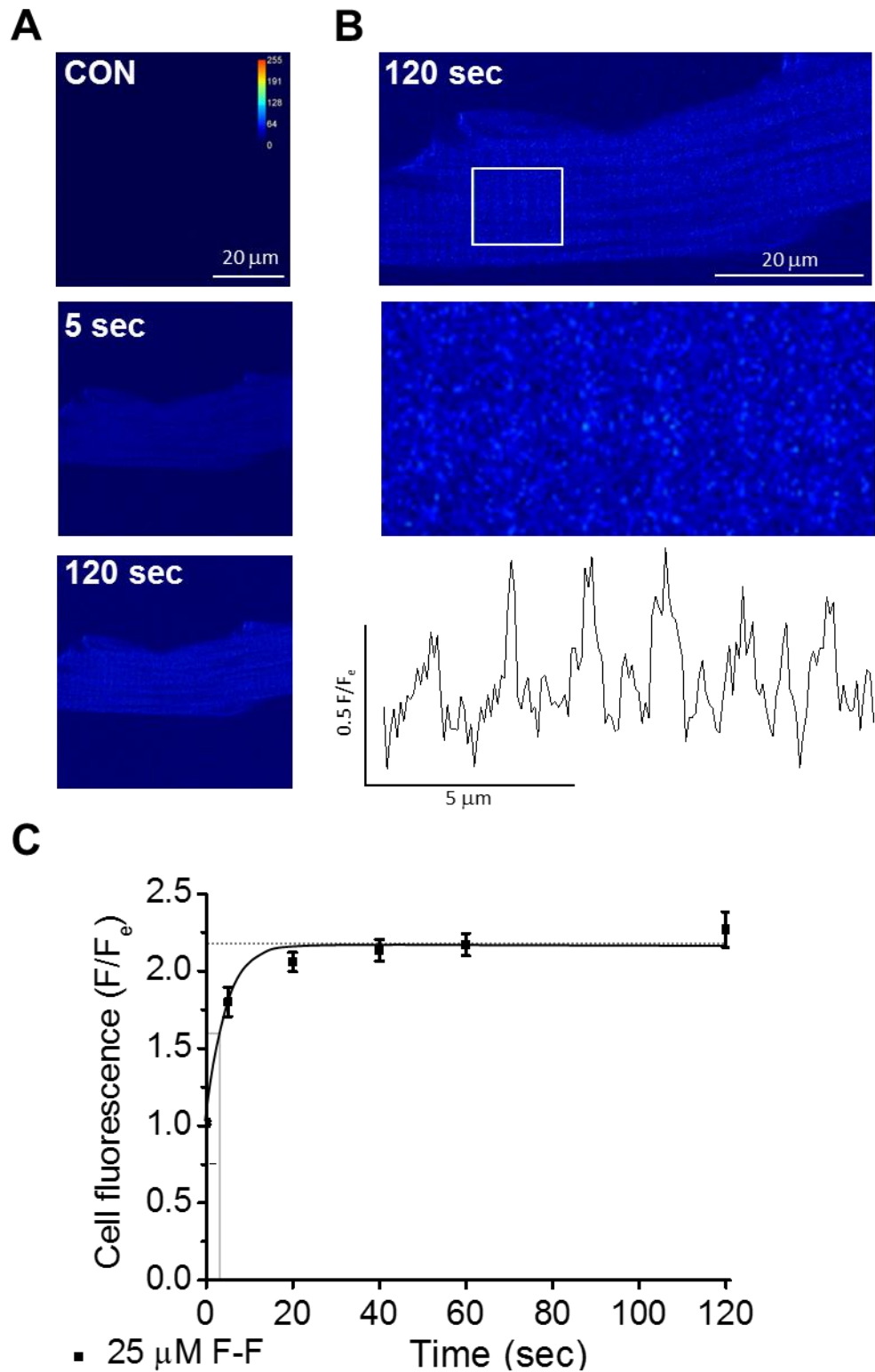


Figure 4.11: Fluorescence pattern of 25 μM flecainide-FITC within Triton-X 100 permeabilised cardiomyocytes

A) Representative XY scans of cells at control and after 5 and 120 sec perfusion with 25 μM flecainide-FITC. **B)** Close up cell section after 120 sec perfusion with flecainide-FITC and fluorescence trace showing transverse striations. **C)** Mean change in cell fluorescence in the presence of flecainide-FITC over 120 sec. $n = 10$ (4).

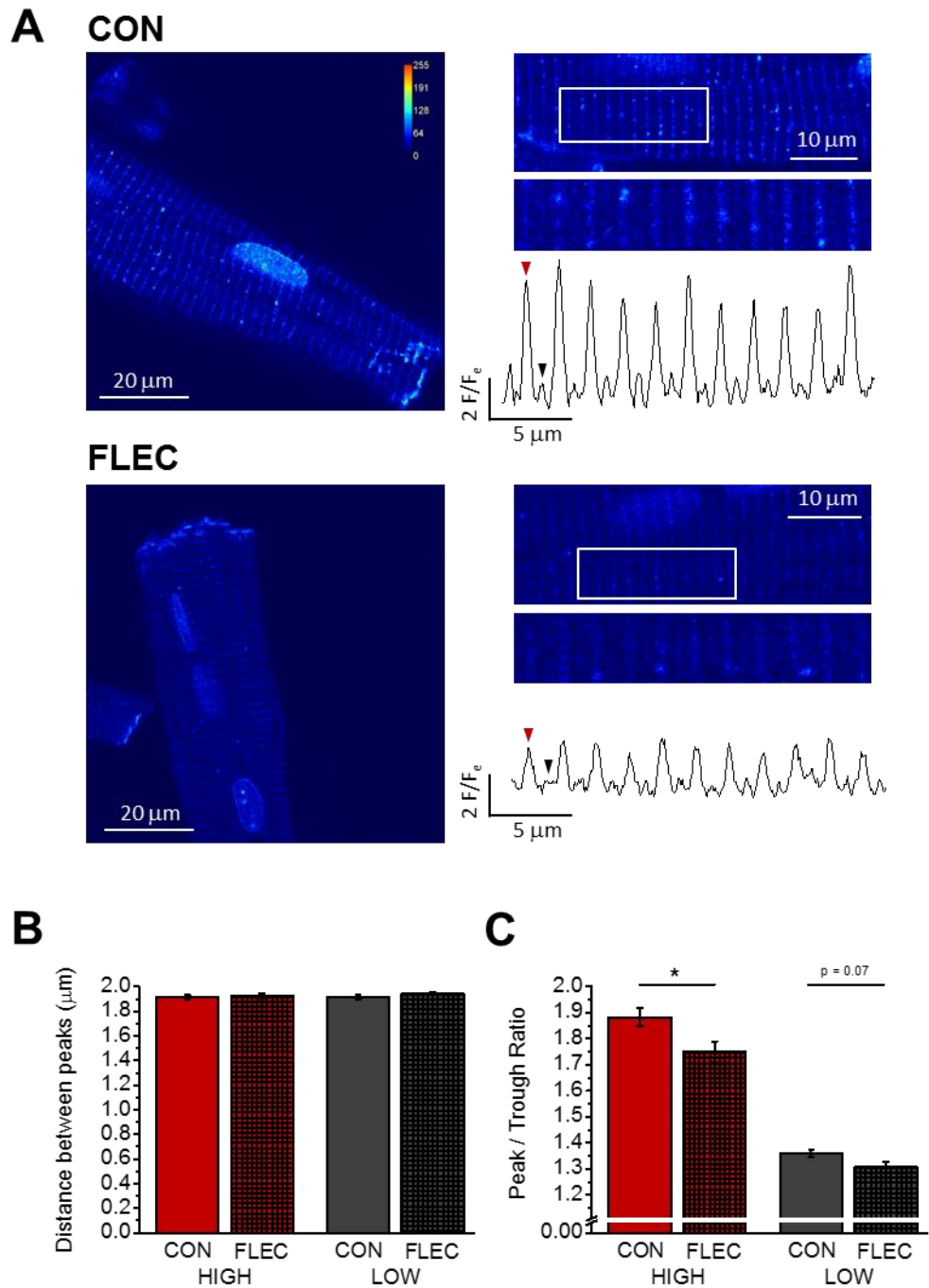


Figure 4.12: Transverse striations visible after 6 μM FITC-flecainide washout with or without 100 μM non-fluorescent flecainide in Triton-X 100 permeabilised cardiomyocytes

A) Representative XY scans and close up sections with fluorescent traces in cells after 7 min washout with 100 μM flecainide (FLEC) or without (CON). **B)** Mean distance between alternate high (HIGH; red triangle) and low (LOW; black triangle) fluorescent peaks in CON and FLEC groups. **C)** Mean peak/trough fluorescence ratio for HIGH and LOW peaks in CON and FLEC groups. Two-tailed unpaired Student's t-test. * = $p < 0.05$. $n = \text{CON} = 21$ (3); FLEC = 26 (3).

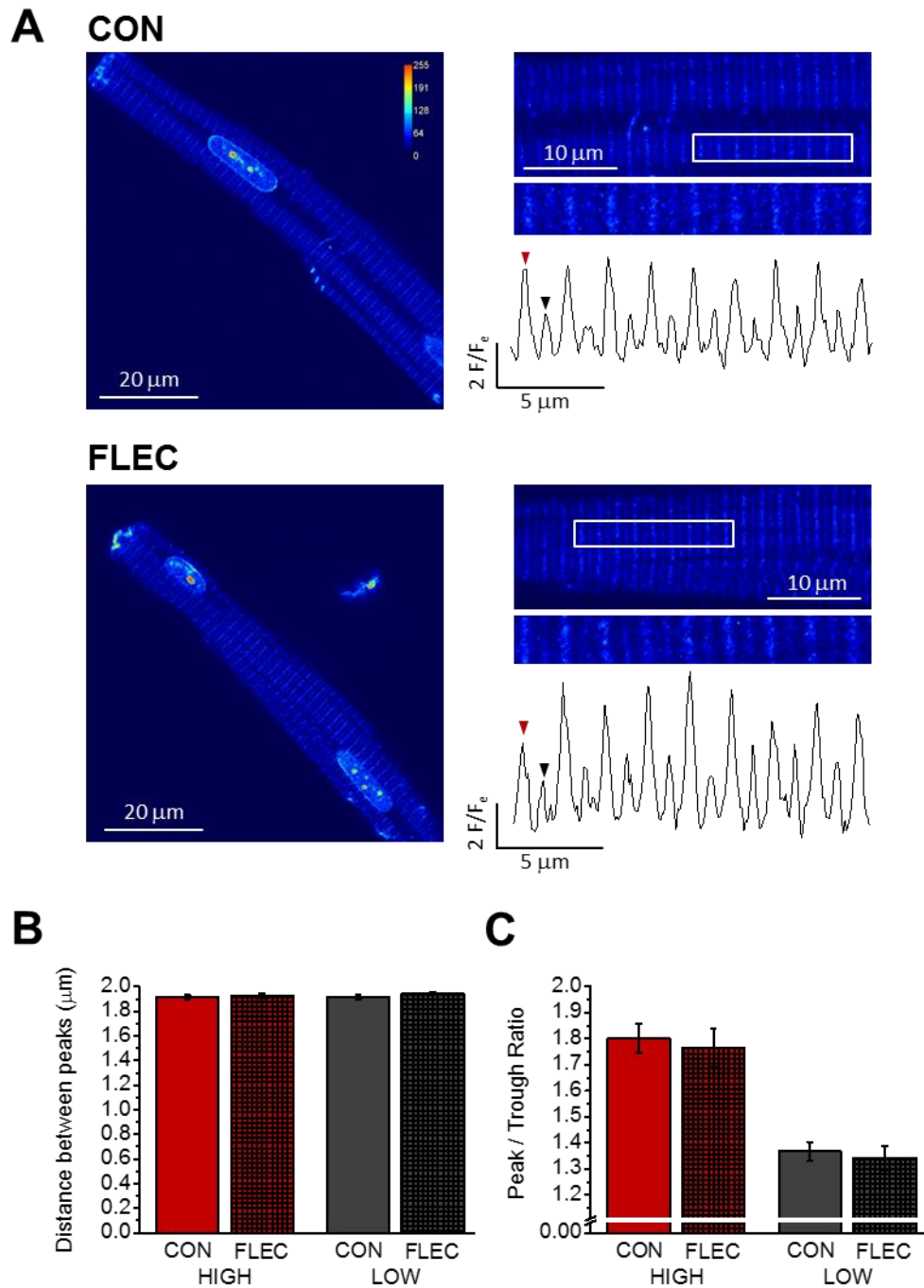


Figure 4.13: Transverse striations visible in Triton-X 100 permeabilised cardiomyocytes after 25 μ M flecainide-FITC washout with or without 100 μ M non-fluorescent flecainide

A) Representative XY scans and dose up sections with fluorescent traces from cells after 7 min washout with 100 μ M non-fluorescent flecainide (FLEC) or without (CON). **B)** Mean distance between alternate high (HIGH; red triangle) and low (LOW; black triangle) fluorescent peaks in CON and FLEC groups. **C)** Mean peak/trough fluorescence ratio for HIGH and LOW peaks in CON and FLEC groups. Two-tailed unpaired Student's t-test. n = CON = 12 (2); FLEC = 12 (2).

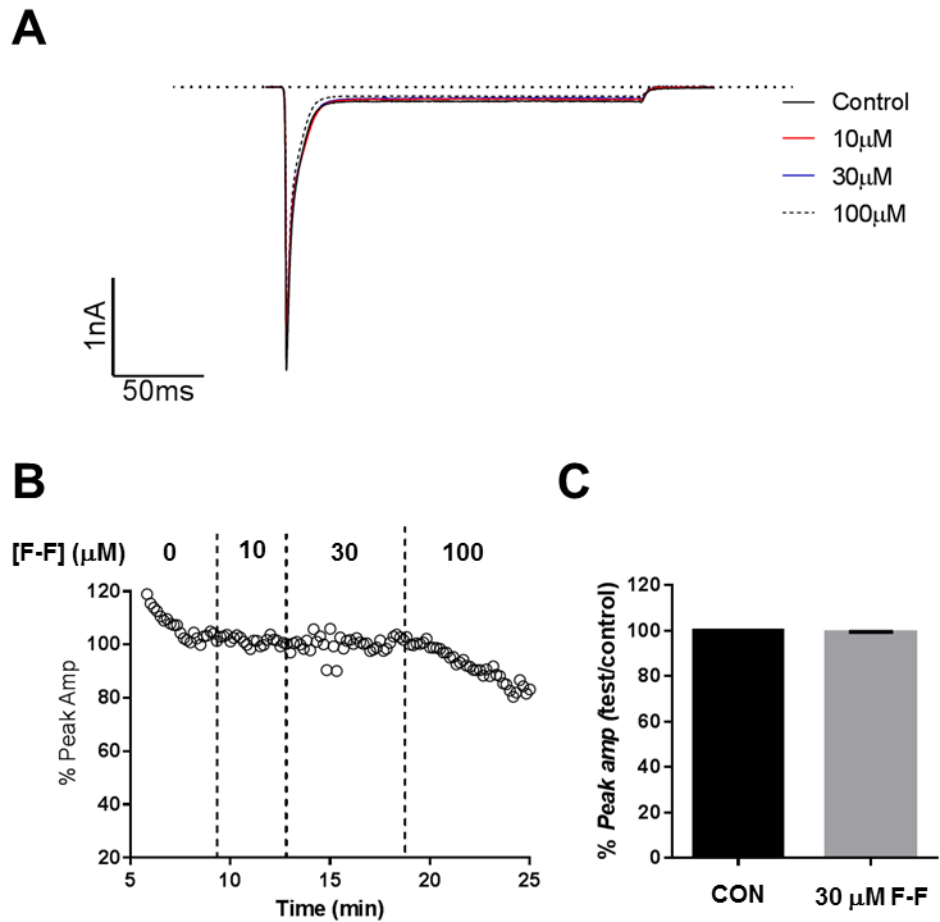


Figure 4.14: Flecainide-FITC block of the cardiac Na⁺ current using patch clamp recording

A) Representative recordings of the peak Na⁺ current at control (black) and with 10 μ M (red), 30 μ M (blue) and 100 μ M (dashed black) flecainide-FITC. **B)** Percentage peak amplitude of the cardiac Na⁺ current upon application of flecainide-FITC. **C)** Mean data of peak amplitude with flecainide-FITC at 30 μ M. n = 2 (1). Patch clamp recordings by Dr Moza Al Owais.

4.4 Discussion

4.4.1 Flecainide-FITC entry into intact cardiomyocytes

In this chapter flecainide-FITC was used to model flecainide entry into intact myocytes. This allowed inferences to be made about the rate and mechanism of flecainide entry, as well as intracellular binding and localization. During cell incubation with flecainide-FITC, cell fluorescence increased over a period of hours, indicating slow flecainide-FITC accumulation into intact cells. The slow accumulation of flecainide is consistent with previous reports that a pre-incubation period of at least 15-30 min is required to observe effects on RyR2 in intact cardiomyocytes isolated from CPVT mice (Hwang et al., 2011b). However, a number of factors including the cellular distribution of flecainide make quantitative conclusions about the concentration of flecainide within the cytosol more difficult.

Movement of flecainide across the cell lipid bilayer will occur via passive diffusion and possibly carrier-mediated transport (Pazdernik and Kerecsen, 2007, Sugano et al., 2010). Passive diffusion of flecainide into the intact cell will occur even though flecainide is ionised at a ratio of 99:1 at physiological pH (7.4) (Liu et al., 2003). Ionised drugs do not readily cross the lipid bilayer. However the lipophilic, neutral proportion of flecainide can move into the cytosol before equilibrating back to its 99:1 charged and uncharged forms, thereby accumulating within the cytosol (Pazdernik and Kerecsen, 2007, Liu et al., 2003). Interestingly, it has been reported that trifluoromethyl groups (-CF₃) such as those incorporated into flecainide's structure (Figure 4.15 A, purple), could increase molecule lipophilicity, thereby increasing passive diffusion of flecainide (Leroux et al., 2008).

The effects of cimetidine suggest that OCTN1 may partially facilitate flecainide-FITC entry into the cell at 25 µM, but not at 6 µM, possibly indicating a low affinity of OCTN1 for flecainide-FITC under these conditions (McBride et al., 2009, Yabuuchi et al., 1998, Yang et al., 2010). Flecainide cell entry via OCTN1 was reported at 4 µM in Chinese Hamster Ovary (CHO) cells (McBride et al., 2009) although this discrepancy may be due to differences in cell types or possible differences in the affinity of OCTN1 for flecainide and flecainide-FITC. OCTN1 uptake of flecainide was reported to be temperature dependent and showed an increased uptake rate at 37 °C compared with experiments performed at room temperature (~22 °C) (McBride et al., 2009). Interestingly, in healthy subjects dosed with flecainide and cimetidine, flecainide plasma levels were increased by ~30% compared with flecainide dosing alone, indicating inhibition of flecainide uptake into organs (BNM-Group, 2013). As clinical administration of flecainide would occur at 37 °C, the proportional effect of OCTN1 may be greater under these

conditions and the relative block by cimetidine, would be greater. The relative lack of effect of cimetidine on flecainide-FITC suggests little effect of OCTN1 under these conditions and that passive diffusion predominantly explains flecainide entry.

All intact cells loaded with flecainide-FITC showed bright, longitudinal “block-like” staining indicative of mitochondrial accumulation (Swift and Sarvazyan, 2000, Boyman et al., 2014a) and the effect of FCCP confirmed this conclusion. The dominance of the flecainide-FITC fluorescence in the mitochondria and the fact that the fluorescence ultimately reached several times that of the drug in the external solution hindered estimation of the cytosolic drug concentration.

In 78.3% of cells, at least one nucleus could be identified and nucleoplasmic fluorescence was analysed separately. The inner and outer nuclear envelope contains nuclear pore complexes which allow the free passage of water soluble molecules < 5000 Da in size (Horowitz, 1972, Bustamante et al., 2000). This should allow flecainide-FITC free passage into the nucleus and provide an estimate of cytosolic flecainide-FITC fluorescence. Flecainide-FITC in the nuclei did not reach the same maximum levels of fluorescence as that measured in the whole cell, indicating a lower concentration of flecainide-FITC within the nuclei compared with the mitochondria at both 6 and 25 μM extracellular flecainide-FITC. Assuming that the drug concentration is the same in the nucleus and the cytosol, it might be possible to use the nucleoplasmic signal as a proxy for cytosolic flecainide-FITC fluorescence. Interestingly, nuclear fluorescence values $>1 F/F_e$ were apparent after 20 min incubation with both flecainide-FITC concentrations, which might suggest that cytosolic as well as mitochondrial accumulation to levels above that present outside the cell. However, FITC fluorescence is likely to be influenced by binding to proteins within each compartment (Thomas et al., 2000). Consequently, a quantitative conclusion about the level of flecainide-FITC within the cytosol is not possible without calibration of the signal.

The acid dissociation constant (pK_a) of a drug and the environmental pH determine the degree of drug ionisation and therefore influence the primary mechanism of transport across biological membranes. The pK_a of flecainide-FITC at physiological pH is currently unknown and therefore it is difficult to interpret if flecainide-FITC movement is truly representative of flecainide. However as detailed above, our data correspond with previous reports of slow flecainide entry and intracellular accumulation (Hwang et al., 2011b), indicating that our extrapolation may be valid.

These experiments suggest that RyR2 mediated effects of flecainide cannot be investigated in intact cardiomyocytes without a prolonged (>20 min) incubation period. This is to ensure that flecainide can cross the lipid bilayer to reach its intracellular target. Therefore, experiments with a 5 min incubation period could not have expected to see any changes in RyR2 function (Sikkel et al., 2013). In contrast, when the incubation period was increased in CPVT models, RyR2 mediated effects were present (Hilliard et al., 2010, Hwang et al., 2011b). However, as this incubation time scale was not appropriate in WT myocytes (Chapter 3) longer incubation period may be required in WT cells to allow further accumulation of flecainide, if the affinity of WT RyR2 for flecainide were decreased. Additionally, drug accumulation into the mitochondria may delay the rise in cytosolic drug content, as is clear when measuring nucleic fluorescence. In which case, equilibrium between the mitochondria and cytosol may be necessary before flecainide functionally affects RyR2. It must also be considered that flecainide may accumulate into the mitochondria and thereby preclude cytosolic accumulation (Chapter 7).

4.4.2 Flecainide-FITC within permeabilised cardiomyocytes

In saponin permeabilised cells the lipid bilayer is disrupted at cholesterol rich lipid raft regions allowing equilibration of the external solution with the intracellular environment (Shany et al., 1974, Goldenthal et al., 1985, Saka et al., 2014). In permeabilised cells the pattern of flecainide fluorescence was similar to that in intact cells and the effects of FCCP confirmed mitochondrial localization. FCCP strongly depolarises the mitochondrial membrane potential by creating proton selective pores which dissipate the proton gradient (Park et al., 2002). These experiments also suggest that mitochondrial concentration of the drug is reliant upon the negative mitochondrial membrane potential. This is consistent with reports from other cationic drugs such as amiodarone, which also accumulate within the mitochondria (Moreau et al., 1999, Szewczyk and Wojtczak, 2002).

The rate of flecainide-FITC movement across the mitochondrial membrane was an order of magnitude greater than across the sarcolemma. Entry through the outer mitochondrial membrane would likely be unimpeded due to the presence of porins or voltage dependent anion channels (VDAC) which allow the free passage of molecules up to 5000 Da into the perimitochondrial space (Colombini, 1979, Alberts et al., 2008). However, the mechanism of entry of flecainide-FITC across the inner mitochondrial membrane is currently unclear as this membrane is reported to be impermeable to the majority of solutes (Fontanesi, 2015). Mitochondria are polarised so that the interior matrix is more negatively charged than the surrounding cytosol giving rise to an electrochemical gradient which ionized flecainide-FITC and flecainide could move down (Perry et al., 2011, Pourahmad et al., 2015). The time to 50%

of the maximal fluorescence was 4.2 times faster at 25 μM flecainide-FITC than at 6 μM . Considering that the concentration of 25 μM flecainide-FITC is 4.2 times greater than at 6 μM , a linear relationship between uptake rate and drug concentration could be assumed, indicative of passive uptake (Sugano et al., 2010). However, if active transport of flecainide-FITC had not yet reached transporter saturation then a similar relationship may be present (Sugano et al., 2010). The inner mitochondrial membrane is reported to have a 3:1 ratio of protein to lipids with many enzymes and transporters present which are necessary for the electron transfer chain (Fontanesi, 2015). Subfamilies of transporters within the Mitochondrial Carrier Family (MCF) facilitate the transport of a variety of highly specific substrates across the inner mitochondrial membrane (Palmieri and Pierri, 2010). Flecainide-FITC may be able to utilise one of these mitochondrial transporters to gain access to the mitochondrial matrix, however, a specific target has not been identified.

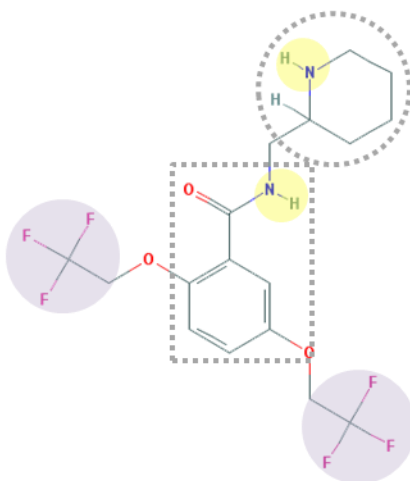
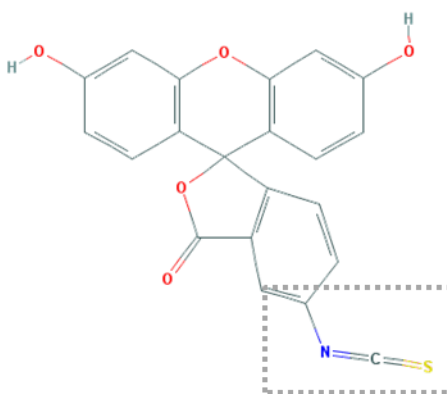
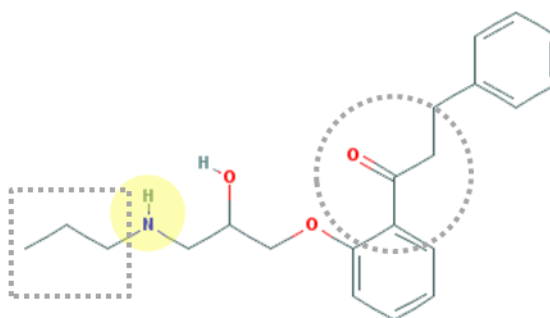
After two of minutes loading with either 6 or 25 μM flecainide-FITC, the cell fluorescence signal was close to, but not at, the saturation point of the detection system (6 μM = 182 ± 7.96 F; 25 μM = 128.45 ± 12.10 F; maximum = 255 F). This indicates that the fluorescence plateau seen at ~ 120 and ~ 10 sec for 6 and 25 μM flecainide-FITC respectively was not limited by the maximum signal intensity able to be obtained by the microscope and attached PMT. Therefore, it can be hypothesised that after this fluorescence plateau has been reached, flecainide-FITC could form a dynamic equilibration between the mitochondria and remaining cytosol. Indeed, during washout of flecainide-FITC in saponin permeabilised cells, a decrease in cell signal was apparent over 10 min indicating flecainide-FITC efflux from the mitochondria (Figure 4.7 and 4.8).

To investigate flecainide-FITC cell localisation without the dominant mitochondrial signal, cells were permeabilised with Triton X-100 before exposure to flecainide-FITC (Willingham, 2010). Prior to flecainide-FITC washout, faint transverse striations were apparent amongst the diffuse and presumably non-specific whole cell staining. Following loss of this background staining during flecainide-FITC washout, transverse striations were clearly observed indicating flecainide-FITC bound to subcellular structures. Binding of 6 μM flecainide-FITC to these transverse structures could be competitively displaced by 100 μM flecainide. Competitive displacement of 25 μM flecainide-FITC was not apparent, likely due to the relative decrease in flecainide competition. However, this is compelling evidence for a true binding site of both flecainide and flecainide-FITC, although it is not clear exactly what the binding site is. Both high and low fluorescent peaks were spaced ~ 1.90 μm apart which is somewhat higher than reported sarcolemmal lengths of between 1.70 – 1.80 μm (Jayasinghe et al., 2009, Bub et al.,

2010) but is consistent with sarcomere lengths measured by colleagues from within the same laboratory (Fowler, 2015). Flecainide has previously been reported to bind to RyR2, which is aligned transversely at the dyadic junctions (Hwang et al., 2011a, Hilliard et al., 2010, Jayasinghe et al., 2009, Hiess et al., 2015), and Na_v1.5, aligned transversely within t-tubule membranes (Wang et al., 2003, Mohler et al., 2004). However, to confirm flecainide-FITC binding to these structures and remove the possibility of non-specific binding (e.g. desmin) (Robinson et al., 2016), co-localisation immunocytochemistry experiments combining flecainide-FITC with specific RyR2 and Na_v1.5 fluorescent antibody staining would be required.

4.4.3 Flecainide-FITC properties

Flecainide-FITC is a novel tool from which valuable information about flecainide's entry and location within intact and permeabilised myocytes could be extrapolated. However, it was observed in preliminary electrophysiological data that flecainide-FITC only shows minor inhibition of the cardiac I_{Na} at 100 μM, whereas flecainide had a pronounced effect at 20 μM. This indicates that the FITC moiety may interfere with flecainide's active site, required for binding to Na_v1.5 (Wang et al., 2003). The decrease in I_{Na} peak amplitude at 100 μM may be indicative of flecainide-FITC inhibition of other Na⁺ channel isoforms (Westenbroek et al., 2013). The exact binding site of FITC to flecainide remains undisclosed by the manufacturer, but it is known that FITC reacts via its isothiocyanato group (Figure 4.15 B, dotted rectangle) to bind with an amine group (Severn-Biotech, 2016). Flecainide has two secondary amine groups (Figure 4.15 A, yellow circles) located at the piperidine ring (Figure 4.15 A, dotted circle) and the benzamide ring (Figure 4.15 A, dotted rectangle). Both the piperidine and benzamide groups have been implicated as active drug sites which can inhibit the hERG or K_v11.1 potassium channel (Melgari et al., 2015a). It is therefore possible that either of these sites could also act as the active site for Na_v1.5 and that FITC binding prevents the binding and functional inhibition of Na_v1.5. Alternatively, the amine groups located at the piperidine and benzamide rings may not be the flecainide binding sites for Na_v1.5, but instead project out into the channel pore to repel positive ions, as is reported to be the case in the K_v2.1 channel (Madeja et al., 2010). If the transverse striations seen in Figure 4.11 and 4.12 were found to co-localise with Na_v1.5, this may explain a loss of flecainide functionality in Na_v1.5 block, without a loss of Na_v1.5 binding. Despite this ambiguity, these potential binding or blocking sites could not be avoided when attaching -FITC or another fluorescent tag. Interestingly, a primary amine group located away from the benzene-like ring structure of another flecainide-like antiarrhythmic drug, propafenone, could provide a suitable conjugation site (Figure 4.15 C, rectangle) (Savio-Galimberti and Knollmann, 2011, Boyle, 2016).

A**B****C****Figure 4.15: Molecular drug structures**

A) Flecainide, with piperidine ring (circle) and bezamide ring (rectangle) emphasised; **B)** FITC with isothiocyanato group (rectangle) emphasised; and **C)** propafenone with propyl (rectangle) and carbonyl (circle) groups emphasised. Yellow circles highlight amine groups present in flecainide and propafenone structures. Purple circles highlight trifluoromethyl groups present in the flecainide structure. Structure images taken from <http://pubchem.ncbi.nlm.nih.gov>.

However, if this amine group also projects into the Na_v1.5 pore to block it, similar problems may arise (Madeja et al., 2010).

Another caveat of FITC is that whilst it was reported to be impermeable to intact cells, a small increase in FITC fluorescence over time has been reported in intact cardiomyocytes (Pan et al., 2014). Unlike at 25 μM FITC, the fluorescence values at 6 μM FITC had not plateaued by 3 hours indicating further uptake was possible. However the uptake rates of flecainide-FITC and FITC were significantly different at both concentrations. It is unknown exactly if or how the FITC tag could aid or hinder flecainide-FITC entry. However due to significant differences in FITC and flecainide-FITC uptake it seems likely that the results observed with flecainide-FITC can be extrapolated to further understand flecainide cell kinetics. Investigating the cellular uptake of FITC conjugated dextran (10 kDa) would control for the possibility of cell permeabilisation with time (Seidel et al., 2017). It is important to note that the level of contaminating free FITC present in the flecainide-FITC drug sample was essentially undetectable in the analysis provided by the company (Severn-Biotech, 2016).

4.4.4 Conclusions and summary

In this chapter, flecainide-FITC was used as a tool to obtain information about the rate of flecainide cell entry and subcellular localization. Based on these novel data, it seems likely that flecainide is capable of entering and accumulating within the intact cardiomyocyte over a period of hours. Entry into the myocyte is likely due to passive diffusion of the neutral portion of the drug. Additionally at higher concentrations, flecainide uptake is partially facilitated by active transport via the OCTN1 transporter. Once within the cell, flecainide accumulation into the mitochondria is fast and dependent upon a negative mitochondrial matrix. Additional binding to transversely orientated structures, possibly Na_v1.5 and/or RyR2, was also apparent although super resolution immunofluorescence microscopy experiments would be required to confirm this.

These findings and the data from Chapter 3 suggest that cell experiments with flecainide require long incubation periods to ensure flecainide has crossed the lipid bilayer barrier and equilibrium between the mitochondria and the cytosol has been reached. In primary cardiomyocytes, extended drug incubation periods are impractical due to limited cell viability. Additionally, cultured cells show t-tubular loss, making them inappropriate to investigate small changes in Ca²⁺ release after incubation with flecainide (Pavlovic et al., 2010) To ensure near immediate application of flecainide to intracellular proteins, saponin permeabilised cells will

henceforth be used to study the effect of flecainide on RyR2. As cell permeabilisation also removes the membrane potential across the cell lipid bilayer, voltage-gated $\text{Na}_v1.5$ are rendered functionless and any effect of flecainide cannot be attributed to its $\text{Na}_v1.5$ inhibition.

Chapter 5: The effect of flecainide on Ca²⁺ handling in permeabilised ventricular myocytes

5.1 Introduction

There is a clear action of flecainide on Ca²⁺ sparks and pro-arrhythmic Ca²⁺ waves in CPVT intact myocytes (Hilliard et al., 2010). However, a similar action on sparks in WT ventricular intact rat myocytes could not be reproduced (Chapter 3) (Sikkel et al., 2013). This might have been due to the short (5 min) incubation time used by Sikkel et al. (2013) as flecainide is mostly charged at physiological pH (Liu et al., 2003) thereby markedly slowing its rate of entry into myocytes (Hwang et al., 2011b, Sikkel et al., 2013). However, even a prolonged incubation period (45-120 min) with flecainide (15 µM) had no effect on Ca²⁺ spark properties in intact WT rat ventricular myocytes (Chapter 3). This might be explained if flecainide has no effect on RyR2 in WT rat cardiomyocytes (Sikkel et al., 2013). Alternatively, flecainide concentration within the cytosol may not be high enough to have a major effect on WT RyR2, even after 2 hours.

XY imaging of intact WT ventricular myocytes after application of flecainide-FITC confirmed the slow trans-sarcolemmal drug entry (Chapter 4). Rather than a simple equilibration between the extracellular solution and the cytosol, flecainide-FITC markedly accumulated into the mitochondria. This may partly explain previous reports in which flecainide accumulates within cardiac tissues (Latini et al., 1987, Mishima et al., 1999). Mitochondrial accumulation of flecainide is likely due to the large electronegative potential across the inner mitochondria membrane and a similar effect has been reported with other cationic drugs, such as amiodarone (Moreau et al., 1999, Westenbroek et al., 2013). By a similar argument, the cytosolic level of flecainide might eventually exceed that outside the cell, as flecainide moves into the negative cytosol (relative to the extracellular matrix) and particularly if an equilibrium between the mitochondria and cytosol is reached. However, given the dominant flecainide-FITC signal in the mitochondria, the experiments described in Chapter 4 did not establish the cytosolic flecainide concentration in intact cells with certainty. In the clinical setting, where regular and long-term dosing is usual, slow trans-sarcolemmal movement of a drug may be unimportant. Yet as evidenced by results presented in Chapter 5 and by Sikkel et al. (2013), this poses a problem experimentally.

One way in which the uncertainty regarding the cytosolic concentration of flecainide could be addressed is via selective permeabilisation of the sarcolemma. Saponin disrupts the sarcolemmal cholesterol rich lipid raft regions, whilst the SR membrane and its associated proteins remain *in situ* and functional (Shany et al., 1974, Goldenthal et al., 1985, Saka et al., 2014, Lukyanenko and Gyorke, 1999). Without a barrier to diffusion, the concentration of flecainide in the space proximal to RyR2 should be equivalent to the surrounding solution, despite persistent mitochondrial accumulation. Additionally, Na_v1.5 is rendered functionless. Thus, changes in Ca²⁺ wave and spark release properties likely reflect an action of flecainide on intracellular proteins, including RyR2. One disadvantage of the saponin permeabilised cell model is that molecules up to 800 kDa in size can diffuse out of the cell (Hudder et al., 2003). This likely includes cytosolic modulators such as CaM (16.7 kDa). SR Ca²⁺ release has been reported to be altered due to lack of CaM-RyR2 binding (Yang et al., 2014, Xu et al., 2010) which in turn may alter the action of flecainide upon RyR2 (Gomez-Hurtado et al., 2015).

In this chapter, the sustained effect of flecainide on Ca²⁺ waves, sparks and SR content was investigated in saponin permeabilised WT rat ventricular myocytes. The possible dependence of flecainide's effect on CaM will also be investigated via restoration of physiological CaM concentration.

5.2 Methods

5.2.1 Permeabilised myocyte imaging protocol

Rat ventricular cardiomyocytes were isolated via retrograde perfusion and enzymatic digestion on a Langendorff apparatus (Chapter 2.2). Cells were saponin permeabilised for 15 min at room temperature (22 ± 2 °C) with 0.01% saponin in permeabilisation solution (Table 2.3). Cells were placed in the experimental chamber on the stage of a Nikon Diaphot inverted microscope and viewed with a $\times 40$ oil immersion lens (Nikon Plan Fluor DLL, numerical aperture 1.3). A confocal laser-scanning unit (Bio-Rad, Cellmap) was attached to the side port of the microscope. Cells were left for 2 min to settle onto the glass cover slip of the experimental chamber and perfusion of control intracellular solution began. The control intracellular solution also contained 10 μM fluo 3 in its free acid form when imaging waves and 15 μM fluo 3 in its free acid form when imaging sparks.

Intracellular solution contained 146 nM free Ca^{2+} (LOW [Ca^{2+}]) or 286 nM free Ca^{2+} (HIGH [Ca^{2+}]) and both solutions contained 0.1 mM EGTA (Table 2.4). Experiments investigating SR Ca^{2+} content used intracellular solution containing HIGH [Ca^{2+}]. An identical solution except for the addition of 20 mM caffeine was briefly applied to the cells to induce SR Ca^{2+} release. In experimental protocols which precluded Ca^{2+} waves, the intracellular solutions were strongly buffered with 0.35 mM EGTA and contained 139 nM free Ca^{2+} (0 waves; Table 2.4). All free [Ca^{2+}] were calculated using REACT software and assumed 10 μM Ca^{2+} contamination and a temperature of 22 °C (Table 2.4) (Orchard et al., 1998, Duncan et al., 1999). The intracellular solutions were freshly prepared on each experimental day and split into control and flecainide solutions to eliminate any differences in [fluo-3] and [Ca^{2+}] differences.

Two scanning protocols were used. The first protocol measured changes in Ca^{2+} wave or spark properties during 3 min perfusion with flecainide in either HIGH [Ca^{2+}], LOW [Ca^{2+}] or in solution that precluded the presence of waves (0 waves). In this protocol, cells were continually scanned. Cells were perfused with control intracellular solution for 3 min before solution was switched to 25 μM flecainide or vehicle (0.001% ethanol) intracellular solution for 4 min (Table 2.3). In the permeabilised cell model, flecainide was used at a concentration 5x greater than that recorded during peak plasma levels (Mano et al., 2015, 3M, 2016). This was to mimic the accumulation of the drug into the cytosol and subcellular compartments, as reported in Chapter 4. Images were acquired in line scan mode at 188 lps, along the longitudinal axis of the cell for 4 min and 45 sec. The first 45 sec of each line scan was under control conditions and the remaining scan period was in the presence of flecainide or vehicle.

The second protocol measured changes in Ca^{2+} wave properties during 6 min perfusion with flecainide in HIGH $[\text{Ca}^{2+}]$. Images were acquired for 30 sec at 60 sec intervals. This protocol aimed to investigate long term changes in SR Ca^{2+} release, whilst minimising the total laser exposure time. Cells were perfused with control intracellular solution for 3 min before introduction of flecainide or vehicle for 6 min. Images were acquired in line scan mode at 188 lps, along the longitudinal axis of the cell. The first line scan imaged the cell under control conditions. The 5 subsequent line scans imaged the cell at 1–5 min after flecainide perfusion had begun.

A higher concentration of flecainide (25 μM) was used in experiments involving permeabilised myocytes. In previous pilot experiments, 25 μM flecainide was found to be the minimum concentration required to affect SR Ca^{2+} release (Steele and Yang, 2017). Peak levels of flecainide in the plasma are reported to be much lower ($\sim 5 \mu\text{M}$) however accumulation of flecainide within the myocyte may occur (Chapter 4) (Latini et al., 1987, Mishima et al., 1999, Mano et al., 2015, 3M, 2016).

5.2.2 Application of exogenous CaM

To investigate the effect of CaM on Ca^{2+} wave properties, 100 nM exogenous CaM (Sigma, bovine brain) was applied to permeabilised myocytes to mimic the physiological level of cytosolic CaM (Wu and Bers, 2007, Gomez-Hurtado et al., 2015, Oo et al., 2015, Maier et al., 2006). Cells were placed in the experimental chamber and perfused with control intracellular solution (HIGH $[\text{Ca}^{2+}]$) or an identical solution containing 100 nM CaM for 2 min. Cells were line scanned for 30 sec at 188 lps, along the longitudinal axis of the cell.

To investigate the effects of flecainide on Ca^{2+} wave properties in the presence of 100 nM exogenous CaM, cells were placed in the experimental chamber and perfused with CaM intracellular solution for 2 min. The cell was initially line scanned for 30 sec under CaM control conditions. Solution was then switched to CaM intracellular solution containing 25 μM flecainide or vehicle and the cell was line scanned for 30 sec at 60 sec intervals for 6 min.

5.2.3 Semi-quantification of CaM in intact and permeabilised ventricular myocytes

Rat ventricular myocytes were isolated via retrograde perfusion and enzymatic digestion on a Langendorff apparatus. All isolated cells were pooled and split into 3 experimental groups.

Cells within group 1 (INTACT) were incubated for 15 min at 22 ± 2 °C in intracellular solution. Cells within group 2 (PERM) were saponin permeabilised (Chapter 2.5.1) for 15 min with 0.01% saponin at 22 ± 2 °C. Cells within group 3 (PERM + 15) were saponin permeabilised (15 min, 0.01%, at 22 ± 2 °C) and remained in intracellular solution for a further 15 min post-permeabilisation.

Samples were re-suspended in 2 ml of homogenisation buffer (Table 2.5) and the protein concentration for each sample was calculated using a BCA assay (Chapter 2.8.2). Equal volumes of protein were loaded into a 12% acrylamide gel and a constant voltage of 50 V was applied for the initial 30 min of protein separation by electrophoresis. Thereafter a constant voltage of 120 V was applied until the 10 kDa MW ladder size ran off the gel (Chapter 2.8.3). All protein was transferred from the acrylamide gel to an activated PVDF membrane via semi-dry transfer (Chapter 2.8.4). Thereafter the membrane was blocked with blocking buffer (Table 2.5) to prevent non-specific antibody binding. Membranes were incubated with rabbit monodonal anti-CaM primary antibody or mouse monodonal anti- β -actin primary antibody each diluted to 1:1000 in blocking buffer, overnight at 4 °C. Excess primary antibody was then washed away with washing buffer (Table 2.5) and the membrane was incubated with anti-rabbit or anti-mouse (as appropriate) secondary antibody conjugated to HRP diluted to 1:15,000 in washing buffer for 90 min at 22 ± 2 °C. Excess secondary antibody was washed away with washing buffer and antibody bound proteins were visualised using an ECL kit and a digital membrane imaging system (G:BOX Genesys, Syngene, UK; Chapter 2.8.5).

5.2.4 Analysis

The time between each Ca^{2+} wave was measured using the ImageJ Line Profile Tool. The number of waves were then presented as a frequency (waves/min). Analysis of Ca^{2+} wave peak amplitude, upstroke rate, duration from the peak to 90% of the Ca^{2+} decline and Ca^{2+} decline time constant was semi-automated as previously described (Chapter 2.7.2) (Benson, 2016). Analysis of Ca^{2+} wave propagation velocity was semi-automated as previously described (Chapter 2.7.3) (Sikora, 2016). Partial waves which propagated <50% of the recorded cell width were not included in the analysis. Ca^{2+} sparks were analysed using the Sparkmaster ImageJ plugin (Chapter 2.7.4) (Picht et al., 2007). Ca^{2+} sparks were measured at HIGH [Ca^{2+}], LOW [Ca^{2+}] and in high EGTA conditions where waves were absent (0 waves). In the presence of Ca^{2+} waves, line scans were cropped into 15 x 1 sec segments, 15 sec prior to a Ca^{2+} wave. Segments that included a wave or were 1 sec post wave were not included in the final analysis.

In the absence of waves, line scans were cropped into 15 x 1 sec consecutive segments within 20 sec of the start of the line scan to ensure comparable cell laser exposure. To investigate changes in Ca²⁺ sparks upon application of flecainide, the intracellular solution, which precluded wave formation (0 waves) was used. Ca²⁺ sparks were analysed under control conditions and after 20, 40, 60 and 180 sec after the solution switch.

5.2.5 Statistics

Two independent groups were statistically analysed with an unpaired two tailed Student's t-test. Three or more independent groups were statistically analysed with a one way ANOVA and a Holm-Sidak *post hoc* test to determine which groups were significantly different. Changes in wave parameters at control and after 3 or 5 min perfusion with experimental solution were displayed as absolute values in a bar graph, in the presence or absence of flecainide. Two tailed paired Student's t-tests were used to test for differences within each group at these two time points. Differences between the absolute values at the control time point were compared between each group using a two tailed unpaired Student's t-test. For each cell scanned, the change in wave properties, as a function of time was also presented as a percentage of control. The differences between control and flecainide groups were compared using a two way repeated measures ANOVA. If a significant difference was identified between the groups, a Holm-Sidak multiple comparisons *post-hoc* test isolated the time points at which the groups were significantly different from one another. Histograms were produced using GraphPad Software. A Gaussian curve was fitted to each dataset and the r^2 goodness of fit was consistently calculated at >0.82. Where the r^2 goodness of fit was <0.90, a Lorentzian curve was also applied, although there was no difference in statistical outcomes between different curve fittings. An extra sum of squares F test was applied to each histogram to test the difference between distributions at control and after perfusion with experimental solution. Statistical analysis was performed using SigmaStat or GraphPad and significance was considered when $p < 0.05$. All data were displayed as mean \pm SEM.

5.3 Results

5.3.1 The effect of $[Ca^{2+}]$ on permeabilised myocyte Ca^{2+} release

Figure 5.1 A shows representative line scans and fluorescence profiles of saponin permeabilised cells which spontaneously and periodically produced Ca^{2+} waves when perfused with intracellular solution containing LOW or HIGH $[Ca^{2+}]$. Individual Ca^{2+} waves at each $[Ca^{2+}]$ are shown in Figure 5.1 B. The wave front was highlighted as a red angled line across the length of the cell and depicted wave propagation velocity. At HIGH $[Ca^{2+}]$, Ca^{2+} wave frequency was 3.3 fold greater than that at LOW $[Ca^{2+}]$ ($p < 0.001$; Figure 5.1 C). There was no significant difference in propagation velocity between groups ($p > 0.05$; Figure 5.1 D; $n = 31$ cells for both groups). Representative line scans and fluorescence profiles of individual Ca^{2+} waves were shown in Figure 5.2 A. Wave amplitude significantly decreased at HIGH $[Ca^{2+}]$ compared with LOW $[Ca^{2+}]$ (4.20 ± 0.18 vs $3.30 \pm 0.12 \Delta F/F_0$; $p < 0.001$; Figure 5.2 B). Similarly wave upstroke rate was significantly decreased at HIGH $[Ca^{2+}]$ (0.050 ± 0.003 vs $0.037 \pm 0.002 (\Delta F/F_0)/ms$; $p < 0.01$; Figure 5.2 C). Free $[Ca^{2+}]$ increased wave duration from the peak to 90% of the Ca^{2+} decline (511.5 ± 27.1 ms vs 611.2 ± 37.8 ms; $p < 0.05$; Figure 5.2 D) but the Ca^{2+} decline time constant was not affected by HIGH or LOW $[Ca^{2+}]$ ($p > 0.05$; Figure 5.2 E; $n = 31$ cells for both groups).

Sparks (red triangles) were imaged in line scan mode and were present in all cells (Figure 5.3 A). Changes in spark frequency, 15 sec prior to a wave or in a time matched section (0 waves), are shown in Figure 5.3 A and the mean values shown in Figure 5.3 B. In cells with 0 waves, spark frequency was unchanged through time (Figure 5.3 B). In cells with waves, spark frequency increased exponentially and spark frequency increased at a greater rate in cells perfused with HIGH $[Ca^{2+}]$ than in cells perfused with LOW $[Ca^{2+}]$ (Figure 5.3 B). The threshold spark frequency immediately prior to a wave release was reached at 4.99 ± 0.47 sparks/100 $\mu m/sec$ and 4.73 ± 0.35 sparks/100 $\mu m/sec$ for LOW $[Ca^{2+}]$ and HIGH $[Ca^{2+}]$ respectively. These values were significantly greater than the time matched spark frequency in cells without waves ($p < 0.01$ (vs. LOW $[Ca^{2+}]$); and $p < 0.05$ (vs HIGH $[Ca^{2+}]$); Figure 5.3 C; $n = 20$ cells (0 waves); $n = 20$ cells (LOW $[Ca^{2+}]$); and $n = 24$ cells (HIGH $[Ca^{2+}]$)). The proportion of cells analysed at each time point, was displayed in Figure 5.3 D as sparks could not be analysed in the presence of a preceding wave.

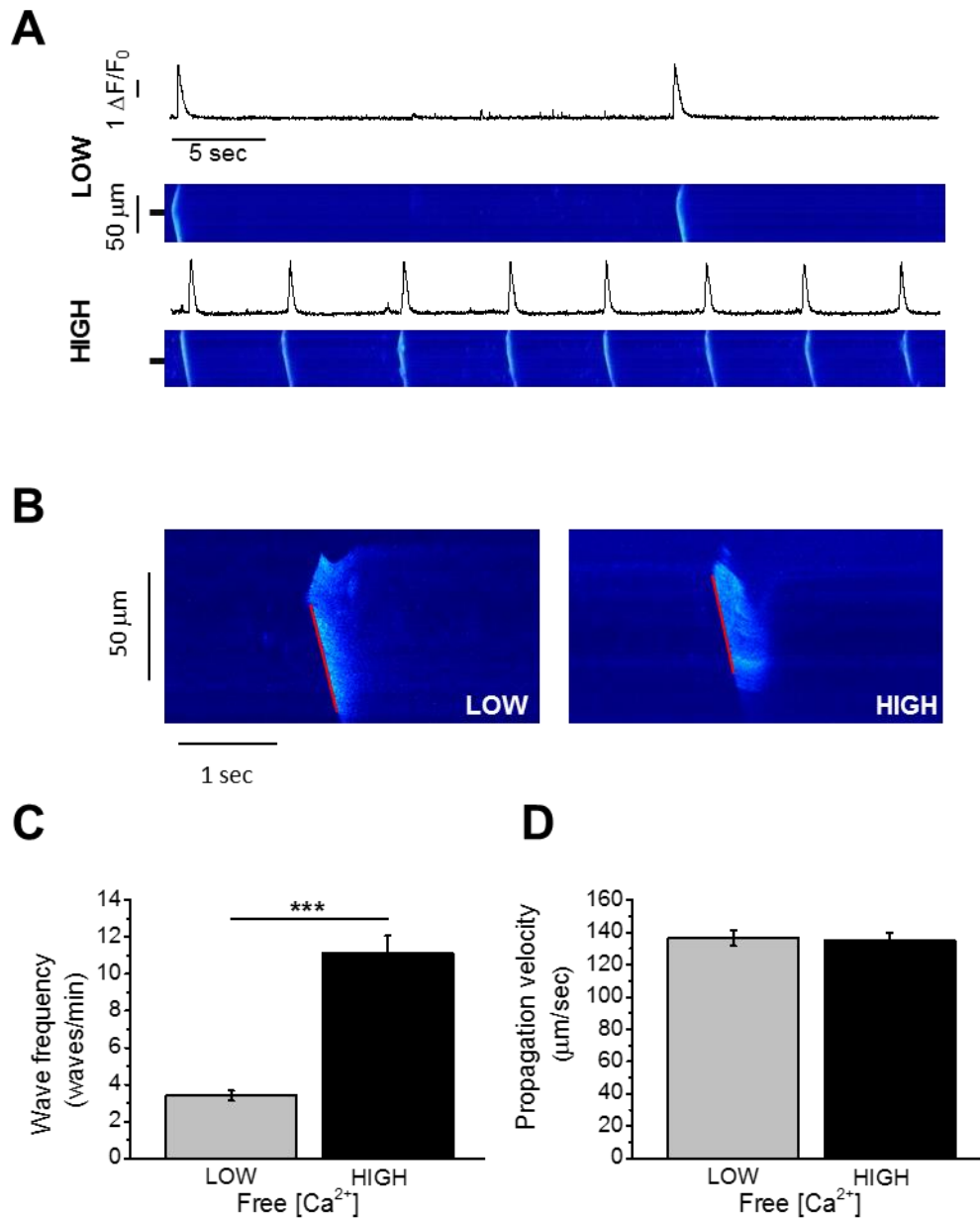


Figure 5.1: The effect of free $[\text{Ca}^{2+}]$ on wave frequency and propagation velocity

A) Representative line scans and fluorescence profiles of waves at 145 nM free $[\text{Ca}^{2+}]$ (LOW) and 282 nM free $[\text{Ca}^{2+}]$ (HIGH) **B)** Representative line scans of waves and their measured wave propagation velocity at LOW and HIGH free $[\text{Ca}^{2+}]$. The red line represents the wave front as identified by the analysis tool. **C)** Differences between LOW and HIGH free $[\text{Ca}^{2+}]$ in wave frequency and **D)** wave propagation velocity. Unpaired two tailed Student's t-test. *** = $p < 0.001$; $n = \text{LOW } [\text{Ca}^{2+}] = 31$ (8); $\text{HIGH } [\text{Ca}^{2+}] = 31$ (8).

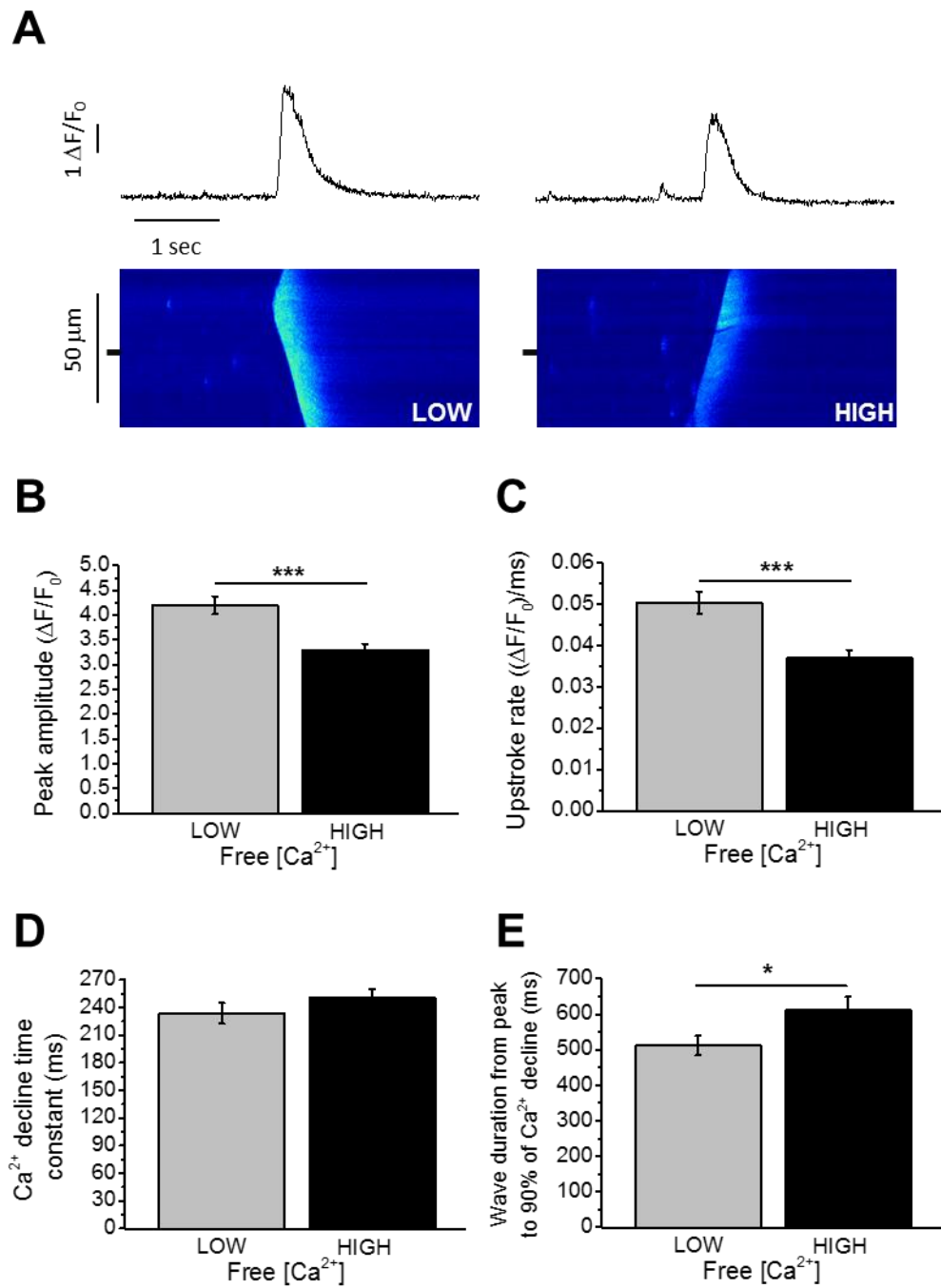


Figure 5.2: The effect of free [Ca²⁺] on wave properties

A) Representative line scans and fluorescence profiles of waves at 145 nM free [Ca²⁺] (LOW) and 282 nM free [Ca²⁺] (HIGH) **B)** Differences between LOW and HIGH free [Ca²⁺] in **B)** peak amplitude, **C)** upstroke rate, **D)** Ca²⁺ decline time constant and **E)** wave duration from wave peak to 90% of the Ca²⁺ decline. Unpaired two tailed Student's t-test. ** = p < 0.01; *** = p < 0.001. n = LOW [Ca²⁺] = 31 (8); HIGH [Ca²⁺] = 31 (8).

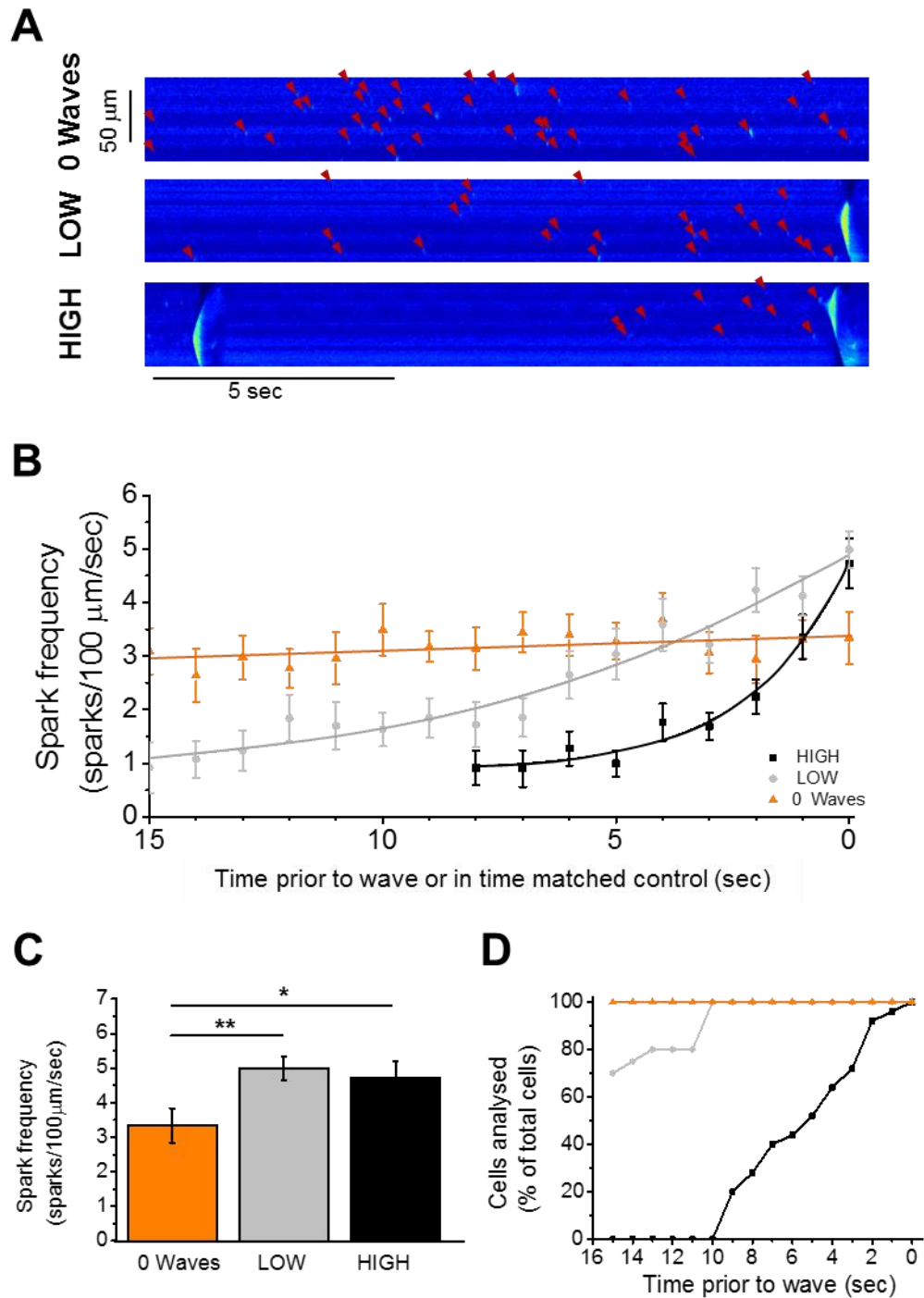


Figure 5.3: The effect of intracellular $[\text{Ca}^{2+}]$ and Ca^{2+} buffering on spark properties

A) Representative line scans in the absence of waves (0 Waves; 139 nM free Ca^{2+}), at LOW $[\text{Ca}^{2+}]$ (146 nM free Ca^{2+}) and at HIGH $[\text{Ca}^{2+}]$ (286 nM free Ca^{2+}). Sparks identified by red triangles. **B)** Changes in spark frequency under each experimental condition. **C)** Spark frequency immediately prior to a wave or in a time matched section of cells with no waves. **D)** The percentage of cells analysed at each time point. Cells were not scanned during a wave or 1 sec post-wave. ANOVA + Holm-Sidak *post hoc* test. * = $p < 0.05$; ** = $p < 0.01$; *** = $p < 0.001$. $n = 0 \text{ Waves} = 20 (3)$; $\text{LOW} = 20 (6)$; $\text{HIGH} = 24 (6)$.

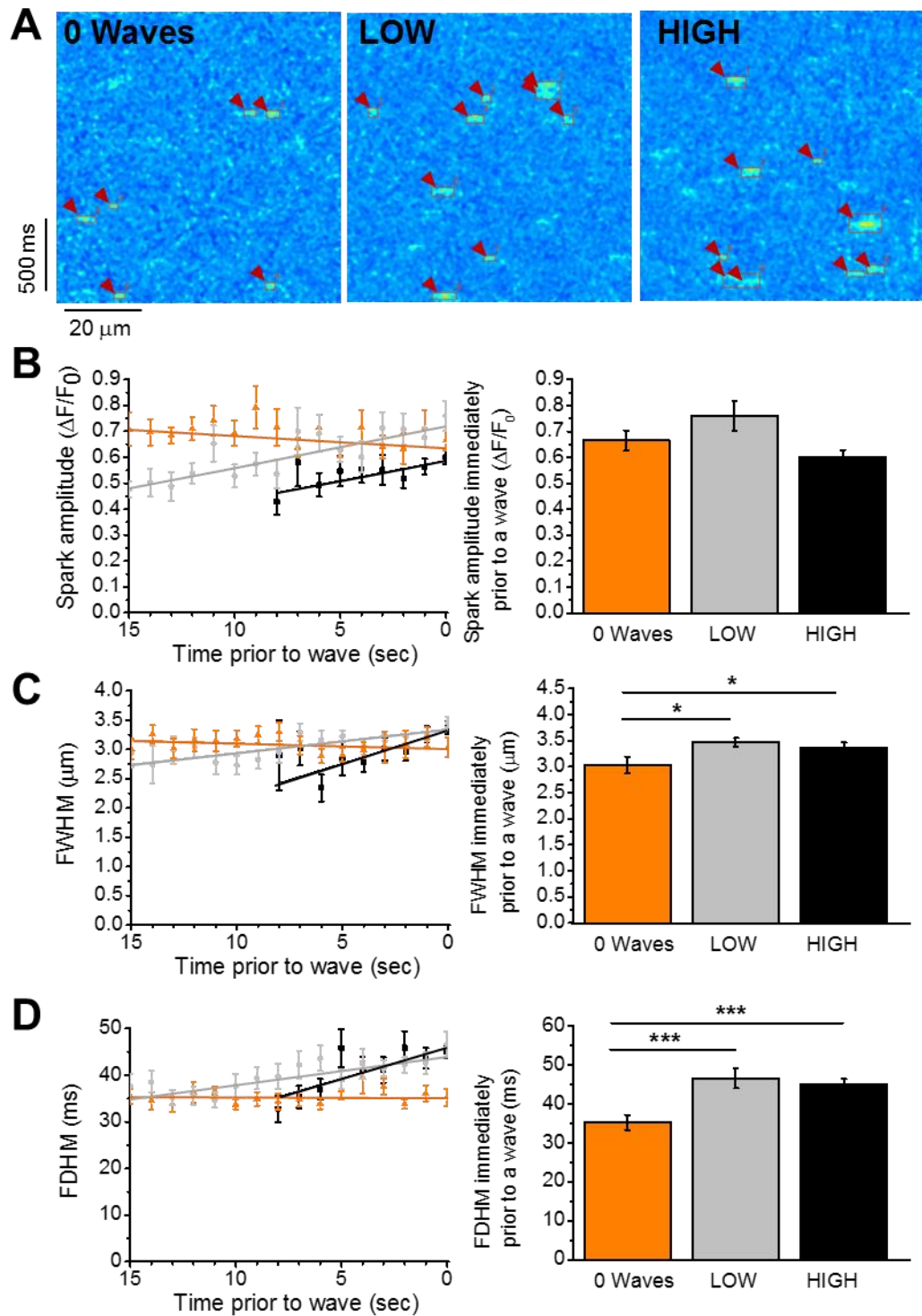


Figure 5.4: The effect of intracellular $[\text{Ca}^{2+}]$ and Ca^{2+} buffering on spark properties

A) Representative line scans in the absence of waves (0 Waves; 139 nM free Ca^{2+}), at LOW $[\text{Ca}^{2+}]$ (146 nM free Ca^{2+}) and at HIGH $[\text{Ca}^{2+}]$ (286 nM free Ca^{2+}). Sparks were identified and numbered by Sparkmaster (Picht et al. 2009). **B)** Rate of change of spark dimensions (L) and spark dimensions immediately prior to a wave or in a time matched control in cells with no waves (R) for spark amplitude **C)** FWHM and **D)** FDHM. ANOVA + Holm-Sidak *post hoc* test. * = $p < 0.05$; *** = $p < 0.001$. $n = 0$ Waves = 20 (3); LOW = 20 (6); HIGH = 24 (6).

Representative sparks released from the SR immediately prior to a Ca^{2+} wave or in a time matched line scan section lacking waves (0 waves) were identified by Sparkmaster and are shown in Figure 5.4 A. In the absence of waves, spark properties were unchanged as a function of time in cells without waves (Figure 5.4 B-D). Spark amplitude linearly increased as a function of time in cells at a rate of $0.019 (\Delta F/F_0)/\text{sec}$ and $0.022 (\Delta F/F_0)/\text{sec}$ for LOW and HIGH $[\text{Ca}^{2+}]$ respectively (Figure 5.4 B (L)). There were no significant differences between groups immediately prior to a wave ($p > 0.05$; Figure 5.4 B (R)). FWHM increased linearly at a rate of $0.035 \mu\text{m}/\text{sec}$ and $0.060 \mu\text{m}/\text{sec}$ for LOW and HIGH $[\text{Ca}^{2+}]$ respectively (Figure 5.4 C (L)). Immediately prior to a wave, spark FWHM was significantly greater in cells at LOW $[\text{Ca}^{2+}]$ ($3.46 \pm 0.09 \mu\text{m}$) and HIGH $[\text{Ca}^{2+}]$ ($3.37 \pm 0.10 \mu\text{m}$) than in cells with 0 waves ($3.03 \pm 0.16 \mu\text{m}$; $p < 0.05$; Figure 5.4 C (R)). FDHM increased linearly at a rate of $0.60 \text{ ms}/\text{sec}$ and $1.53 \text{ ms}/\text{sec}$ for LOW and HIGH $[\text{Ca}^{2+}]$ respectively (Figure 5.4 D (L)). Immediately prior to a wave, spark FDHM was significantly greater in cells at LOW $[\text{Ca}^{2+}]$ ($46.6 \pm 2.61 \text{ ms}$) and HIGH $[\text{Ca}^{2+}]$ ($45.0 \pm 1.36 \text{ ms}$) than in cells with 0 waves ($35.2 \pm 1.87 \text{ ms}$; $p < 0.001$; Figure 5.4 D (R); $n = 20$ cells (0 waves); $n = 20$ cells (LOW $[\text{Ca}^{2+}]$); and $n = 24$ cells (HIGH $[\text{Ca}^{2+}]$)).

5.3.2 The effect of flecainide on Ca^{2+} waves

Figure 5.5 A shows representative line scan images and fluorescence profiles from cells perfused with LOW $[\text{Ca}^{2+}]$ intracellular solution at control (CON) and after 3 min perfusion with vehicle (VEH; 5×10^{-4} % ethanol) or 25 μM flecainide (FLEC) (scanning protocol 1). In LOW $[\text{Ca}^{2+}]$ solution, there was a significant decrease in wave frequency within both VEH ($p < 0.01$) and FLEC groups ($p < 0.001$; Figure 5.5 B) after 3 min. When calculated as a percentage change, FLEC significantly decreased wave frequency by $12.7 \pm 3.45\%$ in comparison to VEH after 3 min perfusion ($p < 0.01$; Figure 5.5 C). Wave propagation velocity was unchanged as a function of time in both VEH and FLEC groups ($p > 0.05$; Figure 5.5 D) and there were no differences between VEH and FLEC groups ($p > 0.05$; Figure 5.5 E; $n = 11$ cells (VEH); and $n = 23$ cells (FLEC)). Representative line scans and fluorescence profiles of individual waves at the control timepoint (CON), and after perfusion with VEH or FLEC are shown in Figure 5.6 A. Peak amplitude significantly decreased after 3 min perfusion with VEH ($p < 0.001$) or FLEC ($p < 0.001$; Figure 5.6 B). Wave amplitude was significantly decreased by $13.9 \pm 4.21\%$ in the VEH group compared with FLEC after 3 min perfusion ($p < 0.05$; Figure 5.6 C). Wave upstroke rate significantly decreased after 3 min perfusion with VEH ($p < 0.001$) or FLEC ($p < 0.001$; Figure 5.6 D). However, there was no significant difference in upstroke rate between VEH and FLEC groups at any time point ($p > 0.05$; Figure 5.6 E). Wave duration from the peak to 90% of the

Ca²⁺ decline was unchanged after 3 min perfusion with VEH or FLEC ($p > 0.05$; Figure 5.7 A) and there were no differences between VEH and FLEC groups at any time points ($p > 0.05$; Figure 5.7 B). Ca²⁺ decline time constant was unchanged as a function of time in VEH and FLEC groups ($p > 0.05$; Figure 5.7 C) and again there were no differences between VEH and FLEC groups ($p > 0.05$; Figure 5.7 D; $n = 11$ cells (VEH); and $n = 23$ cells (FLEC)).

Figure 5.8 A shows representative line scans and fluorescence profiles of Ca²⁺ waves from cells perfused with an intracellular solution at HIGH [Ca²⁺] (scanning protocol 1). Images are shown at CON and after 3 min perfusion with VEH or FLEC. Wave frequency significantly decreased after 3 min perfusion with VEH ($p < 0.05$) or FLEC ($p < 0.001$; Figure 5.8 B). FLEC significantly decreased wave frequency by $9.5 \pm 2.39\%$ compared with VEH after 3 min perfusion ($p < 0.05$; Figure 5.8 C). There were no significant changes in propagation velocity as a function of time in either VEH or FLEC groups ($p > 0.05$; Figure 5.8 D) and FLEC did not alter propagation velocity when compared with VEH ($p > 0.05$; Figure 5.8 E; $n = 12$ cells (VEH); and $n = 24$ cells (FLEC)). Figure 5.9 A shows representative line scans and fluorescence profiles of individual waves at CON and after 3 min perfusion with VEH or FLEC. Peak amplitude significantly decreased after 3 min perfusion with VEH ($p < 0.01$) or FLEC ($p < 0.001$; Figure 5.9 B). FLEC did not significantly alter wave peak amplitude compared to VEH at any time point ($p > 0.05$; Figure 5.9 C). Wave upstroke rate significantly decreased after 3 min perfusion with VEH ($p < 0.01$) or FLEC ($p < 0.001$; Figure 5.9 D). Wave upstroke rate was significantly decreased by $13.7 \pm 3.20\%$ in the FLEC group compared with VEH after 3 min perfusion ($p < 0.05$; Figure 5.9 E). Wave duration from wave peak to 90% of the Ca²⁺ decline was unchanged after 3 min perfusion with VEH ($p > 0.05$) or FLEC ($p > 0.05$; Figure 5.10 A) and there were no differences between VEH and FLEC groups at any time points ($p > 0.05$; Figure 5.10 B). The Ca²⁺ decline time constant was unchanged after 3 min perfusion with VEH ($p > 0.05$), and significantly decreased with FLEC ($p < 0.05$; Figure 5.10 C). Although FLEC did not significantly alter the Ca²⁺ decline time constant at any time point when compared with VEH ($p > 0.05$; Figure 5.10 D; $n = 12$ cells (VEH); and $n = 24$ cells (FLEC)).

The previous results described changes in SR Ca²⁺ wave release upon application of flecainide, when cells were continually scanned over 3 min (scanning protocol 1). The protocol was henceforth altered to investigate the longer-term (5 min) effect of flecainide on Ca²⁺ wave release (scanning protocol 2). To limit the toxic effects of laser exposure, line scanning was discontinuous and cells were scanned for 30 sec at 60 sec intervals (Chapter 5.2.1). Figure 5.11 A shows representative line scans and fluorescence profiles of waves from cells perfused with intracellular solution at HIGH [Ca²⁺], at CON and after 5 min perfusion with VEH or FLEC. Wave

frequency was unchanged after 5 min perfusion in the VEH group ($p > 0.05$), yet significantly decreased as a function of time in the FLEC group (11.01 ± 0.61 waves/min to 7.79 ± 0.54 waves/min; $p < 0.001$; Figure 5.11 B). When compared with VEH, FLEC significantly decreased wave frequency at each time point post-CON ($p < 0.05$) and decreased wave frequency by $22.7 \pm 5.43\%$ after 5 min perfusion ($p < 0.01$; Figure 5.11 C). Using this experimental protocol, the effect of flecainide on Ca^{2+} wave frequency after 3 min was greater than when cells were continually scanned, as in the first protocol. The control response was also more stable.

Wave propagation velocity was not significantly changed after 5 min perfusion with either VEH ($p > 0.05$) or FLEC ($p > 0.05$; Figure 5.11 D) and there was no difference between VEH and FLEC groups at any time point ($p > 0.05$; Figure 5.11 E; $n = 10$ cells (VEH); and $n = 12$ cells (FLEC)). Figure 5.12 A shows representative line scans and fluorescence profiles of individual waves, imaged at HIGH $[\text{Ca}^{2+}]$, at CON and after 5 min perfusion with VEH or FLEC. Peak amplitude significantly decreased after 5 min perfusion with VEH ($p < 0.001$) or FLEC ($p < 0.01$; Figure 5.12 B). There was no significant difference between groups at any time point ($p > 0.05$; Figure 5.12 C). Wave upstroke rate was significantly decreased after 5 min perfusion with VEH ($p < 0.001$) or FLEC ($p < 0.001$). Upstroke rate decreased significantly more with VEH than FLEC, 4 and 5 min after solutions were switched ($p < 0.05$ and $p < 0.001$; Figure 5.12 E). Wave duration from peak to 90% of the Ca^{2+} decline was unchanged after 5 min perfusion with either VEH or FLEC ($p > 0.05$; Figure 5.13 A) and there were no significant differences between groups at any time points ($p > 0.05$; Figure 5.13 B). Similarly, Ca^{2+} decline time constant was unchanged after 5 min perfusion with either VEH or FLEC ($p > 0.05$; Figure 5.13 C) and there were no significant differences between groups at any time points ($p > 0.05$; Figure 5.13 D; $n = 10$ cells (VEH); and $n = 12$ cells (FLEC)). To summarise, at both HIGH and LOW $[\text{Ca}^{2+}]$, flecainide decreased Ca^{2+} wave frequency by $\sim 10\%$ without a consistent effect on any other wave parameters.

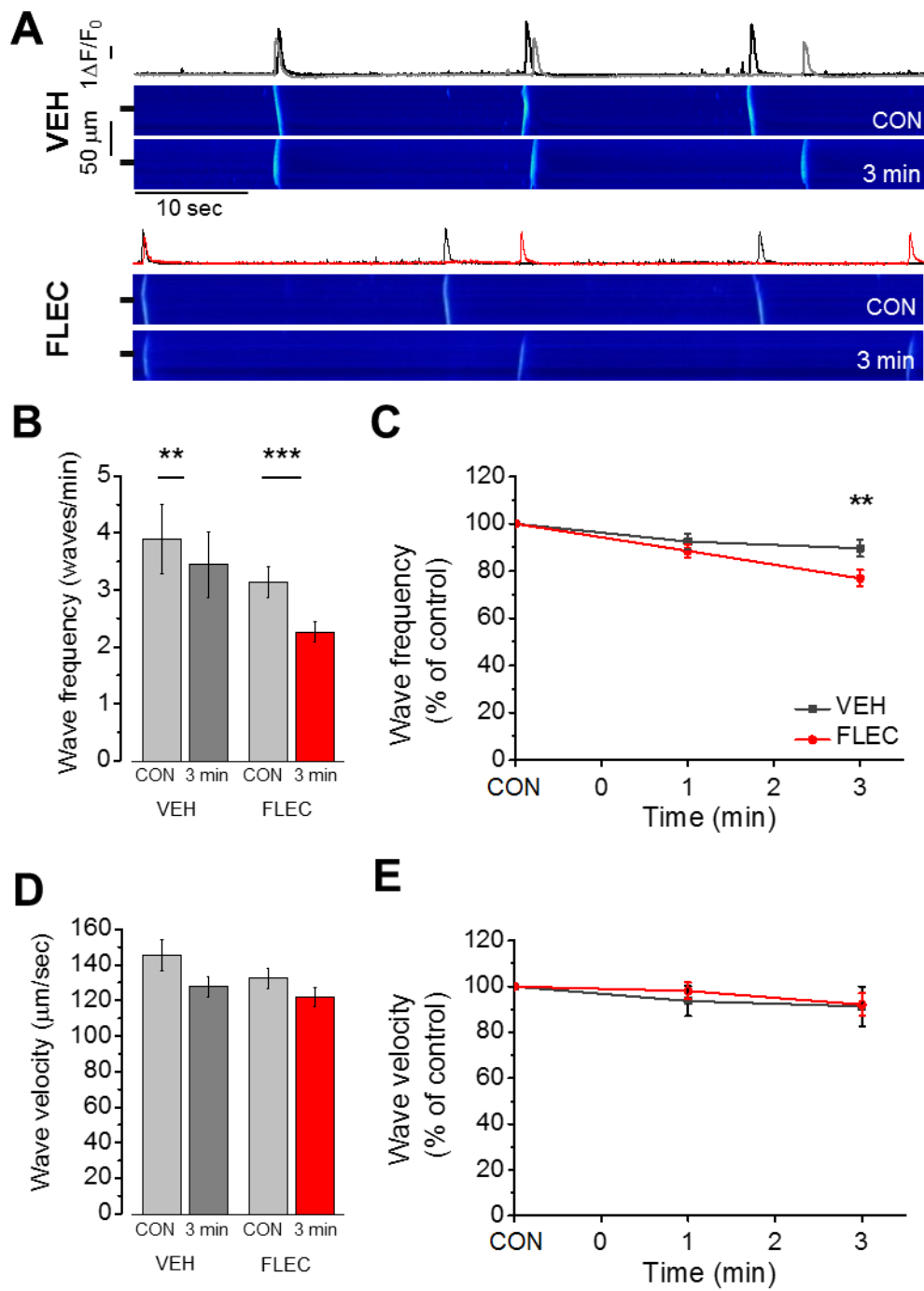


Figure 5.5: The effect of flecainide on wave frequency and propagation velocity over 3 min at LOW free $[Ca^{2+}]$

A) Representative line scans and fluorescence profiles of waves at control (CON) and after 3 min perfusion with vehicle (VEH) or flecainide (FLEC) **B)** Wave frequency for VEH and FLEC groups at CON and after 3 min perfusion. **C)** Percentage change in wave frequency in the VEH and FLEC groups. **D)** Wave propagation velocity for VEH and FLEC groups at CON and after 3 min perfusion. **E)** Percentage change in wave propagation velocity in the VEH and FLEC groups. Paired or unpaired two tailed Student's t-test; or two way repeated measures ANOVA + Holm-Sidak *post hoc* test. ** = $p < 0.01$. *** = $p < 0.001$. $n = \text{VEH} = 11$ (6); $\text{FLEC} = 23$ (8).

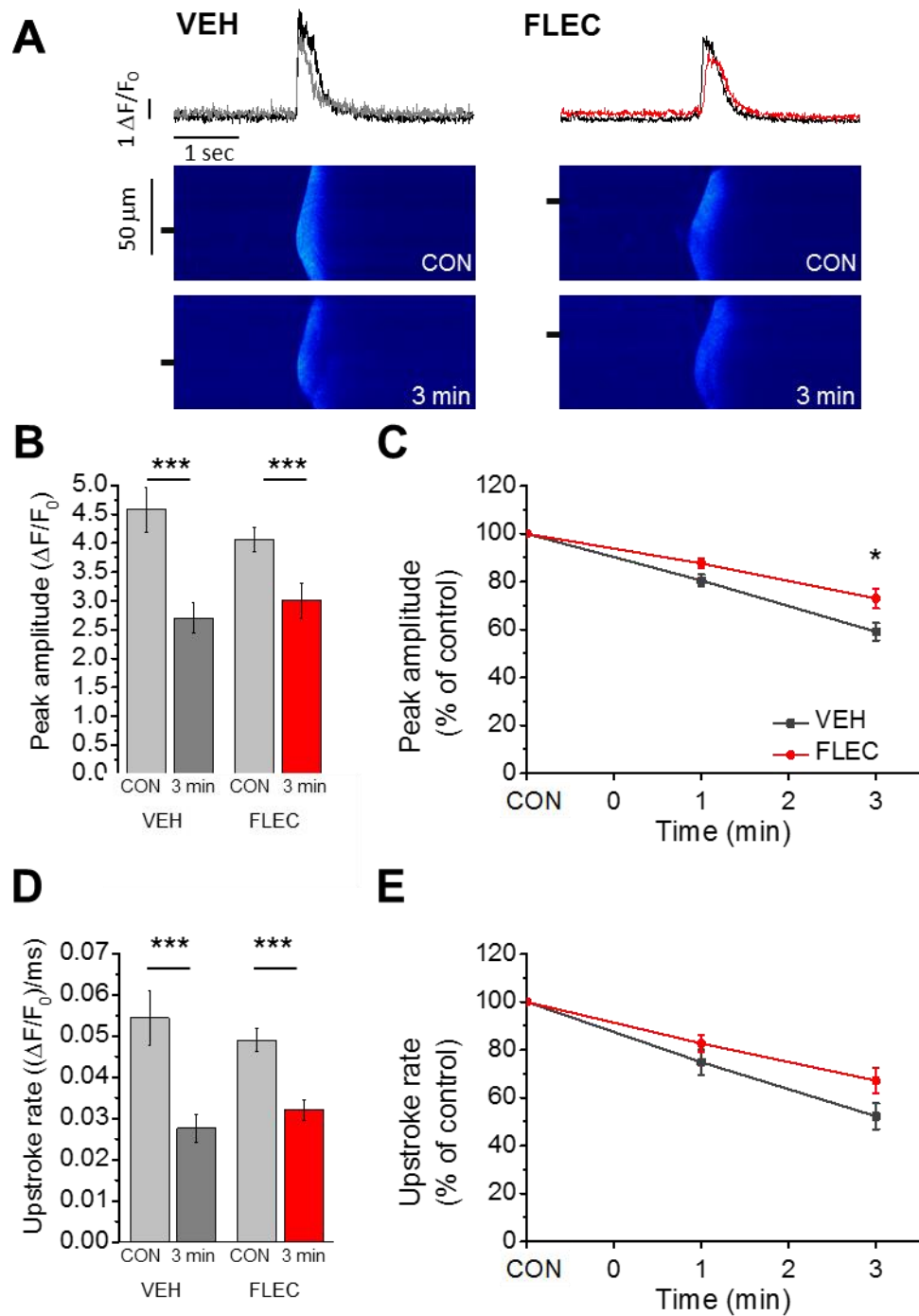


Figure 5.6: The effect of flecainide on wave amplitude and upstroke rate at LOW free $[\text{Ca}^{2+}]$

A) Representative line scans and fluorescence profiles of waves at control (CON) and after 3 min perfusion with vehicle (VEH) or flecainide (FLEC) **B)** Wave amplitude for VEH and FLEC at CON and after 3 min perfusion. **C)** Percentage change in wave amplitude in the VEH and FLEC groups. **D)** Wave upstroke rate for VEH and FLEC at CON and after 3 min perfusion. **E)** Percentage change in wave upstroke rate in the VEH and FLEC groups. Paired or unpaired two tailed Student's t-test; or two way repeated measures ANOVA + Holm-Sidak *post hoc* test. * = $p < 0.05$; *** = $p < 0.001$. $n = \text{VEH} = 11$ (6); $\text{FLEC} = 23$ (8).

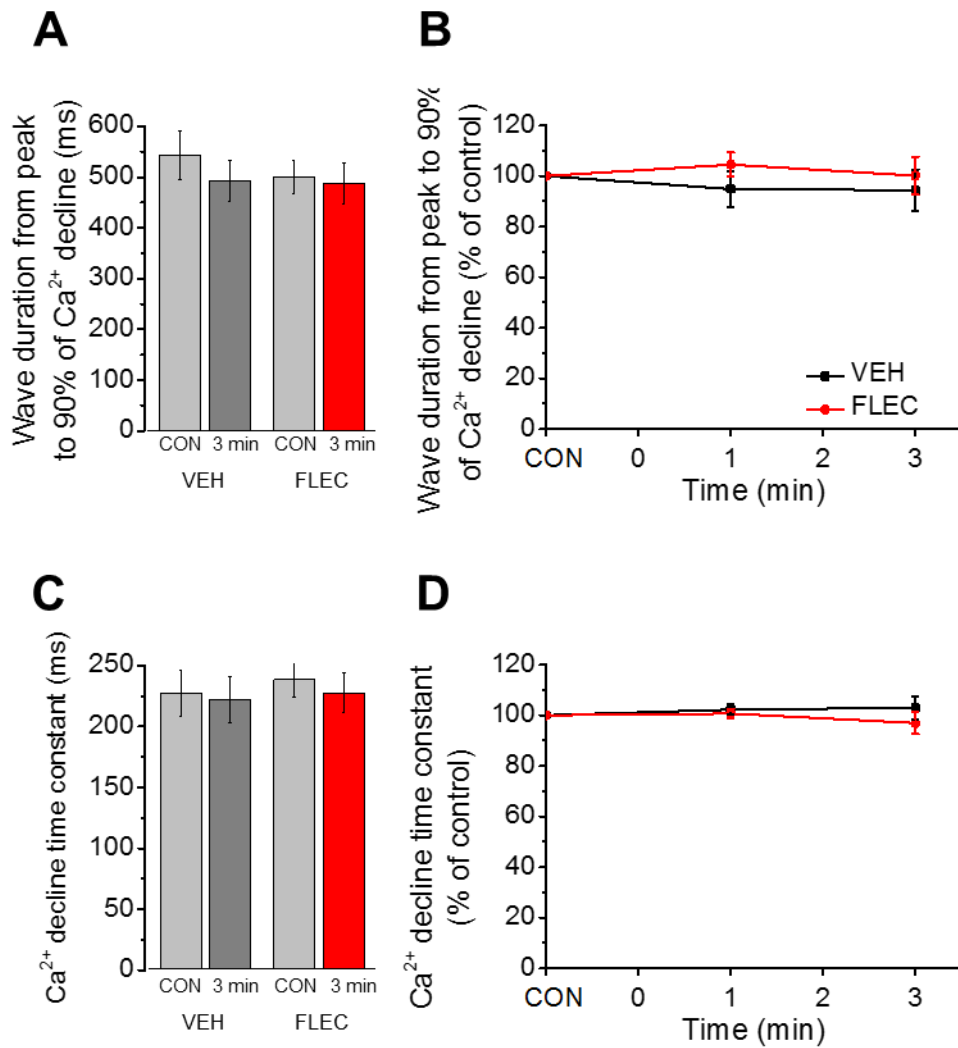


Figure 5.7: The effect of flecainide on wave duration and relaxation time constant at LOW free [Ca²⁺]

A) Wave duration from peak to 90% of Ca²⁺ wave decline for vehicle (VEH) and flecainide (FLEC) treated groups at CON and after 3 min perfusion. **B)** Percentage change in wave duration from peak to 90% of Ca²⁺ wave decline in the VEH and FLEC groups. **C)** Ca²⁺ decline time constant for VEH and FLEC groups at CON and after 3 min perfusion. **D)** Percentage change in Ca²⁺ decline time constant in the VEH and FLEC groups. Paired or unpaired two tailed Student's t-test; or two way repeated measures ANOVA + Holm-Sidak post hoc test. n = VEH = 11 (6); FLEC = 23 (8).

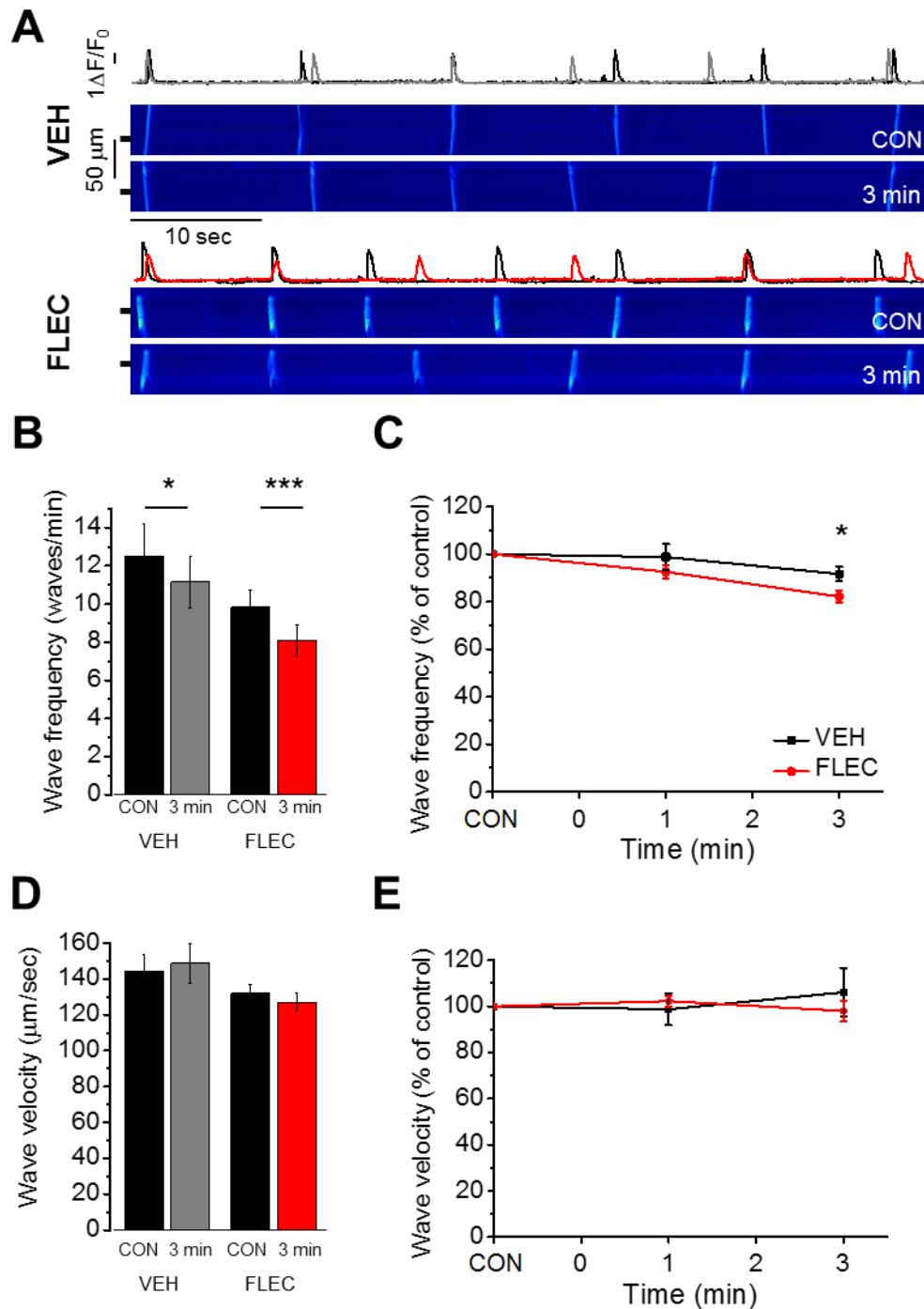


Figure 5.8: The effect of flecainide on wave frequency over 3 min at HIGH free [Ca²⁺]

A) Representative line scans and fluorescence profiles of waves at control (CON) and after 3 min perfusion with vehicle (VEH) or flecainide (FLEC) **B)** Wave frequency for VEH and FLEC groups at CON and after 3 min perfusion. **C)** Percentage change in wave frequency in the VEH and FLEC groups. **D)** Wave velocity for VEH and FLEC groups at CON and after 3 min perfusion. **E)** Percentage change in wave velocity in the VEH and FLEC groups. Paired or unpaired two tailed Student's t-test; or two way repeated measures ANOVA + Holm-Sidak *post hoc* test. * = $p < 0.05$; *** = $p < 0.001$. $n = \text{VEH} = 12 (6)$; $\text{FLEC} = 24 (8)$.

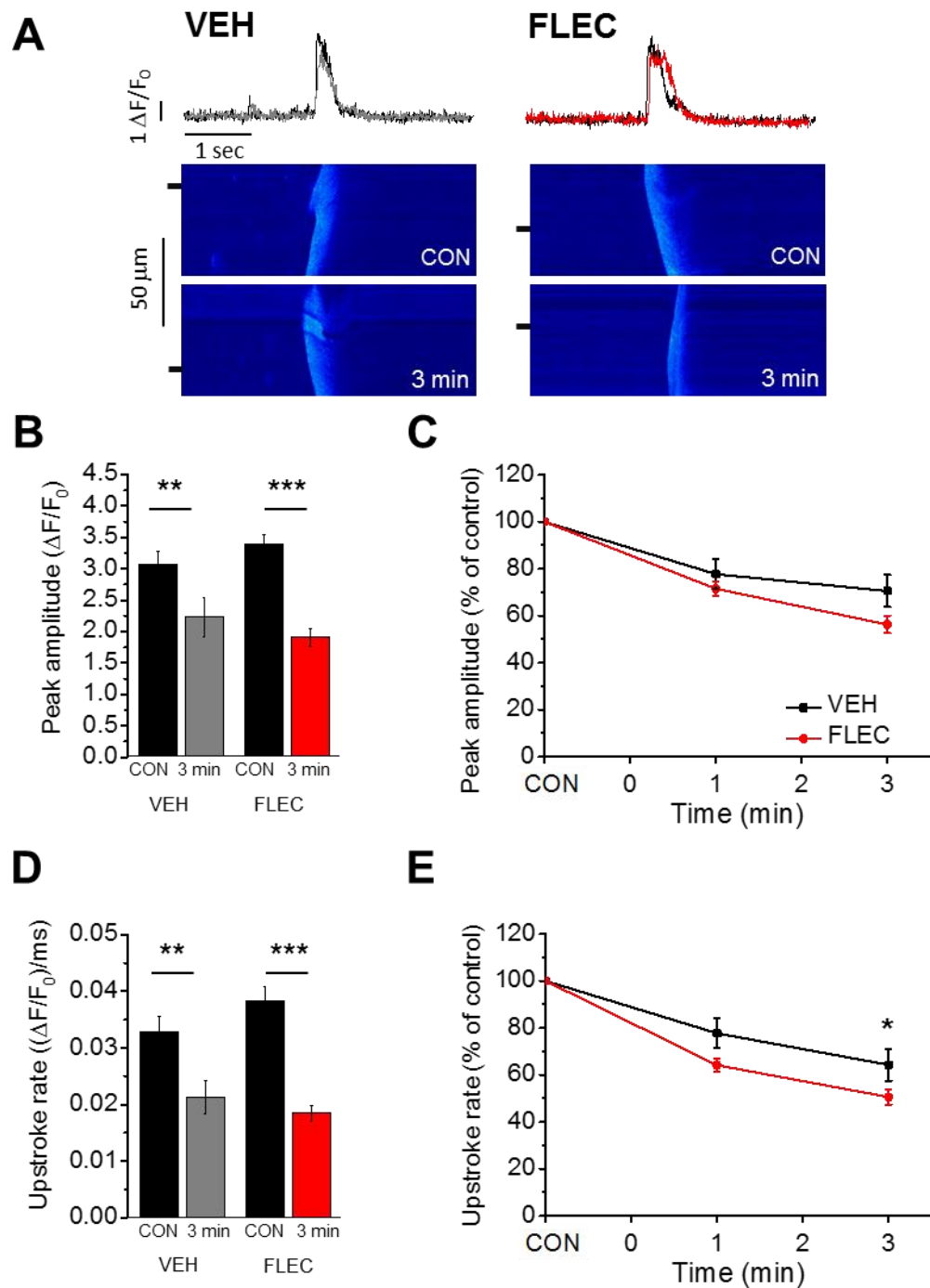


Figure 5.9: The effect of flecainide on wave amplitude and upstroke rate at HIGH free $[Ca^{2+}]$

A) Representative line scans and fluorescence profiles of waves at control (CON) and after 3 min perfusion with vehicle (VEH) or flecainide (FLEC) **B)** Wave amplitude for VEH and FLEC groups at CON and after 3 min perfusion. **C)** Percentage change in wave amplitude in the VEH and FLEC groups. **D)** Wave upstroke rate for VEH and FLEC groups at CON and after 3 min perfusion. **E)** Percentage change in wave upstroke rate in the VEH and FLEC groups. Paired or unpaired two tailed Student's t-test; or two way repeated measures ANOVA + Holm-Sidak *post hoc* test. ** = $p < 0.01$; *** = $p < 0.001$. $n = VEH = 12$ (6); $FLEC = 24$ (8).

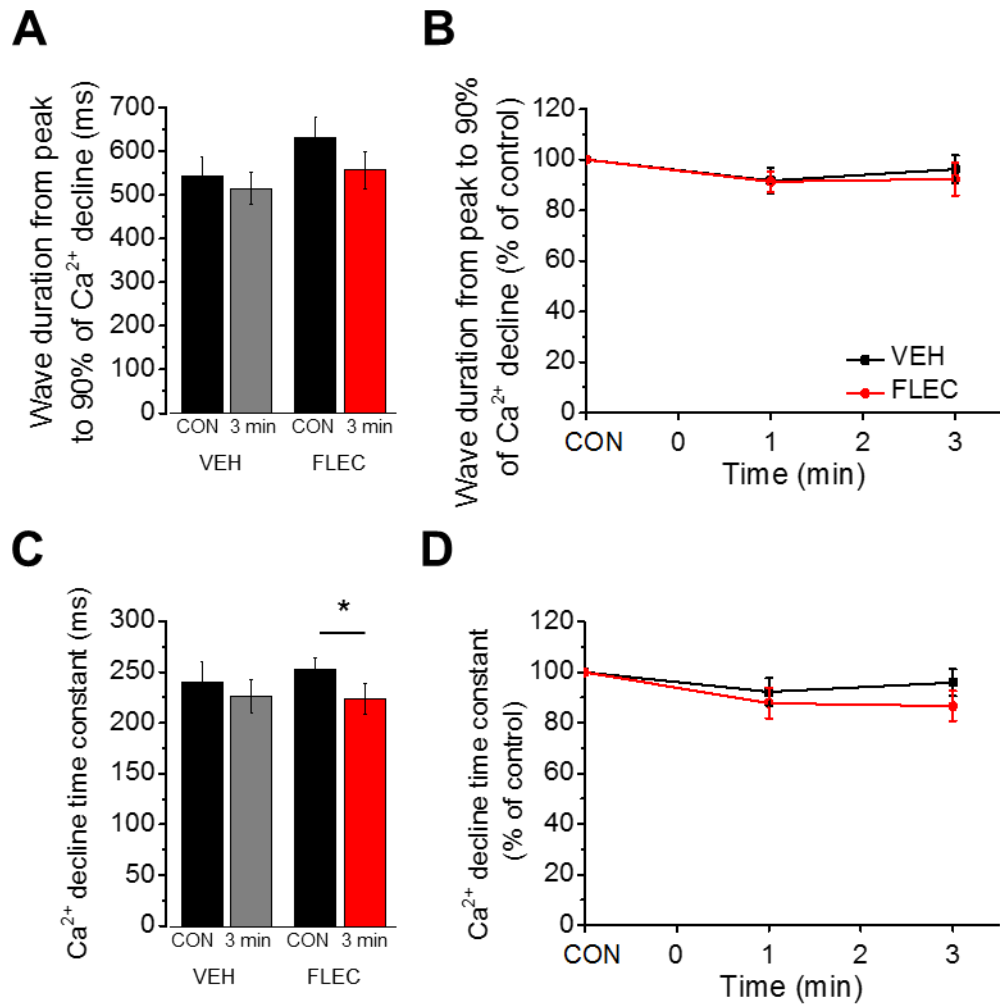


Figure 5.10: Effect of flecainide on wave duration and relaxation time constant at HIGH free [Ca²⁺]
A) Wave duration from peak to 90% of the wave dedine for vehide (VEH) and flecainide (FLEC) treated groups at CON and after 3 min perfusion. **B)** Percentage change in wave duration from peak to 90% of the wave dedine in the VEH and FLEC groups. **C)** Ca²⁺ decline time constant for VEH and FLEC groups at CON and after 3 min perfusion. **D)** Percentage change in Ca²⁺ decline time constant in the VEH and FLEC groups. Paired or unpaired two tailed Student's t-test; or two way repeated measures ANOVA + Holm-Sidak post hoc test. * = p < 0.05. n = VEH = 12 (6); FLEC = 24 (8).

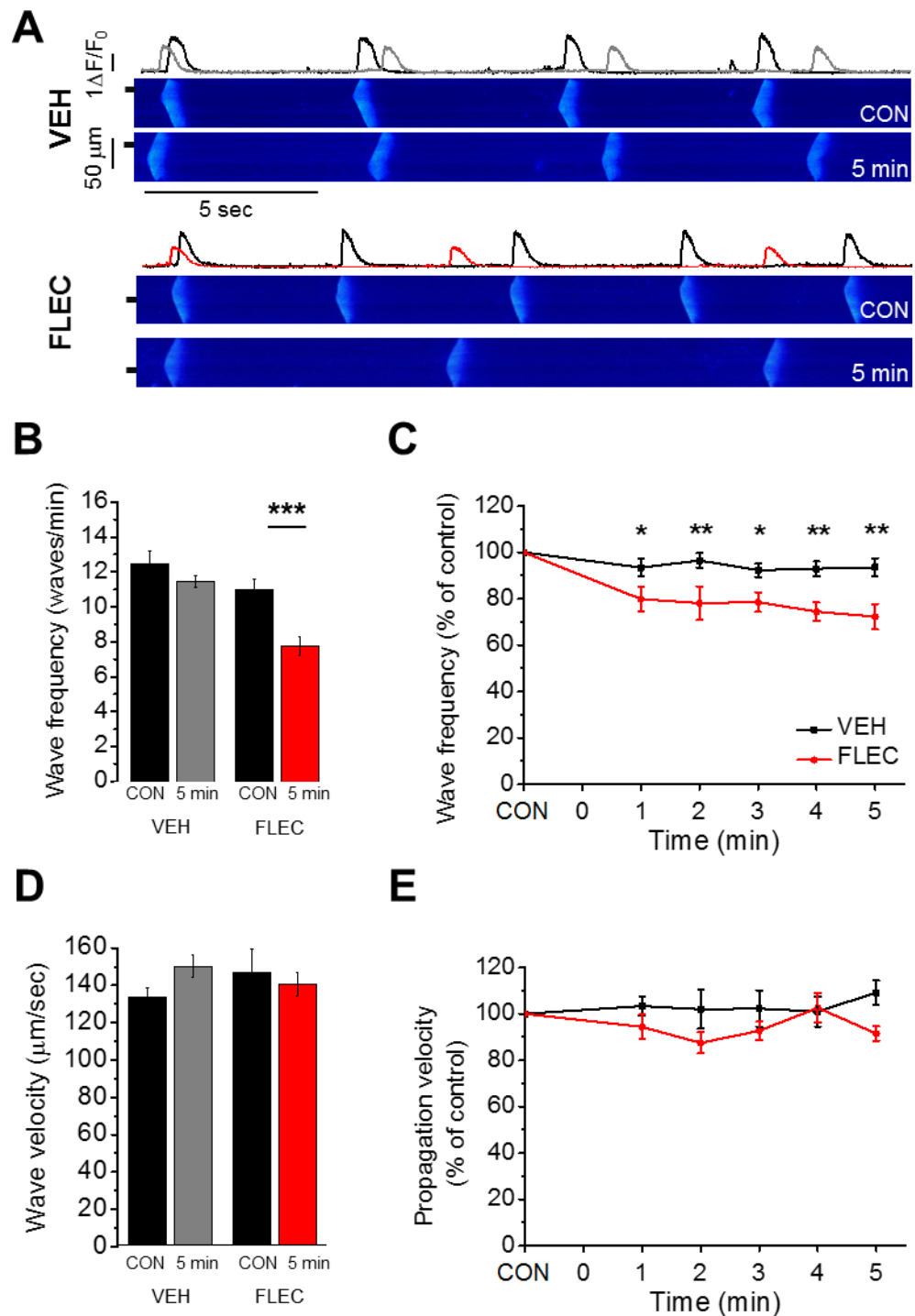


Figure 5.11: The effect of flecainide on wave frequency and propagation velocity over 5 min at HIGH free $[\text{Ca}^{2+}]$

A) Representative line scans and fluorescence profiles of waves at control (CON) and after 5 min perfusion with vehicle (VEH) or flecainide (FLEC) **B)** Wave frequency for VEH and FLEC groups at CON and after 5 min perfusion. **C)** Percentage change in wave frequency in the VEH and FLEC groups. **D)** Wave velocity for VEH and FLEC groups at CON and after 5 min perfusion. **E)** Percentage change in wave velocity in the VEH and FLEC groups. Paired or unpaired two tailed Student's t-test; or two way repeated measures ANOVA + Holm-Sidak *post hoc* test. * = $p < 0.05$; ** = $p < 0.01$; *** = $p < 0.001$. $n = \text{VEH} = 10$ (4); $\text{FLEC} = 12$ (4).

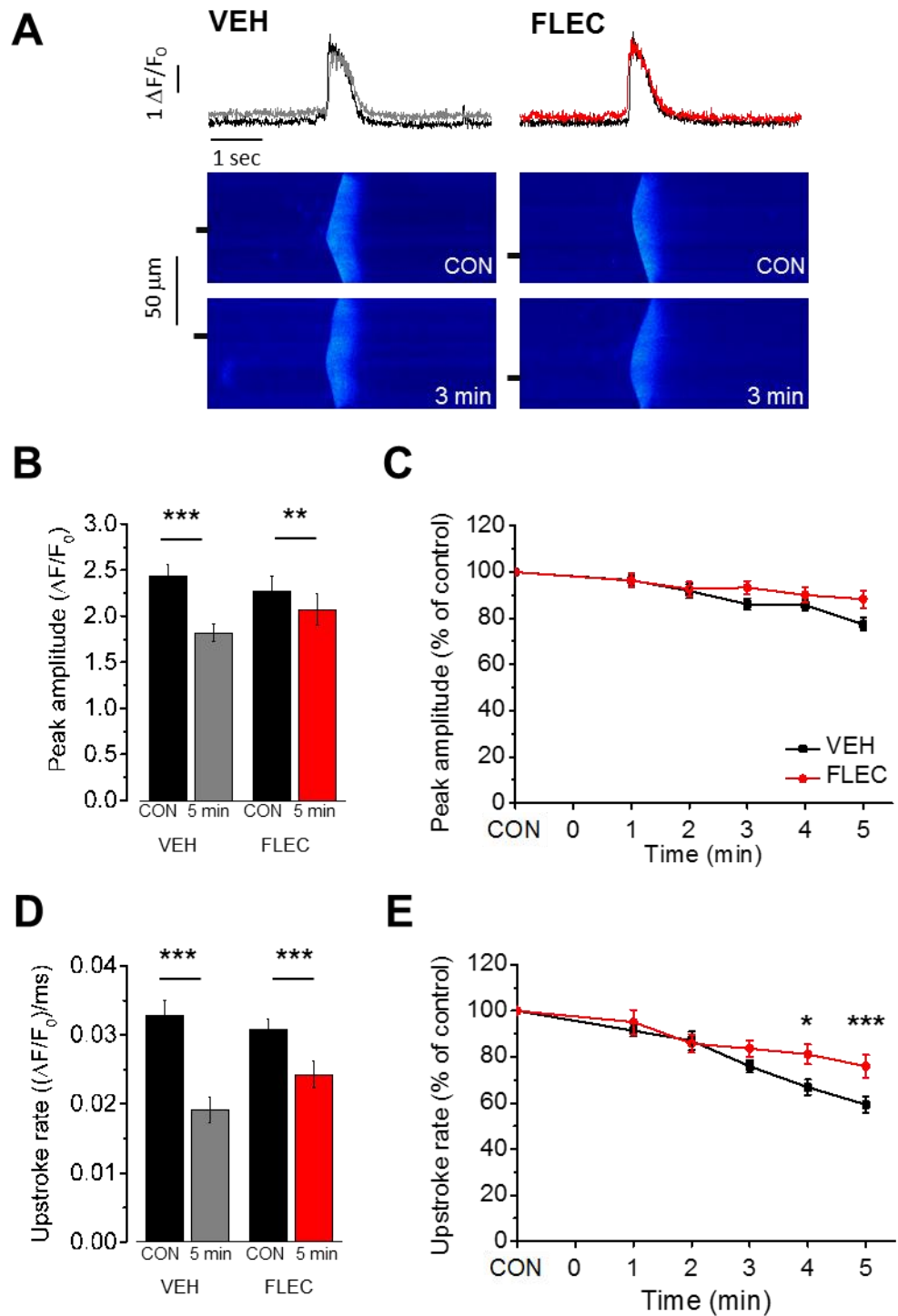


Figure 5.12: The effect of flecainide on wave peak amplitude and upstroke rate over 5 min at HIGH free $[\text{Ca}^{2+}]$

A) Representative line scans and fluorescence profiles of waves at control (CON) and after 5 min perfusion with vehicle (VEH) or flecainide (FLEC) **B)** Peak amplitude for VEH and FLEC groups at CON and after 5 min perfusion. **C)** Percentage change in peak amplitude for VEH and FLEC groups. **D)** Upstroke rate for VEH and FLEC groups at CON and after 5 min perfusion. **E)** Percentage change in upstroke rate for VEH and FLEC groups. Paired and unpaired two tailed Student's t-test; or two way repeated measures ANOVA + Holm-Sidak *post hoc* test. * = $p < 0.05$; ** = $p < 0.01$; *** = $p < 0.001$. $n = \text{VEH} = 10$ (4); $\text{FLEC} = 12$ (4).

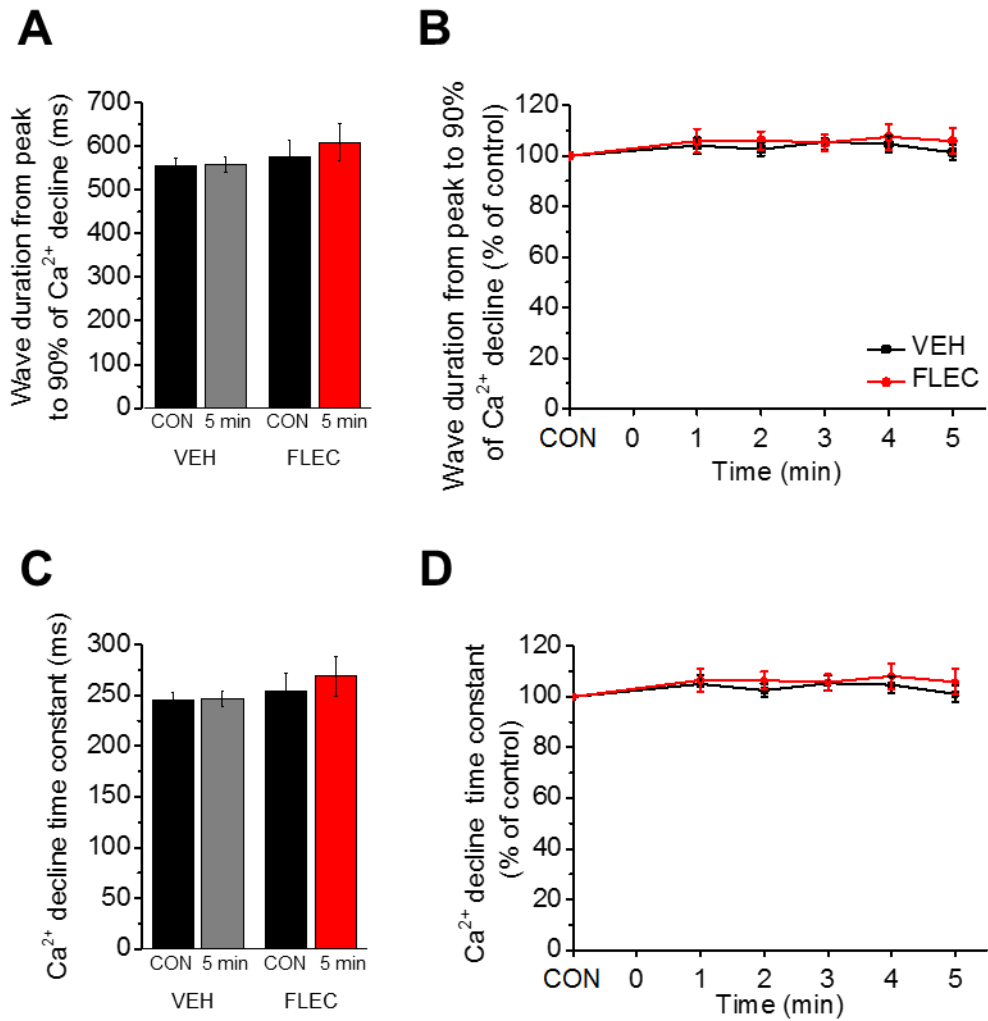


Figure 5.13: The effect of flecainide on wave duration and relaxation constant over 5 min at HIGH free [Ca²⁺]

A) Wave duration from peak to 90% of Ca²⁺ wave decline for vehicle (VEH) and flecainide (FLEC) treated groups at CON and after 5 min perfusion. **B)** Percentage change in wave duration from peak to 90% of the Ca²⁺ wave decline for VEH and FLEC groups. **C)** Ca²⁺ decline time constant for VEH and FLEC at CON and after 5 min perfusion. **D)** Percentage change in Ca²⁺ decline time constant for VEH and FLEC groups. Paired and unpaired two tailed Student's t-test; or two way repeated measures ANOVA + Holm-Sidak post hoc test. n = VEH = 10 (4); FLEC = 12 (4).

5.3.3 The effect of flecainide on Ca²⁺ sparks

Figure 5.14 A shows representative line scans of sparks identified by Sparkmaster at CON and then after 40 sec or 3 min exposure to FLEC (Picht et al., 2007). In these experiments, spark data were collected from permeabilised cells under conditions that precluded wave formation (0 waves; Table 2.3). Spark frequency showed no significant change after 3 min perfusion with VEH ($p > 0.05$) yet significantly increased with FLEC ($p < 0.01$; Figure 5.14 B). When VEH and FLEC groups were compared at 3 min as a percentage change from control, there was a strong trend ($p = 0.053$) for FLEC to increase in spark frequency ($128.2 \pm 8.91\%$; Figure 5.14 C; $n = 13$ cells (VEH); and $n = 31$ cells (FLEC)). Spark amplitude distribution was unchanged after 3 min perfusion with VEH ($p > 0.05$; Figure 5.15 A). Spark amplitude distribution was significantly shifted to the left with FLEC ($p < 0.001$), indicating a decrease in mean spark amplitude after 3 min perfusion (Figure 5.15 B). As a percentage of CON, FLEC significantly decreased spark amplitude by $8.70 \pm 2.54\%$ compared with VEH at 3 min ($p < 0.05$; Figure 5.15 C; $n = 13$ cells (VEH); and $n = 31$ cells (FLEC)). Spark FWHM distribution shifted to the left after 3 min perfusion with VEH ($p < 0.001$ Figure 5.16 A) or FLEC ($p = 0.001$; Figure 5.16 B). As a percentage of CON, FLEC significantly decreased spark FWHM by $6.38 \pm 1.33\%$ compared with VEH at 3 min ($p < 0.05$; Figure 5.16 C; $n = 13$ cells (VEH); and $n = 31$ cells (FLEC)). Spark FDHM distribution was unchanged after 3 min perfusion with VEH ($p > 0.05$; Figure 5.17 A) or FLEC ($p > 0.05$; Figure 5.17 B). There was no difference in FDHM between VEH and FLEC at any time point ($p > 0.05$; Figure 5.17 C; $n = 13$ cells (VEH); and $n = 31$ cells (FLEC)).

5.3.4 The effect of flecainide on Ca²⁺ SR content

Figure 5.18 A shows representative line scans and fluorescence profiles of cells releasing spontaneous Ca²⁺ waves and a Ca²⁺ transient in response to a rapid application of caffeine (caffeine “puff”) applied close to the time point when a wave was expected to occur. Peak amplitude of the Ca²⁺ transient significantly decreased after 5 min perfusion with VEH ($3.15 \pm 0.08 \Delta F/F_0$ vs $1.95 \pm 0.07 \Delta F/F_0$; $p > 0.001$) or FLEC ($2.99 \pm 0.12 \Delta F/F_0$ vs $2.04 \pm 0.07 \Delta F/F_0$; $p < 0.001$; Figure 5.18B). When expressed as a percentage of CON for each cell, there was no significant difference in transient peak amplitude between VEH and FLEC at any time point ($p > 0.05$; Figure 5.18 C). The upstroke rate of the Ca²⁺ transient significantly decreased after 5 min perfusion with VEH ($p < 0.01$) or FLEC ($p < 0.001$; Figure 5.18 D). As a percentage of CON, there was no significant difference in transient upstroke rate between VEH and FLEC at any time point ($p > 0.05$; Figure 5.18 E; $n = 7$ cells (VEH); and $n = 10$ cells (FLEC)).

5.3.5 The effect of calmodulin on permeabilised myocyte Ca²⁺ release with and without flecainide

Relative amounts of endogenous CaM were quantified in intact and in saponin permeabilised ventricular myocytes using Western blotting. Figure 5.19 A shows a representative Western blot probing for CaM (16.7 kDa) and the housekeeping protein β -actin (42 kDa). Immediately after saponin permeabilisation, endogenous CaM decreased to $16.94 \pm 6.78\%$ of that measured in intact cells ($p < 0.001$; Figure 5.19 B). Incubation of the permeabilised cells for a further 15 min (PERM+15) did not further decrease the protein signal ($p > 0.05$; Figure 5.19 B; $n = 4$ hearts for each group).

Figure 5.20 A shows line scans and fluorescence profiles of cells perfused under control (CON) conditions or in the presence of exogenous CaM (100 nM; CaM). Perfusion of CaM significantly increased wave frequency from 6.59 ± 0.40 waves/min to 9.34 ± 0.49 waves/min ($p < 0.001$; Figure 5.20 B). Wave propagation velocity was unchanged ($p > 0.05$; Figure 5.20 C; $n = 17$ (CON); and $n = 20$ (CaM)). Figure 5.21 A shows line scans and fluorescence profiles of individual waves from cells perfused with CON or CaM. Wave amplitude significantly decreased in the presence of exogenous CaM ($3.18 \pm 0.09 \Delta F/F_0$ vs $2.77 \pm 0.08 \Delta F/F_0$; $p < 0.01$; Figure 5.21 B). CaM significantly increased wave upstroke rate from $0.033 \pm 0.002 (\Delta F/F_0)/\text{ms}$ to $0.038 \pm 0.001 (\Delta F/F_0)/\text{ms}$ ($p < 0.05$; Figure 5.21 C). Wave duration from wave peak to 90% of the Ca²⁺ decline was significantly decreased with CaM (543.3 ± 27.8 ms to 402.1 ± 14.7 ms; $p < 0.001$; Figure 5.21 D) and Ca²⁺ decline time constant was significantly decreased with CaM (238.7 ± 12.4 ms to 175.8 ± 6.4 ms; $p < 0.001$; Figure 5.21 E; $n = 17$ (CON); and $n = 20$ (CaM)).

Figure 5.22 A shows line scans and fluorescence profiles of waves from cells imaged under control conditions (CON) and after 5 min perfusion with vehicle (VEH) or flecainide (FLEC). All data were collected in the presence of 100 nM CaM. Wave frequency was unchanged after 5 min perfusion with VEH ($p > 0.05$) and there was a significant decrease in wave frequency with FLEC ($p < 0.001$; Figure 5.22 B). FLEC significantly decreased wave frequency by $14.0 \pm 2.28\%$ compared with VEH after 6 min perfusion ($p < 0.01$; Figure 5.22 C). A significant difference was also apparent after 1, 3, and 4 min of perfusion ($p < 0.01$) and similar trends were shown after 2 and 4 min perfusion ($p = 0.06$ and $p = 0.05$ respectively; Figure 5.22 C). Wave propagation velocity was unchanged after 5 min perfusion with VEH or FLEC ($p > 0.05$; Figure 5.22 D) and there was no significant difference between groups within this parameter ($p > 0.05$; Figure 5.22 E; $n = 9$ (VEH); and $n = 14$ (FLEC)). Figure 5.23 A shows line scans and fluorescence profiles of individual waves at CON and after 5 min perfusion with VEH or FLEC. Peak amplitude significantly decreased after 5 min perfusion with VEH ($p < 0.001$) or CaM FLEC ($p < 0.001$;

Figure 5.23 B). As a percentage of CON, there were no significant differences between groups at any time point ($p > 0.05$; Figure 5.23 C). Wave upstroke rate significantly decreased after 5 min perfusion with VEH ($p < 0.001$) or FLEC ($p < 0.001$; Figure 5.23 D). As a percentage of CON, there were no significant differences between groups at any time point ($p > 0.05$; Figure 5.23 E). Wave duration from the wave peak to 90% of the Ca^{2+} decline was unchanged after 5 min perfusion with VEH ($p > 0.05$) or FLEC ($p > 0.05$; Figure 5.24 A) and there were no significant differences between groups at any time points ($p > 0.05$; Figure 5.24 B). The Ca^{2+} decline time constant of a wave was unchanged after 5 min perfusion with VEH ($p > 0.05$) and was significantly increased with FLEC ($p < 0.001$; Figure 5.24 C). There were no significant differences between groups at any time points within this parameter ($p > 0.05$; Figure 5.24 B; $n = 9$ (VEH); and $n = 14$ (FLEC)). When comparing the size of the effect of flecainide in either the presence or absence of CaM, the effect size was similar.

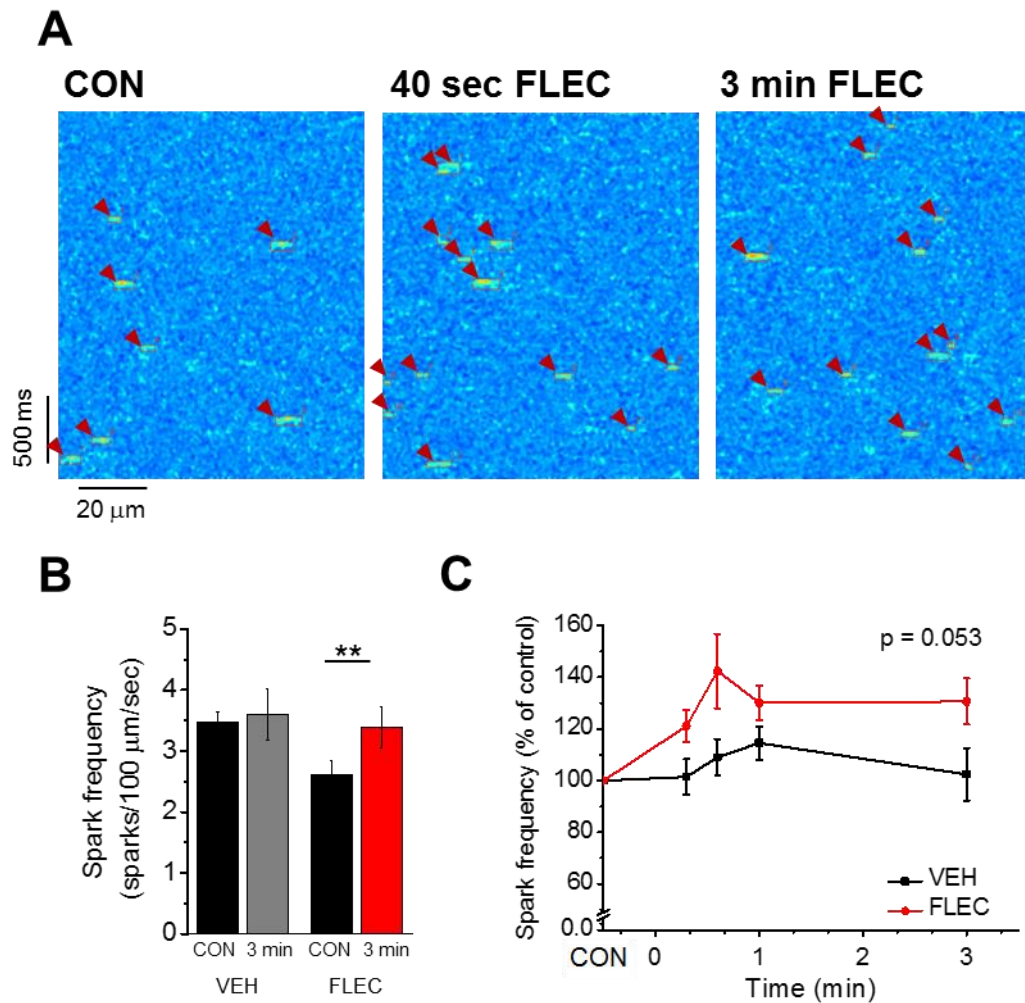


Figure 5.14: The effect of flecainide on spark frequency over 3 min

A) Representative line scans of sparks identified by Sparkmaster at control (CON), after 40 sec and after 3 min of perfusion with flecainide (FLEC) **B)** Spark frequency for vehicle (VEH) and FLEC treated groups at CON and after 3 min perfusion **C)** Percentage change in spark frequency in VEH and FLEC groups. Two way repeated measures ANOVA + Holm-Sidak *post hoc* test. ** = $p < 0.01$. n (cells)=VEH = 13 (6); FLEC = 31 (7).

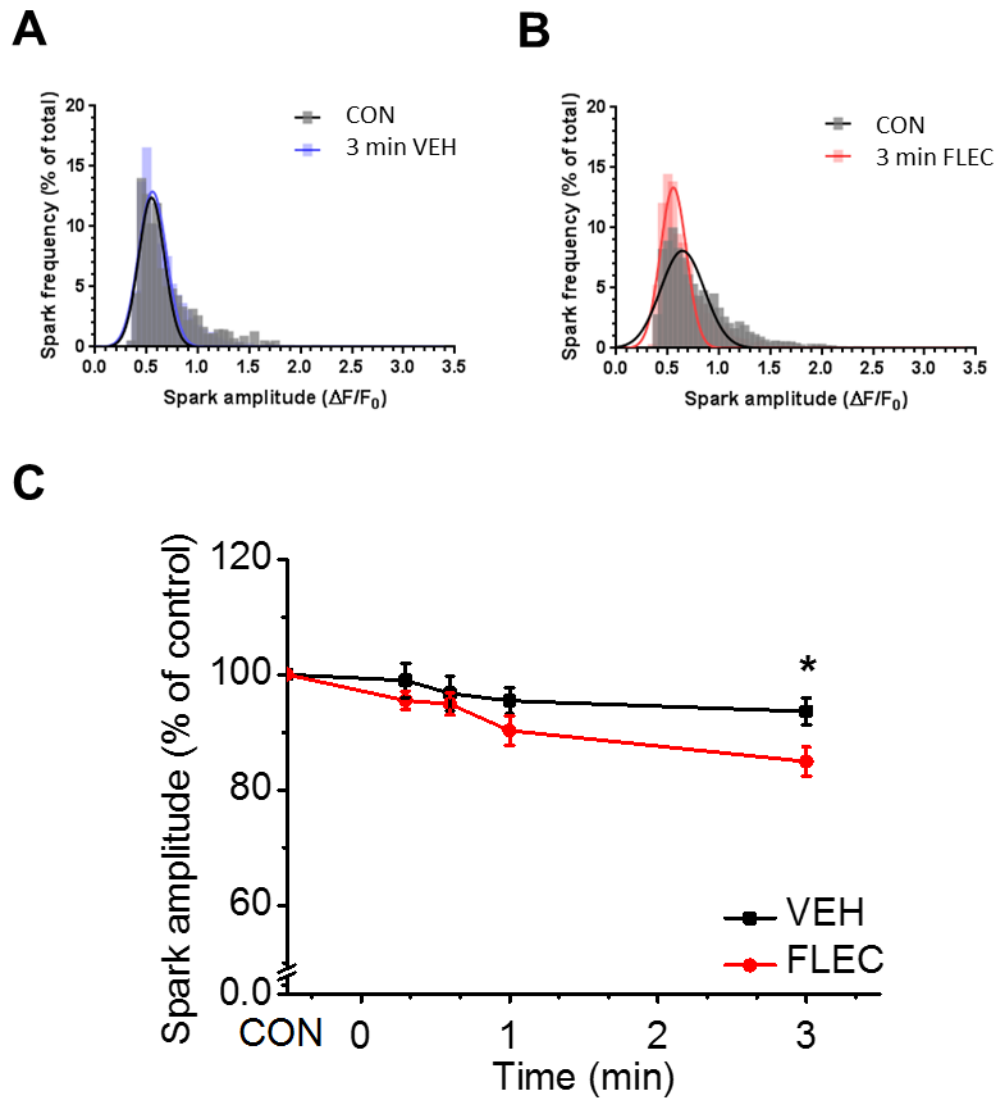


Figure 5.15: The effect of flecainide on spark amplitude over 3 min

A) Spread of individual spark data for spark amplitude in the vehicle (VEH) group at the control time point (CON; black) and after 3 min perfusion (blue). **B)** Spread of individual spark data for spark amplitude in the flecainide (FLEC) group at the control time point (CON; black) and after 3 min (red). **C)** Percentage change in spark amplitude in VEH and FLEC groups. Gaussian curve fit and extra sum of squares F test. Two way repeated measures ANOVA + Holm-Sidak *post hoc* test. * = $p < 0.05$. n (cells) = CON = 13 (6); FLEC = 31 (7). N (sparks) VEH = CON = 705 (6), 3 min = 1108 (6); FLEC = CON = 1545 (7), 3 min = 2270 (7).

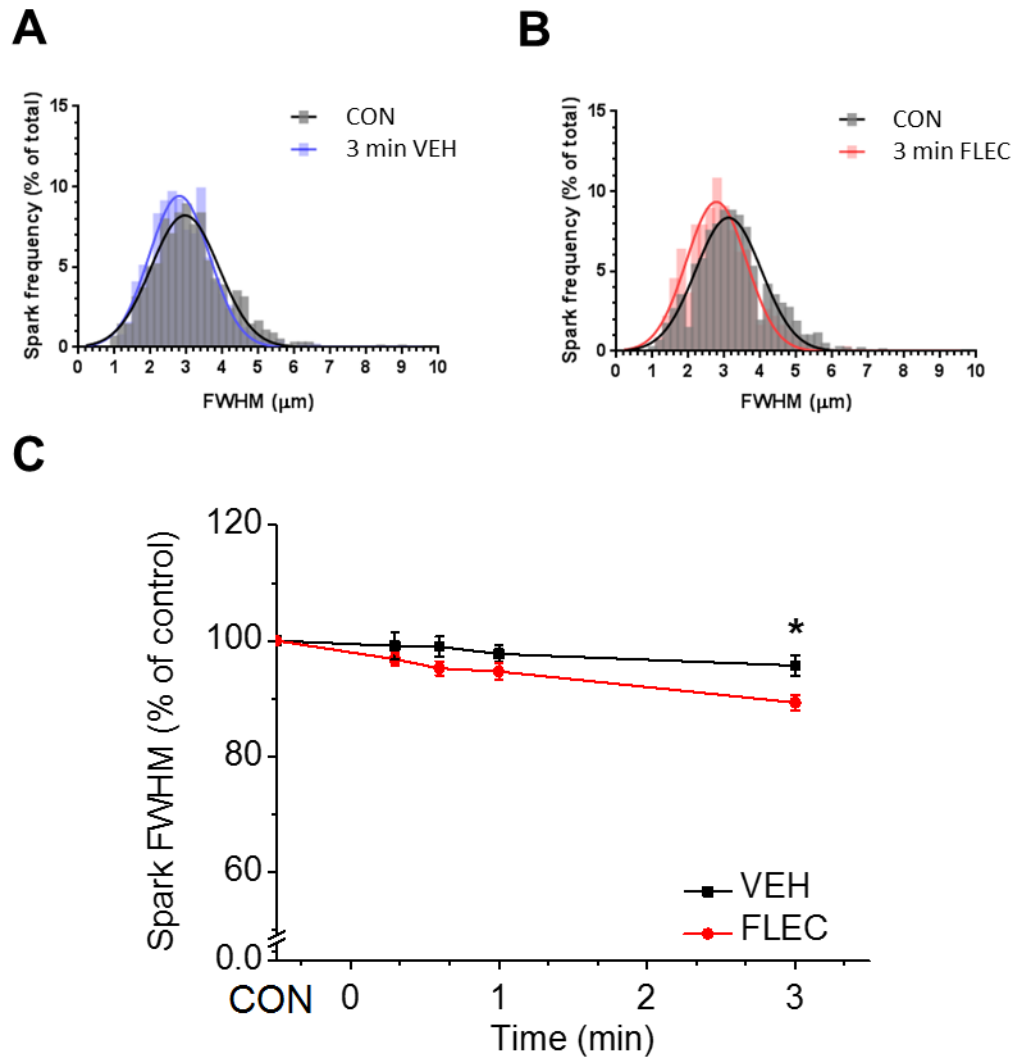


Figure 5.16: The effect of flecainide on spark FWHM over 3 min

A) Spread of individual spark data for FWHM in the vehicle (VEH) group at the control time point (CON; black) and after 3 min perfusion (blue). **B)** Spread of individual spark data for FWHM in the flecainide (FLEC) group at the control time point (CON; black) and after 3 min (red). **C)** Percentage change in spark FWHM in VEH and FLEC groups. Gaussian curve fit and extra sum of squares F test. Two way repeated measures ANOVA + Holm-Sidak *post hoc* test. * = $p < 0.05$. n (cells) = CON = 13 (6); FLEC = 31 (7). N (sparks) VEH = CON = 705 (6), 3 min = 1108 (6); FLEC = CON = 1545 (7), 3 min = 2270 (7).

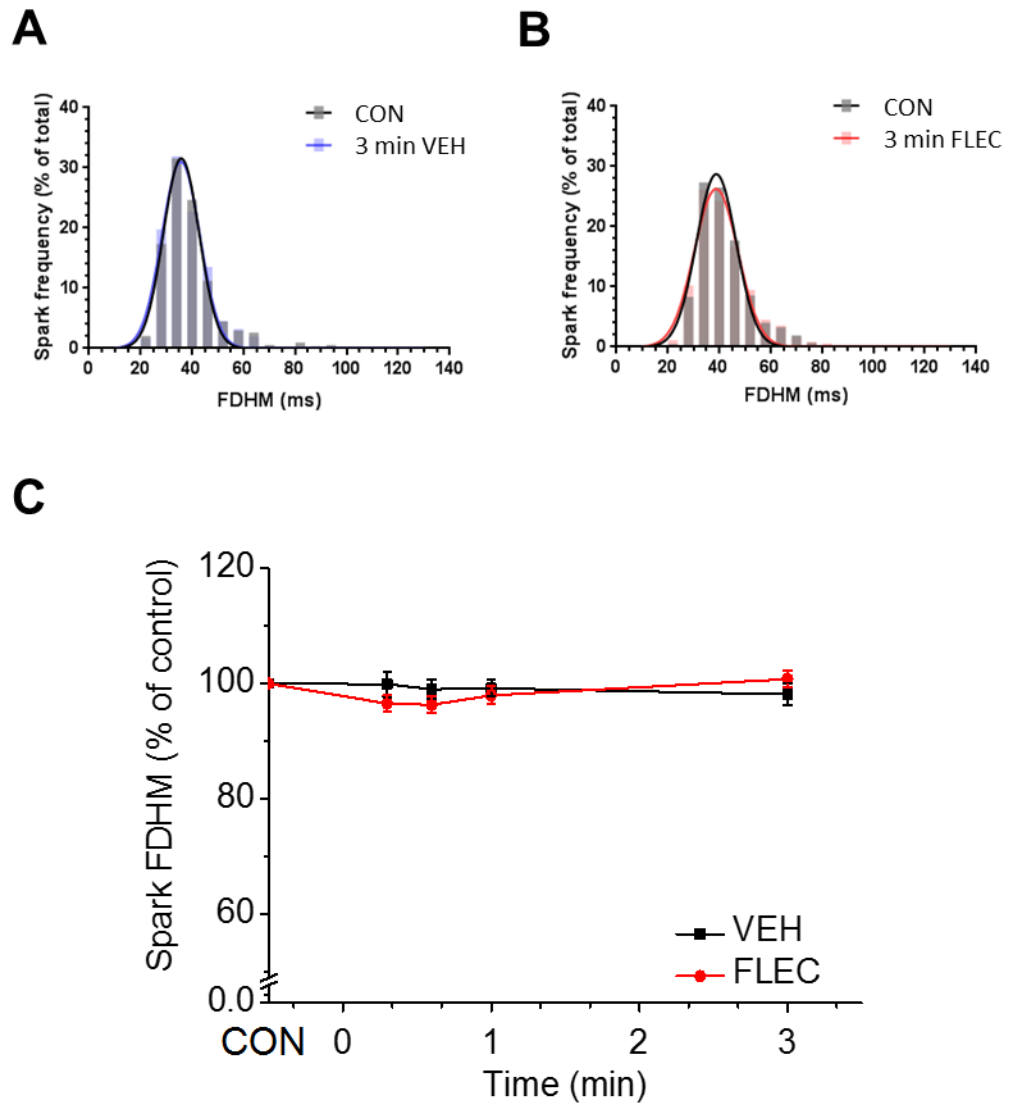


Figure 5.17: Effect of flecainide on spark FDHM over 3 min

A) Spread of individual spark data for FDHM in the vehicle (VEH) group at the control time point (CON; black) and after 3 min perfusion (blue). **B)** Spread of individual spark data for FDHM in the flecainide (FLEC) group at the control time point (CON; black) and after 3 min (red). **C)** Percentage change in spark FDHM in VEH and FLEC groups. Gaussian curve fit and extra sum of squares F test. Two way repeated measures ANOVA + Holm-Sidak *post hoc* test. n (cells) = CON = 13 (6); FLEC = 31 (7). N (sparks) VEH = CON = 705 (6), 3 min = 1108 (6); FLEC = CON = 1545 (7), 3 min = 2270 (7).

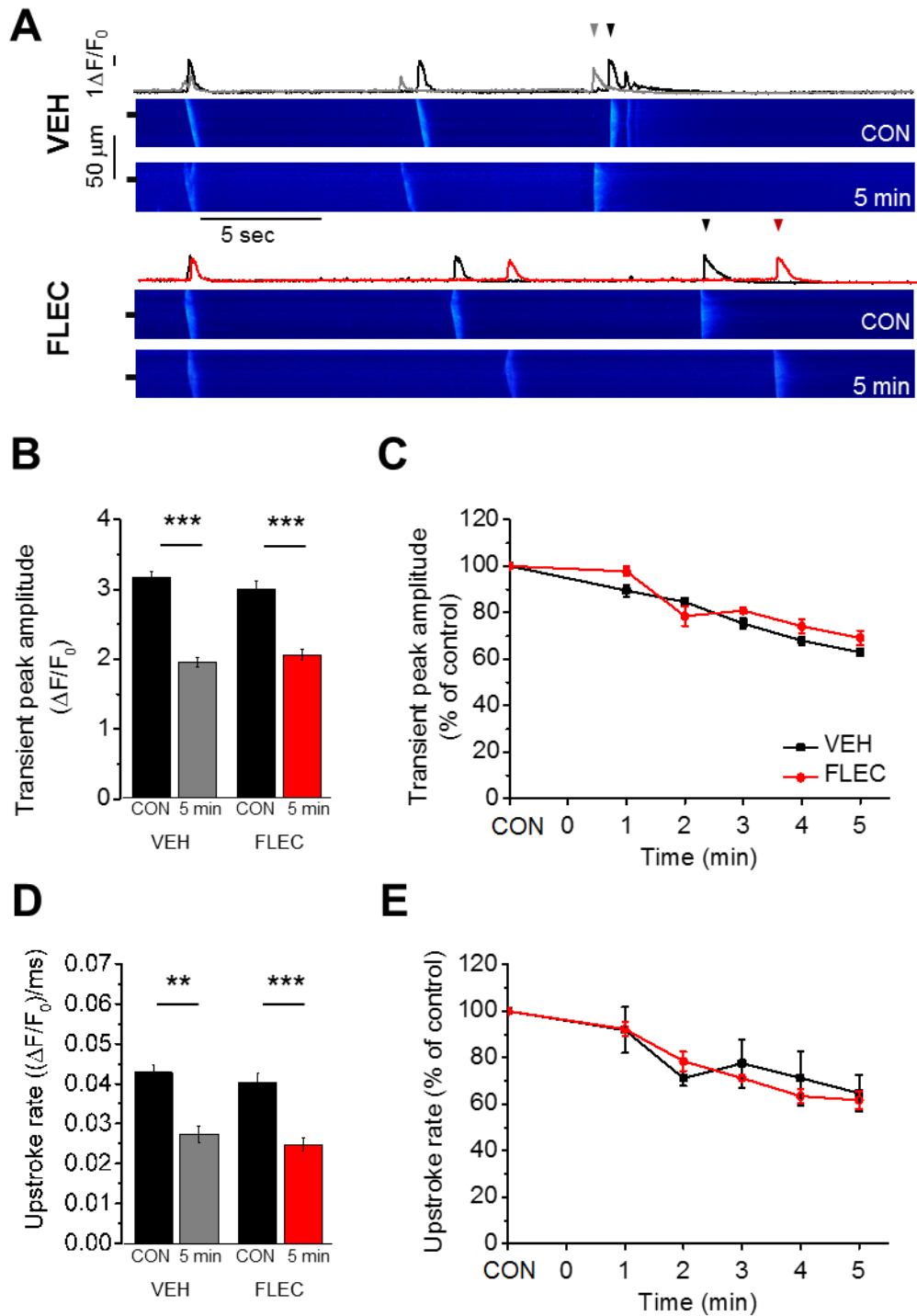


Figure 5.18: The effect of flecainide on SR Ca^{2+} content over 5 min

A) Representative line scans and fluorescence profiles of caffeine induced Ca^{2+} transients at control (CON) and after 5 min perfusion with vehicle (VEH) or flecainide (FLEC). Caffeine induced Ca^{2+} transients indicated with a triangle. **B)** Transient peak amplitude of VEH and FLEC groups at CON and after 5 min perfusion. **C)** Percentage change in transient peak amplitude in VEH and FLEC groups. **D)** Upstroke rate of VEH and FLEC groups at CON and after 5 min perfusion. **E)** Percentage change in upstroke rate in VEH and FLEC groups. Paired and unpaired two tailed Student's t-test; or two way repeated measures ANOVA + Holm-Sidak *post hoc* test. ** = $p < 0.01$; *** = $p < 0.001$. $n = \text{VEH} = 7$ (3); $\text{FLEC} = 10$ (3).

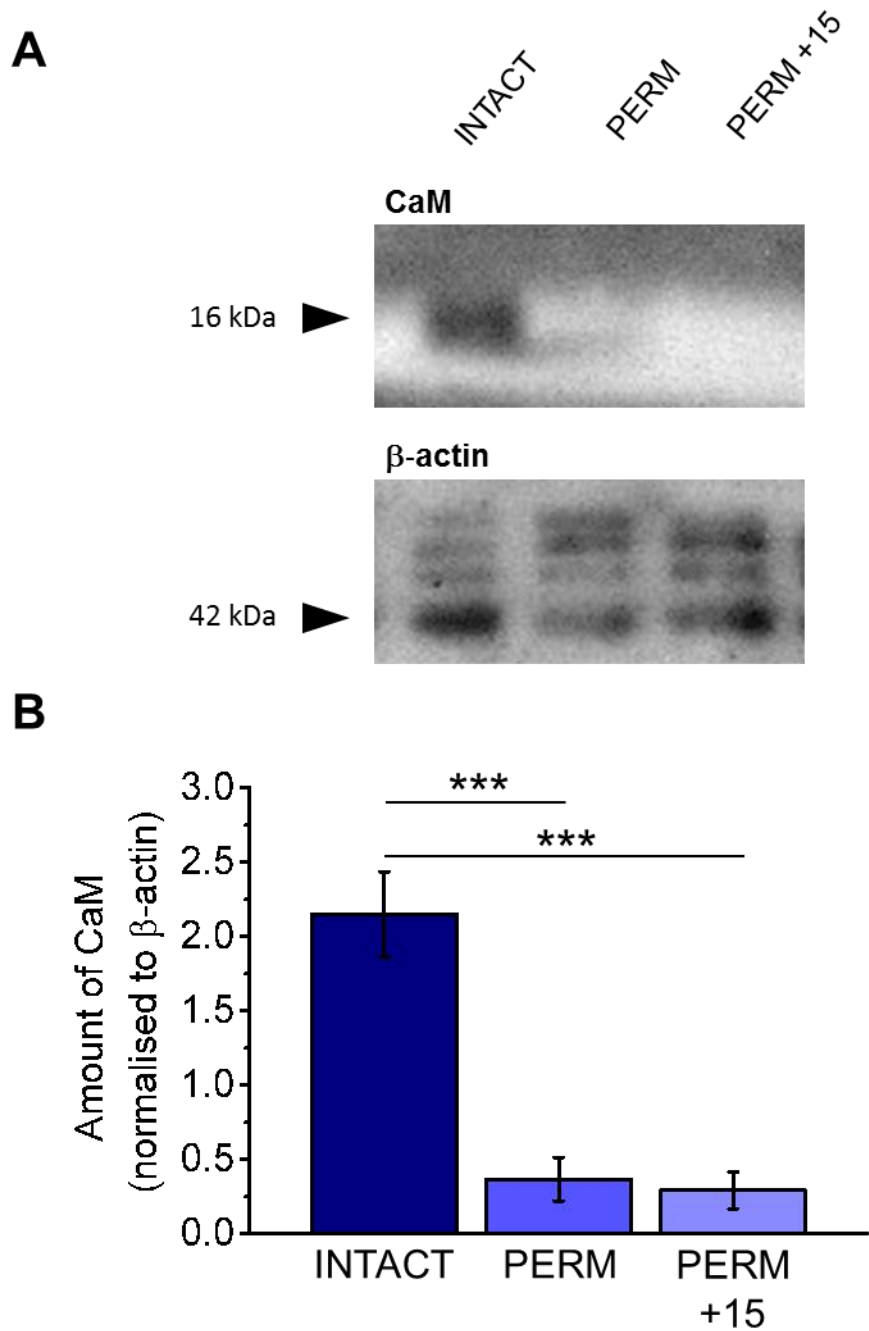


Figure 5.19: The effect of saponin permeabilisation on relative quantity of endogenous intracellular CaM

A) Representative Western blot probing for CaM (16.7 kDa) and the housekeeping protein β -actin (42 kDa) in intact cells (INTACT); saponin permeabilised cells (PERM); and saponin permeabilised cells washed for 15 min in intracellular solution (PERM + 15). **B)** Mean quantity of CaM normalised to β -actin in INTACT, PERM and PERM +15 cells. One way ANOVA + Holm-Sidak *post hoc* test. *** = $p < 0.001$. $n = \text{INTACT} = 4$; $\text{PERM} = 4$; $\text{PERM}+15 = 4$. Data collection and analysis by Dr H M Kirton.

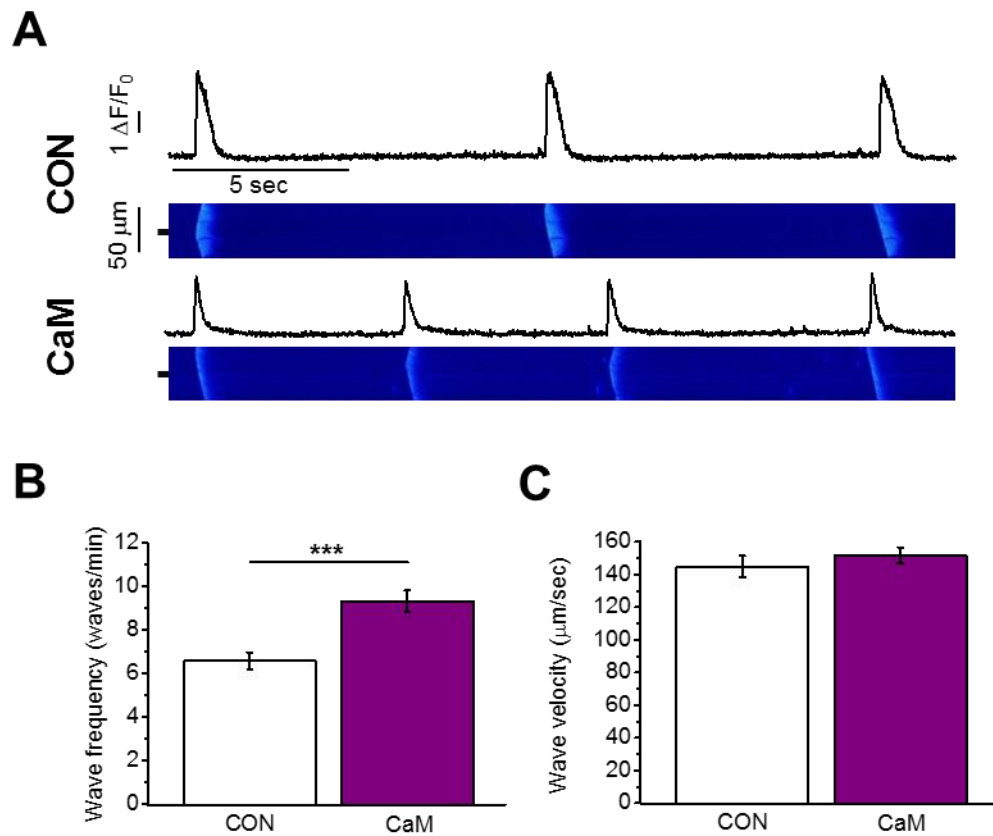


Figure 5.20: The effect of exogenous CaM on wave frequency and propagation velocity

A) Representative line scans and fluorescence profiles of waves at control (CON) and in the presence of exogenous CaM (CaM) **B)** Differences between CON and CaM in wave frequency and **C)** wave propagation velocity. Unpaired two-tailed Student's t-test. *** = $p < 0.001$. $n = \text{CON} = 17$ (3); $\text{CaM} = 20$ (3).

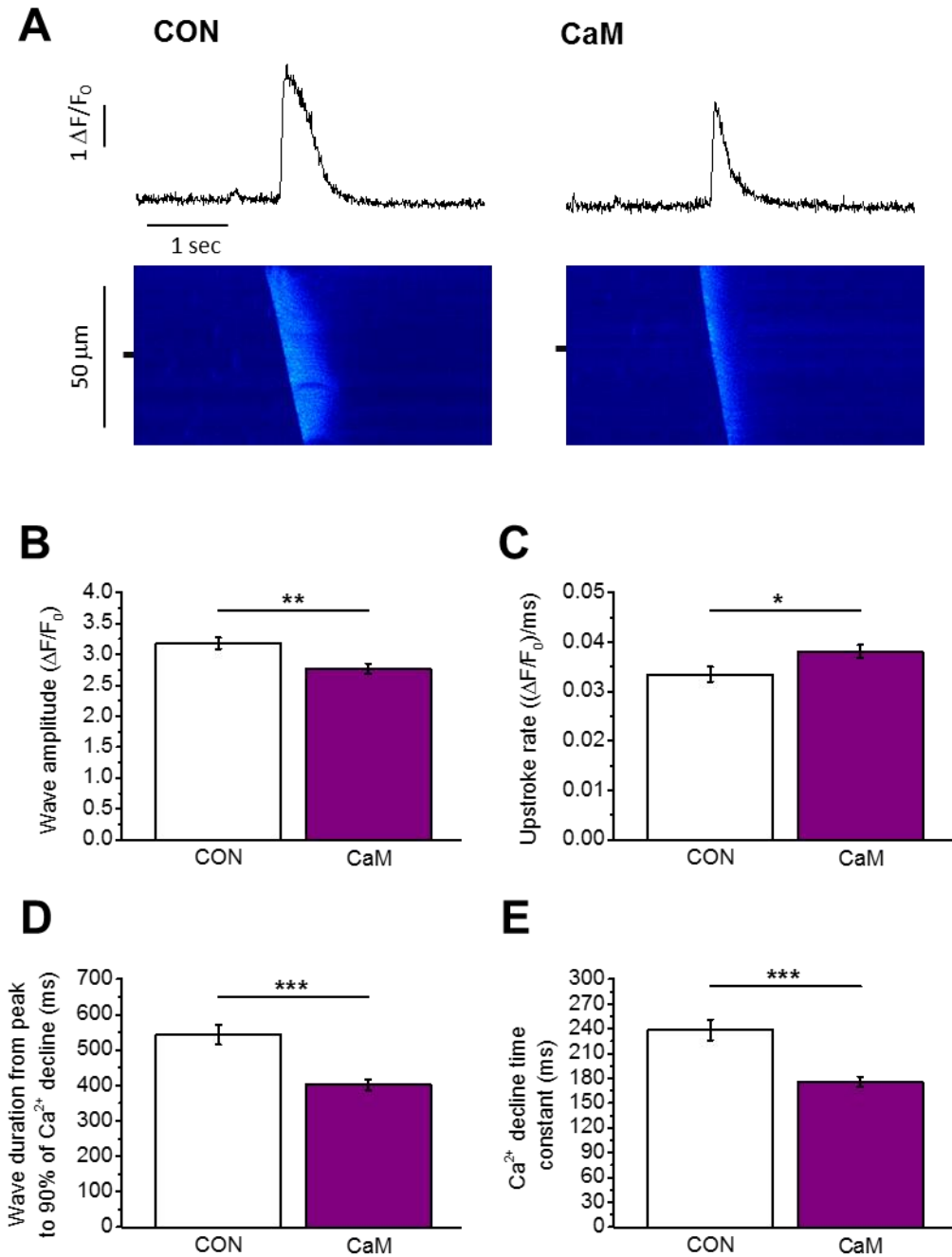


Figure 5.21: The effect of exogenous CaM on wave dimensions

A) Representative line scans and fluorescence profiles of waves at control (CON) and in the presence of exogenous CaM (CaM) **B)** Differences between CON and CaM in **B)** wave peak amplitude, **C)** upstroke rate, **D)** duration from the peak to 90% of Ca^{2+} wave dedine and **E)** Ca^{2+} decline time constant. Unpaired two-tailed Student's t-test. * = $p < 0.05$; *** = $p < 0.001$. $n = \text{CON} = 17$ (3); $\text{CaM} = 20$ (3).

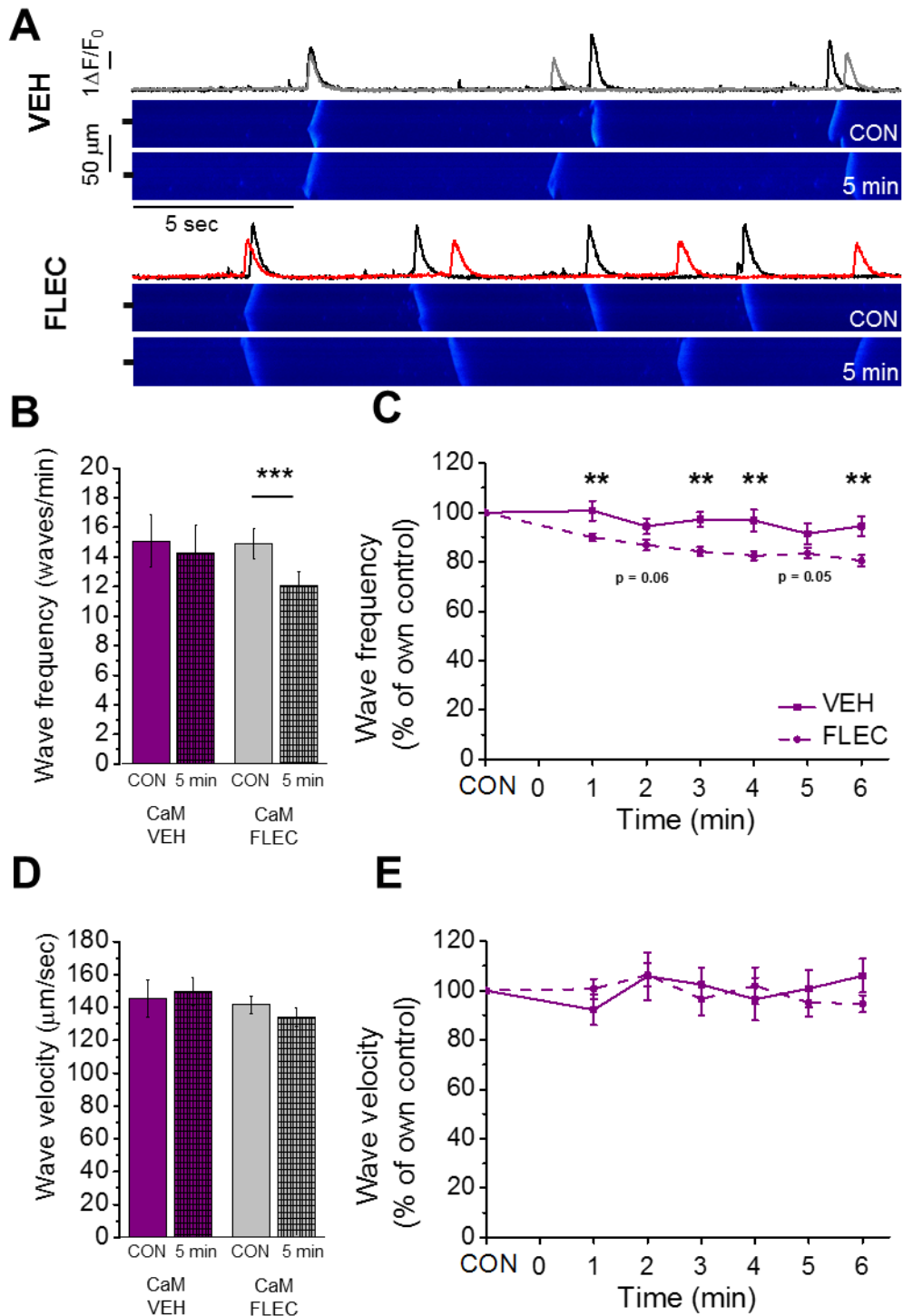


Figure 5.22: The effect of flecainide on wave frequency and propagation velocity in the presence of exogenous CaM

A) Representative line scans and fluorescence profiles of waves at control (CON) and after 5 min perfusion with vehicle (CaM VEH) or flecainide (CaM FLEC), all in the presence of exogenous CaM **B)** Wave frequency for CaM VEH and CaM FLEC at CON and after 5 min perfusion **C)** Percentage change in wave frequency in the CaM VEH and CaM FLEC groups. **D)** Wave velocity for CaM VEH and CaM FLEC at CON and after 5 min perfusion. **E)** Percentage change in wave velocity in the CaM VEH and CaM FLEC groups. Paired and unpaired two tailed Student's t-test; or two way repeated measures ANOVA + Holm-Sidak *post hoc* test. ** = $p < 0.01$; *** = $p < 0.001$. $n = \text{VEH} = 9$ (4); $\text{FLEC} = 14$ (4).

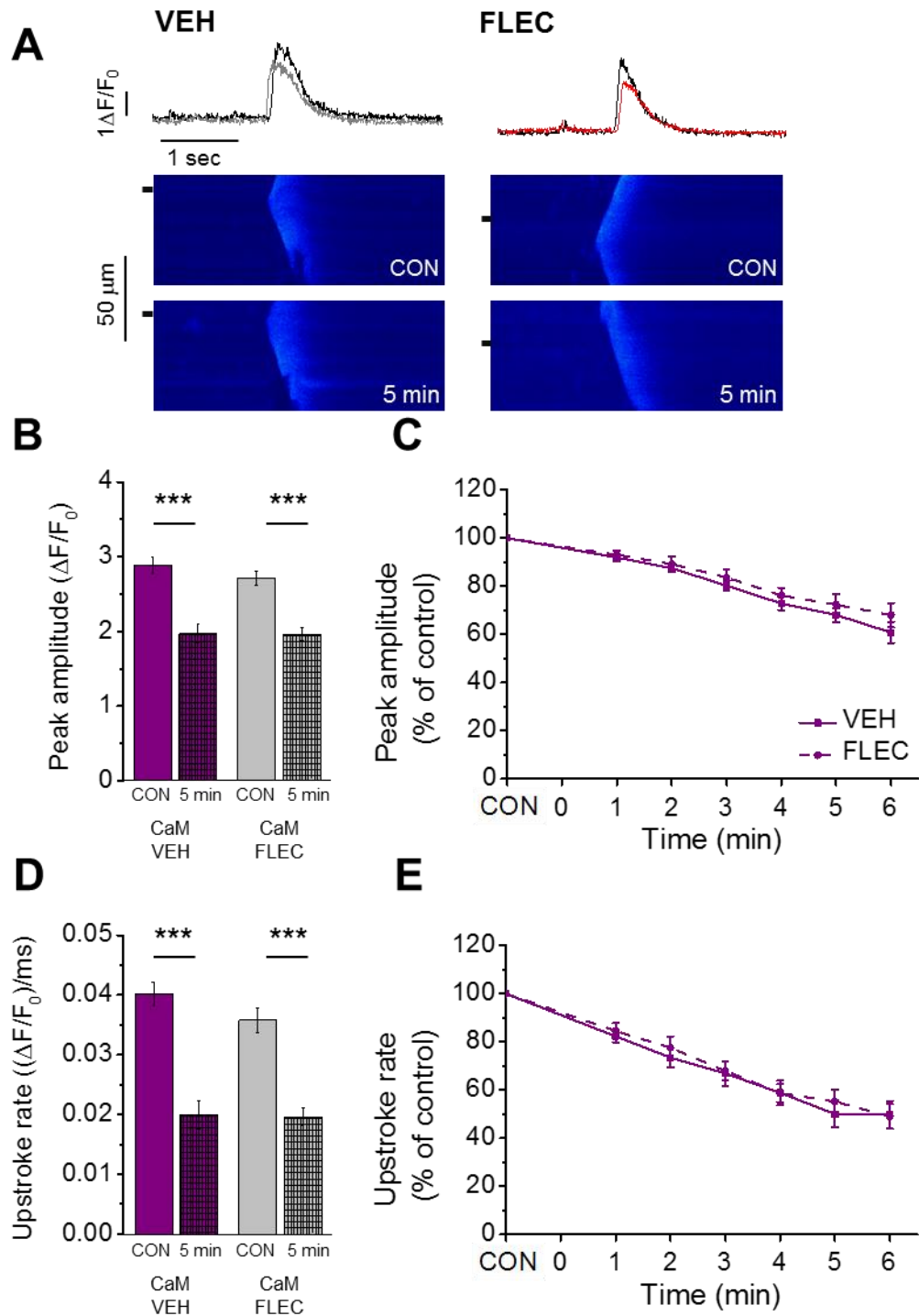


Figure 5.23: The effect of flecainide on wave amplitude and upstroke rate in the presence of exogenous CaM

A) Representative line scans and fluorescence profiles of waves at control (CON) and after 5 min perfusion with vehicle (CaM VEH) or flecainide (CaM FLEC), all in the presence of exogenous CaM **B)** Wave peak amplitude for CaM VEH and CaM FLEC groups at CON and after 5 min perfusion. **C)** Percentage change in wave amplitude in the CaM VEH and CaM FLEC groups. **D)** Wave upstroke rate for CaM VEH and CaM FLEC groups at CON and after 5 min perfusion. **E)** Percentage change in wave upstroke rate in the CaM VEH and CaM FLEC groups. Paired and unpaired two tailed Student's t-test; or two way repeated measures ANOVA + Holm-Sidak *post hoc* test. * = $p < 0.05$; *** = $p < 0.001$. $n = \text{VEH} = 9$ (4); $\text{FLEC} = 14$ (4).

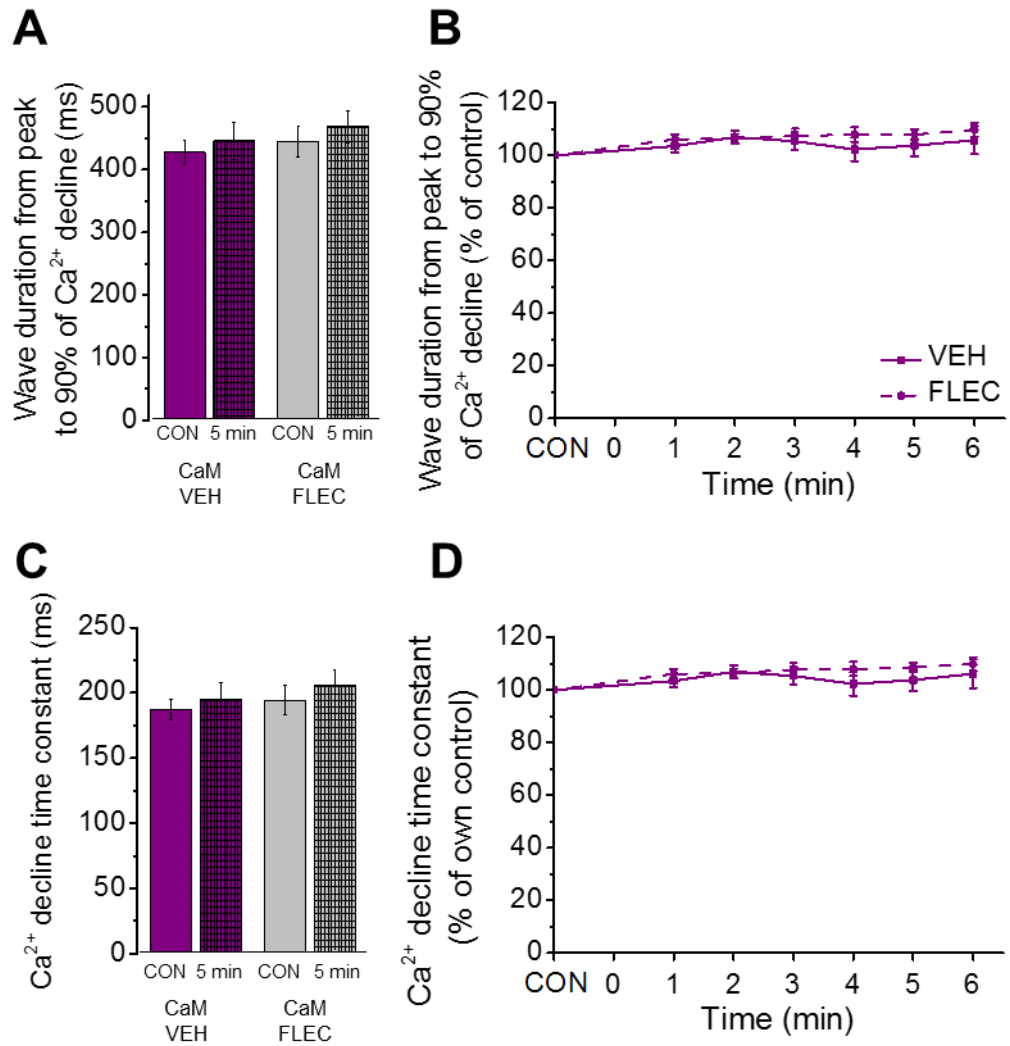


Figure 5.24: The effect of flecainide on wave duration and relaxation time constant in the presence of exogenous CaM

A) Wave duration from the peak to 90% of Ca²⁺ wave decline at control (CON) and after 5 min perfusion with vehicle (CaM VEH) or flecainide (CaM FLEC). **B)** Percentage change in wave duration from the peak to 90% of Ca²⁺ wave decline in the CaM VEH and CaM FLEC groups. **C)** Ca²⁺ decline time constant for CaM VEH and CaM FLEC groups at CON and after 5 min perfusion. **D)** Percentage change in Ca²⁺ decline time constant in the CaM VEH and CaM FLEC groups. Paired and unpaired two-tailed Student's t-test; or two way repeated measures ANOVA + Holm-Sidak post hoc test. n = VEH = 9 (4); FLEC = 14 (4).

5.4 Discussion

5.4.1 The effect of intracellular $[Ca^{2+}]$ on Ca^{2+} waves and sparks

In the current experiments, an increase in $[Ca^{2+}]$ caused an increase in the frequency of Ca^{2+} wave release. This was supported by similar experiments using permeabilised cardiomyocytes or trabeculae (Loughrey et al., 2002, Lukyanenko and Gyorke, 1999, Orchard et al., 1998) and reflects the effects of cytosolic and SR luminal Ca^{2+} on RyR2 activation (Fabiato, 1992, Laver, 2007, Lukyanenko et al., 1996).

Ca^{2+} waves occur at a threshold SR luminal $[Ca^{2+}]$ at which Ca^{2+} spark release is initiated and the propagation of a Ca^{2+} wave is facilitated by an increased cytosolic $[Ca^{2+}]$ (Lukyanenko et al., 1996). Increasing the cytosolic $[Ca^{2+}]$ and the level of SERCA activation also raises luminal Ca^{2+} more rapidly to this threshold point, thereby increasing Ca^{2+} wave frequency (Lukyanenko et al., 1999). In single channel lipid bilayer experiments, increased RyR2 opening times were reported with an increased concentration of luminal Ca^{2+} (Tencerova et al., 2012, Sitsapesan and Williams, 1994). These experiments were performed in the absence of the accessory protein, Casq2, and the presence of a Ca^{2+} activation site on the RyR2 luminal face was inferred (Tencerova et al., 2012, Sitsapesan and Williams, 1994). Indeed, at least one luminal Ca^{2+} activation site has been identified at the helix bundle channel gate of RyR2 (Jiang et al., 2007, Chen et al., 2014). SR Ca^{2+} is also strongly buffered by Casq2 (Mitchell et al., 1988) and there is evidence to suggest that Casq2 also acts as a luminal Ca^{2+} sensor that interacts with RyR2 to influence channel gating (Terentyev et al., 2007).

Permeabilised cardiomyocyte experiments have also inferred the presence of a cytosolic RyR2 Ca^{2+} binding site (Bovo et al., 2011), which underlies the physiological CICR mechanism following Ca^{2+} influx via LTCC (Bers, 2000). Interactions of five amino acid residues located at the C-terminal domain of the skeletal muscle isoform RyR1 were reported to form a Ca^{2+} binding site at the cytosolic face (des Georges et al., 2016). These residues are conserved in the cardiac isoform RyR2, indicating a potential cytosolic Ca^{2+} binding site for the cardiac isoform (des Georges et al., 2016). Recently however, this result has been questioned and instead, the RyR2 central domain of RyR2 has been implicated in cytosolic Ca^{2+} activation (Xiao et al., 2016). A final complicating factor is “feedthrough activation” a mechanism whereby Ca^{2+} released from RyR2 may influence RyR2 activation at cytosolic regulation sites (Laver, 2007).

In the present study, Ca^{2+} wave propagation velocity was unchanged between HIGH and LOW $[Ca^{2+}]$ at $\sim 140 \mu\text{m}/\text{sec}$. Wave propagation along the length of the cell is reported to occur via

saltatory propagation as Ca^{2+} sparks, released from RyR2 clusters, propagate across the cytosol to activate neighbouring RyR2 clusters to release more Ca^{2+} (Cheng et al., 1996, Keizer et al., 1998). 140 $\mu\text{m}/\text{sec}$ is somewhat greater than the published experimental range (70 - 120 $\mu\text{m}/\text{sec}$) (Engel et al., 1995, Engel et al., 1994, Wussling and Salz, 1996, Landgraf et al., 2004, Chen et al., 2014b, Lukyanenko and Gyorke, 1999) yet is within the range simulated by Okada et al. (100 – 150 $\mu\text{m}/\text{sec}$) (Okada et al., 2005).

That peak wave amplitude was decreased with HIGH $[\text{Ca}^{2+}]$ compared with LOW $[\text{Ca}^{2+}]$ is puzzling and may indicate a lower SR Ca^{2+} content at the time of wave release. Spark amplitude immediately prior to wave release also showed a trend to decrease with HIGH $[\text{Ca}^{2+}]$ compared with LOW $[\text{Ca}^{2+}]$. However, this may also be due to the non-linearity of the fluo-3 signal if at HIGH $[\text{Ca}^{2+}]$ the peak wave amplitude were to coincide with the plateau in fluo-3 signal. Indeed, this trend was not apparent for spark frequency, width or duration immediately prior to wave release, indicating that $[\text{Ca}^{2+}]$ did not alter the threshold for Ca^{2+} wave release and therefore did not alter the maximal SR Ca^{2+} content. Hence, once the cytosolic $[\text{Ca}^{2+}]$ has reached a level that induces repetitive waves, increasing $[\text{Ca}^{2+}]$ further only changes the rate at which the SR content rises to that set point.

In cells strongly buffered with EGTA, waves were not apparent and sparks were consistently released at frequencies significantly lower than the maximum seen in HIGH and LOW $[\text{Ca}^{2+}]$ groups. However, it is inappropriate to compare spark frequencies between cells with and without waves due to the differing concentrations of EGTA. The changed Ca^{2+} buffering capacities affect the spatial confinement of sparks differently. Indeed, previous experiments performed in permeabilised myocytes with strong EGTA buffering show Ca^{2+} spark frequency to be highly dependent upon $[\text{Ca}^{2+}]$ and very high spark frequencies were recorded (>60 sparks/100 $\mu\text{m}/\text{sec}$) without inducing waves (Lukyanenko and Gyorke, 1999).

5.4.2 The effect of flecainide on Ca^{2+} waves, sparks and transients

In permeabilised WT myocytes, 3 min of perfusion with 25 μM flecainide induced a ~10% decrease in Ca^{2+} wave frequency when cells were continuously scanned at either LOW or HIGH $[\text{Ca}^{2+}]$. As part of this protocol, there was no significant effect of flecainide after 1 min perfusion. However, in cells with a discontinuous scanning protocol, flecainide induced a ~20% decrease in Ca^{2+} wave frequency and a significant effect was apparent after 1 min of flecainide perfusion. Additionally, when the laser exposure was reduced, as in the second scanning protocol, the variation within groups was less indicating the importance of protocol design. To

minimise the variation in starting wave frequencies due to $[Ca^{2+}]$ variation apparent in permeabilised myocyte experiments (Orchard et al., 1998), the data for each cell were calculated as a percentage change from starting control and the appropriate statistics were used.

In contrast to the present results, experiments performed by Bannister et al. (2015) in permeabilised WT cardiomyocytes, showed no change in wave frequency upon application of flecainide (5 and 25 μ M). However, both cell permeabilisation and data collection occurred during laser exposure and wave frequency variation was high (Bannister et al., 2015). Additionally, whilst the experimental protocol involved paired data, the data analysis clearly stated an unpaired statistical test. Combined, the consequences of these factors probably limited the ability to detect relatively small changes in wave frequency with flecainide, in WT cells. Indeed, in experiments performed by Savio-Galimberti et al. (2015), in which data were compared to vehicle; displayed as a percentage change from control; and cells were not exposed to the laser during permeabilisation, flecainide (25 μ M) significantly decreased Ca^{2+} wave frequency by ~15% in permeabilised WT cardiomyocytes isolated from rabbit and mouse (Savio-Galimberti and Knollmann, 2015).

In comparison to the effect of flecainide on wave frequency in permeabilised $Casq2^{-/-}$ myocytes, the effect of flecainide in WT cells was quantitatively less (~20% vs. ~30%), yet the effect size was similar to that reported in $R4496C^{+/-}$ cardiomyocytes (~20%) (Savio-Galimberti and Knollmann, 2015). Importantly however, the flecainide concentration required to elicit these changes in WT myocytes was 4 fold that required in CPVT myocytes (6 μ M vs. 25 μ M). This indicates that WT RyR2 may have a lower affinity for flecainide than functionally altered RyR2 in CPVT models. Both of these mouse models exhibited a CPVT phenotype in which heart rate and rhythm were normal under basal conditions, yet exhibited exercise-induced arrhythmias (Cerrone et al., 2005, Knollmann et al., 2006). Isolated cells from both CPVT models showed pro-arrhythmic behaviour including increased spontaneous wave frequency, Ca^{2+} spark frequency and duration (Fernandez-Velasco et al., 2009b, Hilliard et al., 2010, Savio-Galimberti and Knollmann, 2015). In the $R4496C^{+/-}$ model however, the *in vitro* CPVT phenotype was less severe compared with the $Casq2^{-/-}$ model (Savio-Galimberti and Knollmann, 2015).

When translated into paced intact cells, a 20% delay in the release of a spontaneous wave is likely to have a substantial anti-arrhythmic effect. This is because pro-arrhythmic waves can only occur between electrically stimulated Ca^{2+} transients. The release of a wave need only be delayed enough to allow a physiological Ca^{2+} transient to occur first, thereby limiting SR Ca^{2+} overload. Thus, a 20% decrease in Ca^{2+} waves in permeabilised cells may equate to a complete

inhibition of waves in intact paced cells, as was apparent in intact Casq2^{-/-} myocytes (Hilliard et al., 2010). A corresponding RyR2 mediated anti-arrhythmic effect was not apparent in paced, intact WT cells (Chapter 3) although this might be explained by a lower affinity of WT RyR2 for flecainide (Chapter 7) or insufficient concentration of flecainide within the cytosolic compartment (Chapter 4). Indeed, an effect of flecainide on RyR2 has been consistently reported in Casq2^{-/-} cells at 6-10 μ M whereas in WT cells, 25 μ M is required (Hilliard et al., 2010, Savio-Galimberti and Knollmann, 2015).

The current results suggest that in WT, permeabilised, ventricular myocytes, flecainide acts independently of Na_v1.5 to elicit a significant anti-arrhythmic effect, likely through an interaction with RyR2. Similar results in Casq2^{-/-} cardiomyocytes concluded that flecainide inhibited RyR2 Ca²⁺ release in an open state block to decrease Ca²⁺ wave frequency (Hilliard et al., 2010). In this way, flecainide imposed a partial block of the RyR2 pore by introducing a sub-state closure to ~20% of the RyR2 channel conductance (Hilliard et al., 2010, Hwang et al., 2011a). Flecainide increased spark frequency alongside a decrease in spark amplitude and width and this was apparent in both the present data, in permeabilised WT cardiomyocytes and to a greater degree, with a lower flecainide concentration, in intact Casq2^{-/-} myocytes (Hilliard et al., 2010). Inhibition of RyR2 by flecainide caused smaller sparks, which may decrease the probability that released Ca²⁺ will propagate to neighbouring RyR2 clusters and form waves. Simultaneously, the increased spark frequency arises to maintain the same Ca²⁺ leak and consequently autoregulation is bypassed (Hilliard et al., 2010, Overend et al., 1997). This was apparent in the present data and in experiments using Casq2^{-/-} cells, whereby SR Ca²⁺ content was maintained upon application of flecainide (Hilliard et al., 2010).

5.4.3 The effect of flecainide on Ca²⁺ waves in the presence of calmodulin

It has been reported that flecainide block of RyR2 is exacerbated in the presence of CaM in single channel RyR2 experiments and in cardiomyocytes isolated from Casq2^{-/-} mice with a CPVT phenotype (Gomez-Hurtado et al., 2015). Similarly, the inhibition of the RyR skeletal muscle isoform RyR1 by dantrolene was apparent only in the presence of CaM, indicating the potential importance of this modulatory protein in pharmaceutical kinetics (Oo et al., 2015a). It was suggested that CaM might be lost during the saponin permeabilisation process due to its small molecular weight (16.7 kDa) relative to the size of sarcolemmal perforations. Proteins 800 kDa in size have been reported to be freely permeable to saponin permeabilised membranes (Hudder et al., 2003). Therefore, the effect of flecainide on wave frequency and

dimensional properties was investigated in the presence of 100 nM exogenous CaM. The total CaM concentration has been reported at $\sim 6 \mu\text{M}$, however the majority of CaM is bound to membrane and cytosolic proteins (Maier et al., 2006). Total available CaM was reported at 50–75 nM, although 100 nM exogenous CaM is consistently used within the literature (Wu and Bers, 2007, Gomez-Hurtado et al., 2015, Oo et al., 2015a, Maier et al., 2006).

CaM is a Ca^{2+} binding protein that binds to and regulates membrane bound proteins such as RyR2 and L-type Ca^{2+} channel; as well as the cytosolic regulatory protein CAMKII (Saucerman and Bers, 2012, Evans and Shea, 2009, Huang et al., 2012, Dixon et al., 2015). There are two Ca^{2+} binding sites at each of the two helix-loop-helix domains (EF hands) located within the C and N terminal lobes respectively (Chattopadhyaya et al., 1992). In its Ca^{2+} bound state, CaM has been reported to bind to RyR2 and decrease RyR2 opening times by $\sim 20\%$ (Smith et al., 1989) (Huang et al., 2012). However, in its unbound form (apoCaM) RyR2 inhibition is diminished (Fruen et al., 2003). In intact myocytes, only 1% of CaM was reported to be free within the cytosol and the majority of CaM was bound to proteins located at the z-lines (Wu and Bers, 2007). Contrary to the current result in which $\sim 85\%$ of CaM was lost after saponin permeabilisation, Wu and Bers reported no change in the amount of CaM between intact and permeabilised cells (Wu and Bers, 2007). A likely explanation for this discrepancy is the permeabilisation methodology used. Wu and Bers exposed myocytes to 50 $\mu\text{g}/\text{ml}$ of saponin for 20 secs, whereas the current protocol incubated myocytes in 0.01 $\mu\text{g}/\text{ml}$ of saponin for 15 min. Whilst both methods resulted in sarcolemmal permeabilisation, endogenous CaM likely unbound from cellular structures to be washed away within the current 15 min saponin incubation period. Indeed, Wu and Bers reported that $>75\%$ of binding between fluorescently labelled CaM and permeabilised cell structures occurred within 15 min of saponin permeabilisation, thus implying that 75% of endogenous CaM unbound from cellular structures within this period (Wu and Bers, 2007).

It was apparent from permeabilised cardiomyocyte experiments in which CaM was minimally present, that CaM is not necessary for Ca^{2+} release and uptake from the SR. However, CaM serves a modulatory role to ensure the physiological release of Ca^{2+} from the SR (Yang et al., 2014, Xu et al., 2010). As a Ca^{2+} binding protein, addition of exogenous CaM to permeabilised cells likely buffered the total $[\text{Ca}^{2+}]$, decreasing the free $[\text{Ca}^{2+}]$ available (Wang et al., 2013), however the exact $[\text{Ca}^{2+}]$ could not be calculated using the REACT $[\text{Ca}^{2+}]$ software (Duncan et al., 1999). It would be expected that wave frequency would decrease, as discussed in Section 5.4.1. However, this was not the case and an increase in Ca^{2+} wave frequency was instead observed. This might indicate that the functional effect of CaM binding to RyR2 counters this

Ca²⁺ buffering effect. Indeed, mutations in CaM specific genes *CALM1-3* have been reported to cause arrhythmogenic disorders with CPVT phenotypes (Nyegaard et al., 2012) and these CaM mutations disrupt the direct binding of CaM to the RyR2-CaM binding domain (CaMBD) and thereby disrupt appropriate CaM modulation of SR Ca²⁺ release (Rebbeck et al., 2016, Sondergaard et al., 2015). This inter-protein interaction causes inhibition of RyR2 opening (Smith et al., 1989, Oda et al., 2013b). In permeabilised myocytes, CaM was reported to stabilise RyR2 activity by promoting RyR2 “zipping” whereby the central and N-terminal domains interact to give rise to a preferentially closed channel state (Figure 1.10) (Oda et al., 2013b). In isolated SR vesicles, addition of CaM was reported to decrease the duration of RyR2 opening times by ~20% in the presence of ATP and at >100 nM free Ca²⁺ (Smith et al., 1989). Additionally, the threshold for wave termination was increased with CaM (Tian et al., 2013). These data correspond with the current results that showed a significant decrease in wave duration from the peak to 63% and 90% of the Ca²⁺ decline in the presence of exogenous CaM. In this case, an increase in the threshold for wave termination would give rise to a greater SR Ca²⁺ content, immediately after the termination of a wave. Thus, the time taken for Ca²⁺ to reach the threshold for wave release would be decreased, leading to an increase in wave frequency (as observed). Experiments by Lukyanenko et al. (1999) observed an increase in spark frequency in the presence of CaM, and SR Ca²⁺ content was increased (Lukyanenko and Gyorke, 1999). It was concluded that the increase in SR content increased the luminal activation of RyR2 causing increased spark release (Lukyanenko and Gyorke, 1999). This may also account for the increased wave frequency observed in the current data due to an increased spark frequency increasing the propensity for Ca²⁺ propagation to form waves.

Despite the significant changes in wave frequency and properties observed in the presence of CaM, flecainide decreased wave frequency to a similar extent in the presence of exogenous CaM in WT cardiomyocytes. This indicates that in WT cardiomyocytes, flecainide was not dependent upon CaM to act on RyR2.

5.4.4 Conclusions and Summary

In saponin permeabilised WT myocytes where drug access to RyR2 was immediate and Na_v1.5 was functionally absent, flecainide induced a sustained decrease in the frequency of spontaneous Ca²⁺ waves. This is consistent with a direct action of flecainide on RyR2. When the experimental design was modified to allow prolonged flecainide perfusion, whilst limiting laser exposure, the effects of flecainide on Ca²⁺ wave frequency were more similar to that described in CPVT myocytes; however, in WT cells these effects occurred at a much higher concentration of flecainide than in CPVT myocytes. This may explain why clear effects on RyR2 were not

observed in intact WT myocytes (Chapter 3) (Sikkel et al., 2013). In intact myocytes, flecainide applied at plasma concentrations or higher (6 μ M or 15 μ M), may not have accumulated sufficiently within the cytosol during the experimental protocol, especially considering that trans-sarcolemmal movement is slow and flecainide preferentially accumulates within the mitochondria (Chapter 4). Whilst a previous study suggested that restoration of physiological levels of CaM increased the effects of flecainide in permeabilised CPVT myocytes, this could not be replicated in WT cells.

Chapter 6: The effect of flecainide on RyR2 after inhibition of the SR counter-current in permeabilised myocytes

6.1 Introduction

Release of SR Ca^{2+} via RyR2 occurs spontaneously in the form of sparks and pro-arrhythmic waves; and as transients in response to caffeine or electrical field stimulation. Flux of Ca^{2+} from the SR lumen to the cytosol is accompanied by the movement of positively charged ions in the opposite direction (Coronado et al., 1980). This 'counter-current' is mostly carried by K^+ and without it, the SR membrane would rapidly polarise towards the Ca^{2+} equilibrium potential resulting in cessation of Ca^{2+} release within <1 ms (Gillespie and Fill, 2008). For the same reason, an 'outward' counter-current, in the luminal to cytosolic direction, must accompany the reuptake of Ca^{2+} into the SR via SERCA.

During diastole, the potential difference across the SR membrane is generally assumed to be at 0 mV (Somlyo et al., 1977, Venturi et al., 2013, Guo et al., 2013). Although there is some computational and experimental evidence to suggest that the SR lumen is slightly inside negative at ~ -2 mV (Yazawa et al., 2007, Gillespie and Fill, 2008). While the existence of a transient voltage change across the SR membrane coinciding with Ca^{2+} release has been hypothesised (Beeler, 1980, Laver and Lamb, 1998), the magnitude and time course of such an effect has not been established. This is largely due to the technical difficulties involved in calibrating measurements of SR membrane potential, using voltage-sensitive dyes or electrophysiological recordings of SR vesicles (Meissner, 1983, Portele et al., 1997, Chang and Jackson, 2003). However, the occurrence of transient voltage changes across the SR may indirectly be supported by the presence of a subset of SR-specific, voltage-dependent channels such as RyR2 and trimeric intracellular cation-specific (TRIC) channels (Diaz-Sylvester et al., 2011, Venturi et al., 2013).

It is currently unclear which channels within the SR membrane facilitate the ionic movements that underlie the counter-current. There is convincing evidence to suggest that the K^+ flux is carried by TRIC A and B subtype channels (Section 6.4.1) (Yazawa et al., 2007, Pitt et al., 2010, Venturi et al., 2013) or by RyR2 (Gillespie and Fill, 2008, Guo et al., 2013). There is speculation that other unidentified K^+ and Cl^- specific channels may also contribute to the SR counter-current (Zhou et al., 2014, Townsend and Rosenberg, 1995) and at least in skeletal muscle, proton channels may contribute 5 -10 % of the SR counter-current (Kamp et al., 1998).

The possibility of a transient polarisation of the SR membrane during Ca^{2+} release is of relevance to the present work because a recent study on RyR2 channels incorporated into lipid bilayers suggested that flecainide inhibits RyR2 when the inside of the SR is negatively charged with respect to the cytosol (Bannister et al., 2015). It was suggested that under these conditions, flecainide partially blocked RyR2-mediated K^+ movement, but without a physiologically relevant effect on Ca^{2+} efflux (Bannister et al., 2016). These authors assumed that the SR membrane potential is always zero under physiological conditions and therefore, the reported effects of flecainide on intact cells must reflect a non-RyR2 target, such as sarcolemmal $\text{Na}_v1.5$. However both our group (Chapter 5), and others (Hilliard et al., 2010, Savio-Galimberti and Knollmann, 2015) reported changes in Ca^{2+} waves and sparks upon application of flecainide to permeabilised myocytes, where $\text{Na}_v1.5$ is not functional.

Previous studies have shown that the SR counter-current can be inhibited by substitution of K^+ with Cs^+ (Kawai et al., 1998) or facilitated by addition of the K^+ ionophore valinomycin (Kometani and Kasai, 1978). Therefore, the aim of the work described in this chapter was to investigate whether modulating the SR counter-current influences the effect of flecainide on SR Ca^{2+} regulation. Specifically, if transient polarisation of the SR facilitates the action of flecainide on RyR2, then inhibition or facilitation of the counter-current might be expected to increase or decrease the effect of flecainide respectively.

6.2 Methods

6.2.1 SR K⁺ counter-current block protocol

Rat ventricular cardiomyocytes were isolated via retrograde perfusion and enzymatic digestion on a Langendorff apparatus (Chapter 2.2). Cells were permeabilised in intracellular solution containing 0.01% saponin for 15 min at room temperature (22.0 ± 2 °C) (Chapter 2.5.1). Cells were then placed in the experimental chamber on the microscope stage and left for 2 min to settle onto the glass cover slip before perfusion with intracellular solution (146 nM free Ca²⁺ buffered with 0.1 mM EGTA; Table 2.4), whilst a suitable cell was identified for scanning (Chapter 2.5.3). To inhibit the SR counter-current, cells were bathed in an intracellular solution designed to minimize the K⁺ and Cl⁻ content. Potassium chloride was substituted with caesium methanesulphonate; magnesium chloride for magnesium sulphate; and caesium hydroxide was used to adjust the pH (Table 2.3) (Kawai et al., 1998, Zhou et al., 2014). In experiments investigating the effect of SR K⁺ counter-current block on wave properties, cells were line scanned at 188 lps in the presence of K⁺ solution (45 sec) and then switched to Cs⁺ solution (1 min 45 sec). Measurements for analysis were taken at the control time point (K⁺) and 1 min after the solution switch (Cs⁺).

To investigate the effect of 25 µM flecainide during SR counter-current block, each cell was equilibrated in Cs⁺ solution for 2 min prior to line scanning. Laser intensity was maintained at 7% of the maximum laser intensity throughout. This scan time included a 15 sec interval at 2 min 45 sec where the scan was stopped, saved and a new scan was started. The first 45 sec of scanning was analysed as the control time point. Thereafter, the first and third minutes after the control scan section were analysed for the time control and flecainide groups. Flecainide was used at a concentration 5x greater than that recorded during peak plasma levels (Mano et al., 2015, 3M, 2016). This was to mimic the accumulation of the drug into the cytosol and subcellular compartments, as reported in Chapter 4 and to remain consistent with results presented in Chapter 5.

6.2.2 Valinomycin protocol

Isolated, saponin permeabilised cardiomyocytes were placed in the experimental chamber on the microscope stage and left for 2 min to settle onto the glass cover slip before being perfused with intracellular solution (146 nM free Ca^{2+} ; Table 2.4). A suitable cell was selected and line scanned under control conditions for 2 min 45 sec at 188 lps with an interval time of 5.3 ms between lines. The laser intensity was maintained at 7% of the maximum intensity throughout. The solution was switched to intracellular solution containing 2 μM valinomycin; or 2 μM valinomycin and 25 μM flecainide. The cell was scanned for 2 min 45 sec at 0 and 3 min after perfusion with valinomycin or valinomycin and flecainide began.

6.2.3 Analysis and statistics

Line scans were viewed using ImageJ software. To measure wave frequency, the time between the start of each wave was measured using the Line Profile Tool. Aborted wavelets were classed as waves which propagated <50% of the scanned cell width and were not included in the wave frequency analysis. However, they were included in the wave spatial spread analysis. The length of the cell and the length of the wave were measured using the ImageJ Line Tool at the time at which the wave occurred. The percentage of the cell length occupied by a wave was calculated to normalise for differences in cell length both within and across datasets. Wave propagation velocity was analysed using a Python encoded image analysis tool (Sikora, 2016) (Chapter 2.7.3). Waves were manually cropped from the original scan file in ImageJ to include the full wave duration and a minimum of 1 sec of quiescent cell background before and after the wave event. Cropped images were inputted into the analysis tool. Wave fronts were identified at a range of different sensitivity thresholds and the propagation velocity was calculated from a fitted linear gradient. All outputted files were manually checked for erroneous wave front identification and these were omitted from the final analyses. Wave peak amplitude, upstroke rate, duration from wave peak to 90% of the wave decline and Ca^{2+} decline time constant were analysed using the C++ encoded image analysis tool (Benson, 2016). Waves were cropped as previously described and saved as a text file that was inputted into the wave dimension analysis tool (Chapter 2.7.2). Identified wave parameters included the time values for the wave start, peak and end; peak fluorescence values; and an exponential fit along the wave decline. From these parameters, the peak amplitude, upstroke rate, duration from the peak to 90% of the wave decline and Ca^{2+} decline time constant were calculated.

Changes in wave parameters at control and after 3 min perfusion with experimental solution were displayed as absolute values in a bar graph, in the presence or absence of flecainide. Two

tailed paired Student's t-tests were used to test for differences within each group at these time points. Differences between the absolute values at the control time point were compared between each group using a two tailed unpaired Student's t-test. For each cell scanned, the change in its wave properties over time was also presented as a percentage of control. The differences between control and flecainide groups was compared using a two way repeated measures ANOVA. If a significant difference was identified between the groups, a Holm-Sidak multiple comparisons *post-hoc* test isolated the time points at which the groups were significantly different from one another. Significance was considered when $p < 0.05$. All data were displayed as mean \pm SEM.

6.3 Results

6.3.1 Cs⁺ ion exchange decreased wave frequency and prolonged wave duration

It was hypothesised that the SR counter-current could be blocked by Cs⁺ ion exchange. The effect of Cs⁺ ion exchange on wave frequency; spatial spread; propagation velocity; and wave upstroke rate, amplitude, duration from the peak to 90% of the wave decline and Ca²⁺ decline time constant was investigated in permeabilised ventricular myocytes. Figure 6.1 A shows representative line scans of a cell perfused with K⁺ control solution (CON) and the same cell after 1 min perfusion with Cs⁺ solution (Cs⁺). The [Ca²⁺] was maintained throughout. Cs⁺ exchange significantly decreased wave frequency by 61.3% ($p < 0.05$; Figure 6.1 B; $n = 6$ cells for both groups). The spatial spread of each wave across the length of the cell and the wave propagation velocity did not change between CON and Cs⁺ groups ($p > 0.05$; Figure 6.1 C and D; $n = 6$ cells for both groups).

Close up line scans and fluorescence profiles of individual waves illustrate the change in wave duration upon application of Cs⁺ (Figure 6.2 A). Cs⁺ exchange significantly decreased wave peak amplitude ($p < 0.01$; Figure 6.2 B) and the peak upstroke rate ($p < 0.01$; Figure 6.2 C). Wave duration from the peak to 90% of the wave decline and wave Ca²⁺ decline time constant significantly increased upon perfusion with Cs⁺ by 49.2% ($p < 0.01$) and 50.1% respectively ($p < 0.01$; Figure 6.2 D and E; $n = 6$ cells for both groups).

6.3.2 Flecaïnide decreased wave frequency after counter-current inhibition

Figure 6.3 A shows representative line scans and fluorescence profiles illustrating changes in wave frequency after 3 min of perfusion with Cs⁺ and vehicle (Cs⁺ VEH) or Cs⁺ and flecaïnide (Cs⁺ FLEC). After 3 min perfusion, wave frequency was unchanged in the vehicle control ($p > 0.05$) and significantly decreased from 2.7 ± 0.3 waves/min to 1.5 ± 0.3 waves/min with the addition of flecaïnide ($p < 0.01$; Figure 6.3 B). Figure 6.3 C shows changes in wave frequency as a percentage of control (CON) for Cs⁺ VEH and Cs⁺ FLEC groups. After 3 min perfusion, Cs⁺ FLEC decreased wave frequency by $38.1 \pm 10.1\%$ in comparison to Cs⁺ VEH. Groups were significantly different at 3 min ($p < 0.01$; $n = 13$ cells for both groups). In the Cs⁺ FLEC group, 23.1% of cells (3/14 cells) did not display any waves during the final minute of scanning.

The distance propagated by a wave across the length of a cell is shown in Figure 6.4 A as a white double-headed arrow. Wave propagation velocity is shown as a red line along the edge

of the wave front. A small decrease in the spatial spread of a wave occurred in both the Cs⁺ VEH ($p = 0.06$) and Cs⁺ FLEC groups after 3 min perfusion ($p < 0.05$; Figure 6.4 B) although no significant difference between groups was apparent at any time point when measured as a percentage of control ($p > 0.05$; Figure 6.4 C). Propagation velocity did not significantly change after 3 min in either Cs⁺ VEH ($p > 0.05$) or Cs⁺ FLEC ($p > 0.05$; Figure 6.4 D) and there was no significant difference between groups at any time point ($p > 0.05$; Figure 6.4 E; $n = 13$ cells for both groups).

Close up line scans and fluorescence profiles of individual waves illustrate changes in wave properties after 3 min in Cs⁺ VEH and Cs⁺ FLEC (Figure 6.5 A). Peak amplitude decreased significantly after 3 min perfusion with Cs⁺ VEH ($p < 0.001$) and Cs⁺ FLEC ($p < 0.001$; Figure 6.5 B). As a percentage of control there was no significant differences between the groups at any time point ($p > 0.05$; Figure 6.5 C). Upstroke rate decreased significantly after 3 min perfusion with Cs⁺ VEH ($p < 0.01$) and Cs⁺ FLEC ($p < 0.001$; Figure 6.5 D). There were no significant differences between the groups at any time point ($p > 0.05$; Figure 6.5 E). Wave duration from the peak to 90% of the wave decline decreased significantly after 3 min perfusion with Cs⁺ VEH ($p < 0.05$) or Cs⁺ FLEC ($p > 0.01$; Figure 6.6 A). As a percentage of control, wave duration from the peak to 90% of the wave decline decreased in both groups by ~16% after 3 min and there were no significant differences between the groups at any time point ($p > 0.05$; Figure 6.6 B). Ca²⁺ decline time constant decreased significantly after 3 min perfusion with Cs⁺ VEH ($p < 0.05$) but was unchanged with Cs⁺ FLEC ($p > 0.05$; Figure 6.6 C). As a percentage of control, the wave Ca²⁺ decline time constant for both groups decreased by ~16% after 3 min and there were no significant differences between the groups at any time point ($p > 0.05$; Figure 6.6 D; $n = 13$ cells for both groups). To summarise, in the presence of Cs⁺, flecainide significantly decreased wave frequency by ~40% without an effect on any other wave parameter.

6.3.3 Flecainide countered the decrease in wave frequency caused by valinomycin

Figure 6.7 A shows representative line scans and fluorescence profiles illustrating changes in wave frequency after 3 min of perfusion with valinomycin and vehicle (VAL VEH) or valinomycin and flecainide (VAL FLEC). Wave frequency significantly decreased to $34.1 \pm 6.8\%$ of control in the VAL VEH group after 3 min perfusion. 18.2% of cells (2/11 cells) did not exhibit a wave in the final 2 min 45 sec of scanning.

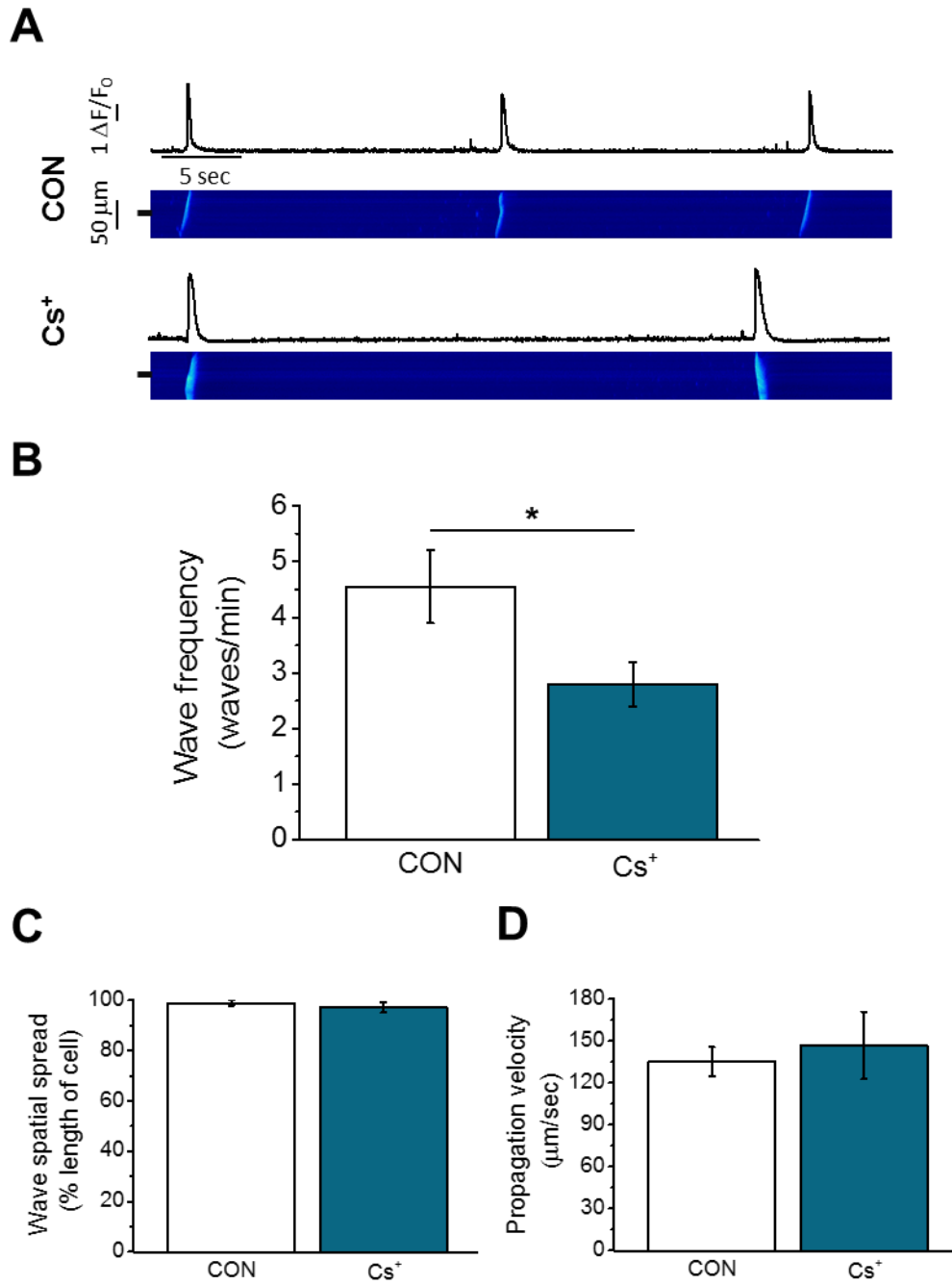


Figure 6.1: Effect of Cs⁺ on wave frequency and wave propagation

A) Representative line scans of waves at control (CON) and after Cs⁺ perfusion (Cs⁺), within the same cell. Representative fluorescence profiles taken at black lines next to each line scan. **B)** Differences between CON and Cs⁺ wave frequency, **C)** spatial spread across the cell length and **D)** propagation velocity. Paired two-tailed Student's t-tests. * = $p < 0.05$. $n = \text{CON} = 6$ (5); $\text{Cs}^+ = 6$ (5).

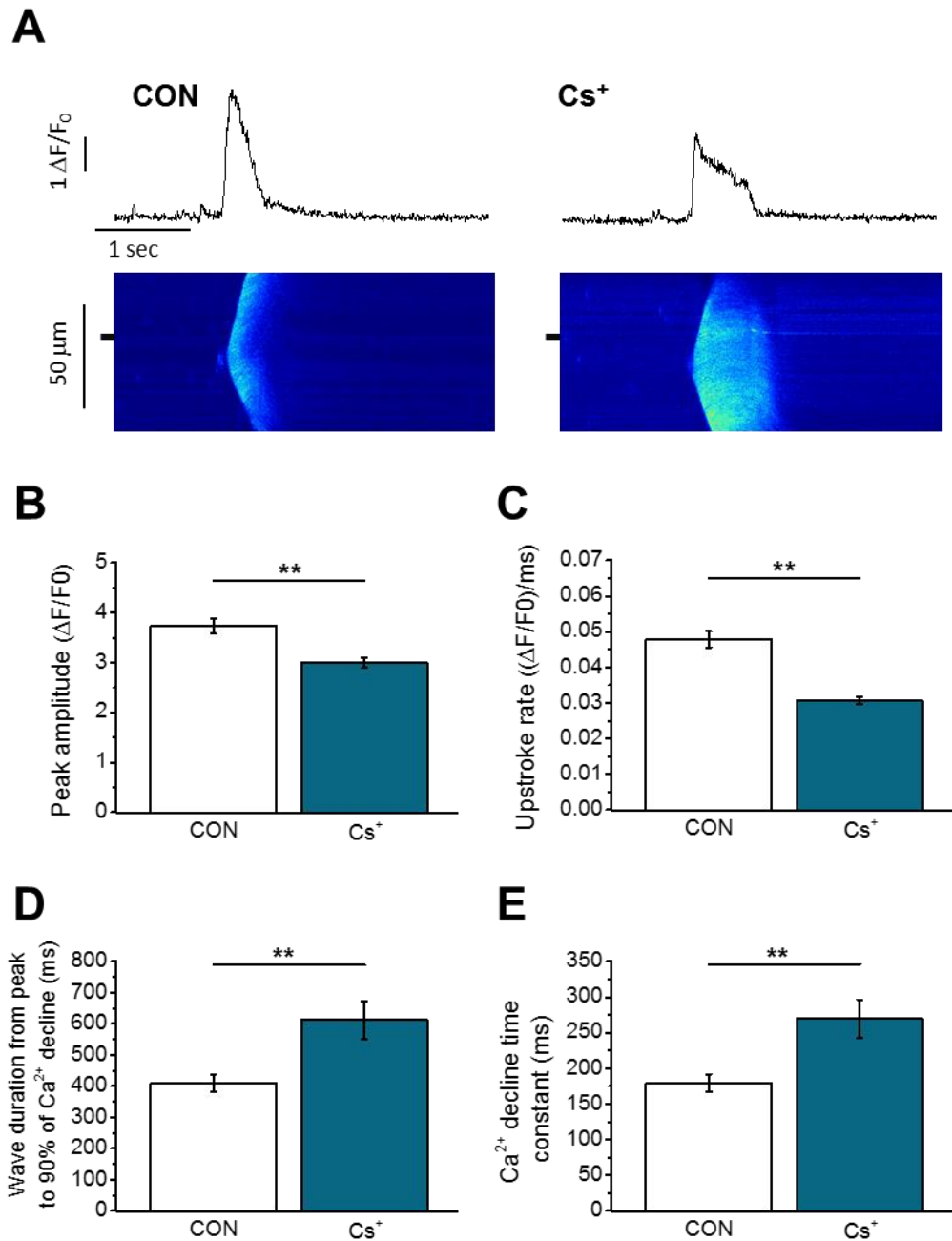


Figure 6.2: Effect of Cs^+ on wave properties

A) Representative line scans of waves at control (CON) and after Cs^+ perfusion (Cs^+) within the same cell. Representative fluorescence profiles taken at black lines next to each line scan. **B)** Differences between CON and Cs^+ peak amplitude, **C)** upstroke rate, **D)** duration from peak to 90% of Ca^{2+} wave decline and **E)** Ca^{2+} decline time constant. Paired two-tailed Student's t-tests. ** = $p < 0.01$; *** = $p < 0.001$. $n = \text{CON} = 6$ (5); $\text{Cs}^+ = 6$ (5).

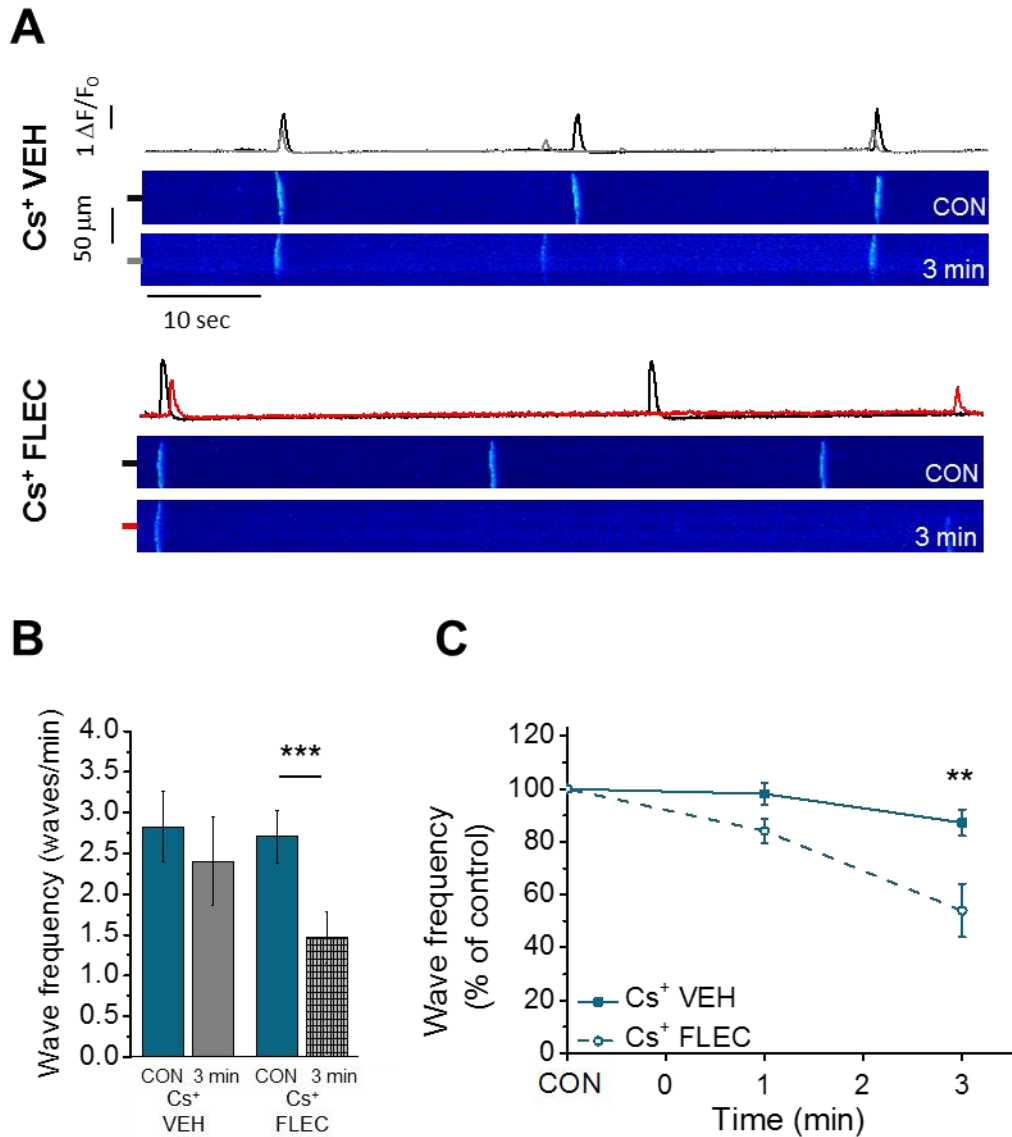


Figure 6.3: Effect of flecainide on wave frequency in the presence of Cs⁺

A) Representative line scans of cells at Cs⁺ control conditions (CON) and after 3 min perfusion with vehicle (Cs⁺ VEH, grey) or flecainide (Cs⁺ FLEC, red). Representative fluorescence profiles taken at correspondingly coloured lines next to each line scan. **B)** Wave frequency at CON and after 3 min perfusion with Cs⁺ VEH or Cs⁺ FLEC. **C)** Percentage change in wave frequency in Cs⁺ VEH (solid) or Cs⁺ FLEC (dashed). Paired or unpaired Student's t-tests; or two way repeated measures ANOVA + Holm-Sidak *post hoc* test where appropriate. ** = $p < 0.01$; *** = $p < 0.001$. $n = \text{Cs}^+ \text{CON} = 13$ (5); $\text{Cs}^+ \text{FLEC} = 13$ (5).

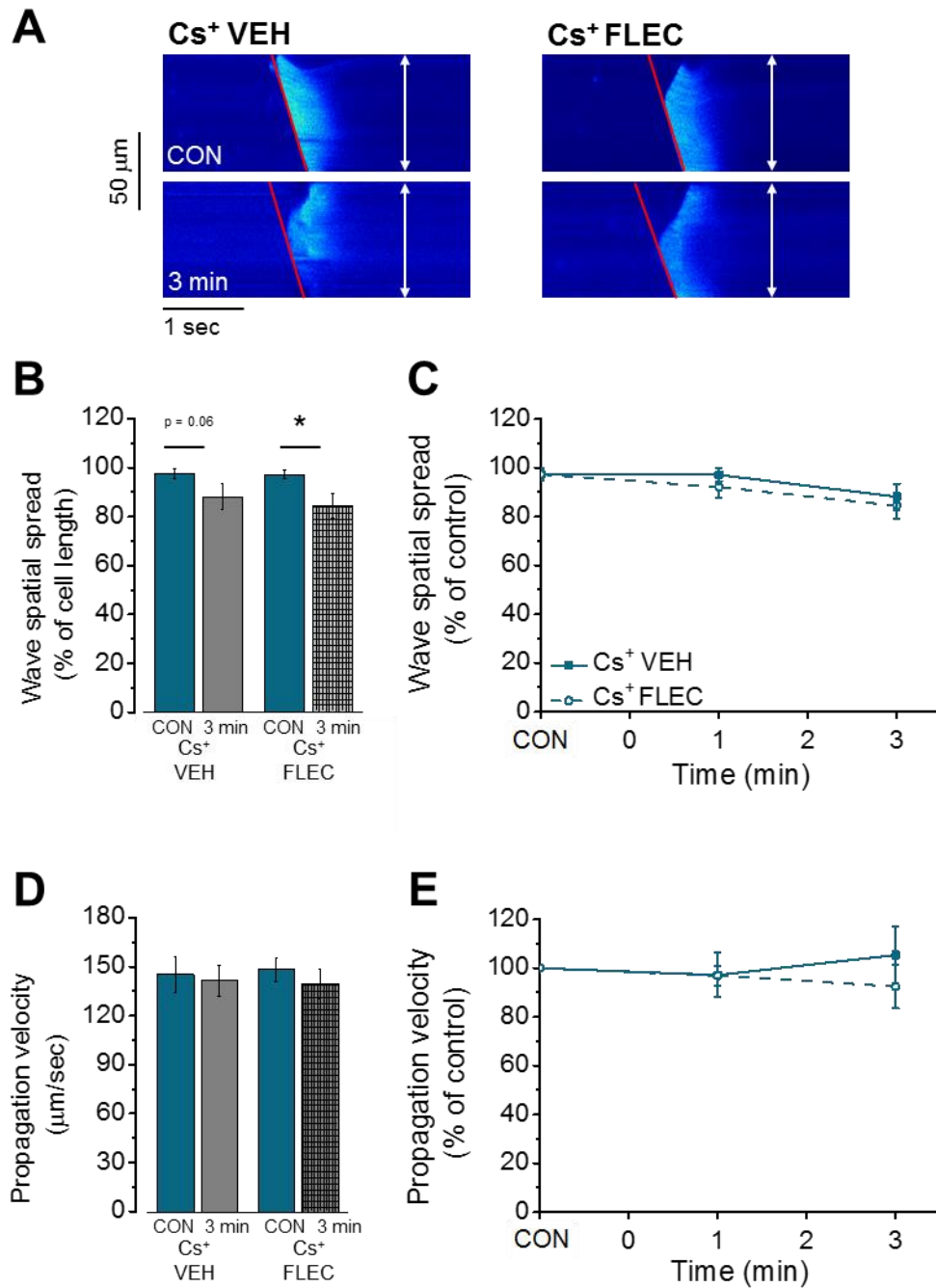


Figure 6.4: Effect of flecainide on wave propagation in the presence of Cs⁺

A) Representative line scans showing wave propagation across the length of the cell (white arrows) and propagation velocity (red lines) at Cs⁺ control (CON) and after 3 min perfusion with vehicle (Cs⁺ VEH) or flecainide (Cs⁺ FLEC). **B)** Spatial spread of a wave at CON and after 3 min perfusion with Cs⁺ VEH or Cs⁺ FLEC. **C)** Percentage change in spatial spread in Cs⁺ VEH (solid) and Cs⁺ FLEC (dashed). **D)** Propagation velocity at CON and after 3 min perfusion with Cs⁺ VEH or Cs⁺ FLEC. **E)** Percentage change in propagation velocity in Cs⁺ VEH (solid) and Cs⁺ FLEC (dashed). Paired or unpaired Student's t-tests; or two way repeated measures ANOVA + Holm-Sidak *post hoc* test where appropriate. * = $p < 0.05$. $n = \text{Cs}^+ \text{CON} = 13$ (5); $\text{Cs}^+ \text{FLEC} = 13$ (5).

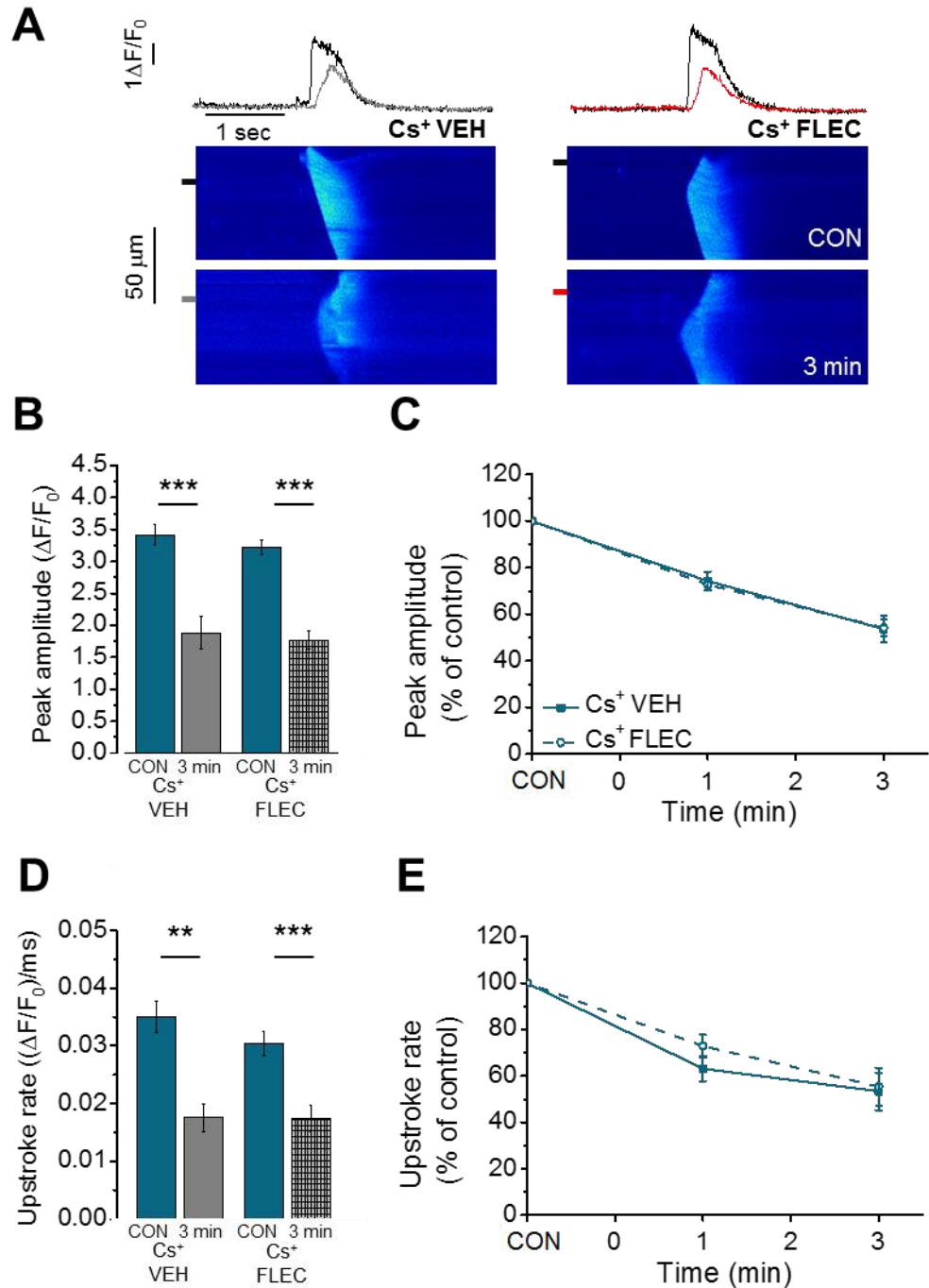


Figure 6.5: Effect of flecainide on wave properties in the presence of Cs⁺

A) Representative line scans of waves at Cs⁺ control (CON) and after 3 min perfusion with vehicle (Cs⁺ VEH, grey) or flecainide (Cs⁺ FLEC, red). Representative fluorescence profiles taken at correspondingly coloured lines next to each line scan. **B)** Peak amplitude at CON and after 3 min perfusion with Cs⁺ VEH or Cs⁺ FLEC. **C)** Percentage change in peak amplitude in Cs⁺ VEH (solid) and Cs⁺ FLEC (dashed). **D)** Upstroke rate at CON and after 3 min perfusion with Cs⁺ VEH or Cs⁺ FLEC. **E)** Percentage change in upstroke rate in Cs⁺ VEH (solid) and Cs⁺ FLEC (dashed). Paired or unpaired Student's t-test; or two way repeated measures ANOVA + Holm-Sidak *post hoc* test where appropriate. ** = $p < 0.01$; *** = $p < 0.001$. $n = \text{Cs}^+ \text{CON} = 13$ (5); $\text{Cs}^+ \text{FLEC} = 13$ (5).

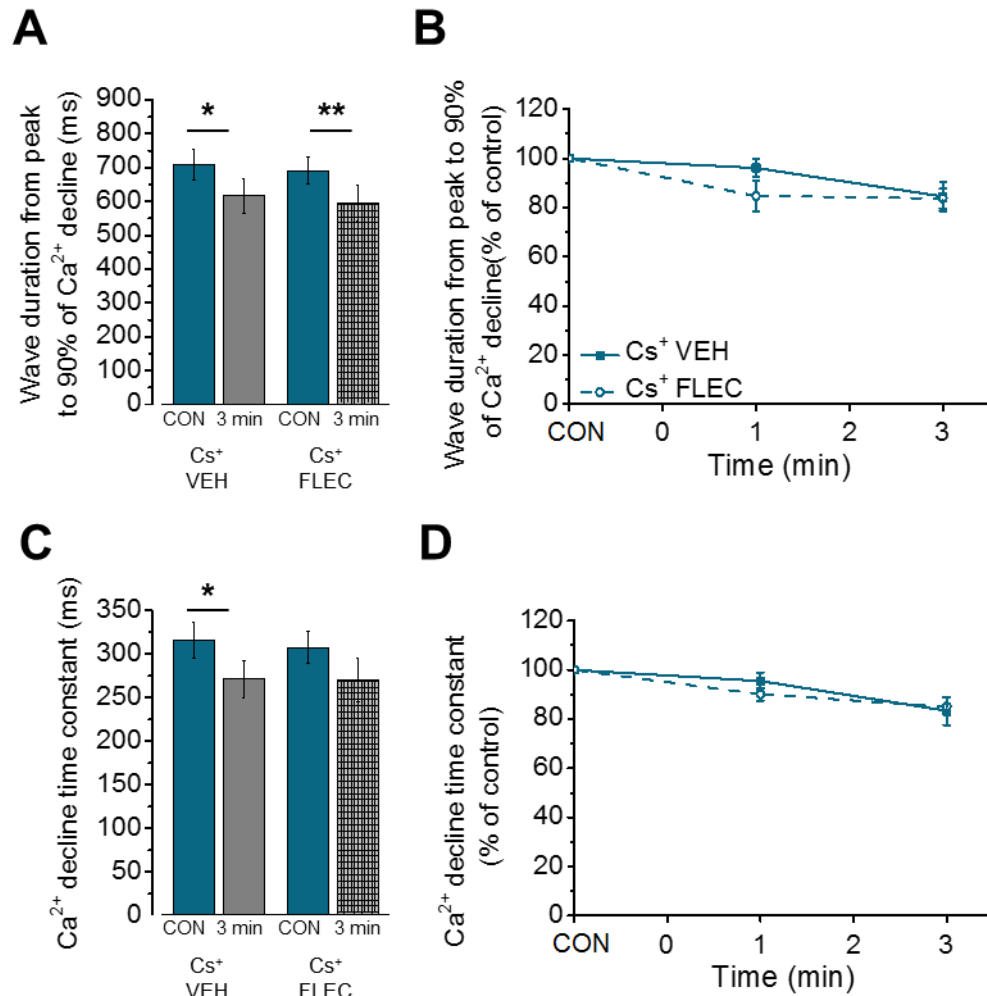


Figure 6.6: Effect of flecainide on wave properties in the presence of Cs⁺

A) Wave duration from wave peak to 90% of the Ca²⁺ decline at Cs⁺ control (CON) and after 3 min perfusion with vehicle (Cs⁺ VEH) or flecainide (Cs⁺ FLEC). **B)** Percentage change in wave duration from wave peak to 90% of the Ca²⁺ decline in Cs⁺ VEH (solid) and Cs⁺ FLEC (dashed). **C)** Ca²⁺ decline time constant at CON and after 3 min perfusion with Cs⁺ VEH or Cs⁺ FLEC. **D)** Percentage change in Ca²⁺ decline time constant in Cs⁺ VEH (solid) and Cs⁺ FLEC (dashed). Paired or unpaired Student's t-test; or two way repeated measures ANOVA + Holm-Sidak post hoc test where appropriate. * = p < 0.05; ** = p < 0.01; *** = p < 0.001. n = Cs⁺ CON = 13 (5); Cs⁺ FLEC = 13 (5).

Flecainide decreased wave frequency to $61.8 \pm 3.0\%$ of control. A significant difference between vehicle and flecainide groups was apparent at 3 min ($p < 0.01$; Figure 6.7 C; $n = 11$ cells (VALVEH) and 9 cells (VALFLEC)).

Representative images illustrating the distance propagated by the wave across the length of the cell (white arrows) and the propagation velocity of a wave (red lines) are shown in Figure 6.8 A. The distance propagated by a wave was significantly decreased from $99.4 \pm 0.43\%$ of the cell length to $51.5 \pm 9.73\%$ of the cell length after 3 min perfusion with VAL VEH ($p < 0.001$). There was no significant change in the spatial spread of a wave after 3 min with VAL FLEC ($p > 0.05$; Figure 6.8B). As a percentage of control, significant differences between vehicle and flecainide groups were apparent at 3 min ($p < 0.001$). Despite significant changes in the spatial spread of a wave, wave propagation velocity was unchanged over time in both VAL VEH and VAL FLEC groups ($p > 0.05$; Figure 6.8 D and E; $n = 11$ cells (VALVEH) and 9 cells (VALFLEC)).

Figure 6.9 A shows dose up line scans and fluorescence profiles of waves under control conditions and after 3 min perfusion with vehicle or flecainide. After 3 min perfusion, peak amplitude significantly decreased in VALVEH ($p < 0.001$) and VAL FLEC ($p < 0.001$; Figure 6.9 B). Wave peak amplitude was decreased to $\sim 50\%$ of control in both groups and there were no significant differences between groups at any time point ($p > 0.05$; Figure 6.9 C). Similarly, wave upstroke rate significantly decreased after 3 min in VAL VEH ($p < 0.001$) and VAL FLEC groups ($p < 0.001$; Figure 6.9 D). Wave upstroke rate was decreased to $\sim 44\%$ of control in both groups and there were no significant differences between groups at any time point ($p > 0.05$; Figure 6.9 E). Wave duration from the wave peak to 90% of the wave decline was unchanged after 3 min in VAL VEH ($p > 0.05$) or VAL FLEC ($p > 0.05$; Figure 6.10 A) and there was no significant difference between groups at any time ($p > 0.05$; Figure 6.10 B). There was no significant change in Ca^{2+} decline time constant after 3 min in either the VAL VEH or VAL FLEC group ($p > 0.05$; Figure 6.10 C) and there were no significant differences between the groups at any time point ($p > 0.05$; Figure 6.10 D; $n = 11$ cells (VALVEH) and 9 cells (VALFLEC)).

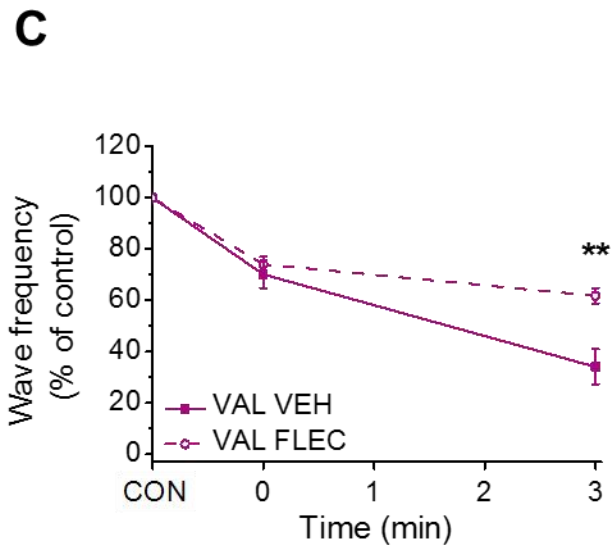
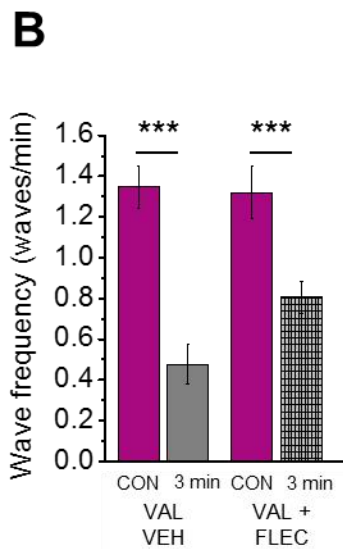
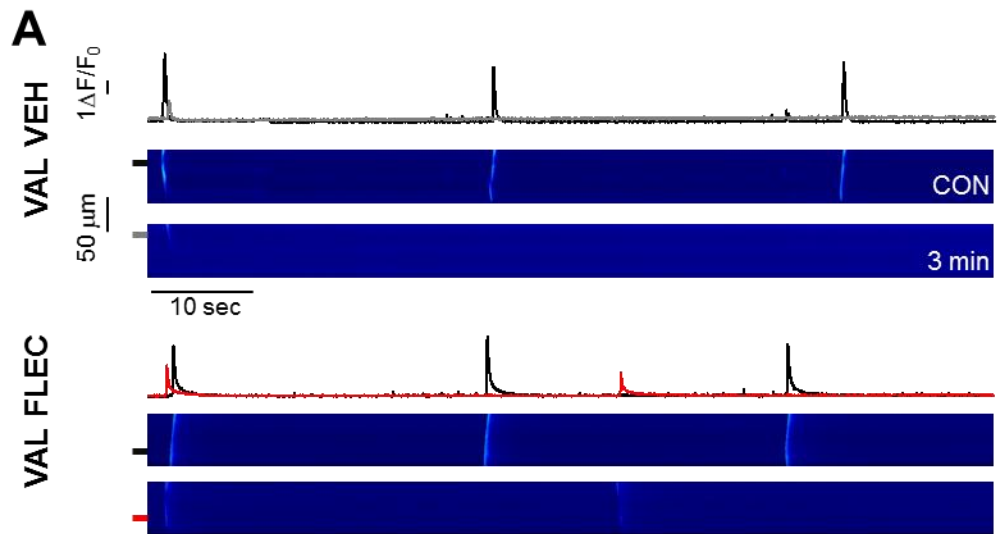


Figure 6.7: Effect of valinomycin or valinomycin + flecainide on wave frequency

A) Representative line scans of cells at control conditions (CON) and after 3 min perfusion with valinomycin and vehicle (VAL VEH, grey) or valinomycin and flecainide (VAL FLEC, red). Representative fluorescence profiles taken at correspondingly coloured lines next to each line scan. **B)** Wave frequency at CON and after 3 min perfusion with VAL VEH or VAL FLEC. **C)** Percentage change in wave frequency in VAL VEH (solid) or VAL FLEC (dashed). Paired or unpaired Student's t-test; or two way repeated measures ANOVA + Holm-Sidak *post hoc* test where appropriate. ** = $p < 0.01$. *** = $p < 0.001$. $n = \text{VAL VEH} = 11$ (4); $\text{VAL FLEC} = 9$ (4).

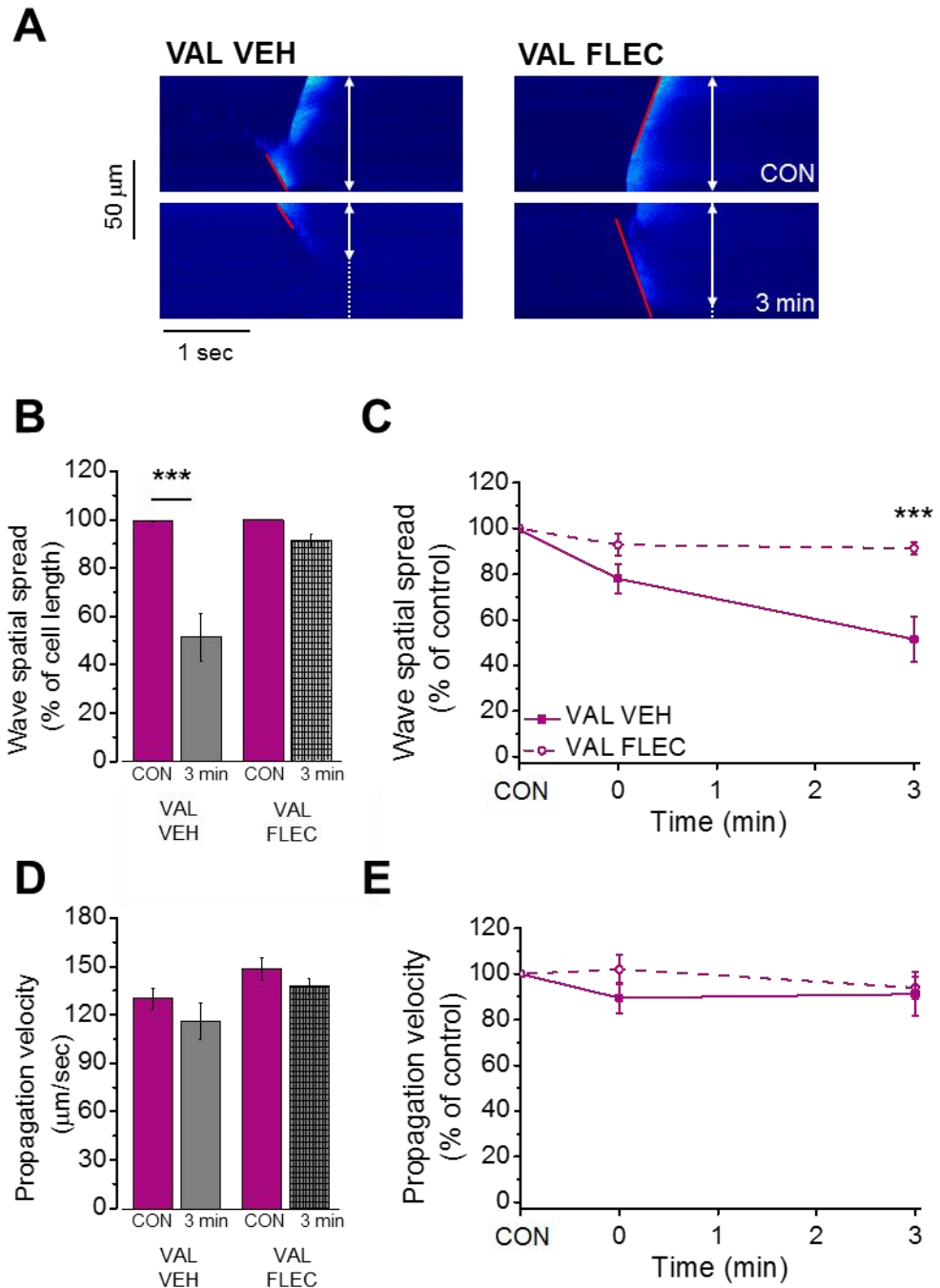


Figure 6.8: Effect of valinomycin or valinomycin + flecainide on wave propagation

A) Representative line scans showing wave propagation across the length of the cell (white arrows) and propagation velocity (red lines) at control (CON) and after 3 min perfusion with valinomycin and vehicle (VAL VEH) or valinomycin and flecainide (VAL FLEC). **B)** Spatial spread of a wave at CON and after 3 min perfusion with VAL VEH or VAL FLEC. **C)** Percentage change in spatial spread in VAL VEH (solid) or VAL FLEC (dashed). **D)** Propagation velocity at CON and after 3 min perfusion with VAL VEH or VAL FLEC. **E)** Percentage change in propagation velocity in VAL VEH (solid) or VAL FLEC (dashed). Paired or unpaired Student's t-test; or two way repeated measures ANOVA + Holm-Sidak *post hoc* test where appropriate. ** = $p < 0.01$. *** = $p < 0.001$. $n = \text{VAL VEH} = 11$ (4); $\text{VAL FLEC} = 9$ (4).

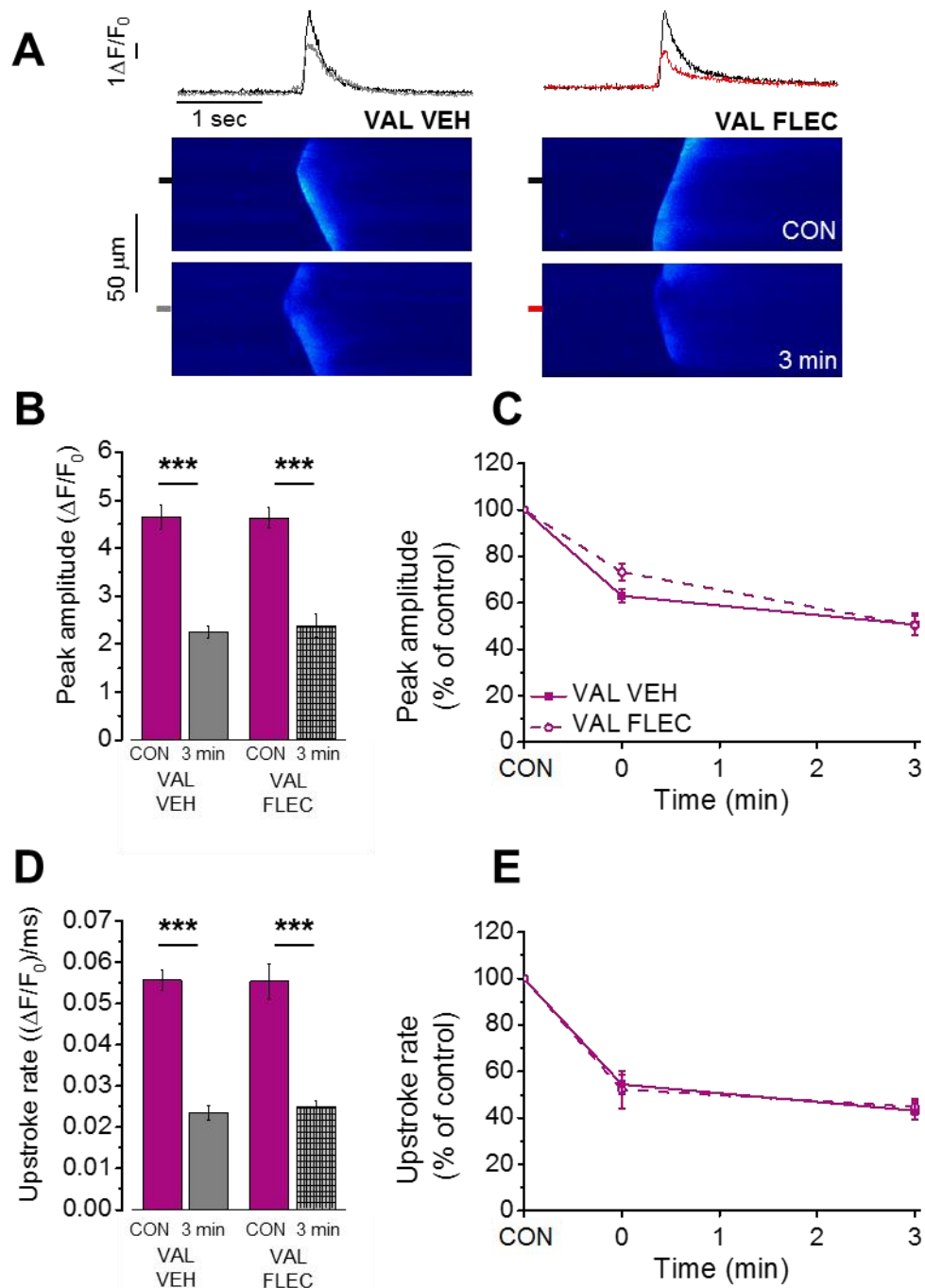


Figure 6.9: Effect of valinomycin or valinomycin + flecainide on wave properties

A) Representative line scans of waves at control (CON) and after 3 min perfusion with valinomycin and vehicle (VAL VEH, grey) or valinomycin and flecainide (VAL FLEC, red). Representative fluorescence profiles taken at correspondingly coloured lines next to each line scan. **B)** Peak amplitude at CON and after 3 min perfusion with VAL VEH or VAL FLEC. **C)** Percentage change in peak amplitude in VAL VEH (solid) or VAL FLEC (dashed). **D)** Upstroke rate at CON and after 3 min perfusion with VAL VEH or VAL FLEC. **E)** Percentage change in upstroke rate in VAL VEH (solid) or VAL FLEC (dashed). Paired or unpaired Student's t-test; or two way repeated measures ANOVA + Holm-Sidak *post hoc* test where appropriate. * = $p < 0.05$; *** = $p < 0.001$. $n = \text{VAL VEH} = 11$ (4); $\text{VAL FLEC} = 9$ (4).

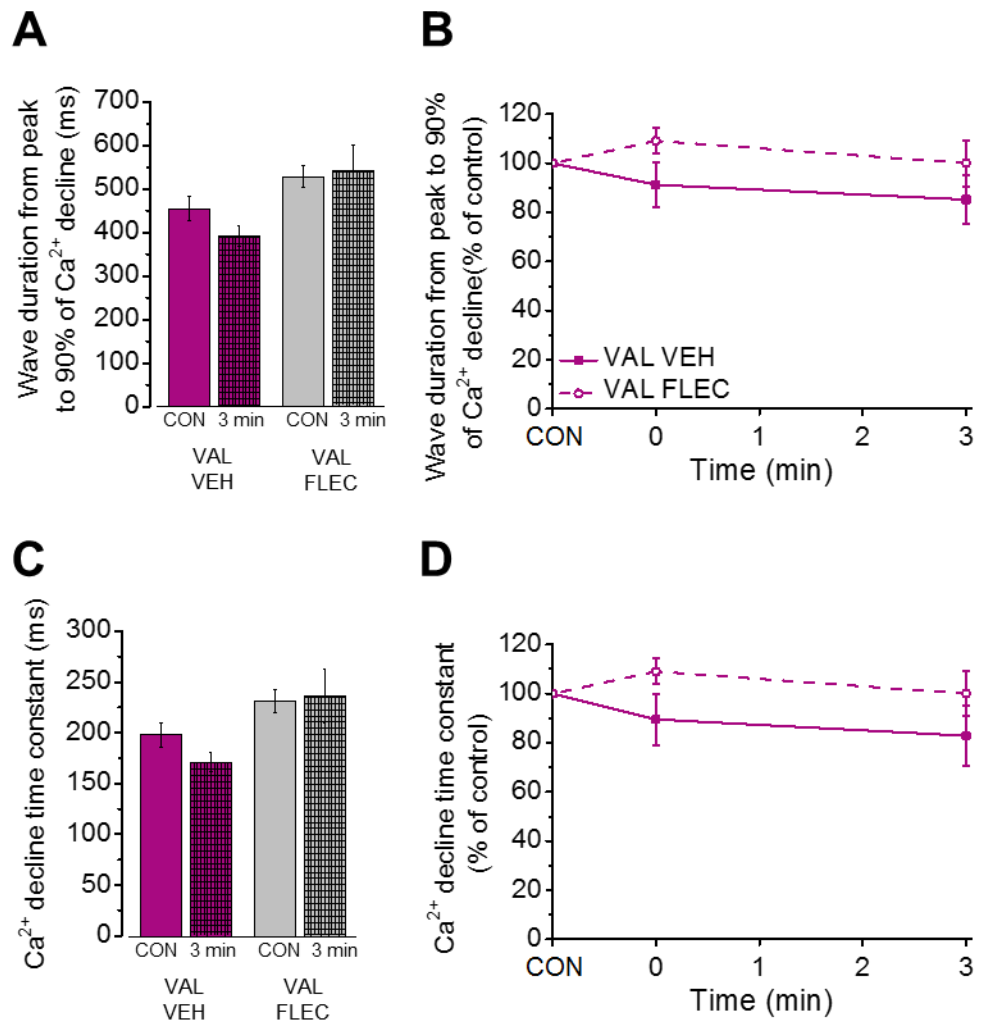


Figure 6.10: Effect of valinomycin or valinomycin + flecainide on wave properties

A) Wave duration from wave peak to 90% of the Ca²⁺ decline at CON and after 3 min perfusion with valinomycin and vehicle (VAL VEH) or valinomycin and flecainide (VAL FLEC). **B)** Percentage change in wave duration from wave peak to 90% of the Ca²⁺ decline in VAL VEH (solid) or VAL FLEC (dashed). **C)** Ca²⁺ decline time constant at CON and after 3 min perfusion with VAL VEH or VAL FLEC. **D)** Percentage change in Ca²⁺ decline time constant in VAL VEH (solid) or VAL FLEC (dashed). Paired or unpaired Student's t-test; or two way repeated measures ANOVA + Holm-Sidak post hoc test where appropriate. * = p < 0.05; ** = p < 0.01. n = VALVEH = 11 (4); VALFLEC = 9 (4).

6.4 Discussion

As shown in Chapter 5, flecainide significantly decreases Ca^{2+} wave frequency and alters Ca^{2+} spark properties in permeabilised myocytes where sarcolemmal $\text{Na}_v1.5$ channels are not functional. These findings suggest that flecainide modifies RyR2 gating. However, work on single RyR channels has provided evidence that flecainide's action only occurs when the inside of the SR is negatively polarised; a condition met to an unknown extent during SR Ca^{2+} release. In this chapter, the possibility that flecainide's action depends on polarisation of the SR membrane was investigated by modulating the counter-current, which serves to limit the development of a potential difference across the SR membrane during Ca^{2+} release.

6.4.1 Channels which mediate the K^+ SR counter-current

The SR counter-current is predominantly carried by the cytosolic to luminal movement of K^+ during and immediately after the release of Ca^{2+} from the SR (Coronado et al., 1980). TRIC B and RyR2 channels have been implicated in facilitating this role (Venturi et al., 2013, Guo et al., 2013). Single channel experiments investigating native TRIC B channels from a TRIC A knockout mouse model showed at least two different gating mechanisms (Venturi et al., 2013). The majority of recorded TRIC B channels were highly voltage sensitive and their P_o increased as the SR 'lumen' became more negative, as is thought to be the case during SR Ca^{2+} efflux (Venturi et al., 2013). Whilst not definitive proof, the presence of voltage sensitive channels located at the SR is teleologically consistent with transient changes in SR membrane potential. Interestingly, purified TRIC B was blocked by 'luminal' Ca^{2+} indicating a Ca^{2+} -dependent gating mechanism (Pitt et al., 2010) and this is supported by a previous report of an unidentified SR K^+ channel which could be blocked by Ca^{2+} in a voltage-dependent manner (Liu and Strauss, 1991). Although the majority of TRIC B channels were voltage dependent, a subset of channels showed voltage-independent gating, indicating a degree of free movement of K^+ across the SR membrane (Venturi et al., 2013). It is possible that both voltage dependent and independent gating kinetics could be governed by post-translational modifications (Venturi et al., 2013).

RyR2 has also been reported to act as a counter-current channel, alongside its undisputed role in Ca^{2+} release (Guo et al., 2013). Experiments on single channels within lipid bilayers have shown that the RyR2 Ca^{2+} current in intracellular solution reversed at -2.7 mV, instead of the calculated Ca^{2+} reversal potential of ~ -120 mV (Guo et al., 2013). This led the authors to conclude that RyR2 mediated counter-current was sufficient to maintain a stable SR

membrane potential during SR Ca^{2+} release and that current fluxes that occur via K^+ channels are functionally unimportant (Gillespie and Fill, 2008, Guo et al., 2013). Whilst there is convincing evidence to suggest that RyR2 conductance of K^+ from the cytosol to the SR lumen contributes to the SR counter-current, that RyR2 is the sole contributor is unlikely. TRIC-knockout mice suffer embryonic cardiac failure and show severe dysfunction in intracellular Ca^{2+} handling, implicating a role for TRIC in facilitating the SR counter-current (Yazawa et al., 2007). Moreover, specific block of SR K^+ channels via Cs^+ substitution markedly alters SR Ca^{2+} and will be further discussed in Section 6.4.2 (Kawai et al., 1998).

Our working hypothesis is that during SR Ca^{2+} release, the movement of K^+ in the cytosolic to luminal direction mostly occurs via both RyR2 and the voltage-dependent subtype of TRIC B. The counter-current via TRIC channels may persist briefly after RyR2 channels have returned to their closed state to dissipate any residual polarization of the membrane. During the 'diastolic period', SR Ca^{2+} uptake via SERCA also requires K^+ to move in the opposite direction (lumen to cytosol) to limit the generation of an inside-positive SR membrane potential. In this case, the voltage-independent subtype of TRIC B may be predominantly responsible allowing free movement of K^+ .

While experimental evidence addressing the specific roles of TRIC A and B channels is lacking, the neonatal mortality of the TRIC A and B double knockout mouse due to cardiac dysfunction is evidence that both forms are important in the heart (Yazawa et al., 2007). The role of Cl^- and H^+ channels has also not been addressed despite evidence of their presence within the cardiac SR (Townsend and Rosenberg, 1995, Kamp et al., 1998). Additionally, there is little information available to further understand the time course of any of these events, although computational modelling of RyR2 counter-current conductance has indicated rapid changes in SR membrane potential in the order of tens of milliseconds (Gillespie and Fill, 2008). Despite these limitations, this hypothesis can be used as a starting point to investigate the effect of flecainide on SR membrane potential changes and Ca^{2+} handling.

6.4.2 Block of SR counter-current with Cs⁺ and effect on Ca²⁺ release

Inhibition of sarcolemmal K⁺ currents by exchange of K⁺ for Cs⁺ in experimental solutions has been reported for the transient outward potassium current (I_{to}) (Matsuda, 1996) and the inwardly rectifying potassium current (I_{K1}) (Harvey and Ten Eick, 1989). Similarly, K⁺ exchange for Cs⁺ inhibited the SR counter-current in lipid bilayer experiments mimicking the SR membrane (Guo et al., 2013); and in saponin permeabilised ventricular myocytes during SR Ca²⁺ waves (Kawai et al., 1998, Guo et al., 2013). In lipid bilayers, Cs⁺ inhibited the SR counter-current by ~88% through unidentified SR K⁺ channels only; the cytosolic to luminal passage of monovalent cations through RyR2 was unaffected (Guo et al., 2013). TRIC B channels have recently been reported to be blocked by Cs⁺, confirming this channel as a potential target (Yang et al., 2016). This suggests that in experiments using permeabilised myocytes, including those reported here, RyR2 conductance of monovalent cations was likely unaffected during Cs⁺ substitution.

Interestingly, Guo et al. reported unchanged spark properties and caffeine induced transients during Cs⁺ substitution and the authors concluded that SR K⁺ channels had no important role in sustaining normal Ca²⁺ release. In contrast, our findings and those of others (Kawai et al., 1998) provide evidence of a pronounced decrease in Ca²⁺ wave frequency and prolongation of wave duration following Cs⁺ substitution. This discrepancy might reflect differences in the form of Ca²⁺ release studied. Sparks and triggered Ca²⁺ transients are considered 'physiological' forms of Ca²⁺ release (Cheng et al., 1996, Bers, 2001). Ca²⁺ waves are considered pathological due to their occurrence under pathological or Ca²⁺ overloaded conditions (Hilliard et al., 2010, Diaz et al., 1997). It is possible that the changes observed in the presence of Cs⁺ occur only when the SR Ca²⁺ store reaches its threshold for spontaneous Ca²⁺ wave release (Salazar-Cantu et al., 2016); SR Ca²⁺ sparks and triggered Ca²⁺ transients occur at a lower SR Ca²⁺ content.

Our data clearly indicate that inhibiting the SR counter-current had a significant effect on Ca²⁺ waves and these are supported by similar results by Kawai et al. (Kawai et al., 1998). Prolongation of the time to wave peak is indicative of slowed Ca²⁺ release. Additionally, a decrease in wave frequency and the increased Ca²⁺ decline time constant are indicative of slowed Ca²⁺ uptake, prolonging the time required for the SR Ca²⁺ release threshold to be reached (Kawai et al., 1998). We propose that during Ca²⁺ release, changes in the SR membrane potential would be increased or prolonged following Cs⁺ substitution. Conversely, slowed luminal to cytosolic movement of K⁺ during Ca²⁺ uptake could also slow Ca²⁺ movement across the SR membrane (Kawai et al., 1998).

Experiments involving direct measurement of SR membrane potential are needed to test this hypothesis directly. However, due to limitations further discussed in Section 6.4.7, the use of potential sensitive dyes is unlikely to work in isolated cells. In short, changes in the SR membrane are likely to be small relative to that of the sarcolemma or the mitochondria and SR fluorescence signals would be dwarfed (Section 6.4.7) (Portele et al., 1997). An alternative approach using the voltage sensitive fluorescent protein, ArcLight is discussed in Chapter 8 (Leyton-Mange et al., 2014).

6.4.3 The effect of flecainide on wave frequency was exacerbated when SR counter-current was slowed with Cs⁺

In the previous chapter, flecainide significantly decreased wave frequency, increased spark frequency and decreased spark amplitude and width in saponin permeabilised myocytes perfused with intracellular solution. In this cell model, RyR2 remained *in situ*, whilst Na_v1.5 was rendered functionless. It was concluded by us and others that flecainide inhibited RyR2 in its open channel state to elicit the changes observed in SR Ca²⁺ release (Hilliard et al., 2010, Savio-Galimberti and Knollmann, 2015).

Since these results, the direct effect of flecainide on RyR2 has been called into question (Bannister et al., 2016, Bannister et al., 2015). In part, this may be due to an inability to reproduce an effect of flecainide in WT permeabilised myocytes, due to previously discussed discrepancies (Chapter 5.). An interesting point was raised however, in that flecainide was capable of blocking ion movement through the RyR2 pore, but only under certain electrophysiological conditions (Bannister et al., 2016, Bannister et al., 2015). The results by Bannister et al. suggested that flecainide's block of cation movement through RyR2 only occurred when the SR lumen was held at a negative potential in relation to the cytosolic space (Bannister et al., 2016). Under these conditions in single channel-lipid bilayer experiments, cations moved in the cytosolic to luminal direction. It was concluded that this direction of cation movement was non-physiological and that therefore, the effect of flecainide on RyR2 should be considered irrelevant (Bannister et al., 2016, Bannister et al., 2015).

Before accepting this conclusion, two criticisms must be considered. Firstly, the cytosolic to luminal movement of K⁺ via RyR2 is present physiologically as a contributor to the SR counter-current (Tinker et al., 1992, Guo et al., 2013, Gillespie and Fill, 2008, Coronado et al., 1980). This partial block of this SR counter-current by flecainide may indirectly alter Ca²⁺ release and a qualitative parallel could be drawn between flecainide block of RyR2-mediated counter-

current and Cs⁺ block of SR K⁺ channel-mediated counter-current. Bannister et al. theorised that Ca²⁺ would push the relatively weakly bound flecainide out of the RyR2 pore in this situation, thereby preventing a sustained effect. However this could not be directly investigated due to the non-physiological salt content of the lipid bilayer experiments which did not contain both K⁺ and Ca²⁺ (Bannister et al., 2016, Bannister et al., 2015). The experiments documented in Chapter 5 ensured physiologically relevant concentrations of K⁺ and Ca²⁺; and RyR2 remained *in situ*. Under these conditions, a significant effect of flecainide on Ca²⁺ wave and spark release was apparent and was supported by qualitatively similar results observed in CPVT myocytes (Savio-Galimberti and Knollmann, 2015). Therefore, an indirect effect of flecainide on RyR2 Ca²⁺ release might occur due to an inhibition of the RyR2-mediated SR counter-current.

Secondly, the holding potential at which flecainide blocked RyR2 current flux in the cytosolic to luminal direction was experimentally contrived. However, it is conceivable that this lumen-negative SR membrane potential could exist to a small extent during diastole (Gillespie and Fill, 2008, Yazawa et al., 2007) and/or transiently to a greater extent during SR Ca²⁺ release (Beeler, 1980, Laver and Lamb, 1998). We have hypothesised that Cs⁺ substitution results in a larger and/or more prolonged polarization of the SR membrane (Figure 7.1 A). Under these conditions in WT cells, the decrease in wave frequency induced by flecainide was almost doubled (~38%) compared to experiments performed using control solution (Chapter 5), and was comparable to that reported in the permeabilised Casq2^{-/-} cardiomyocyte upon application of 100 μM flecainide (Savio-Galimberti and Knollmann, 2015). Flecainide is >99% protonated at physiological pH (Liu et al., 2003). In the presence of Cs⁺, when the SR is likely at an increased or prolonged negative membrane potential, charged flecainide binding affinity to the already negative RyR2 pore may be increased (Mead-Savery et al., 2009), thereby eliciting a greater effect on Ca²⁺ wave frequency. Interestingly, the neutral and fully-charged derivatives of flecainide (NU-FL and QX-FL respectively) elicited a significantly weaker block of RyR2 than flecainide indicating that the flecainide's positive charge may not be the sole contributor to its mechanism of action on RyR2 (Bannister et al 2016). Despite this, flecainide block of RyR2 increased linearly from 0 mV, showing a clear voltage dependent block of RyR2 channels in lipid bilayers as the SR 'lumen' became more negative (Bannister et al., 2016). Similar preliminary experiments also performed in Casq2^{-/-} permeabilised mouse myocytes also reported a greater effect of flecainide on wave frequency in the presence of Cs⁺ (Gomez-Hurtado and Knollmann, 2016).

6.4.4 The effect of flecainide on wave frequency when SR counter-current was increased with valinomycin

Valinomycin is a K^+ ionophore which acts to create K^+ selective pores across biological membranes (Favero et al., 2003). To facilitate this conduction, K^+ binds to 6 of the 12 carbonyl groups located within the dodecadeptide ring structure of valinomycin (Varma et al., 2008). Increased K^+ conductance due to application of valinomycin has been reported in the cardiac sarcolemma (Bartschat et al., 1980), mitochondrial membrane (Kaasik et al., 2004, Miro-Casas et al., 2009) and the SR (Kometani and Kasai, 1978). Depending on the ionic concentration of K^+ across each membrane, valinomycin can elicit differing effects.

Under physiological conditions, the intracellular K^+ concentration (~ 140 mM) is greater than the extracellular concentration (~ 5 mM). The high K^+ permeability across the sarcolemma is predominantly responsible for holding the membrane potential of ventricular cells at ~ -85 mV (Opie, 2004). Application of valinomycin further decreases the membrane potential to < -100 mV due to the amplified K^+ permeability (Bartschat et al., 1980). Across the inner mitochondrial membrane, ATP-regulated (mitoK_{ATP}), Ca^{2+} -activated (mitoBK_{Ca}), voltage-gated (mitoK_v1.3) and two pore domain (mitoTASK) K^+ channels control K^+ entry into the mitochondria (Laskowski et al., 2016). Despite these varied channels, low mitochondrial permeability to K^+ has been reported (Bednarczyk et al., 2008). The application of valinomycin induced mitochondrial swelling (Kaasik et al., 2004) and decreased the mitochondrial membrane potential (Inai et al., 1997, Diaz et al., 2013) due to an increased mitochondrial K^+ concentration.

During cell diastole, equal concentrations of K^+ across the SR membrane were reported by Somlyo et al. (1977) indicating the free movement of K^+ across the SR, which may be facilitated by voltage-independent TRIC B channels (Somlyo et al., 1977, Venturi et al., 2013). However, it is likely that a proportion of K^+ flux across the SR may be regulated or restricted due to the presence of K^+ permeable voltage-dependent TRIC B and RyR2 channels (Coronado et al., 1980, Guo et al., 2013, Venturi et al., 2013, Diaz-Sylvester et al., 2011). After application of valinomycin it is assumed that the proportion of K^+ flux which occurs immediately during and after SR Ca^{2+} release is unrestricted and may move through valinomycin induced pores instead (Kometani and Kasai, 1978). Therefore, transient changes in the SR membrane potential during Ca^{2+} release may be less pronounced and/or briefer.

Upon the application of valinomycin in saponin permeabilised cardiomyocytes, a significant decrease in wave frequency was apparent with $\sim 18\%$ of cells exhibiting no waves after 3 min

of perfusion. Such a dramatic decrease in wave frequency is typically indicative of a decrease in SR Ca^{2+} uptake (Venetucci et al., 2007) and consequential decrease in SR Ca^{2+} content. However, the limited evidence available is contradictory. Ca^{2+} uptake into SR vesicles has been reported to increase (Beeler, 1980, Caswell and Brandt, 1981) or decrease (Vladimirov et al., 1978, Arav et al., 1983) in the presence of valinomycin. This discrepancy might be explained by differences in the relative quantities of SERCA, RyR and calsequestrin in SR vesicle preparations as Ca^{2+} uptake rate is faster in SERCA rich “light” SR vesicles, compared with RyR2 rich “heavy” vesicles in the presence of valinomycin (Inui et al., 1988, Nigro et al., 2009). Moreover, valinomycin activity on SERCA is dependent upon $[\text{Ca}^{2+}]$. At high intra-luminal SR $[\text{Ca}^{2+}]$ (35 μM), valinomycin increases Ca^{2+} uptake via SERCA; yet in the presence of the Ca^{2+} ionophore A23187, luminal Ca^{2+} remains low and valinomycin inhibits SERCA uptake of Ca^{2+} (Beeler and Gable, 1994). In the current experiments, free $[\text{Ca}^{2+}]$ was relatively low (146 nM) indicating that valinomycin would likely inhibit SERCA uptake rate (Beeler and Gable, 1994). Indeed, in similar experiments using cardiomyocytes isolated from the $\text{CASQ2}^{-/-}$ CPVT mouse model, valinomycin did not significantly decrease wave frequency (Gomez-Hurtado and Knollmann, 2016). This may be due to the very high $[\text{Ca}^{2+}]$ used, which elicited a starting wave frequency of ~ 1.6 waves/sec (Gomez-Hurtado and Knollmann, 2016, Savio-Galimberti and Knollmann, 2015). Under these conditions, valinomycin inhibition of SERCA uptake may be greatly reduced or reversed (Beeler and Gable, 1994).

6.4.5 The effect on wave frequency in the presence of valinomycin and flecainide

In the presence of Cs^+ , it was hypothesised that a transient polarisation of the SR membrane would be greater or prolonged. Under these conditions, a more pronounced decrease in wave frequency was apparent upon application of flecainide, consistent with dependence of flecainide on a negative SR membrane potential. To further investigate this dependence, valinomycin was applied to myocytes to induce the free movement of K^+ across the SR which was posited to abolish the SR membrane potential. In doing so, it was hypothesised that flecainide would have no effect on wave frequency. In fact, the effect of flecainide was reversed. Perfusion with valinomycin alone decreased wave frequency by $\sim 70\%$. However, the joint perfusion of valinomycin and flecainide somewhat maintained wave frequency and only a $\sim 40\%$ decrease from control was observed. Several speculative discussion points could be initiated from this result.

It is unlikely that flecainide directly inhibits the valinomycin pore in a similar fashion to its block of the $K_v11.1$ and $K_v2.1$ channels (Melgari et al., 2015a, Madeja et al., 2010). This is due to significant structural differences between K^+ specific channel pores and the valinomycin pore (Varma et al., 2008). However, there is the potential that currently un-investigated flecainide interaction with other mitochondrial or SR membrane proteins, could elicit a positive effect on Ca^{2+} regulation in the permeabilised myocyte. For example, flecainide may directly compete with valinomycin for functional access to SERCA, thereby limiting the inhibitory effect of valinomycin on SERCA and the consequential changes in SR Ca^{2+} uptake and release (Beeler and Gable, 1994). Although, no significant changes in Ca^{2+} decline time were apparent, indicating no effect of flecainide on SERCA. Alternatively, if flecainide inhibition of RyR2 were to persist, passive Ca^{2+} leak via RyR2 may be reduced and SR Ca^{2+} content somewhat maintained. Under these conditions, the Ca^{2+} dependent effect of valinomycin on SERCA may be partially opposed (Beeler and Gable, 1994).

In intact cardiomyocytes, valinomycin was reported to increase ROS production (Heinzel et al., 2005b) which may induce detrimental changes to SERCA cycling and RyR2 leak (Kuster et al., 2010, Eager et al., 1997). There is a preliminary report of flecainide inhibiting ROS production via the tumour necrosis factor- α (TNF- α) pathway (Nojima et al., 1995). Additionally, a preliminary report exists which suggests that flecainide is able to maintain normal mitochondrial function within the ischaemic myocardium (Sugiyama et al., 1989). However, this may be due to an indirect effect of flecainide on the mitochondria via $Na_v1.5$ or RyR2 rather than a potential direct effect on mitochondrial channels.

Whilst the effect of flecainide in the presence of valinomycin is clear and indeed interesting, ultimately the reasons for its effect on wave frequency are inconclusive. This is partly due to the multi-faceted effect of valinomycin in the current cell model. However, potential alternative interactions of flecainide with other SR or mitochondrial proteins remain unreported in the literature.

6.4.6 Limitations

The aim of these experiments was to investigate the mechanism of action of flecainide on RyR2. It was hypothesised that flecainide inhibition of RyR2 may be dependent upon transient SR membrane potential changes that have been speculated to occur during SR Ca^{2+} release (Yazawa et al., 2007, Beeler, 1980, Laver and Lamb, 1998). However, little direct evidence exists to directly measure SR membrane potential changes during Ca^{2+} release. Unlike the sarcolemma, patch clamp recordings of SR membrane *in situ* are not technically possible due

to the dense and lattice-like network of the SR (Pinali et al., 2013). SR vesicles can be isolated, however a risk of contamination with sarcolemmal or mitochondrial membranes exists, giving rise to vesicles comprised of ~20% non-SR membrane (Byrd et al., 1989). Additionally, longitudinal and junctional SR membrane vesicles are comprised of differing proportions of RyR2, SERCA and CASQ2 proteins (Inui et al., 1988) which in turn can alter vesicle behaviour (Nigro et al., 2009). To measure physiological changes in membrane potential, physiological proportions of SR vesicle types are also required.

Potentiometric dyes such as ANNINE 6 and tetramethylrhodamine methyl ester (TMRM) have been successful in measuring sarcolemmal and mitochondrial changes in membrane potential respectively (Bu et al., 2009, Scaduto and Grotyohann, 1999). However, dyes used to measure membrane potential changes across the SR have been criticised for their difficulty in calibration (Portele et al., 1997) and variability in results due to tissue thickness or dye density (Chang and Jackson, 2003). Alongside this, transient changes in SR membrane potentials were reported by Beeler et al. (1979) using 3, 3'-diethyloxycarbocyanine (DiOC₂(3)) applied to SR vesicles. However, it was concluded that these changes were caused by Ca²⁺ binding to the SR membrane and were therefore artefacts. Additionally, due to the self-reported insensitivity of the dye, any changes in SR membrane potential <30 mV would not be recorded (Beeler et al., 1979). The above aims to illustrate the technical difficulties involved in experimentally investigating SR membrane potential changes. Computational models may begin to decipher the elusive changes across the SR membrane, which likely occur on the millisecond timescale (Gillespie and Fill, 2008). These may be further refined as and when experimental findings concerning channel protein identification and function become clear within the literature.

Permeabilised myocytes may begin to overcome some of the discussed difficulties, as SR proteins are *in situ* at physiologically relevant proportions. However, permeabilised myocytes are a reduced model of cardiomyocyte Ca²⁺ handling. CICR via Ca²⁺ influx through LTCC cannot occur and necessary regulatory proteins such as calmodulin (Terentyev et al., 2003a) are lost in the permeabilisation process (Chapter 5). SR and mitochondrial bound membrane proteins are still intact and likely to be functioning on a reduced level.

As discussed, the effects of valinomycin as a K⁺ ionophore are not limited to the SR and therefore changes in cell function may be due to increased K⁺ movement across the SR (Kometani and Kasai, 1978), mitochondria (Kaasik et al., 2004, Heinzl et al., 2005b), or even the nucleus (Bolkent and Zierold, 2002). The effect on valinomycin across the nucleus was not discussed as the nucleus does not directly modulate cytosolic [Ca²⁺] at the time scale of Ca²⁺ release and uptake (Zhong et al., 2012). Alongside this, a K⁺ equilibrium already exists between

the cytosol and the nuclei (Bolkent and Zierold, 2002) indicating a minimal effect of valinomycin on this organelle.

6.4.7 Conclusions and Summary

The hypothesis underlying the experiments described in this chapter is that during SR Ca^{2+} release, transient polarisation of the SR membrane is opposed by the SR counter-current, which is likely carried by TRIC B and RyR2 (Guo et al., 2013, Venturi et al., 2013, Zhou et al., 2014). Replacement of K^+ with Cs^+ reduces the SR counter-current to around 10 – 20 % of its normal magnitude (Guo et al., 2013). As found in this and previous studies (Kawai et al., 1998), when the counter-current is inhibited, the rate of spontaneous Ca^{2+} release and re-uptake was significantly slowed giving rise to a decrease in wave frequency. As Cs^+ blocks K^+ via SR K^+ channels (likely TRIC channels) but not RyR2 (Guo et al., 2013), this supports a role for the counter-current in global SR Ca^{2+} release, albeit during pathological Ca^{2+} waves. Furthermore, given the marked effect of Cs^+ substitution on SR Ca^{2+} waves, it seems likely that counter-current inhibition results in a greater polarisation of the SR during Ca^{2+} efflux, which then limits the rate of Ca^{2+} efflux.

During counter-current inhibition, the effect of flecainide on wave frequency was greater than previously seen in the control intracellular solution (Chapter 5). This might be explained if presence of an SR membrane potential facilitates the action of flecainide on RyR2. This is appealing, because it appears consistent with findings in isolated RyR2 channels that the blocking action of flecainide only occurred when the 'luminal' side of the membrane was negatively charged (Bannister et al., 2016, Bannister et al., 2015). A reported blocking effect of flecainide on the counter-current (Bannister et al., 2015) would additionally serve to amplify any change in membrane potential.

In the presence of valinomycin, wave frequency was higher in the added presence of flecainide and the drug failed to prevent the dispersion of waves into aborted wavelets. This suggests that when the K^+ permeability of the SR is increased, the beneficial effect of flecainide on waves is lost. This might be explained by reduced generation of a potential difference across the SR membrane. Unfortunately, the fact that valinomycin itself has a marked and as yet unclear effect on SR Ca^{2+} regulation means that these experiments are inconclusive. Measurement of SR Ca^{2+} content via caffeine "puff" experiments may begin to clarify the effect of valinomycin on permeabilised cardiomyocytes as well as support the effects observed in the presence of Cs^+ .

Chapter 7: General Discussion

7.1 Introduction

This research investigated the controversial hypothesis that flecainide acts directly on RyR2 to alter SR Ca^{2+} release and suppress pro-arrhythmic behaviour in WT cardiomyocytes. Flecainide is a well-characterised inhibitor of $\text{Na}_v1.5$ (Belardinelli et al., 2013, Nitta et al., 1992, Ramos and O'Leary, 2004) yet an additional mechanism of action on RyR2 has been reported in cardiomyocytes with CPVT mutations (Hilliard et al., 2010, Savio-Galimberti and Knollmann, 2015, Watanabe et al., 2009). In this series of studies, the permeabilised ventricular myocyte model was predominantly used to separate the cellular effects of flecainide on $\text{Na}_v1.5$ and RyR2 in WT myocytes. In the absence of functional $\text{Na}_v1.5$ channels, flecainide consistently suppressed pro-arrhythmic Ca^{2+} waves and altered Ca^{2+} spark properties, supporting the hypothesis that flecainide directly affected RyR2 function. It also became apparent that the effect of flecainide on RyR2 might depend upon transient changes in SR membrane potential during Ca^{2+} release. This final chapter will summarise the key findings of this thesis, speculate on some of the previously discussed conclusions and identify new avenues of research and clinical implications.

7.2 The diffusion of flecainide across the sarcolemma and its effects in intact and permeabilised myocytes

Electrical pacing and superfusion of intact WT cardiomyocytes with 100 nM isoprenaline induced spontaneous Ca^{2+} waves during and immediately after field stimulation (Chapter 3). After incubation with flecainide (45 min, 15 μM), spontaneous Ca^{2+} wave frequency was significantly decreased. However, there were no additional effects of flecainide on Ca^{2+} spark properties. The results were similar when Ca^{2+} wave and spark properties were re-investigated in intact myocytes with an increased flecainide incubation period (2 hours) or in myocytes isolated from the MCT model of right-sided heart failure. It was concluded that flecainide likely inhibited Ca^{2+} waves via inhibition of $\text{Na}_v1.5$ without an effect on RyR2. It was postulated by Sikkel et al. (2013) that flecainide inhibition of $\text{Na}_v1.5$ could have decreased intracellular $[\text{Na}^+]$, thereby facilitating Ca^{2+} efflux via NCX and decreasing cytosolic $[\text{Ca}^{2+}]$ to decrease Ca^{2+} propagation and wave formation (Sikkel et al., 2013). However, these parameters were not directly measured by Sikkel (2013).

Intact cardiomyocytes were periodically imaged immediately after application of flecainide-FITC (Chapter 4). Flecainide-FITC moved across the sarcolemma to accumulate within the myocyte over the recorded 3-hour period; however, equilibrium within the cytosol was not reached after this time. The majority of trans-sarcolemmal movement was passive, although a small component was dimetidine sensitive, consistent with active transport via OCT1N1 at higher drug concentrations (25 μ M). Interestingly, flecainide-FITC accumulation in the myocyte was predominantly targeted to the mitochondria and was dependent upon the negatively charged mitochondrial matrix. This was likely due to the highly protonated nature of flecainide at physiological pH (Liu et al., 2003). However, these results also indicate that an effect of flecainide on RyR2 may not have been apparent in Chapter 3 due to the slow trans-sarcolemmal movement and predominant mitochondrial accumulation of flecainide in intact cardiomyocytes. When flecainide is given clinically this may not pose a problem due to regular dosing, allowing time for trans-sarcolemmal movement and eventual equilibrium between the mitochondria and the cytosol. In this case, flecainide may eventually accumulate within the cytosol to a concentration capable of modulating RyR2 activity (Chapter 4). Experimentally however, this slow movement across the sarcolemma has led to misleading results (Sikkel et al., 2013).

In order to bypass the problem of slow trans-sarcolemmal movement of flecainide, the sarcolemma was permeabilised with saponin to allow flecainide immediate access to SR membrane proteins (Chapter 5). In doing so, Na_v1.5 was rendered functionless whilst RyR2 remained *in situ*, allowing a clear separation of flecainide's effects on the two channels. The concentration of flecainide used in permeabilised myocyte experiments (25 μ M) was greater than that reported in the plasma 0.2 – 5 μ M (trough to peak concentrations) (Mano et al., 2015, 3M, 2016). Initial experiments in WT permeabilised myocytes found 25 μ M flecainide was required to produce an effect on Ca²⁺ release (Hilliard et al., 2010, Steele and Yang, 2017). In the permeabilised myocyte model, flecainide significantly and consistently suppressed pro-arrhythmic Ca²⁺ waves by 10-20% and this effect was sustained. Additionally, spark frequency was increased and spark width and amplitude significantly decreased. These effects were similar to those seen in intact and permeabilised CPVT cardiomyocytes, yet ~4x the concentration of flecainide was required (6 μ M vs. 25 μ M) (Hilliard et al., 2010, Savio-Galimberti and Knollmann, 2015) and are indicative of a direct effect of flecainide on RyR2. Interestingly, the size of flecainide's effect on RyR2 was unaffected by the presence of CaM indicating that the loss of this cytosolic mediator during myocyte permeabilisation was unimportant in WT cells. This was in contrast to effects seen in Casq2^{-/-} myocytes whereby CaM potentiated the effect of flecainide (Gomez-Hurtado et al., 2015).

The effect of flecainide on Ca^{2+} wave frequency was consistent with a dependence on SR membrane potential (Chapter 6). By inhibiting the SR counter-current via K^+ exchange for Cs^+ and minimising Cl^- content, the membrane potential across the SR which likely occurs transiently during and immediately after each Ca^{2+} release, was predicted to have been increased in magnitude or duration. The experimental exacerbation of this mechanism resulted in a ~40% suppression of Ca^{2+} wave frequency by flecainide, an effect size similar to that seen in CPVT models at 100 μM flecainide (Savio-Galimberti and Knollmann, 2015)

7.3 Proposed mechanism of action of flecainide on RyR2

A direct effect of flecainide on RyR2 has been observed in all single channel lipid bilayer experiments (Hilliard et al., 2010, Bannister et al., 2016, Bannister et al., 2015, Hwang et al., 2011a). However, the question of its physiological relevance is still contested in the literature (Bannister et al., 2016, Bannister et al., 2015). In cardiomyocytes isolated from animal models with a CPVT phenotype, pro-arrhythmic Ca^{2+} waves are suppressed in the absence of functional $\text{Na}_v1.5$, consistent with an effect of flecainide on RyR2 in these cells at a relatively low flecainide concentration (6 μM) (Savio-Galimberti and Knollmann, 2015, Hilliard et al., 2010). In WT intact cardiomyocytes, the effect of flecainide on RyR2 could not be convincingly demonstrated (Chapter 3) (Bannister et al., 2015). Yet in permeabilised myocytes, in which $\text{Na}_v1.5$ is rendered functionless, significant changes in Ca^{2+} spark properties were observed and the suppression of pro-arrhythmic waves was reproducible across different datasets and under different experimental conditions (Chapter 5).

One proposal put forward by Hilliard et al. (2010) concerning flecainide's mechanism of action on RyR2 is that flecainide blocks the RyR2 pore in its open state resulting in smaller and more frequent sparks. The smaller amplitude and width of sparks might then explain the reduced probability of sparks propagating to form pro-arrhythmic waves whilst the increased spark frequency maintains normal SR leak. However, the relationship between these findings on permeabilised cells and studies on isolated channels is unclear. As noted by Bannister et al. (2015), the effect of flecainide on isolated RyR2 in lipid bilayers was apparent only when the SR lumen was negative with respect to the cytosol; a situation assumed to have no physiological relevance. However, we have proposed that SR polarization may occur transiently during and immediately after Ca^{2+} release (Figure 7.1 and 7.2). Specifically, it seems likely that during diastole when RyR2 is predominantly closed there should be little or no voltage difference across the SR membrane, primarily due to the free movement of K^+ via SR K^+

channels (Figure 7.2 A and B) (Yazawa et al., 2007, Gillespie and Fill, 2008, Somlyo et al., 1977). In contrast, during Ca^{2+} spark or wave release, the rapid Ca^{2+} efflux may transiently polarize the SR membrane if the counter current compensation is not instantaneous (Figure 7.2 A and B ii) (Beeler, 1980, Laver and Lamb, 1998). This situation may transiently fulfil the conditions identified in lipid bilayer experiments where flecainide induced open state block of RyR2 (Hilliard et al., 2010, Bannister et al., 2016, Bannister et al., 2015, Hwang et al., 2011a).

Inhibition of SR K^+ channels and the associated counter current by the application of Cs^+ (Kawai et al., 1998) would be expected to increase the magnitude of any SR polarization during Ca^{2+} release. The inside-negative potential temporarily persists along with flecainide inhibition of RyR2 (Figure 7.2). As the net movement of Ca^{2+} and K^+ through the RyR2 shifts to prioritise K^+ movement into the SR lumen, the inside negative potential subsides, preventing further inhibition of RyR2 by flecainide (Figure 7.2) (Bannister et al., 2016, Bannister et al., 2015). Thereafter, the myocyte enters diastole and RyR2 is closed (Figure 7.2). It could be speculated that RyR2 in mutant myocytes are subject to greater or more prolonged SR membrane potential differences, thereby increasing flecainide block of RyR2.

7.4 The effect of flecainide on other intracellular membrane bound proteins

Within this thesis, the anti-arrhythmic effect of flecainide on RyR2 function has been the primary focus and there is evidence from single channel experiments to show a direct effect of flecainide on RyR2 (Bannister et al., 2016, Bannister et al., 2015, Hilliard et al., 2010, Hwang et al., 2011a). However, in the current cell model, channels and transporters located at the SR, mitochondria and nuclear membranes exist which have the potential to be modulated by flecainide. Flecainide is a promiscuous drug, showing modulation of $\text{Na}_v1.5$, sarcolemmal K^+ channels and RyR2 (Belardinelli et al., 2013, Hilliard et al., 2010, Madeja et al., 2010). K^+ channels are also located at the mitochondria, where flecainide accumulation was reported to occur (Chapter 4) and it is possible that flecainide will inhibit mitochondrial K^+ channels too (Madeja et al., 2010, Melgari et al., 2015b). Under physiological conditions, this may not elicit a large response as mitochondrial K^+ channels are reported to be relatively inactive within cardiomyocytes (Bednarczyk et al., 2008). However, the role of mitochondrial K^+ channels in pathological conditions is still unclear, as is their potential to be modulated pharmacologically (Schulz and Di Lisa, 2016).

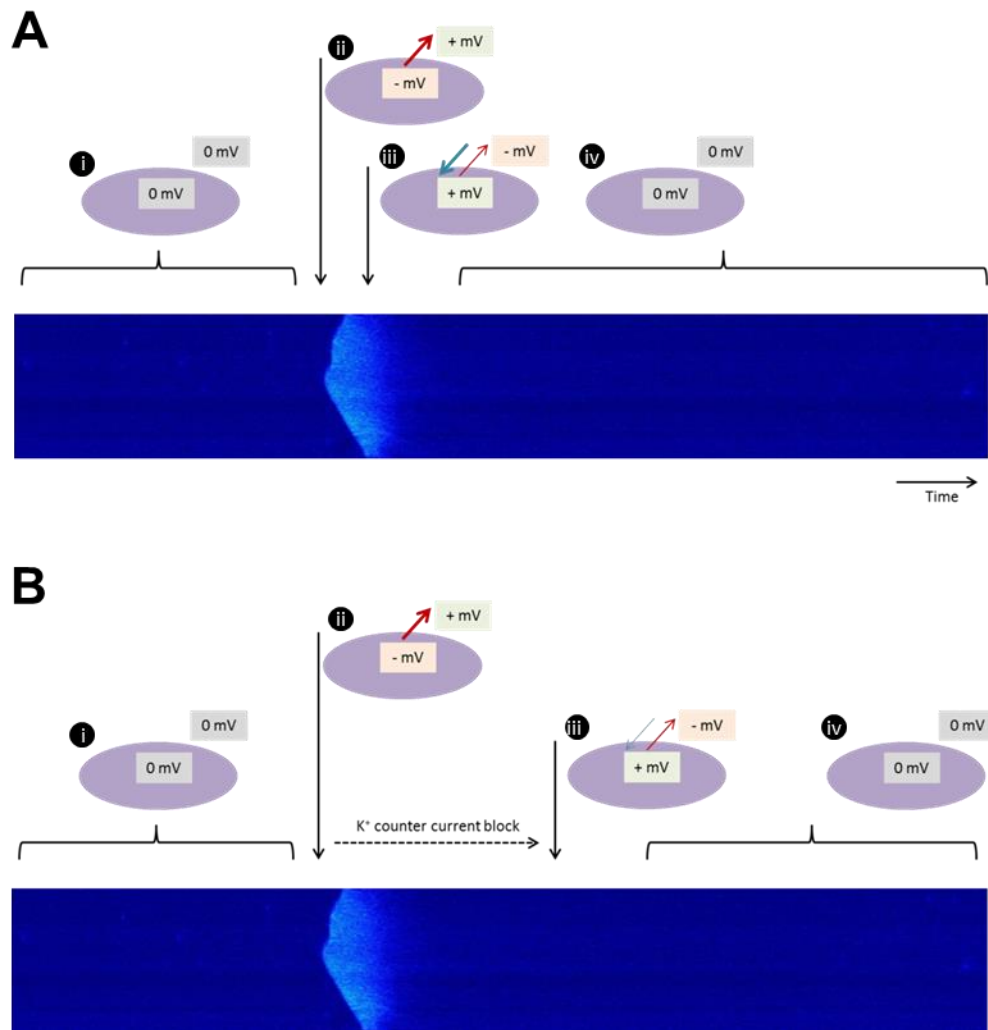


Figure 7.1: Hypothesised transient changes in SR membrane potential during a Ca^{2+} wave

A) Schematic representation of the hypothesised changes in SR membrane potential before, during and immediately after the release of a spontaneous Ca^{2+} wave. i) During cell diastole, there is little or no difference in voltage across the SR membrane. ii) At the start of a Ca^{2+} wave, a large volume of Ca^{2+} (red arrow) moves from the SR to into the cytosol, carrying a large movement of positive charge. A transient negative potential is created inside the SR lumen. Under these conditions, a significant inhibition of RyR2 P_o by flecainide was apparent in single channel lipid bilayer experiments. iii) Initiation of the SR counter-current causes K^+ to flow into the SR via RyR2 and SR K^+ (TRIC) channels, lessening the SR membrane potential and preventing further flecainide block of RyR2. iv) RyR2 is predominantly closed and a balance between the SR lumen and cytosol is restored producing no potential difference across the SR. **B)** Schematic representation of the hypothesised changes in SR membrane potential before, during and immediately after the release of a spontaneous Ca^{2+} wave in the presence of Cs^+ . Cs^+ partially inhibits SR counter current, thereby increasing the duration required for the SR membrane potential to equilibrate or increasing the magnitude of the SR membrane potential after the release of Ca^{2+} . During this period (ii), the transient negative potential created inside the SR lumen is prolonged or increased, thereby increasing the inhibition of RyR2 by flecainide.

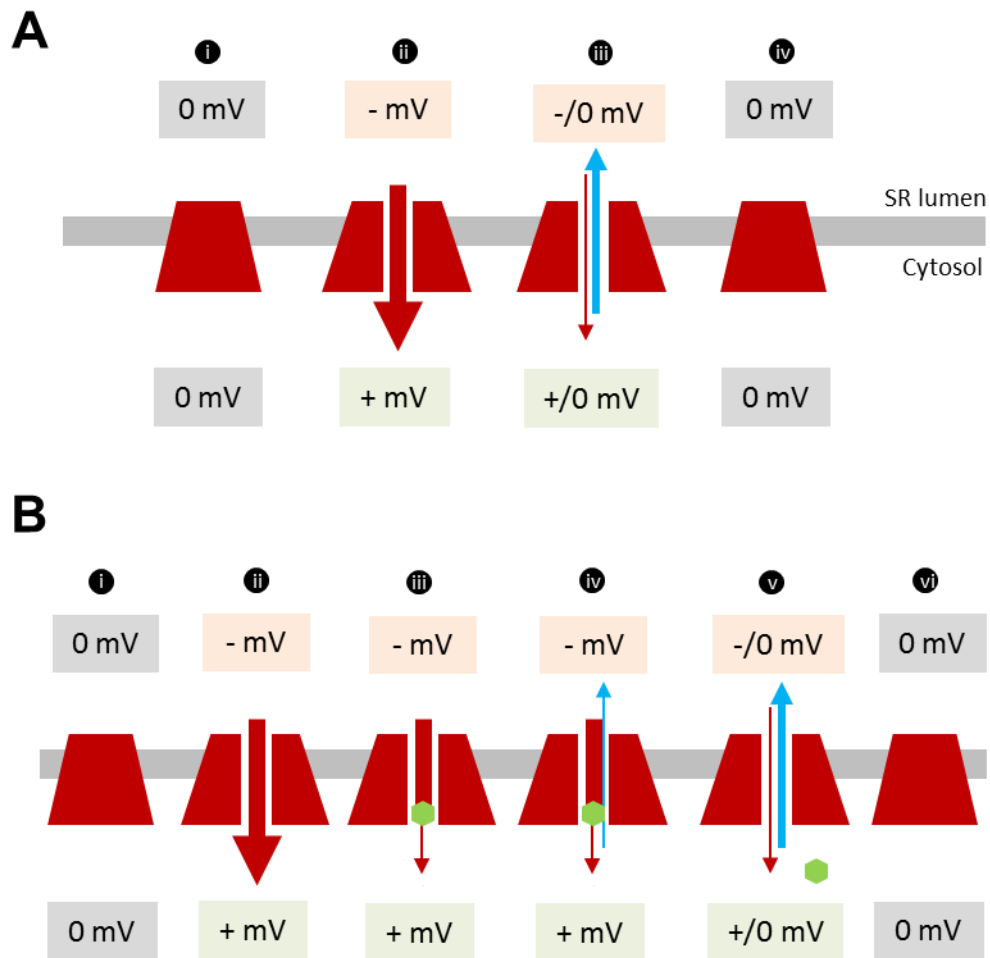


Figure 7.2: Hypothesised block of RyR2 by flecainide during SR Ca²⁺ release

A) Schematic representation of RyR2 opening, flow of Ca²⁺ and K⁺ currents and relative changes in membrane potential across the SR. i) RyR2 is predominantly in its closed state and there is no voltage difference across the SR. ii) Ca²⁺ is released (red arrow) through the open RyR2 channel pore. A transient negative potential inside the SR lumen is created by the large movement of positive charge. iii) K⁺ counter-current (blue arrow) moves into the SR through RyR2, lessening the transient membrane potential. iv) RyR2 is predominantly in its closed state and there is little or no voltage difference across the SR. **B)** Schematic representation of flecainide block of RyR2 during SR Ca²⁺ release. i) RyR2 is predominantly in its closed state and there is little or no voltage difference across the SR. ii) Ca²⁺ release through the open RyR2 channel pore. A transient negative potential inside the SR lumen is created. iii) Under these conditions, flecainide (green) inhibits RyR2 Ca²⁺ conductance and a sub-conductance state is generated. iv) Flecainide inhibition of RyR2 persists as K⁺ counter-current is initiated. Partial block of the SR counter current by Cs⁺ prolongs the membrane potential difference and flecainide block of RyR2. v) K⁺ counter current persists as SR Ca²⁺ content depletes. The transient membrane potential is lessened as the net ion movement through RyR2 shifts to favour K⁺. This prevents further inhibition of RyR2 by flecainide. vi) RyR2 closes and there is little or no voltage difference across the SR during diastole. Arrows represent net movement of ions.

Efsevin, a newly patented anti-arrhythmic drug affecting VDAC2 function on the mitochondrial membrane also modulates spark properties and wave frequency in isolated cardiomyocytes, yet does not directly affect RyR2 function (Shimizu et al., 2015, Chen, 2016). Efsevin increased Ca^{2+} uptake into the mitochondria thereby causing shorter and narrower Ca^{2+} sparks. In doing so, spark propagation was suppressed and Ca^{2+} wave frequency was decreased (Shimizu et al., 2015). The total uptake of cytosolic Ca^{2+} via the mitochondria is likely to be very small (Boyman et al., 2014b), yet local regulation of Ca^{2+} by the mitochondria may modulate arrhythmogenicity (Shimizu et al., 2015, Loughrey et al., 2002). Efsevin serves as an example that changes in spark size may not necessarily equate to direct changes in RyR2 function and the effect of flecainide has not yet been investigated from this perspective.

When valinomycin was applied to the myocyte, it was expected that K^+ would move freely across the SR membrane to remove the occurrence of a transient membrane potential and flecainide would have no effect on Ca^{2+} wave frequency. In fact, Ca^{2+} wave frequency significantly decreased in the presence of valinomycin, potentially due to an unexpected effect of valinomycin on SERCA activity. Under these conditions, flecainide partially maintained wave frequency yet these results remain inconclusive. Valinomycin is also an activator of ROS production in intact cardiomyocytes (Heinzel et al., 2005a). ROS have been reported to induce detrimental changes to SERCA cycling and RyR2 leak (Kuster et al., 2010, Eager et al., 1997) leading to a significantly decreased SR Ca^{2+} content and a significant decrease in wave frequency, such as that seen in Chapter 6. Mitochondrial ROS production is possible in permeabilised myocytes (Kuznetsov et al., 2004) indicating that a preliminary report of flecainide inhibiting ROS production via the Tumour Necrosis Factor- α (TNF- α) pathway may be relevant (Nojima et al., 1995). This could begin to explain the unexpected effect of flecainide in the presence of valinomycin, although other aspects of the ROS pathways need to be considered, such as the likely loss of caspases, the predominate proteins within the TNF- α signalling pathway (Zhu et al., 2006, Chen et al., 2010).

The above discussion is speculation and is largely unsupported by experimental evidence. Yet, these possibilities may be interesting to bear in mind, considering the controversy and unexpected results, surrounding flecainide.

7.5 Differences in effect seen with flecainide in WT and CPVT animal models

As observed in Chapter 5, the effect of flecainide on Ca^{2+} waves was qualitatively comparable in WT rat to $\text{Casq2}^{-/-}$ and $\text{R4496C}^{+/-}$ mouse models with a CPVT phenotype, however a greater concentration of flecainide was required to elicit a similar effect (Chapter 5) (Hilliard et al., 2010, Savio-Galimberti and Knollmann, 2015). Whilst differences in experimental protocol are also likely to be present, the continuation of this pattern was apparent in preliminary experiments reported by Gomez-Hurtado and Knollmann 2016 which were investigating the effect of flecainide in the presence of Cs^+ or valinomydin in $\text{Casq2}^{-/-}$ myocytes (Gomez-Hurtado and Knollmann, 2016).

It is possible that species differences associated with Ca^{2+} handling may partially account for differences in the effect of flecainide (Bers, 2001). However, the effect of flecainide in WT mouse and rabbit cardiomyocytes was similar to results observed in WT rat (Chapter 5) (Savio-Galimberti and Knollmann, 2015). This indicates that species differences are unlikely to play a major role in explaining the differences in flecainide's effect.

RyR2 protein structure may be altered in the $\text{R4496C}^{+/-}$ mutant mouse model due to the altered genomic sequencing of RyR2. If these structural changes coincide with the RyR2-flecainide binding site, the affinity of flecainide to RyR2 may be altered, giving rise to an altered effect of flecainide. However, as RyR2 is a large protein (~565 kDa) (Tunwell et al., 1996), the chance of the RyR2 structure being modified at the relatively small flecainide binding site are small. Additionally, in the $\text{Casq2}^{-/-}$ mutant mouse, RyR2 structure remains unaltered, yet an increased effect of flecainide on Ca^{2+} waves was also apparent.

Differences in RyR2 function between WT and mutant animal models might also govern the differences in the effect of flecainide observed. Cardiomyocytes from both $\text{Casq2}^{-/-}$ and $\text{R4496C}^{+/-}$ mice display a similar CPVT phenotype and in both cases, RyR2 displays an increased sensitivity to Ca^{2+} (Liu et al., 2011, Fernandez-Velasco et al., 2009a, Savio-Galimberti and Knollmann, 2015). In both CPVT models, Ca^{2+} waves were more frequent and exhibited a faster propagation velocity compared with WT. Additionally, Ca^{2+} spark frequency and duration was increased, although spark mass was significantly smaller than WT. The increased RyR2 Ca^{2+} sensitivity and more frequent Ca^{2+} release in both CPVT models may underlie the increased effect of flecainide. For example, it is speculated that more frequent Ca^{2+} release or increased spark duration may give rise to an increased SR membrane potential if the counter current cannot match this increased Ca^{2+} release (Guo et al., 2013, Yazawa et al., 2007). This may cause to greater or more prolonged transient membrane potential differences across the SR. Under

these conditions, flecainide's affinity to RyR2 and blocking capacity may be increased (Chapter 6) (Figure 7.2). Additionally, increased RyR2 P_o in the CPVT model could allow increased drug access to potential binding sites within the open channel pore.

Whilst drug accumulation into the mitochondria was apparent, it must be considered that cytosolic flecainide accumulation may not reach concentrations high enough to affect RyR2 activity in WT cells. Despite this, this study serves as a proof of concept, that RyR2 activity can be affected in WT cells and supports the development of mechanistically similar but kinetically altered pharmacological compounds.

7.6 Future perspectives

To further investigate the differences in the effect of flecainide observed in WT or CPVT mutant cardiomyocytes, the synthetic domain peptide, DPc10 could be utilised. DPc10 is a synthetic peptide which binds to a region on the RyR2 N-terminal, inhibiting intra-RyR2 binding between the N-terminal and central domain (Figure 1.10) (Yamamoto and Ikemoto, 2002). This increases Ca^{2+} sensitivity giving rise to a CPVT phenotype in WT cells (Yang et al., 2006). It would be interesting to establish whether the effect of flecainide in the presence of DPc10 could be achieved at concentrations observed in $Casq2^{-/-}$ and $R4496C^{+/-}$ cardiomyocytes.

Interestingly, flecainide is not the only drug to exhibit an apparent dependence upon changes in SR membrane potential. The experimental RyR2 modulator, JTV-519, has also been reported to block RyR2 to intermediate conductance states, yet only when the SR is held at a negative potential (Darcy et al., 2016). Several clinical drugs have recently been hypothesised to exhibit an inhibitory action upon RyR, although their dependence upon changes in SR membrane potential are unknown. Flecainide and, to a less well-published extent, R-propafenone, are the only two $Na_v1.5$ channel inhibitors suggested to act on RyR2 (Hwang et al., 2011a, Hilliard et al., 2010). Additionally, two enantiomer specific β -blockers R-carvedilol and S-nebivolol suppressed Ca^{2+} release, without traditional β -blocker actions on heart rate and blood pressure, indicating an effect on RyR2 (Zhang et al., 2015, Tan et al., 2016). Dantrolene, a CaM-dependent drug, inhibited skeletal RyR1 in response to triggered malignant hyperthermia (Oo et al., 2015b, Wang et al., 2011).

Further investigations into the mechanisms of action of these drugs may begin to advance our understanding of how RyR2 can be modulated without activating autoregulation. Single channel lipid bilayer experiments are valuable in gaining an initial understanding of RyR2-drug

interactions. However, in this experimental model the environment of the isolated RyR2 channel differs markedly from the physiological state. Experiments utilising permeabilised myocytes, such as those described within this thesis are ideal. Measurement of RyR2 Ca^{2+} release can be imaged using confocal microscopy line scanning whilst RyR2 remains *in situ* and the cytosolic environment can be better physiologically mimicked. In the case of R-propafenone, complicating actions on $\text{Na}_v1.5$ can also be removed. Enantiomer specific R-carvedilol and S-nebivolol do not exhibit β -adrenoceptor blockade (Nichols et al., 1989, Siebert et al., 2008), indicating that intact cardiomyocytes could be utilised without a second mechanism complicating the results. Additionally, computational molecular modelling can begin to predict RyR2 binding sites for pharmacological targets such as flecainide, R-propafenone, R-carvedilol and S-nebivolol. Molecular docking software maps the quaternary protein structure and identifies and ranks potential binding sites for specific small molecules in response to the molecule's structure and chemical properties (Morris et al., 2009).

Most importantly, further investigation of physiologically relevant transient SR membrane potentials is required. The effect of flecainide on Ca^{2+} waves was clearly altered in response to experimental interventions assumed to modify any transient change in SR membrane potential during SR Ca^{2+} release (Chapter 6). It may be possible to study this directly using an expressed fluorescent voltage-sensor protein known as ArcLight, which can be targeted to specific membranes (Cao et al., 2013). Using this methodology, fast changes in sarcolemmal membrane potential have been demonstrated in cardiac stem cells (Leyton-Mange et al., 2014, Song et al., 2015). In future experiments, the ArcLight protein could be targeted to the SR membrane in adult cardiac myocytes using adenoviral expression. This may enable the visualisation of transient changes in SR membrane potential, without signal contamination from the mitochondria or sarcolemma. The action of Cs^+ and valinomycin on SR membrane counter-current could then be confirmed in WT and CPVT cell models.

7.7 Clinical implications

RyR2 has long been regarded as a lucrative potential pharmacological target (Santonastasi and Wehrens, 2007) as RyR2 plays a prominent role in pathological Ca^{2+} release and initiation of potentially fatal ventricular arrhythmias (Marjamaa et al., 2011, Fujiwara et al., 2008, Chang et al., 2013, Benoist et al., 2012). As 700,000 people are affected by arrhythmias in the UK alone, the clinical application for an RyR2 modulator is great (BHF, 2016). However, due to SR auto-regulation, changes in RyR2 P_o are short-lived upon drug application at low concentrations, and

toxic at high concentrations (Santonastasi and Wehrens, 2007, Lukyanenko et al., 2001, Overend et al., 1997) . Drugs that modulate RyR2, whilst bypassing SR autoregulation would be a prerequisite for clinical application.

Small clinical studies have indicated a beneficial effect of flecainide in CPVT patients (Khoury et al., 2013, Mantziari et al., 2013, Lieve et al., 2016, van der Werf et al., 2011a). However, further research is required to develop new drugs that selectively target RyR2, without an effect on Na_v1.5; as it is flecainide's inhibition of I_{Na} that causes fatal arrhythmias in patients with structural heart disease (CAST, 1989, Anderson et al., 1994). The present data adds to the growing number of preclinical studies that demonstrate a preserved effect of flecainide on RyR2, alongside its inhibition of Na_v1.5 (Hilliard et al., 2010, Savio-Galimberti and Knollmann, 2015, Watanabe et al., 2009). Importantly, this data indicates that flecainide also affects RyR2 in WT myocytes, thereby potentially increasing the demographic of patients that may benefit from RyR2 selective drugs.

Appendix

Chemical Name	Company, Country
Acrylamide	National Diagnostics, UK
BSA	Sigma, UK
CaCl ₂	Sigma, UK
Caffeine	Sigma, UK
Cimetidine	Sigma, UK
Collagenase	Worthington Biochemical Corporation, NJ, USA
Creatine	Sigma, UK
Cs hydroxide hydrate	Sigma, UK
Cs methanesulfonate	Sigma, UK
EGTA	Sigma, UK
Ethanol	Sigma, UK
Exogenous CaM	Sigma, UK
FCCP	Sigma, UK
FITC	Sigma, UK
Flecainide acetate	Sigma, UK
Flecainide-FITC	Severn Biotech, UK
Fluo-3	Biotium, CA, USA
Fluo-4 AM	Life Technologies, CA, USA
Glucose	Sigma, UK
Glycerol	Fisher Scientific, UK
Glycine	Fisher Scientific, UK
HEPES	Sigma, UK
Isoprenaline	Sigma, UK
KCl	Sigma, UK
KOH	Sigma, UK
Methanol	Sigma, UK
Mg sulphate	Sigma, UK
MgCl ₂	PanReac AppliChem, DE
Na ₂ ATP	Sigma, UK
Na ₂ CrP	Sigma, UK
NaCl	Fisher Scientific, UK
NaH ₂ PO ₄	BDH Laboratory Supplies/VWR, UK
NaOH	Fisher Scientific, UK
Protease from <i>Streptomyces griseus</i>	Sigma, UK
Protease inhibitor mix	Roche Applied Sciences, CH
Resolving buffer	National Diagnostics, UK
Saponin	Sigma, UK
Skimmed milk	Milipore, UK
Stacking buffer	National Diagnostics, UK
Tank buffer	National Diagnostics, UK
Taurine	Sigma, UK
TEMED	Sigma, UK
Triton X-100	Sigma, UK
TWEEN-20	Sigma, UK
Valinomycin	Sigma, UK

Table 8.1: Chemical names and sources

References

- 3M 2016. Tambacor - flecainide acetate tablet. *In:* 3M (ed.). <https://dailymed.nlm.nih.gov/dailymed/archives/fdaDrugInfo.cfm?archiveid=223644>: NIH.
- AL-HASSNAN, Z. N., TULBAH, S., AL-MANEA, W. & AL-FAYYADH, M. 2013. The phenotype of a CASQ2 mutation in a Saudi family with catecholaminergic polymorphic ventricular tachycardia. *Pacing and Clinical Electrophysiology*, 36, e140-2.
- ALBERTS, B., WILSON, J. & HUNT, T. 2008. *Molecular biology of the cell*, New York, Garland Science.
- ALCALAI, R., WAKIMOTO, H., ARAD, M., PLANER, D., KONNO, T., WANG, L., SEIDMAN, J. G., SEIDMAN, C. E. & BERUL, C. I. 2011. Prevention of ventricular arrhythmia and calcium dysregulation in a catecholaminergic polymorphic ventricular tachycardia mouse model carrying calsequestrin-2 mutation. *Journal of Cardiovascular Electrophysiology*, 22, 316-24.
- ALLOT, E., CAPUCCI, A., CRIJNS, H. J., GOETTE, A. & TAMARGO, J. 2011. Twenty-five years in the making: flecainide is safe and effective for the management of atrial fibrillation. *Europace*, 13, 161-73.
- ALLOUIS, M., PROBST, V., JAAFAR, P., SCHOTT, J. J. & LE MAREC, H. 2005. Unusual clinical presentation in a family with catecholaminergic polymorphic ventricular tachycardia due to a G14876A ryanodine receptor gene mutation. *The American Journal of Cardiology*, 95, 700-2.
- ALTAMIRANO, J. & BERS, D. M. 2007. Voltage dependence of cardiac excitation-contraction coupling: unitary Ca²⁺ current amplitude and open channel probability. *Circulation Research*, 101, 590-7.
- ALTSCHAFL, B. A., ARVANITIS, D. A., FUENTES, O., YUAN, Q., KRANIAS, E. G. & VALDIVIA, H. H. 2011. Dual role of junctin in the regulation of ryanodine receptors and calcium release in cardiac ventricular myocytes. *J Physiol*, 589, 6063-80.
- ANDERSON, J. L., PLATIA, E. V., HALLSTROM, A., HENTHORN, R. W., BUCKINGHAM, T. A., CARLSON, M. D. & CARSON, P. E. 1994. Interaction of baseline characteristics with the hazard of encainide, flecainide, and moricizine therapy in patients with myocardial infarction. A possible explanation for increased mortality in the Cardiac Arrhythmia Suppression Trial (CAST). *Circulation*, 90, 2843-52.
- ANDERSON, J. L., STEWART, J. R., PERRY, B. A., VAN HAMERSVELD, D. D., JOHNSON, T. A., CONARD, G. J., CHANG, S. F., KVAM, D. C. & PITT, B. 1981. Oral flecainide acetate for the treatment of ventricular arrhythmias. *The New England Journal of Medicine*, 305, 473-7.
- ANDRIENKO, T. N., PICHT, E. & BERS, D. M. 2009. Mitochondrial free calcium regulation during sarcoplasmic reticulum calcium release in rat cardiac myocytes. *Journal of Molecular and Cellular Cardiology*, 46, 1027-36.
- ANNO, T. & HONDEGHEM, L. M. 1989. Interactions of flecainide with guinea pig cardiac sodium channels. *Circulation Research*, 66, 789.
- ANTZELEVITCH, C., BELARDINELLI, L., ZYGMUNT, A. C., BURASHNIKOV, A., DI DIEGO, J. M., FISH, J. M., CORDEIRO, J. M. & THOMAS, G. 2004. Electrophysiological effects of ranolazine, a novel antianginal agent with antiarrhythmic properties. *Circulation*, 110, 904-10.
- ANTZELEVITCH, C., NESTERENKO, V., SHRYOCK, J. C., RAJAMANI, S., SONG, Y. & BELARDINELLI, L. 2014. The role of late I_{Na} in development of cardiac arrhythmias. *Handb Exp Pharmacol*, 221, 137-68.
- ANTZELEVITCH, C., SICOURI, S., LITOVSKY, S. H., LUKAS, A., KRISHNAN, S. C., DI DIEGO, J. M., GINTANT, G. A. & LIU, D. W. 1991. Heterogeneity within the ventricular wall.

- Electrophysiology and pharmacology of epicardial, endocardial, and M cells. *Circulation Research*, 69, 1427-49.
- ARAV, R., ADEREM, A. A. & BERMAN, M. C. 1983. Interaction of nucleotides and cations with the (Ca²⁺, Mg²⁺)-ATPase of sarcoplasmic reticulum as determined by fluorescence changes of bound 1-anilino-8-naphthalenesulfonate. *Journal of Biological Chemistry*, 258, 10433-8.
- ARNOULD-TAYLOR, W. 1998. *A Textbook of Anatomy and Physiology*, Stanley Thornes.
- BAARTSCHEER, A., SCHUMACHER, C. A., BELTERMAN, C. N. W., CORONEL, R. & FIOLET, J. W. T. 2003. SR calcium handling and calcium after-transients in a rabbit model of heart failure. *Cardiovascular Research*, 58, 99-108.
- BADDELEY, D., JAYASINGHE, I. D., LAM, L., ROSSBERGER, S., CANNELL, M. B. & SOELLER, C. 2009. Optical single-channel resolution imaging of the ryanodine receptor distribution in rat cardiac myocytes. *Proc Natl Acad Sci U S A*, 106, 22275-80.
- BAHER, A. A., UY, M., XIE, F., GARFINKEL, A., QU, Z. & WEISS, J. N. 2011. Bidirectional ventricular tachycardia: ping pong in the His-Purkinje system. *Heart Rhythm*, 8, 599-605.
- BANERJEE, I., FUSELER, J. W., PRICE, R. L., BORG, T. K. & BAUDINO, T. A. 2007. Determination of cell types and numbers during cardiac development in the neonatal and adult rat and mouse. *American Journal of Physiology: Heart and Circulatory Physiology*, 293, H1883-91.
- BANITT, E. H., BRONN, W. R., COYNE, W. E. & SCHMID, J. R. 1977. Antiarrhythmics. 2. Synthesis and antiarrhythmic activity of N-(piperidylalkyl)trifluoroethoxybenzamides. *Journal of Medicinal Chemistry*, 20, 821-6.
- BANNISTER, M. L., ALVREZ-LAVIADA, A., THOMAS, N. L., MASON, S. A., COLEMAN, S., DU PLESSIS, C. L., MORAN, A. T., NEILL-HALL, D., OSMAN, H., BAGLEY, M. C., MACLEOD, K. T., GEORGE, C. H. & WILLIAMS, A. J. 2016. Effects of flecainide derivatives on sarcoplasmic reticulum calcium release suggests a lack of direct action on the cardiac ryanodine receptor. *British Journal of Pharmacology*, 173, 2446 - 2459.
- BANNISTER, M. L., THOMAS, N. L., SIKKEL, M. B., MUKHERJEE, S., MAXWELL, C., MACLEOD, K. T., GEORGE, C. H. & WILLIAMS, A. J. 2015. The mechanism of flecainide action in CPVT does not involve a direct effect on RyR2. *Circulation Research*, 116, 1324-35.
- BAO, M., KANTER, E. M., HUANG, R. Y., MAXEINER, S., FRANK, M., ZHANG, Y., SCHUESSLER, R. B., SMITH, T. W., TOWNSEND, R. R., ROHRS, H. W., BERTHOUD, V. M., WILLECKE, K., LAING, J. G. & YAMADA, K. A. 2011. Residual Cx45 and its relationship to Cx43 in murine ventricular myocardium. *Channels*, 5, 489-99.
- BARTSCHAT, D. K., CYR, D. L. & LINDENMAYER, G. E. 1980. Depolarization-induced calcium uptake by vesicles in a highly enriched preparation from canine vesicle. *The Journal of Biological Chemistry*, 255, 10044 - 10047.
- BASSANI, J. W., YUAN, W. & BERS, D. M. 1995a. Fractional SR Ca release is regulated by trigger Ca and SR Ca content in cardiac myocytes. *American Journal of Physiology*, 268, C1313-9.
- BASSANI, R. A., ALTAMIRANO, J., PUGLISI, J. L. & BERS, D. M. 2004. Action potential duration determines sarcoplasmic reticulum Ca²⁺ reloading in mammalian ventricular myocytes. *The Journal of Physiology*, 559, 593-609.
- BASSANI, R. A., MATTIAZZI, A. & BERS, D. M. 1995b. CaMKII is responsible for activity-dependent acceleration of relaxation in rat ventricular myocytes. *American Journal of Physiology*, 268, H703-12.
- BEDNARCZYK, P., BARKER, G. D. & HALESTRAP, A. P. 2008. Determination of the rate of potassium movement through potassium channels in isolated rat heart and liver mitochondria. *Biochimica et Biophysica ACTA*, 1777, 540 - 548.
- BEELER, T., RUSSELL, J. T. & MARTONOSI, A. 1979. Optical probe responses on sarcoplasmic reticulum: oxocarbocyanines as probes of membrane potential. *European Journal of Biochemistry*, 95, 579-91.

- BEELER, T. J. 1980. Calcium uptake and membrane potential in sarcoplasmic reticulum. *The Journal of Biological Chemistry*, 255, 9156 - 9161.
- BEELER, T. J. & GABLE, K. S. 1994. Phosphate, nitrendipine and valinomycin increase the Ca²⁺/ATP coupling ratio of rat skeletal muscle sarcoplasmic reticulum Ca²⁺-ATPase. *Biochimica et Biophysica ACTA*, 1189, 189-94.
- BEERY, T. A., SHAH, M. J. & BENSON, D. W. 2009. Genetic characterization of familial CPVT after 30 years. *Biological Research for Nursing*, 11, 66-72.
- BELARDINELLI, L., LIU, G., SMITH-MAXWELL, C., WANG, W.-Q., EL-BIZRI, N., HIRAKAWA, R., KARPINSKI, S., HONG LI, C., HU, L., LI, X.-J., CRUMB, W., WU, L., KOLTUN, D., ZABLOCKI, J., YAO, L., DHALLA, A. K., RAJAMANI, S. & SHRYOCK, J. C. 2013. A novel, potent and selective inhibitor of cardiac late sodium channel suppresses experimental arrhythmias. *Journal of Pharmacology and Experimental Therapeutics*, 344, 23 - 32.
- BENITO, B., BRUGADA, R., PERICH, R. M., LIZOTTE, E., CINCA, J., MONT, L., BERRUEZO, A., TOLOSANA, J. M., FREIXA, X., BRUGADA, P. & BRUGADA, J. 2008. A mutation in the sodium channel is responsible for the association of long QT syndrome and familial atrial fibrillation. *Heart Rhythm*, 5, 1434-40.
- BENOIST, D. 2012. University of Leeds.
- BENOIST, D., STONES, R., DRINKHILL, M. J., BENSON, A. P., YANG, Z., CASSAN, C., GILBERT, S. H., SAINT, D. A., CAZORIA, O., STEELE, D. S., BERNUS, O. & WHITE, E. 2012. Cardiac arrhythmia mechanisms in rats with heart failure induced by pulmonary hypertension. *American Journal of Physiology: Heart and Circulatory Physiology*, 302, H2381-95.
- BENSLEY, J. G., DE MATTEO, R., HARDING, R. & BLACK, M. J. 2016. Three-dimensional direct measurement of cardiomyocyte volume, nuclearity, and ploidy in thick histological sections. *Scientific Reports*, 6, 23756.
- BENSON, A. P. 2016. Wave dimension analysis tool. 2 ed.
- BERS, D. A. 2001. *Excitation-Contraction Coupling and Cardiac Contractile Force*, The Netherlands, Kluwer Academic Publishers.
- BERS, D. M. 2000. Calcium fluxes involved in control of cardiac myocyte contraction. *Circulation Research*, 87, 275-81.
- BERS, D. M., DESPA, S. & BOSSUYT, J. 2006a. Regulation of Ca²⁺ and Na⁺ in normal and failing cardiac myocytes. *Ann NY Acad Sci*, 1080, 165-77.
- BERS, D. M., DESPA, S. & BOSSUYT, J. 2006b. Regulation of Ca²⁺ and Na⁺ in normal and failing cardiac myocytes. *Annals of the New York Academy of Sciences*, 1080 165-77.
- BERS, D. M. & STIFFEL, V. M. 1993. Ratio of ryanodine to dihydropyridine receptors in cardiac and skeletal muscle and implications for E-C coupling. *Am J Physiol*, 264, C1587-93.
- BEYER, E. C., KISTLER, J., PAUL, D. L. & GOODENOUGH, D. A. 1989. Antisera directed against connexin43 peptides react with a 43-kD protein localized to gap junctions in myocardium and other tissues. *The Journal of Cell Biology*, 108, 595-605.
- BEYER, E. C., PAUL, D. L. & GOODENOUGH, D. A. 1987. Connexin43: a protein from rat heart homologous to a gap junction protein from liver. *J Cell Biol*, 105, 2621-9.
- BHF 2016. Heart Rhythms. In: FOUNDATION, B. H. (ed.). British heart Foundation.
- BIRKEDAL, R., SHIELS, H. A. & VENDELIN, M. 2006. Three-dimensional mitochondrial arrangement in ventricular myocytes: from chaos to order. *American Journal of Physiology: Cell Physiology*, 291, C1148-58.
- BLATTER, L. A. & WIER, W. G. 1990. Intracellular diffusion, binding, and compartmentalization of the fluorescent calcium indicators indo-1 and fura-2. *Biophysical Journal*, 58, 1491-9.
- BNF 2015. *British National Formulary*, London, BMJ Group and Pharmaceutical Press.
- BNM-GROUP 2013. New Zealand Data Sheet: Flecainide BNM. medsafe.govt.nz.
- BOLKENT, S. & ZIEROLD, K. 2002. Effects of the ionophores valinomycin, ionomycin and gramicidin A on the element compartmentation in cultured rat hepatocytes. *Toxicology In Vitro*, 16, 159-65.

- BOVO, E., HUKE, S., BLATTER, L. A. & ZIMA, A. V. 2017. The effect of PKA-mediated phosphorylation of ryanodine receptor on SR Ca²⁺ leak in ventricular myocytes. *J Mol Cell Cardiol*, 104, 9-16.
- BOVO, E., MAZUREK, S. R., BLATTER, L. A. & ZIMA, A. V. 2011. Regulation of sarcoplasmic reticulum Ca²⁺(+) leak by cytosolic Ca²⁺(+) in rabbit ventricular myocytes. *Journal of Physiology*, 589, 6039-50.
- BOVO, E., MAZUREK, S. R., FILL, M. & ZIMA, A. V. 2015. Cytosolic Ca²⁺(+) buffering determines the intra-SR Ca²⁺(+) concentration at which cardiac Ca²⁺(+) sparks terminate. *Cell Calcium*, 58, 246-53.
- BOYLE, R. 12/10/2016 2016. RE: *Flecainide and propafenone FITC conjugation*. Type to STEELE, D. S.
- BOYLE, W. A. & NERBONNE, J. M. 1991. A novel type of depolarization-activated K⁺ current in isolated adult rat atrial myocytes. *American Journal of Physiology*, 260, H1236-47.
- BOYMAN, L., CHIKANDO, A. C., WILLIAMS, G. S., KHAIRALLAH, R. J., KETTLEWELL, S., WARD, C. W., SMITH, G. L., KAO, J. P. & LEDERER, W. J. 2014a. Calcium movement in cardiac mitochondria. *Biophysical Journal*, 107, 1289-301.
- BOYMAN, L., CHIKANDO, A. C., WILLIAMS, G. S., KHAIRALLAH, R. J., KETTLEWELL, S., WARD, C. W., SMITH, G. L., KAO, J. P. & LEDERER, W. J. 2014b. Calcium movement in cardiac mitochondria. *Biophys J*, 107, 1289-301.
- BRIDGE, J. H., SMOLLEY, J. R. & SPITZER, K. W. 1990. The relationship between charge movements associated with I_{Ca} and I_{Na-Ca} in cardiac myocytes. *Science*, 248, 376-8.
- BROCHET, D. X., XIE, W., YANG, D., CHENG, H. & LEDERER, W. J. 2011. Quarky calcium release in the heart. *Circulation Research*, 108, 210-8.
- BROWN, H. F., CLARK, A. & NOBLE, S. J. 1976. Identification of the pace-maker current in frog atrium. *Journal of Physiology*, 258, 521-45.
- BU, G., ADAMS, H., BERBARI, E. J. & RUBART, M. 2009. Uniform action potential repolarization within the sarcolemma of in situ ventricular cardiomyocytes. *Biophysical Journal*, 96, 2532-46.
- BUB, G., CAMELLITI, P., BOLLENSDORF, C., STUCKEY, D. J., PICTON, G., BURTON, R. A. B., CLARKE, K. & KOHL, P. 2010. Measurement and analysis of sarcomere length in rat cardiomyocytes. *American Journal of Physiology. Heart and Circulatory Physiology*, 298, H1616 - H1625.
- BUCCHI, A., BARBUTI, A., BARUSCOTTI, M. & DIFRANCESCO, D. 2007. Heart rate reduction via selective 'funny' channel blockers. *Current Opinion in Pharmacology*, 7, 208-13.
- BUSTAMANTE, J. O., MICHELETTE, E. R., GEIBEL, J. P., HANOVER, J. A., MCDONNELL, T. J. & DEAN, D. A. 2000. Dendrimer-assisted patch-clamp sizing of nuclear pores. *European Journal of Physiology*, 439, 829 - 837.
- BYRD, S. K., BODE, A. K. & KLUG, G. A. 1989. Effects of exercise of varying duration on sarcoplasmic reticulum function. *Journal of Applied Physiology*, 66, 1383-9.
- CALAGHAN, S. & WHITE, E. 2006. Caveolae modulate excitation-contraction coupling and beta₂-adrenergic signalling in adult rat ventricular myocytes. *Cardiovascular Research*, 69, 816-24.
- CALAGHAN, S. C., WHITE, E. & COLYER, J. 1998. Co-ordinated changes in cAMP, phosphorylated phospholamban, Ca²⁺ and contraction following beta-adrenergic stimulation of rat heart. *European Journal of Physiology*, 436, 948-56.
- CALLAMARAS, N. & PARKER, I. 1999. Construction of line-scan confocal microscope for physiological recording. *Methods in Enzymology*, 307, 152-69.
- CALLOE, K., GOODROW, R., OLESEN, S. P., ANTZELEVITCH, C. & CORDEIRO, J. M. 2013. Tissue-specific effects of acetylcholine in the canine heart. *Am J Physiol Heart Circ Physiol*, 305, H66-75.
- CANNELL, M. B. & SOELLER, C. 1998. Sparks of interest in cardiac excitation-contraction coupling. *Trends Pharmacol Sci*, 19, 16-20.

- CAO, G., PLATISA, J., PIERIBONE, V. A., RACCUGLIA, D., KUNST, M. & NITABACH, M. N. 2013. Genetically targeted optical electrophysiology in intact neural circuits. *Cell*, 154, 904-13.
- CAPOGROSSI, M. C., SUAREZ-ISLA, B. A. & LAKATTA, E. G. 1986. The interaction of electrically stimulated twitches and spontaneous contractile waves in single cardiac myocytes. *J Gen Physiol*, 88, 615-33.
- CARTLEDGE, J. E., KANE, C., DIAS, P., TEFOM, M., CLARKE, L., MCKEE, B., AL AYOUBI, S., CHESTER, A., YACOUB, M. H., CAMELLITI, P. & TERRACCIANO, C. M. 2015. Functional crosstalk between cardiac fibroblasts and adult cardiomyocytes by soluble mediators. *Cardiovascular Research*, 105, 260-70.
- CAST 1989. Preliminary report: effect of encainide and flecainide on mortality in a randomized trial of arrhythmia suppression after myocardial infarction. The Cardiac Arrhythmia Suppression Trial (CAST) Investigators. *The New England Journal of Medicine*, 321, 406-12.
- CASWELL, A. H. & BRANDT, N. R. 1981. Ion-induced release of calcium from isolated sarcoplasmic reticulum. *Journal of Membrane Biology*, 58, 21 - 33.
- CERRONE, M., COLOMBI, B., SANTORO, M., DI BARLETTA, M. R., SCELSI, M., VILLANI, L., NAPOLITANO, C. & PRIORI, S. G. 2005. Bidirectional ventricular tachycardia and fibrillation elicited in a knock-in mouse model carrier of a mutation in the cardiac ryanodine receptor. *Circulation Research*, 96, e77-82.
- CHANG, M. G., DE LANGE, E., CALMETTES, G., GARFINKEL, A., QU, Z. & WEISS, J. N. 2013. Pro- and antiarrhythmic effects of ATP-sensitive potassium current activation on reentry during early afterdepolarization-mediated arrhythmias. *Heart Rhythm*, 10, 575-82.
- CHANG, P. Y. & JACKSON, M. B. 2003. Interpretation and optimization of absorbance and fluorescence signals from voltage-sensitive dyes. *Journal of Membrane Biology*, 196, 105 - 116.
- CHASE, A. & ORCHARD, C. H. 2011. Ca efflux via the sarcolemmal Ca ATPase occurs only in the t-tubules of rat ventricular myocytes. *Journal of Molecular and Cellular Cardiology*, 50, 187-93.
- CHATTOPADHYAYA, R., MEADOR, W. E., MEANS, A. R. & QUIOCHO, F. A. 1992. Calmodulin structure refined at 1.7 Å resolution. *Journal of Molecular Biology*, 228, 1177-92.
- CHEN, H., VALLE, G., FURLAN, S., NANI, A., GYORKE, S., FILL, M. & VOLPE, P. 2013. Mechanism of calsequestrin regulation of single cardiac ryanodine receptor in normal and pathological conditions. *J Gen Physiol*, 142, 127-36.
- CHEN, J.-N. 2016. *Anti-arrhythmicity agents* WO2016100379 A1.
- CHEN, W., WANG, R., CHEN, B., ZHONG, X., KONG, H., BAI, Y., ZHOU, Q., XIE, C., ZHANG, J., GUO, A., TIAN, X., JONES, P. P., O'MARA, M. L., LIU, Y., MI, T., ZHANG, L., BOLSTAD, J., SEMENIUK, L., CHENG, H., ZHANG, J., CHEN, J., TIELEMAN, D. P., GILLIS, A. M., DUFF, H. J., FILL, M., SONG, L. S. & CHEN, S. R. 2014. The ryanodine receptor store-sensing gate controls Ca²⁺ waves and Ca²⁺-triggered arrhythmias. *Nature Medicine*, 20, 184-92.
- CHEN, Y., PAT, B., ZHENG, J., CAIN, L., POWELL, P., SHI, K., SABRI, A., HUSAIN, A. & DELL'ITALIA, L. J. 2010. Tumor necrosis factor- α produced in cardiomyocytes mediates a predominant myocardial inflammatory response to stretch in early volume overload. *Journal of Molecular and Cellular Cardiology*, 49, 70-8.
- CHENG, H., LEDERER, M. R., LEDERER, W. J. & CANNELL, M. B. 1996. Calcium sparks and intracellular calcium waves in cardiac myocytes. *The American Physiological Society*, 148 - 159.
- CHENG, H. & LEDERER, W. J. 2008. Calcium sparks. *Physiological Review*, 88, 1491-545.
- CHING, L. L., WILLIAMS, A. J. & SITSAPESAN, R. 2000. Evidence for Ca²⁺ activation and inactivation sites on the luminal side of the cardiac ryanodine receptor complex. *Circ Res*, 87, 201-6.

- CHOI, H. S. & EISNER, D. A. 1999. The effects of inhibition of the sarcolemmal Ca-ATPase on systolic calcium fluxes and intracellular calcium concentration in rat ventricular myocytes. *European Journal of Physiology*, 437, 966-71.
- CHOPRA, N., KANNANKERIL, P. J., YANG, T., HLAING, T., HOLINSTAT, I., ETTENSOHN, K., PFEIFER, K., AKIN, B., JONES, L. R., FRANZINI-ARMSTRONG, C. & KNOLLMANN, B. C. 2007. Modest reductions of cardiac calsequestrin increase sarcoplasmic reticulum Ca²⁺ leak independent of luminal Ca²⁺ and trigger ventricular arrhythmias in mice. *Circ Res*, 101, 617-26.
- CLAYTON, R. H. & HOLDEN, A. V. 2002. Dynamics and interaction of filaments in a computational model of re-entrant ventricular fibrillation. *Physics in Medicine and Biology*, 47, 1777-92.
- COLOMBINI, M. 1979. A candidate for the permeability pathway of the outer mitochondrial membrane. *Nature*, 279, 643 - 645.
- COROMILAS, J., SALTMAN, A. E., WALDECKER, B., DILLON, S. M. & WIT, A. L. 1995. Electrophysiological effects of flecainide on anisotropic conduction and reentry in infarcted canine hearts. *Circulation*, 91, 2245-63.
- CORONADO, R., ROSENBERG, R. L. & MILLER, C. 1980. Ionic selectivity, saturation and block in a potassium selective channel from sarcoplasmic reticulum. *Journal of General Physiology*, 76, 425 - 446.
- CROSSMAN, D. J., YOUNG, A. A., RUYGROK, P. N., NASON, G. P., BADDELELY, D., SOELLER, C. & CANNELL, M. B. 2015. T-tubule disease: Relationship between t-tubule organization and regional contractile performance in human dilated cardiomyopathy. *Journal of Molecular and Cellular Cardiology*, 84, 170-8.
- CURRAN, J. W., HINTON, M. J., RIOS, E., BERS, D. M. & SHANNON, T. R. 2007. Beta-adrenergic enhancement of sarcoplasmic reticulum calcium leak in cardiac myocytes is mediated by calcium/calcium-dependent protein kinase. *Circulation Research*, 100, 391 - 398.
- DARCY, Y. L., DIAZ-SYLVESTER, P. L. & COPELLO, J. A. 2016. K201 (JTV519) is a Ca²⁺-Dependent Blocker of SERCA and a Partial Agonist of Ryanodine Receptors in Striated Muscle. *Molecular Pharmacology*, 90, 106-15.
- DES GEORGES, A., CLARKE, O. B., ZALK, R., YUAN, Q., CONDON, K. J., GRASSUCCI, R. A., HENDRICKSON, W. A., MARKS, A. R. & FRANK, J. 2016. Structural Basis for Gating and Activation of RyR1. *Cell*, 167, 145-157 e17.
- DIAZ-SYLVESTER, P. L., PORTA, M. & COPELLO, J. A. 2011. Modulation of cardiac ryanodine receptor channels by alkaline earth cations. *PLOS ONE*, 6, e26693.
- DIAZ, M. E., TRAFFORD, A., O'NEILL, S. C. & EISNER, D. A. 1997. Measurement of sarcoplasmic reticulum calcium content and sarcolemmal calcium fluxes in isolated rat ventricular myocytes during spontaneous calcium release. *Journal of Physiology*, 501, 3 - 16.
- DIAZ, R. J., FERNANDEZ, K., LYTVYN, Y., HAWRYLYSHYN, K., HARVEY, K., HOSSAIN, T., HINEK, A. & WILSON, G. J. 2013. Enhanced cell-volume regulation in cyclosporin A cardioprotection. *Cardiovascular Research*, 98, 411 - 419.
- DIBB, K. M., CLARKE, J. D., EISNER, D. A., RICHARDS, M. A. & TRAFFORD, A. W. 2013. A functional role for transverse (t-) tubules in the atria. *Journal of Molecular and Cellular Cardiology*, 58, 84-91.
- DIBB, K. M., CLARKE, J. D., HORN, M. A., RICHARDS, M. A., GRAHAM, H. K., EISNER, D. A. & TRAFFORD, A. W. 2009. Characterization of an extensive transverse tubular network in sheep atrial myocytes and its depletion in heart failure. *Circulation: Heart Failure*, 2, 482-9.
- DIBB, K. M., EISNER, D. A. & TRAFFORD, A. W. 2007. Regulation of systolic [Ca²⁺]_i and cellular Ca²⁺ flux balance in rat ventricular myocytes by SR Ca²⁺, L-type Ca²⁺ current and diastolic [Ca²⁺]_i. *J Physiol*, 585, 579-92.
- DIGMAN, M. A., STAKIC, M. & GRATTON, E. 2013. Raster image correlation spectroscopy and number and brightness analysis. *Methods Enzymology*, 518, 121-44.

- DIXON, R. E., MORENO, C. M., YUAN, C., OPITZ-ARAYA, X., BINDER, M. D., NAVEDO, M. F. & SANTANA, L. F. 2015. Graded Ca(2+)/calmodulin-dependent coupling of voltage-gated CaV1.2 channels. *eLife*, 4.
- DOBREV, D. & WEHRENS, X. H. 2014. Role of RyR2 phosphorylation in heart failure and arrhythmias: Controversies around ryanodine receptor phosphorylation in cardiac disease. *Circ Res*, 114, 1311-9; discussion 1319.
- DOBRYNSKI, H., LI, J., TELLEZ, J., GREENER, I. D., NIKOLSKI, V. P., WRIGHT, S. E., PARSON, S. H., JONES, S. A., LANCASTER, M. K., YAMAMOTO, M., HONJO, H., TAKAGISHI, Y., KODAMA, I., EFIMOV, I. R., BILLETER, R. & BOYETT, M. R. 2005. Computer three-dimensional reconstruction of the sinoatrial node. *Circulation*, 111, 846-54.
- DOMEI, T. L., MAXWELL, J. T. & BLATTER, L. A. 2012. Beta-adrenergic stimulation increases the intra-sarcoplasmic reticulum calcium threshold for calcium wave generation. *Journal of Physiology*, 590, 6093 - 6108.
- DRIES, E., BITO, V., LENAERTS, I., ANTOONS, G., SIPIDO, K. R. & MACQUAIDE, N. 2013. Selective modulation of coupled ryanodine receptors during microdomain activation of calcium/calmodulin-dependent kinase II in the dyadic cleft. *Circ Res*, 113, 1242-52.
- DUAN, J., GHERGHE, C., LIU, D., HAMLETT, E., SRIKANTHA, L., RODGERS, L., REGAN, J. N., ROJAS, M., WILLIS, M., LEASK, A., MAJESKY, M. & DEB, A. 2012. Wnt1/betacatenin injury response activates the epicardium and cardiac fibroblasts to promote cardiac repair. *Emboj*, 31, 429-42.
- DUBELL, W. H., GIGENA, M. S., GUATIMOSIM, S., LONG, X., LEDERER, W. J. & ROGERS, T. B. 2002. Effects of PP1/PP2A inhibitor calyculin A on the E-C coupling cascade in murine ventricular myocytes. *Am J Physiol Heart Circ Physiol*, 282, H38-48.
- DUNCAN, L., BURTON, F. L. & SMITH, G. L. 1999. REACT: Calculation of free metal and ligand concentrations using a Windows-based computer programme. *Journal of Physiology*, 517, P, 2P.
- DZBEK, J. & KORZENIEWSKI, B. 2007. Control over action potential, calcium peak and average fluxes in the cyclic quasi-steady-state ion transport system in cardiac myocytes: in silico studies. *Biochemical Journal*, 404, 227-33.
- EAGER, K. R., RODEN, L. D. & DULHUNTY, A. F. 1997. Actions of sulfhydryl reagents on single ryanodine receptor Ca(2+)-release channels from sheep myocardium. *American Journal of Physiology*, 272, C1908-18.
- EGOM, E. E., BAE, J. S., CAPEL, R., RICHARDS, M., KE, Y., PHARITHI, R. B., MAHER, V., KRZULIAK, P. & LEI, M. 2016. Effect of sphingosine-1-phosphate on L-type calcium current and Ca(2+) transient in rat ventricular myocytes. *Molecular and Cellular Biochemistry*, 419, 83-92.
- EISNER, D., BODE, E., VENETUCCI, L. & TRAFFORD, A. 2013. Calcium flux balance in the heart. *J Mol Cell Cardiol*, 58, 110-7.
- EISNER, D. A., TRAFFORD, A. W., DIAZ, M. E., OVEREND, C. L. & O'NEILL, S. C. 1998. The control of Ca release from the cardiac sarcoplasmic reticulum: regulation versus autoregulation. *Cardiovasc Res*, 38, 589-604.
- EVANS, T. I. & SHEA, M. A. 2009. Energetics of calmodulin domain interactions with the calmodulin binding domain of CaMKII. *Proteins*, 76, 47-61.
- FABIATO, A. 1992. Two kinds of calcium-induced release of calcium from the sarcoplasmic reticulum of skinned cardiac cells. *Advances in Experimental Medicine and Biology*, 311, 245-62.
- FABIATO, A. & FABIATO, F. 1975. Effects of magnesium on contractile activation of skinned cardiac cells. *Journal of Physiology*, 249, 497-517.
- FAGUNDES, A., DE MAGALHAES, L. P., RUSSO, M. & XAVIER, E. 2010. Pharmacological Treatment of Electrical Storm in Catecholaminergic Polymorphic Ventricular Tachycardia. *Pacing and Clinical Electrophysiology*, 33, e27-e31.
- FARKAS, V., SZENTANDRASSY, N., BARANDI, L., HEGYI, B., RUZSNAVSZKY, F., RUZSNAVSZKY, O., HORVATH, B., BANYASZ, T., MAGYAR, J., MARTON, I. & NANASI, P. P. 2012. Interaction

- between Ca(2+) channel blockers and isoproterenol on L-type Ca(2+) current in canine ventricular cardiomyocytes. *Acta Physiologica*, 206, 42-50.
- FAVERO, G., CAMPANELLA, L., ANNIBALE, A. D., SANTUCCI, R. & FERRI, T. 2003. Mixed hybrid bilayer lipid membrane incorporating valinomycin: improvements in preparation and functioning. *Microchemical Journal*, 74, 141 - 148.
- FERNANDEZ-VELASCO, M., RUEDA, A., RIZZI, N., BENITAH, J. P., COLOMBI, B., NAPOLITANO, C., PRIORI, S. G., RICHARD, S. & GOMEZ, A. M. 2009a. Increased Ca²⁺ sensitivity of the ryanodine receptor mutant RyR2R4496C underlies catecholaminergic polymorphic ventricular tachycardia. *Circ Res*, 104, 201-9, 12p following 209.
- FERNANDEZ-VELASCO, M., RUEDA, A., RIZZI, N., BENITAH, J. P., COLOMBI, B., NAPOLITANO, C., PRIORI, S. G., RICHARD, S. & GOMEZ, A. M. 2009b. Increased Ca²⁺ sensitivity of the ryanodine receptor mutant RyR2R4496C underlies catecholaminergic polymorphic ventricular tachycardia. *Circulation Research*, 104, 201-9, 12p following 209.
- FOLLMER, C. H., CULLINAN, C. A. & COLATSKY, T. J. 1992. Differential block of cardiac delayed rectifier current by class Ic antiarrhythmic drugs: evidence for open channel block and unblock. *Cardiovascular Research*, 26, 1121-30.
- FONTANESI, F. 2015. Mitochondria: Structure and Role in Respiration.
- FOWLER, E. 2015. *Beta 1 adrenoceptor blockade treatment of right ventricular dysfunction caused by pulmonary hypertension*. PhD, University of Leeds.
- FOWLER, E., DRINKHILL, M. J., STONES, R., PERVOLARAKI, E., NORMAN, R., STEER, E., BENOIST, D., YANG, Z., HAUTON, D., EGGINGTON, S., STEELE, D. S., CALAGHAN, S. & WHITE, E. In preparation. Beta1-adrenoceptor antagonist, metoprolol, prolongs survival and attenuates electrical, metabolic and Ca²⁺ handling dysfunction in rats with right heart failure and pulmonary artery hypertension
- FOZZARD, H. A. & SHEU, S. S. 1982. The resting potential in heart muscle. *Advances in Myocardiology*, 3, 125-33.
- FRAMPTON, J. E., ORCHARD, C. H. & BOYETT, M. R. 1991. Diastolic, systolic and sarcoplasmic reticulum [Ca²⁺] during inotropic interventions in isolated rat myocytes. *Journal of Physiology*, 437, 351-75.
- FRANK, K., TILGMANN, C., SHANNON, T. R., BERS, D. M. & KRANIAS, E. G. 2000. Regulatory role of phospholamban in the efficiency of cardiac sarcoplasmic reticulum Ca²⁺ transport. *Biochemistry*, 39, 14176-82.
- FRIDOLFSSON, H. N., ROTH, D. M., INSEL, P. A. & PATEL, H. H. 2014. Regulation of intracellular signaling and function by caveolin. *Fasebj*, 28, 3823-31.
- FRISK, M., KOIVUMAKI, J. T., NORSENG, P. A., MALECKAR, M. M., SEJERSTED, O. M. & LOUCH, W. E. 2014. Variable t-tubule organization and Ca²⁺ homeostasis across the atria. *American Journal of Physiology: Heart and Circulation Physiology*, 307, H609-20.
- FRUEN, B. R., BLACK, D. J., BLOOMQUIST, R. A., BARDY, J. M., JOHNSON, J. D., LOUIS, C. F. & BALOG, E. M. 2003. Regulation of the RYR1 and RYR2 Ca²⁺ release channel isoforms by Ca²⁺-insensitive mutants of calmodulin. *Biochemistry*, 42, 2740-7.
- FUJIWARA, K., TANAKA, H., MANI, H., NAKAGAMI, T. & TAKAMATSU, T. 2008. Burst emergence of intracellular Ca²⁺ waves evokes arrhythmogenic oscillatory depolarization via the Na⁺-Ca²⁺ exchanger: simultaneous confocal recording of membrane potential and intracellular Ca²⁺ in the heart. *Circulation Research*, 103, 509-18.
- GATTONI, S., ROE, A. T., FRISK, M., LOUCH, W. E., NIEDERER, S. A. & SMITH, N. P. 2016. The calcium-frequency response in the rat ventricular myocyte: an experimental and modelling study. *Journal of Physiology*, 594, 4193-224.
- GEE, K. R., BROWN, K. A., CHEN, W. N., BISHOP-STEWART, J., GRAY, D. & JOHNSON, I. 2000. Chemical and physiological characterization of fluo-4 Ca(2+)-indicator dyes. *Cell Calcium*, 27, 97-106.
- GEORGE, C. H., HIGGS, G. V. & LAI, F. A. 2003. Ryanodine receptor mutations associated with stress-induced ventricular tachycardia mediate increased calcium release in stimulated cardiomyocytes. *Circulation Research*, 93, 531-40.

- GILBERT, S. H., BENSON, A. P., LI, P. & HOLDEN, A. V. 2007. Regional localisation of left ventricular sheet structure: integration with current models of cardiac fibre, sheet and band structure. *European Journal of Cardio-Thoracic Surgery*, 32, 231-49.
- GILLESPIE, D., CHEN, H. & FILL, M. 2012. Is ryanodine receptor a calcium or magnesium channel? Roles of K⁺ and Mg²⁺ during Ca²⁺ release. *Cell Calcium*, 51, 427-33.
- GILLESPIE, D. & FILL, M. 2008. Intracellular calcium release channels mediate their own countercurrent: the ryanodine receptor case study. *Biophysical Journal*, 95, 3706 - 3714.
- GILLESPIE, D. & FILL, M. 2013. Pernicious attrition and inter-RyR2 CICR current control in cardiac muscle. *J Mol Cell Cardiol*, 58, 53-8.
- GOLDENTHAL, K. L., HEDMAN, K., CHEN, J. W., AUGUST, J. T. & WILLINGHAM, M. C. 1985. Postfixation detergent treatment for immunofluorescence suppresses localisation of some integral membrane proteins. *The Journal of Histochemistry and Cytochemistry*, 33, 813 - 820.
- GOMEZ-HURTADO, N. & KNOLLMANN, B. C. 2016. RE: *Flecainide effect in CASQ knockout and wild type cells with caesium and valinomycin*. Type to STEELE, D. S. & STEER, E.
- GOMEZ-HURTADO, N., OO, Y. W., LAVER, D. & KNOLLMANN, B. C. 2015. Calmodulin potentiates RyR2 block and calcium wave suppression by flecainide. *Biophysical Journal*, 108, 264a - 265a.
- GOMEZ, A. M., CHENG, H., LEDERER, W. J. & BERS, D. M. 1996. Ca²⁺ diffusion and sarcoplasmic reticulum transport both contribute to [Ca²⁺]_i decline during Ca²⁺ sparks in rat ventricular myocytes. *Journal of Physiology*, 496 (Pt 2), 575-81.
- GOURDIE, R. G., SEVERS, N. J., GREEN, C. R., ROTHERY, S., GERMROTH, P. & THOMPSON, R. P. 1993. The spatial distribution and relative abundance of gap-junctional connexin40 and connexin43 correlate to functional properties of components of the cardiac atrioventricular conduction system. *Journal of Cell Science*, 105 (Pt 4), 985-91.
- GRAY, B., BAGNALL, R. D., LAM, L., INGLES, J., TURNER, C., HAAN, E., DAVIS, A., YANG, P. C., CLANCY, C. E., SY, R. W. & SEMSARIAN, C. 2016. A novel heterozygous mutation in cardiac calsequestrin causes autosomal dominant catecholaminergic polymorphic ventricular tachycardia. *Heart Rhythm*, 13, 1652-60.
- GRIMM, M. & BROWN, J. H. 2010. Beta-adrenergic receptor signaling in the heart: role of CaMKII. *Journal of Molecular and Cellular Cardiology*, 48, 322-30.
- GROS, D. B. & JONGSMA, H. J. 1996. Connexins in mammalian heart function. *Bioessays*, 18, 719-30.
- GUO, T., NANI, A., SHONTS, S., PERRYMAN, M., CHEN, H., SHANNON, T. R., GILLESPIE, D. & FILL, M. 2013. Sarcoplasmic reticulum potassium (TRIC) channel does not carry essential countercurrent during calcium release. *Biophysical Journal*, 105, 1151 - 1160.
- GUSEV, K. & NIGGLI, E. 2008. Modulation of the local SR Ca²⁺ release by intracellular Mg²⁺ in cardiac myocytes. *Journal of General Physiology*, 132, 721-30.
- GYORKE, I. & GYORKE, S. 1998. Regulation of the cardiac ryanodine receptor channel by luminal Ca²⁺ involves luminal Ca²⁺ sensing sites. *Biophys J*, 75, 2801-10.
- GYORKE, S., LUKYANENKO, V. & GYORKE, I. 1997. Dual effects of tetracaine on spontaneous calcium release in rat ventricular myocytes. *Journal of Physiology*, 500 (Pt 2), 297-309.
- HAGEMANN, D., KUSCHEL, M., KURAMOCHI, T., ZHU, W., CHENG, H. & XIAO, R. P. 2000. Frequency-encoding Thr17 phospholamban phosphorylation is independent of Ser16 phosphorylation in cardiac myocytes. *Journal of Biological Chemistry*, 275, 22532-6.
- HALL, J. E. & GUYTON, A. C. 2016. *Guyton and Hall textbook of medical physiology: Textbook of medical physiology*, Philadelphia, USA, Elsevier.
- HAMAMATSU-PHOTONICS, K. K. 2007. Photomultiplier Tubes. In: HAKAMATA, T. (ed.) *Basics and Applications*. 3a ed.: Hamamatsu Photonics K. K.
- HANDHLE, A., ORMONDE, C. E., THOMAS, N. L., BRALESFORD, C., WILLIAMS, A. J., LAI, F. A. & ZISSIMOPOULOS, S. 2016. Calsequestrin interacts directly with the cardiac ryanodine receptor luminal domain. 129, 3983-3988.

- HARVEY, R. D. & TEN EICK, R. E. 1989. Voltage-dependent block of cardiac inward-rectifying potassium current by monovalent cations. *Journal of General Physiology*, 94, 349 - 361.
- HAYASHI, T., MARTONE, M. E., YU, Z., THOR, A., DOI, M., HOLST, M. J., ELLISMAN, M. H. & HOSHIJIMA, M. 2009. Three-dimensional electron microscopy reveals new details of membrane systems for Ca²⁺ signaling in the heart. *Journal of Cell Science*, 122, 1005-13.
- HAYWARD, C., PATEL, H. C., PATEL, K., DI MARIO, C., LYON, A. R., AHSAN, S. Y. & ROWLAND, E. 2016. The evolving landscape of oral anti-arrhythmic prescriptions for atrial fibrillation in England: 1998-2014. *European Heart Journal: Cardiovascular Pharmacotherapy*, 2, 90-4.
- HEAD, B. P., PATEL, H. H., ROTH, D. M., LAI, N. C., NIESMAN, I. R., FARQUHAR, M. G. & INSEL, P. A. 2005. G-protein-coupled receptor signaling components localize in both sarcolemmal and intracellular caveolin-3-associated microdomains in adult cardiac myocytes. *Journal of Biological Chemistry*, 280, 31036-44.
- HEINZEL, F. R., LUO, Y., LI, X., BOENGLER, K., BUECHERT, A., GARCIA-DORADO, D., DI LISA, F., SCHULZ, R. & HEUSCH, G. 2005a. Impairment of diazoxide-induced formation of reactive oxygen species and loss of cardioprotection in connexin 43 deficient mice. *Circ Res*, 97, 583-6.
- HEINZEL, F. R., LUO, Y., LI, X., BOENGLER, K., BUECHERT, A., GARCIA-DORADO, D., DI LISA, F., SCHULZ, R. & HEUSCH, G. 2005b. Impairment of diazoxide-induced formation of reactive oxygen species and loss of cardioprotection in connexin 43 deficient mice. *Circulation Research*, 97, 583-6.
- HELM, P. A., TSENG, H. J., YOUNES, L., MCVEIGH, E. R. & WINSLOW, R. L. 2005. Ex vivo 3D diffusion tensor imaging and quantification of cardiac laminar structure. *Magnetic Resonance in Medicine*, 54, 850-9.
- HIESS, F., VALLMITJANA, A., WANG, R., CHENG, H., TER KEURS, H. E., CHEN, J., HOVE-MADSEN, L., BENITEZ, R. & CHEN, S. R. 2015. Distribution and Function of Cardiac Ryanodine Receptor Clusters in Live Ventricular Myocytes. *Journal of Biological Chemistry*, 290, 20477-87.
- HILLIARD, F. A., STEELE, D. S., LAVER, D., YANG, Z., LE MARCHAND, S. J., CHOPRA, N., PISTON, D. W., HUKU, S. & KNOLLMANN, B. C. 2010. Flecainide inhibits arrhythmogenic calcium waves by open state block of RyR2 calcium release channels and reduction of calcium spark mass. *Journal of Molecular and Cellular Cardiology*, 48, 293-301.
- HOROWITZ, S. B. 1972. The permeability of the amphibian oocyte nucleus, in situ. *The Journal of Cell Biology*, 54, 609 - 625.
- HOU, Y., JAYASINGHE, I., CROSSMAN, D. J., BADDELEY, D. & SOELLER, C. 2015. Nanoscale analysis of ryanodine receptor clusters in dyadic couplings of rat cardiac myocytes. *J Mol Cell Cardiol*, 80, 45-55.
- HOUSER, S. R. 2014. Role of RyR2 phosphorylation in heart failure and arrhythmias: protein kinase A-mediated hyperphosphorylation of the ryanodine receptor at serine 2808 does not alter cardiac contractility or cause heart failure and arrhythmias. *Circulation Research*, 114, 1320-7; discussion 1327.
- HU, R. M., TAN, B. H., ORLAND, K. M., VALDIVIA, C. R., PETERSON, A., PU, J. & MAKIELSKI, J. C. 2013. Digenic inheritance novel mutations in SCN5a and SNTA1 increase late I(Na) contributing to LQT syndrome. *American Journal of Physiology: Heart and Circulation Physiology*, 304, H994-h1001.
- HUANG, C. F., CHEN, Y. C., YEH, H. I. & CHEN, S. A. 2012. Mononucleated and binucleated cardiomyocytes in left atrium and pulmonary vein have different electrical activity and calcium dynamics. *Progress in Biophysics and Molecular Biology*, 108, 64-73.
- HUANG, T., LONG, M. & HUO, B. 2010. Competitive Binding to Cuprous Ions of Protein and BCA in the Bicinchoninic Acid Protein Assay. *The Open Biomedical Engineering Journal*, 4, 271-8.

- HUDDER, A., NATHANSON, L. & DEUTSCHER, M. P. 2003. Organization of mammalian cytoplasm. *Molecular and Cellular Biology*, 23, 9318-26.
- HUKE, S. & BERS, D. M. 2008. Ryanodine receptor phosphorylation at Serine 2030, 2808 and 2814 in rat cardiomyocytes. *Biochem Biophys Res Commun*, 376, 80-5.
- HUXLEY, H. E. 1967. Recent x-ray diffraction and electron microscope studies of striated muscle. *Journal of General Physiology*, 50, Suppl:71-83.
- HWANG, H. S., HASDEMIR, C., LAVER, D., MEHRA, D., TURHAN, K., FAGGIONI, M., YIN, H. & KNOLLMANN, B. C. 2011a. Inhibition of cardiac calcium release channels (RyR2) determines efficacy of Class I antiarrhythmic drugs in catecholaminergic polymorphic ventricular tachycardia. *Circulation Arrhythmia Electrophysiology*, 4, 128-135.
- HWANG, H. S., SAVIO-GALIMBERTI, E. & KNOLLMANN, B. C. 2011b. Slow diffusion across membrane delays onset of RyR2 channel block and calcium wave suppression by flecainide in intact myocytes. *Biophysical Journal: Abstract Issue*.
- IAIZO, P. A. 2015. *Handbook of Cardiac Anatomy, Physiology, and Devices*, Springer.
- IKEDA, N., SINGH, B. N., DAVIS, L. D. & HAUSWIRTH, O. 1985. Effects of flecainide on the electrophysiologic properties of isolated canine and rabbit myocardial fibers. *Journal of the American College of Cardiology*, 5, 303 - 310.
- INAI, Y., YABUKI, M., KANNO, T., AKIYAMA, J., YASUDA, T. & UTSUMI, K. 1997. Valinomycin induces apoptosis of ascites hepatoma cells (AH-130) in relation to mitochondrial membrane potential. *Cell Structure and Function*, 22, 555 - 563.
- INUI, M., WANG, S., SAITO, A. & FLEISCHER, S. 1988. Characterization of junctional and longitudinal sarcoplasmic reticulum from heart muscle. *J Biol Chem*, 263, 10843-50.
- JAFRI, M. S. 2012. Models of excitation-contraction coupling in cardiac ventricular myocytes. *Methods Mol Biol*, 910, 309-35.
- JANUARY, C. T. & RIDDLE, J. M. 1989. Early afterdepolarizations: mechanism of induction and block. A role for L-type Ca²⁺ current. *Circulation Research*, 64, 977-90.
- JAYASINGHE, I. D., CANNELL, M. D. & SOELLER, C. 2009. Organization of ryanodine receptors, transverse tubules and sodium-calcium exchanger in rat myocytes. *Biophysical Journal*, 97, 2664 - 2673.
- JIANG, D., CHEN, W., WANG, R., ZHANG, L. & CHEN, S. R. 2007. Loss of luminal Ca²⁺ activation in the cardiac ryanodine receptor is associated with ventricular fibrillation and sudden death. *Proceedings of the National Academy of Sciences*, 104, 18309-14.
- JONES, L. R., ZHANG, L., SANBORN, K., JORGENSEN, A. O. & KELLEY, J. 1995. Purification, primary structure, and immunological characterization of the 26-kDa calsequestrin binding protein (junctin) from cardiac junctional sarcoplasmic reticulum. *Journal of Biological Chemistry*, 270, 30787-96.
- JONES, S. A. & LANCASTER, M. K. 2015. Progressive age-associated activation of JNK associates with conduction disruption in the aged atrium. *Mechanisms of Ageing and Development*, 146-148, 72-80.
- JOSEPHSON, I. R., SANCHEZ-CHAPULA, J. & BROWN, A. M. 1984a. A comparison of calcium currents in rat and guinea pig single ventricular cells. *Circulation Research*, 54, 144-56.
- JOSEPHSON, I. R., SANCHEZ-CHAPULA, J. & BROWN, A. M. 1984b. Early outward current in rat single ventricular cells. *Circulation Research*, 54, 157-62.
- JOUSILAHTI, P., VARTIAINEN, E., TUOMILEHTO, J. & PUSKA, P. 1999. Sex, age, cardiovascular risk factors, and coronary heart disease: a prospective follow-up study of 14 786 middle-aged men and women in Finland. *Circulation*, 99, 1165-72.
- JUNG, D. W., BAYSAL, K. & BRIERLEY, G. P. 1995. The sodium-calcium antiport of heart mitochondria is not electroneutral. *Journal of Biological Chemistry*, 270, 672-8.
- KAASIK, A., JOUBERT, F., VENTURA-CLAPIER, R. & VEKSLER, V. 2004. A novel mechanism of regulation of cardiac contractility by mitochondrial functional state. *Official Publication of the Federation of American Societies for Experimental Biology*, 18, 1219 - 1227.
- KALYANASUNDARAM, A., BAL, N. C., FRANZINI-ARMSTRONG, C., KNOLLMANN, B. C. & PERIASAMY, M. 2010. The calsequestrin mutation CASQ2D307H does not affect protein

- stability and targeting to the junctional sarcoplasmic reticulum but compromises its dynamic regulation of calcium buffering. *J Biol Chem*, 285, 3076-83.
- KAMP, F., DONOSO, P. & HIDALGO, C. 1998. Changes in luminal pH caused by calcium release in sarcoplasmic reticulum vesicles. *Biophysical Journal*, 74, 290 - 296.
- KANNANKERIL, P. J. 2010. Flecainide for Catecholaminergic Polymorphic Ventricular Tachycardia. *Identifier: NCT01117454*. <https://clinicaltrials.gov/ct2/home>: US National Institutes of Health.
- KANZAKI, Y., TERASAKI, F., OKABE, M., FUJITA, S., KATASHIMA, T., OTSUKA, K. & ISHIZAKA, N. 2010. Three-dimensional architecture of cardiomyocytes and connective tissue in human heart revealed by scanning electron microscopy. *Circulation*, 122, 1973-4.
- KASHIMURA, T., BRISTON, S. J., TRAFFORD, A., NAPOLITANO, C., PRIORI, G. P., EISNER, D. A. & VENETUCCI, L. A. 2010. In the RyR2R4496C mouse model of CPVT, beta adrenergic stimulation induces calcium waves by increasing SR calcium content and not by decreasing the threshold for calcium waves. *Circulation Research*, 107, 1483 - 1489.
- KAWAI, M., HUSSAIN, M. & ORCHARD, C. H. 1998. Caesium inhibits spontaneous calcium release from the sarcoplasmic reticulum of skinned cardiac myocytes. *The American Physiological Society*, 275, H422 - H430.
- KAWAI, M., HUSSAIN, M. & ORCHARD, C. H. 1999. Excitation-contraction coupling in rat ventricular myocytes after fomamide-induced detubulation. *American Journal of Physiology*, 277, H603-9.
- KENTISH, J. C., MCCLOSKEY, D. T., LAYLAND, J., PALMER, S., LEIDEN, J. M., MARTIN, A. F. & SOLARO, R. J. 2001. Phosphorylation of troponin I by protein kinase A accelerates relaxation and crossbridge cycle kinetics in mouse ventricular muscle. *Circulation Research*, 88, 1059-65.
- KHOURY, A., MARAI, I., SULEIMAN, M., BLICH, M., LORBER, A., GEPSTEIN, L. & BOULOS, M. 2013. Flecainide therapy suppresses exercise-induced ventricular arrhythmias in patients with CASQ2-associated catecholaminergic polymorphic ventricular tachycardia. *Heart Rhythm*, 10, 1671-5.
- KIRCHHOF, P., ENGELEN, M., FRANZ, M. R., RIBBING, M., WASMER, K., BREITHARDT, G., HAVERKAMP, W. & ECKARDT, L. 2005. Electrophysiological effects of flecainide and sotalol in the human atrium during persistent atrial fibrillation. *Basic Research in Cardiology*, 100, 112-21.
- KIRICHOK, Y., KRAPIVINSKY, G. & CLAPHAM, D. E. 2004. The mitochondrial calcium uniporter is a highly selective ion channel. *Nature*, 427, 360-4.
- KIRK, M. M., IZU, L. T., CHEN-IZU, Y., MCCULLE, S. L., WIER, W. G., BALKE, C. W. & SHOROFKY, S. R. 2003. Role of the transverse-axial tubule system in generating calcium sparks and calcium transients in rat atrial myocytes. *Journal of Physiology*, 547, 441-51.
- KNOLLMANN, B. C., CHOPRA, N., HLAING, T., AKIN, B., YANG, T., ETTENSOHN, K., KNOLLMANN, B. E., HORTON, K. D., WEISSMAN, N. J., HOLINSTAT, I., ZHANG, W., RODEN, D. M., JONES, L. R., FRANZINI-ARMSTRONG, C. & PFEIFER, K. 2006. Casq2 deletion causes sarcoplasmic reticulum volume increase, premature Ca²⁺ release, and catecholaminergic polymorphic ventricular tachycardia. *The Journal of Clinical Investigation*, 116, 2510-20.
- KOBAYASHI, Y. M., ALSEIKHAN, B. A. & JONES, L. R. 2000. Localization and characterization of the calsequestrin-binding domain of triadin 1. Evidence for a charged beta-strand in mediating the protein-protein interaction. *Journal of Biological Chemistry*, 275, 17639-46.
- KOMETANI, T. & KASAI, M. 1978. Ionic permeability of sarcoplasmic reticulum vesicles measured by light scattering method. *Journal of Membrane Biology*, 41, 295 - 308.
- KORECKY, B. & RAKUSAN, K. 1978. Normal and hypertrophic growth of the rat heart: changes in cell dimensions and number. *American Journal of Physiology*, 234, H123-8.

- KORT, A. A., CAPOGROSSI, M. C. & LAKATTA, E. G. 1985. Frequency, amplitude and propagation velocity of spontaneous calcium dependent contractile waves in intact adult rat cardiac myocyte and isolated myocytes. *Circulation Research*, 57, 844 - 855.
- KRAHN, A. D., GOLLOB, M., YEE, R., GULA, L. J., SKANES, A. C., WALKER, B. D. & KLEIN, G. J. 2005. Diagnosis of unexplained cardiac arrest: role of adrenaline and procainamide infusion. *Circulation*, 112, 2228-34.
- KRISHNAN, S. C. & ANTZELEVITCH, C. 1991. Sodium channel block produces opposite electrophysiological effects in canine ventricular epicardium and endocardium. *Circulation Research*, 69, 277-91.
- KRISHNAN, S. C. & ANTZELEVITCH, C. 1993. Flecainide-induced arrhythmia in canine ventricular epicardium. Phase 2 reentry? *Circulation*, 87, 562-72.
- KUSTER, G. M., LANCEL, S., ZHANG, J., COMMUNAL, C., TRUCILLO, M. P., LIM, C. C., PFISTER, O., WEINBERG, E. O., COHEN, R. A., LIAO, R., SIWIK, D. A. & COLUCCI, W. S. 2010. Redox-mediated reciprocal regulation of SERCA and Na⁺-Ca²⁺ exchanger contributes to sarcoplasmic reticulum Ca²⁺ depletion in cardiac myocytes. *Free Radical Biology and Medicine*, 48, 1182-7.
- KUZNETSOV, A. V., SCHNEEBERGER, S., SEILER, R., BRANDACHER, G., MARK, W., STEURER, W., SAKS, V., USSON, Y., MARGREITER, R. & GNAIGER, E. 2004. Mitochondrial defects and heterogeneous cytochrome c release after cardiac cold ischemia and reperfusion. *Am J Physiol Heart Circ Physiol*, 286, H1633-41.
- LAFUENTE-LAFUENTE, C., VALEMBOSIS, L., BERGMANN, J. F. & BELMIN, J. 2015. Antiarrhythmics for maintaining sinus rhythm after cardioversion of atrial fibrillation. *Cochrane Database System Review*, Cd005049.
- LASKOWSKI, M., AUGUSTYNEK, B., KULAWIAK, B., KOPROWSKI, P., BEDNARCZYK, P., JARMUSZKIEWICZ, W. & SZEWCZYK, A. 2016. What do we not know about mitochondrial potassium channels? *Biochimica et Biophysica ACTA*, 1857, 1247 - 1257.
- LATINI, R., CAVALLI, A., MAGGIONI, A. P. & VOLPI, A. 1987. Flecaïnide distribution in human tissues. *British Journal of Clinical Pharmacology*, 24, 820 - 822.
- LAVIER, D. & LAMB, G. D. 1998. Inactivation of calcium release channels (ryanodine receptors RyR1 and RyR2) with rapid steps in calcium concentration and voltage. *Biophysical Journal*, 74, 2352 - 2364.
- LAVIER, D. R. 2007. Ca²⁺ stores regulate ryanodine receptor Ca²⁺ release channels via luminal and cytosolic Ca²⁺ sites. *Biophysical Journal*, 92, 3541-55.
- LAVIER, D. R., BAYNES, T. M. & DULHUNTY, A. F. 1997. Magnesium inhibition of ryanodine-receptor calcium channels: evidence for two independent mechanisms. *J Membr Biol*, 156, 213-29.
- LAVIER, D. R. & HONEN, B. N. 2008. Luminal Mg²⁺, a key factor controlling RYR2-mediated Ca²⁺ release: cytoplasmic and luminal regulation modeled in a tetrameric channel. *J Gen Physiol*, 132, 429-46.
- LAVIER, D. R. & VAN HELDEN, D. F. 2011. Three independent mechanisms contribute to tetracaine inhibition of cardiac calcium release channels. *J Mol Cell Cardiol*, 51, 357-69.
- LAYLAND, J. & KENTISH, J. C. 1999. Positive force- and [Ca²⁺]_i-frequency relationships in rat ventricular trabeculae at physiological frequencies. *American Journal of Physiology*, 276, H9-h18.
- LEREN, I. S., SABERNIAK, J., MAJID, E., HALAND, T. F., EDVARSDEN, T. & HAUGAA, K. H. 2016. Nadolol decreases the incidence and severity of ventricular arrhythmias during exercise stress testing compared with beta1-selective beta-blockers in patients with catecholaminergic polymorphic ventricular tachycardia. *Heart Rhythm*, 13, 433-40.
- LEROUX, F. R., MANTEAU, B. & VORS, J.-P. 2008. Trifluoromethyl ethers - synthesis and properties of an unusual substituent. *Beilstein Journal of Organic Chemistry*, 4.
- LEYTON-MANGE, J. S., MILLS, R. W., MACRI, V. S., JANG, M. Y., BUTTE, F. N., ELLINOR, P. T. & MILAN, D. J. 2014. Rapid cellular phenotyping of human pluripotent stem cell-derived

- cardiomyocytes using a genetically encoded fluorescent voltage sensor. *Stem Cell Reports*, 2, 163-70.
- LI, L., DESANTIAGO, J., CHU, G., KRANIAS, E. G. & BERS, D. M. 2000. Phosphorylation of phospholamban and troponin I in beta-adrenergic-induced acceleration of cardiac relaxation. *American Journal of Physiology: Heart and Circulation Physiology*, 278, H769-79.
- LI, L., MIRZA, S., RICHARDSON, S. J., GALLANT, E. M., THEKKEDAM, C., PACE, S. M., ZORZATO, F., LIU, D., BEARD, N. A. & DULHUNTY, A. F. 2015. A new cytoplasmic interaction between junctin and ryanodine receptor Ca²⁺ release channels. *J Cell Sci*, 128, 951-63.
- LI, X., HUSTON, E., LYNCH, M. J., HOUSLAY, M. D. & BAILLIE, G. S. 2006. Phosphodiesterase-4 influences the PKA phosphorylation status and membrane translocation of G-protein receptor kinase 2 (GRK2) in HEK-293beta2 cells and cardiac myocytes. *Biochem J*, 394, 427-35.
- LI, Y., KRANIAS, E. G., MIGNERY, G. A. & BERS, D. M. 2002. Protein kinase A phosphorylation of the ryanodine receptor does not affect calcium sparks in mouse ventricular myocytes. *Circ Res*, 90, 309-16.
- LIEVE, K. V., WILDE, A. A. & VAN DER WERF, C. 2016. The Role of Flecainide in the Management of Catecholaminergic Polymorphic Ventricular Tachycardia. *Arrhythmia and Electrophysiology Review*, 5, 45-9.
- LIPP, P. & BOOTMAN, M. D. 1997. To quark or to spark, that is the question. *Journal of Physiology*, 502 (Pt 1), 1.
- LIU, H., ATKINS, J. & KASS, R. S. 2003. Common molecular determinants of flecainide and lidocaine block of heart sodium channels: Evidence from experiments with neutral and quaternary flecainide analogues. *The Journal of General Physiology*, 121, 199-214.
- LIU, N., COLOMBI, B., MEMMI, M., ZISSIMOPOULOS, S., RIZZI, N., NEGRI, S., IMBRIANI, M., NAPOLITANO, C., LAI, F. A. & PRIORI, S. G. 2006. Arrhythmogenesis in catecholaminergic polymorphic ventricular tachycardia: insights from a RyR2 R4496C knock-in mouse model. *Circulation Research*, 99, 292-8.
- LIU, N., DENEGRI, M., RUAN, Y., AVELINO-CRUZ, J. E., PERISSI, A., NEGRI, S., NAPOLITANO, C., COETZEE, W. A., BOYDEN, P. A. & PRIORI, S. G. 2011. Short communication: flecainide exerts an antiarrhythmic effect in a mouse model of catecholaminergic polymorphic ventricular tachycardia by increasing the threshold for triggered activity. *Circulation Research*, 109, 291-5.
- LIU, Q.-Y. & STRAUSS, H. 1991. Blockade of cardiac sarcoplasmic reticulum potassium channel by Ca: Two binding-site model of blockade. *Biophysical Journal*, 60, 198 - 203.
- LIU, Y., KIMLICKA, L., HIESS, F., TIAN, X., WANG, R., ZHANG, L., JONES, P. P., VAN PETEGEM, F. & CHEN, S. R. 2013a. The CPVT-associated RyR2 mutation G230C enhances store overload-induced Ca²⁺ release and destabilizes the N-terminal domains. *Biochem J*, 454, 123-31.
- LIU, Y., KIMLICKA, L., HIESS, F., TIAN, X., WANG, R., ZHANG, L., JONES, P. P., VAN PETEGEM, F. & CHEN, S. R. 2013b. The CPVT-associated RyR2 mutation G230C enhances store overload-induced Ca²⁺ release and destabilizes the N-terminal domains. *Biochemical Journal*, 454, 123-31.
- LIU, Z., WANG, R., TIAN, X., ZHONG, X., GANGOPADHYAY, J., COLE, R., IKEMOTO, N., CHEN, S. R. & WAGENKNECHT, T. 2010. Dynamic, inter-subunit interactions between the N-terminal and central mutation regions of cardiac ryanodine receptor. *J Cell Sci*, 123, 1775-84.
- LIU, Z., ZHANG, J., LI, P., CHEN, S. R. & WAGENKNECHT, T. 2002. Three-dimensional reconstruction of the recombinant type 2 ryanodine receptor and localization of its divergent region 1. *Journal of Biological Chemistry*, 277, 46712-9.
- LJUBOJEVIC, S. & BERS, D. M. 2015. Nuclear calcium in cardiac myocytes. *Journal of Cardiovascular Pharmacology*, 65, 211-7.

- LOGOTHETIS, D. E., KURACHI, Y., GALPER, J., NEER, E. J. & CLAPHAM, D. E. 1987. The beta gamma subunits of GTP-binding proteins activate the muscarinic K⁺ channel in heart. *Nature*, 325, 321-6.
- LOUCH, W. E., MORK, H. K., SEXTON, J., STROMME, T. A., LAAKE, P., SJAASTAD, I. & SEJERSTED, O. M. 2006. T-tubule disorganization and reduced synchrony of Ca²⁺ release in murine cardiomyocytes following myocardial infarction. *Journal of Physiology*, 574, 519-33.
- LOUGHREY, C. M., MACEACHERN, K. E., NEARY, P. & SMITH, G. L. 2002. The relationship between intracellular [Ca²⁺] and Ca²⁺ wave characteristics in permeabilised cardiomyocytes from the rabbit. *Journal of Physiology*, 543, 859-70.
- LU, L., XIA, L. & ZHU, X. 2012. Simulation of arrhythmogenic effect of rogue RyRs in failing heart by using a coupled model. *Comput Math Methods Med*, 2012, 183978.
- LUKYANENKO, V., GYORKE, I. & GYORKE, S. 1996. Regulation of calcium release by calcium inside the sarcoplasmic reticulum in ventricular myocytes. *European Journal of Physiology*, 432, 1047 - 1054.
- LUKYANENKO, V. & GYORKE, S. 1999. Ca²⁺ sparks and Ca²⁺ waves in saponin-permeabilized rat ventricular myocytes. *Journal of Physiology*, 521 Pt 3, 575-85.
- LUKYANENKO, V., SUBRAMANIAN, S., GYORKE, I., WIESNER, T. F. & GYORKE, S. 1999. The role of luminal Ca²⁺ in the generation of Ca²⁺ waves in rat ventricular myocytes. *Journal of Physiology*, 518, 173-86.
- LUKYANENKO, V., VIATCHENKO-KARPINSKI, S., SMIRNOV, A., WIESNER, T. F. & GYORKE, S. 2001. Dynamic regulation of sarcoplasmic reticulum Ca²⁺ content and release by luminal Ca²⁺-sensitive leak in rat ventricular myocytes. *Biophysical Journal*, 81, 785-98.
- MACKIEWICZ, U. & LEWARTOWSKI, B. 2006. Temperature dependent contribution of Ca²⁺ transporters to relaxation in cardiac myocytes: important role of sarcolemmal Ca²⁺-ATPase. *J Physiol Pharmacol*, 57, 3-15.
- MADEJA, M., STEFFEN, W., MESIC, I., GARIC, B. & ZHOROV, B. S. 2010. Overlapping binding sites of structurally different antiarrhythmics flecainide and propafenone in the subunit interface of potassium channel Kv2.1. *The Journal of Biological Chemistry*, 285, 33898 - 33905.
- MAIER, L. S., ZIOLO, M. T., BOSSUYT, J., PERSECHINI, A., MESTRIL, R. & BERS, D. M. 2006. Dynamic changes in free Ca-calmodulin levels in adult cardiac myocytes. *Journal of Molecular and Cellular Cardiology*, 41, 451-8.
- MANO, Y., ASAKAWA, Y., KITA, K., ISHII, T., HOTTA, K. & KUSANO, K. 2015. Validation of an ultra-performance liquid chromatography-tandem mass spectrometry method for the determination of flecainide in human plasma and its clinical application. *Biomedical Chromatography*, 29, 1399-405.
- MANTZIARI, L., VASSILIKOS, V., ANASTASAKIS, A., KOTSAKA, X., PARASKEVAIDIS, S., STYLIADIS, I. H. & LURIA, D. 2013. A de novo novel cardiac ryanodine mutation (Ser4155Tyr) associated with catecholaminergic polymorphic ventricular tachycardia. *Annals of Noninvasive Electrocardiology*, 18, 571-6.
- MARJAMAA, A., LAITINEN-FORSBLOM, P., WRONSKA, A., TOIVONEN, L., KONTULA, K. & SWAN, H. 2011. Ryanodine receptor (RyR2) mutations in sudden cardiac death: studies in extended pedigrees and phenotypic characterization in vitro. *International Journal of Cardiology*, 147, 246-52.
- MARKS, A. R., PRIORI, S., MEMMI, M., KONTULA, K. & LAITINEN, P. J. 2002. Involvement of the cardiac ryanodine receptor/calcium release channel in catecholaminergic polymorphic ventricular tachycardia. *Journal of Cell Physiology*, 190, 1-6.
- MARX, S. O., REIKEN, S., HISAMATSU, Y., JAYARAMAN, T., BURKHOFF, D., ROSEMBLIT, N. & MARKS, A. R. 2000. PKA phosphorylation dissociates FKBP12.6 from the calcium release channel (ryanodine receptor): defective regulation in failing hearts. *Cell*, 101, 365-76.

- MASON, F. E. & SOSSALLA, S. 2016. The Significance of the Late Na⁺ Current for Arrhythmia Induction and the Therapeutic Antiarrhythmic Potential of Ranolazine. *Journal of Cardiovascular Pharmacology and Therapeutics*.
- MATSUDA, H. 1996. Rubidium, caesium ions and the inwardly rectifying potassium channels in guinea-pig ventricular cells. *European Journal of Physiology*, 432, 26 - 33.
- MATSUYAMA, T. A., HO, S. Y., MCCARTHY, K. P., UEDA, A., MAKIMOTO, H., SATOMI, K., KAMAKURA, S., INOUE, S. & ISHIBASHI-UEDA, H. 2012. Anatomic assessment of variations in myocardial approaches to the atrioventricular node. *Journal of Cardiovascular Electrophysiology*, 23, 398-403.
- MATSUYAMA, T. A., TANAKA, H., ADACHI, T., JIANG, Y., ISHIBASHI-UEDA, H. & TAKAMATSU, T. 2013. Intrinsic left atrial histoanatomy as the basis for reentrant excitation causing atrial fibrillation/flutter in rats. *Heart Rhythm*, 10, 1342-8.
- MAYAMA, T., MATSUMURA, K., LIN, H., OGAWA, K. & IMANAGA, I. 2007. Remodelling of cardiac gap junction connexin 43 and arrhythmogenesis. *Experimental and Clinical Cardiology*, 12, 67-76.
- MCBRIDE, B. F., YANG, T., LIU, K., URBAN, T. J., GIACIMINI, K. M., KIM, R. B. & RODEN, D. M. 2009. The organic cation transporter, OCTN1, expressed in the human heart potentiates antagonism of the HERG potassium channel. *Journal of Cardiovascular Pharmacology*, 54, 63 - 71.
- MCCALL, E., HRYSHKO, L. V., STIFFEL, V. M., CHRISTENSEN, D. M. & BERS, D. M. 1996. Possible functional linkage between the cardiac dihydropyridine and ryanodine receptor: acceleration of rest decay by Bay K 8644. *J Mol Cell Cardiol*, 28, 79-93.
- MCMORN, S. O., HARRISON, S. M., ZANG, W. J., YU, X. J. & BOYETT, M. R. 1993. A direct negative inotropic effect of acetylcholine on rat ventricular myocytes. *Am J Physiol*, 265, H1393-400.
- MEAD-SAVERY, F. C., WANG, R., TANNA-TOPAN, B., WAYNE CHEN, S. R., WELCH, W. & WILLIAMS, A. J. 2009. Changes in negative charge at the luminal mouth of the pore alter ion handling and gating in the cardiac ryanodine-receptor. *Biophysical Journal*, 96, 1374 - 1387.
- MEDEIROS-DOMINGO, A., BHUIYAN, Z. A., TESTER, D. J., HOFMAN, N., BIKKER, H., VAN TINTELEN, J. P., MANNENS, M. M., WILDE, A. A. & ACKERMAN, M. J. 2009. The RYR2-encoded ryanodine receptor/calcium release channel in patients diagnosed previously with either catecholaminergic polymorphic ventricular tachycardia or genotype negative, exercise-induced long QT syndrome: a comprehensive open reading frame mutational analysis. *Journal of the American College of Cardiology*, 54, 2065-74.
- MEISSNER, G. 1983. Monovalent ion and calcium ion fluxes in sarcoplasmic reticulum. *Molecular and Cellular Biochemistry*, 55, 62 - 82.
- MELGARI, D., EL HARACHI, A., ZHANG, Y., DEMPSEY, C. E. & HANCOX, J. C. Identification of the flecainide binding site on the hERG potassium channel. Physiological Society Annual Meeting, 2015a Cardiff, UK. Proceedings of the Physiological Society.
- MELGARI, D., ZHANG, Y., EL HARCHI, A., DEMPSEY, C. E. & HANCOX, J. C. 2015b. Molecular basis of hERG potassium channel blockade by the class Ic antiarrhythmic flecainide. *Journal of Molecular and Cellular Cardiology*, 86, 42-53.
- MIKI, M., MAKIMURA, S., SUGAHARA, Y., YAMADA, R., BUNYA, M., SAITOH, T. & TOBITA, H. 2012. A three-dimensional FRET analysis to construct an atomic model of the actin-tropomyosin-troponin core domain complex on a muscle thin filament. *Journal of Molecular Biology*, 420, 40-55.
- MIRO-CASAS, E., RUIZ-MEANA, M., AGULLO, E., STAHLHOFEN, S., RODRIGUEZ-SINOVAS, A., CABESTRERO, A., JORGE, I., TORRE, I., VAZQUEZ, J., BOENGLER, K., SCHULZ, R., HEUSCH, G. & GARCIA-DORADO, D. 2009. Connexin43 in cardiomyocyte mitochondria contributes to mitochondrial potassium uptake. *Cardiovasc Research*, 83, 747-56.
- MISHIMA, M., UEDA, M., TAKAO, A., INABA, A., KAMIYA, K., MORIKI, H., KIRIYA, H., TAGUCHI, M. & YUZURIHA, T. 1999. Studies on the metabolic fate of flecainide acetate: Blood

- levels, distribution, metabolism and excretion in rats after IV administration. *Drug Metabolism and Pharmacokinetics*, 14, 201-213.
- MITCHELL, R. D., SIMMERMAN, H. K. & JONES, L. R. 1988. Ca²⁺ binding effects on protein conformation and protein interactions of canine cardiac calsequestrin. *The Journal of Biological Chemistry*, 263, 1376-81.
- MOHLER, P. J., RIVOLTA, I., NAPOLITANO, C., LEMAILLET, G., LAMBERT, S., PRIORI, S. G. & BENNETT, V. 2004. Nav1.5 E1053K mutation causing Brugada syndrome blocks binding to ankyrin-G and expression of Nav1.5 on the surface of cardiomyocytes. *Proceedings of the National Academy of Sciences*, 101, 17533 - 17538.
- MOREAU, D., CLAUW, F., MARTINE, L., GRYNBERG, A., ROCHETTE, L. & DEMAISON, L. 1999. Effects of amiodarone on cardiac function and mitochondrial oxidative phosphorylation during ischemia and reperfusion. *Molecular and Cellular Biochemistry*, 194, 291-300.
- MORRIS, G. M., HUEY, R., LINDSTROM, W., SANNER, M. F., BELEW, R. K., GOODSSELL, D. S. & OLSON, A. J. 2009. AutoDock4 and AutoDockTools4: Automated docking with selective receptor flexibility. *Journal of Computational Chemistry*, 30, 2785-91.
- MOSS, A. J., WINDLE, J. R., HALL, W. J., ZAREBA, W., ROBINSON, J. L., MCNITT, S., SEVERSKI, P., ROSERO, S., DAUBERT, J. P., QI, M., CIECIORKA, M. & MANALAN, A. S. 2005. Safety and efficacy of flecainide in subjects with Long QT-3 syndrome (DeltaKPQ mutation): a randomized, double-blind, placebo-controlled clinical trial. *Annals of Noninvasive Electrocardiology*, 10, 59-66.
- MUKHERJEE, R., CRAWFORD, F. A., HEWETT, K. W. & SPINALE, F. G. 1993. Cell and sarcomere contractile performance from the same cardiocyte using video microscopy. *Journal of Applied Physiology*, 74, 2023-33.
- MURPHY, M. P. 2009. How mitochondria produce reactive oxygen species. *Biochemical Journal*, 417, 1-13.
- MYLES, R. C., WANG, L., KANG, C., BERS, D. M. & RIPPLINGER, C. M. 2012. Local beta-adrenergic stimulation overcomes source-sink mismatch to generate focal arrhythmia. *Circulation Research*, 110, 1454-64.
- NÄBAUER, M., CALLEWAERT, G., CLEEMANN, L. & MORAD, M. 1989. Regulation of calcium release is gated by calcium current, not gating charge, in cardiac myocytes. *Science*, 244, 800-3.
- NAG, A. C. 1980. Study of non-muscle cells of the adult mammalian heart: a fine structural analysis and distribution. *Cytobios*, 28, 41-61.
- NAGATOMO, T., JANUARY, C. T. & MAKIELSKI, J. C. 2000. Preferential block of late sodium current in the LQT3 DeltaKPQ mutant by the class I(C) antiarrhythmic flecainide. *Molecular Pharmacology*, 57, 101-7.
- NAGY, Z. A., VIRAG, L., TOTH, A., BILICZKI, P., ACSAI, K., BANYASZ, T., NANASI, P., PAPP, J. G. & VARRO, A. 2004. Selective inhibition of sodium-calcium exchanger by SEA-0400 decreases early and delayed after depolarization in canine heart. *British Journal of Pharmacology*, 143, 827-31.
- NAIR, K., UMAPATHY, K., FARID, T., MASSE, S., MUELLER, E., SIVANANDAN, R. V., POKU, K., RAO, V., NAIR, V., BUTANY, J., IDEKER, R. E. & NANTHAKUMAR, K. 2011. Intramural activation during early human ventricular fibrillation. *Circulation: Arrhythmia and Electrophysiology*, 4, 692-703.
- NAM, G. B., BURASHNIKOV, A. & ANTZELEVITCH, C. 2005. Cellular mechanisms underlying the development of catecholaminergic ventricular tachycardia. *Circulation*, 111, 2727-33.
- NAPOLITANO, C., PRIORI, G. P. & BLOISE, R. 2016. *Catecholaminergic Polymorphic Ventricular Tachycardia*, Seattle (WA), University of Washington, Seattle.
- NAPOLITANO, C., PRIORI, S. G. & BLOISE, R. 1993. Catecholaminergic Polymorphic Ventricular Tachycardia. In: PAGON, R. A., ADAM, M. P., ARDINGER, H. H., WALLACE, S. E., AMEMIYA, A., BEAN, L. J. H., BIRD, T. D., LEDBETTER, N., MEFFORD, H. C., SMITH, R. J. H. & STEPHENS, K. (eds.) *Gene Reviews*. Seattle (WA): University of Washington, Seattle

- NEGASH, S., YAO, Q., SUN, H., LI, J., BIGELOW, D. J. & SQUIER, T. C. 2000. Phospholamban remains associated with the Ca²⁺- and Mg²⁺-dependent ATPase following phosphorylation by cAMP-dependent protein kinase. *Biochemical Journal*, 351, 195-205.
- NENASHEVA, T. A., NEARY, M., MASHANOV, G. I., BIRDSALL, N. J., BRECKENRIDGE, R. A. & MOLLOY, J. E. 2013. Abundance, distribution, mobility and oligomeric state of M(2) muscarinic acetylcholine receptors in live cardiac muscle. *Journal of Molecular and Cellular Cardiology*, 57, 129-36.
- NERBONNE, J. M. & KASS, R. S. 2005. Molecular physiology of cardiac repolarization. *Physiological Review*, 85, 1205-53.
- NETTER, F. 2014. Atlas of Human Anatomy. Saunders.
- NICHOLS, A. J., SULPIZIO, A. C., ASHTON, D. J., HIEBLE, J. P. & RUFFOLO, R. R., JR. 1989. The interaction of the enantiomers of carvedilol with alpha 1- and beta 1-adrenoceptors. *Chirality*, 1, 265-70.
- NIGRO, M., ARRUDA, A. P. & DE MEIS, L. 2009. Ca²⁺ transport and heat production in vesicles derived from the sarcoplasmic reticulum terminal cisternae: regulation by K⁺. *Biochimica et Biophysica ACTA*, 1788, 1517-22.
- NING, W. & WIT, A. L. 1983. Comparison of the direct effects of nifedipine and verapamil on the electrical activity of the sinoatrial and atrioventricular nodes of the rabbit heart. *Am Heart J*, 106, 345-55.
- NITTA, J., SUNAMI, A., MARUMO, F. & HIRAOKA, M. 1992. States and sites of actions of flecainide on guinea-pig cardiac sodium channels. *European Journal of Pharmacology*, 214, 191 - 197.
- NOJIMA, S., KOBUCHI, H., SAIBARA, T., YASUDA, T. & UTSUMI, K. 1995. Selective inhibition of human TNF-alpha action by flecainide acetate, an antiarrhythmic drug. *Physiol Chem Phys Med NMR*, 27, 77-89.
- NYEGAARD, M., OVERGAARD, M. T., SONDERGAARD, M. T., VRANAS, M., BEHR, E. R., HILDEBRANDT, L. L., LUND, J., HEDLEY, P. L., CAMM, A. J., WETTRELL, G., FOSDAL, I., CHRISTIANSEN, M. & BORGLUM, A. D. 2012. Mutations in calmodulin cause ventricular tachycardia and sudden cardiac death. *The American Journal of Human Genetics*, 91, 703-12.
- O'LEARY, M. E., CHEN, L. Q., KALLEN, R. G. & HORN, R. 1995. A molecular link between activation and inactivation of sodium channels. *J Gen Physiol*, 106, 641-58.
- ODA, T., YANG, Y., NITU, F. R., SVENSSON, B., LU, X., FRUEN, B. R., CORNEA, R. L. & BERS, D. M. 2013a. In cardiomyocytes, binding of unzipping peptide activates ryanodine receptor 2 and reciprocally inhibits calmodulin binding. *Circ Res*, 112, 487-97.
- ODA, T., YANG, Y., NITU, F. R., SVENSSON, B., LU, X., FRUEN, B. R., CORNEA, R. L. & BERS, D. M. 2013b. In cardiomyocytes, binding of unzipping peptide activates ryanodine receptor 2 and reciprocally inhibits calmodulin binding. *Circulation Research*, 112, 487-97.
- OGRODNIK, J. & NIGGLI, E. 2010. Increased calcium leak and spatiotemporal coherence of calcium release in cardiomyocytes during beta adrenergic stimulation. *Journal of Physiology*, 588, 225 - 242.
- OLIVETTI, G., CIGOLA, E., MAESTRI, R., CORRADI, D., LAGRASTA, C., GAMBERT, S. R. & ANVERSA, P. 1996. Aging, cardiac hypertrophy and ischemic cardiomyopathy do not affect the proportion of mononucleated and multinucleated myocytes in the human heart. *Journal of Molecular and Cellular Cardiology*, 28, 1463-77.
- OLSON, B. J. & MARKWELL, J. 2007. Assays for determination of protein concentration. *Current Protocols of Pharmacology*, Appendix 3, 3A.
- OO, Y. W., GOMEZ-HURTADO, N., WALWEEL, K., VAN HELDEN, D. F., IMTIAZ, M. S., KNOLLMANN, B. C. & LAVER, D. R. 2015a. Essential Role of Calmodulin in RyR Inhibition by Dantrolene. *Molecular Pharmacology*, 88, 57-63.

- OO, Y. W., GOMEZ-HURTADO, N., WALWEEL, K., VAN HELDEN, D. F., IMTIAZ, M. S., KNOLLMANN, B. C. & LAVER, D. R. 2015b. Essential Role of Calmodulin in RyR Inhibition by Dantrolene. *Mol Pharmacol*, 88, 57-63.
- OPIE, L. H. 2004. *Heart physiology: From cell to circulation*, Lippincott Williams & Wilkins.
- ORCHARD, C. H., SMITH, G. L. & STEELE, D. S. 1998. Effects of cytosolic Ca²⁺ on the Ca²⁺ content of the sarcoplasmic reticulum in saponin-permeabilized rat ventricular trabeculae. *European Journal of Pharmacology*, 435, 555-63.
- OTSU, K., FUJII, J., PERIASAMY, M., DIFILIPPANTONIO, M., UPPENDER, M., WARD, D. C. & MACLENNAN, D. H. 1993. Chromosome mapping of five human cardiac and skeletal muscle sarcoplasmic reticulum protein genes. *Genomics*, 17, 507-9.
- OVALLE, W. K. & NAHIRNEY, P. C. 2013. *Netter's Essential Histology E-Book*. Elsevier Health Sciences.
- OVEREND, C. L., EISNER, D. A. & O'NEILL, S. C. 1997. The effect of tetracaine on spontaneous Ca²⁺ release and sarcoplasmic reticulum calcium content in rat ventricular myocytes. *Journal of Physiology*, 502 (Pt 3), 471-9.
- PAGE, E., MCCALLISTER, L. P. & POWER, B. 1971. Stereological measurements of cardiac ultrastructures implicated in excitation-contraction coupling. *Proceedings of the National Academy of Sciences*, 68, 1465-6.
- PALMIERI, F. & PIERRI, C. L. 2010. Mitochondrial metabolite transport. *Biochemical Society: Essays in Biochemistry*, 47, 37 - 52.
- PAN, D., HU, Z., QIU, F., HUANG, Z.-L., MA, Y., WANG, Y., QIN, L., ZHANG, Z., ZENG, S. & ZHANG, Y.-H. 2014. A general strategy for developing cell-permeable photo-modulatable organic fluorescent probes for live-cell super-resolution imaging. *Nature Communications*, 5, 1 - 8.
- PARK, H., WU, S., DUNKER, A. K. & KANG, C. 2003. Polymerization of calsequestrin. Implications for Ca²⁺ regulation. *Journal of Biological Chemistry*, 278, 16176-82.
- PARK, K.-S., I, J., PAK, Y. K., BAE, S.-W., RHIM, H., SUH, S.-H., PARK, S. J., ZHU, M. H., SO, I. & KIM, W. K. 2002. FCCP Depolarises plasma membrane potential by activating proton and sodium current in bovine aortic endothelial cells. *European Journal of Physiology*, 443, 344 - 352.
- PATLAK, J. 1991. Molecular kinetics of voltage-dependent Na⁺ channels. *Physiological Review*, 71, 1047-80.
- PAUL, A. A., WITCHEL, H. J. & HANCOX, J. C. 2002. Inhibition of the current of heterologously expressed HERG potassium channels by flecainide and comparison with quinidine, propafenone and lignocaine. *Br J Pharmacol*, 136, 717-29.
- PAVLOVIC, D., MCLATCHIE, L. M. & SHATTOCK, M. J. 2010. The rate of loss of T-tubules in cultured adult ventricular myocytes is species dependent. *Experimental Physiology*, 95, 518-27.
- PAZDERNIK, T. L. & KERECSEN, L. 2007. *Rapid Review Pharmacology*, Philadelphia, USA, Mosby Elsevier.
- PEETERS, G. A., SANGUINETTI, M. C., EKI, Y., KONARZEWSKA, H., RENLUND, D. G., KARWANDE, S. V. & BARRY, W. H. 1995. Method for isolation of human ventricular myocytes from single endocardial and epicardial biopsies. *American Journal of Physiology*, 268, H1757-64.
- PERRY, S. W., NORMAN, J. P., BARBIERI, J., BROWN, E. B. & GELBARD, H. A. 2011. Mitochondrial membrane potential probes and the proton gradient: a practical usage guide. *Biotechniques*, 50, 98 - 115.
- PETROVIC, P., VALENT, I., COCHEROVA, E., PAVELKOVA, J. & ZAHRADNIKOVA, A. 2015. Ryanodine receptor gating controls generation of diastolic calcium waves in cardiac myocytes. *Journal of General Physiology*, 145, 489-511.
- PFLAUMER, A. & DAVIS, A. M. 2012. Guidelines for the diagnosis and management of Catecholaminergic Polymorphic Ventricular Tachycardia. *Heart Lung and Circulation*, 21, 96-100.

- PICHT, E., ZIMA, A. V., BLATTER, L. A. & BERS, D. A. 2007. Sparkmaster: automated calcium spark analysis with ImageJ. *American Journal of Physiology: Cell Physiology*, 293, 1073 - 1081.
- PIESKE, B., MAIER, L. S., BERS, D. M. & HASENFUSS, G. 1999. Ca²⁺ handling and sarcoplasmic reticulum Ca²⁺ content in isolated failing and nonfailing human myocardium. *Circ Res*, 85, 38-46.
- PINALI, C., BENNETT, H., DAVENPORT, J. B., TRAFFORD, A. W. & KITMITTO, A. 2013. Three-dimensional reconstruction of cardiac sarcoplasmic reticulum reveals a continuous network linking transverse-tubules: this organization is perturbed in heart failure. *Circulation Research*, 113, 1219-30.
- PITT, S. J., PARK, K.-S., NISHI, M., URASHIMA, T., AOKI, S., YAMAZAKI, D., MA, J., TAKESHIMA, H. & SITSAPESAN, R. 2010. Charade of the SR potassium channel: Two ion channels, TRIC-A and TRIC-B masquerade as a single potassium channel. *Biophysical Journal*, 99, 417 - 426.
- PONICKE, K., HEINROTH-HOFFMANN, I. & BRODDE, O. E. 2003. Role of beta 1- and beta 2-adrenoceptors in hypertrophic and apoptotic effects of noradrenaline and adrenaline in adult rat ventricular cardiomyocytes. *Naunyn Schmiedebergs Archives of Pharmacology*, 367, 592-9.
- PORTA, M., ZIMA, A. V., NANI, A., DIAZ-SYLVESTER, P. L., COPELLO, J. A., RAMOS-FRANCE, J., BLATTER, L. A. & FILL, M. 2011. Single ryanodine receptor channel basis of caffeine's action on calcium sparks. *Biophysical Journal*, 100, 931 - 938.
- PORTELE, A., LENZ, J. & HOEFER, M. 1997. Estimation of membrane potential in reconstituted plasma membrane vesicles using a numerical model of oxonol VI distribution. *Journal of Bioenergetics and Biomembranes*, 29, 603 - 609.
- POSTMA, A. V., DENJOY, I., KAMBLOCK, J., ALDERS, M., LUPOGLAZOFF, J. M., VAKSMANN, G., DUBOSQ-BIDOT, L., SEBILLON, P., MANNENS, M. M., GUICHENEY, P. & WILDE, A. A. 2005. Catecholaminergic polymorphic ventricular tachycardia: RYR2 mutations, bradycardia, and follow up of the patients. *Journal of Medical Genetics*, 42, 863-70.
- POURAHMAD, J., SAJIMI, A. & SEYDI, E. 2015. Mitochondrial Targeting for Drug Development, Toxicology Studies - Cells, Drugs and Environment. In: CHRISTINA, A. (ed.). <http://www.intechopen.com/books/toxicology-studies-cells-drugs-and-environment/mitochondrial-targeting-for-drug-development>: InTech.
- PRIORI, S. G. & CHEN, S. R. 2011. Inherited dysfunction of sarcoplasmic reticulum Ca²⁺ handling and arrhythmogenesis. *Circ Res*, 108, 871-83.
- RADERMACHER, M., RAO, V., GRASSUCCI, R., FRANK, J., TIMERMAN, A. P., FLEISCHER, S. & WAGENKNECHT, T. 1994. Cryo-electron microscopy and three-dimensional reconstruction of the calcium release channel/ryanodine receptor from skeletal muscle. *Journal of Cell Biology*, 127, 411-23.
- RAJAMANI, S., LIU, G., EL-BIZRI, N., GUO, D., LI, C., CHEN, X. L., KAHLIG, K. M., MOLLOVA, N., ELZEIN, E., ZABLOCKI, J. & BELARDINELLI, L. 2016. The novel late Na⁺ current inhibitor, GS-6615 (eledazine) and its anti-arrhythmic effects in rabbit isolated heart preparations. *British Journal of Pharmacology*, 173, 3088-3098.
- RAMOS, E. & O'LEARY, M. E. 2004. State-dependent trapping of flecainide in the cardiac sodium channel. *Journal of Physiology*, 560, 37 - 49.
- REBBECK, R. T., NITU, F. R., ROHDE, D., MOST, P., BERS, D. M., THOMAS, D. D. & CORNEA, R. L. 2016. S100A1 Protein Does Not Compete with Calmodulin for Ryanodine Receptor Binding but Structurally Alters the Ryanodine Receptor-Calmodulin Complex. *Journal of Biological Chemistry*, 291, 15896-907.
- REDINGTON, A. N., GRAY, H. H., HODSON, M. E., RIGBY, M. L. & OLDERSHAW, P. J. 1988. Characterisation of the normal right ventricular pressure-volume relation by biplane angiography and simultaneous micromanometer pressure measurements. *British Heart Journal*, 59, 23-30.

- ROBINSON, P., CAPORIZZO, M. A., AHMADZADEH, H., BOGUSH, A. I., CHEN, C. Y., MARGULIES, K. B., SHENOY, V. B. & PROSSER, B. L. 2016. Detyrosinated microtubules buckle and bear load in contracting cardiomyocytes. *Science*, 352, 428 - 439.
- ROCCHETTI, M., SALA, L., RIZZETTO, R., STASZEWSKY, L. I., ALEMANNI, M., ZAMBELLI, V., RUSSO, I., BARILE, L., CORNAGHI, L., ALTOMARE, C., RONCHI, C., MOSTACCIUOLO, G., LUCCHETTI, J., GOBBI, M., LATINI, R. & ZAZA, A. 2014. Ranolazine prevents INaI enhancement and blunts myocardial remodelling in a model of pulmonary hypertension. *Cardiovascular Research*, 104, 37-48.
- ROOK, M. B., EVERS, M. M., VOS, M. A. & BIERHUIZEN, M. F. A. 2012. Biology of cardiac sodium channel Nav1.5 expression. *Cardiovascular Research*, 93, 12 - 23.
- ROSES-NOGUER, F., JARMAN, J. W., CLAGUE, J. R. & TILL, J. 2014. Outcomes of defibrillator therapy in catecholaminergic polymorphic ventricular tachycardia. *Heart Rhythm*, 11, 58-66.
- ROSSO, R., KALMAN, J. M., ROGOWSKI, O., DIAMANT, S., BIRGER, A., BINER, S., BELHASSEN, B. & VISKIN, S. 2007. Calcium channel blockers and beta-blockers versus beta-blockers alone for preventing exercise-induced arrhythmias in catecholaminergic polymorphic ventricular tachycardia. *Heart Rhythm*, 4, 1149-54.
- ROUX-BUISSON, N., CACHEUX, M., FOUREST-LIEUVIN, A., FAUCONNIER, J., BROCARD, J., DENJOY, I., DURAND, P., GUICHENEY, P., KYNDT, F., LEENHARDT, A., LE MAREC, H., LUCET, V., MABO, P., PROBST, V., MONNIER, N., RAY, P. F., SANTONI, E., TREMEAUX, P., LACAMPAGNE, A., FAURE, J., LUNARDI, J. & MARTY, I. 2012. Absence of triadin, a protein of the calcium release complex, is responsible for cardiac arrhythmia with sudden death in human. *Human Molecular Genetics*, 21, 2759-67.
- SAHARA, M., SATA, M., MORITA, T., NAKAMURA, K., HIRATA, Y. & NAGAI, R. 2007. Diverse contribution of bone marrow-derived cells to vascular remodeling associated with pulmonary arterial hypertension and arterial neointimal formation. *Circulation*, 115, 509-17.
- SAKA, S. K., HONIGMANN, A., EGGELING, C., HELL, S. W., LANG, T. & RIZZOLI, S. O. 2014. Multi-protein assemblies underlie the mesoscale organisation of the plasma membrane. *Nature Communications*, 5.
- SALAZAR-CANTU, A., PEREZ-TREVINO, P., MONTALVO-PARRA, D., BALDERAS-VILLALOBOS, J., GOMEZ-VIQUEZ, N. L., GARCIA, N. & ALTAMIRANO, J. 2016. Role of SERCA and the sarcoplasmic reticulum calcium content on calcium waves propagation in rat ventricular myocytes. *Archives of Biochemistry and Biophysics*, 604, 11-9.
- SANTIAGO, D. J., CURRAN, J. W., BERS, D. M., LEDERER, W. J., STERN, M. D., RIOS, E. & SHANNON, T. R. 2010. Ca sparks do not explain all ryanodine receptor-mediated SR Ca leak in mouse ventricular myocytes. *Biophysical Journal*, 98, 2111-20.
- SANTIAGO, D. J., RIOS, E. & SHANNON, T. R. 2013. Isoproterenol increases the fraction of spark-dependent RyR-mediated leak in ventricular myocytes. *Biophysical Journal*, 104, 976-85.
- SANTONASTASI, M. & WEHRENS, X. H. 2007. Ryanodine receptors as pharmacological targets for heart disease. *Acta Pharmacologica Sinica*, 28, 937-44.
- SAUCERMAN, J. J. & BERS, D. M. 2012. Calmodulin binding proteins provide domains of local Ca²⁺ signaling in cardiac myocytes. *Journal of Molecular and Cellular Cardiology*, 52, 312-6.
- SAVIO-GALIMBERTI, E., FRANK, J., INOUE, M., GOLDBABER, J. I., CANNELL, M. B., BRIDGE, J. H. & SACHSE, F. B. 2008. Novel features of the rabbit transverse tubular system revealed by quantitative analysis of three-dimensional reconstructions from confocal images. *Biophysical Journal*, 95, 2053-62.
- SAVIO-GALIMBERTI, E. & KNOLLMANN, B. C. 2011. Efficacy and potency of class I antiarrhythmic drugs for suppression of calcium waves in permeabilised myocytes lacking calsequestrin. *Journal of Molecular and Cellular Cardiology*, 51, 760 - 768.

- SAVIO-GALIMBERTI, E. & KNOLLMANN, B. C. 2015. Channel activity of cardiac ryanodine receptors (RyR2) determines potency and efficacy of flecainide and R-propafenone against arrhythmogenic calcium waves in ventricular cardiomyocytes. *Public Library of Science*, 10, e0131179.
- SCADUTO, R. C., JR. & GROTYOHANN, L. W. 1999. Measurement of mitochondrial membrane potential using fluorescent rhodamine derivatives. *Biophysical Journal*, 76, 469-77.
- SCHAMPAERT, S., VAN 'T VEER, M., RUTTEN, M. C., VAN TUIJL, S., DE HART, J., VAN DE VOSSE, F. N. & PIJLS, N. H. 2013. Autoregulation of coronary blood flow in the isolated beating pig heart. *Artificial Organs*, 37, 724-30.
- SCHLOTTHAUER, K. & BERS, D. M. 2000. Sarcoplasmic reticulum calcium release causes myocyte depolarisation. Underlying mechanism and threshold for triggered action potentials. *Circulation Research*, 87, 774 - 780.
- SCHNEIDER, C. A., RASBAND, W. S. & ELICEIRI, K. W. 2012. NIH Image to ImageJ: 25 years of image analysis. *Nature Methods*, 9, 671-675.
- SCHULZ, R. & DI LISA, F. 2016. Mitochondrial potassium homeostasis: a central player in cardioprotection. *Cardiovascular Research*, 110, 4-5.
- SCRIVEN, D. R., ASGHARI, P., SCHULSON, M. N. & MOORE, E. D. 2010. Analysis of Cav1.2 and ryanodine receptor clusters in rat ventricular myocytes. *Biophys J*, 99, 3923-9.
- SEIDEL, T., NAVANKASATTUSAS, S., AHMAD, A. A., DIAKOS, N. A., XU, W. D., TRISTANI-FIROUZI, M., BONIOS, M., TALEB, I., LI, D. Y., SELZMAN, C. H., DRAKOS, S. G. & SACHSE, F. B. 2017. Sheet-Like Remodeling of the Transverse Tubular System in Human Heart Failure Impairs Excitation-Contraction Coupling and Functional Recovery by Mechanical Unloading. *Circulation*.
- SEVERN-BIOTECH. 2016. RE: *Flecainide-FITC binding site*. Type to STEELE, D. S.
- SEVERS, N. J. 1982. Cholesterol distribution and structural differentiation in the sarcoplasmic reticulum of rat cardiac muscle cells. A freeze-fracture cytochemical investigation. *Cell Tissue Res*, 224, 613-24.
- SHANY, S., BERNHEIMER, A. W., GRUSHOFF, P. S. & KIM, K.-S. 1974. Evidence for membrane cholesterol as the common binding site for cereolysin, streptolysin O and saponin. *Molecular and Cellular Biochemistry*, 3, 179 - 186.
- SHATTOCK, M. J. & BERS, D. M. 1989. Rat vs. rabbit ventricle: Ca flux and intracellular Na assessed by ion-selective microelectrodes. *American Journal of Physiology*, 256, C813-22.
- SHIMIZU, H., SCHREDELSEKER, J., HUANG, J., LU, K., NAGHDI, S., LU, F., FRANKLIN, S., FUJI, H. D., WANG, K., ZHU, H., TIAN, C., LIN, B., NAKANO, H., EHRlich, A., NAKAI, J., STIEG, A. Z., GIMZEWSKI, J. K., NAKANO, A., GOLDHABER, J. I., VONDRISKA, T. M., HAJNOCZKY, G., KWON, O. & CHEN, J. N. 2015. Mitochondrial Ca(2+) uptake by the voltage-dependent anion channel 2 regulates cardiac rhythmicity. *Elife*, 4.
- SHKRYL, V. M. & BLATTER, L. A. 2013. Ca(2+) release events in cardiac myocytes up close: insights from fast confocal imaging. *Public Library of Science*, 8, e61525.
- SIEBERT, C. D., HANSICKE, A. & NAGEL, T. 2008. Stereochemical comparison of nebivolol with other beta-blockers. *Chirality*, 20, 103-9.
- SIKKEL, M. B., COLLINS, T. P., ROWLANDS, C., SHAH, M., O'GARA, P., WILLIAMS, A. J., HARDING, S. E., LYON, A. R. & MACLEOD, K. T. 2013. Flecainide reduces calcium spark and wave frequency via inhibition of the sarcolemmal sodium current. *Cardiovascular Research*, 98, 286-296.
- SIKORA, S. N. F. 2016. Wave velocity analysis tool. 1 ed.
- SITSAPESAN, R., MONTGOMERY, R. A., MACLEOD, K. T. & WILLIAMS, A. J. 1991. Sheep cardiac sarcoplasmic reticulum calcium-release channels: modification of conductance and gating by temperature. *J Physiol*, 434, 469-88.
- SITSAPESAN, R. & WILLIAMS, A. J. 1994a. Gating of the native and purified cardiac SR Ca(2+)-release channel with monovalent cations as permeant species. *Biophys J*, 67, 1484-94.

- SITSAPESAN, R. & WILLIAMS, A. J. 1994b. Regulation of the gating of the sheep cardiac sarcoplasmic reticulum Ca²⁺-release channel by luminal Ca²⁺. *J Membr Biol*, 137, 215-26.
- SMITH, A. J., LEWIS, F. C., AQUILA, I., WARING, C. D., NOCERA, A., AGOSTI, V., NADAL-GINARD, B., TORELLA, D. & ELLISON, G. M. 2014. Isolation and characterization of resident endogenous c-Kit⁺ cardiac stem cells from the adult mouse and rat heart. *Nature Protocols*, 9, 1662-81.
- SMITH, J. S., ROUSSEAU, E. & MEISSNER, G. 1989. Calmodulin modulation of single sarcoplasmic reticulum Ca²⁺-release channels from cardiac and skeletal muscle. *Circulation Research*, 64, 352-9.
- SOBIE, E. A., GUATIMOSIM, S., GOMEZ-VIQUEZ, L., SONG, L. S., HARTMANN, H., SALEET JAFRI, M. & LEDERER, W. J. 2006. The Ca²⁺ leak paradox and rogue ryanodine receptors: SR Ca²⁺ efflux theory and practice. *Prog Biophys Mol Biol*, 90, 172-85.
- SOELLER, C. & CANNELL, M. B. 1999. Examination of the transverse tubular system in living cardiac rat myocytes by 2-photon microscopy and digital image-processing techniques. *Circulation Research*, 84, 266-75.
- SOELLER, C. & CANNELL, M. B. 2002. Estimation of the sarcoplasmic reticulum Ca²⁺ release flux underlying Ca²⁺ sparks. *Biophysical Journal*, 82, 2396-414.
- SOLARO, R. J., PANG, D. C. & BRIGGS, F. N. 1971. The purification of cardiac myofibrils with Triton X-100. *Biochimica et Biophysica ACTA*, 245, 259-62.
- SOMLYO, A. V., SHULMAN, H. & SOMLYO, A. P. 1977. Composition of sarcoplasmic reticulum in situ by electron probe X-ray microanalysis. *Nature*, 268, 556 - 558.
- SONDERGAARD, M. T., TIAN, X., LIU, Y., WANG, R., CHAZIN, W. J., CHEN, S. R. & OVERGAARD, M. T. 2015. Arrhythmogenic Calmodulin Mutations Affect the Activation and Termination of Cardiac Ryanodine Receptor-mediated Ca²⁺ Release. *Journal of Biological Chemistry*, 290, 26151-62.
- SONG, L., ALCALAI, R., ARAD, M., WOLF, C. M., TOKA, O., CONNER, D. A., BERUL, C. I., ELGAR, M., SEIDMAN, C. E. & SEIDMAN, J. G. 2007. Calsequestrin 2 (CASQ2) mutations increase expression of calreticulin and ryanodine receptors, causing catecholaminergic polymorphic ventricular tachycardia. *Journal of Clinical Investigation*, 117, 1814-23.
- SONG, L., AWARI, D. W., HAN, E. Y., UCHE-ANYA, E., PARK, S. H., YABE, Y. A., CHUNG, W. K. & YAZAWA, M. 2015. Dual optical recordings for action potentials and calcium handling in induced pluripotent stem cell models of cardiac arrhythmias using genetically encoded fluorescent indicators. *Stem Cells Translational Medicine*, 4, 468-75.
- SONG, L. S., SOBIE, E. A., MCCULLE, S., LEDERER, W. J., BALKE, C. W. & CHENG, H. 2006. Orphaned ryanodine receptors in the failing heart. *Proc Natl Acad Sci U S A*, 103, 4305-10.
- SONG, Y., SHRYOCK, J. C., WU, L. & BELARDINELLI, L. 2004. Antagonism by ranolazine of the pro-arrhythmic effects of increasing late I_{Na} in guinea pig ventricular myocytes. *Journal of Cardiovascular Pharmacology*, 44, 192-9.
- SPACH, M. S., DOLBER, P. C. & ANDERSON, P. A. 1989. Multiple regional differences in cellular properties that regulate repolarization and contraction in the right atrium of adult and newborn dogs. *Circulation Research*, 65, 1594-611.
- STEELE, D. S., S, H. H. & KNOLLMANN, B. C. 2013. Triple mode action of flecainide in catecholaminergic polymorphic ventricular tachycardia. *Cardiovascular Research*, 98, 326 - 327.
- STEELE, D. S. & YANG, Z. 2017. RE: Preliminary flecainide experiments in permeabilised myocytes. Type to STEER, E.
- STERN, M. D. & CHENG, H. 2004. Putting out the fire: what terminates calcium-induced calcium release in cardiac muscle? *Cell Calcium*, 35, 591-601.
- STERN, M. D., RIOS, E. & MALTSEV, V. A. 2013. Life and death of a cardiac calcium spark. *J Gen Physiol*, 142, 257-74.

- STOKOE, K. S., THOMAS, G., GODDARD, C. A., COLLEDGE, W. H., GRACE, A. A. & HUANG, C. L. 2007. Effects of flecainide and quinidine on arrhythmogenic properties of Scn5a+/Delta murine hearts modelling long QT syndrome 3. *Journal of Physiology*, 578, 69-84.
- STOSCHITZKY, K., KOSHCHAROVA, G., LERCHER, P., MAIER, R., SAKOTNIK, A., KLEIN, W., LIEBMANN, P. M. & LINDNER, W. 2001. Stereoselective effects of (R)- and (S)-carvedilol in humans. *Chirality*, 13, 342-6.
- SUGANO, K., KANSY, M., ARTURSSON, P., AVDEEF, A., BENDELS, S., DI, L., ECKER, G. F., FISCHER, H., GEREBTZOFF, G., LENNERNAES, H. & SENNER, F. 2010. Coexistence of passive and carrier-mediated processes in drug transport. *Nature Review: Drug Discovery*, 9, 597 - 614.
- SUGIYAMA, S., HIEDA, N., OZAWA, T., FUKUSHIMA, A., OGAWA, T. & HANAKI, Y. 1989. [The effect of flecainide on 2 hour occlusion-induced myocardial damages in dog]. *Kokyu To Junkan*, 37, 443-7.
- SWIFT, L. M. & SARVAZYAN, N. 2000. Localisation of dichlorofluorescein in cardiac myocytes: implications for assessment of oxidative stress. *American Journal of Physiology. Heart and Circulatory Physiology*, 278, 982 - 990.
- SZEWCZYK, A. & WOJTCZAK, L. 2002. Mitochondria as a pharmacological target. *Pharmacological Review*, 54, 101-27.
- SZIGLIGETI, P., PANKUCSI, C., BANYASZ, T., VARRO, A. & NANASI, P. P. 1996. Action potential duration and force-frequency relationship in isolated rabbit, guinea pig and rat cardiac muscle. *Journal of Comparative Physiology B*, 166, 150-5.
- TAN, Z., XIAO, Z., WEI, J., ZHANG, J., ZHOU, Q., SMITH, C. D., NANI, A., WU, G., SONG, L. S., BACK, T. G., FILL, M. & CHEN, S. R. 2016. Nebivolol suppresses cardiac ryanodine receptor-mediated spontaneous Ca²⁺ release and catecholaminergic polymorphic ventricular tachycardia. *Biochemical Journal*, 473, 4159-4172.
- TENCEROVA, B., ZAHRADNIKOVA, A., GABURJAKOVA, J. & GABURJAKOVA, M. 2012. Luminal Ca²⁺ controls activation of the cardiac ryanodine receptor by ATP. *Journal of General Physiology*, 140, 93-108.
- TERENTYEV, D., VIATCHENKO-KARPINSKI, S., GYORKE, I., TERENTYEVA, R. & GYORKE, S. 2003a. Protein phosphatases decrease sarcoplasmic reticulum calcium content by stimulating calcium release in cardiac myocytes. *J Physiol*, 552, 109-18.
- TERENTYEV, D., VIATCHENKO-KARPINSKI, S., GYORKE, I., TERENTYEVA, R. & GYORKE, S. 2003b. Protein phosphatases decrease sarcoplasmic reticulum calcium content by stimulating calcium release in cardiac myocytes. *Journal of Physiology*, 552, 109-18.
- TERENTYEV, D., VIATCHENKO-KARPINSKI, S., VEDAMOORTHYRAO, S., ODURU, S., GYORKE, I., WILLIAMS, S. C. & GYORKE, S. 2007. Protein protein interactions between triadin and calsequestrin are involved in modulation of sarcoplasmic reticulum calcium release in cardiac myocytes. *J Physiol*, 583, 71-80.
- THOMAS, D., TOVEY, S. C., COLLINS, T. J., BOOTMAN, M. D., BERRIDGE, M. J. & LIPP, P. 2000. A comparison of fluorescent Ca²⁺ indicator properties and their use in measuring elementary and global Ca²⁺ signals. *Cell Calcium*, 28, 213-23.
- TIAN, X., TANG, Y., LIU, Y., WANG, R. & CHEN, S. R. 2013. Calmodulin modulates the termination threshold for cardiac ryanodine receptor-mediated Ca²⁺ release. *Biochemical Journal*, 455, 367-75.
- TINKER, A., LINDSAY, A. R. G. & WILLIMAS, A. J. 1992. A model for ionic conduction in the ryanodine receptor channel for sheep cardiac muscle sarcoplasmic reticulum. *Journal of General Physiology*, 100, 495 - 517.
- TOISCHER, K., HARTMANN, N., WAGNER, S., FISCHER, T. H., HERTING, J., DANNER, B. C., SAG, C. M., HUND, T. J., MOHLER, P. J., BELARDINELLI, L., HASENFUSS, G., MAIER, L. S. & SOSSALLA, S. 2013. Role of late sodium current as a potential arrhythmogenic mechanism in the progression of pressure-induced heart disease. *Journal of Molecular and Cellular Cardiology*, 61, 111-22.

- TOWNSEND, C. & ROSENBERG, R. L. 1995. Characterisation of a chloride channel reconstituted from cardiac sarcoplasmic reticulum. *Journal of Membrane Biology*, 147, 121 - 136.
- TUNWELL, R. E., WICKENDEN, C., BERTRAND, B. M., SHEVCHENKO, V. I., WALSH, M. B., ALLEN, P. D. & LAI, F. A. 1996. The human cardiac muscle ryanodine receptor-calcium release channel: identification, primary structure and topological analysis. *Biochemical Journal*, 318 (Pt 2), 477-87.
- TYSKA, M. J., DUPUIS, D. E., GUILFORD, W. H., PATLAK, J. B., WALLER, G. S., TRYBUS, K. M., WARSHAW, D. M. & LOWEY, S. 1999. Two heads of myosin are better than one for generating force and motion. *Proceedings of National Academy of Sciences*, 96, 4402-7.
- ULLRICH, N. D., VALDIVIA, H. H. & NIGGLI, E. 2012. PKA phosphorylation of cardiac ryanodine receptor modulates SR luminal Ca²⁺ sensitivity. *Journal of Molecular Cellular Cardiology*, 53, 33-42.
- UNITT, J. F., MCCORMACK, J. G., REID, D., MACLACHLAN, L. K. & ENGLAND, P. J. 1989. Direct evidence for a role of intramitochondrial Ca²⁺ in the regulation of oxidative phosphorylation in the stimulated rat heart. Studies using ³¹P n.m.r. and ruthenium red. *Biochemical Journal*, 262, 293-301.
- VAN DER WERF, C., KANNANKERIL, P. J., SACHER, F., KRAHN, A. D., VISKIN, S., LEENHARDT, A., SHIMIZU, W., SUMITOMO, N., FISH, F. A., BHUIYAN, Z. A., WILLEMS, A. R., VAN DER VEEN, M. J., WATANABE, H., LABORDERIE, J., HAISSAGUERRE, M., KNOLLMANN, B. C. & WILDE, A. A. 2011a. Flecainide therapy reduces exercise-induced ventricular arrhythmias in patients with catecholaminergic polymorphic ventricular tachycardia. *Journal of the American College of Cardiology*, 57, 2244-54.
- VAN DER WERF, C., KANNANKERIL, P. J., SACHER, F., KRAHN, A. D., VISKIN, S., LEENHARDT, A., SHIMIZU, W., SUMITOMO, N., FISH, F. A., BHUIYAN, Z. A., WILLEMS, A. R., VAN DER VEEN, M. J., WATANABE, H., LABORDERIE, J., HAISSAGUERRE, M., KNOLLMANN, B. C. & WILDE, A. A. 2011b. Flecainide therapy reduces exercise-induced ventricular arrhythmias in patients with catecholaminergic polymorphic ventricular tachycardia. *J Am Coll Cardiol*, 57, 2244-54.
- VAN DER WERF, C. & WILDE, A. A. 2013. Catecholaminergic polymorphic ventricular tachycardia: from bench to bedside. *Heart*, 99, 497-504.
- VANHOUTTE, P. M. & LEVY, M. N. 1980. Prejunctional cholinergic modulation of adrenergic neurotransmission in the cardiovascular system. *American Journal of Physiology*, 238, H275-81.
- VARELA, M., COLMAN, M. A., HANCOX, J. C. & ASLANIDI, O. V. 2016. Atrial Heterogeneity Generates Re-entrant Substrate during Atrial Fibrillation and Anti-arrhythmic Drug Action: Mechanistic Insights from Canine Atrial Models. *Public Library of Science: Computational Biology*, 12, e1005245.
- VARMA, S., SABO, D. & REMPE, S. B. 2008. K⁺/Na⁺ selectivity in K channels and valinomycin: over-coordination versus cavity-size constraints. *Journal of Molecular Biology*, 376, 13-22.
- VASEGHI, M. & SHIVKUMAR, K. 2008. The role of the autonomic nervous system in sudden cardiac death. *Progress in Cardiovascular Disease*, 50, 404-19.
- VENETUCCI, L. A., TRAFFORD, A. W. & EISNER, D. A. 2007. Increasing ryanodine receptor open probability alone does not produce arrhythmogenic calcium waves: threshold sarcoplasmic reticulum calcium content is required. *Circulation Research*, 100, 105-11.
- VENETUCCI, L. A., TRAFFORD, A. W., O'NEILL, S. C. & EISNER, D. A. 2008. The sarcoplasmic reticulum and arrhythmogenic calcium release. *Cardiovasc Res*, 77, 285-92.
- VENTURI, E., MATYJASZKIEWICZ, A., PITT, S. J., TSANEVA-ATANASOVE, K., NISHI, M., YAMAZAKI, D., TAKESHIMA, H. & SITSAPESAN, R. 2013. TRIC-B channels display labile gating: Evidence from the TRIC-A knockout mouse model. *European Journal of Physiology*, 465, 1135 - 1148.

- VIATCHENKO-KAPINSKI, S. & GYORKE, S. 2001. Modulation of the calcium induced calcium release cascade by beta-adrenergic stimulation in rat ventricular myocytes. *Journal of Physiology*, 533, 837 - 848.
- VIGNESWARAN, T. V., CALLAGHAN, N., ANDREWS, R. E., MILLER, O., ROSENTHAL, E., SHARLAND, G. K. & SIMPSON, J. M. 2014. Correlation of maternal flecainide concentrations and therapeutic effect in fetal supraventricular tachycardia. *Heart Rhythm*, 11, 2047-53.
- VIITASALO, M., OIKARINEN, L., SWAN, H., VAANANEN, H., JARVENPAA, J., HIETANEN, H., KARJALAINEN, J. & TOIVONEN, L. 2006. Effects of beta-blocker therapy on ventricular repolarization documented by 24-h electrocardiography in patients with type 1 long-QT syndrome. *Journal of the American College of Cardiology*, 48, 747-53.
- VLADIMIROV, A., SERGEEVA, N. S., RUBTSOV, B. & KLEBANOV, G. I. 1978. Effect of valinomycin on structural and functional transitions in sarcoplasmic reticulum membranes. *Biofizika*, 23, 165 - 167.
- WALKER, M. A., WILLIAMS, G. S., KOHL, T., LEHNART, S. E., JAFRI, M. S., GREENSTEIN, J. L., LEDERER, W. J. & WINSLOW, R. L. 2014. Superresolution modeling of calcium release in the heart. *Biophys J*, 107, 3018-29.
- WALKER, M. J. 2006. Antiarrhythmic drug research. *British Journal of Pharmacology*, 147 Suppl 1, S222-31.
- WALSH, M. A., STUART, A. G., SCHLECHT, H. B., JAMES, A. F., HANCOX, J. C. & NEWBURY-ECOB, R. A. 2016. Compound Heterozygous Triadin Mutation Causing Cardiac Arrest in Two Siblings. *Pacing and Clinical Electrophysiology*, 39, 497-501.
- WALWEEL, K., MOLENAAR, P., IMTIAZ, M. S., DENNISS, A., DOS REMEDIOS, C., VAN HELDEN, D. F., DULHUNTY, A. F., LAVER, D. R. & BEARD, N. A. 2017. Ryanodine receptor modification and regulation by intracellular Ca²⁺ and Mg²⁺ in healthy and failing human hearts. *Journal of Molecular and Cellular Cardiology*.
- WANG, G. K., RUSSELL, C. & WANG, S.-Y. 2003. State-dependent block of wild-type and inactivation deficient sodium channels by flecainide. *The Journal of General Physiology*, 122, 365 - 374.
- WANG, R., ZHONG, X., MENG, X., KOOP, A., TIAN, X., JONES, P. P., FRUEN, B. R., WAGENKNECHT, T., LIU, Z. & CHEN, S. R. 2011. Localization of the dantrolene-binding sequence near the FK506-binding protein-binding site in the three-dimensional structure of the ryanodine receptor. *Journal of Biological Chemistry*, 286, 12202-12.
- WANG, W., BARNABEI, M. S., ASP, M. L., HEINIS, F. I., ARDEN, E., DAVIS, J., BRAUNLIN, E., LI, Q., DAVIS, J. P., POTTER, J. D. & METZGER, J. M. 2013. Noncanonical EF-hand motif strategically delays Ca²⁺ buffering to enhance cardiac performance. *Nat Med*, 19, 305-12.
- WANG, Z., FERMINI, B. & NATTEL, S. 1993a. Delayed rectifier outward current and repolarization in human atrial myocytes. *Circulation Research*, 73, 276-85.
- WANG, Z., FERMINI, B. & NATTEL, S. 1993b. Mechanism of flecainide's rate-dependent actions on action potential duration in canine atrial tissue. *Journal of Pharmacology and Experimental Therapeutics*, 267, 575-81.
- WATANABE, H., CHOPRA, N., LAVER, D., HWANG, H. S., DAVIE, S. S., ROACH, D. E., DUFF, H. J., RODEN, D. M., WILDE, A. A. M. & KNOLLMANN, B. C. 2009. Flecainide prevents catecholaminergic polymorphic ventricular tachycardia in mice and humans. *Nature Medicine*, 15, 380-383.
- WATANABE, H. & KNOLLMANN, B. C. 2011. Mechanism underlying catecholaminergic polymorphic ventricular tachycardia and approaches to therapy. *Journal of Electrocardiology*, 44, 650-5.
- WEHRENS, X. H., LEHNART, S. E., HUANG, F., VEST, J. A., REIKEN, S. R., MOHLER, P. J., SUN, J., GUATIMOSIM, S., SONG, L. S., ROSEMBLIT, N., D'ARMIENTO, J. M., NAPOLITANO, C., MEMMI, M., PRIORI, S. G., LEDERER, W. J. & MARKS, A. R. 2003. FKBP12.6 deficiency and defective calcium release channel (ryanodine receptor) function linked to exercise-induced sudden cardiac death. *Cell*, 113, 829-40.

- WEHRENS, X. H. T., LEHNART, S. E., REIKEN, S. R. & MARKS, A. R. 2004. Calcium/Calmodulin-dependent protein kinase II phosphorylation regulates RyR2. *Circulation Research*, 94, 61 - 70.
- WEITL, N. & SEIFERT, R. 2008. Distinct interactions of human beta1- and beta2-adrenoceptors with isoproterenol, epinephrine, norepinephrine, and dopamine. *Journal of Pharmacology and Experimental Therapeutics*, 327, 760-9.
- WESTCOTT, A. P., JAFRI, M. S., LEDERER, W. J. & WILLIAMS, G. S. B. 2016. RyR2 sensitivity governs the stability and synchrony of local calcium release during cardiac excitation-contraction coupling. *Journal of Molecular and Cellular Cardiology*, 92, 82 - 92.
- WESTENBROEK, R. E., BISCHOFF, S., FU, Y., MAIER, S. K., CATTERALL, W. A. & SCHEUER, T. 2013. Localization of sodium channel subtypes in mouse ventricular myocytes using quantitative immunocytochemistry. *Journal of Molecular and Cellular Cardiology*, 64, 69-78.
- WILLIAMS, G. S., BOYMAN, L., CHIKANDO, A. C., KHAIRALLAH, R. J. & LEDERER, W. J. 2013. Mitochondrial calcium uptake. *Proc Natl Acad Sci U S A*, 110, 10479-86.
- WILLIAMS, G. S., CHIKANDO, A. C., TUAN, H. T., SOBIE, E. A., LEDERER, W. J. & JAFRI, M. S. 2011. Dynamics of calcium sparks and calcium leak in the heart. *Biophysical Journal*, 101, 1287-96.
- WILLINGHAM, M. C. 2010. *Immunocytochemical Methods and Protocol, Methods in Molecular Biology*, Humana Press.
- WINSLOW, R. L., TANSKANEN, A., CHEN, M. & GREENSTEIN, J. L. 2006. Multiscale modeling of calcium signaling in the cardiac dyad. *Annals of the New York Academy of Sciences*, 1080, 362-75.
- WOLF, P. A., ABBOTT, R. D. & KANNEL, W. B. 1991. Atrial fibrillation as an independent risk factor for stroke: the Framingham Study. *Stroke*, 22, 983-8.
- WU, X. & BERS, D. M. 2007. Free and bound intracellular calmodulin measurements in cardiac myocytes. *Cell Calcium*, 41, 353-64.
- XIAO, Z., GUO, W., SUN, B., HUNT, D. J., WEI, J., LIU, Y., WANG, Y., WANG, R., JONES, P. P., BACK, T. G. & CHEN, S. R. 2016. Enhanced Cytosolic Ca²⁺ Activation Underlies a Common Defect of Central Domain Cardiac Ryanodine Receptor Mutations Linked to Arrhythmias. *Journal of Biological Chemistry*, 291, 24528-24537.
- XU, F., ZHANG, M., HE, W., HAN, R., XUE, F., LIU, Z., ZHANG, F., LIPPINCOTT-SCHWARTZ, J. & XU, P. 2016. Live cell single molecule-guided Bayesian localization super resolution microscopy. *Cell Research*.
- XU, X., YANO, M., UCHINOUMI, H., HINO, A., SUETOMI, T., ONO, M., TATEISHI, H., ODA, T., OKUDA, S., DOI, M., KOBAYASHI, S., YAMAMOTO, T., IKEDA, Y., IKEMOTO, N. & MATSUZAKI, M. 2010. Defective calmodulin binding to the cardiac ryanodine receptor plays a key role in CPVT-associated channel dysfunction. *Biochemical and Biophysical Research Communications*, 394, 660-6.
- YABUUCHI, H., TAMAI, I., NEZU, J.-I., SAKAMOTO, K., OKU, A., SHIMANE, M., SAI, Y. & TSUJI, A. 1998. Novel membrane and transporter OCTN1 mediates multispecific, bidirectional and pH dependent transport of organic cations. *The Journal of Pharmacology and Experimental Therapeutics*, 289, 768 - 773.
- YAMAMOTO, T. & IKEMOTO, N. 2002. Spectroscopic monitoring of local conformational changes during the intramolecular domain-domain interaction of the ryanodine receptor. *Biochemistry*, 41, 1492-501.
- YANG, H., HU, M., GUO, J., OU, X., CAI, T. & LIU, Z. 2016. Pore architecture of TRIC channels and insights into their gating mechanism. *Nature*, 538, 537-541.
- YANG, T., MCBRIDE, B. F., LEAKE, B. F., KIM, R. B. & RODEN, D. M. 2010. Modulation of drug block by the cardiac potassium channel KCNA5 by the drug transporters OCTN1 and MDR1. *British Journal of Pharmacology*, 161, 1023 - 1033.
- YANG, Y., GUO, T., ODA, T., CHAKRABORTY, A., CHEN, L., UCHINOUMI, H., KNOWLTON, A. A., FRUEN, B. R., CORNEA, R. L., MEISSNER, G. & BERS, D. M. 2014. Cardiac myocyte Z-line

- calmodulin is mainly RyR2-bound, and reduction is arrhythmogenic and occurs in heart failure. *Circulation Research*, 114, 295-306.
- YANG, Z., IKEMOTO, N., LAMB, G. D. & STEELE, D. S. 2006. The RyR2 central domain peptide DPc10 lowers the threshold for spontaneous Ca²⁺ release in permeabilized cardiomyocytes. *Cardiovascular Research*, 70, 475-85.
- YANG, Z., PASCAREL, C., STEELE, D. S., KOMUKAI, K., BRETTE, F. & ORCHARD, C. H. 2002. Na⁺-Ca²⁺ exchange activity is localized in the T-tubules of rat ventricular myocytes. *Circulation Research*, 91, 315-22.
- YANG, Z. & STEELE, D. S. 2002. Effects of phosphocreatine on SR Ca(2+) regulation in isolated saponin-permeabilized rat cardiac myocytes. *Journal of Physiology*, 539, 767-77.
- YAO, J. A., JIANG, M., FAN, J. S., ZHOU, Y. Y. & TSENG, G. N. 1999. Heterogeneous changes in K currents in rat ventricles three days after myocardial infarction. *Cardiovascular Research*, 44, 132-45.
- YAZAWA, M., FERRANTE, C., FENG, J., MIO, K., OGURA, T., ZHANG, M., LIN, P.-H., PAN, Z., KOMAZAKI, S., KATO, K., NISHI, M., ZHAO, X., WEISLEDER, N., SATO, C., MA, J. & TAKESHIMA, H. 2007. TRIC channels are essential for calcium handling in intracellular stores. *Nature*, 448, 78 - 83.
- YEOLA, S. W. & SNYDERS, D. J. 1997. Electrophysiological and pharmacological correspondence between Kv4.2 current and rat cardiac transient outward current. *Cardiovasc Res*, 33, 540-7.
- YU, J. Z. & RASENICK, M. M. 2002. Real-time visualization of a fluorescent G(alpha)(s): dissociation of the activated G protein from plasma membrane. *Mol Pharmacol*, 61, 352-9.
- ZHANG, J., ZHOU, Q., SMITH, C. D., CHEN, H., TAN, Z., CHEN, B., NANI, A., WU, G., SONG, L. S., FILL, M., BACK, T. G. & CHEN, S. R. 2015. Non-beta-blocking R-carvedilol enantiomer suppresses Ca²⁺ waves and stress-induced ventricular tachyarrhythmia without lowering heart rate or blood pressure. *Biochemical Journal*, 470, 233-42.
- ZHANG, Z., ZHAO, Z., LIU, Y., WANG, W., WU, Y. & DING, J. 2013. Kinetic model of Nav1.5 channel provides a subtle insight into slow inactivation associated excitability in cardiac cells. *Public Library of Science*, 8, e64286.
- ZHONG, X., LIU, J., LU, F., WANG, Y., ZHAO, Y., DONG, S., LENG, X., JIA, J., REN, H., XU, C. & ZHANG, W. 2012. Calcium sensing receptor regulates cardiomyocyte function through nuclear calcium. *Cell Biology International*, 36, 937-43.
- ZHOU, Q., XIAO, J., JIANG, D., WANG, R., VEMBAIYAN, K., WANG, A., SMITH, C. D., XIE, C., CHEN, W., ZHANG, J., TIAN, X., JONES, P. P., ZHONG, X., GUO, A., CHEN, H., ZHANG, L., ZHU, W., YANG, D., LI, X., CHEN, J., GILLIS, A. M., DUFF, H. J., CHENG, H., FELDMAN, A. M., SONG, L. S., FILL, M., BACK, T. G. & CHEN, S. R. 2011. Carvedilol and its new analogs suppress arrhythmogenic store overload-induced Ca²⁺ release. *Nature Medicine*, 17, 1003-9.
- ZHOU, X., LIN, P.-H., YAMAZAKI, D., PARK, K.-S., KOMAZAKI, S., WAYNE CHEN, S. R., TAKESHIMA, H. & MA, J. 2014. Trimeric intracellular cation channels and sarcoplasmic/endoplasmic reticulum calcium homeostasis. *Circulation Research*, 114, 706 - 716.
- ZHU, J., LIU, M., KENNEDY, R. H. & LIU, S. J. 2006. TNF-alpha-induced impairment of mitochondrial integrity and apoptosis mediated by caspase-8 in adult ventricular myocytes. *Cytokine*, 34, 96-105.
- ZIMA, A. V., BARE, D. J., MIGNERY, G. A. & BLATTER, L. A. 2007. IP3-dependent nuclear Ca²⁺ signalling in the mammalian heart. *Journal of Physiology*, 584, 601-11.
- ZIMA, A. V. & BLATTER, L. A. 2004. Inositol-1,4,5-trisphosphate-dependent Ca(2+) signalling in cat atrial excitation-contraction coupling and arrhythmias. *Journal of Physiology*, 555, 607-15.
- ZIMA, A. V., BOVO, E., BERS, D. M. & BLATTER, L. A. 2010. Calcium spark-dependent and -independent sarcoplasmic reticulum calcium leak in normal and failing rabbit ventricular myocytes. *Journal of Physiology*, 588, 4743 - 4757.

